THE JOURNAL
OF
CHEMICAL PHYSICS

VOLUME 17, NUMBER 10 OCTOBER, 1949

Editorial

THE tremendous increase in research since the close of the war, added to the considerable broadening in the field of chemical physics, has resulted in an enormous growth in the number of manuscripts submitted to the editorial office of the *Journal of Chemical Physics*. Whereas, before the war the *Journal of Chemical Physics* had gradually increased to 1128 pages in the year 1939, which was the largest volume prior to 1948, the number of manuscripts submitted and accepted for publication during 1949 would probably amount to approximately 2000 pages in the Journal.

With the increase in all publication costs, the current subscription rate would not be adequate to keep the finances of the Journal out of the deficit column if all these manuscripts were published. This is in spite of an increase in the number of subscribers and a considerable effort to effect all economies possible.

The Executive Committee of the American Institute of Physics had decided to budget the *Journal of Chemical Physics* to 1200 pages for the 1949 volume which was estimated to result in zero profit. The result has been evident to the authors and readers in that the time elapsed between receipt of an article and eventual publication has been increasing steadily to approximately ten months at the present time, while only approximately three months is required by the techniques of publication.

In view of the obvious undesirability of delaying publication, the Executive Committee of the American Institute of Physics recently agreed to increase the budget sufficiently to permit the publication of as many as 2000 pages for the year 1949, subject only to the capacity of the printer to absorb the sudden increase without delaying publication dates. Presumably the latter limitation will not permit the publication of quite as many pages in this year as has been allowed. This decision of the Executive Committee of the Institute was taken in spite of the fact that it would result in a very serious deficit in the finances of the Journal.

In order to attempt to maintain a considerably increased number of pages in the future, consistent with the quantity of valuable research published in the field of chemical physics, it is necessary to increase the subscription price of the Journal. The new prices will be

Members of the Institute	$12.00
Non-members	15.00
Foreign members	13.00
Foreign non-members	16.00

In addition an increase in the page charge for publication will shortly be adopted.

It is hoped that with these changes in subscription rates and in the page charge the *Journal of Chemical Physics* can continue to exist and to perform the same service of prompt publication that it has in the past.

JOSEPH E. MAYER
Editor

The Normal Vibrations of Polyatomic Molecules as Calculated by Urey-Bradley Field. III. A Table of Force Constants

TAKEHIKO SIMANOUTI
Chemical Institute, Faculty of Science, Tokyo University, Tokyo, Japan
(Received February 23, 1949)

Assuming the Urey-Bradley field for various chemical structures, stretching, bending and repulsive force constants were determined so as to give the best fit with the observed vibration frequencies. The magnitude of these force constants, especially of repulsive constants, was discussed.

INTRODUCTION

IN the preceding two papers[1,2] in which consistent normal coordinate treatments were applied to twenty simple polyatomic molecules, it was concluded that the Urey-Bradley field is an adequate type of potential energy in analysing the vibrational spectra. The potential energy of molecules due to this field is expressed as follows:[3]

$$V=\sum_i [K_i' r_{i0}\Delta r_i+\tfrac{1}{2}K_i(\Delta r_i)^2]+\sum_{i<j} [H_{ij}' r_{ij0}^2\Delta\alpha_{ij}+\tfrac{1}{2}H_{ij}(r_{ij0}\Delta\alpha_{ij})^2]+\sum_{i<j} [F_{ij}' q_{ij0}\Delta q_{ij}+\tfrac{1}{2}F_{ij}(\Delta q_{ij})^2], \quad (1)$$

where r_i is the bond length C$-$X$_i$, α_{ij} is the bond angle X$_i-$C$-$X$_j$, q_{ij} is the distance between atoms (X$_i$ and X$_j$) which are not bonded directly, r_{ij} represents $(r_i r_j)^{\frac{1}{2}}$, r_{i0}, r_{ij0}, and q_{ij0} denote the equilibrium values of these distances, and Δ refers to the change in the following symbol from its equilibrium values. K' and K are stretching constants, H' and H are bending constants, and F' and F are repulsive constants.

The purpose of this paper is to apply this potential to the calculation of frequencies of other polyatomic molecules and to obtain a table of force constants K, H, F', F, and intramolecular tensions κ, for various chemical structures.*

CALCULATION

Three types of molecules, CX$_4$, CX$_3-$CX$_3$, and $-$CX$_2-$CX$_2-$, have been dealt with. Since the technique developed by Wilson[4] is quite straightforward, we have used this procedure. Assuming tetrahedral angles ($\alpha_0=109°\,28'$), and using the G and F matrices, the secular equations for these molecules are found to be

$$|\mathbf{GF}-3M_C\lambda\mathbf{E}|=0, \quad (2)$$

where M_C is the mass of C atom, $\mathbf{E}$ is the unit matrix, and λ is $4\pi^2c^2\nu^2$, c and ν being, respectively, the velocity of light and the vibration frequency (cm^{-1}).

For the $\mathbf{G}$ and $\mathbf{F}$ matrices of CX$_4$ molecule we have

$$\mathbf{G}_A=m,\quad \mathbf{F}_A=a+3c,\quad \mathbf{G}_E=3m,\quad \mathbf{F}_E=2b-4e,\quad \mathbf{G}_T=\begin{pmatrix}4+m, & -8\\ -8, & 16+2m\end{pmatrix},\quad \mathbf{F}_T=\begin{pmatrix}a-c, & 2k\\ 2k, & 2b\end{pmatrix}. \quad (3)$$

TABLE I. Force constants and intramolecular tensions.

Stretching force constants K (10^5 dynes/cm)

C$-$H	4.8$\sim$3.9[a]	Si$-$H	2.7
C$-$C	2.8$\sim$2.0[b]	Si$-$Si	1.25
C$-$F	3.75	Si$-$F	5.4
C$-$CH$_3$	3.7	Si$-$CH$_3$	3.05
C$-$Cl	1.75	Si$-$Cl	2.6
C$-$Br	1.45	Si$-$Br	2.0

Bending force constants H (10^5 dynes/cm)

H$-$C$-$H	0.4	C$-$C$-$H	0.15	H$-$Si$-$H	0.15
CH$_3-$C$-$CH$_3$	0.2	C$-$C$-$F	0.15	CH$_3-$Si$-$CH$_3$	0.1
F$-$C$-$F	0.15	C$-$C$-$Cl	0.1	F$-$Si$-$F	0.02
Cl$-$C$-$Cl	0.1	C$-$C$-$Br	0.1	Cl$-$Si$-$Cl	0.04
Br$-$C$-$Br	0.05	H$-$C$-$Cl	0.05	Br$-$Si$-$Br	0.04
		Cl$-$C$-$Br	0.05		

Repulsive force constants F' (10^5 dynes/cm)

H...H	0.0	C...H	-0.05	H...H[c]	-0.03
CH$_3$...CH$_3$	-0.05	C...F	-0.1	CH$_3$...CH$_3$[c]	-0.02
F...F	-0.3	C...Cl	-0.1	F...F[c]	-0.31
Cl...Cl	-0.1	C...Br	-0.1	Cl...Cl[c]	-0.06
Br...Br	-0.1	H...Cl	-0.05	Br...Br[c]	-0.04
		Cl...Br	-0.1		

Repulsive force constants F (10^5 dynes/cm)

H...H	0.1	C...H	0.4	H...H[c]	0.04
CH$_3$...CH$_3$	0.3	C...F	1.3	CH$_3$...CH$_3$[c]	0.03
F...F	1.35	C...Cl	0.6	F...F[c]	0.43
Cl...Cl	0.65	C...Br	0.5	Cl...Cl[c]	0.3
Br...Br	0.5	H...Cl	0.8	Br...Br[c]	0.23
		Cl...Br	0.55		

Intramolecular tensions κ (10^{-11} dynes·cm)

CH$_4\sim$CD$_4$	0	$-$CH$_2-$CH$_2-$	0.2	SiH$_4$	0.05
C(CH$_3$)$_4$	0.1	C$_2$H$_6$, C$_2$D$_6$	0.05	Si(CH$_3$)$_4$	0.05
CF$_4$	0.5	$-$CF$_2-$CF$_2-$	0.3	SiF$_4$	0.7
CCl$_4$	0.3	C$_2$F$_6$	0.3	SiCl$_4$	0.25
CBr$_4$	0.3	C$_2$Cl$_6$	0.1	SiBr$_4$	0.15
		C$_2$Br$_6$	0.1		
		CCl$_3$Br, CCl$_2$Br$_2$, CClBr$_3$	0.3		

[a] K_{CH}=4.8 (CH$_4$), 4.5 (CH$_3-$), 4.2 (CH$_2-$), 3.9 (CH$-$).
[b] K_{CC}=2.8 (C$_2$H$_6$), 2.0 (C$_2$Cl$_6$, C$_2$Br$_6$, C$_2$F$_6$).
[c] Values for SiX$_4$.

[1] T. Simanouti, J. Chem. Phys. **17**, 245 (1949).
[2] T. Simanouti, J. Chem. Phys. **17**, 734 (1949).
[3] H. C. Urey and C. A. Bradley, Phys. Rev. **38**, 1969 (1931).
* The other constants K' and H' are represented in terms of F' and κ (see reference 1, Eqs. (7) and (8)).
[4] E. B. Wilson, Jr., J. Chem. Phys. **7**, 1047 (1939); **9**, 76 (1941).

In the case of CX_3-CX_3 molecule,[5]

$$\mathbf{G}_{A1g}=\begin{pmatrix} 36, & -6, & -24 \\ -6, & 1+m, & 4 \\ -24, & 4, & 16+2m \end{pmatrix},$$

$$\mathbf{F}_{A1g}=\begin{pmatrix} a_0/6, & c_1, & k_1 \\ c_1, & a'+2c, & k_2-2k \\ k_1, & k_2-2k, & b_1+b \end{pmatrix},$$

$$\mathbf{G}_{A2u}=\begin{pmatrix} 1+m, & 4 \\ 4, & 16+2m \end{pmatrix},$$

$$\mathbf{F}_{A2u}=\begin{pmatrix} a'+2c, & k_2-2k \\ k_2-2k, & b_1+b \end{pmatrix}, \qquad (4)$$

$$\mathbf{G}_{Eg}=\begin{pmatrix} 4+m, & -2p, & 8 \\ -2p, & p^2+2m, & -4p+m \\ 8, & -4p+m, & 16+5m \end{pmatrix},$$

$$\mathbf{G}_{Eu}=\begin{pmatrix} 4+m, & -2, & 8 \\ -2, & 1+2m, & -4+m \\ 8, & -4+m, & 16+5m \end{pmatrix},$$

$$\mathbf{F}_{Eg}=\mathbf{F}_{Eu}=\begin{pmatrix} a'-c, & k_2, & -k \\ k_2, & b_1-e, & -e \\ -k, & -e, & b-e \end{pmatrix}.$$

And for the infra-red active vibrations of $-CX_2-CX_2-$ molecule (linear extended form) we have**

$$\mathbf{G}_{A2u}=9+3m,$$

$$\mathbf{F}_{A2u}=b_1,$$

$$\mathbf{G}_{A1u}=\begin{pmatrix} 2+m, & 4 \\ 4, & 8+2m \end{pmatrix},$$

$$\mathbf{F}_{A1u}=\begin{pmatrix} a''+c, & k_2-2k \\ k_2-2k, & (b_1+4b-6e)/2 \end{pmatrix}, \qquad (5)$$

$$\mathbf{G}_{B1u}=\begin{pmatrix} 4+m, & -4 \\ -4, & 4+2m \end{pmatrix},$$

$$\mathbf{F}_{B1u}=\begin{pmatrix} a''-c, & k_2 \\ k_2, & b_1/2 \end{pmatrix}.$$

Here

$$\begin{aligned} a&=K_{CX}+F_{XX'}+2F_{XX}, \\ a'&=K_{CX}+\tfrac{2}{3}F_{XX'}+(4/3)F_{XX}+2t_1^2F_{CX'}+s_1^2F_{CX}, \\ a''&=K_{CX}+\tfrac{1}{3}F_{XX'}+\tfrac{2}{3}F_{XX}+4t_1^2F_{CX'}+2s_1^2F_{CX}, \\ a_0&=K_{CC}+6(2t_0^2F_{CX'}+s_0^2F_{CX}), \\ b&=(H_{XCX}-\tfrac{2}{3}F_{XX'}+\tfrac{1}{3}F_{XX})/2+(3\kappa/4\sqrt{2}r_1^2), \\ b_1&=(H_{CCX}-s_0s_1F_{CX'}+2t_0t_1F_{CX})(r_0/2r_1) \\ &\qquad +(3\kappa/4\sqrt{2}r_1^2), \\ c&=-\tfrac{1}{3}F_{XX'}+\tfrac{2}{3}F_{XX}, \\ c_1&=-2t_0t_1F_{CX'}+s_0s_1F_{CX}, \\ k&=\tfrac{1}{3}(F_{XX'}+F_{XX}), \\ k_1&=t_0s_1F_{CX'}+t_1s_0F_{CX}, \\ k_2&=(t_1s_0F_{CX'}+t_0s_1F_{CX})(r_0/r_1), \\ e&=(\kappa/2\sqrt{2}r_1^2), \\ m&=3M_C/M_X, \\ p&=(6r_1/r_0)+1, \end{aligned} \qquad (6)$$

with the abbreviations

$$\begin{aligned} s_0&=(3r_0+r_1)/3q_{CX}, \\ s_1&=(3r_1+r_0)/3q_{CX}, \\ t_0&=2r_1/3q_{CX}, \\ t_1&=2r_0/3q_{CX}, \end{aligned} \qquad (7)$$

M_X, r_0, and r_1 being respectively the mass of X atom, C−C bond length, and C−X bond length.

The force constants obtained from these equations are tabulated in Table I,*** and the frequencies calculated for various molecules are compared with the observed values in Table II.

DISCUSSION

In 1941 a table of force constants was given by Crawford and Brinkley.[6] Since that time the table has been extended for various molecules by several authors. These sets of force constants are fairly reliable, being based upon a treatment of sufficient generality and consistency. The table given in the present paper, however, is different from those tables in that it involves *repulsive force constants* (F' and F) and *intramolecular tensions* (κ) instead of *interaction terms*.

Whether or not this approximation method is more physically significant depends of course upon the molecule discussed. But in the case of heavy atoms such as chlorine and bromine, the approximation of the Urey-Bradley field seems to be more adequate, because it is mainly valency electron that gives too complex potential energy to be expressed by the Urey-Bradley field. In fact the calculated frequencies of CCl_3-CCl_3 and CBr_3-CBr_3 as well as those of $CClBr_3$, CCl_2Br_2, and CCl_3Br treated in the preceding paper[1] are in satisfactory agreement with the observed. In the case of molecules which have hydrogen atoms the results also seems better than expected.

The magnitude of stretching force constants (K) given in Table I are found to be reasonable when we

[5] These **G** matrices are in agreement with those given by E. L. Pace, J. Chem. Phys. **16**, 74 (1948).

** These formulas are in agreement with those described in reference 2. Details of the normal coordinate treatment of extended linear polymers and the selection rule for infra-red absorption and Raman effect will be given in near future.

*** Table I includes force constants obtained in the previous papers.

[6] B. L. Crawford, Jr. and S. R. Brinkley, Jr., J. Chem. Phys. **9**, 69 (1941).

TABLE II. Calculated and observed vibration frequencies (cm^{-1}).

		Obs.	Calc.	Δν Percent			Obs.	Calc.	Δν Percent
CH_4	A	2916[a]	2960	1.5	SiH_4	A	2187[b,c,d]	2195	0.4
	E	1499	1480	1.3		E	975	936	4.0
	T	1306	1324	1.4		T	910	885	2.7
		3018	3037	0.6			2183	2189	0.3
$C(CH_3)_4$	A	734[e,f]	744	1.4	$Si(CH_3)_4$	A	598[g]	598	0.0
	E	336	328	2.4		E	202	199	1.5
	T	415	426	2.6		T	239	240	0.4
		(925) (1253)	1133	...			696 863	782	...
CF_4	A	904[h,i,j]	904	0.0	SiF_4	A	797[h,i,k]	798	0.1
	E	437	433	0.9		E	268	267	0.4
	T	635	628	1.1		T	463	462	0.2
		1265	1239	2.1			1022	1023	0.1
CCl_4	A	460[l,m]	456	0.9	$SiCl_4$	A	424[n]	426	0.5
	E	218	224	2.7		E	150	152	1.3
	T	314	318	1.3		T	221	224	1.4
		761 787	787	...			608	612	0.7
CBr_4	A	269[l]	271	0.7	$SiBr_4$	A	249[n]	249	0.0
	E	123	126	2.4		E	90	91	1.0
	T	183	188	2.7		T	137	137	0.0
		654 672	696	...			487	487	0.0
C_2Cl_6 (C−C=1.54A, C−Cl=1.77A)					C_2Br_6 (C−C=1.54A, C−Br=1.92A)				
	A_{1g}	170[o,p]	185	8.8		A_{1g}	...	110	...
		431	432	0.2			255[o]	258	1.2
		975	982	0.7			...	944	...
	A_{2u}	...	368	...		A_{2u}	...	222	...
		...	696	...			...	596	...
	E_u	...	130	...		E_u	...	80	...
		...	271	...			...	158	...
		...	743	...			...	640	...
	E_g	223	205	8.1		E_g	139	121	13.0
		340	322	5.3			204	195	4.4
		859	885	2.9			768	828	7.8
C_2F_6 (C−C=1.54A, C−F=1.36A)					$-CF_2-CF_2-$ (C−C=1.54A, C−F=1.36A)				
	A_{1g}	349[q,r,s]	391	12.0		A_{1u}	...	573	...
		809	846	4.6			1150[t] ~1250	1191	...
		1420	1231	13.3					
	A_{2u}	714	698	2.2		B_{1u}	719 ~787	665	...
		1117	1154	3.3					
	E_u	216	248	14.8		B_{2u}	...	209	...
		523	531	1.5			1150 ~1250	1137	...
		1251	1159	7.3					
	E_g	380	376	1.1					
		620	612	1.3					
		1237	1224	1.1					

[a] D. M. Dennison, Rev. Mod. Phys. **12**, 208 (1940).
[b] W. B. Steward and H. H. Nielsen, Phys. Rev. **47**, 828 (1935).
[c] F. Stitt and D. M. Yost, J. Chem. Phys. **4**, 82 (1936).
[d] Straley, Tindal, and Nielsen, Phys. Rev. **58**, 1002 (1940).
[e] K. W. F. Kohlrausch and F. Köppl, Zeits. f. physik. Chemie **B26**, 209 (1934).
[f] D. H. Rank, J. Chem. Phys. **1**, 572 (1933).
[g] F. T. Wall and C. R. Eddy, J. Chem. Phys. **6**, 107 (1938).
[h] Yost, Lassetre, and Gross, J. Chem. Phys. **4**, 325 (1936).
[i] A. Eucken and A. Betram, Zeits. f. physik. Chemie **B31**, 361 (1936).
[j] Bailey, Hale, and Thompson, Proc. Roy. Soc. (London) **A167**, 555 (1938).
[k] D. M. Yost, Proc. Ind. Acad. Sci. **8A**, 333 (1938).
[l] A. Langseth, Zeits. f. Physik **72**, 350 (1931).
[m] Morino, Watanabe, and Mizushima, Sci. Pap. I.P.C.R. (Tokyo) **39**, 348 (1938).
[n] K. W. F. Kohlrausch, *Der Smekal-Raman-Effect, Ergänzungsband 1931-1937* (Verlag. Julius Springer, Berlin, 1938).
[o] D. T. Hamilton and F. F. Cleveland, J. Chem. Phys. **12**, 249 (1944). See also references in this article.
[p] S. Mizushima and co-workers, unpublished.
[q] P. Torkington and H. W. Thompson, Trans. Faraday Soc. **41**, 236 (1945).
[r] D. H. Rank and E. L. Pace, J. Chem. Phys. **15**, 39 (1947).
[s] Nielsen, Richards, and McMurry, J. Chem. Phys. **16**, 67 (1948).
[t] W. E. Hanford and R. M. Joyce, J. Am. Chem. Soc. **68**, 2082 (1946).

compare them with the corresponding values calculated by Badger's rule[7] which was proposed to give force constants for diatomic molecules. The details will be discussed in the following paper in which we shall treat various oxide molecules.

The bending force constants (H) are small (0.1∼0.05) in the case of Cl−C−Cl and Br−C−Br, and large (0.4) in the case of H−C−H. This fact gives some suggestions as to the density distribution of valency electron clouds for these molecules. We wish that these values may be extended and be compared with theoretical values which will in future be obtained by the theory of chemical bond.

From the magnitude of repulsive force constants (F' and F) we may justify the present assumption. The

[7] R. M. Badger, J. Chem. Phys. **2**, 128 (1934).

TABLE III. Constants for interatomic potential energy.

	Neon[a]	Argon[a]	Krypton[b]
r_0 (A)	3.08	3.83	4.06
ϕ_0 (10^{15} erg)	4.89	16.5	22.6

[a] R. H. Fowler and E. A. Guggenheim, *Statistical Thermodynamics* (Cambridge University Press, London, 1939), p. 285.
[b] T. Kihara and M. Kotani, Proc. Phys. Math. Soc. Japan **25**, 602 (1943).

exact magnitude of those repulsive forces, when atoms are so close together, has not yet been published so far as we know. But it seems likely that the corresponding extrapolation of interatomic forces of neon, argon, and krypton empirically obtained from interatomic distances, heats of sublimation, second virial coefficients and other methods gives the right order of magnitude as the values of F_{FF}', F_{FF}, F_{ClCl}', F_{ClCl}, F_{BrBr}', and F_{BrBr}.

The interatomic potential energy of neon etc., is expressed by Lennard-Jones as

$$U(q)=\phi_0[(r_0/q)^{12}-2(r_0/q)^6], \tag{8}$$

where r_0 is the value of interatomic distance q at which $U(q)$ has a minimum value equal to $-\phi_0$. The values of ϕ_0 and r_0 used are tabulated in Table III. From this equation F' and F defined in Eq. (1) are expressed by

$$F'=\left(\frac{1}{q}\frac{dU}{dq}\right)_{q=q_0}=\frac{12\phi_0}{q_0^2}\left[-\left(\frac{r_0}{q_0}\right)^{12}+\left(\frac{r_0}{q_0}\right)^6\right], \tag{9}$$

$$F=\left(\frac{d^2U}{dq^2}\right)_{q=q_0}=\frac{12\phi_0}{q_0^2}\left[13\left(\frac{r_0}{q_0}\right)^{12}-7\left(\frac{r_0}{q_0}\right)^6\right]. \tag{10}$$

TABLE IV. Force constants, F' and F, and interatomic forces (10^5 dynes/cm).

	F	F'		F	F'
F...F (CF_4)	1.35	−0.30	F...F (SiF_4)	0.43	−0.31
Ne...Ne (2.22A)	0.75	−0.05	Ne...Ne (2.51A)	0.12	−0.01
Cl...Cl (CCl_4)	0.65	−0.10	Cl...Cl ($SiCl_4$)	0.30	−0.06
Ar...Ar (2.87A)	0.91	−0.06	Ar...Ar (3.30A)	0.11	−0.01
Br...Br (CBr_4)	0.50	−0.10	Br...Br ($SiBr_4$)	0.23	−0.04
Kr...Kr (3.12A)	0.75	−0.05	Kr...Kr (3.50A)	0.13	−0.01

We can calculate from these equations the values of F' and F when the two neon (argon, krypton) atoms are so close together as the two fluorine (chlorine, bromine) atoms are in CF_4 (CCl_4, CBr_4) and in SiF_4 ($SiCl_4$, $SiBr_4$). The calculated values are compared with the repulsive force constants obtained from normal coordinate treatment in Table IV. The agreement of these two kinds of values seems to be of significant. That the repulsive force constants for CF_4 molecule are large as compared with those of others is to be attributed partly to the shortness of the CF bond length and partly to the ionic nature of CF bond. In view of these facts it is not a good approximation to neglect interactions between two CF_3- groups in the normal coordinate treatment of CF_3-CF_3 molecule.

The author wishes to express his sincere thanks to Professor S. Mizushima for many helpful discussions.

Note added in proof.—Since some revisions have been made in proof, the calculated frequencies of C_2Cl_6 molecule given in Table II are somewhat different from those reported in the article by Mizushima, Morino, Simanouti, and Kuratani, J. Chem. Phys. **17**, 838 (1949). The conclusion of our previous paper, however, is not affected by this revision.

THE JOURNAL OF CHEMICAL PHYSICS VOLUME 17, NUMBER 10 OCTOBER, 1949

The Kinetics of Membrane Processes. I. The Mechanism and the Kinetic Laws for Diffusion through Membranes*

K. J. LAIDLER AND K. E. SHULER**
Department of Chemistry, The Catholic University of America, Washington, D. C.
(Received August 9, 1948)

The equations for diffusion in binary systems are extended to the case of diffusion through a membrane. Three elementary rate processes are considered at a solution-membrane interface: (1) adsorption of the diffusing species, (2) desorption back into the solution, and (3) diffusion into the membrane, and an expression for the rate constant of the over-all process of surface penetration is developed in terms of three specific rate constants. Various special cases are considered and discussed with reference to the experimental data. A general expression for the rate of diffusion of a species through a membrane under steady-state conditions is derived, the rate being expressed as a function of activities. It is shown that the application of this expression to the case of a solvent passing through a membrane which is impermeable to the solute leads to the thermodynamically exact equation for the osmotic pressure. Expressions are given for the rate of flow of solvent and solute through a membrane as a function of the osmotic and hydrostatic pressures across the membrane.

INTRODUCTION

IN a paper on the diffusion laws in liquid systems[1] it has been shown on both statistical and thermodynamical grounds that the proper composition unit to be used is the mole fraction activity Nf, and that more constant diffusion coefficients are found if the equations are formulated on this basis. In the present paper this treatment is extended to the case in which phase boundary processes occur in addition to diffusion, i.e., to the permeation of a solid by molecules in solution. The kinetic laws for the penetration of membranes, in the steady state of flow, are derived, and

* Parts I, II, and III of this series have been accepted as the dissertation of Kurt E. Shuler, submitted to the Faculty of the Graduate School of Arts and Sciences of the Catholic University of America in partial fulfillment of the requirements for the degree of Doctor of Philosophy in Chemistry.
** Present address: Applied Physics Laboratory, The Johns Hopkins University, Silver Spring, Maryland.
[1] K. E. Shuler and K. J. Laidler (to be published).

equations for various special cases of interest are developed.

DIFFUSION INTO A SOLID

When a molecular species in solution penetrates a solid it can generally be assumed, especially if the solution be well stirred, that the rate of diffusion in the liquid is sufficiently rapid so that it need not be taken into consideration; if this is the case the elementary processes occurring at the interface are

(1) Adsorption on the interface
(2) Desorption at the interface back into the solution
(3) Diffusion into the solid.

For convenience it will be assumed that the molecules undergoing these processes are solute molecules, but the treatment can, as will be seen, be applied equally well to the solvent. As a result of the three elementary processes occurring above, a certain concentration of solute molecules will be maintained at the interface, the amount being controlled by the relative magnitudes of the three rates.

The rates of the adsorption and desorption processes may be formulated by a modification of the procedure used previously for gas-solid interfaces,[2] the change being that mole fractions will here be used instead of concentrations; that mole fractions should be used in formulating the kinetic laws for liquid systems has already been noted by G. Scatchard.[3] For convenience of representation, mole fractions, N, will be used instead of mole fraction activities, Nf, but the application to non-ideal solutions can easily be made.

The process of adsorption may be regarded as a bimolecular reaction between solute molecules in solution of mole fraction N and bare sites; if the mole fraction of adsorbed solute molecules on the surface is N', that of the bare sites is $1-N'$. The rate of adsorption, v_1, is therefore given by

$$v_1=k_1N(1-N'), \tag{1}$$

where k_1 is a specific rate constant for the process; its value can, in principle, be calculated using the theory of absolute reaction rates,[2] although the procedure would be difficult for a liquid system. The process of desorption can be regarded as a unimolecular dissociation; since the mole fraction of the adsorbed molecules is N', the rate of the process is

$$v_{-1}=k_{-1}N', \tag{2}$$

where k_{-1} is the specific rate constant for desorption.

The rate, v_2, of the diffusion into the solid is obtained by integrating the diffusion equation

$$(\partial N/\partial t)_x=D_N(\partial^2N/\partial x^2)_t, \tag{3}$$

subject to the correct boundary conditions. Explicit solutions are not required for the present purposes, but have been collected by R. M. Barrer[4] who uses the concentration law. It is sufficient to note here that the rate of disappearance from the surface by the process of diffusion is proportional to the first power of the mole fraction of the solute molecules, i.e.,

$$v_2=k_2N', \tag{4}$$

where k_2 is a function of the diffusion coefficient D.

The rate of entry into the solid will be much greater than the rate of change of concentration of adsorbed molecules, so that steady-state conditions may be assumed, i.e.,

$$k_1N(1-N')-k_{-1}N'-k_2N'=0. \tag{5}$$

This gives

$$N'=k_1N/(k_1N+k_{-1}+k_2), \tag{6}$$

so that the rate of entry into the solid, k_2N', is

$$v=k_1k_2N/(k_1N+k_{-1}+k_2). \tag{7}$$

An equation of similar form, involving concentrations instead of mole fractions, has been shown[5] to account for the rate of uptake of gases by surfaces into which penetration will occur.

Two special cases of Eq. (7) are of interest:

Case I—If $k_1N\gg k_{-1}+k_2$, the rate is given approximately by

$$v=k_2, \tag{8}$$

which means that the diffusion in the solid is rate controlling; the adsorption rate is sufficiently rapid to maintain a fully covered surface, so that the rate of uptake is independent of the composition of the liquid phase. For gas-solid systems this type of law is usually obeyed in corrosion processes.

Case II—If $k_{-1}+k_2\gg k_1N$, the rate is given by

$$v=(k_1k_2/k_{-1}+k_2)N, \tag{9}$$

i.e., it is now proportional to the first power of the mole fraction. In this case the rate of entry is in general determined by the three specific rate constants k_1, k_{-1}, and k_2. If, in addition, $k_{-1}\gg k_2$, the rate is given by

$$v=(k_1/k_{-1})k_2N, \tag{10}$$

so that the rate is determined by the diffusion rate and the adsorption equilibrium constant k_1/k_{-1}. If on the other hand $k_2\gg k_{-1}$ the rate is given by

$$v=k_1N, \tag{11}$$

and the rate of adsorption controls the over-all rate. In gas-solid systems this linear rate of uptake is obeyed for example in the uptake of hydrogen gas by palladium.

[2] Laidler, Glasstone, and Eyring, J. Chem. Phys. **8**, 659 (1940); Glasstone, Laidler, and Eyring, *The Theory of Rate Processes* (McGraw-Hill Book Company, Inc., New York, 1941) Chapter VII.

[3] G. Scatchard, J. Chem. Phys. **7**, 657 (1939).

[4] R. M. Barrer, *Diffusion in and through Solids* (Cambridge University Press, London, 1941), Chapter I.

[5] K. J. Laidler, J. Phys. Colloid Chem. **53**, 712 (1949); K. J. Laidler, *Symposium on Reactions in the Solid State* (Paris, 1948).

STEADY FLOW THROUGH MEMBRANES

When two solutions, which may be designated α and β, are separated by a membrane which is initially free of the solute, the solute molecules enter the membrane at both interfaces, the rates of uptake obeying the law represented by Eq. (7) or one of its special cases. Under these circumstances the concentration of solute builds up within the membrane and there is at first no steady state, except (to a good approximation) at the two interfaces. After a certain time, however, a steady state is established at all points within the membrane, and there is a net flow of solute from the more concentrated to the more dilute solution. For a steady state it follows that $(\partial N/\partial t)_x=0$ at all points on the membrane, so that according to Eq. (3)

$$(\partial^2 N/\partial x^2)_t=0 \tag{12}$$

or

$$(\partial N/\partial x)_t=\text{const.}, \tag{13}$$

i.e., the mole fraction gradient is a constant. If the mole fraction in the membrane at the interface with solution α be denoted N'^{α} and that at solution β as N'^{β}, as represented in Fig. 1, the mole fraction gradient within the membrane is given by

$$(\partial N/\partial x)_t=(N'^{\beta}-N'^{\alpha})/d', \tag{14}$$

where d' is the thickness of the membrane. The integrated form of Eq. (3) is[1]

$$dn^{\beta}/dt=-D_N A c_t(dN/dx), \tag{15}$$

where dn^{β} is the number of moles passing from α into β through a cross-sectional area A in time dt, and c_t is the total concentration of all species present, which is essentially constant. The net rate of flow through the membrane is therefore

$$dn^{\beta}/dt=-D_N A c_t(N'^{\beta}-N'^{\alpha})/d', \tag{16}$$

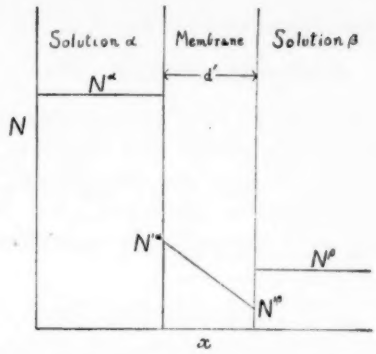

FIG. 1. The variation of the mole fraction of a species in two solutions α and β separated by a membrane. The species is less soluble in the membrane than in the solvent ($k_1/k_{-1}<1$), and the mole fraction gradient within the membrane is $(N'^{\alpha}-N'^{\beta})/d'$ which is less than $(N^{\alpha}-N^{\beta})/d'$, the reduction factor being k_1/k_{-1}.

in which N'^{β} and N'^{α} have still to be expressed in terms of the mole fractions in the two solutions, N^{β} and N^{α}. Equation (16) may be written in the form

$$dn^{\beta}/dt=-k_2(N'^{\beta}-N'^{\alpha}), \tag{17}$$

where k_2 is equal to $D_N A c_t/d'$.

The rate of flow may be expressed in terms of the mole fractions N^{α} and N^{β} by obtaining the steady-state expression at the two interfaces. At the interface α the rates of adsorption, desorption, and diffusion are

$$v_1=k_1 N^{\alpha}(1-N'^{\alpha}), \tag{18}$$

$$v_{-1}=k_{-1}N'^{\alpha}, \tag{19}$$

$$v_2=-k_2(N'^{\beta}-N'^{\alpha}), \tag{20}$$

and the steady-state expression is therefore

$$k_1 N^{\alpha}(1-N'^{\alpha})-k_{-1}N'^{\alpha}+k_2(N'^{\beta}-N'^{\alpha})=0. \tag{21}$$

Similarly, at interface β the expression is

$$k_1 N^{\beta}(1-N'^{\beta})-k_{-1}N'^{\beta}-k_2(N'^{\beta}-N'^{\alpha})=0. \tag{22}$$

Solution of these two simultaneous equations gives

$$N'^{\beta}-N'^{\alpha}=\frac{N^{\beta}-N^{\alpha}}{(2k_2+k_{-1})/k_1+[(k_2/k_{-1})+1](N^{\beta}+N^{\alpha})+(k_1/k_{-1})N^{\alpha}N^{\beta}}. \tag{23}$$

In the case that $k_2 \ll k_{-1} \gg k_1$, i.e., the rates of diffusion in the membrane and of adsorption are small compared with the rate of desorption, Eq. (23) reduces to

$$N'^{\beta}-N'^{\alpha}=(k_1/k_{-1})(N^{\beta}-N^{\alpha}), \tag{24}$$

and the rate of flow from α to β is given by

$$dn^{\beta}/dt=k_1 k_2/k_{-1}(N^{\alpha}-N^{\beta}). \tag{25}$$

The rate is therefore proportional to the difference between the mole fractions in the two solutions, and examination of Eq. (23) shows that this result will only arise if $k_2 \ll k_{-1} \gg k_1$. Since the ratio k_1/k_{-1} is the equilibrium constant for the adsorption process, Eq. (25) corresponds to the slow step being diffusion through the membrane; this can therefore be inferred if the results show that the rate of flow is proportional to $N^{\alpha}-N^{\beta}$. It is to be noted that the ratio k_1/k_{-1} is required by the above conditions to be small; the distribution coefficient of the diffusing species between the membrane and the solution must therefore be small for the above result to be obtained.

Equation (25) may be written as

$$\frac{dn^{\beta}}{dt}=\frac{k_1}{k_{-1}}\frac{D_N A c_t}{d'}(N^{\alpha}-N^{\beta}), \tag{26}$$

which it is convenient to write as

$$dn^\beta/dt=(QAc_t/d')(N^\alpha-N^\beta), \tag{27}$$

where Q, equal to $(k_1/k_{-1})\,D_N$, may be called the permeation coefficient of the species with respect to the membrane; it is seen to have the dimensions L^2T^{-1} (like the Fick's law diffusion coefficient), and will be expressed in the units cm^2 $sec.^{-1}$. For a non-ideal solution the rate of flow is

$$dn^\beta/dt=(QAc_t/d')(N^\alpha f^\alpha-N^\beta f^\beta). \tag{28}$$

The permeation constant Q defined above differs from the permeability constant P used by Barrer;[4] Q is the product of the diffusion coefficient and the ratio of the concentrations, i.e., solubilities, in the membrane and in the solvent, while P is the product of the diffusion coefficient and the solubility of the diffusing species in the membrane. Whereas Q has the same dimensions as D, P involves the concentration; the use of Q thus has a distinct advantage in comparing permeation with free diffusion.

Rates of Flow of Solvent and Solute: Influence of Pressure

Expressions will now be deduced for the rates of flow of solvent and solute molecules through a membrane separating two solutions. The solutions are designated α and β, the solvent and solute 1 and 2 respectively, and the permeation constants of solvent and solute as Q_1 and Q_2 respectively. The influence of hydrostatic pressure on the rates of flow will be taken into account, and it will be supposed that the hydrostatic pressure on solution β exceeds that on solution α by an amount P.

The hydrostatic pressure influences the rates by modifying the activities of the species in solution β. The change in partial vapor pressure (dp_i) of a species i brought about by the imposition of the hydrostatic pressure dP is[6]

$$dp_i/p_i=(\bar{V}_i/RT)\cdot dP \tag{29}$$

where $\bar{V}_i$ is the molar volume of the species i; this integrates to

$$p_i=p_i^0\exp(P\bar{V}_i/RT) \tag{30}$$

where p_i^0 is the partial vapor pressure corresponding to zero hydrostatic pressure (relative to atmospheric). The activity coefficient at pressure P of a component which at zero pressure has an activity coefficient of f_i^0 is therefore $f_i^0\exp(P\bar{V}_i/RT)$, and the activity is $N_if_i^0\exp(P\bar{V}_i/RT)$. The activity of the solvent in solution β is therefore $N_1f_1^0\exp(P\bar{V}_1/RT)$, and that of the solute is $N_2f_2^0\exp(P\bar{V}_2/RT)$, where f_1^0 and f_2^0 are the activity coefficients at atmospheric pressure.

[6] Cf. E. A. Guggenheim, *Modern Thermodynamics by the Methods of Willard Gibbs* (Methuen and Company, Ltd., London, 1933), p. 63.

The activity differences $N^\beta f^\beta-N^\alpha f^\alpha$ may now be written down; for the solvent we have

$$N_1^\beta f_1^\beta-N_1^\alpha f_1^\alpha=N_1^\beta f_1^{0\beta}\exp(P\bar{V}_1/RT)-N_1^\alpha f_1^{0\alpha} \tag{31}$$

and for the solute

$$N_2^\beta f_2^\beta-N_2^\alpha f_2^\alpha=N_2^\beta f_2^{0\beta}\exp(P\bar{V}_2/RT)-N_2^\alpha f_2^{0\alpha}. \tag{32}$$

According to Eq. (28) the rates of flow from α to β are thus: For the solvent

$$dn_1^\beta/dt=(Q_1Ac_t/d')\{N_1^\alpha f_1^{0\alpha}-N_1^\beta f_1^{0\beta}\exp(P\bar{V}_1/RT)\}; \tag{33}$$

and for the solute

$$dn_2^\beta/dt=(Q_2Ac_t/d')\{N_2^\alpha f_2^{0\alpha}-N_2^\beta f_2^{0\beta}\exp(P\bar{V}_2/RT)\}. \tag{34}$$

The Osmotic Pressure

Since it is convenient to express the rates of flow as functions of the osmotic pressures π^α and π^β of the two solutions, equations for these quantities will be derived. The pressure π^β is the pressure developed at equilibrium when α is pure solvent ($N_1^\alpha f_1^{0\alpha}=1$) and when there is no diffusion of the solute, i.e., when $Q_2=0$, so that $dn_2^\beta/dt=0$. The condition for equilibrium is defined by $dn_1^\beta/dt=0$, from which, using Eq. (33), it follows that

$$1-N_1^\beta f_1^{0\beta}\exp(\pi^\beta\bar{V}_1/RT)=0 \tag{35}$$

since $(Q_1Ac_t/d')\neq 0$; this rearranges to

$$\pi^\beta=(RT/\bar{V}_1)\ln(1/N_1^\beta f_1^{0\beta}) \tag{36}$$

which is the exact thermodynamic relationship between osmotic pressure and mole fraction.[7] At low concentrations for which $f_1^{0\beta}=1$ it becomes[1] $\pi^\beta V_1=n_2^\beta RT$ (Morse's equation) where V_1 is the total volume of solvent associated with n_2^β moles of solute. Similarly the osmotic pressure of solution α is given by

$$\pi^\alpha=(RT/\bar{V}_1)\ln(1/N_1^\alpha f_1^{0\alpha}). \tag{37}$$

Equations analogous to (36) and (37) could also be written down for the solute, the osmotic pressure now being that which would be developed if the membrane were impermeable to the solvent and permeable to the solute, the distinction between solute and solvent being completely arbitrary. Such equations will not, however, be used here since it is more convenient to relate the mole fraction of the solute molecules to the osmotic pressures of Eqs. (36) and (37); this will be done in deriving the rate of flow of the solute molecules.

Rate of Flow as Functions of Osmotic and Hydrostatic Pressures

The rates of flow will now be expressed in terms of osmotic pressures instead of in mole fractions as in

[7] F. G. Donnan and E. A. Guggenheim, Zeits. f. physik. Chemie **A162**, 346 (1932).

Eqs. (33) and (34). From Eq. (37) it follows that

$$N_1{}^{\alpha}f_1{}^{0\alpha}=\exp(-\pi^{\alpha}\bar{V}_1/RT), \tag{38}$$

and from Eq. (36) that

$$N_1{}^{\beta}f_1{}^{0\beta}=\exp(-\pi^{\beta}\bar{V}_1/RT). \tag{39}$$

Substitution of these expressions into Eq. (33) gives, for the net rate of flow of the solvent from α to β,

$$dn_1{}^{\beta}/dt=(Q_1Ac_t/d')\{\exp(-\pi^{\alpha}\bar{V}_1/RT) -\exp((P-\pi^{\beta})\bar{V}_1/RT)\}. \tag{40}$$

If the solutions are sufficiently dilute so that $\pi^{\alpha}\bar{V}_1/RT \ll 1$ and $(\pi^{\beta}-P)\bar{V}_1/RT \ll 1$ the exponentials can be expanded with the neglect of terms beyond the first; the error introduced by expanding the exponentials and taking the first term only is very slight for all solutions in which one would be interested. Even for a three-normal ($3N$) sucrose solution in water, the error is only 0.5 percent. Expansion of the exponentials then gives

$$dn_1{}^{\beta}/dt=(Q_1Ac_t/d')(\bar{V}_1/RT)(\pi^{\beta}-\pi^{\alpha}-P). \tag{41}$$

This may be written as

$$dn_1{}^{\beta}/dt=(Q_1Ac_t\bar{V}_1/d'RT)(\pi-P), \tag{42}$$

where $\pi=\pi^{\beta}-\pi^{\alpha}$ is the difference between the osmotic pressures of the two solutions. Apart from the restriction, introduced by the inequalities, that the solutions be fairly dilute, this rate equation is exact and does not require that the solution be ideal.

A similar treatment for the rate of flow of solute leads to expressions of great complexity; to simplify the treatment the assumption will be made that the solution is sufficiently dilute so as to be ideal. Then, the rate of flow in terms of mole fractions will be (cf. Eq. (34))

$$dn_2{}^{\beta}/dt=(Q_2Ac_t/d')\{N_2{}^{\alpha}-N_2{}^{\beta}\exp(P\bar{V}_2/RT)\}. \tag{43}$$

The mole fraction $N_2{}^{\alpha}$ is given by

$$N_2{}^{\alpha}=1-N_1{}^{\alpha}=1-\exp(-\pi^{\alpha}\bar{V}_1/RT), \tag{44}$$

using Eq. (38), and similarly, using Eq. (39)

$$N_2{}^{\beta}=1-\exp(-\pi^{\beta}\bar{V}_1/RT). \tag{45}$$

The rate of flow is, therefore,

$$\frac{dn_2{}^{\beta}}{dt}=\frac{Q_2Ac_t}{d'}\{1-\exp(-\pi^{\alpha}\bar{V}_1/RT) -(1-\exp(-\pi^{\beta}\bar{V}_1/RT)\exp(P\bar{V}_2/RT)\}. \tag{46}$$

Expansion of these exponentials gives

$$\frac{dn_2{}^{\beta}}{dt}=\frac{Q_2Ac_t}{d'}\left\{\frac{\pi^{\alpha}\bar{V}_1}{RT}-\frac{\pi^{\beta}\bar{V}_1}{RT}\left(1+\frac{P\bar{V}_2}{RT}\right)\right\} \tag{47}$$

$$\frac{dn_2{}^{\beta}}{dt}=\frac{Q_2Ac_t\bar{V}_1}{d'RT}(\pi^{\alpha}-\pi^{\beta}) \tag{48}$$

$$\frac{dn_2{}^{\beta}}{dt}=-\frac{Q_2Ac_t\bar{V}_1}{d'RT}\pi. \tag{49}$$

In going from Eq. (47) to Eq. (48), the small term $\pi^{\beta}P\bar{V}_1\bar{V}_2/(RT)^2$ has been neglected. This approximation introduces only a very small error in the usual type of membrane experiments with fairly dilute solutions in which the hydrostatic pressure P is only a few hundred mm of solution; thus for a rise of 500 mm occurring with a sucrose solution, $1+P\bar{V}_2/RT$ differs from unity by only 0.04 percent. In Eq. (41), however, P must not be neglected since it may be of comparable magnitude with π, however small it may be. It is to be noted that according to Eq. (49) the hydrostatic pressure P does not influence the rate of flow of the solute in a dilute solution.

Equations similar to (42) and (49), but without explicit coefficients, were proposed in 1911 by A. von Antropoff[8] on intuitive grounds. The application of our equations to osmotic experiments with membranes permeable to both solvent and solute will be considered in subsequent papers..

[8] A. von Antropoff, Zeits. f. physik. Chemie **76**, 721 (1911).

The Kinetics of Membrane Processes. II. Theoretical Pressure-Time Relationships for Permeable Membranes

K. J. LAIDLER AND K. E. SHULER
Department of Chemistry, The Catholic University of America, Washington, D. C.
(Received August 9, 1948)

The rate equations developed in Part I for the flow of solvent and solute through a permeable membrane have been extended to the case in which the flow is measured by the rise and fall in a capillary inserted into the more concentrated solution. The differential equation obtained for this case has been integrated to give an explicit relationship between the height of rise in the capillary and the time. The equation is shown to give the height-time relationship in the form found by experiment. It is shown that the osmotic pressure obtained with a semipermeable membrane is a special case of the more general theory of diffusion through membranes permeable to both solvent and solute. The possibility of positive and negative values of P, i.e., of *initial* rise or fall respectively in the capillary, is discussed, and the significance of these cases evaluated in terms of the molar volumes and permeation constants of solvent and solute.

INTRODUCTION

IN the previous paper[1] (Part I), equations have been derived for the rates of flow of solvent and solute molecules from a solution α to a solution β separated from it by a membrane which is permeable, to different extents, to both species. For the solvent it was found that the number n_1^β of molecules entering solution β in time t is given fairly accurately by the expression

$$dn_1^\beta/dt=\frac{Q_1Ac_t\bar{V}_1}{d'RT}(\pi-P), \tag{1}$$

where Q_1 is the permeation constant for the solvent, A the area and d' the thickness of the membrane, c_t is the total molar concentration in the membrane, $\bar{V}_1$ the molar volume of the solvent, π the difference $(\pi^\beta-\pi^\alpha)$ between the true osmotic pressures for the two solutions, and P is the hydrostatic pressure acting on solution β, solution α being maintained at atmospheric pressure. This equation was shown to be accurate for fairly dilute solutions, whether ideal or not. For the solute a rate expression was obtained on the assumption of ideality; it was

$$dn_2^\beta/dt=-\frac{Q_2Ac_t\bar{V}_1}{d'RT}\pi, \tag{2}$$

the symbols having the same meaning as before, the subscript 2 indicating that the properties of the solute are now referred to.

On the basis of these equations, kinetic laws will be derived which should be applicable to the following type of experiment. Two solutions of a non-electrolyte at different concentrations of the same solute are separated by a membrane, the pressure of one being maintained at atmospheric pressure; the pressure and volume of the other are allowed to vary, and the changes are measured by observing the level in a capillary tube. In practice it is most convenient to arrange the solutions so that the level rises rather than falls in the capillary tube, the more dilute solution usually being the one to be maintained at atmospheric pressure. Measurements are made of the level of the meniscus as a function of the time, a correction being made for capillarity within the tube.

If the membrane is semipermeable and separates a solution from the pure solvent maintained at atmospheric pressure, the level of the meniscus rises owing to the passage of pure solvent into the solution, and continues to rise until it reaches a maximum pressure, which is the osmotic pressure of the solution (somewhat diluted by the passage of the solvent); the change of pressure with time in this case is represented by curve I in Fig. 1. If, on the other hand, the solute also diffuses through the membrane, but passes through it less rapidly than the solvent, the curve will be as represented in curve II; the pressure rises to a maximum and then falls to zero. If the solute diffuses through the membrane sufficiently rapidly as compared with the solvent, the pressure falls initially, reaches a minimum, and then rises to zero (curve III); this last case is realized only infrequently. The general laws governing these types of behavior will now be derived on the basis of the equations developed in Part I for the kinetics of flow of solvent and solute through a membrane permeable to both.

PRESSURE-TIME CURVES FOR OSMOTIC FLOW

The Differential Equation

Equations (1) and (2) may now be used to relate the rates of change of volume and pressure in terms of the osmotic pressure difference π and the hydrostatic pressure P. The equations give the rate of flow from α to β, so that the rate of increase of volume of solution β due to the flow of solvent is

$$dV_1^\beta/dt=\frac{Q_1Ac_t\bar{V}_1^2}{d'RT}(\pi-P). \tag{3}$$

Similarly the rate of increase of volume due to the flow

[1] K. J. Laidler and K. E. Shuler, J. Chem. Phys. 17, 851 (1949).

of solute is

$$dV_2^\beta/dt = -\frac{Q_2 A c_i \bar{V}_1 \bar{V}_2}{d'RT}\pi. \quad (4)$$

The net rate of increase of volume of solution β is thus

$$dV^\beta/dt = dV_1^\beta/dt + dV_2^\beta/dt$$

$$= \frac{Q_1 A c_i \bar{V}_1^2}{d'RT}(\pi - P) - \frac{Q_2 A c_i \bar{V}_1 \bar{V}_2}{d'RT}\pi. \quad (5)$$

If a is the area of cross section of the capillary tube and the pressure P is expressed as centimeters of rise in the tube,[2] the rate of increase of volume is $d(aP)/dt$, and it follows that

$$dP/dt = \frac{Q_1 A c_i \bar{V}_1^2}{d'RTa}(\pi - P) - \frac{Q_2 A c_i \bar{V}_1 \bar{V}_2}{d'RTa}\pi. \quad (5)$$

This equation may be written as

$$dP/dt = \lambda_1(\pi - P) - \lambda_2\pi, \quad (7)$$

where

$$\lambda_1 = \frac{Q_1 A c_i \bar{V}_1^2}{d'RTa} \quad (8)$$

and

$$\lambda_2 = \frac{Q_2 A c_i \bar{V}_1 \bar{V}_2}{d'RTa}. \quad (9)$$

The Rate of Change of Osmotic Pressure

In order for Eq. (7) to be solved, the variation of the osmotic pressure difference π with time must be known. The change in the concentrations of the two solutions with time is determined largely by the diffusion of the solute molecules, since this produces a much greater proportional change in concentration than does the diffusion of the solvent molecules. The rate of increase of the number of moles of solute in solution β is equal to the rate of decrease in solution α, and is given by Eq. (2). If V^β liters is the total volume of solution β the rate of decrease of the mole fraction N_2^β is given to a good approximation by[3]

$$-dN_2^\beta/dt = -(\bar{V}_1/V^\beta)(dn_2^\beta/dt). \quad (10)$$

Introducing Eq. (2) gives

$$-dN_2^\beta/dt = \frac{Q_2 A c_i \bar{V}_1^2}{V^\beta d'RT}\pi \quad (11)$$

and similarly the rate of increase of the mole fraction of the solute in solution α of volume V^α, is

$$dN_2^\alpha/dt = \frac{Q_2 c_i A \bar{V}_1^2}{V^\alpha d'RT}\pi. \quad (12)$$

[2] The osmotic pressure difference π must also be in the same units, and RT must be expressed as cm^4.

[3] In dilute solutions, $n_1^\beta = V^\beta/\bar{V}_1$ and $N_2^\beta = n_2^\beta/n_1^\beta$; hence $N_2^\beta/n_2^\beta = \bar{V}_1/V^\beta$.

Since the rate of change of osmotic pressure is related to the sum of these quantities it is sufficiently accurate to introduce the osmotic pressures π^α and π^β by the approximate expressions

$$\pi^\alpha = N_2^\alpha(RT/\bar{V}_1) \quad (13)$$

and

$$\pi^\beta = N_2^\beta(RT/\bar{V}_1). \quad (14)$$

Substitution for N_2^α and N_2^β in Eqs. (11) and (12) gives

$$-\frac{d\pi^\beta}{dt} = \frac{Q_2 A c_i \bar{V}_1}{d'V^\beta}\pi \quad (15)$$

and

$$\frac{d\pi^\alpha}{dt} = \frac{Q_2 A c_i \bar{V}_1}{d'V^\alpha}\pi. \quad (16)$$

The rate of change of the osmotic pressure difference π is thus given by

$$\frac{d\pi}{dt} = \frac{d(\pi^\beta - \pi^\alpha)}{dt} = -\frac{Q_2 A c_i \bar{V}_1}{d'}\pi(1/V^\beta + 1/V^\alpha). \quad (17)$$

This may be written as

$$-d\pi/dt = \lambda_3\pi \quad (18)$$

where

$$\lambda_3 = \frac{Q_2 A c_i \bar{V}_1}{d'}(1/V^\beta + 1/V^\alpha). \quad (19)$$

Solution of the Equations

The equations to be solved are (7) and (18), *viz.*,

$$dP/dt = \lambda_1(\pi - P) - \lambda_2\pi \quad (20)$$

and

$$-d\pi/dt = \lambda_3\pi. \quad (21)$$

The solution of Eq. (21) subject to the boundary condition $\pi = \pi_0$, $t = 0$, where π_0 is the theoretical equilibrium value of $\pi^\beta - \pi^\alpha$ as given by the Morse equation at the beginning of the experiment, is

$$\pi = \pi_0 e^{-\lambda_3 t}. \quad (22)$$

Substitution of this into Eq. (20) gives

$$dP/dt = \lambda_1(\pi_0 e^{-\lambda_3 t} - P) - \lambda_2\pi_0 e^{-\lambda_3 t}, \quad (23)$$

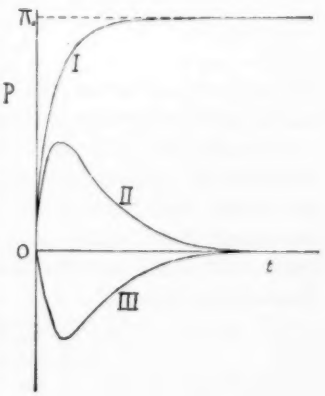

FIG. 1. The variation of pressure with time when a solution is separated from the pure solvent by a membrane, the solvent being maintained at atmospheric pressure. For a semipermeable membrane (curve I) the pressure rises exponentially to the osmotic pressure π_0. Curves II and III are for membranes permeable to both solvent and solute; for curve II the membrane is more permeable to the solvent; for curve III to the solute.

which rearranges to

$$dP/dt+P\lambda_1=\pi_0(\lambda_1-\lambda_2)e^{-\lambda_3 t}. \quad (24)$$

This is a linear differential equation of the first order and with the boundary condition $t=0$, $P=0$ integrates to

$$P=\pi_0\frac{\lambda_1-\lambda_2}{\lambda_1-\lambda_3}(e^{-\lambda_3 t}-e^{-\lambda_1 t}). \quad (25)$$

There has thus been obtained an explicit relationship between pressure and time, involving the initial osmotic pressure difference π_0 and the three parameters λ_1, λ_2, and λ_3. The three parameters are functions of the known volumes and other dimensions of the system, and also of the two permeation constants Q_1 and Q_2. It will now be shown that Eq. (25) is of the proper form to explain curves I, II, and III in Fig. 1.

For a semipermeable membrane, for which $Q_2=0$, it follows that $\lambda_2=\lambda_3=0$, and the equation becomes

$$P=\pi_0(1-e^{-\lambda_1 t}). \quad (26)$$

This corresponds to an exponential rise from $P=0$ to $P=\pi_0$ (curve I).

Whatever the relative magnitudes of λ_1 and λ_3 the function $(e^{-\lambda_3 t}-e^{\lambda_1-t})/(\lambda_1-\lambda_3)$ is always positive. Consequently if $\lambda_1>\lambda_2$ the curve rises initially and reaches a maximum after which it falls to zero (curve II). If $\lambda_2>\lambda_1$ the curve falls initially and shows a minimum before returning to zero (curve III).

The expression for the maximum pressure rise in the capillary is

$$P_{\max}=\pi_0\frac{(\lambda_1-\lambda_2)}{\lambda_1}\left(\frac{\lambda_3}{\lambda_1}\right)^{\lambda_3/(\lambda_1-\lambda_3)}. \quad (27)$$

For a semipermeable membrane, $\lambda_2=\lambda_3=0$, and the expression reduces to $P_{\max}=\pi_0$ in accordance with the definitions of these quantities, after evaluation of the indeterminate form resulting from the above substitutions.

It can furthermore be seen that if $\lambda_3>\lambda_1$, which is usually the case, the exponential $e^{-\lambda_3 t}$ is much smaller than $e^{-\lambda_1 t}$ for sufficiently large values of t, so that Eq. (25) approximates to

$$\ln P=\ln\left\{\pi_0\frac{(\lambda_1-\lambda_2)}{(\lambda_3-\lambda_1)}\right\}-\lambda_1 t. \quad (28)$$

The plot of ln P *versus* t should therefore be a straight line for sufficiently large values of t, the slope being $-\lambda_1$.

In testing Eq. (25) against the experimental results, the following procedure is adopted, since Eq. (25) does not readily lend itself to the usual least square method treatment. Two points P_1, t_1 near the beginning of the graph, and P_2, t_2 near the end of the graph, are chosen. Then, using Eq. (25),

$$\frac{P_1}{P_2}=\frac{(e^{-\lambda_3 t_1}-e^{-\lambda_1 t_1})}{(e^{-\lambda_3 t_2}-e^{-\lambda_1 t_2})}. \quad (29)$$

Since λ_1 is known from the slope, the above equation can be solved for λ_3, and then λ_2 can be found by substitution in (25). Doing this for several pairs of points, the proper values for λ_3 and λ_2 can readily be found. The permeation constants Q_1 and Q_2 can then be calculated from Eq. (8) and (9).

The Change of Concentration with Time

By a modification of the above procedure it is also possible to derive an expression for the concentration of the solute in solutions α and β at any time t. Equation (22) may be written as

$$\pi^\beta-\pi^\alpha=(\pi_0{}^\beta-\pi_0{}^\alpha)e^{-\lambda_3 t}, \quad (30)$$

and since by van't Hoff's law for dilute solutions, the osmotic pressures are proportional to the concentrations of the solute, it follows that

$$c_2{}^\beta-c_2{}^\alpha=({}^0c_2{}^\beta-{}^0c_2{}^\alpha)e^{-\lambda_3 t}, \quad (31)$$

where $c_2{}^\alpha$ is the concentration of the solute in solution α at time t and ${}^0c_2{}^\alpha$ is the initial concentration at $t=0$. Using the auxiliary condition that at any time t

$$c_2{}^\alpha=n_2{}^\alpha/V^\alpha, \quad (32)$$

and that

$${}^0n_2{}^\beta+{}^0n_2{}^\alpha=n_2{}^\beta+n_2{}^\alpha, \quad (33)$$

it can be deduced that

$$c_2{}^\alpha=\frac{{}^0n_2{}^\beta(1-e^{-\lambda_3 t})+{}^0n_2{}^\alpha[1+(V^\beta/V^\alpha)e^{-\lambda_3 t}]}{V^\beta+V^\alpha}, \quad (34)$$

and a similar expression for $c_2{}^\beta$ can be obtained. The concentration of the solute in the two solutions after time t can therefore be calculated in terms of the constant λ_3, itself a function of Q_2.

The special case in which $\pi^\alpha=$ constant is of practical interest since it can easily be realized in the laboratory by using a flow system or making one volume much larger than the other. Applying the condition $\pi^\alpha=$ constant to the equations previously developed, it is found that Eq. (25) is still obeyed, but now λ_3 is given by

$$\lambda_3=Q_2 A c_i\bar{V}_1/d'V^\beta. \quad (35)$$

The relationship between λ_2 and λ_3 is now

$$\lambda_3=\lambda_2(RTa/\bar{V}_2V^\beta), \quad (36)$$

and expressions in terms of concentrations may readily be obtained.

DISCUSSION

General

The treatment given has led to a general equation for the pressure and volume of a solution separated by a membrane from another solution, expressed as a function of the time. It enables these relationships to be predicted from the known dimensions of the system and from the permeation constants of solvent and

solute; conversely the permeation constants can be evaluated from the pressure-time relationships.

The theory is applicable directly to experiments in which the pressure and volume of one system are allowed to increase simultaneously by the expansion of one solution into a capillary tube; this implies a particular linear relationship between the volume and the pressure. For other types of relationships, such as will obtain in biological cells where there is an actual expansion of the cell instead of an expansion into a capillary, a different treatment is necessary.

It is to be noted that the hydrostatic pressure exerted by the column in the capillary upon the solution must be explicitly taken into account. The importance of including it is shown by Eq. (3) according to which the hydrostatic pressure P and the osmotic pressure difference π enter into the rate of flow of solvent as $\pi - P$. If π and P are of comparable magnitude, the neglect of P naturally introduces considerable error; moreover, neglect of P would lead to equations which would be at variance with the experimental pressure-time curves which will be described in Part III.

According to the theoretical treatment given in this paper a membrane is characterized with respect to the flow of the components of a binary solution by the permeation constants of the two species. Upon the values of these constants depends the general shape of the pressure-time relationship; changes in either or both of them will influence the initial pressure rise, the height of the maximum, and the rise at any arbitrary time. These quantities are also dependent upon the molar volumes, the total volumes, and the cross-sectional area of the capillary.

Maximum Height of Rise in the Capillary

Since for semipermeable membranes the height of rise, i.e., the osmotic pressure, is a linear function of the composition of the solution according to the laws of van't Hoff and Morse, it might be thought that the maximum height of rise in the type of system and experiment discussed here would also bear the same relationship, especially since the Morse law was used as one of the starting points of this treatment. However, an examination of Eq. (27) for the maximum height of rise will show that this is not the case; thus π_0 which is a linear factor of the composition is multiplied by a complicated expression involving the permeation constants of solvent and solute. This is very similar to the case of a consecutive, first-order reaction

$$A \xrightarrow{k_1} B \xrightarrow{k_2} C \tag{37}$$

where the maximum concentration of B is given by

$$(C_B)_{max} = a_0 (k_2/k_1)^{k_2/(k_1-k_2)}, \tag{38}$$

where a_0 is the initial concentration of A. This similarity is of course due to the fact that Eqs. (20) and (21) are formally the rate equations for consecutive first order reactions with three instead of two rate constants.

P_{max} being a complicated function of the initial concentration and the permeation constants, it is impossible to draw any direct conclusions as to the initial concentration or the permeation constants of the system involved from its value alone; a complete analysis of the pressure-time curve obtained must be made, as described earlier in this paper, to obtain this information. For the characterization of a given membrane, the rate constants λ_1, λ_2, and λ_3, and hence Q_1 and Q_2, are therefore much more fundamental quantities than the maximum height of rise.

Initial Rise or Fall in the Capillary

When two solutions of different concentrations of the same solute are separated by a permeable membrane, and the change in the system is measured by the change in the level of a capillary inserted into the more concentrated solution, there is the possibility of either an *initial* rise or *initial* fall in the capillary (curves II and III, Fig. 1) in contrast to the case of a semipermeable membrane where there will *always* be a rise in the capillary (curve I, Fig. 1).

The explanation for this is contained in Eq. (25) which shows that the sign of P depends upon the sign of $(\lambda_1 - \lambda_2)$; this arises, as mentioned before, because the function $(e^{-\lambda_2 t} - e^{-\lambda_1 t})/(\lambda_1 - \lambda_2)$ is always positive whatever the relative values of λ_1 and λ_2. Therefore if $\lambda_1 > \lambda_2$, the value of P is always positive, while if $\lambda_1 < \lambda_2$, its value is always negative. For the case of a semipermeable membrane for which Eq. (26) applies, P is always positive, whatever the value of λ_1, the other constants not entering in the equation. Expressing λ_1 and λ_2 by means of Eqs. (8) and (9) it is seen that the condition for a positive P, i.e., an initial rise in the capillary, is given by

$$\frac{Q_1 c_t A \bar{V}_1^2}{d' RTa} > \frac{Q_2 c_t A \bar{V}_1 \bar{V}_2}{d' RTa} \tag{39}$$

which reduces to

$$Q_1 \bar{V}_1 > Q_2 \bar{V}_2. \tag{40}$$

The condition for a negative P, i.e., an initial fall in the capillary is conversely that

$$Q_1 \bar{V}_1 < Q_2 \bar{V}_2. \tag{41}$$

These simple conditions could have been arrived at intuitively, since the rates of volume increase due to solvent and solute are clearly proportional to $Q_1 \bar{V}_1$ and $Q_2 \bar{V}_2$, the product of the permeation constant of the substance and its molar volume, the mole fraction gradient at any time being the same for both solvent and solute. If $Q_2 \bar{V}_2 = Q_1 \bar{V}_1$ the concentrations of the two solutions will equalize without the development of any pressure between the two solutions.

The collodion membranes with which we have ex-

perimented so far have been much more permeable to water than to the solutes used, and for aqueous solutions it has always been found that $Q_1\bar{V}_1 > Q_2\bar{V}_2$, i.e., there was always an initial rise in the capillary inserted into the more concentrated solution. Attempts to obtain an initial fall in the capillary with aqueous solutions of non-electrolytes have failed, and this is attributed to the fact that the values of $Q_2\bar{V}_2$ do not change very much from solute to solute. A solute with a larger value of Q_2 generally has to be one of smaller molar volume $\bar{V}_2$, and in general it has been noted that Q_2 is approximately inversely proportional to $\bar{V}_2$.

It has been possible, however, to obtain an initial fall in the capillary, and thus negative values of P, using glycerol as a solvent and urea as the solute. Since in this case $\bar{V}_1$ is of about the same order as $\bar{V}_2$, this must have been due to $Q_1 < Q_2$, where the deciding factor probably is the low diffusion coefficient for the self diffusion of glycerol. The system was picked for that reason; the experimental details and results will be given in Part III.

This discussion of the initial rise and fall in the capillary pertains directly only to solutions of non-electrolytes. For electrolytes, the electro-osmotic effect caused by the potential differences across the membrane and the zeta-potential on the membrane complicate matters; we hope to give an extension of the above treatment to electrolytes in a later paper.

THE JOURNAL OF CHEMICAL PHYSICS VOLUME 17, NUMBER 10 OCTOBER, 1949

The Kinetics of Membrane Processes. III. The Diffusion of Various Non-Electrolytes through Collodion Membranes

K. E. SHULER, C. A. DAMES, AND K. J. LAIDLER
Department of Chemistry, The Catholic University of America, Washington, D. C.
(Received October 15, 1948)

Measurements have been made of the rates of diffusion of various non-electrolytes, and of water, through a collodion membrane separating a dilute solution from pure water. The determinations were made by measuring the rate of rise and fall in a capillary tube in the solution, and analyzing the results using the procedure described in a previous paper. The work was done with 0.25N solutions of sucrose, lactose, raffinose and mannitol, and was carried out at different temperatures so that energies and entropies of activation could be determined. The energy of activation for diffusion through the membranes was found in all cases to be slightly less than for free diffusion, a result that is shown to be consistent with a positive heat of adsorption of the solute and solvent at the membrane. Analogously the entropies of activation for membrane diffusion are somewhat less than for free diffusion, since the process of adsorption brings about a decrease in entropy. The rate of diffusion of water through a membrane is shown to depend upon the nature of the solute diffusing, a result which arises from the fact that diffusion is a mutual process. An experiment is described in which there is an initial net flow from the solution into the solvent.

INTRODUCTION

In previous papers (Parts I and II)[1,2] equations have been developed which are relevant to experiments in which a solution and the pure solvent are separated by a membrane permeable, to different degrees, to both solvent and solute, and in which the level in a capillary tube connected to the solution is measured as a function of time. An equation (Eq. (25) of Part II) was derived expressing pressure as a function of time: it involved, besides the relevant dimensions of the reaction system, the permeation constants for solvent and solute. A method was outlined for analyzing the experimental pressure-time curves so as to obtain the values of the two permeation constants.

In the present paper this procedure is applied to experimental results obtained with dilute aqueous solutions of four non-electrolytes, using collodion membranes. The object of the experiments has been the establishment of the fundamental kinetic laws obeyed when there is simultaneous flow of two substances, the solvent and the solute; the determination of absolute values of the permeation constants, and the energies and entropies of activation, has been regarded as incidental, since they are relevant only to the particular membranes used. It has been possible, however, to show that the equations developed in the previous papers are applicable, and to arrive at some general conclusions as to the mechanism of flow through membranes of this type.

[1] K. J. Laidler and K. E. Shuler, J. Chem. Phys. **17**, 851 (1949).
[2] K. J. Laidler and K. E. Shuler, J. Chem. Phys. **17**, 856 (1949).

Experimental Procedure

(1) *The Membranes.* The collodion membranes used were prepared from collodion cotton, pyroxylin, manufactured by the J. T. Baker Chemical Company. The membranes used in the experiments were strong enough to hold about 60 cc of solution without tearing, but thin and porous enough to permit completion of a run within a reasonable length of time.

The membranes were prepared by standard methods. The collodion solution (about 7 percent) was prepared

by dissolving 35 g of collodion in 160 cc absolute ethyl alcohol and 475 cc of absolute ether. This solution was then poured into a 3.5×17 cm test tube, poured out again and the residue allowed to evaporate with rotation for $3\frac{3}{4}$ minutes. Water was then added, and the resulting membrane was removed by injecting water down the side between the membrane and the test tube. The collodion bag was then cut down to a length of about 8 cm and fastened to the outside of a short glass tube (about 2 cm long) by means of rubber bands. The total volume of the bag was about 60 cc.

The membranes were stored in a large Erlenmeyer flask filled with water, to which had been added a few

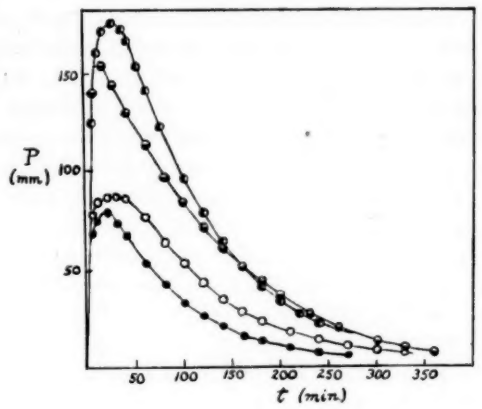

FIG. 1. Pressure-time curves for membrane diffusion at 30°C. ○ = sucrose solution, ● = mannitol, ◒ = raffinose, ◐ = lactose.

crystals of thymol as a preservative. A rubber stopper was inserted into the glass tube to which the membrane was fastened, and this stopper was attached to the stopper closing the Erlenmeyer flask by means of a hook and eye arrangement. This permitted storing the collodion bag under water at all times, and thus prevented any change due to loss of water from taking place in the membrane. Membranes have been kept this way for several months without changes in their properties.

After use, the membrane was washed several times with water, both inside and outside, and the water in the Erlenmeyer flask was changed several times after each run; this removes any solute dissolved in the membrane.

(2) *The Measuring System.* Measurements were made by noting the height of rise in a capillary tube of 0.4-mm internal radius. The capillary was fastened to a meter rule by means of two clamps which permitted the tube to be adjusted in position. The collodion bag was fastened to the capillary tube by means of a rubber stopper in such a way that the capillary came to about 2 cm below the level of the solution in the collodion bag. Collodion solution was then applied with a fine brush at the junction of the rubber stopper and the glass tube to which the membrane was fastened; this held the membrane tightly on the capillary and eliminated the possibility of leakage between the stopper and the glass holder for the membrane.

TABLE I. Data for diffusion through membrane I. 0.25*N* sucrose solution.

Temperature	10.0°C	20.0°C	30.0°C	40.0°C
$\lambda_1 \times 10^3$ (min.$^{-1}$)	7.10	9.52	11.0	12.7
$\lambda_2 \times 10^3$ (min.$^{-1}$)	6.84	9.15	10.6	12.1
$(\lambda_1 - \lambda_2) \times 10^4$ (min.$^{-1}$)	2.6	3.7	4.0	6.0
$\lambda_3 \times 10^3$ (min.$^{-1}$)	36.4	50.9	54.0	74.1
P_{max} exp. (mm)	289	324	352	390
P_{max} calc. (mm)	283	330	348	394

(3) *The Measuring Technique.* A vessel of about 6 liters capacity filled with distilled water was placed in a large thermostatted water bath. The membrane was filled with the solution to be tested, which had first been brought to the temperature of the water bath. The membrane was then fastened to the capillary in the way described above, and by moving the capillary, the solution level in it was brought to the zero mark on the meter stick. The membrane was then submerged in the beaker in such a way that the water level in the beaker coincided with the zero mark on the measuring stick. The water in the beaker was stirred continuously so that the concentration of the solution surrounding the membrane was uniform. Due to surface tension, the level in the capillary rose to a certain height above the level of the surrounding water as soon as the membrane was submerged in the water. This height of capillary rise was determined experimentally before the run was begun, and it was assumed that the height of capillary rise due to surface tension was constant throughout the run, although the solution inside the membrane continuously changed in concentration. This error, however, would only be of a magnitude of 1–2 mm at the most.

Readings were taken as soon as the level of the solution in the capillary reached the predetermined height corresponding to the capillary rise due to surface tension. This took only about 1 second after immersion. This point then is the zero point and all other readings

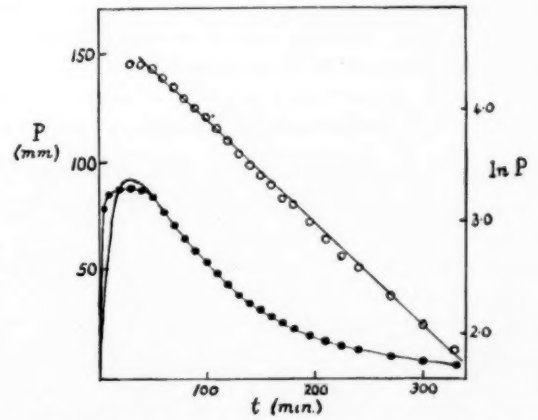

FIG. 2. Pressure-time and ln(pressure)-time curves for membrane diffusion. The black circles are experimental points on the pressure-time curve for sucrose solution, the line without points being the calculated curve. The open circles are ln*P* *vs.* *t* points and fall about a straight line.

TABLE II.

Data for diffusion through membrane II at 30.0°C

Solution 0.25N	Sucrose	Lactose	Mannitol	Raffinose
$\lambda_1\times10^2$ (min.$^{-1}$)	1.00	1.00	1.15	0.89
$\lambda_2\times10^2$ (min.$^{-1}$)	0.99	0.97	1.13	0.87
$(\lambda_1-\lambda_2)\times10^4$ (min.$^{-1}$)	1.4	2.9	2.3	1.9
$\lambda_3\times10^2$ (min.$^{-1}$)	7.80	9.10	16.0	8.00
P_{max} exp. (mm)	87	175	80	154
P_{max} calc. (mm)	92	169	80	137

Data for diffusion through membrane II at 46.5°C

Solution 0.25N	Sucrose	Lactose	Mannitol	Raffinose
$\lambda_1\times10^2$ (min.$^{-1}$)	1.30	1.14	1.375	1.24
$\lambda_2\times10^2$ (min.$^{-1}$)	1.27	1.13	1.350	1.23
$(\lambda_1-\lambda_2)\times10^4$ (min.$^{-1}$)	2.80	1.29	2.07	1.40
$\lambda_3\times10^2$ (min.$^{-1}$)	15.3	15.0	27.0	12.0
P_{max} exp. (mm)	111	73	63	87
P_{max} calc. (mm)	108	52	46	72

are referred to it. Readings were taken every minute for the first 5 minutes, every two minutes after that up to the maximum height of rise, and then every 5 minutes until the conclusion of the experiment.

After completion of the run, the membrane was carefully washed and stored as described above. The two membranes used in the experiments were checked periodically with a 0.25*N* sucrose solution to determine if there were any changes; as already stated, the membranes still gave reproducible results after several months. The experiments were carried out with sucrose, lactose, mannitol and raffinose, all in 0.25*N* solution in water as solvent. In addition a 0.5*N* solution of urea with glycerol as solvent was investigated.

(4) *The Measurements.* Membrane I was used with an 0.25*M* solution of sucrose, and several runs were made at each of the temperatures 10°, 20°, 30° and 40°C; the object of this was the determination of the variation of the permeation constants with temperature, and a comparison with the results obtained for free diffusion in water. Membrane II was used with 0.25*M* solutions of sucrose, lactose, raffinose and mannitol, and measurements were made at 30° and at 46.5°C.

Experimental Results

Pressure-time curves obtained with membrane II at 30°C using the four different solutes are reproduced in Fig. 1. In Fig. 2 is shown a P *vs.* t curve and a log$P$ *vs.* t curve for sucrose at 30°C, also obtained with membrane II; the curves obtained at other temperatures and with other solutes are similar. The final slope of ln$P$ *vs.* t gives the value of λ_1; values for λ_2 and λ_3 are then found using Eqs. (29) and (25) of Part II. The value of π_0, the osmotic pressure at zero time, is obtained using the Morse equation; since P, the height of rise in the capillary, is expressed in terms of mm of water, π_0 is expressed in the same units, the value for the sucrose solution at 30°C being 7.01×10^4 mm.

In Fig. 2 a calculated curve, obtained from the values of λ_1, λ_2, and λ_3 derived, is shown. It is seen that there is excellent agreement with the observed curve during the later stages of the run, that the maximum heights of rise are in satisfactory agreement, but that initially the deviations are greater. The deviations at the beginning of the experiment are expected to be greatest, since the initial slope is given by $\pi_0(\lambda_1-\lambda_2)$, and since λ_1 and λ_2 are very close to one another the initial slope will be very sensitive to their actual values. Thus in the case of sucrose, λ_1 and λ_2 are both approximately 1×10^{-2}, while $\lambda_1-\lambda_2$ is 1.39×10^{-4}; poor initial agreement is therefore to be expected even if λ_1 and λ_2 are known quite accurately.

The results obtained for membrane I at the four temperatures are shown in Table I, and those for membrane II, for the four solutes at two temperatures, in Table II. The maximum heights of rise calculated using these constants are shown and are compared with the experimental values. The values given in the tables are the means of three independent determinations which gave very concordant results.

The Energies of Activation. The values of λ_1 and λ_2 are related to those of the permeation constants Q_1 (for the solvent) and Q_2 (for the solute) by (cf. Eqs. (8) and (9) of Part II)

$$\lambda_1=(Q_1c_t\bar{V}_1^2A/dRTa) \quad (1)$$

and

$$\lambda_2=(Q_2c_t\bar{V}_2\bar{V}_1A/dRTa), \quad (2)$$

where $\bar{V}_1$ and $\bar{V}_2$ are the partial molar volumes of solvent and solute, A is the surface area and d the thickness of membrane, a the cross-sectional area of the capillary, c_t the total concentration of solvent and solute, and R is the gas constant. Since $\bar{V}_1$, $\bar{V}_2$, c_t, A, d and a are practically independent of temperature, it follows that the energies of activation for Q_1 and Q_2 can be obtained by plotting ln(λ_1T) and ln(λ_2T) respectively against $1/T$.

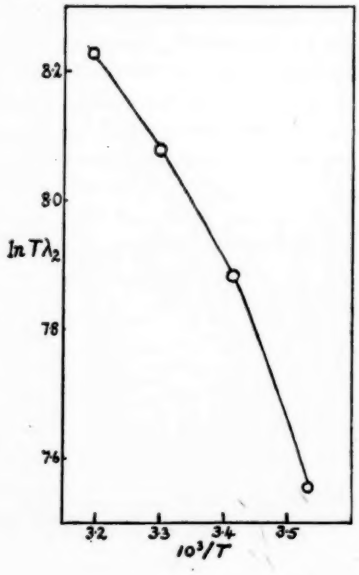

FIG. 3. A plot of ln$T\lambda_2$ for the diffusion of sucrose through membrane I. The curvature indicates that the energy of activation decreases with rising temperature.

Such a plot is shown in Fig. 3, the data being for the diffusion of sucrose through membrane I. A slight curvature is to be noted, and will be seen later to be characteristic of diffusion in aqueous systems. The energy of activation therefore varies (it actually decreases) with a rise in temperature. By taking tangents to the curve, activation energies corresponding to various temperature ranges may be obtained, and are shown in Table III for both sucrose and water. In Table IV are given activation energies for the four solutes and water using membrane II, the values being obtained from the rates at the two temperatures 30° and 46.5°C, and therefore being relevant to this temperature range. It is to be noted that the values for the sucrose-water system using the two membranes agree fairly well.

The Permeation Constants. The permeation constants Q_1 and Q_2 for membrane II were calculated using Eqs. (1) and (2). The average value of the membrane thickness d was determined at various points using a micrometer caliper graduated in 1/10,000 of an inch, while the area A was measured geometrically. The values thus determined are not of high accuracy, but the *relative* values of Q_1 and Q_2 will be correct (the same approximate values for A and d being used throughout), while their absolute values are sufficiently accurate to be used for calculating the entropies. Values of the permeation constant at 30°C are included in Table V, which also gives the diffusion constants D_f for free diffusion in water and the ratio Q/D_f; the values of D_f were not all available at 30°C, but were estimated as accurately as possible from the values at other temperatures.

The Entropies of Activation. According to Eyring and his co-workers,[3] the diffusion constant D is expressible as

$$D = e\sigma^2(kT/h)\exp(\Delta S^{\ddagger}/R)\exp(-E/RT), \qquad (3)$$

where e is the base of the natural logarithms, k is the Boltzmann constant, h is Planck's constant, σ is the average distance between equilibrium positions in the process of diffusion, $\Delta S^{\ddagger}$ is the entropy of activation and E is the experimental energy of activation determined in the manner described above. According to the theoretical treatment of membrane diffusion given in Parts I and II, this equation is equally applicable to membrane diffusion, the diffusion constant now being replaced by the permeation constant Q.

Utilizing the data of Tables IV and V for membrane II, values of the function $[\exp(\Delta S^{\ddagger}/R)]^{\frac{1}{2}}$ have been calculated and are given in Table VI, which includes also some values for diffusion of gases through glass and Neoprene obtained by R. M. Barrer.[4]

[3] H. Eyring, J. Chem. Phys. 4, 283 (1936); Hirschfelder, Stevenson, and Eyring, *ibid.* 5, 896 (1937); for reviews see Kincaid, Eyring, and Stearn, Chem. Rev. 28, 301 (1941), Glasstone, Laidler, and Eyring, *The Theory of Rate Processes* (McGraw-Hill Book Company, Inc., New York, 1941), Chapter XI.

[4] R. M. Barrer, J. Chem. Soc. 278 (1934); Trans. Faraday Soc. 35, 628, 644 (1939); cf. Glasstone, Laidler, and Eyring, reference (3), pp. 543–544.

TABLE III. Energy of activation for diffusion through membrane I (10°–40°C; 0.25N sucrose).

Temp.°C	E_{act} H_2O, (kcal.)	E_{act} sucrose, (kcal.)
10°–20°C	5.4	5.4
20°–30°C	3.2	3.4
30°–40°C	3.1	3.2

TABLE IV. Energies of activation for diffusion through membrane II (30°C–46.5°C).

Substance	E_{act} for H_2O through membrane, (kcal.)	E_{act} for solute through membrane, (kcal.)
Sucrose	3.7	3.5
Lactose	2.3	2.4
Mannitol	2.8	2.7
Raffinose	4.5	4.7

The value of σ for diffusion through membranes is probably similar to that for free diffusion, where it is usually 1A; assuming this value the data of Table VI for the collodion membrane gives values of $\Delta S^{\ddagger}$ of from -10 to -20 cal./degree.

"Negative Osmosis." Various attempts were made to achieve negative osmosis, i.e., an initial fall instead of a rise in the tube when the capillary is attached to the more concentrated solution (Case III of Fig. 1, Part II). This was finally accomplished using an 0.5N solution of urea in glycerol. For convenience the solvent, glycerol, was placed in the collodion bag to which the tube was attached, and the bag immersed in the solution. A rise of several millimeters was observed, followed by a fall. No further work was carried out on this as the system would seem to be of negligible theoretical importance.

GENERAL DISCUSSION

Permeation of the Solutes

The permeation constants for the solutes are seen from Table V to fall in the order

mannitol > sucrose, lactose > raffinose.

This is the inverse of the order of the molar volumes, the larger molecules diffusing least rapidly. As discussed in Part I the ratio Q_2/D_M, where D_M is the constant for diffusion through the membrane, is equal to the adsorption equilibrium constant k_1/k_{-1};* values of this quantity are included in Table V. The values are all of the order of 10^{-4}, and this may be associated in a qualitative manner with the ratio of pore area to the total area of the membrane, this ratio probably being the dominant factor in determining the distribution of solute molecules between solution and membrane. The small value of k_1/k_{-1} is consistent with one of the

* Since for the porous types of collodion membranes used the diffusion coefficient for free diffusion, D_f, is probably not much different from that of membrane diffusion in order of magnitude, the ratio Q/D_f was formed in the absence of exact knowledge of D_M.

TABLE V. Permeation constants for membrane II and constants for free diffusion in water $T=30°C$.

	Sucrose	Lactose	Mannitol	Raffinose
$Q_1\times10^9$ (cm^2 $sec.^{-1}$)	7.8	7.8	8.8	7.2
$Q_2\times10^{10}$ (cm^2 $sec.^{-1}$)	6.5	5.8	12.7	4.0
$D_f\times10^6$ [a] (cm^2 $sec.^{-1}$)	5.6	5.2	7.2	4.0
$\frac{Q_2}{D_f}\times10^4\approx\frac{k_1}{k_{-1}}10^4$	1.2	1.1	1.8	1.0

[a] Estimated for 30°C where not given at that temperature in the literature.

TABLE VI. Entropy factors for diffusion through membranes.

Diffusing species	Membrane	$\sigma(e^{\Delta S^\ddagger/R})^{\frac{1}{2}}$(A)
Sucrose	Collodion membrane II	1.1×10^{-2}
Lactose	Collodion membrane II	4.3×10^{-2}
Mannitol	Collodion membrane II	8.1×10^{-2}
Raffinose	Collodion membrane II	2.4×10^{-2}
H_2O (sucrose solution)	Collodion membrane II	1.2×10^{-2}
Hydrogen	Glass	4×10^{-2}
Helium	Glass	4×10^{-2}
Hydrogen	Neoprene	74
Argon	Neoprene	185
Nitrogen	Neoprene	215

conditions (cf. Eq. (24) of Part I) that diffusion through the membrane shall be the rate-determining step.

The Permeation of Water

An interesting and significant fact about the data presented in Table V is that the permeation constants Q_1 for water depend upon the solute used: the variations are seen to be much too great to be explained as experimental error.

That such behavior is to be expected follows at once if the viewpoint of Eyring[3] regarding diffusion processes is adopted. According to this concept, a diffusing molecule passes from one equilibrium position to the next by pushing aside neighboring molecules, a process which involves movement on the part of not only the molecule under consideration, but of other molecules which must adjust their positions in order to allow the molecule to move. The rate of diffusion of a given molecule will therefore depend not only upon the nature of the molecule itself but on that of the other species present in solution.

If one is dealing with free diffusion in a solution, the diffusion constants for solvent and solute are necessarily related to one another in a simple manner. Consider a given surface of cross section in the solution: the number of solvent molecules passing from left to right is proportional to the diffusion constant D_1, and to the mole fraction gradient; similarly the number of solute molecules moving from right to left is proportional to D_2 and to the mole-fraction gradient. Since the mole fraction gradients bringing about diffusion of the two species are necessarily the same, one can write, for the number of moles moving across the surface in a given time

$$n_1=kD_1, \tag{4}$$

$$n_2=kD_2. \tag{5}$$

The corresponding volume changes are therefore

$$V_1=kD_1\bar{V}_1, \tag{6}$$

$$V_2=kD_2\bar{V}_2, \tag{7}$$

where $\bar{V}_1$ and $\bar{V}_2$ are as before the molar volumes. Since the imaginary surface is kept fixed and there is no net movement of the solution these volume changes must be the same, so that

$$D_1\bar{V}_1=D_2\bar{V}_2. \tag{8}$$

This is therefore a necessary relationship between the diffusion constants of solvent and solute in free diffusion.

For diffusion through a membrane the corresponding relationship

$$Q_1\bar{V}_1=Q_2\bar{V}_2 \tag{9}$$

is not necessarily obeyed, since the molecules are now not only flowing past one another but past the molecules constituting the membrane. When Eq. (9) is not obeyed there is a net movement in the system, which was forbidden in the case of free diffusion. It was seen in Part II that Eq. (9) is in fact the condition that the concentration of the two solutions will equalize without the development of any pressure between the two solutions, and that according as $Q_1\bar{V}_1$ is greater or less than $Q_2\bar{V}_2$ the osmosis is respectively "positive" or "negative." If a membrane were of such a nature that it offered very little resistance to the flow of the solvent and solute molecules the deviations from Eq. (9) would be small. On the other hand a membrane that interfered seriously with the flow of either or both species would introduce marked deviations; an extreme example of this is the semipermeable membrane which reduces Q_2 to zero. The membranes used in the present work are clearly of the first type, since Eq. (9) is found to be approximately obeyed.

Applying these considerations qualitatively to the experimental data it is found that the permeation constant Q_1 for water is smallest for the solution of raffinose; anhydrous raffinose has the lowest value of $Q_2\bar{V}_2$ of the solutes tested, in spite of having the highest value of $\bar{V}_2$. The permeation constant for water is largest for mannitol, which has the largest $Q_2\bar{V}_2$; it is intermediate and practically equal for sucrose and lactose for which $Q_2\bar{V}_2$ is intermediate. That the permeation coefficients do not vary as much for the different solutions as for the various solutes is due to the smaller molar volume of the water, the change in the equilibrium distance for the water molecules for different solutes not being as large as that for the solute molecules themselves.

The Energies of Activation

In discussing diffusion constants in aqueous solutions attention must be paid to the fact that the activation energies are dependent upon the temperature; when one plots the logarithm of the diffusion constant against the reciprocal of the absolute temperature T one obtains not a straight line but one which is slightly concave towards the axes.[5] This implies that the activation energy decreases with increasing temperature, a phenomenon which has been explained by Eyring and his co-workers on the basis of the hydrogen-bonded structure of water,[6,3] the amount of bonding becoming less at higher temperatures and therefore allowing diffusion to take place more readily. As examples of this type of behavior may be quoted the data for the diffusion of mannitol in water,[7] which give[5] an activation energy of 6.59 kcal. between 10° and 20°C and of 3.77 between 60° and 70°C. For the diffusion of heavy water into light water,[8] which within an error of 2 percent may be considered as the self-diffusion of water, the results indicate an activation energy of 7.06 kcal. between 25° and 35°C and of 3.93 kcal. between 35° and 45°C.

The same type of variation of the activation energy for permeation has been noted in the present work (cf. Fig. (3)), the value for sucrose falling from 5.4 kcal. at 5° to 3.2 at 35°C. In comparing activation energies for permeation the same temperature range must be considered in each case. The observed variation of the activation energy for permeation is probably not only due to the associated nature of the solvent, as in free diffusion, but also to the reversible change of the membrane structure due to the increased thermal motion of the chain molecules at higher temperatures, as has been found by Barrer[9] for the passage of gases through elastomers.

Free diffusion data for the interval between 30° and 46.5° are only available for mannitol, the value being about 4.1 kcal.; however, for the other three substances used in this range the values can be estimated, and are found to be somewhat higher than for mannitol. The energies of activation for permeation of the membrane are thus somewhat smaller than for free diffusion in water. It is readily seen from the treatment given in Part I that the over-all energy of activation for permeation is less than that for the diffusion through the membrane by the heat of adsorption of the substance in the membrane. According to the pore theory of membrane diffusion the energy of activation for diffusion in the membrane may be very close to that for free diffusion; the difference between this value and that for permeation is therefore the heat of adsorption in the membrane. That this heat should be positive is consistent with the fact that adsorption involves a decrease in entropy. The situation here is closely analogous to that in the case of reactions on surfaces, for which the over-all energy of activation is less than that for the actual process on the surface by the heat of adsorption of the reacting species.

The fact that the energy of activation for the permeation of sucrose is higher than that of lactose is of interest in view of the chemical similarity and almost identical molar volumes. The same result is found with free diffusion in water; between 10° and 20°C the values are 4.85 kcal. for sucrose and 4.07 for lactose. The higher values for sucrose, implying that this molecule must pass over a higher energy barrier in moving from one equilibrium position to the next, may be due to its tendency to associate with water molecules,[10] some of which may be dragged along in the diffusion process.

The Entropy of Activation

According to the views of Eyring and his co-workers,[3] the value of $\Delta S^{\ddagger}$, the entropy of activation for permeation, gives an indication of the mechanism of flow; large positive values indicate that the permeation is accompanied by breakage of bonds, while low values of $\Delta S^{\ddagger}$ indicate that permeation has taken place without bond breaking. The slightly negative values encountered with some systems can then be explained by the partial immobilization of the diffusing molecules in the membrane as they permeate it without breaking, or loosening, the membrane structure.

This view has been criticized recently by Barrer in a series of publications in which the alternative view of the "activation zone" is applied to this problem.[9] According to this view, the value of $\Delta S^{\ddagger}$ cannot be interpreted in terms of a mechanical picture so simply as has been done by Eyring. According to Barrer a high $\Delta S^{\ddagger}$, which is correlated with a high activation energy for diffusion, may mean either a large zone of activation or the reversible loosening of more chain segments of the membrane; which is the case depends upon whether or not the heat of adsorption of the diffusing molecule remains constant as the structure, i.e., cross linking, of the membrane changes. A low $\Delta S^{\ddagger}$ is then associated with either a small zone of activation or very little or no loosening of the membrane structure on permeation.

Whichever viewpoint may be accepted in the interpretation of $\Delta S^{\ddagger}$ it seems clear that the low value of $\Delta S^{\ddagger}$ found for the sugar-water-collodion system indicates that the permeation of the species through the membrane occurs with a minimum of disturbance of the membrane structure, and a small zone of disorder; it therefore would probably be correct to interpret the small negative values of $\Delta S^{\ddagger}$ mechanically as interstitial permeation of the membrane (minimum of chain loosening) with partial immobilization in the membrane (small zone of disorder).

[5] H. S. Taylor, J. Chem. Phys. **6**, 331 (1938).
[6] R. H. Ewell and H. Eyring, J. Chem. Phys. **5**, 726 (1937).
[7] J. D. R. Schaffer and F. E. C. Schaffer, Proc. Acad. Sci. Amsterdam **19**, 148 (1916).
[8] J. C. Orr and J. A. V. Butler, J. Chem. Soc. 1273 (1935).
[9] R. M. Barrer, Trans. Faraday Soc. **38**, 322 (1942), **39**, 48 (1943), **39**, 59 (1943); R. M. Barrer and G. Skirrow, J. Polymer Sci. **4**, 549 (1948) and several other papers.
[10] G. Scatchard, J. Am. Chem. Soc. **43**, 2406 (1921).

On Permanent Charges in Solid Dielectrics. II.* Surface Charges and Transient Currents in Carnauba Wax

B. GROSS
National Institute of Technology, Rio de Janeiro, Brazil
(Received September 23, 1948)

Permanent surface charges are produced in disks of carnauba wax by exposure to an external electric field. The nature of these charges is studied with a new method of analysis, which is based on the simultaneous measurement of the external current and of the induced charges on the electrodes of the capacitor containtaining the dielectric. The observed effects are explained by dielectric absorption and by transfer of charge from the electrode to the surface of the dielectric; this latter phenomenon is due to surface breakdown and continuous conduction currents. The results provide an adequate explanation for the electret.

DISPLACEMENTS of charge carriers within the dielectric and exchange of carriers between dielectric and electrodes take place during exposure of a solid dielectric to an external field and after withdrawal of the field and short-circuiting. These effects manifest themselves by the production of time-dependent currents in the external circuit and by the induction of electric charges on the electrodes of the capacitor containing the dielectric. This paper reports a systematic study of the permanent surface charges and transient currents for disks of carnauba wax and discusses their bearing on the interpretation of the electret. Use is made of the results achieved in a former research and published as Part I of this paper.[1] A preliminary report[2] has already been published. A list of pertinent papers is given below;[3] for a more complete bibliography we refer to the recent report given by Gutmann.[4]

I. DIELECTRIC TESTING WITH THE DISSECTIBLE CAPACITOR

1. The Dissectible Capacitor

Current and induced charges are measured with the dissectible capacitor[5] (Fig. 1). The dielectric, in the form of a disk (diameter 7 cm, height 7–10 mm) is clamped to the lower, fixed electrode of the capacitor by means of a guard ring. The upper electrode (diameter 6.5 cm) can be lifted; it is suspended on an iron piston which moves in the field of a coil. Passing the current through the coil lifts piston and electrode; interruption of the current brings the electrode again into contact with the dielectric. Since the electrode is not rigidly fixed to the piston, but is allowed a certain freedom of motion, it adjusts itself easily to the surface of the dielectric and an adequate contact between dielectric and electrode is achieved. The weight of the movable system is 815 g; an airdamping device makes the movement of the system sufficiently smooth. Nickel-plated and steel electrodes have been used without measurable difference in the results. A special shielding device closes over the dielectric every time the electrode is lifted, avoiding any influence of the polarized dielectric upon the measuring electrode during the act of measuring. The closing and opening of this device is accomplished by the movement of the piston. The movable electrode is connected with the measuring system, which is constituted by a one-fiber string electrometer and an adjustable air capacitor; this electrode and the connecting wires are insulated by sulphur insulators. The lower electrode is during polarization connected with the high voltage source; otherwise it is grounded. The guard ring and other metal parts of the capacitor are always grounded. Heating coils are placed around the electrode system for measurements at elevated temperatures. Temperature is read on a mercury thermometer; a thermocouple is also provided for. The entire capacitor, including the heater, is enclosed in a desiccator.

2. Technique of Measurement

All measurements were made with samples of first-grade (yellow) filtered carnauba wax under conditions of very low humidity. For obtaining quantitative results one should avoid operations involving uncontrolled handling of the samples, like taking them out of the capacitor, exposing them to humid air, and wrapping them in tinfoil and unwrapping them. Thus during one experimental cycle the sample remained always in the

* Paper handled by the Committee on Inter-American Scientific Publication.

[1] B. Gross and L. F. Dennard, Phys. Rev. **67**, 253 (1945).

[2] Bernhard Gross, Phys. Rev. **66**, 26 (1944).

[3] O. Heaviside, Electrical Papers, Vol. 1, pp. 488; M. Eguchi, Proc. Phys. Math. Soc. Japan. Ser. 3, **1**, 326 (1919); **2**, 169 (1920); Phil. Mag. **49**, 179 (1925); S. Mikola, Zeits. f. Physik **32**, 476 (1925); K. Nakata, Proc. Phys. Math. Soc. Japan. Ser. 3, **9**, 179 (1927); E. P. Adams, J. Frank. Inst. **204**, 469 (1927); M. Ewing, Phys. Rev. **36**, 378 (1930); R. D. Bennett, Phys. Rev. **37**, 103 (1931); O. J. Johnson and P. H. Carr, Phys. Rev. **42**, 912 (1932); P. Jaeger, Ann. d. Physik **21**, 481 (1934); A. Gemant, Phil. Mag. **20**, 929 (1935); Rev. Sci. Inst. **11**, 65 (1940); Phys. Rev. **61**, 79 (1942); G. Groetzinger and H. Kretsch, Zeits. f. Physik **103**, 337 (1936); Thiessen, Winkel, and Herrmann, Physik. Zeits. **37**, 511 (1936); H. Frei and G. Groetzinger, Physik. Zeits. **37**, 720 (1936); W. M. Good and J. D. Stranathan, Phys. Rev. **56**, 810 (1939); G. E. Sheppard and J. D. Stranathan, Phys. Rev. **60**, 360 (1941); B. Gross, Anais Acad. Brasil. Ci. **15**, 63 (1943); **17**, 219 (1945); Partington, Planer, and Boswell, Nature **158**, 835 (1946).

[4] Felix Gutmann, Rev. Mod. Phys. **20** 457 (1948).

[5] The origin of the dissectible capacitor as a tool in the study of dielectric phenomena goes back to Benjamin Franklin; See Bernhard Gross, Am. J. Phys. **12**, 324 (1944), and J. Zeleny, *ibid.* **12**, 329 (1944).

capacitor and the desiccator was not opened. This excluded the possibility of polarizing the dielectric in the molten state. But the samples, which we have polarized at an elevated temperature below the melting point, produce electric fields, the intensity and permanency of which reach the values mentioned in the literature for polarization in the molten state.

The circuit employed (Fig. 2) allows for measurement of *the total external current* $J(t)$ and *the induced charge* $q(t)$ of the removable electrode.

3. Analysis of the Currents

The electric charges $\pm q$ found on the electrodes of a shorted capacitor are due to induction by fields, which originate in other charges residing in the dielectric. Observation of the induced charges of the electrodes therefore gives information about the nature and time-dependence of the charges in the dielectric. Quantitative information is gained, when use is made of the general equation, which according to Maxwell's theory connects currents and charges:

$$J(t)=i(t)+dq/dt, \tag{1}$$

where $J(t)$ is the external current, $i(t)$ is the conduction current across the dielectric-electrode interface, and dq/dt is the displacement current across the interface.

The simultaneous measurement of $J(t)$ and $q(t)$ permits the decomposition of the current across the interface into its two components; $i(t)$ is a measure for the transfer of charge carriers between dielectric and electrode and dq/dt is a measure for the displacement of charge carriers within the dielectric. This method of measurement gives more insight into dielectric behavior than the usual practice of measuring either J or q; its field of application may conveniently be extended to dielectric testing in general.

4. The Field at the Surface of the Dielectric

The electric field E produced by the dielectric (in a shorted condition) is given by

$$E=1.16\times10^{13}q/A \text{ volt/cm}, \tag{2}$$

where the area A is given in cm² and q in coulombs.

II. EXPERIMENTAL RESULTS

1. Dielectric Absorption and Heterocharge

All effects, which occur when low or medium polarizing voltage is applied at room temperature, can be explained by dielectric absorption. Figure 3 gives the typical aspect of the curves obtained under such conditions ($V=950$ volt and $T=30°$C). The *current* shows the familiar behavior characteristic for every solid dielectric and for carnauba wax already discussed in I. The *charge* of the electrode jumps from zero to a finite initial value, when the polarizing voltage is applied; then it increases continuously. At the moment of the short-circuit a jump of q of the same value as before, but in the contrary direction, is observed, followed by a slow decrease. The polarity of q does not change; the electrode, which during polarization was connected with the positive pole, carries always a positive charge, the adjacent surface of the dielectric a negative one. The displacement current obtained by differentiation of the function $q(t)$ (actually $\Delta q/\Delta t$ is given) is found to coincide within the precision of the measurement with the measured values of the external current $J(t)$. Thus no conduction current flows across the dielectric-electrode interface; this proves that no exchange of charge carriers between dielectric and electrode is taking place.

The jumps of q in phase with the voltage jumps of course are caused by the charging and discharging of the geometrical capacitance. The behavior of the time-dependent currents and the coincidence of the $J(t)$ and dq/dt curves is explained by dielectric absorption and agrees with the conclusions of the generally ac-

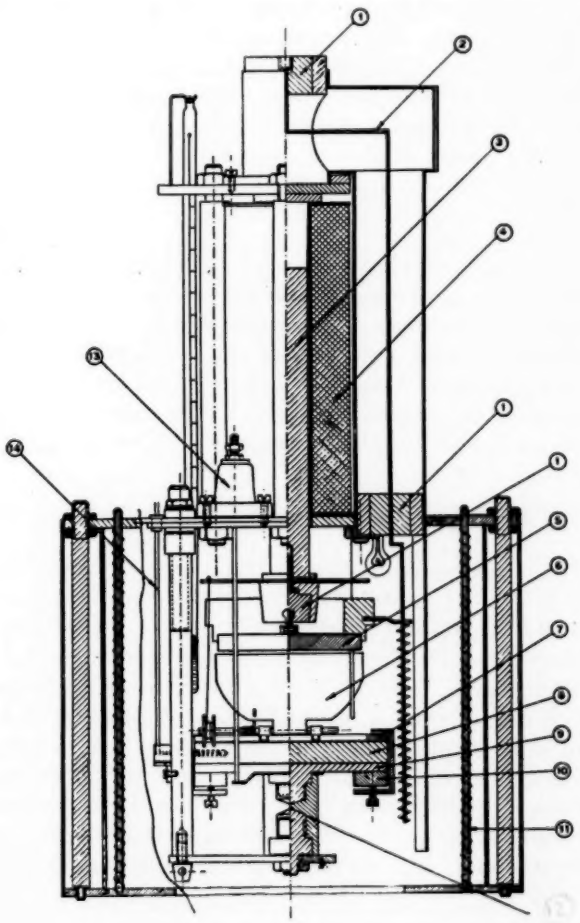

FIG. 1. Dissectible condenser.

(1) Sulfur insulator
(2) Lead to measuring electrode
(3) Iron piston
(4) Magnetic coil
(5) Removable electrode
(6) Shielding device
(7) Guard ring
(8) Dielectric
(9) Fixed electrode
(10) Clamps
(11) Heater coil
(12) Insulator
(13) High voltage pole
(14) Thermocouple

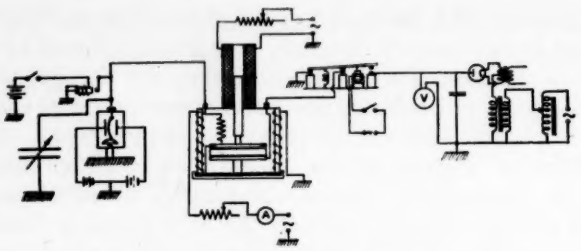

FIG. 2. Diagram of the circuit.

cepted theories of this effect. According to them, the following mechanisms may be effective: (a) hindered dipole orientation (Debye), associated with the rotation of dipole systems; (b) microscopical heterogeneity of structure (Maxwell-Wagner), associated with the displacement of ions over microscopical distances; (c) ionic conduction, associated with the formation of space charges.[6] The two former effects do not involve any transfer of charge carriers between dielectric and electrodes and in the case of the last one this transfer plays a minor role. This being so, there is $J=dq/dt$.[7] Formally absorption can always be accounted for by a time-dependent component of the volume polarization $P(t)$. This leads to the appearance of surface charges $s=-PA$. It follows that

$$s(t)=\int_t^\infty J(t)dt. \tag{3}$$

The polarity of s is contrary to that of the corresponding electrode during polarization; thus according to Gemant's terminology s is a *heterocharge*.[8] The relation (3) can be used generally for the computation of the heterocharge, if it is applied to the shorted system. Thus the value of the heterocharge at a time t after the short-circuit is given by the integral over the total discharge current from 0 to ∞.

2. "Freezing-in" of the Heterocharge

A considerable fraction of the absorbed charge can be frozen in by an adequate heat treatment, as has been shown by Frei and Groetzinger[9] and later discussed in I. Since dielectric absorption is always associated with a heterocharge, production of a permanently polarized dielectric carrying a heterocharge only is feasible. Such an experiment is shown in Fig. 4. A voltage of 175 v was applied at 70°C; after 30 min. the temperature was reduced to 40°C, then the system was short-circuited. Figure 4a shows the behavior immediately after the short-circuit, Fig. 4b that during reheating 2 weeks later. The current behaves much as in I; the current surge during reheating indicates the liberation of a frozen-in charge. The sign of q again is that of a heterocharge; the value of q at first decreases, later it stays constant over the period of two weeks, which passes between the two phases of the experiment.[10]

3. Surface Breakdown

A new effect, transfer of charge from the electrode to the surface of the dielectric, sets in, when the applied voltage is sufficiently high and the temperature well above room temperature, or even when a very high voltage is applied at room temperature. This is shown in Fig. 5 giving the results of an experiment, in which 2500 v were applied at 50°C. Comparison with Fig. 3a shows various conspicuous differences: (a) The charge of the electrode repeatedly undergoes strong discontinuous variations. (b) The current now contains a steady state component; this is the ohmic current which appears at high temperatures. (c) The analysis of the current shows the existence of a conduction current between dielectric and electrode (by the inequality of J and dq/dt), which seems connected at least in part with the steady state current. The inset of Fig. 5 gives again the charge in function of time, but in such a way that the discontinuous variations of q are disregarded; thus after each jump the q values have been increased by an amount equal to the height of the jump.

We conclude that a jump gives evidence for an instantaneous breakdown of the interface.[11] With in-

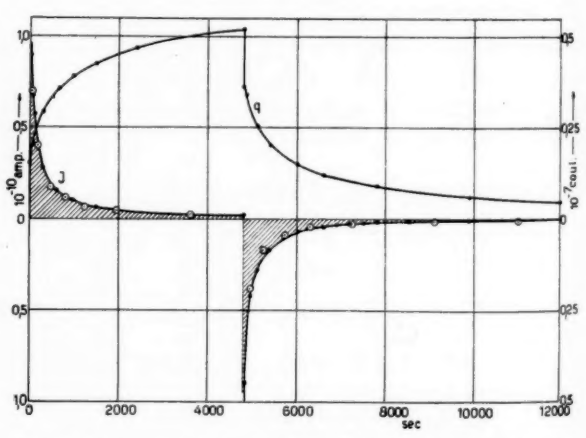

FIG. 3. Currents and charges for dielectric absorption. (Points: measured values; circles: calculated values of the displacement current.)

[6] The theory of this effect is due to G. Jaffé, Ann. d. Physik **16**, 217 (1933). Space charges in electrets, which were polarized in the molten state, have been observed by Gemant (see reference 3) and by Thiessen, Winkel, and Herrmann (see reference 3).

[7] This relation between the absorption current and the surface charges of the electrodes of an absorptive capacitor is found in many papers on absorption, i.e. G. Jaffe (see reference 6).

[8] A. Gemant, see reference 3.

[9] H. Frei and G. Groetzinger, reference 3.

[10] It has already been reported by Johnson and Carr, reference 3, that polarization with very low voltages yields electrets with heterocharges; for further measurements see Gemant, reference 3.

[11] Since evidence for a crystalline structure of the electret has been found (M. Ewing, reference 3; A. Gemant, reference 3), a jump could possibly be thought of as being due to an adjustment of domains (see reference 4, p. 463). In the formal theory this effect is described by a discontinuous variation of the volume polarization $P(t)$; thus it must be accompanied by a jump of $J(t)$. But we have never observed discontinuous phenomena in the current-time curve except those caused by variations of the applied voltage.

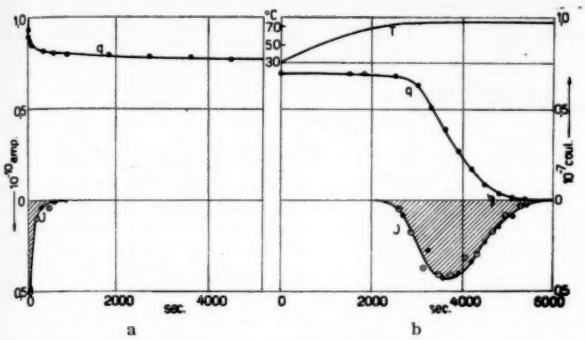

FIG. 4. "Freezing-in" of the absorbed charge. (a) Current and charge after the short-circuit. (b) Current and charge during reheating, 2 weeks later. (Points: measured values; circles: calculated values of the displacement current.)

creasing polarization of the dielectric, the surface charges and, consequently, the field in the interface rise to high values. Finally the interface breaks down and a considerable amount of electricity is rushed from the electrode to the surface of the dielectric. This charge has a polarity, which is contrary to that of the original charge of the dielectric; it neutralizes part of the latter and thus reduces the field in the interface below sparking threshold.

During this experiment the density of the surface charge reached about 4.7×10^{-9} coul./cm^2 and the electric field 54,000 v/cm. But occasionally we have observed still higher values, in one instance a surface charge of 5.7×10^{-9} coul./cm^2, giving a field of 66,000 v/cm.[12]

4. The Homocharge

The charge, which during a surface breakdown is transferred to the dielectric, does not dissipate at once. This can be inferred from the study of the behavior after short-circuit of a sample, where surface breakdown has occurred; (Fig. 6) (9800 v applied at 29°C for 2 hr.). Figure 6a shows that the behavior of $J(t)$ and the slope of $q(t)$ are very much the same as before (Fig. 3) and there is still $i=0$. But there is one significant new feature: the position of the $q(t)$ curve relative to the vertical axis has changed, the whole curve being displaced downward by a constant amount; in consequence of this downward shift q undergoes a polarity reversal. Thus some time after the short-circuit, the electrode which was connected with the positive pole of the voltage source, carries a negative charge and the other electrode a positive one, the polarities of the corresponding surfaces of the dielectric being, respectively, positive and negative. Figure 6b shows, that heating (22 hr. after the short-circuit) destroys these charges. But during this heating period there is $J\neq dq/dt$ and $i\neq0$ over a considerable interval. This proves the occurrence of a continuous transfer of charge carriers between dielectric and electrode. The small external current flows in the same direction as during the period of application of the polarizing voltage. This is just what one has to expect when an ionic charge which during the application of the external field has gathered on the surface of the dielectric, dissipates by conduction within the dielectric (internal decay). But the fact that the measured current J is much smaller than the calculated displacement current dq/dt proves that only a small fraction of the ionic charge dissipates in this way; the bulk of the ionic charge dissipates by conduction across the dielectric-electrode interface (external decay). The value of $i(t)$ is a measure for the rate of the external decay.

Thus one reaches the conclusion that at the moment of the short-circuit the dielectric carried two types of surface charges:[13] (a) The charge s associated with dielectric absorption and (b) the charge f associated with surface breakdown. After the short-circuit, s decays according to the law of decay of the absorbed charge; since in the present case no heat treatment was

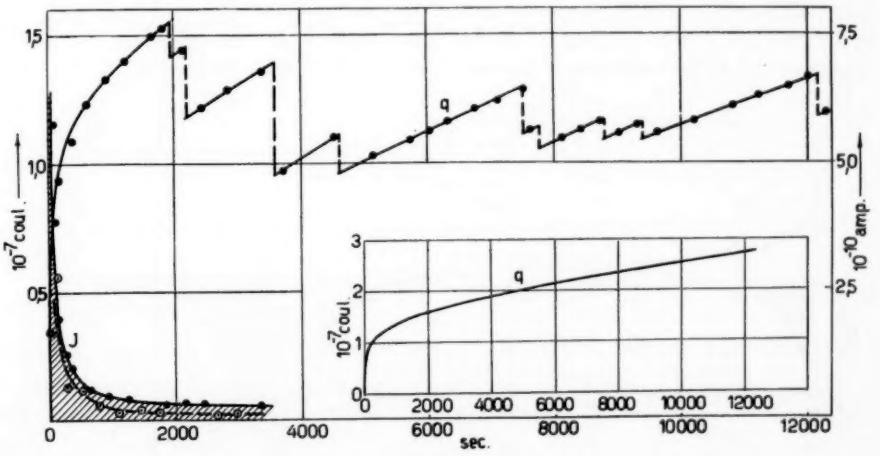

FIG. 5. Transfer of charge from the electrode to the surface of the dielectric during polarization. Inset: charge $q(t)$; the curve is made continuous by adding at every jump the corresponding loss of charge of the electrode. Circles: dq/dt.

[12] The role of breakdown phenomena has been emphasized by Mikola (see reference 3) and by Thiessen, Winkel, and Herrmann (see reference 3). Mikola's external polarization is to some extent the counterpart of the homocharge effect of the present paper, and his internal polarization is the counterpart of the heterocharge effect.

[13] A two-charge theory was first formulated by Adams, reference 3.

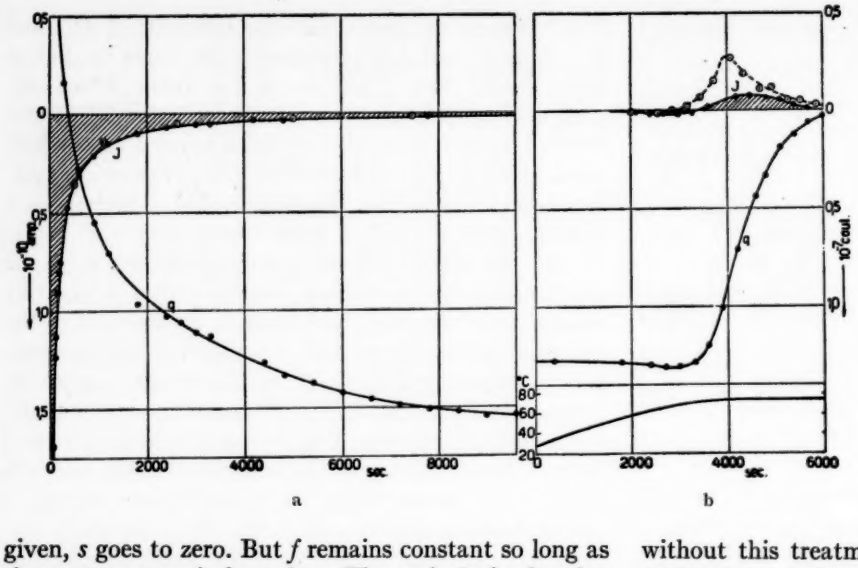

FIG. 6. Evidence for the existence of an ionic surface charge due to transfer of charge from the electrode to the dielectric. (a) Current and charge immediately after short-circuit. (b) Current and charge during heating, 1 day later. Circles: dq/dt.

given, s goes to zero. But f remains constant so long as the temperature is kept low. Thus when the heating started, only the charge f was left on the dielectric. The opposite polarities and different values of relaxation times of the two charges show that these charges are not of the same kind: s is due to a homogeneous volume polarization of the dielectric; f is an ionic surface charge. This explains why these charges coexist without mutual recombination. Since the sign of f is the same as that of the corresponding polarizing electrode, in Gemant's terminology f is a *homocharge*.

The induced charge of the electrode is now generally given by

$$q-q_0=-(s+f), \tag{4}$$

where q_0 is the charge of the geometrical capacitance. It is to be noted that the sign of f is contrary to that of s.

5. Coexistence of Homocharge and Heterocharge

Homocharge and heterocharge can be preserved together on the dielectric over long periods of time. For this purpose the volume polarization, and with it the heterocharge, must be frozen in by the usual heat treatment; the homocharge can be preserved even without this treatment. Thus a sample was polarized with 950 v during 30 min. at 69°C; then the temperature was reduced to 35°C and the system was shorted. The behavior immediately after the short-circuit does not reveal any novel feature, in particular no conduction current. A polarity reversal does occur, but later than in the foregoing experiment. Reheating started 19 hours after the short-circuit. It causes the appearance of a discharge current associated with the liberation of a frozen-in charge. But at the same time the absolute value of the induced charge of the electrode at first goes up, not down; later a maximum is reached and finally q tends to zero. During the period of increase there is still $i=0$, but shortly before the maximum of q is reached, a strong conduction current sets in, which soon predominates over the displacement current. No current reversal is observed (Fig. 7).

Interpretation in terms of the two-charge theory is straightforward. After the short-circuit a part of the absorbed charge decays, another bigger part remains frozen-in; the ionic charge remains undiminished. In consequence of the reheating, both charges decay, but the decay of the ionic charge begins later than that of

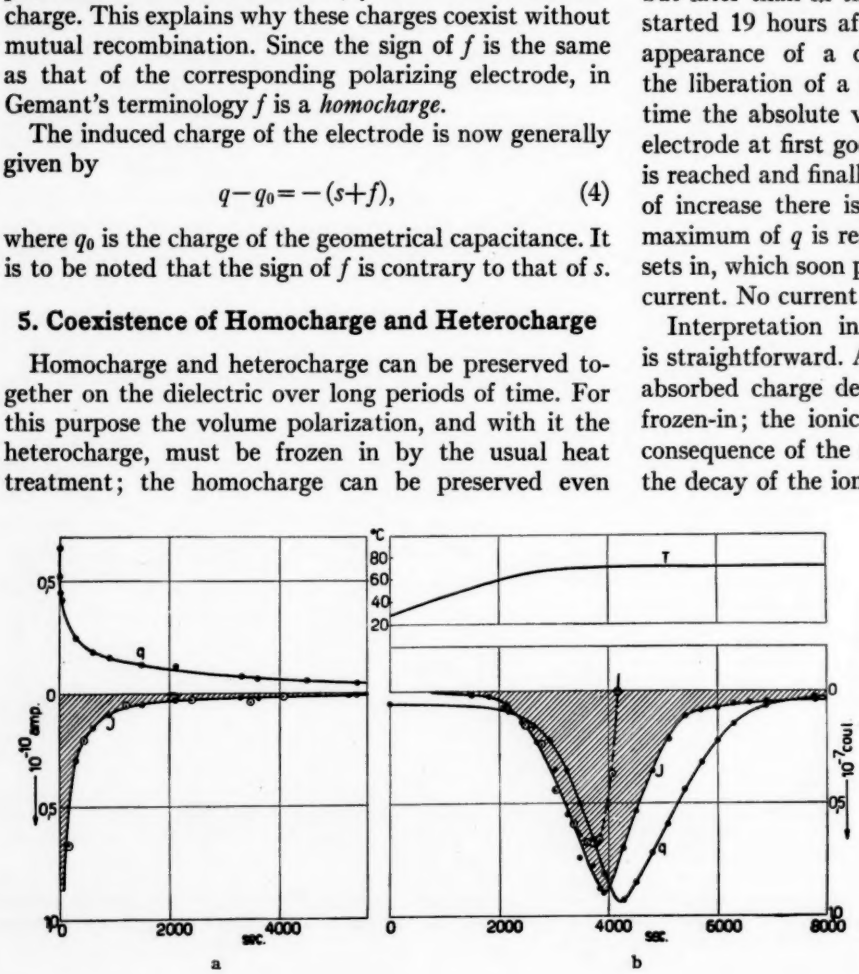

FIG. 7. Evidence for the coexistence of 2 types of charges on the surface of the dielectric. (a) Current and charge immediately after short-circuit. (b) Current and charge during reheating, 19 hours later. Circles: dq/dt.

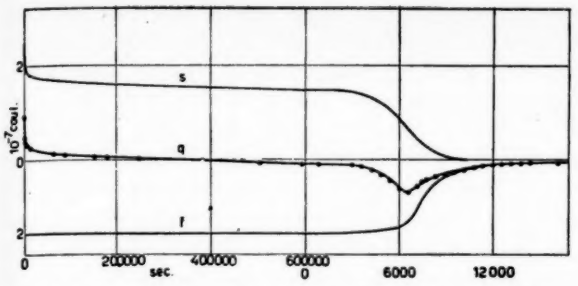

FIG. 8. Decomposition of the surface charge into homocharge f and heterocharge s. Reheating begins 600,000 sec. after the short-circuit. The time-scale for the heating period is changed.

the frozen-in volume polarization. Therefore at first only s decreases, while f remains constant; later f too decreases. This behavior, according to Eq. (4), gives the temporary increase of q shown in the measurement. The dissipation of f proceeds by continuous conduction currents across the dielectric-electrode interface and can be computed from the values of the conduction current $i(t)$.

6. Computation of Heterocharge and Homocharge

The discharge current $J(t)$ in the external circuit is due almost entirely to the decay of the volume polarization. Neglecting altogether the small contribution possibly arising from an internal decay of the homocharge, one obtains the value of the heterocharge $s(t)$ at the time t from Eq. (3) as the integral over $J(t)$ from 0 to ∞. The value of the homocharge f then follows from Eq. (4) as the difference between the induced charge of the electrode and the value of the heterocharge. Such a computation is shown in Fig. 8 for an experiment similar to that just described, with a polarizing voltage of 2000 v applied at 65°C. It is worth mentioning that over a considerable period of time q is nearly zero; the current (not shown in the figure) is then very small also. An observer confining his attention to this interval, could easily conclude that "the electret has been discharged." But the analysis of the data in terms of heterocharge and homocharge shows that the measured value of q represents here as in many other cases but a small difference effect; both s and f exceed q by a considerable amount. It is in the range of possibility to avoid formation of one or the other of the two charges and to get in this way electrets, which produce much higher fields than those employed hitherto.

7. Behavior of an Uncovered Dielectric

The surface charge of an uncovered dielectric decreases rapidly after the electrode has been withdrawn. When the electrode is again brought into contact with the dielectric, the charge recovers.[14] This is shown in Fig. 9 for a sample which initially carried an ionic charge

[14] Such effects have already been observed by M. Eguchi, reference 3.

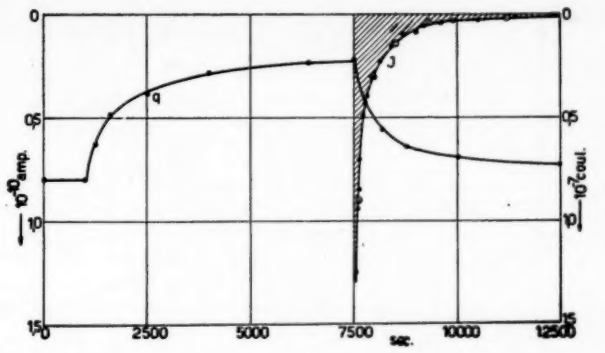

FIG. 9. Uncovering of a charged dielectric. The electrode is lifted at the point corresponding to 1000 sec. and is depressed at 7500 sec. (Points: measured values; circles: calculated values of the displacement current).

only. The reason for this behavior is found in the difference between the fields of the shorted and of the open electret. When the electrode is in contact with the dielectric, the field of the charge of the dielectric is concentrated mainly in the dielectric-electrode interface and the field in the interior of the dielectric is weak.[15] When the electrode is removed, the situation is reversed and the main field of the charge of the dielectric is now concentrated in the interior of the dielectric. Thus removing of an electrode produces the same effect as does application of an external field; volume polarization and absorption occur. Accordingly new surface charges appear and partially neutralize the previously existing charges. But when the electrode system is reassembled, the primitive field distribution is reestablished and the field in the interior of the dielectric

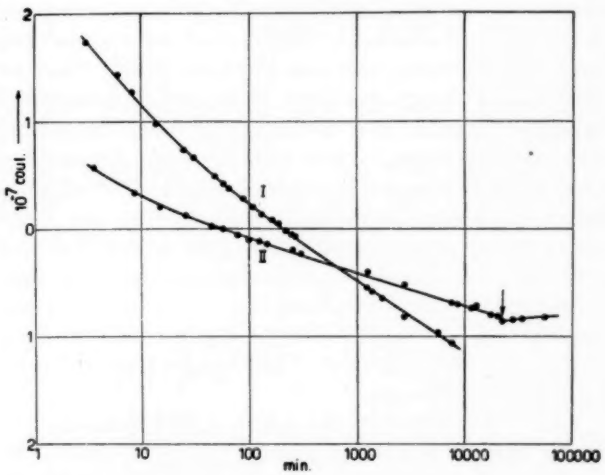

FIG. 10. Charge of the electrode against logarithm of time; I. Applied voltage 4500 v. II. Applied voltage 3000 v. At the point indicated by an arrow, the sample was reheated until the volume polarization had been destroyed.

[15] The precise values of the field at every point depend on the thickness of the interface, the ratio of the dielectric constants of interface and dielectric, and the space charge distribution in the dielectric; but for the following qualitative considerations the knowledge of these precise values is not essential.

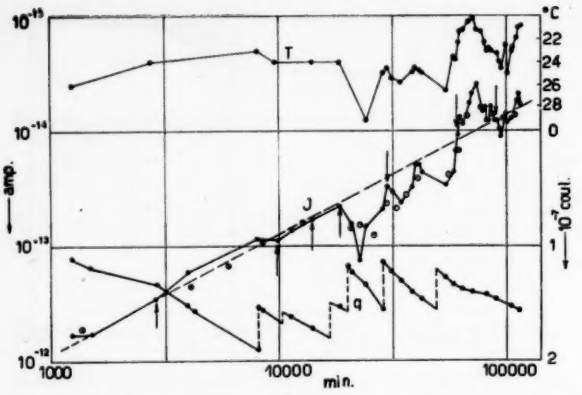

FIG. 11. Current, charge, and temperature of a sample polarized with a high voltage. The measurements extend over 80 days. The arrows indicate current values corresponding to a temperature of 24°C. Circles: dq/dt.

is reduced to its former low level. This is similar to the short-circuiting of a previously energized capacitor. The ensuing decay of the recently formed polarization restores the initial high value of q; it manifests itself also by the appearance of a discharge current $J(t)$ of the same type as that observed after the short-circuit of an absorptive capacitor. Figure 9 shows this discharge current, which strongly confirms the ideas outlined here.

8. Decay of the Polarization of the Dielectric

Figure 10 gives for two experiments the value of q against the logarithm of time. In one case 3000 v were applied at 56°C during 10 min., in the other 4500 v at 67°C during 150 min.; in both cases the system was shorted when room temperature had been reached. The systematic variation of q was observed over several weeks; one and the same effect, the slow decay of the frozen-in charge, manifests itself over this period of time. In one of the experiments, the sample was reheated after 16 days of observation for a short time and only as much as was necessary for removing the frozen-in heterocharge. From this moment on (indicated in the figure by an arrow), the trend of $q(t)$ is different; the increase of q now has given way to a very slow decrease obviously caused by a slow decay of the homocharge which after the short reheating had been left alone on the dielectric. This decrease was observed for nearly four weeks.

Finally Fig. 11 gives the result of an experiment, in which 9,000 v were applied at 71°C for 3 hours; the system was shorted, when room temperature had been reached. These measurements extend over 80 days. In a logarithmic time scale, log J, the temperature, q and dq/dt, are given. The current undergoes a series of fluctuations. Inspection shows that they are correlated with fluctuations of the temperature and, therefore, caused by the enormous value of the temperature coefficient of the discharge current. When the current values corresponding to a temperature of 24°C are selected (in the figure pointed out by arrows), they define with good approximation a straight line, with a slope equal to 1. Thus during all this time the current obeys the well-known, and frequently questioned, power law. The charge q at first increases regularly just as happened in the two former experiments. But when the intensity of the field in the interface attained a sufficiently high value, several discontinuous variations do occur. The slope of the curve $q(t)$ coincides amazingly well with the measured values of $J(t)$, following all the irregularities of the latter. Thus except during a surface breakdown there is no indication of conduction across the interface in spite of the high value of the field existing there. Thus the ionic charge does not dissipate unless breakdown occurs, and this is a rather rare event. One must conclude, that at room temperature a strong potential barrier impedes the transfer of carriers between dielectric and electrode; the height of the barrier is reduced at elevated temperatures.

III. SUMMARY

Our experiments lead us to the following conclusions: (a) The heterocharge is due to a volume polarization of the dielectric.[16] It is preserved, because this volume polarization can be frozen in. (b) The homocharge is an ionic surface charge caused by surface breakdown. (c) The sum of heterocharge and homocharge gives the free surface charge of the dielectric. This free charge together with the corresponding induced charge of the electrode constitutes an electric double layer. (d) At room temperature the double layer does not disappear by surface conduction, because the potential barrier at the surface of the electrode then prevents transfer of charge between dielectric and electrode; it does not decay by volume conduction, because it does not set up an electric field within the dielectric, provided its thickness is small compared with the thickness of the sample. (e) At elevated temperature continuous conduction currents flow between dielectric and electrode. because the height of the potential barrier is reduced, (f) The electric moment of the double layer is limited by breakdown phenomena occurring in the dielectric-electrode interface.

I am greatly indebted to the Director of the Institute, Professor E. L. da Fonseca Costa, who made this study possible.

[16] We do not in general exclude the possibility of an ionic effect and of space charges of the type found by Jaeger (reference 3) and Gemant (reference 3). This effect will contribute to the heterocharge. But as Gemant has already pointed out, the time constant for the decay of the space charges will be much smaller than that for the decay of the frozen-in volume polarization, in consequence of the finite volume conductance of the dielectric. Therefore the permanent component of the heterocharge of the present paper must be due to a volume polarization. Unpublished measurements about discharge currents, in which the surface layers on both sides of the samples were mechanically removed before the sample was reheated, prove this point of view.

The Magnetic Susceptibility of Organic Compounds

S. BROERSMA†
Laboratory for Technical Physics, Delft, Holland
(Received September 2, 1948)

With the object to obtain new data for the statistical analysis of hydrocarbon mixtures, measurements on diamagnetic organic compounds at room temperature have been performed. The precision was of the order of 1 per mil (10^{-3}) of the diamagnetic effect. We checked the additivity rule and found it to be applicable within 5 per mil on the average. Mixtures were also investigated. A linear relation with the concentration was found to hold for hydrocarbon mixtures within the precision of measurement. For liquids containing electric dipole deviations up to 6 per mil were observed. We applied the results to the analysis of unknown mixtures.

I. EXPERIMENTAL RESULTS

IN this paper we shall deal with the susceptibilities of organic compounds. As the apparatus used is described elsewhere,[1] we shall, as far as concerns the measurements, restrict ourselves to some general remarks.

We applied two types of apparatus, *viz.*, a torsion balance (T.B.) and an inductance apparatus. (I.A.) This made it possible to avoid system errors which are often present, and indeed some were observed. In the author's thesis[1] more details about the work can be found.

The purity of the samples is of great importance. To avoid the effect of ferromagnetics we use a special filter, consisting of a funnel placed in a small magnet. If we pour the liquid through the funnel, on filling the cuvette it is found experimentally that most iron particles are withheld and that the measurement is not affected. A calculation shows that in the filter the magnetic forces exerted on the ferromagnetic particles are one thousand times larger than the forces of viscosity pushing them through the funnel. In the estimate we assume particles to be present, each producing one per mil of our diamagnetic effect. ($0.4 \cdot 10^{-8}$ g iron in 8 g of substance.)

The presence of paramagnetic oxygen is also of great interest. For water differences up to 3 per mil were found, after boiling for some time. Hydrocarbons never showed differences larger than our precision of measurement in this respect. However, measuring the effect of the cuvette filled with air, the barometric pressure has to be taken into account. A change of 15 mm in the pressure gives rise to 1 per mil change in the result.

For the *calibration* it is useful to fill the cuvette with N_2 or CO_2 and to close the cuvette with a greased plug. Their volume susceptibilities* are 0.4 and 0.1, respectively. In order to calibrate the instrument we used the following volume susceptibilities at 20°C: κ (water) = 903.1, κ (air) = −36.9, the difference being 940.

It appeared that the proportionality constant of the torsion balance changed no more than two per mil during a series of some weeks. The error in the adjustment proved to be 0.2 per mil, adding only a small contribution to the error in the susceptibility, which was probably due to a displacement of the balance or ferromagnetic impurities situated on the moving part of the balance.

Comparison of the results of both apparatus helped us to remove systematic errors, as we can expect entirely different errors to be present in the inductance apparatus. We performed two series with the balance, the second one with an improvement, and one series with the inductance apparatus.

Plotting the differences between the values obtained with the different apparatus for the same sample against the density, system differences of the order of some per mil were found. It appeared that during the first series the balance changed its position when the cuvette contained a liquid of different density. In the second series the change in density was compensated by shifting a weight. After that the differences, being three per mil at the most, agreed better with the estimate of the separate errors (Fig. 1).

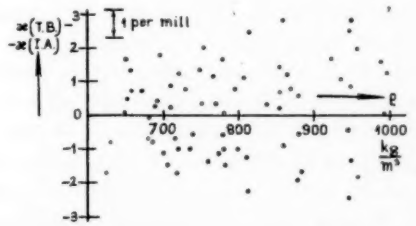

FIG. 1. The difference between the volume susceptibilities, as found with a torsion balance and an inductance apparatus, is plotted *vs.* the density of the liquids (ρ in kg/m³).

† Now at University of Indonesia, Bandung, Indonesia.

[1] S. Broersma, *Magnetic Measurements on Organic Compounds* (Martinus Nyhoff, The Hague, 1947). Also Rev. Sci. Inst. **20**, 660 (1949).

* We use the rationalized Giorgi system. The susceptibility referring to unit volume is given by $\kappa = \mu_r - 1$, that referring to unit mass by $\chi = \kappa/\rho$. The unit employed is -10^{-8}. The magnetic moment is defined by $M = v\kappa H = v\kappa\mu_0^{-1}B$; v = volume, ρ = density (kg/m³), μ_0 = permeability of vacuum, and μ_r = relative permeability.

TABLE I. Values of the volume, mass, and molar susceptibility, unit -10^{-6}.

	$\kappa=\mu_r-1$			χ	$\chi_M=M\chi$			
	T.B.	I.A.	Average	$=\kappa/\rho$	Meas.	Calc.	Meas. — calc.	C.g.s. units, meas.
n-pentane	687.6		687.6	1.0981	79.23	78.6	+0.6	6305
2-methyl-butane	695.0		695.0	1.1215	80.92	79.9	+1.0	6440
n-hexane	712.1		712.1	1.0799	93.05	92.9	+0.2	7405
2-methyl-pentane	716.9		716.9	1.0975	94.57	94.2	+0.4	7526
3-methyl-pentane	731.7		731.7	1.1013	94.90	94.2	+0.7	7552
2,2-dimethyl-butane	721.8		721.8	1.1118	95.80	95.5	+0.3	7624
2,3-dimethyl-butane	735.5		735.5	1.1115	95.78	95.5	+0.3	7622
n-heptane	730.9	731.0	731.0	1.0690	107.11	107.2	−0.1	8524
2-methyl-hexane	734.0		734.0	1.0815	108.37	108.5	−0.1	8624
2,2-dimethyl-pentane	735.0		735.0	1.0907	109.29	109.8	−0.5	8697
2,3-dimethyl-pentane	762.8		762.8	1.0974	109.96	109·8	+0.2	8751
2,4-dimethyl-pentane	738.4		738.4	1.0972	109.94	109.8	+0.2	8748
2,2,3-trimethyl-butane	764.8		764.8	1.1081	111.03	111.1	0.0	8836
n-octane	747.5	747.7	747.6	1.0631	121.43	121.4	0.0	9663
3-methyl-heptane	760.2	761.7	761.0	1.0781	123.14	122.7	+0.4	9799
2,3-dimethyl-hexane	775.1	774.1	774.6	1.0867	124.12	124.0	+0.1	9877
3,4-dimethyl-hexane	784.7	783.4	784.1	1.0898	124.48	124.0	+0.5	9906
2,5-dimethyl-hexane	751.0	749.2	750.1	1.0798	123.33	124.0	−0.7	9815
2,2,3-trimethyl-pentane	786.3	787.1	786.7	1.0987	125.49	125.3	+0.2	9986
2,2,4-trimethyl-pentane	748.3	749.0	748.7	1.0819	123.57	125.3	−1.7	9834
n-nonane	760.5	761.7	761.1	1.0594	135.87	135.7	+0.2	10813
n-decane	771.1	770.2	770.7	1.0555	150.18	150.0	+0.2	11951
n-hexadecane	806.4	807.4	806.9	1.0412	235.77	235.7	+0.1	18763
2,2,4,7,9,9-hexamethyl-decane	828.8	828.7	828.8	1.0628	240.66	243.5	−2.8	19152
cyclopentane	790.4		790.4	1.0604	74.37	72.7	+1.7	5918
methyl-cyclopentane	785.0	784.5	784.8	1.0478	88.18	88.3	−0.1	7017
1,2- and 1,3-dimethyl-cyclopentanes	782.8	781.4	782.1	1.0406	102.17	103.9	−1.7	8131
cyclohexane	768.1	768.7	768.4	0.9868	83.05	83.5	−0.4	6609
methyl cyclohexane	775.8	777.6	776.7	1.0100	99.16	99.1	+0.1	7891
ethyl-cyclohexane	794.7	794.7	794.7	1.0201	114.47	113.3	+1.1	9109
isopropyl-cyclohexane	819.7	820.8	820.3	1.0218	128.99	128.9	+0.1	10265
tert. butyl-cyclohexane	837.5	838.9	838.2	1.0311	144.62	144.5	+0.1	11509
heptyl-cyclohexane	823.0	825.4	824.2	1.0158	185.22	184.7	+0.5	14740
octyl-cyclohexane	827.9	825.3	826.6	1.0117	198.66	199.0	−0.4	15809
decalin	856.6	855.9	856.3	0.9699	134.08	133.8	+0.3	10670
dicyclohexyl	864.8	866.5	865.7	0.9771	162.49	162.4	+0.1	12931
1,1-dicyclohexyl-nonane	879.8		879.8	0.9965	291.50	292.2	−0.7	23198
perhydro anthracene	902.0		902.0	0.9540	183.48	184.1	−0.6	14601
benzene	773.3	774.1	773.7	0.8807	68.80	67.5	+1.3	5475
toluene	776.5		776.5	0.9017	83.07	83.1	0.0	6611
ethyl-benzene	797.3	796.4	796.8	0.9138	97.01	97.3	−0.3	7720
n-heptyl-benzene	820.3		820.3	0.9581	168.90	168.7	+0.2	13441
o-xylene	809.0	809.6	809.3	0.9207	97.74	98.6	−0.9	7778
m-xylene	784.9	782.0	783.5	0.9063	96.21	98.6	−2.4	7656
p-xylene	781.8	782.8	782.3	0.9088	96.48	98.6	−2.2	7678
1,3,5-trimethyl-benzene	795.8		795.8	0.9653	116.01	114.2	+1.8	9232
1,6-diphenyl-hexane	865.5	862.9	864.2	0.9058	215.90	216.0	−0.1	17181
1,1-diphenyl-nonane	870.7	872.1	871.4	0.9245	259.26	260.3	−1.0	20632

The physical error in the average value of κ will be of the order of one per mil. The error in the density (<0.5 per mil) has to be added. Chemical errors such as impurities in the form of isomers have only a small effect according to the additivity rule. Assuming a relative proportion of isomers of $3\cdot10^{-2}$ and relative differences in the κ of $3\cdot10^{-2}$, their effect is one part in thousand at the most.

So for the hydrocarbons, being highly purified, the error in $\chi_M=\chi\cdot M$ will be of the order of 1.5 per mil. The other substances may have a lower purity. Their density and refractive index were observed and compared with a literature. Here the chemical error may be some per mil, the precision of χ_M 2 to 3 per mil.

Tables I and II** contain the susceptibilities, referring to the unit volume (κ), mass (χ), and kilomole (χ_M), expressed in units of the rationalized Giorgi system. The last column gives χ_M in c.g.s. units (ratio: $4\pi\cdot10^{-3}$). All numbers have to be multiplied with -10^{-6}.

Comparison with literature shows large differences. We therefore collected the values found for 18 substances and measured by several investigators. Excepting by the author, only force methods have been used.

On comparing the values no correlation seems to exist between the precision mentioned by the authors and the deviation from the average values. In order to prevent one value from disturbing the estimate of the average, we assigned half the weight to the values lying far away from a preliminary mean. The number of these values was at the most $\frac{1}{3}$ of the total number of values. The rounded-off results are listed in Table III. In the second column the number of values of the main group with weight one is given. The largest deviation in this group from the average value is taken as a measure for the error.

The table shows directly that only for 15 substances the susceptibilities are known with a precision better than 10 per mil. Therefore the values of Table II, referring to compounds measured only once by the author, *viz.*, with the balance and probably not having the high purity of those of Table I, have been rounded off at one or two per mil. Our values differ up to 5 per mil from the averages of Table III, the average deviation being less than 2.5 per mil. In the mean our values lie 1.5 per mil below those found in literature.

II. PURE COMPOUNDS

The best expression for the susceptibility has been given by Van Vleck,[2] calculating the susceptibility of an assembly of independent molecules. If we omit the paramagnetic term, dependent on the temperature, then:

$$\chi_M\mu_0^{-1}=\tfrac{2}{3}N\sum_{n'}{}'\frac{|m(n,n')|^2}{h\nu(n',n)}-\tfrac{1}{4}N\sum_i\frac{e_i^2}{m_i}\langle x_i^2+y_i^2\rangle_{Av}. \quad (1)$$

Here N is the number of Avogadro, e_i and m_i are the charge and mass of the ith electron or nucleus, x_i and y_i are its coordinates in a plane perpendicular to the field. $m(n,n')$ represents the high frequency

** The compounds mentioned in Table I were put at our disposal by Professor H. I. Waterman and the Bataafsche Petroleum Maatschappy. (Wibaut, Hoog, Langedyk, Overhoff, and Smittenberg, Rec. Trav. Chim. **58**, 329 (1939)) measured several other properties of these samples. The compounds in Table II from erythritol up to rhamnose were put at our disposal by Dr. J. van Alphen.

[2] J. H. Van Vleck, *The Theory of Electric and Magnetic Susceptibilities* (Oxford University Press, London, 1932). Here the equations have been written according to the rationalized Giorgi system.

TABLE II. Values of the volume, mass, and molar susceptibility, unit -10^{-6}.

		κ	χ	$\chi_M = M\chi$			
		T.B.	$=\kappa/\rho$	Meas.	Calc.	Meas. — calc.	C.g.s. units, meas.
chloroform	$CHCl_3$	930	0.624	74.5			5930
carbon tetrachloride	CCl_4	868	0.544	83.7			6660
prim. propyl chloride	$C_2H_5CH_2Cl$	795	0.898	70.5	70.1	+0.4	5610
prim. *n*-butyl chloride	$C_3H_7CH_2Cl$	807	0.911	84.3	84.4	−0.1	6710
sec. *n*-butyl chloride	$C_2H_5CHClCH_3$	798	0.915	84.7	84.4	+0.3	6740
bromine	Br_2	1319	0.422	67.4			5360
methylene bromide	CH_2Br_2	1175	0.471	81.8			6510
bromoform	$CHBr_3$	1191	0.411	103.8			8260
ethyl bromide	C_2H_5Br	903	0.631	68.7	67.4	+1.3	5470
ethylene dibromide	CH_2BrCH_2Br	1150	0.527	99.0	99.0	0.0	7880
methylene iodide	CH_2I_2	1453	0.437	117.0	117.1	−0.1	9310
methyl alcohol	HCH_2OH	666	0.840	26.9	27.3	−0.4	2140
ethyl alcohol	CH_3CH_2OH	723	0.915	42.2	42.2	0.0	3360
prim. propyl alcohol	$C_2H_5CH_2OH$	760	0.945	56.8	56.5	+0.3	4520
prim. *n*-butyl alcohol	$C_3H_7CH_2OH$	768	0.948	70.3	70.7	−0.4	5590
prim. *n*-hexyl alcohol	$C_5H_{11}CH_2OH$	800	0.973	99.5	99.3	+0.2	7920
formic acid	$HCOOH$	662	0.543	25.0	25.3	−0.3	1990
acetic acid	CH_3COOH	698	0.665	40.0	40.2	−0.2	3180
propionic acid	C_2H_5COOH	731	0.736	54.6	54.5	+0.1	4350
n-butyric acid	C_3H_7COOH	752	0.785	69.2	68.7	+0.5	5510
n-heptoic acid	$C_6H_{13}COOH$	787	0.855	111.3	111.6	−0.3	8860
ethyl formate	$HCOOC_2H_5$	667	0.729	54.0	53.4	+0.6	4300
methyl acetate	CH_3COOCH_3	675	0.723	53.6	54.0	−0.4	4260
ethyl acetate	$CH_3COOC_2H_5$	696	0.771	68.0	68.2	−0.2	5410
iso-amyl acetate	$CH_3COO(CH_2)_2CH(CH_3)_2$	753	0.863	112.3	112.4	−0.1	8940
glycol	CH_2OHCH_2OH	877	0.784	48.7	48.6	+0.1	3880
hexamethylene glycol	$CH_2OH(CH_2)_4CH_2OH$		0.896	105.9	105.7	+0.2	8430
glycerol	$CH_2OHCHOHCH_2OH$	979	0.778	71.7	71.0	+0.7	5706
erythritol	$CH_2OH(CHOH)_2CH_2OH$		0.759	92.7	93.4	(−0.7)	7380
adonitol	$CH_2OH(CHOH)_3CH_2OH$		0.754	114.7	115.8	(−1.1)	9130
sorbitol	$CH_2OH(CHOH)_4CH_2OH$		0.744	135.5	138.2	(−2.7)	10780
mannitol	the same		0.767	139.7	138.2	(+1.5)	11120
dulcitol	the same		0.775	141.2	138.2	(+3.0)	11240
arabinose	$OCH(CHOH)_3CH_2OH$		0.718	107.7	107.0	(+0.7)	8570
xylose	the same		0.710	106.6	107.0	(−0.4)	8480
glucose	$OCH(CHOH)_4CH_2OH$		0.716	129.0	129.4	(−0.4)	10260
mannose	the same		0.718	129.3	129.4	(−0.1)	10290
galactose	the same		0.719	129.5	129.4	(+0.1)	10300
fructose	$CH_2OHCO(CHOH)_3CH_2OH$		0.716	129.0			10260
rhamnose	$OCH(CHOH)_4CH_3$		0.760	124.6	123.0	(+1.6)	9920
acetone	CH_3COCH_3	580	0.732	42.5			3380
diethylether	$C_2H_5OC_2H_5$	671	0.934	69.2			5510
diethyl malonate	$COOC_2H_5CH_2COOC_2H_5$	750	0.720	115.3	115.0	+0.3	9180
allyl alcohol	$CH_2{:}CHCH_2OH$	679	0.794	46.1	46.1	0.0	3670
cyclohexanol	$C_6H_{11}OH$	872	0.920	92.2	91.6	+0.6	7340
phenyl chloride	C_6H_5Cl	860	0.777	87.4	87.6	−0.2	6960
benzyl chloride	$C_6H_5CH_2Cl$	890	0.806	102.1	103.2	−1.1	8120
α-napthyl chloride	$C_6H_4{:}C_4H_3Cl$	992	0.831	135.2	134.7	+0.5	10760
phenyl bromide	C_6H_5Br	936	0.625	98.2	99.1	−0.9	7810
α-napthyl bromide	$C_6H_4{:}C_4H_3Br$	1053	0.704	145.7	146.2	−0.5	11590
phenyl iodide	C_6H_5I	1038	0.567	115.6	115.6	0.0	9200
nitrobenzene	$C_6H_5NO_2$	759	0.631	77.7			6180
o-cresol	$C_6H_4(OH)CH_3$	872	0.823	89.0	89.7	−0.7	7080
m- and *p*-cresol	the same	871	0.835	90.3	89.7	+0.6	7190
methyl salicylate (*O*)	$C_6H_4(OH)COOCH_3$	840	0.712	108.4	107.9	+0.5	8630

TABLE III. Average values of the mass susceptibilities as found in literature. Unit -10^{-6}.

		Giorgi	C.g.s.			Giorgi	C.g.s.
water		0.905	72.0	5 per mil			
2 per mil				chloroform	5	0.625	49.7
				propyl alcohol	4	0.944	75.1
carbon tetrachloride	5	0.543	43.2	butyl alcohol	4	0.949	75.5
ethyl acetate	4	0.770	61.3	acetic acid	5	0.668	53.2
benzene	8	0.882	70.2	propionic acid	2	0.737	58.7
				n-butyric acid	4	0.789	62.8
10 to 20 per mil				ethyl formate	2	0.729	58.0
acetone	8	0.736	58.6	methyl acetate	3	0.720	57.3
methyl alcohol	6	0.842	67.0	propyl acetate	3	0.809	64.4
ethyl alcohol	6	0.920	73.2	toluene	4	0.903	71.9
formic acid	4	0.543	43.2	nitrobenzene	6	0.630	50.1

elements of the magnetic moment occurring in the atoms and $h\nu(n', n)$ the energy difference of the two states between which a transition occurs. The first term represents a paramagnetic effect which is independent of the temperature. The effect of the nucleus on the diamagnetic term is small.

It can be proven that the paramagnetic term is zero in the case of atoms, if we take their nuclei as a zero point for the coordinates x and y. Now forming the molecules from independent atoms, we can describe the new situation by using for each atom its own nucleus as zero point, and correct the diamagnetic term for changes in the charge distribution. At the same time we add a high frequency term, which is caused by the non-central fields due to the adjoining atoms.

If these extra terms are smaller than the main effect, it is obvious that an additivity rule will be fulfilled in a first approximation. Furthermore, deviations from this rule can be expected to give us information about the structure of the molecule.

Hydrogen atoms represent the simplest case of Eq. (1). For this we find:

$$\chi_H = -\mu_0(Ne^2/2m)a_0^2 = -2.98\cdot 10^{-6}, \qquad (2)$$

in which a_0 is the radius of the smallest orbit in the classical theory of hydrogen. The size of this effect is a convenient unit for both magnetic terms in Eq. (1).

We can estimate the first term by replacing $\nu(n', n)$ by an average frequency ν_0, for which we write with the aid of Rydberg's constant:

$$\nu_0 = \alpha \dot{R}c,$$

ν_0 being, in general, of the order of the resonance frequency of hydrogen and hence α of the order of 1.

Now we can replace:

$$\sum_{n'}{}' |m(n, n')|^2 = m^2(n, n) = (geh/4\pi m)^2 P^2(n, n),$$

where $P(n, n)$ is the angular momentum measured in units $h/2\pi$. Furthermore, we have

$$\langle x_i^2 + y_i^2 \rangle_{Av} = \tfrac{2}{3}\langle r_i^2 \rangle_{Av}.$$

TABLE IV. The dia, para, and total molar susceptibility of H_2.

	Dia	Para	Total
Van Vleck (1929)	5.92	−0.64	5.28
Witmer (1942)	5.17	−0.12	5.05
Experimental			5.03
Two H atoms	5.96		5.96

Substituting this in (1) we get

$$\chi_M = \tfrac{1}{3}\chi_H[\sum_i (r_i/\alpha_0)^2 - 2g^2P^2(n, n)/\alpha]. \qquad (3)$$

Equation (3) has been applied for the calculation of the effect of hydrogen molecules. Here refractive data give $\alpha = 1.23$, while $g = 1$. Applying known wave functions, Van Vleck and Frank[3] found the first row in Table IV. The value of Witmer[4] agrees better with the experimental results.

For inert gases there exists a rather large difference between the calculated and measured values. This is mainly due to the fact that the largest contributions come from the outer electrons for which the calculations are less reliable. Obviously, in other cases the computations will be even more difficult.

Therefore, the main result obtainable from theory is that we can expect an additivity rule to hold while deviations due to atomic interaction occur. The latter will often reproduce for different molecules and can be introduced as separate terms. Extensive experimental investigations of Pascal[5] first established this additivity rule.

In this section we shall consider some pure compounds, mainly hydrocarbons. After that the effects on mixing will be discussed, showing the molecular interactions, and also the application to mixtures of unknown structure.

According to the *additivity rule* the following holds:

$$\chi_M = \sum_k n_k \chi_M{}^k, \qquad (4)$$

where n_k is the number of contributing elements of the kind k present in the molecules. In this chapter we shall try to derive the values $\chi_M{}^k$ which represent the separate terms in Eq. (1) and which are due to the several elements, from the experimental values of χ_M, obtained for the several compounds.

We shall start with the homologous series. The main contribution is given by the CH_2- group. In Fig. 2 we have plotted $\chi_M - n\cdot 14.3$ against n, the number of CH_2- groups present in the molecule. In a graphic representation the deviations are easily recognizable, the more so as we subtract the average

[3] J. H. Van Vleck and H. Frank, Proc. Nat. Acad. Sci. **15**, 539 (1929).
[4] E. E. Witmer, Phys. Rev. **61**, 387 (1942).
[5] P. Pascal, see Auwers, Jahrbuch der Radio aktivitat und Elektronik **17**, 181 (1921).

effect of the CH_2- group (14.3) and hence obtain almost horizontal lines.

The normal alphatic compounds (a) show only small deviations from a straight line. The mean slope corresponds to a value for the CH_2- group of 14.28, with a precision of about 2 per mil. Only *n*-pentane shows an important deviation. The other lines representing the average increment in other series of compounds, apart from *k*, were drawn parallel to this line.

On comparing compounds with an equal number of branches (b), larger deviations appear. On the basis of their magnetic behavior such compounds can be further divided into a few groups, *viz.*, with respect to the position of the branches in the chain. We shall discuss this below.

The series of cyclohexane (c) also shows deviations as regards additivity. For the higher compounds this may be due to impurities. For cyclohexane itself it can be real. In (d) compounds with 2 cyclohexane rings are represented. Benzene and its homologues (e) show a similar additivity. The values of the alcohols (f) and the acids (g) fit the drawn lines rather well. Line (h) represents the position of the values of some esters. Glycol and homologous compounds (i) show good agreement with the assumed average effect of a CH_2- group.

Though lines with different inclination could also have been drawn, a change by 5 per mil in the CH_2- value would already cause large deviations from the points indicated. A comparison with literature, however, shows far larger differences. For the CH_2- group values have been found ranging from 14.28,[6] 14.43,[7] 14.63,[8] 14.66,[9] up to 14.69.[10] The fact that we examine longer molecules than the other authors can partially explain why our value is among the lower ones.

Line (*k*) in Fig. 2 gives the results for the alcohols from glycerol up to mannitol and isomers (the average of the isomers has been used). For each CHOH− group 22.4 is subtracted. The deviations are not very large.

For calculations with *other compounds* the estimate of a mean value for a chain branching is very convenient. It appears to be about 1.3. For two branches roughly double this value is found, also on attaching the branches to the same carbon atom. Sometimes this value was already applied in the data of Fig. 2.

For a further analysis we shall distinguish between primary, secondary, tertiary, and quarternary C-atoms, depending upon the number of C−C-bonds starting from these carbon atoms. We shall use the value for a secondary C-atom in a long chain as a basis and attribute to the other C-atoms an extra effect equal to the difference with this value.

In Fig. 2 the points of intersection of the several lines with the axis of ordinate directly yield the value for the different groups. They are given in Table V. We observe that these values include both the effect of a group and a term related to the structure, so that another step has to be done in order to find the single contributions.

Considering formic acid and methylalcohol in Fig. 2, *f*, *g*, and *h*, we see that their points lie somewhat below the drawn lines. In formic acid only the COOH− group is present, connected to hydrogen, without further C-atoms. In methylalcohol there is only the CH_2OH- group and hydrogen. We shall therefore assume that these observed differences in the series *f*, *g*, and *h* account for the effect of a primary C-atom, which is 0.6 on the average. Now, also, the other values $\chi_M{}^k$ can be derived.

We find for H, 3.0. As has been mentioned, the calculated value for H-atoms is 2.98; half the experimental value of pure H_2 is 2.52; the contribution of

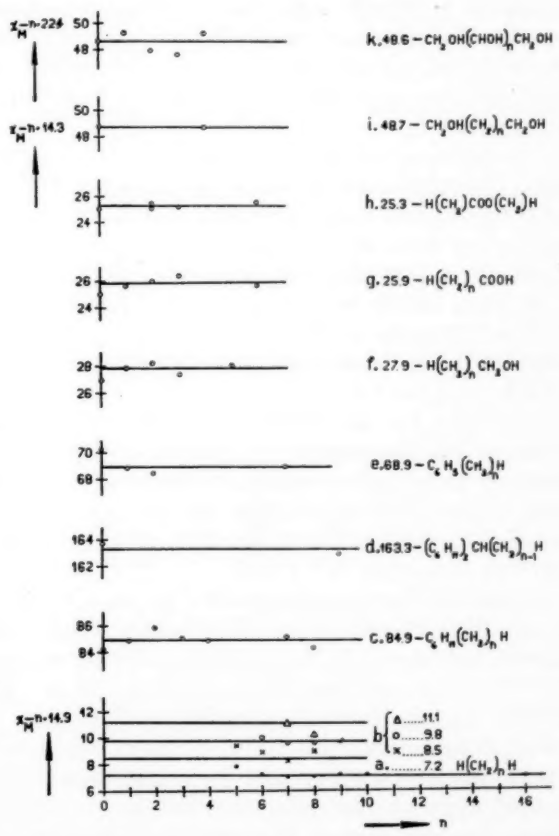

FIG. 2. The molar susceptibilities of members of homologous series are plotted *vs.* the number of carbon atoms. A constant amount is subtracted for each CH_2- group present; the unit is -10^{-6}.

[6] S. S. Bhatnagar, N. G. Mitra, and G. D. Tuli, Phil. Mag. **18**, 449 (1934).
[7] B. Cabrera and H. Fahlenbrach, Zeits. f. Physik **85**, 568 (1933).
[8] J. Farquharson and M. V. C. Sastri, Trans. Faraday Soc. **33**, 1472 (1937).
[9] D. B. Woodbridge, Phys. Rev. **48**, 672 (1935).
[10] W. R. Angus and W. K. Hill, Trans. Faraday Soc. **39**, 187 (1943).

TABLE V. Contributions to the molar susceptibility as found in Fig. 2.

H+primary C-atom	3.6	HCH_2OH+primary C-atom	27.9
Chain branching	1.3	HCOOH+primary C-atom	25.9
C_6H_{12}+branch	84.9	HCOOH+prim. C-atoms (esters)	25.3
$C_6H_{11}\cdot C_6H_{11}$+branch	163.3	CH_2OH (CH_2-homologs)	24.3[5]
C_6H_6+branch	68.9	CH_2OH (CHOH-homologs)	24.3
		CHOH	22.4

C is 8.3. For some sorts of pure carbon one has found $\chi_M = 7.6$. These values agree more or less.

From the average value of 1.3 for a branch there follows, after subtraction of the effect of a primary C-atom, the value of a tertiary C-atom: +0.7.

Now we can examine the saturated rings. The extra contribution due to the 6-membered ring in the cyclohexane series (Table I) appears to be −2.1. From dicyclohexyl follows $2\cdot -2.3$, from decalin $2\cdot -2.1$, and from perhydroanthracene $3\cdot -2.4$. This gives an average value of −2.2 for the 6-membered ring.

The 5-membered ring shows more irregular contributions to the magnetic effect. As an order of magnitude we can use +1.3 for the few compounds available.

Examining the homologs of benzene, we find an effect due to the ring of −0.2. For 1.6-diphenylhexane we obtain $2\cdot -0.4$, for 1.1-diphenyl-nonane $2\cdot -0.8$. Benzene itself and 1, 3, 5-trimethylbenzene give positive values. The xylenes demonstrate the large influence of the relative position of branches in the ring.

The mono-substituted compounds with Cl show fairly constant contributions for chlorine, ranging for 6 substances from 22.0 to 23.7. In chloroform and carbon tetrachloride the Cl-atoms give different effects: 21.1 and 18.8, respectively.

Bromine shows effects ranging from 33.7 to 35.9 in 4 compounds. It becomes lower when there is more Br in the molecule. For pure bromine we find $2\cdot 33.7$.

The value for the COOH− group is found, considering the homologs of formic acid and the esters. The former give 22.3, the latter 21.2. We shall assume 22.3 for COOH and subtract 1.1 for esters. This means that the effect of H in CH_2 is different from that in COOH.

Examining the alcohols, we find for the CH_2OH− group 24.3; from glycerol-homologs with CH_2 substituted there follows 24.3[5]; substances with CHOH− groups substituted give 24.3. The CHOH− group then also can be derived.

For these compounds, containing electric dipoles, interaction effects occur, and the values found might depend upon the temperature. Below we shall examine this by mixing the liquids. Effects of the order of 5 per mil may occur.

Investigation of some sugar solutions suggests that the effect of stereo-isomerism probably will not exceed 10 per mil, being about the precision of measurement here.

TABLE VI. Contributions by the several groups; unit -10^{-6}.

	Giorgi	C.g.s.		Giorgi	C.g.s.		Giorgi	C.g.s.
CH_2	14.28	1136	primary C-atom	0.6	50	COOH	22.3	1770
H	3.0	238	tertiary C-atom	0.7	60	esters	−1.1	−90
C	8.28	659	double bond	(−4.4)	(−350)	CH_2OH	24.3	1930
Cl	23.1	1840	saturated 5-ring	(+1.3)	(+100)	CHOH	22.4	1780
Br	34.6	2750	saturated 6-ring	−2.2	−180	OCH	15.5	1230
I	51.1	4070	benzene ring	−0.2	− 20			
			naphthalene ring	+7.8	+620			

Table VI contains the results as concerns the several contributions to the susceptibility. In Tables I and II they have been applied. The differences between the measured and calculated values of χ_M are most often smaller than 8 per mil, less than 5 per mil on the average. We omitted the calculated values of those compounds, of which the measured value had not been taken into account in the previous calculation of the group values.

Up to now we used an average value for a *branch* consisting of the effect of a primary and a tertiary C-atom. As the aliphatic hydrocarbons containing branches have been extremely purified, it has significance to extend the analysis somewhat. We have 20 hydrocarbons at our disposal and therefore can introduce some new variables.

Apart from the effect of an isolated branch (r), one can have the extra effect on attaching two primary C-atoms to the same C-atom in a chain (p_0), on attaching them to two neighboring C-atoms (p_1), and on attaching them to two atoms with one secondary in between (p_2). Furthermore, there is the extra effect of a quarternary C-atom compared with two tertiary apart (t_0), of two neighboring tertiary C-atoms (t_1) and of two tertiary C-atoms with one secondary in between (t_2).

For a definite compound we then have to count the number of times such relative positions occur. By successive approximation the unknown values can be estimated. In Table VII the results are given. The three rows with p refer to the position of the primary C-atoms, the following three (t) to the position of the tertiary C-atoms.

Using these constants we get an agreement with the measured values within 2 per mil; applying an average value for a branch alone, the differences are 4 per mil.

The two branches themselves contribute about 20 per mil to the effect. Though the gain is not large, having introduced another 5 constants, still we can expect that the data of Table VII reveal some of the peculiarities in the susceptibility of the compounds. In the calculation of χ_M as given in Table I, these data were not applied.

We also performed this analysis with the data of the Faraday effect, obtained by the author

measuring the same hydrocarbons.[11] Although the effects are far stronger here, the agreement is much better, compared with the application of one single value for a branch (D in Table VII). Only 3 more constants are needed here. With one constant the deviations are 25 per mil, which is roughly equal to the total effect of two branches. With 4 constants the deviation is 4 per mil only.

In the last four rows of Table VII we give the total effect of two branches placed in different positions in a long chain. In both magnetic data an oscillating effect may be seen.

III. MIXTURES

In II we investigated the susceptibilities of pure compounds. Here, we shall examine the influence of the interaction effects between the molecules. These effects can be examined in the dependence of the susceptibility upon the temperature and on melting, also by diluting a liquid with other liquids.

When there are no dipoles, association is not likely to occur, and on mixing the liquids the susceptibility will be linearly related to the concentration. When there are dipoles, non-linearities will appear on mixing, and the susceptibility will also depend upon the temperature.

We shall again apply Eq. (4), now supposing n_k to be the fraction of the kth component. For the mean molecular weight the following equation holds:

$$M=\sum_k n_k M_k, \tag{5}$$

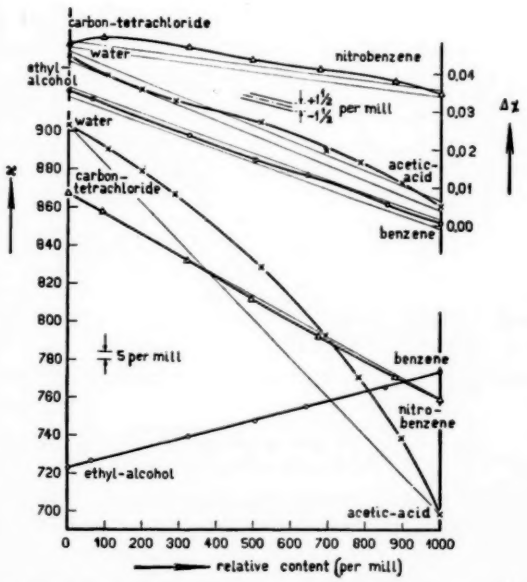

FIG. 3. The volume and mass susceptibilities of liquid mixtures, containing molecules with electric dipoles, plotted *vs.* the relative content of mass (in parts per thousand).

[11] Broersma, Waterman, Westerdyk, and Wiersma, Physica 10, 97 (1943).

TABLE VII. The dependence of the contributions upon the relative positions of the branches in the molecule.

		χ_M	D
	r	+1.2	+2.2
C XXXXX C	p_0	—	+1.45
XXXXX CC	p_1	+0.3	—
C C XXXXX	p_2	+0.1	—
X XXCXX X	t_0	−0.5	+1.1
XX XXCCXX	t_1	−0.5	−3.8
X X XXCXCXX	t_2	−0.6	—
C XXCXX C	$(r+p+t)_0$	1.9	7.0
CC XXCCXX	$(r+p+t)_1$	2.2	0.4
C C XCXCX	$(r+p+t)_2$	1.9	4.4
C C XCXXCX	$(r+p+t)_3$	2.4	4.4

so that we easily find

$$\chi=\sum_k m_k \chi^k, \tag{6}$$

where m_k is the fraction of mass of the kth component and χ^k the susceptibility per unit mass. Hence χ is linearly related with the fraction of mass. The same follows for the susceptibility per unit volume κ and the fraction of volume v_k, provided no contraction occurs.

For the investigation mixtures were chosen of which one or both of the components contained electric dipoles, *viz.*, ethyl alcohol-benzene, carbon tetrachloride-nitrobenzene, water-acetic acid, and water-ethyl alcohol.

In Figs. 3 and 4 the results are given. The points representing the two pure compounds have been connected by two straight lines at a distance +1.5 and −1.5 per mil from the average.

In Fig. 3, κ and $\Delta\chi$, the difference between χ and a constant value for each of the systems, both have been plotted against the relative content of mass. We see that the values for ethyl alcohol-benzene mixtures deviate less than 1 per mil from a straight line. The mixtures of carbon tetrachloride and nitrobenzene show a deviation in χ of 6 per mil. Although the κ-curve of water-acetic acid shows

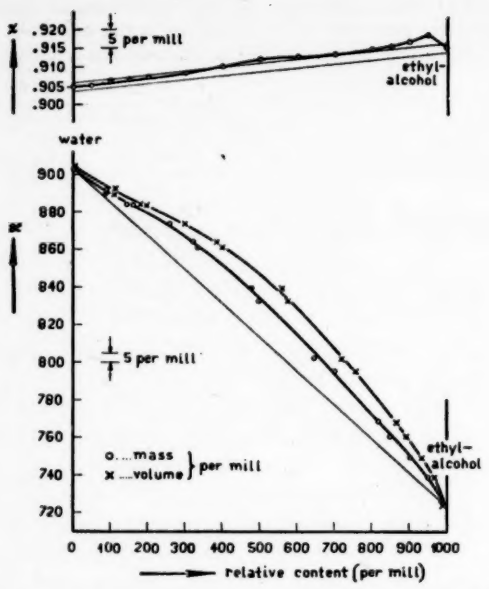

FIG. 4. The volume and mass susceptibilities of ethylalcohol-water mixtures plotted *vs.* the concentration (in parts per thousand).

departures up to 40 per mil from the straight line, still the χ-curve deviates no more than 4 per mil.

Figure 4 gives the volume susceptibility of water-ethyl alcohol mixtures plotted against the relative content of mass and relative content of volume. There are deviations of 25 and 40 per mil, respectively. The χ-curve, however, shows only a deviation of 5 per mil for high alcohol concentrations; for low concentrations the curve follows the straight line.

Roughly speaking, the observed maximum deviations are about 5 per mil. We can expect the effects of the interaction in pure compounds to be of this order of magnitude, which is also, as Table I and II show, the limit of the applicability of the additivity rule, using the constants of Table VI.

After this we performed measurements with 7 sets of mixtures of hydrocarbons. In Fig. 5 the measurements with the torsion balance (T.B.) and inductance apparatus (I.A.) are indicated. The following maximum deviations from the average of the values occur:

n-heptane—*n*-octane	0.5 per mil,
n-heptane—2,2,4-trimethyl-pentane	1.0 per mil,
n-heptane—*n*-hexadecane	1.0 per mil,
n-heptane—methyl-cyclohexane	1.5 per mil,
cyclohexane—methyl-cyclopentane	1.0 per mil,
cyclohexane—methyl-cyclohexane	1.5 per mil,
decalin—methyl-cyclohexane	1.0 per mil.

This means that within the precision of measurement there exists a linear relation between the susceptibility and the concentration. As no dipoles are present here and no contraction occurs, the deviations will probably be even much smaller.

The above data and results have been applied to experiments dealing with *research on mixtures of hydrocarbons*, such as oil fractions which cannot be separated by means of the normal chemical or physico-chemical methods. The range of molecular weights in these mixtures is about 150 to 350, so that the number of C-atoms present will be 10 to 25, giving the possibility of a great number of isomers.

The best description of these mixtures can be given by means of a statistical analysis.[12] The fact that the magnetic susceptibility has additive properties and is not affected by mixing makes statistical analysis a convenient tool for this purpose. Also, other physical quantities can serve for the purpose. They are needed because there are several variables, such as have been listed in Table VI. Furthermore, by means of slow chemical reactions, e.g., hydrogenation, one has been able to remove some properties without changing other aspects of the constitution—such as, e.g., saturated rings. Therefore, we shall only examine saturated hydrocarbons, consisting of carbon and hydrogen atoms, rings, and branches.

Waterman and collaborators determined already several constants for the three series: tin I (7 fractions), tin V*** (7 fractions), and tin VIII (5 fractions). The mean molecular weight is known with an accuracy of about 10 per mil, the other data within a fraction of one per mil.

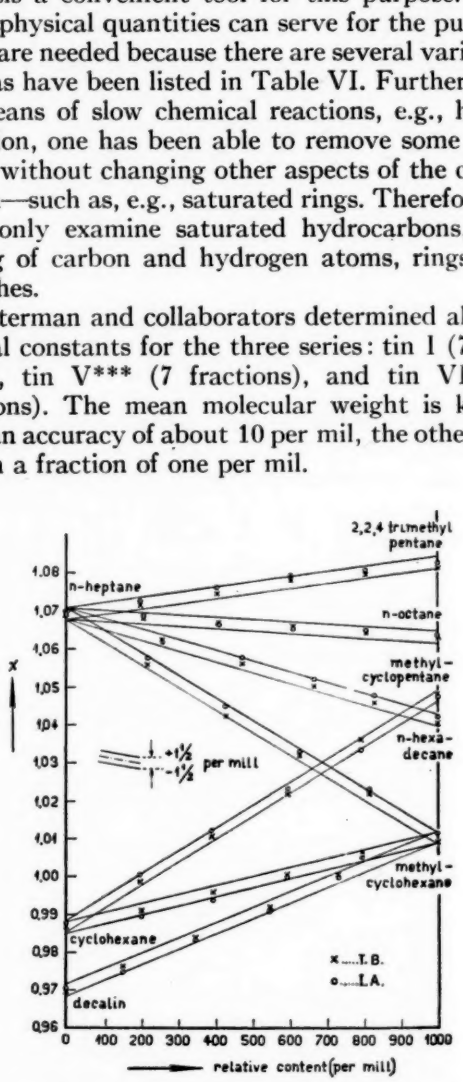

FIG. 5. The mass susceptibilities of hydrocarbon mixtures plotted *vs.* the relative content, showing a linear relation.

[12] Waterman, Vlugter, Van Westen, J. Inst. Petr. Tech. **21**, 661, 701 (1935); Waterman, Leendertse, J. Inst. Petr. Tech. **24**, 16 (1938).

*** The word "tin" refers to a sample of crude oil taken from a certain well. Here we are only interested in a comparison of the physical data of some of the fractions, obtained from three of those samples.

As the precision of M is far less than that of the other constants, we shall change the expression for the additivity rule somewhat, by using Eqs. (4) and (5). Furthermore, in connection with the valency picture, the introduction of certain elements will change the number of H-atoms. From C_nH_{2n+2} there follows $n_H = 2n_c + 2$. The introduction of double bonds, saturated rings, and the coupling of rings, will decrease n_H by 2 for each change so that

$$n_H = 2(n_c + 1 - n_k'),$$

in which n_k' indicates the number of these constitutive elements.

With these three equations n_H and n_c can be eliminated. We then obtain:

$$(\chi - A)M = B + \sum_k n_k'(\chi_k' - B) + \sum_k n_k''\chi_k'', \quad (7)$$

where

$$A = (\chi/M)_{CH_2} \quad \text{and} \quad B = \chi_{H_2} - M_{H_2} \cdot A. \quad (8)$$

A represents the effect of the CH_2- group, the main element in long chains. B indicates the change in the content of hydrogen in the molecule. The property with a double prime affects the susceptibility, without changing the hydrogen content.

Formula (7) is very well adapted to our problem. The influence of the molecular weight agrees with its precision of measurement. The main effect due to the CH_2- group is eliminated from the start, although its precise knowledge of course is necessary. Obviously the formula holds for every additive property.

The molecular refraction has been shown to be additive within a high precision, while only a small number of structural effects are of interest. The influence of the rings and other constitutional effects prove to be much smaller than the effect of the carbon and hydrogen atom itself. Applying Eq. (7), only A and B are important. If n_r is the number of rings and R_s the specific refraction, we find

$$(R_s - A_r)M = B_r(1 - n_r).$$

Waterman and collaborators carried out the analysis more empirically and were able to determine the *number of rings* with an accuracy of about 5 percent. Applying our formula to their published data, we get

$$(R_s - 0.3294)M = 1.50(1 - n_r).$$

The values of A and B thus found agree with the values found for pure compounds by applying Eq. (8). We find: $A = 0.3292$; $B = 1.54$.

The parachor has been investigated in the same way. According to Sugden this quantity is roughly additive and appears to be very sensitive for structural effects. Following Waterman *et al.*, *the number of tertiary C-atoms* can be estimated with it, assuming a special sort of rings. The values for the constants of Eq. (7) again agree with those found with (8) from pure compounds.

TABLE VIII. Structural and magnetic data of unknown hydrocarbon mixtures.

	M	n_r	n_t	n_p	κ	χ	$\frac{\chi_r}{\chi_b = 1.3}$	$\frac{a_r}{a_b = 2}$
Tin I								
1	166	0.9	2^5	2^5	832	1.0406	+0.2	−0.2
2	185	0.9	3	3^5	843	1.0428	0.0	−2.4
3	201	1.0	3	3	847	1.0390	+0.2	−2.3
4	235	1.0	3^5	3^5	851	1.0378	0.0	−2.3
5	247	1.1	4	4	857	1.0373	+0.1	−2.6
6	275	1.1	4	4	862	1.0359	+0.1	−2.6
7	304	1.3	5	4^5	869	1.0360	+0.4	−4.1
Tin V								
1	164	0.7	2	2^5	819	1.0402	−0.9	+0.3
2	175	0.8	2	2^5	832	1.0448	+1.2	+1.2
3	199	0.9	3	3	839	1.0407	+0.2	−4.8
4	219	0.9	3^5	3^5	847	1.0391	−0.1	−4.1
5	240	1.0	4	4	852	1.0365	−1.2	−3.4
6	277	1.1	4^5	4^5	852	1.0263	−2.9	−5.7
7	300	1.3	4^5	4	858	1.0222	−2.2	−4.8
Tin VIII								
1	176	1.1	3	2^5	849	1.0327	−0.3	−1.3
2	205	1.5	4	3	872	1.0326	0.0	−2.6
3	255	1.9	5	3^5	888	1.0280	+0.3	−2.5
4	303	2.2	7	5				
5	351	2.6	8^5	5	907	1.0219	−0.5	−2.1
Effect 5-ring							(+1.3)	1.1
Effect 6-ring							−2.2	−4.0
Difference when changing χ_M or D by 1 per mil							0.2	0.2

After this *the number of primary C-atoms* can be calculated, assuming a certain molecular model (see 11, p. 124). The values for n_r, n_t, and n_p thus obtained are given in Table VIII; n_t and n_p are less precise than n_r and have been rounded off for that reason. Table VIII contains also the *measured susceptibilities*, χ has not been rounded off.

Now we shall have to adapt Eq. (7) to these results. This gives 18 equations of the form

$$(\chi - A)M = B(1 - n_r) - \chi_r n_r - \chi_p n_p - \chi_t n_t, \quad (9)$$

containing the variables A, B, χ_r, χ_p, and χ_t. By successive approximation these values can be estimated.

It appears that A agrees within 2 per mil with the result for the pure substances and B within 5 per mil, while the order of magnitude of the other quantities fit well.

Applying now the values found for the pure compounds, we can start with

$$(\chi - 1.018)M = 3.95(1 - n_r) + \chi_r n_r + \tfrac{1}{2}(n_p + n_t)\chi_b + \epsilon,$$

where $\chi_b = \chi_p + \chi_t$, while $\epsilon = \frac{1}{2}(n_t - n_p)(\chi_t - \chi_p)$ is small and can also be substituted.

Now only the constants χ_r and χ_b are left, while both 5-rings and 6-rings can occur in the mixtures.

We shall assume that the ratio n_{5r} to n_{6r} is constant for each of the tins separately. In the preliminary calculation we assumed it to be constant for all of the mixtures. We then examine the reproducibility of χ_r for the several mixtures of one tin, applying some different values for χ_b.

It appears that χ_r has a fairly constant value for the tins if $\chi_b = 1.3 \pm 0.1$[5], while then $\chi_r = +0.1$ for tin I and $\chi_r = -0.1$ for tin VIII. According to Table VII, $\chi_{6r} = -2.2$ and an average value of $\chi_{5r} = +1.3$ so that both 5-membered and 6-membered rings are present.

The author also measured the constant D, as given by the Faraday effect (see 11), and applied Eq. (7) to it. The analysis shows that the effect of the ring, a_r (last column in Table VIII), as present in the mixtures, is constant for the fractions 1–6 of tin I, and 2, 3, and 5 of tin VIII. This result agrees to that obtained with the susceptibility, although there are differences in the relative concentration of 5-rings and 6-rings. Tin V shows irregularities for both effects; probably non-magnetic data are disturbing here.

As a result we can state that the magnetic data seem to be able to give some additional information as concerns the structure of the substances. The results for mixtures, applying also other physical constants, agree in several respects with those obtained for pure compounds.

The work described was carried out in the Laboratory for Technical Physics in the department of the late Professor E. C. Wiersma during and after the war years. His valuable criticism and guidance will always remain in my memory. The experimental problems were often discussed with Professor P. van der Leeden. The physico-chemical possibilities of the magnetic work were proposed by Professor H. I. Waterman and Professor R. Kronig.

THE JOURNAL OF CHEMICAL PHYSICS VOLUME 17, NUMBER 10 OCTOBER, 1949

The Ultraviolet Absorption and Luminescence of Decaborane*

GEORGE C. PIMENTEL AND KENNETH S. PITZER
Department of Chemistry, University of California, Berkeley, California

(Received January 3, 1949)

The ultraviolet absorption spectrum of decaborane in cyclohexane shows a broad absorption with a maximum molecular extinction coefficient of 3200±100A at wave-length 2720±50A. The luminescence of decaborane dissolved in a glass at 77°K shows a continuous fluorescence extending from 3630±50A to about 6000A with a broad maximum at 4520A. No further luminescence was observed at wave-lengths shorter than 9000A. The 0—0 transition is located at 3600±50A. The energy levels of a particle in a rectangular, hemispherical, and spherical box were used to test the applicability of a metallic model to decaborane. Agreement with the absorption spectrum and the molecular dimensions was obtained.

THE structure of decaborane has recently been determined by x-ray analysis.[1] Silibiger and Bauer concluded that the structures inferred by extrapolation from the lighter boron hydrides[2] cannot be correct. Kasper, Lucht, and Harker[1] then determined the structure, and it is fundamentally different from the earlier proposals.

Decaborane may be described as a ten-atom fragment of boron metal with hydrogen atoms around the outside. Thus each boron is bound to five or six other atoms. A study of the electronic spectrum of decaborane[3] is particularly interesting as a means of investigating the electronic binding associated with this structure.

EXPERIMENTAL RESULTS

Decaborane was prepared by heating diborane at 140–160°C for about one hour.[4] The product was sublimed twice into a receiver at 0°C with rejection of very volatile and non-volatile portions. The melting point of the final product was 98.1–99.6°C (corr); the reported melting point is 99.7°C.

The ultraviolet spectrum was taken in cyclohexane solution with a Beckmann spectrometer. Absorption was observed with a maximum molecular extinction coefficient of 3200±100 at wave-length 2720±50A. The absorption curve as observed between 2200A and 3700A is shown in Fig. 1a.[5]

The fluorescence spectrum of decaborane at the temperature of liquid nitrogen was also taken. A few

* This work was supported by the ONR under contract N 7 onr-295, Task Order X as Project No. NR-058-097. This aid is gratefully acknowledged.

[1] G. Silibiger and S. H. Bauer, J. Am. Chem. Soc. **70**, 115–119 (1948); Kasper, Lucht, and Harker, *ibid.* **70**, 881 (1948).

[2] B. V. Nebrasov, J. Gen. Chem. (U.R.S.S.) **10**, 1021, 1156 (1940); K. S. Pitzer, J. Am. Chem. Soc. **67**, 1126 (1945); and other references there cited.

[3] This spectrum was also of interest in connection with an attempt, so far unsuccessful, to obtain spectroscopic evidence for BH_3 in diborane at elevated temperatures.

[4] H. Schlesinger and A. B. Burg, Chem. Rev. **31**, 13 (1942).

[5] The decaborane solution of highest concentration, 0.1601 m/l, as well as all fluorescence solutions were made up using a sample of decaborane (m.p. 99.3–99.6°C, corr.) kindly furnished by Dr. D. Harker, Research Laboratory, General Electric Company, Schenectady, New York. In view of the sharp melting point of this sample, it seems unlikely that the longwave tail of the absorption could be due to impurities.

milligrams of decaborane[5] were dissolved in sixteen cc of methylcyclopentane, four cc of isopentane were added, and the solution was quickly cooled to a glass. As exciting source, the emission of a mercury arc in the spectral region between 2900A and 3400A was used. This spectral region was isolated by the filter system designated C[1] by Kasha.[6] The spectrum was photographed in a Hilger E-2 quartz spectrograph. A continuous luminescence extending from 3630±50A to about 6000A with a broad maximum at 4520A was observed. The microphotometer tracing of the photographed spectrum, reproduced by a smooth curve in Fig. 1b, evidenced no fine structure whatsoever. The quantum yield of the luminescence was estimated[7] to be in the range 0.5 to 1. The fluorescence lifetime was found to be of short duration (too short to be observed with a phosphoroscope having a resolving time of less than 0.001 second) and hence the existence of an additional discrete and weak absorption band on the long wave-length side of the main absorption is considered to be very unlikely. Observations were made through the visible region and extending to 9000A under experimental conditions where a luminescence of about one-hundredth of the intensity of the 4520A emission could have been detected and no further luminescence appeared.

Assuming the luminescence corresponds to a singlet-singlet transition, the two spectra shown in Fig. 1 locate the zero-zero transition at 3600A. It is also possible that the luminescence is a triplet-singlet transition corresponding to a weak singlet-triplet absorption obscured by the main absorption band. If this is true, the excited triplet level must be lower in energy than the excited singlet. Hence, the zero-zero band would still be between the toe of the absorption band and the short wave-length end of the fluorescence. The zero-zero transition is thus located in either case to be 3600±50A.

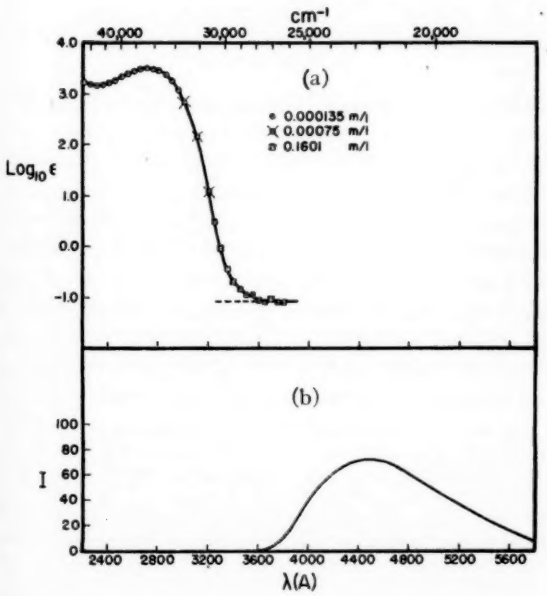

FIG. 1. (a) Absorption spectrum of $B_{10}H_{14}$ dissolved in cyclohexane. Dotted line indicates threshold of sensitivity. (b) Luminescence spectrum of $B_{10}H_{14}$ at 77°K. Exciting source 2900–3400A. Intensity on arbitrary scale; 100=total plate blackening.

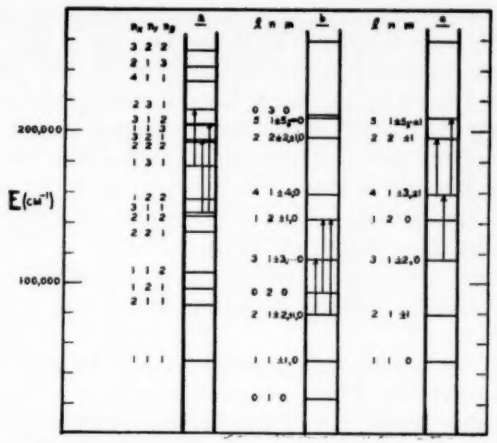

FIG. 2. Energy level diagrams for a particle in a three-dimensional box. (a) Rectangular box; $a=4.98$A, $b=4.34$A, $c=3.94$A. (b) Spherical box; $r=3.60$A. (c) Hemispherical box; $r=3.60$A. Lowest allowed transitions shown from ground state of a system containing twenty electrons.

THEORETICAL INTERPRETATION

Recently it has been shown that the electronic spectra of conjugated double bond systems in organic molecules may be treated successfully on a "metallic" model.[8] The term "metallic" indicates that some of the binding electrons are free to move within the confines of the molecule without substantial change in potential energy. In the Kasper, Lucht, and Harker structure of decaborane, each boron must be bonded to five or six other atoms in spite of an over-all electron deficiency. Hence, the electronic orbitals can hardly correspond to localized bonds between pairs of atoms but rather must be of

TABLE I.

	Rectangular box	Hemispherical box	Spherical box
Dimensions	Length 4.98A	Radius 3.60A	Radius 3.60A
Orbital extension	0.79A	1.65A	2.10A
Allowed spectrum	(2720A) 2065A 1700A 1630A	(2720A) 2320A 2005A	(2720A) 2065A 1585A

[5] M. Kasha, J. Opt. Soc. Am. **38**, 929 (1948).

[6] This estimate was made by Dr. M. Kasha by intensity comparison with substances of known fluorescence yield in a fixed geometry apparatus.

[8] Noel S. Bayliss, J. Chem. Phys. **16**, 287 (1948); W. Simpson, Ph.D. dissertation, University of California (1948); Hans Kuhn, J. Chem. Phys. **16**, 840 (1948); Helv. Chim. Acta **31**, 91 (1948).

large amplitude over a considerable region of space, possibly over the entire molecule. In view of the fairly uniform potential which would exist in the central region defined by the boron shell, it seems appropriate to apply the metallic model to decaborane. In this case, however, the electrons to be classed as "metallic" include all the binding electrons not localized in B—H bonds and the molecule is formed so as to allow these electrons a considerable amplitude of free motion in three dimensions. Interactions will be neglected between electrons and individual nuclei and between pairs of electrons.

The decaborane molecule has a shape somewhat like a tub or cradle. Three models were taken to approximate this shape, a rectangular box, a hemispherical box, and a spherical box. The structure of decaborane[2] shows twelve hydrogens bonded each to one boron atom. We assume these B—H bonds to contain one localized electron pair which does not enter into the metallic system. The location of the last two hydrogen atoms is somewhat uncertain,[9] but they appear to be definitely included in the metallic system. The number of metallic electrons is thus the total of 44 less 24 in localized B—H bonds or a net of 20 electrons. These twenty electrons were placed in the ten lowest orbitals for the ground state of each model. The energy levels for a particle in a rectangular box are given by most treatises on quantum theory; those for the spherical box by Margenau and Murphy.[10] The solutions for the hemispherical box are just those of the spherical box whose wave functions have a node in the equatorial plane. The excited states of decaborane are obtained by moving one of the higher energy electrons to an unoccupied orbital. The selection rules for these transitions are readily obtained by standard methods and are such that only a small fraction of the transitions are permitted.

It is hardly possible to select an exact box size, *a priori*, although Simpson[9] found that the box wall should lie about three quarters of an angstrom unit beyond the outermost carbon nuclei. It is possible, however, to choose the dimensions for each model which cause the first allowed transition to coincide with the observed absorption peak. The applicability of the model may then be judged by the comparison to the observed molecular dimensions. The calculated dimensions are given in Table I together with the average orbital extension beyond the outermost boron nuclei. The corresponding spectra of allowed transitions are shown in Fig. 2. The observed dimensions of the boron skeleton, measuring to boron centers, as obtained from the bond lengths given in reference 2 are:

maximum length	3.40±0.10A
maximum width	2.76±0.04A
maximum depth	2.36±0.05A

It is to be noted that an allowed transition for the rectangular box is concerned with a change of only one quantum number. Assuming the orbital extensions are about the same in the three dimensions, then the smallest energy change in an allowed transition is found to occur when only the quantum number associated with the longest molecular dimension changes. Fitting this particular transition to the 2720A absorption, it is possible to calculate an orbital extension for this dimension. Orbital extensions for the other two rectangular box dimensions can be calculated only if other absorption bands are known which could be attributed to transitions involving changes of the quantum numbers appropriate to these dimensions.

It should be noted that the metallic model does not differentiate between singlet and triplet states. Thus the model cannot hope for accuracy exceeding the separation of singlet and triplet. Since the orbitals are presumed to extend over the entire molecule, the exchange integrals involving the electronic interaction would be expected to be small and the singlet-triplet splitting not too serious.

We wish to thank Dr. D. Harker for supplying the sample of decaborane and Dr. M. Kasha for assistance with the luminescence spectrum.

CONCLUSION

The absorption and luminescence spectra of decaborane have been studied and the applicability of the metal model to decaborane has been tested. The energy levels of a single particle in a rectangular, hemispherical, or a spherical box are in agreement with the absorption spectrum and molecular dimensions. Assuming validity of the particle in a box model, the orbital extension beyond the boron centers is about 1.5A. Within the assumption that the single particle in a box approximates the metal model, the spectrum of decaborane is in qualitative agreement with the view that decaborane is a metal of molecular dimensions.[11]

[9] D. Harker, private communication.

[10] H. Margenau and G. M. Murphy, *The Mathematics of Physics and Chemistry* (D. Van Nostrand Company, Inc., New York, 1943), p. 252.

[11] *Note added in proof:* At the March, 1949 meeting of the American Chemical Society in San Francisco, J. S. Kasper indicated that there remains doubt as to whether ten or twelve hydrogens are bonded on the periphery of the boron skeleton, each to a single boron. If only ten are so located (instead of twelve as indicated in reference 1), the number of electrons to be classed as metallic is 24. This necessitates the use of two more levels to make up the ground configuration but does not alter the lowest allowed transition or the box dimensions for any of the three models discussed here.

Internal Rotation IV. The Optical Activity and Isomerization Energy of the Rotational Isomers of *D*-Secondary Butyl Alcohol

H. J. BERNSTEIN
National Research Council, Ottawa, Canada

AND

E. EGELUND PEDERSEN*
University of Copenhagen, Copenhagen, Denmark

(Received December 14, 1948)

The specific rotation of secondary butyl alcohol was measured in dilute solutions of cyclohexane at intervals of 5° between 20°C and 70°C inclusive.

After corrections for solvent effect and change of refractive index with temperature had been made there remained a definite temperature dependence of the rotivity.

Interpretation of the results on the basis of three optically active rotational isomers (two of equal energy and the third less stable) gave the rotivity of the third isomer as $-21°$ and the sum of the other two as $+21°$.

The heat of isomerization was found to be 803 cal. per mole.

The concentrations of the three rotational isomers at 20° are calculated as 42.3 percent, 42.3 percent, and 15.3 percent.

INTRODUCTION

A MOLECULE such as secondary butyl alcohol $CH_3CH_2-C^*HOHCH_3$, has an asymmetric carbon atom (marked with the asterisk) and exists therefore as a *d* and an *l* form. Due to the hindered rotation about the C−C* bond each of the optically active forms may have three rotational isomers shown in Fig. 1 for one of the optical isomers. In this figure the molecules are viewed along the C−C* axis with the CH_3CH_2 groups below the plane of the paper and the C^*HOHCH_3 groups above the plane. Further, it is assumed that the pictured configurations correspond to the minima of the energy curve as a function of azimuthal angle and are therefore considered more stable than the "eclipsed" forms.

It is to be expected that each of the rotational isomers will rotate the plane of polarization of incident light to a different degree.[1] Since the angle of rotation is proportional to the number of active molecules present the rotation of the equilibrium mixture of the 3 rotational isomers will depend on the equilibrium concentrations of the three forms. Thus the rotation of *d*-2-butanol, for example, should be a function of temperature since the concentrations of the 3 isomers in thermal equilibrium are a function of temperature.

This temperature dependence is accurately expressed in terms of heats of reactions when the material is in the gaseous phase. However, since the measurements of this work were carried out in solution both concentration and solvent effects have to be eliminated or accounted for.

NOTATION

When plane-polarized light of wave-length λ vac. traverses a medium whose refractive index is n the plane of polarization is rotated by an angle[2]

$$\alpha = 16\pi^3/\lambda^2 \text{ vac.} \cdot n^2+2/3 \cdot N/v \cdot g \text{ radians per cm}, \quad (1)$$

or

$$\alpha = 16\pi^2/\lambda^2 \text{ vac.} \cdot 180n^2+2/3 \cdot N/v \cdot g \text{ degrees per cm}, \quad (2)$$

where N is Avogadro's number, v is the volume in cm^3 occupied by 1 mole of the optically active substance, and g is a rotatory parameter (see Appendix, Eq. (16)). The specific rotation is

$$[\alpha] = \alpha v/lM, \quad (3)$$

where l is the length of the path through the medium in dm, and M the molecular weight of the active substance. Substituting for α from (1) in (3) and using the sodium D line λ vac. = 5893A one obtains

$$[\alpha]_D = 4.960 \times 10^{37} n^2+2/3M \cdot g. \quad (4)$$

Since in this work only the sodium D line was used the subscript D will be deleted from all symbols measuring the rotation.

Further, Ω, called the rotivity,[3] is defined as $\Omega = [\alpha]/n^2+2$ so that from (4) one obtains

$$\Omega = 4.960 \times 10^{37}/3M \cdot g. \quad (5)$$

TEMPERATURE EFFECT

Since the rotational isomers have different rotivities the rotivity of the equilibrium mixture obtained from

* National Research Laboratories Postdoctorate Fellow 1948-19.

[1] J. G. Kirkwood, J. Chem. Phys. 5, 487 (1937).

[2] See reference 1, p. 481.

[3] C. O. Beckmann and K. Cohen, J. Chem. Phys. 4, 784 (1936).

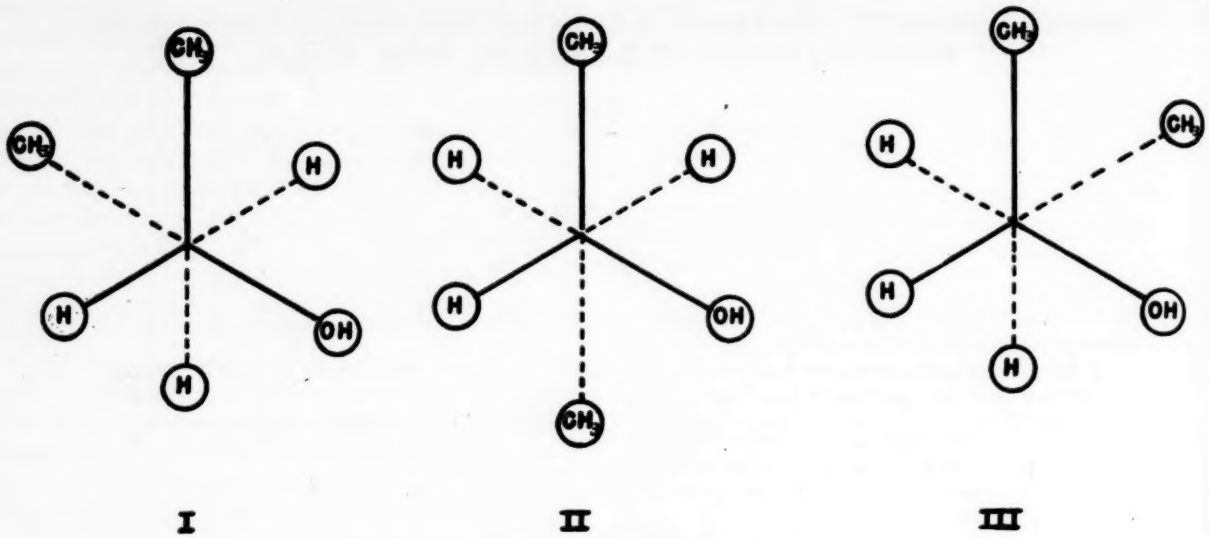

FIG. 1. Rotational isomers of secondary butyl alcohol.

observations in the gas phase is

$$\Omega_0 = N_I\Omega_I/N + N_{II}\Omega_{II}/N + N_{III}\Omega_{III}/N, \quad (6)$$

where Ω_I, Ω_{II}, Ω_{III} are the rotivities of configurations I, II, III respectively, and N_I/N, N_{II}/N, N_{III}/N are the concentrations of I, II, III respectively, expressed as mole fractions, and $N = N_I + N_{II} + N_{III}$.

Since the 3 rotational isomers are in thermal equilibrium

$$\frac{N_{II}}{N_I} = A_1 \exp[-(\Delta H_1^0/RT)], \quad (7)$$

$$\frac{N_{III}}{N_{II}} = A_2 \exp[-(\Delta H_2^0/RT)], \quad (8)$$

where A_1, A_2 are constants and ΔH_1^0, ΔH_2^0 are the heats of reaction over the temperature range studied. Thus

$$\left.\begin{aligned}
\frac{N_I}{N} &= \frac{1}{1 + A_1 \exp[-(\Delta H_1^0/RT)] + A_1A_2 \exp[-(\Delta H_1^0 + \Delta H_2^0/RT)]} \\
\frac{N_{II}}{N} &= \frac{A_1 \exp[-(\Delta H_1^0/RT)]}{1 + A_1 \exp[-(\Delta H_1^0/RT)] + A_1A_2 \exp[-(\Delta H_1^0 + \Delta H_2^0/RT)]} \\
\frac{N_{III}}{N} &= \frac{A_1A_2 \exp[-(\Delta H_1^0 + \Delta H_2^0/RT)]}{1 + A_1 \exp[-(\Delta H_1^0/RT)] + A_1A_2 \exp[-(\Delta H_1^0 + \Delta H_2^0/RT)]}
\end{aligned}\right\} \quad (9)$$

Hence

$$\Omega_0 = \frac{1}{1 + A_1 \exp[-(\Delta H_1^0/RT)] + A_1A_2 \exp[-(\Delta H_1^0 + \Delta H_2^0/RT)]} \times \{\Omega_I + A_1 \exp[-(\Delta H_1^0/RT)]\Omega_{II} + A_1A_2 \exp[-(\Delta H_1^0 + \Delta H_2^0/RT)]\Omega_{III}\}. \quad (10)$$

As was mentioned previously, this relation is valid only for the vapor.

SOLVENT EFFECT

Since the measurements are carried out in solution certain corrections must be applied in order to obtain the gas value Ω_0. As shown in the experimental part of this paper, the association effect can be eliminated entirely by sufficient dilution in a non-polar solvent such as cyclohexane.

The dilute solution values of Ω thus obtained are related to the gas values Ω_0 by the relation[4]

$$\Omega = \Omega_0 + B(\epsilon - 1/\epsilon + 2), \quad (11)$$

where B is a constant for solvents of similar structure[4,5] at a given temperature, and ϵ is the dielectric constant of the medium at that temperature. For non-polar

[4] See reference 3, p. 784.
[5] N. Gutzwiller, Helv. Phys. Acta 18, 497 (1945).

TABLE I. *D*-secondary butyl alcohol in cyclohexane at 20°C.

$1/C$	d	α	$[\alpha]$	n	P/M	$\Omega_{90\text{ percent}}=\frac{[\alpha]}{n^2+2}$	Ω_{pure}
1.244	0.8060	20.15	12.50	1.3970	0.2988	3.163	3.510
2.851	0.7861	9.65	13.75	1.4108	0.3157	3.446	3.824
5.702	0.7784	5.14	14.65	1.4177	0.3225	3.653	4.053
11.32	0.7784	2.67	15.11	1.4216	0.3262	3.758	4.170
11.40	0.7784	2.65	15.11	1.4216	0.3262	3.758	4.170
20.00	0.7784	1.555	15.55	1.4233	0.3273	3.863	4.286
22.81	0.7784	1.36	15.51	1.4238	0.3277	3.851	4.273
32.23	0.7784	0.955	15.39	1.4243	0.3280	3.820	4.239
45.61	0.7784	0.69	15.74	1.4250	0.3285	3.905	4.333
49.07	0.7784	0.64	15.70	1.4250	0.3285	3.895	4.323

solvents Eq. (11) can be approximated closely by

$$\Omega=\Omega_0+B(n^2-1/n^2+2). \qquad (11a)$$

In order to make the solvent correction Ω is obtained for non-polar solvents of different n at different temperatures. Plots of Ω *versus* (n^2-1/n^2+2) will give straight lines whose slopes are the B's for the particular temperatures.

SUPERPOSITION RULE FOR OPTICALLY ACTIVE ROTATIONAL ISOMERS

It will be found later that in order to interpret the Ω *vs.* T data any information about the Ω's of configurations I, II, III would be most helpful. In Fig. 2 configuration I of Fig. 1 is redrawn so that the OH group is coplanar with the CH_3-CH_2 groups and the CH_3 group is above the plane of the paper and the H below

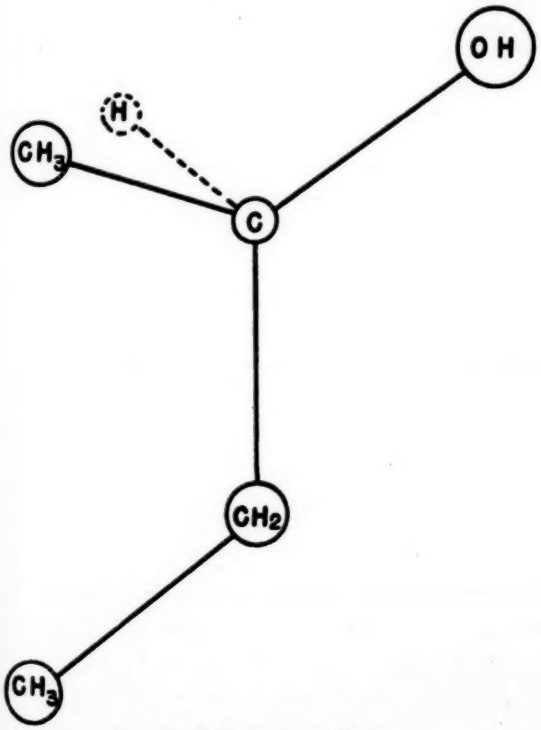

FIG. 2. Configuration I of Fig. 1.

TABLE II. *D*-secondary butyl alcohol in cyclohexane at different temperatures and dilutions.

t°C	$1/C$	d	α	$[\alpha]$	$\Omega_{90\text{ percent}}=\frac{[\alpha]}{3}(1-P/M\cdot d)$	Ω_{pure}
25°	11.41	0.7722	2.61	14.89	3.713	4.11
	20.16	0.7722	1.50	15.12	3.766	4.18
	32.49	0.7722	0.93	15.11	3.761	4.17
	49.46	0.7722	0.615	15.21	3.784	4.19
30°C	11.50	0.7661	2.56	14.72	3.680	4.08
	20.32	0.7661	1.46	14.83	3.704	4.11
	32.75	0.7661	0.90	14.74	3.679	4.08
	49.86	0.7661	0.60	14.96	3.732	4.13
35°C	11.59	0.7605	2.50	14.49	3.632	4.02
	20.47	0.7605	1.425	14.58	3.650	4.05
	32.99	0.7605	0.88	14.52	3.633	4.02
	50.22	0.7605	0.58	14.57	3.643	4.04
40°C	2.925	0.7663	9.04	13.22	3.341	3.71
	5.901	0.7595	4.78	14.10	3.549	3.94
	11.67	0.7551	2.45	14.30	3.593	3.99
	11.87	0.7551	2.45	14.54	3.653	4.05
	20.62	0.7551	1.39	14.33	3.796	3.99
	23.64	0.7551	1.23	14.54	3.647	4.05
	33.23	0.7551	0.86	14.29	3.584	3.98
	47.28	0.7551	0.615	14.54	3.644	4.04
	50.49	0.7551	0.56	14.17	3.552	3.94
45°C	11.75	0.7500	2.40	14.10	3.550	3.94
	20.76	0.7500	1.36	14.12	3.551	3.94
	33.45	0.7500	0.85	14.22	3.574	3.96
	50.93	0.7500	0.55	14.01	3.519	3.90
50°C	11.82	0.7452	2.35	13.89	3.505	3.88
	20.89	0.7452	1.33	13.89	3.501	3.88
	33.67	0.7452	0.83	13.97	3.518	3.89
	51.26	0.7452	0.54	13.84	3.484	3.86
55°C	11.90	0.7407	2.31	13.74	3.473	3.84
	21.02	0.7407	1.31	13.77	3.477	3.84
	33.87	0.7407	0.81	13.72	3.462	3.83
	51.57	0.7407	0.52	13.42	3.385	3.76
60°C	11.96	0.7366	2.26	13.51	3.421	3.78
	21.13	0.7366	1.28	13.52	3.420	3.78
	34.06	0.7366	0.79	13.45	3.400	3.77
	51.85	0.7366	0.51	13.22	3.340	3.70
65°C	12.03	0.7326	2.215	13.32	3.379	3.74
	21.25	0.7326	1.26	13.39	3.393	3.75
	34.24	0.7326	0.78	13.35	3.381	3.74
	52.14	0.7326	0.50	13.04	3.301	3.68
70°C	3.039	0.7375	8.14	12.37	3.163	3.51
	6.093	0.7308	4.25	12.95	3.299	3.65
	12.08	0.7290	2.18	13.17	3.346	3.70
	12.17	0.7290	2.18	13.27	3.372	3.73
	21.36	0.7290	1.24	13.24	3.360	3.72
	24.36	0.7290	1.09	13.28	3.369	3.73
	34.42	0.7290	0.76	13.10	3.323	3.68
	48.74	0.7290	0.55	13.40	3.397	3.76
	52.41	0.7290	0.50	13.10	3.321	3.68

the plane. It is a general result of optical activity theory that molecules which have a plane of symmetry are not optically active. As a result the interaction of the C—OH and CH_3-CH_2 groups will not contribute to the rotivity. If the contribution to the rotivity of this molecule from the CH_3 group is g_{CH_3}, it would be $-g_{CH_3}$ if the CH_3HOH groups were rotated 120° so that the CH_3 group were below the plane of the paper since, in general, mirror images have rotations of oppo-

TABLE III. The rotivity of *l*-secondary butyl alcohol in dilute solutions of different solvents.

Solvent	n^{20}	d^{20}	d^{40}	$1/C$	α^{40}	$[\alpha]^{40}$	Ω^{40}	$(n^2-1/n^2+2)_{40°}$
n hexane	1.3860	0.6895	0.6712	18.20	−0.695	−6.33	−1.63	0.2286
n heptane	1.4034	0.7295	0.7116	18.08	−0.70	−6.33	−1.61	0.2382
cyclohexane	1.4230	0.7784	0.7551	18.32	−0.69	−6.32	−1.59	0.2470
CCl_4	1.4548	1.533	1.498	18.16	−0.695	−6.31	−1.55	0.2650

site sign. As a result if groups above the plane of the paper make a positive contribution to the rotivity, groups below make a negative contribution. Therefore

$$\Omega_{\mathrm{I}}=\frac{4.960\times10^{37}}{3M}(g_{CH_3}-g_{\mathrm{H}}),$$

$$\Omega_{\mathrm{II}}=\frac{4.960\times10^{37}}{3M}(g_{\mathrm{H}}-g_{\mathrm{OH}}),$$

$$\Omega_{\mathrm{III}}=\frac{4.960\times10^{37}}{3M}(g_{\mathrm{OH}}-g_{CH_3}).$$

The sum $\Omega_{\mathrm{I}}+\Omega_{\mathrm{II}}+\Omega_{\mathrm{III}}$ is then zero. This is strictly true only when there is no asymmetry other than that given to the molecule by rotation. If there is asymmetry due to a C atom then there is a definite rotivity due to this asymmetric C which is present in all the rotational configurations. In what follows the rotivity due to the asymmetric C has been neglected. This seems reasonable since it would approximate the rotivity of isopropyl alcohol which is zero. Accordingly a general rule for rotational isomers with groups which make angles that are symmetrically disposed about the rotation axis, is

$$\sum_{i=1}^{m}\Omega_i=0, \tag{12}$$

where $m=2, 3, \cdots$ is the total number of minima in the energy curve as a function of azimuthal angle. In the Appendix the polarizability theory of Kirkwood[1] is used to compute the value of Ω_{III}. As already mentioned this involves only interaction of the OH and CH_3 groups and thus avoids the calculations involving H which are at the present moment inexact.

From the superposition rule and the calculated value of Ω_{III} the value of $\Omega_{\mathrm{I}}+\Omega_{\mathrm{II}}$ which involve H interactions and which would otherwise have been difficult to evaluate individually, may be obtained.

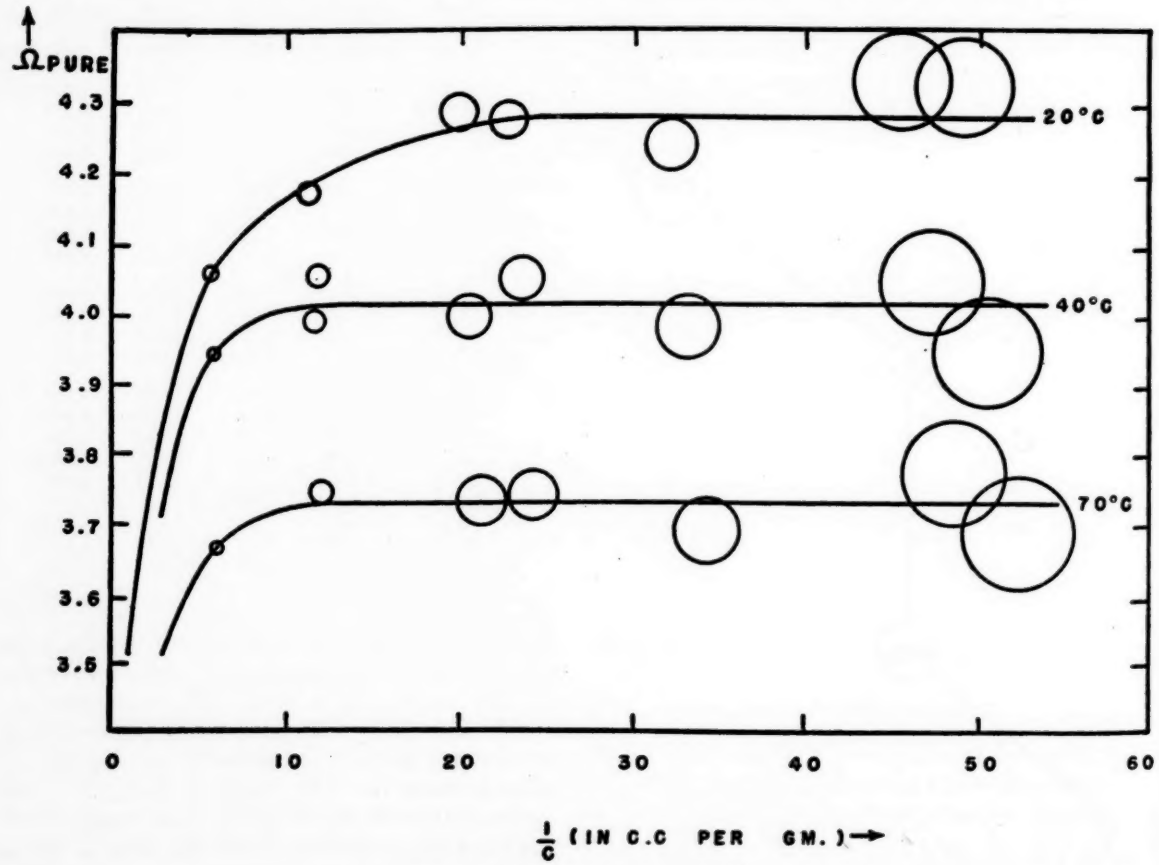

FIG. 3. Rotivity Ω *versus* concentration.

EXPERIMENTAL

Inactive 2-butanol (b.p. 99.5°) was partially resolved into optically active components through the brucine salt of the acid phthalate by the method of Pickard and Kenyon[6,7] as presented by R. Adams.[8] The *d*-alcohol thus obtained had the following properties b.p. 99.8°C, $d^{20}=0.8060$, $\alpha^{20}=+20.15°$ in a 2 dm tube. The specific rotation is $[\alpha]^{20}=\alpha^{20}/2C=12.50°$ where C is the concentration in g per cc. According to Pickard and Kenyon[7] the specific rotation of the optically pure compound is 13.87°. Our sample of *d*-butanol contains then 90 percent of the dextro compound and 10 percent of the racemic mixture.

The rotation measurements were carried out in a 2 dm tube surrounded by a jacket through which water was circulated from a thermostat. The temperature was controlled to ±0.1°C.

In the following Tables I, II the rotivity for various dilutions is given for temperatures at every 5° between 20° and 70° inclusive. The Lorentz-Lorentz equation, *viz.*, $P=M/d\cdot n^2-1/n^2+2$ gives $1/n^2+2=\frac{1}{3}(1-P/M\cdot d)$. Hence the rotivity for the 90 percent *d*-alcohol is $\Omega_{90\text{ percent}}=[\alpha]/n^2+2=[\alpha]/3(1-P/M\cdot d)$. P/M is calculated from the data at 20° and used throughout since it is independent of temperature. The value for the optically pure alcohol, Ω_{pure}, is obtained by multiplying $\Omega_{90\text{ percent}}$ by the factor 1.109. In Fig. 3 Ω_{pure} is plotted against 1/C for 20°C, 40°C, and 70°C. The circles about the experimental points indicate the experimental errors. As can be seen from the graphs the rotivity finally reaches a value which is independent of concentration. In order to evaluate the dilute solution value of Ω the experimental Ω's for solutions of greater dilution than 11 were weighted according to their experimental errors and the weighted average calculated. For 20°C, however, only the values of Ω for solutions of dilution greater than 20 were used to obtain the average value. In order to determine the extent of the correction due to the solvent, rotation measurements at different temperatures were to be performed on 5 percent solutions of the *l*-alcohol ($\alpha^{25}=-9.20°$) in *n*-hexane, *n*-heptane, cyclohexane and carbon tetrachloride. The first temperature at which these measurements were made was 40° and the results are given in Table III. In order to get $B^{40°}$ of Eq. (11a) Ω^{40} was plotted against $(n^2-1/n^2+2)_{40°}$ and the resulting straight line is shown

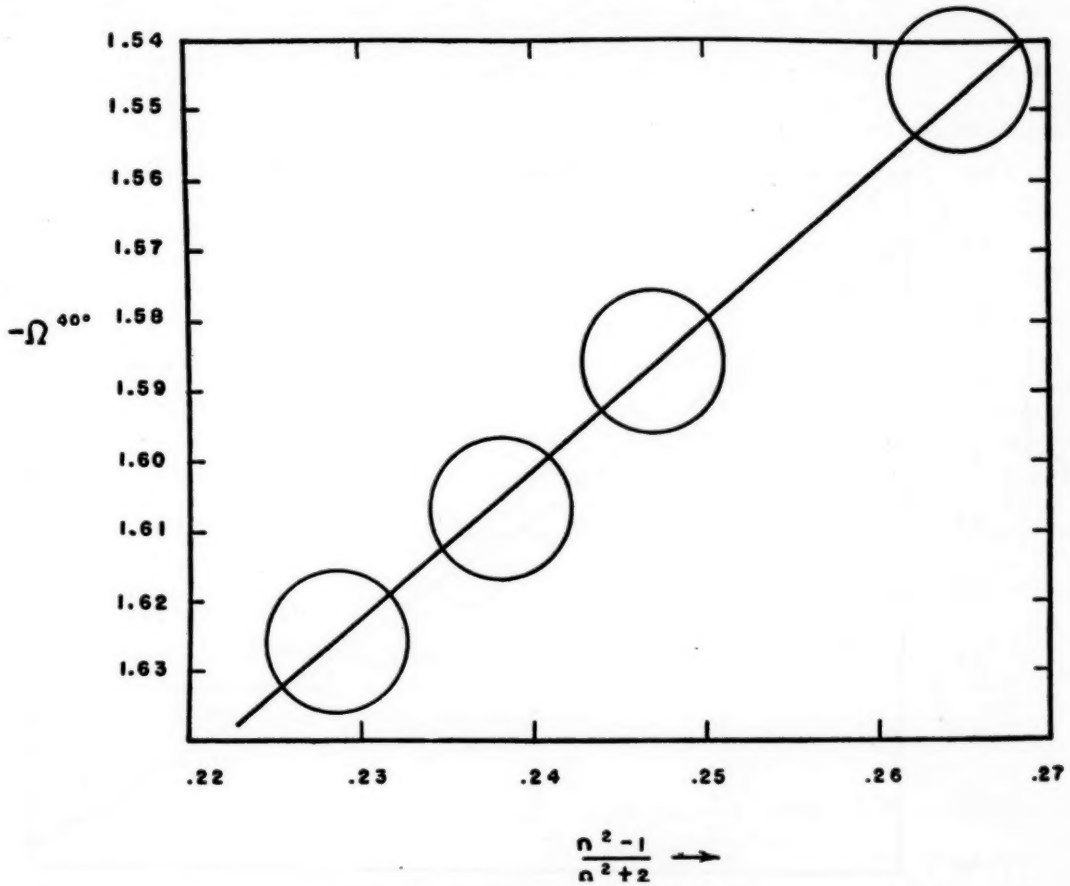

FIG. 4. Rotivity Ω against $(n^2-1)/(n^2-2)$.

[6] Pickard and Kenyon, J. Chem. Soc. London **99**, 45 (1911).
[7] See reference 6, **103**, 1923 (1913).
[8] Edited by Roger Adams, *Organic Reactions* (John Wiley and Sons, Inc., New York, 1944), Vol. 2, p. 403.

TABLE IV. The rotivity of *d*-secondary butyl alcohol at different temperatures.

t°C	$[\alpha]_{pure}$	Ω_0
20	17.25	5.75
25	16.80	5.60
30	16.39	5.46
35	16.11	5.37
40	15.97	5.32
45	15.68	5.23
50	15.42	5.14
55	15.21	5.07
60	14.93	4.98
65	14.79	4.93
70	14.67	4.89

in Fig. 4. The slope of this line is -2.10. Since this was obtained for an alcohol whose optical purity was 39.6 percent the value of $B^{40°}$ corrected for optical purity is -5.31.

As can be seen from Table III, $[\alpha]$ for the alcohol in the four solvents is a constant. Now since

$$\Omega=[\alpha]/n^2+2=[\alpha]/3-[\alpha]/3\cdot(n^2-1/n^2+2),$$

and $[\alpha]/3$ is a constant, the slope of Ω *versus* (n^2-1/n^2+2) (B of Eq. (11a)) is $[\alpha]/3$, and $\Omega_0=[\alpha]/3$, where of course only the dilute solution values of specific rotation are involved.

If we assume that $[\alpha]$ in the 4 solvents will be constant at the other temperatures (certainly not an unreasonable assumption) then the gas values are obtained immediately from $\Omega_0=[\alpha]/3$ at the particular temperature. In this way the evaluation of B at all the temperatures studied could be avoided and the true correction for the solvent effect made at all temperatures from the dilute solution value of $[\alpha]$.

If $[\alpha]$ for dilute solutions from Tables I, II is weighted according to its experimental error and the average obtained, it must be multiplied by 1.109 to correct for optical purity and then divided by three to get Ω_0.

Table IV gives the dilute solution values of $[\alpha]_{pure}$ and Ω_0 at the different temperatures studied. The percentage error in Ω_0 is the same as for $[\alpha]$ and is about 1 percent. The possible error in Ω_0 is then ± 0.05.

INTERPRETATION OF THE RESULTS

Ω_0 as a function of T is given by Eq. (10) which involves Ω_I, Ω_{II}, Ω_{III}, A_1, A_2, ΔH_1^0, ΔH_2^0 as unknowns. Making use of the superposition rule (Eq. (12)) the number of unknowns is reduced to six. The temperature range studied is not wide enough, however, to permit evaluation of these unknowns from data which are accurate only to ± 1 percent.

On the other hand it is very reasonable to suppose that configurations I and II have about the same energy, and that III is less stable than either I or II.

In this case $\Delta H_1^0=0$ and $A_1=1$ since the two isomers are equally probable, and, since $\Omega_I+\Omega_{II}+\Omega_{III}=0$, Eq.

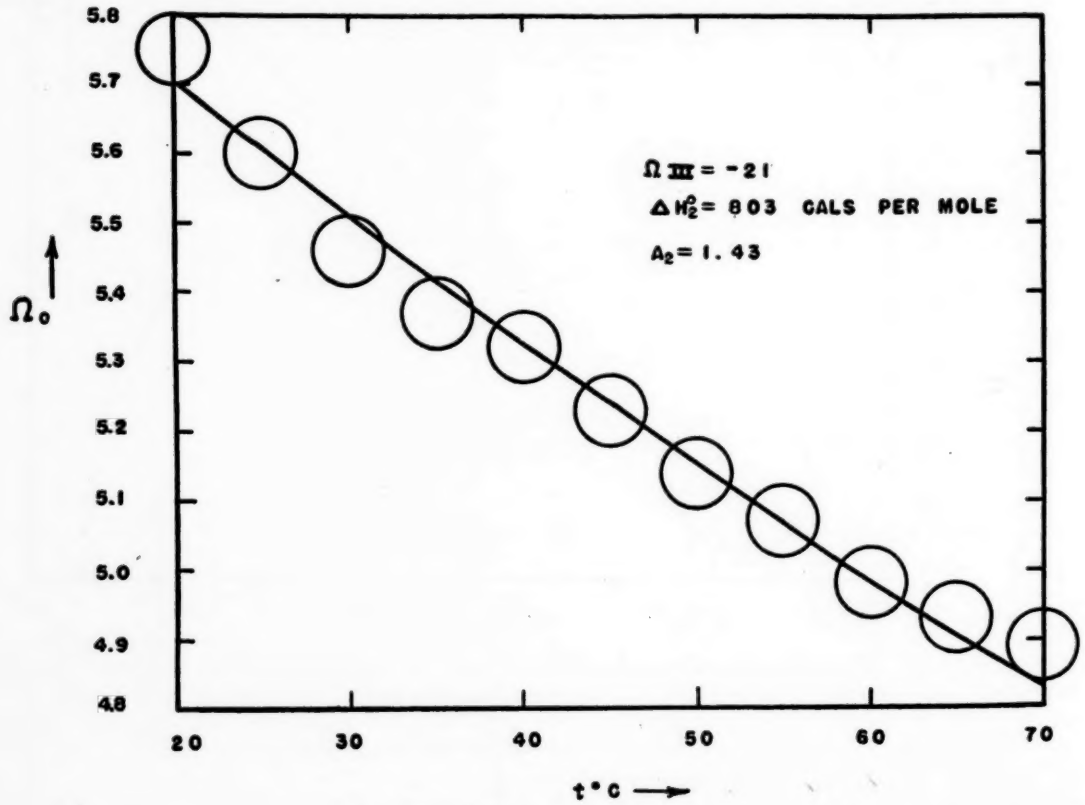

FIG. 5. Temperature dependence of rotivity.

(10) becomes

$$\Omega_0=-\frac{\Omega_{III}\{1-A_2\exp[-(\Delta H_2^0/RT)]\}}{2+A_2\exp[-(\Delta H_2^0/RT)]}. \quad (13)$$

This equation may be rewritten as

$$\ln\frac{\Omega_{III}-2\Omega_0}{\Omega_0-\Omega_{III}}=\ln A_2-(\Delta H_2^0/RT). \quad (14)$$

Plotting the left-hand side against $1/T$ should give a straight line for the proper value of Ω_{III}. A satisfactory straight line is obtained for $\Omega_{III}=-21\pm1.0$. The slope of this line gives $\Delta H_2^0=803\pm60$ cal. per mole and hence $A_2=1.43\pm0.10$. The temperature dependence of Ω_0 is given by

$$\Omega_0=\frac{21.0-31.0\exp(-803/RT)}{2+1.43\exp(-803/RT)}. \quad (15)$$

In Table V the computed Ω_0's are compared with the observed, and in Fig. 5, the computed curve has been drawn along with the experimental points circled by their experimental error for comparison. As can be seen the data are represented by Eq. (15) to within the experimental error.

The concentrations of rotational isomers I, II, III at 20°C are 42.35 percent, 42.35 percent, and 15.3 percent, respectively, and at 70°C are 43.0 percent, 43.0 percent, and 14.0 percent respectively.

The value for Ω_{III} computed from the polarizability theory of Kirkwood (see Appendix) to be -12.3 is in tolerable agreement with the experimental value.

To obtain an independent check on the value of ΔH_2^0 the infra-red spectrum of the gas should be obtained at several temperatures, in order to compare intensity ratios of bands due to the different isomers at these temperatures.

Unfortunately the spectrum could not be resolved with a Perkin-Elmer spectrometer.

ACKNOWLEDGMENT

The authors are indebted to Dr. L. Marion for placing the polarimeter at our disposal.

APPENDIX

If the electrons of a molecule may be considered as assignable to definite groups between which there is no exchange, and all molecular transitions are localized in a distinct group, g of Eq. (5) is given by[1]

$$g=-\tfrac{1}{6}\sum_{i>k=1}^{N}\alpha_i\alpha_k\beta_i\beta_kG_{ik}\mathbf{R}_{ik}(\mathbf{b}_i\times\mathbf{b}_k), \quad (16)$$

TABLE V.

t°C	$\Omega_{obs.}$	$\Omega_{calc.}$	$\Omega_{obs.}-\Omega_{calc.}$
20	5.75	5.70	+0.05
25	5.60	5.61	−0.01
30	5.46	5.51	−0.05
35	5.37	5.42	−0.05
40	5.32	5.32	0.00
45	5.23	5.24	−0.01
50	5.14	5.16	−0.02
55	5.07	5.07	0.00
60	4.98	4.98	0.00
65	4.93	4.90	+0.03
70	4.89	4.83	+0.06

where

$$G_{ik}=\frac{1}{R_{ik}^3}\left[\mathbf{b}_i\mathbf{b}_k-\frac{3\mathbf{b}_i\mathbf{R}_{ik}\cdot\mathbf{b}_k\mathbf{R}_{ik}}{R_{ik}^3}\right],$$

$\mathbf{R}_{ik}=\mathbf{R}_k-\mathbf{R}_i$,

$\mathbf{b}_i$, $\mathbf{b}_k$ are unit vectors defining the optical axes of groups i, k,

α_i, α_k are the mean polarizabilities of groups i, k,

β_i, β_k are the anisotropies of groups i, k.

In order to calculate g it is necessary to know the α's, β's, the dimensions of the molecule, the directions of the optical axes, and the direction of $\mathbf{R}_{ik}$.

In the following, g_{III} the rotatory parameter for configuration III, will be computed. The value of g_{III} is given by

$$g_{III}=-\tfrac{1}{6}\{\alpha_{OH}\alpha_{C_2H_5}\beta_{OH}\beta_{C_2H_5}\times G_{OHC_2H_5}\mathbf{R}_{OHC_2H_5}(\mathbf{b}_{OH}\times\mathbf{b}_{C_2H_5})+\alpha_{CH_3}\alpha_{C_2H_5}\beta_{CH_3}\beta_{C_2H_5}\times G_{CH_3C_2H_5}\mathbf{R}_{CH_3C_2H_5}(\mathbf{b}_{CH_3}\times\mathbf{b}_{C_2H_5})\},$$

since the terms in H, C_2H_5 do not contribute because of coplanarity of H and CH_3-CH_2. The values of α_{OH}, α_{CH_3}, $\alpha_{C_2H_5}$, and β_{OH}, β_{CH_3}, $\beta_{C_2H_5}$ are those used by Kirkwood. The molecular dimensions are taken as C−C=1.54A, C−O=1.43A, C−H=1.09A, and all angles tetrahedral. The $\mathbf{b}$ vectors are assumed to be in the direction of the bond which joins the active group to the C atom and the $\mathbf{R}_{ik}$ are measured from the mid-point of the C−C bond in the CH_3-CH_2 or C_2H_5 groups to the group in question. Evaluation of g_{III} gives -5.47×10^{-35} whence $\Omega_{III}=-12.30$. From the superposition rule, Eq. (12), $\Omega_I+\Omega_{II}=+12.30$.

If α_H is taken as 0.4×10^{-24} and β_H as 0.35 then

$$g_I=8.67\times10^{-35},\quad \Omega_I=19.50,$$
$$g_{II}=-3.20\times10^{-35},\quad \Omega_{II}=-7.20,$$

which may be considered as reasonable estimates for configurations I and II.

Polymorphism and Anion Rotational Disorder in the Alkaline Earth Carbonates

J. J. LANDER
*Bell Telephone Laboratories, Murray Hill, New Jersey**
(Received December 26, 1948)

X-ray diffraction methods have been developed for the study of materials at high temperatures under controlled atmospheres, and an investigation of the high temperature phases of the alkaline earth carbonates has been made. $BaCO_3$ was found to change from orthorhombic (aragonite type) to hexagonal (calcite type) at 803°C, and to cubic (sodium chloride type) at 976°C. $SrCO_3$ was found to change from orthorhombic (aragonite type) to hexagonal (calcite type) at 912°C. A few experiments with mixtures, which go through similar transitions, are described.

These transitions are related to the rotational activity of the carbonate ions and consideration of the nature of the transitions leads to a description of the probable rotational behavior of these ions in the various phases.

PART I. EXPERIMENTAL X-RAY DIFFRACTION STUDY

ONE of the earliest cases of polymorphism investigated by means of x-ray diffraction is that of $CaCO_3$. Calcite (rhombohedral) and aragonite (orthorhombic) are well understood from the crystallographic point of view but a complete identification of vaterite (hexagonal) has not been reported. Aragonite is presumably the stable form at low temperatures and high pressures. It is rapidly and irreversibly converted to calcite at about 470°C. Vaterite is so unstable that large crystals have not been obtained. A fourth modification has been reported by Boeke.[1] He observed a reversible change in heat content of calcite at 975°C but found that the optical properties did not change in the transition.

Strontianite, ismorphous with aragonite, is the only form of strontium carbonate which has been observed at room temperature. Boeke[2] reported a transition to a hexagonal form occurring at 929°C on heating and at 920°C on cooling. These transition temperatures are very sensitive to impurities. For example, he had reported earlier that the temperature of transition on heating was 830°C, and this lower result he thought due to admixed $CaCO_3$.

Witherite, ismorphous with aragonite, is the only form of barium carbonate which has been observed at room temperature. Boeke reported (reference 2) that witherite changes to a hexagonal form at 811°C and to a cubic form at 982°C. On cooling a hysteresis of about 50°C was observed in the case of the first transition. He also found that the admixture of 30 mole percent $CaCO_3$ lowered the orthorhombic to hexagonal transition temperature by about 150°C. However Cork and Gerhard,[3] having completed an x-ray study of $BaCO_3$ at temperatures up to 1000°C stated, "In pure $BaCO_3$ no change in structure occurred, but the lattice enlarged."

Since the existence of at least one of these alkaline earth carbonate modifications has been questioned, and since in any case the crystallographic data given by Boeke are necessarily meager (he was limited to optical techniques), the x-ray diffraction study reported herein has been made. The results, besides being of general chemical interest, are of immediate importance to determinations of rates of decomposition and of equilibria between carbonate and oxide. Moreover they appear to provide an interesting set of examples of order-disorder transitions produced by anion rotational oscillation in the solid state, and this aspect of their behavior will be considered in detail in Part II.

Experimental Procedure

The crystallographic data reported below were obtained with x-ray diffraction accessories designed for the study of materials at high temperatures in controlled atmospheres or in a vacuum.[4] Transition temperatures were observed precisely and rapidly with an x-ray spectrometer and one of these accessories. More detailed information was obtained from powder patterns for which CuK_α radiation and a nickel filter were used. Some of these patterns are reproduced in Figs. 1, 2, and 3.

The transition temperatures reported are averages of results obtained with the spectrometer as well as from measurements of rates of heating and cooling. Agreement to ± 5°C was obtained for corresponding points in all cases except that of the cubic transition of $BaCO_3$ for which an initial set of runs in the spectrometer gave too low a value. In this method a very small amount of material is used and one cannot be sure that its quality is as pure as that of the source. For this reason the transition temperatures were also measured using much larger samples and the usual differential method of observing heating and cooling rates as a function of temperature. The results of these measurements have been given heavier weight in the reported results.

* Presented at the First International Congress of Crystallography, held at Harvard University, July 28 to August 3, 1948.
[1] H. E. Boeke, Neues Yahrb. Min. Geol. I, 91 (1912).
[2] H. E. Boeke, Chem. Zentr. I, 1909 (1913).
[3] J. M. Cork and S. L. Gerhard, Am. Min. 16, 71 (1931).
[4] J. J. Lander, Rev. Sci. Inst. 20, 82 (1949).

The carbonates were obtained from batches of exceptionally high purity with respect to the cation. They had been dried at room temperature after precipitation from water solution. In all experiments at higher than ambient temperature of the laboratory they were maintained in 99.8 percent pure CO_2 at one atmosphere. Noticeable decomposition to oxide did not occur below 1300°C in the case of $BaCO_3$ or of $SrCO_3$ but occurred at about 900°C in the case of $CaCO_3$. There was no noticeable reaction with the platinum supports.

Experimental Results with $BaCO_3$

Aragonite Type

As received barium carbonate gave only a few extremely broad features. After heating to 200°C an identifiable witherite pattern was obtained. The pattern of Fig. 1(a) was obtained from material at room temperature after it had been heated to 700°C. The lines are quite sharp and the pattern is identical with that obtained from a powdered crystal of witherite.[5] Measurements of a pattern from the former material into which sodium chloride was ground to serve as standard are given in Table I. The lattice constants $a_0=5.30$A, $b_0=8.88$A and $c_0=6.42$A are believed to be accurate to 0.2 percent. They are compared in Table II with those found by Wilson,[6] by Cork and Gerhard (reference 3), and by Colby and LaCoste.[7]

Figure 1(b) is a pattern obtained from $BaCO_3$ at 750°C. Most of its features correspond with those of 1(a), however it will be found that a few lines are markedly displaced. Measurements of the most accurately determinable spacings, given in Table I, reveal an unusually large expansion along the c_0 direction, the direction normal to the plane of the carbonate ion. In order to obtain more accurate values for the changes in cell constants produced by heating from 20°C to 750°C the x-ray spectrometer was used. This method gives a greater relative accuracy than can be obtained

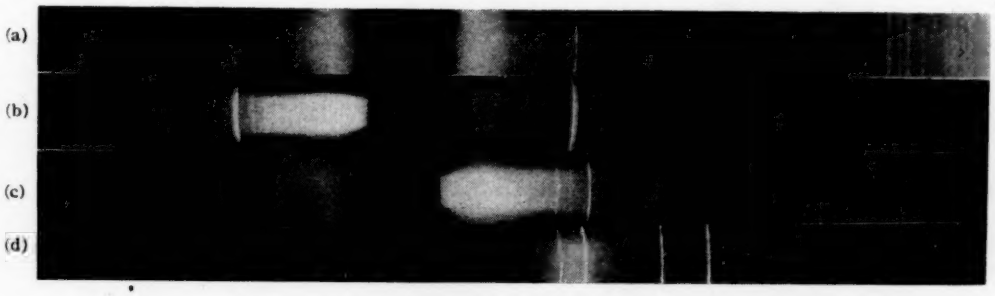

FIG. 1. Patterns from $BaCO_3$: (a) orthorhombic form at 20°C after heating to 700°C; (b) the same at 750°C; (c) hexagonal form at 830°C; (d) cubic form at 960°C after heating to 980°C.

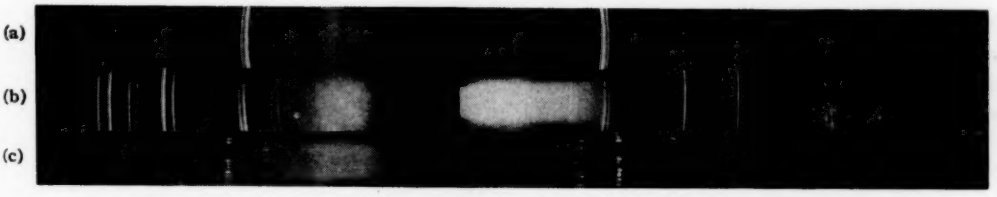

FIG. 2. Patterns from $SrCO_3$: (a) orthorhombic form at 20°C after heating to 700°C; (b) hexagonal form at 860°C; (c) hexagonal form at 920°C.

FIG. 3. "Triple carbonate" patterns: (a) orthorhombic form, no heat treatment; (b) hexagonal form at 750°C; (c) hexagonal form at 20°C after heating to 750°C.

[5] Crystals of witherite were obtained from Wards Natural Science Museum. They contained about one percent of strontium.
[6] T. A. Wilson, Phys. Rev. **31**, 305 (1928).
[7] M. Y. Colby and L. J. B. LaCoste, Zeits. f. Krist. **90**, 1 (1935).

TABLE I. X-ray data from aragonite-type carbonates.

hkl	$BaCO_3$ at 20°C			$BaCO_3$ at 750°C		$SrCO_3$ at 20°C			Triple Carbonate at 20°C	
	I(obs.)	d(obs.)	d(calc.)	d(obs.)	d(calc.)	I(obs.)	d(obs.)	d(calc.)	I(obs.)	d(obs.)
110	½	4.54	4.55	4.52	4.57	¼	4.32	4.34	½	4.38
020	¼	4.45	4.44	4.45	4.46	¼	4.18	4.18	¼	4.22
101	...	...	...	4.10	4.15	¼	3.90	3.88	...	...
111	10	3.70	3.71	3.71	3.76	10	3.50	3.51	10	3.56
021	3	3.65	3.65	3.66	3.70	5	3.42	3.48	5	3.49
002	1	3.22	3.21	3.31	3.32	2	2.98	3.00	1	3.08
012	½	3.02	3.02	3.09	3.11	2	2.81	2.82	1	2.89
102	...	...	...	2.80	2.82	1	2.58	2.58	½	2.64
031	1	2.66	2.69	2.69	2.72	2	2.54	2.53	3	2.57
200			2.65	2.66	2.66			2.54		
112	2	2.62	2.62	2.69	2.69	3	2.46	2.47	3	2.52
022	2	2.59	2.60	2.66	2.66	3	2.44	2.44	5	2.48
130			2.58	2.59				2.43		
210	...	...	...	2.54	2.55	½	2.25	2.25	½	2.28
220	1	2.28	2.28	2.27	2.28	1½	2.17	2.17	½	2.19
040	½	2.22	2.22	2.22	2.23	½	2.090	2.092	1	2.128
221	4	2.15	2.15	2.15	2.16	5	2.040	2.041	7	2.073
041	2	2.101	2.103	2.110	2.110	3	1.973	1.973	5	2.015
202	2	2.052	2.050	2.075	2.076	3	1.936	1.938	3	1.975
132	3	2.020	2.012	2.040	2.043	4	1.893	1.894	5	1.938
113	4	1.937	1.936	2.000	1.991	3	1.816	1.816	5	1.862
023	...	...	...	...	...	1	1.804	1.803	½	1.822
222	½	1.858	1.857	...	...	½	1.758	1.758	1	1.793
042	¼	1.827	1.827	1.850	1.848	¼	1.716	1.716	½	1.750
310	¼	1.731	1.732	1.736	1.739	½	1.660	1.660	1	1.680
240	¼	1.705	1.702	1.705	1.708	¼	1.617	1.612	¾	1.645
311	1½	1.672	1.673	1.683	1.683	2	1.602	1.600	3	1.622
241	1½	1.645	1.645	1.653	1.654	2	1.562	1.560	3	1.586
151	2	1.626	1.628	1.639	1.639	2	1.537	1.535	3	1.567
004	¼	1.606	1.606	...	...	¼	1.500	1.500	½	1.541
223	½	1.558	1.558	1.595	1.590	¾	1.473	1.471	1	1.505
330	½	1.517	1.517	1.522	1.523	...	...	...	1	1.468
114	...	...	...	...	...	1	1.420	1.417	1½	1.453

by measurement of the photographic patterns.** Displacements of the lines due to the 221, 132, and 113 planes were observed. The cell constants at 750°C given in Table IV were obtained in this manner.

Calcite Type

The pattern of Fig. 2(c) was produced by $BaCO_3$ at 830°C. Measured values for intensities and spacings are given in Table III as well as spacings calculated for a calcite-type structure with $a_0=5.205$A and $c_0=10.55$A. The spacings which occur are those of the rhombohedral division of the hexagonal system and the observed intensities are in qualitative agreement with intensities calculated for the calcite structure in which scattering by the carbonate ion is neglected. For such a structure the intensities of all lines which appear are equal to a constant multiplied by the plane multiplicity and the angular scattering function. In the case of calcite it has been shown that carbonate ions are ordered in the manner shown in Fig. 4, and therefore the smallest rhombohedral cell contains two molecules. However, such ordering would be more difficult to observe in calcite-type structures containing much heavier metal ions and at comparatively high temperatures. The hexagonal indexing of Table III assumes the smaller rhombohedral cell which contains one molecule and it is to be noted that all the observed features can be indexed on this basis, but the absence of reflections such as the 210, from which the ordering of carbonate ions can be inferred, is not accepted herein as evidence of disorder in either hexagonal $BaCO_3$ or $SrCO_3$. It is not unlikely that a more thorough study, preferably with monochromatic radiation, would decide this important point.

The transition temperature observed on heating was 803°C and that on cooling was 750°C. It was found that both transitions occurred abruptly. Material was held for an hour with no observable change at temperatures which, when shifted in the right direction by 10°C, produced the transitions in a matter of seconds.

Lower transition temperatures were obtained by adding $CaCO_3$, as was observed by Boeke. Approximately 2 mole percent lowered the temperatures of transition by approximately 25°C. Measurements of the transition in air also yielded lower results, presumably caused by a small amount of decomposition.

Sodium Chloride Type

The pattern reproduced in Fig. 1(d) was obtained from $BaCO_3$ at 960°C after heating to 980°C. Spacings in intensities correspond to those of the sodium chloride-

** The back-reflection technique would yield much more accurate results but could not be used because of the diffuseness of the features in the back reflection region. However, to obtain the highest precision, coefficients of linear expansion should be measured directly, for example, by interferometric measurements of single crystals.

type cubic structure with a_0 equal to 6.96A. It is to be noted that the unit rhombohedral cell of calcite can be regarded as a distorted sodium chloride-type cell. Conversely a sodium chloride-type structure can be regarded as a special case of the calcite-type structure and may be given a similar indexing. The constants for the orthohexagonal cell (which is based on a (111) plane of the cubic cell) of cubic $BaCO_3$ are given in Table IV. This method of representing constants facilitates comparison among the polymorphic forms.

Tests to 1300°C revealed no further change in structure and none is to be expected.

The transition from hexagonal to cubic occurred at 976°C and the reverse transition about 20°C lower. Both were abrupt. Admixture of 2 mole percent $CaCO_3$ was observed to raise the temperatures of transition by about 20°C, and, as will be described below, it was found that large amounts of $SrCO_3$ or $CaCO_3$ tend to stabilize the hexagonal form.

Experimental Results with $SrCO_3$

Aragonite Type

Natural crystals were not obtained. As received, the powder gave a recognizable strontianite pattern. After heating to 700°C and cooling slowly the pattern of Fig. 2(a) was obtained. The close correspondence between this and the witherite pattern is obvious. Observed spacings and intensities are given in Table I as well as spacings calculated with $a_0=5.08$A, $b_0=8.36$A and $c_0=6.00$A. As in the case of $BaCO_3$ an unusually large thermal expansion along the c_0 axis was observed. The results of measurements of the change in lattice constants made with the spectrometer are given in Table IV.

Calcite Type

The intensities and indexing of spacings of the pattern of Fig. 2(c), produced by $SrCO_3$ at 920°C, parallel those found for hexagonal $BaCO_3$ and therefore the structure is that of calcite with anions possibly disordered. The calculated spacings given in Table III were obtained with a_0 equal to 5.092A and c_0 equal to 9.53A.

The orthorhombic to hexagonal transition occurred at about 912°C. Boeke obtained 929°C. Transitions were abrupt and admixture of 2 mole percent $CaCO_3$ lowered the temperatures of transition by about 40°C.

TABLE II. Reported lattice constants of aragonite type $BaCO_3$ and $SrCO_3$.

Material	a_0	b_0	c_0	Reference
$BaCO_3$ (20°C)	5.30	8.88	6.42	Lander
$BaCO_3$ (20°C)	5.252	8.828	6.544	Wilson
$BaCO_3$ (20°C)	5.28	8.83	6.39	Colby and LaCoste
$BaCO_3$ (20°C)	5.256	9.172	6.412	Cork and Gerhard
$SrCO_3$ (20°C)	5.08	8.36	6.00	Lander
$SrCO_3$ (20°C)	5.12	8.40	6.08	Wilson

TABLE III. X-ray data from calcite-type carbonates.

	$BaCO_3$ at 830°C			$SrCO_3$ at 920°C			Triple Carbonate at 20°C		
hkl	I	d(obs.)	d(calc.)	I	d(obs.)	d(calc.)	I	d(obs.)	d(calc.)
10.1	7	4.12	4.14	5	3.98	4.00	5	3.96	3.99
00.3	3	3.48	3.52	—	—	—	—	—	—
01.2	10	3.40	3.42	10	3.22	3.18	10	3.17	3.18
11.0	6	2.59	2.60	5	2.53	2.54	5	2.58	2.56
10.4	6	2.27	2.28	5	2.094	2.098	—	—	—
02.1	5	2.20	2.20	3	2.140	2.140	5	2.155	2.155
11.3	2	2.09	2.09	(5)	1.993	1.988	5	1.956	1.960
20.2	2	2.07	2.07			2.000	2	1.988	1.994
01.5	2	1.910	1.910	2	1.752	1.749	½	1.692	1.692
00.6	½	1.760	1.758	½	1.593	1.589	½	1.525	1.525
02.4	½	1.711	1.713	1	1.622	1.618	¼	1.592	1.592
21.1	2	1.682	1.682	3	1.639	1.643	1	1.648	1.648
12.2	1½	1.622	1.622	2	1.573	1.573	¾	1.573	1.575
20.5	½	1.538	1.539	½	1.446	1.441	—	—	—
03.0	½	1.503	1.503	1	1.470	1.471	¼	1.478	1.478
11.6	1	1.456	1.457	½	1.349	1.347	½	1.311	1.311
21.4	(1)	1.429	1.430	1	1.366	1.365	½	1.352	1.351
10.7			1.429	—	—	—	—	—	—
30.3	½	1.382	1.382	½	1.334	1.334	½	1.311	1.330
12.5	½	1.323	1.325	¼	1.255	1.254	—	—	—
01.8	¼	1.266	1.266	—	—	—	—	—	—
22.0	—	—	—	¼	1.273	1.272	½	1.281	1.280

Heating to 1300°C produced no further change in structure. It is possible that a transition to a cubic form exists at a higher temperature and would be observed in experiments carried out with the material under a high pressure of CO_2.

Experimental Results with $CaCO_3$

$CaCO_3$ was examined in the temperature range between 20°C and 900°C with the spectrometer. No transition was observed. At 900°C decomposition set in, the equilibrium pressure of CO_2 being about one atmosphere. Thus it was impossible to check the result obtained by Boeke at 975°C with the available equipment.

Lattice constants at 20°C and at 750°C are given in Table IV. These were obtained from measurements made of line displacements with the spectrometer. From these data the average coefficient of linear expansion in the c_0 direction is calculated to be 25×10^{-6} per °C and in the a_0 direction -2×10^{-6} per °C. Geiss[8] measured these coefficients by a direct method in the range 0° to 80°C and obtained $(25.57+0.016t)\times10^{-6}$ for the first and $(-5.05+0.008t)\times10^{-6}$ for the second. Obviously third-order terms, negative in each case, must be added to cover the range 0° to 800°C. However, these terms cannot be obtained very precisely from the x-ray data reported here.

Experimental Results with a Triple Carbonate

A mixture of 46 percent $BaCO_3$, 46 percent $SrCO_3$ and 8 percent $CaCO_3$ (percentages by weight) obtained by precipitation from a solution of the three metallic ions gave the barely recognizable aragonite-type pat-

[8] Geiss, Ann. d. Physik **76**, 403 (1925).

TABLE IV. Orthorhombic and hexagonal cell constants.

Material	Temp. (°C)	Structure*	a_0	b_0	c_0	Volume in A³ per mole
$BaCO_3$	20	Orthorhombic	5.30	8.88	6.42	76.0
$BaCO_3$	750	Orthorhombic	4.32	8.92	6.64	78.6
$BaCO_3$	830	Hexagonal	5.205	9.02	10.55	82.6
$BaCO_3$	960	Cubic	4.92	8.52	12.05	84.2
$SrCO_3$	20	Orthorhombic	5.08	8.36	6.00	63.7
$SrCO_3$	850	Orthorhombic	5.10	8.39	6.19	66.2
$SrCO_3$	920	Hexagonal	5.092	8.82	9.53	71.4
$CaCO_3$	20	Hexagonal	4.97	8.64	8.51	61.1
$CaCO_3$	750	Hexagonal	4.976	8.64	8.67	62.0

* In the hexaxonal and cubic structures a_0, b_0 and c_0, refer to the orthohexagonal cells and these cells contain eight molecules, whereas the orthorhombic cells contain four molecules. Anion disorder is implied by the values of c_0 given for all hexagonal cells. This is not valid in the case of $CaCO_3$ and may not be for the others. For an ordered cell this dimension is actually $2 \times c_0$.

tern reproduced in Fig. 3(a). After heating to 700°C and cooling to room temperature the material gave a good pattern very similar to those of Figs. 1(a) and 2(a). Observed intensities and spacings are given in Table I and the calculated lattice constants are $a_0 = 5.14$A, $b_0 = 8.52$A and $c_0 = 6.16$A.

Calcite Type

A pattern of hexagonal "triple carbonate" was obtained from the material at 750°C, and it was found that this structure was retained on cooling to room temperature at a moderate rate. However by very slow cooling the aragonite structure was obtained. The hexagonal patterns are reproduced in Fig. 3 and the observed intensities and spacings of the room temperature pattern are given in Table III. The spacings calculated from $a_0 = 5.12$A and $c_0 = 9.15$A agree very well with the observed values. The expansion between 20°C and 750°C along the c_0 direction, as measured with the spectrometer, was 3.8 percent whereas in the a_0 direction it was 0.4 percent.

Examination with the spectrometer revealed that the transition from orthorhombic to hexagonal on heating occurred rapidly at 710°C (±5°) and again it was found that the hexagonal structure was retained when the material was cooled at a moderate rate. Thus the structure of the "triple carbonate" may be either orthorhombic or hexagonal depending on the heat treatment, and this may be true of a wide range of mixtures of two or more of the carbonates.

Huber and Wagener[9] made an x-ray examination of mixtures of the alkaline earth carbonates, and they report complete solution and the orthorhombic structure for mixtures of $BaCO_3$ or $SrCO_3$ with less than about 20 mole percent $CaCO_3$.

R. Faivre has made x-ray studies of mixtures of $SrCO_3$ with $CaCO_3$ and of $BaCO_3$ with $CaCO_3$.[10] After heating to 900°C he found miscibility and the orthorhombic structure for mixtures containing more than 50 mole percent $SrCO_3$ in $CaCO_3$ but a solubility limit of 11 percent was observed for $SrCO_3$ in the calcite form of $CaCO_3$. He also found that $BaCO_3$ takes up 35 percent $CaCO_3$ without change in structure but when more than this amount was present he observed the hexagonal structure.

[9] H. Huber and S. Wagener, Zeits. f. tech. Physik **23**, 1 (1942).
[10] R. Faivre, Comptes Rendus **219**, 73 (1944); **222**, 227 (1946).

Volume Considerations

The volumes in cubic angstroms per molecule of the alkaline earth carbonates at various temperatures are listed in Table IV and are plotted in Fig. 5. The full lines indicate average volume expansions and for the hexagonal forms of $BaCO_3$ and $SrCO_3$ and the cubic form of $BaCO_3$ they are estimates made on the assumption that the coefficients of volume expansion are the same as those of the orthorhombic forms. X-ray measurements were made but the temperature ranges are too small to obtain very accurate results. However, such measurements did prove that the expansions cannot be much larger than those estimated. The volume increases at the transition points are believed to be accurate to about 10 percent. The discontinuity indicated for $CaCO_3$ at 975°C is based on the assumption that the transition observed by Boeke is accompanied by a marked expansion along the c_0 axis.

PART II. ANION ROTATIONAL DISORDER

Introduction

A large number of transitions in solids have been associated with increased rotational activity of asymmetric ions or asymmetric molecular groups. In general it is expected that rotation remains effectively hindered

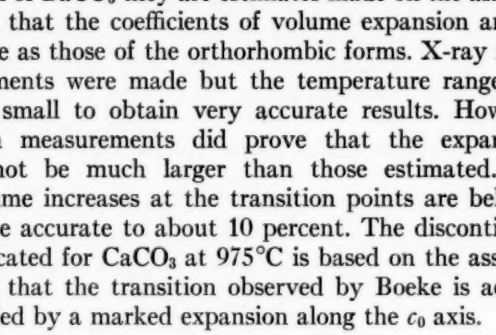

FIG. 4. Projection, along trigonal axis, of a carbonate ion and its nearest neighbors of both kinds in the ordered calcite structure. Circles represent metal ions, full lines a central plane and adjacent planes, dotted lines more distant planes, heavy lines upper planes and light lines lower planes.

above the transition temperature. Extensive investigations by means of the nuclear magnetic resonance method provide the most conclusive experimental evidence for this point of view.[11,12]

In the argument which follows, and which concerns the alkaline earth carbonates, stress is placed on the possibility of a transition being determined or characterized by an increase in the number of configurations of rotational oscillation available to the carbonate ion. For example, constrained to a plane with a field of threefold symmetry, three configurations of rotational oscillation are available to the ion. If the symmetry of field changes to sixfold, six configurations are available. A transition which involves such an increase in configurations apparently takes place with a large increase in ionic rotational activity; but considerations of detailed dynamical behavior such as relative amplitudes of modes of oscillation, the persistence of ordered domains, and average rotational frequencies are not a part of the formal argument of this paper. An increase in the number of available configurations is described as a decrease in order, and it is assumed that the increase proceeds stepwise. It is recognized that this treatment represents a limited aspect of both disordering processes and changes in structure.

It is not at all obvious that the transition phases of barium and strontium carbonate are disordered and no direct experimental evidence for disorder has been offered. Moreover it is to be noted that in the related aragonite to calcite transition of $CaCO_3$ one type of ordered anion configurations simply gives way to another, there being no decrease in order since the number of configurations available to an anion is three in each case. Nevertheless it is argued that the transitions to hexagonal forms of barium and strontium carbonate are quite different in character. Furthermore the very interesting results of an x-ray study of $NaNO_3$ made by L. A. Siegel,[13] and described below, indicate in detail the probable behavior of the hexagonal phases of the carbonates.

Comparison of Alkaline Earth Carbonates with Alkaline Nitrates

The alkali nitrates undergo transitions similar to those observed in the alkaline earth carbonates and it is to be noted that the nitrate ion is almost identical with the carbonate ion morphologically. Both ions are clover-shaped and only very careful x-ray examination reveals dimensional differences. KNO_3 is orthorhombic (aragonite structure) at room temperature but changes to a disordered hexagonal (calcite) structure at 127.7°C.[14]

$NaNO_3$ is hexagonal (calcite structure) at room temperature and it undergoes a transition at 275°C.

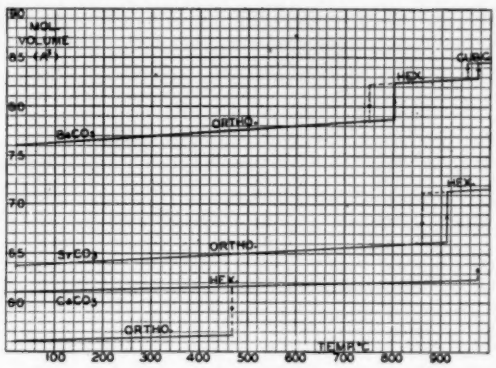

FIG. 5. Volumes per molecule in cubic angstroms plotted against temperature.

X-ray examination indicated that the nitrate ions rotate above the transition temperature but that no other change in structure takes place.[15] A large expansion along the trigonal axis accompanies the transition (see Table V). In this case the more accurate analysis made by L. A. Siegel results in a more detailed description of the rotational behavior of the nitrate ion.

NH_4NO_3 undergoes six-phase transitions.[16] A cubic form of the CsCl type is observed between 125.2 and 169.5°C, a tetragonal form between 84.2 and 125.2°C, an orthorhombic form between 32.3 and 84.2°C, etc. Free rotation about three mutually perpendicular axes was assumed to explain the x-ray data obtained from the cubic form, but apparently rotation was not required to interpret data obtained from the other modifications. A transition to a CsCl-type cubic phase is also exhibited by $CsNO_3$ (at 170°C), $RbNO_3$ (210°C) and by $TlNO_3$ (at 170°C). Finbak and Hassel[17] made a study of these materials as well as of NH_4NO_3 and they pointed out that the cell dimensions of the cubic phases were too small to permit perfectly free rotation of any reasonably sized nitrate ions. However they did not assign more probable locations to the nitrate ions.

It is apparent that the phase transitions of alkali nitrates and of alkaline earth carbonates have a number of features in common. The temperature range of the transitions of interest in the case of the carbonates is quite different, but this is to be expected as a result of the stronger electrostatic and repulsive forces acting between the doubly charged ions. If anion rotational disorder exists in the hexagonal and the cubic forms of the carbonates, the analogy is almost complete. Pertinent crystallographic data are collected in Table V.

The cubic phases listed in Table V are too dense to contain anions occupying a volume corresponding to that of spheres circumscribed about a reasonably sized anion. The case of NH_4NO_3 has been discussed by Fin-

[11] Bitter, Alpert, Poss, Lehr, and Lin, Phys. Rev. **71**, 738 (1947).
[12] N. L. Alpert, Phys. Rev. **75**, 398 (1949).
[13] Presented at the First International Congress of Crystallography, held at Harvard University, July 28 to August 3, 1948.
[14] Kracek, Barth, and Ksanda, Phys. Rev. **40**, 1034 (1932).
[15] Kracek, Posnjak, and Hendricks, J. Am. Chem. Soc. **53**, 1183, 2609, 339 (1931).
[16] Hendricks, Posnjak, and Kracek, J. Am. Chem. Soc. **54**, 2766 (1932).
[17] C. Finbak and O. H. Hassel, Zeits. f. physik Chemie **B35**, 25 (1937).

TABLE V.

Material	Str.	Temp. (°C)	a_0	b_0	c_0	r_M
$BaCO_3$	Ortho.*	20	5.30	8.88	6.42	1.35
$BaCO_3$	Hex.	750	5.20	9.02	10.55	1.35
$BaCO_3$	NaCl	950	4.92	8.52	12.05	1.35
$SrCO_3$	Ortho.	20	5.08	8.36	6.00	1.13
$SrCO_3$	Hex.	920	5.09	8.82	9.53	1.13
$CaCO_3$	Ortho.	20	4.94	7.94	5.72	0.99
$CaCO_3$	Hex.	20	4.96	8.49	2×8.48	0.99
$NaNO_3$	Hex.	20	5.06	8.76	2×8.39	0.95
$NaNO_3$	Hex. (rot.)	275	5.08	8.80	8.82	0.95
KNO_3	Ortho.	20	5.42	9.17	6.45	1.33
KNO_3	Hex. (rot.)	127	5.27	9.13	9.54	1.33
NH_4NO_3	Hex.	−18	5.75	9.96	2×7.95	1.48
NH_4NO_3	CsCl (rot.)	126	6.22	7.62	7.62	1.48

* Cell constants are for orthorhombic or orthohexagonal cells. Unless c_0 for hexagonal cells is multiplied by 2, disorder is implied. Metal radii r_M are from L. C. Pauling [*The Nature of the Chemical Bond* (Cornell University Press, Ithaca, 1940), p. 346]. The approximate *C-O* distance is 1.31 and the *N-O* distance is 1.21. Dimensions are in A units. Where the structure is marked (rot.) the original data were interpreted as evidence for free rotation by Kracek *et al.*

bak and Hassel and a simple calculation leads to this conclusion in the case of $BaCO_3$. The shortest Ba–O distance calculated for the hexagonal phase is 2.65. Allowing 1.35 for the radius of the barium ion leaves 1.30 for the outer radius of an oxygen ion in the carbonate ion. Since the hexagonal (calcite) structure is simply a distortion of the cubic (NaCl) structure, it is expected that the value for the outer radius of the oxygen ion will not change much in the transition. From the above values the diameter of the sphere circumscribing the carbonate ion is calculated to be 5.22 and the diameter of the barium ion to be 2.70. Thus the unit cell edge for the sodium chloride structure, assuming completely free rotation, might be expected to be 7.92. The observed value is 6.96, about 12 percent lower, and therefore, on the average, carbonate groups do not occupy a maximum volume. This argument suggests an assignment of positions which do not have spherical symmetry (free rotation about three mutually perpendicular axes).

It is to be noted that an approach to spherical symmetry can be obtained with an ordered arrangement of nitrate groups in which the anions are distributed with planes perpendicular to the four trigonal axes of a cube. The alkaline earth nitrates actually crystallize in a CaF_2-type cubic structure and an ordered arrangement has been assigned to the nitrate ions with planes perpendicular to the four trigonal axes.[18]

Mechanisms for Disorder in a Calcite-Type Structure

In calcite-type structures containing a planar anion with threefold symmetry the ordered arrangement of Fig. 4 is generally observed. All anions in a given plane have the same orientation, but are rotated through 60° with respect to all anions in the two adjacent planes. Only three equivalent positions are available to a given anion. This ordering is not due to the metal ions. With respect to these alone the potential field in the plane of any anion has sixfold symmetry, which leaves six equivalent positions for all anions. Order is created by the anions themselves in setting up maximum distances between nearest oxygen ions. The metal ions offer a considerable barrier to the rotation of a single anion, but it is conceivable that a relative minimum exists in potential energy for the position obtained by rotating through 60°. An important consequence of such a rotation is that the energy levels of similar wrong orientations for all neighboring anions are temporarily lowered, so that there is a tendency for one such transition to produce another nearby.

This model of disorder is analogous to that for order-disorder in some alloys in which no gross change in structure takes place. A qualitative treatment of the Bragg-Williams type, which assumes complete disorder and neglects differences in vibrational entropy, is easily adapted to the situation. In the partially disordered crystal of N anions there are $2N$ non-equivalent orientations, therefore the maximum entropy change is $k \ln 2^N$. The change in internal energy is proportional to the energy Vo required to disorder an anion in the completely ordered crystal. It follows that the critical temperature is proportional to Vo. Since the ordered and disordered orientations are identical with respect to metal ions Vo is determined, to a first approximation, by the "repulsive" interactions between oxygen ions. It is obvious that with increasing cell size the distances between oxygen ions increase and therefore that Vo decreases. Thus critical temperatures should decrease in the series $CaCO_3$, $SrCO_3$, and $BaCO_3$. Moreover if the critical temperature of one of the series is known, then these temperatures may be calculated readily for the rest of the series, since some of the factors which are difficult to evaluate can be eliminated as a result of similarity in structure and other properties. If the Born-Mayer[19] equation be used to calculate Vo it is found that

$$Vo = A\sum_s a_s e^{-r_s/\rho},$$

where A contains factors which should have identical values for the members of the series, a_s is the number of identical distances r_s between interaction centers for oxygen ions, and ρ is a constant which should be about 0.34×10^{-8} cm. The ratio of two critical temperatures is given by

$$T/T' = [\sum_s a_s e^{-r_s/\rho}]/[\sum_s a_s e^{-r_s'/\rho}],$$

in which the constant of proportionality in the expression for the critical temperature is also eliminated. If the disordered structure for $CaCO_3$ is more stable above 975°C, then with reasonable values for r_s and r_s' it has been calculated that $BaCO_3$ should disorder at a temperature about 400°C lower. The critical temperature

[18] Structurbericht, Band II, p. 73.

[19] M. Born and J. E. Mayer, Zeits. f. Physik **71**, 1 (1932).

for $SrCO_3$ should be intermediate. Since the only transition which has been observed in $BaCO_3$ below 975°C is the orthorhombic to hexagonal one at about 800°C, the above treatment predicts that the hexagonal form is disordered. A similar argument holds for the hexagonal form of $SrCO_3$.

A more detailed treatment of this simplest type of rotational disorder has not been given because this mechanism is probably not the correct one in the case of the carbonates. The analysis is of interest insofar as this simplest mechanism is a plausible one which may apply in some other cases, and it may serve to highlight the difficulties of more complicated situations.

L. A. Siegel (reference 13) has found in his x-ray study of $NaNO_3$ that the disordered configurations of the nitrate ion are the six orientations obtained by aligning oxygen ions with nearest metallic ions in the c_0 projection as shown in Fig. 6. It seems likely that the same mechanism holds for the carbonates. This type of disorder is not equivalent to that already discussed and in particular it is to be noted that in such a transition interactions of all types between ions change significantly. Thus it appears that in neither the alkali nitrates nor in the alkaline earth carbonates does there exist a transition of anion rotational disorder uncomplicated by further structural change.

Siegel pointed out that the type of disorder which he observed is more directly related to the aragonite structure so far as anion orientations are concerned. If the hexagonal forms of $BaCO_3$ and $SrCO_3$ are disordered in this way the transitions from the aragonite-type structure of these compounds are very logical. Consider a calcite-type structure but with anion orientations of the ordered aragonite type. Upon examining various possible arrangements it is found that, to obtain a stable configuration, either the cations or the anions or both must be displaced from their lattice points, i.e., the calcite structure cannot be stable. As a more exact solution of the problem nature provides the aragonite structure. But it is apparent that the calcite-type structure is stabilized by disordering these anion orientations of the aragonite type.

The above considerations lend a plausibility to the argument that the hexagonal forms of $BaCO_3$ and $SrCO_3$ have a disordered structure. A more convincing argument may be developed if it is assumed that $CaCO_3$ is disordered above 975°C according to the second mechanism. If this is a stable high temperature form for the calcite-type arrangement, then it should be stable at lower temperatures if oxygen-oxygen interactions are decreased, and this is accomplished by replacing calcium ions by the larger strontium or barium ions. A quantitative calculation will not be attempted. Such a calculation presumably requires a generalized Bragg-Williams-type theory which takes structural differences into account.

The argument that disorder, if it exists, is of the type described by Siegel may be supported by a consideration more specific than the general analogy between alkali nitrates and alkaline earth carbonates. Consider a carbonate ion rotated in the ordered hexagonal structure from the 0° position through 30° and 60°. In a static structure the 30° rotation results in large overlap between oxygen ions and nearest metal ions and the 60° rotation in large overlap between nearest oxygen ions. From data given in Table V for hexagonal $SrCO_3$ and $CaCO_3$ the outer radius of an oxygen ion is calculated to be about 1.35A. In $CaCO_3$ with a_0 equal to 4.96A this results in an oxygen to oxygen overlap of 0.36A in the 60° position. Estimating c_0 as 8.70A at 975°C results in an overlap between calcium and oxygen ions in the 30° position equal to about 0.34A. In the two cases the amount of overlapping is calculated to be approximately the same, but electrostatic interaction favors the 30° position and furthermore the "repulsive" interaction calculated with the Born-Mayer equation is a factor of 3 larger for doubly charged like ions than for doubly charged unlike ions, other factors being equal. According to this argument the 30° position has a significantly lower energy and therefore in the initial stages of disordering jumps to this alternative set of configurations with sixfold symmetry seem more likely.

Rotational Disorder in Cubic Structures

The transitions of $BaCO_3$ and NH_4NO_3 to cubic structures remain to be considered. It has been argued that anion-free rotation about all axes is improbable but it was pointed out that a cubic structure may result from an arrangement of these anions with planes perpendicular to the four trigonal axes (body diagonals) of a cube. In the case of $BaCO_3$ with the NaCl structure the projection along the trigonal axis of any anion so

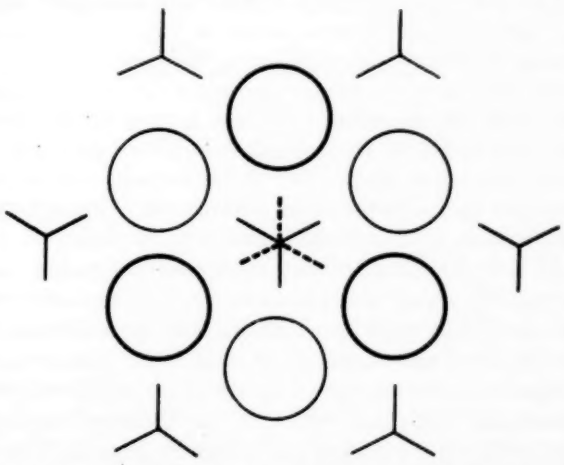

FIG. 6. Projection, along pseudotrigonal axis, of a carbonate ion and its nearest neighbors of both kinds in the aragonite structure. Light circles represent metal ions at the zero level and heavier circles metal ions at one-half. The three carbonate ions along the center line are at approximately one-third and those above and below at approximately one-sixth. The carbonate ions represented by the dashed lines are at approximately five-sixths and minus one-sixth.

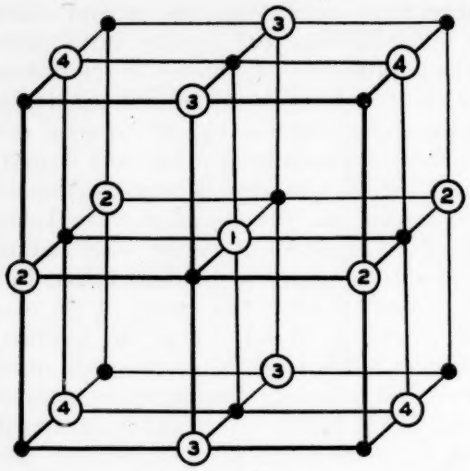

FIG. 7. Representation of a possible structure for cubic $BaCO_3$. Carbonate ions are indicated by the open circles and numbers refer to the four ways of orienting an ion with its plane perpendicular to a trigonal axis. This cell is ordered with respect to these orientations.

oriented on a Cl lattice point and of its nearest neighbor cations is identical with a similar projection for the hexagonal calcite-type structure. Such an ordered arrangement has, of course, less rotational order than the ordered hexagonal arrangement, but two additional types of disorder may exist. Disorder may arise in a manner similar to that described above for the hexagonal structure in which disordering was brought about by increased rotational activity of an anion in its plane, in which process six rotational configurations, probably of the aragonite type, become available; and disorder may also arise by rotations to wrong trigonal axes, that is, by rotations about axes lying in the planes of the ions.

Consider a likely ordered arrangement of a type which should result in the cubic NaCl structure. Such an arrangement is represented in Fig. 7. The open circles represent carbonate ions. The four orientations with the plane of the ion perpendicular to a trigonal axis may be distributed in any fashion on the four carbonate sites of an elementary cube but once this is done the requirement that the unit cubic cell be repeatable in space fixes the distribution. Note that no two nearest neighbors are identically oriented.

If one calculates minimum oxygen to oxygen and oxygen to metal ion distances for this arrangement, assuming only rotation about the axis perpendicular to the plane of anions, one finds that these distances are larger than the corresponding distances calculated for a disordered hexagonal structure and therefore one concludes that if the hexagonal phase is disordered with respect to rotation of an anion in its plane, according to the first or the second mechanism discussed above, then the cubic phase is also disordered with respect to the same rotational mode and probably according to the corresponding mechanism. One might argue that oxygen to oxygen interactions are so much smaller than in the hexagonal phase that an approach to completely free rotation may take place, but the amplitudes of rotational oscillations in directions perpendicular to the plane of an anion must be large, as is indicated by the transition to the cubic structure, and an adequate estimate of the various interactions must take this into account.

The cubic phase of $BaCO_3$ may be disordered with respect to the four orientations of anions on the body diagonals. Such a disordering process might appear as a separate transition and be characterized by an increase from one to four in the number of equivalent orientations of the axis of the ion.

Summary and Conclusion

Transitions in the solid state of both the first and the second kinds which are obviously due to increased rotational activity of an asymmetric ion are well known. In general the experimental evidence favors a theory of disordered configurations of rotational oscillation, and this theory is assumed *a priori*. The high temperature transitions of the alkaline earth carbonates apparently fall into this classification. No direct experimental evidence has been offered in proof of this argument. It is supported (1) by analogy with the behavior of alkali-nitrates, (2) by the evidence of increased rotational activity offered by the very large coefficients of thermal expansion in the direction perpendicular to the plane of the carbonate ion in both orthorhombic and hexagonal forms, (3) by the anomalous heat in $CaCO_3$ at 975°C, (4) by the existence of plausible mechanisms for rotational disorder which may be, in effect, first approximations to the rotational activity of the anions in these substances, and (5) by the transition of $BaCO_3$ to a cubic structure, which transition clearly implies an advance stage of rotational disorder.

For these reasons, and since no evidence for order exists, it has been argued that the hexagonal phases of both $BaCO_3$ and $SrCO_3$ and also of $CaCO_3$ above 975°C are disordered, the most likely mechanism being one in which the number of equivalent orientations obtained by rotation of a carbonate ion in its plane changes from three to six. These may be assigned in two different ways, and the more likely is that observed by Siegel in $NaNO_3$. It also seems probable that the cubic phase of $BaCO_3$ is disordered in the same sense, but cubic symmetry implies a rotation of the axis of the carbonate ion. The four body diagonals of a cube provide four preferred orientations for the axis of the ion. An ordered arrangement exists and also one of disorder in which case the configurations of rotational oscillation of an ion in this mode increase from one to four.

The configurations of rotational oscillation available to an asymmetric ion or molecule are an important property of transitions involving rotational disorder.

The transitions described above appear to be relatively simple from this point of view. In an extreme type of disorder the configurations may be uniformly distributed in space, but the most extreme case is one of free or nearly free rotation in space in which case configurations of rotational oscillation are no longer significant. It is doubtful that a precise determination of the rotational behavior of $BaCO_3$ or $SrCO_3$ can be made by means of x-ray diffraction studies if the transition forms are disordered.

THE JOURNAL OF CHEMICAL PHYSICS VOLUME 17, NUMBER 10 OCTOBER, 1949

Rotational Absorption Spectrum of HDO*

M. W. P. STRANDBERG
Research Laboratory of Electronics, Massachusetts Institute of Technology, Cambridge, Massachusetts
(Received December 13, 1948)

The 2_2-2_1, 3_0-3_1, $4_{-3}-3_1$, and the 5_0-5_1 rotational absorption transitions of HDO have been observed and identified on the basis of their Stark effect. By comparing the theoretical and experimental Stark shift, the dipole moment for all these transitions has been measured as $1.84\pm.01$. The effective HOD angle is also determined as $104°\pm30'$ and the parameter of asymmetry, κ, as about -0.696. The line breadth $\Delta\nu$ at one atmosphere is 0.38 ± 0.04 cm^{-1}. None of these quantities is in disagreement with independent determinations.

INTRODUCTION

THE intermediate heavy water molecule, HDO, has not been studied as fruitfully as have the H_2O and D_2O isotopic forms. The pure rotational spectrum of the intermediate molecule observed in the infra-red is, of course, hopelessly complicated by absorption due to the inevitable H_2O and D_2O impurities. However, King, Hainer, and Cross[1] (KHC) have reanalyzed existing vibration-rotation data and on the basis of a rigid rotor model have published a table of expected absorption frequencies in the microwave region.

One might expect that little could be said about the HDO molecule if these absorption frequencies were measured since, for example, centrifugal distortion of the energy levels would obscure any relation between the absorption frequencies and the molecular structure. It is inevitable that with a molecule as complicated as HDO, an asymmetric top, those rotational energy levels having magnitudes of several hundred wave numbers may not be calculated exactly from measured energy-level differences of the order of one wave number.

On the other hand, such measurements are of value in determining the usefulness of a rigid rotor analysis of infra-red data, and in supplementing infra-red data used in assigning term values. Stark effect measurements also provide additional structure data in the case of HDO, as we shall show below. A study of the absorption due to HDO in the microwave region can thus be of use, although application of the data is certainly more limited than in the case of a linear or a symmetric top molecule.

* This work has been supported in part by the Signal Corps, the Air Materiel Command and ONR.

[1] King, Hainer, and Cross, Phys. Rev. **71**, 433 (1947).

EXPERIMENTAL MEASUREMENTS

The sweep spectroscope and frequency standard used in these measurements have been described elsewhere.[2] Since KHC have pointed out that centrifugal distortion effects cancel out rather well in $\Delta J=0$ transitions, these transitions were first studied. The 5_0-5_1** line at 22307.67 Mc/sec has been reported by Townes and Merritt,[3] and by us.[4] To obtain a more accurate analysis the Stark effect for this transition was remeasured, and two other transitions, the 2_1-2_2 and the 3_0-3_1 were also measured at 10,278.99 Mc/sec and 50,236.90 Mc/sec, respectively. The Stark measurements on these lines enable positive identification to be made.

INTERPRETATION RESULTS

The theoretical Stark effect may be calculated for these transitions to compare with the observed perturbation. For perturbation energies ($\mu\cdot E$, where μ is the electric dipole moment, E is the electric field) much less than the energy difference between the asymmetric-top term values, the Stark effect is a second-order perturbation. The problem is one of calculating the quantum mechanical matrix elements of the direction cosines of the molecule-fixed axes to the space-fixed electric field axis. Induced polarization may generally be ignored as Golden and Wilson[5] have shown. Fortunately, necessary direction-cosine matrix elements have been tabu-

[2] Strandberg, Wentink, and Kyhl, Phys. Rev. **75**, 270 (1949).

** The $J\tau$ notation will be used. J is the total angular momentum quantum number, and τ is a running index over the energy levels within the given J group.

[3] C. H. Townes and F. R. Merritt, Phys. Rev. **70**, 558 (1946).

[4] Strandberg *et al.*, Phys. Rev. **73**, 188 (1948).

[5] S. Golden and E. B. Wilson, Jr., J. Chem. Phys. **16**, 669 (1948).

lated by CHK[6] in the form of line strengths, for various degrees of asymmetry of the molecule. They have also outlined a convenient method for calculating these matrix elements for any asymmetry. Some arithmetical juggling is necessary to recover the direction cosines themselves from the line strengths tabulated by CHK, since the line strengths are the sums of the squares of the direction-cosine matrix elements over the magnetic quantum numbers and the three space directions. The term values in the presence of an electric field are given by conventional perturbation theory[7, 8]

$$W_{J,\tau}=W^{(0)}{}_{J,\tau}+W^{(2)}{}_{J,\tau} \text{ ergs}, \tag{1a}$$

where $W^{(2)}{}_{J,\tau}$ is the second-order correction to the unperturbed energy $W^{(0)}{}_{J,\tau}$ and is calculated as

$$W^{(2)}{}_{J,\tau}=E^2\sum{}'_{J',\tau'}\frac{\mu_g{}^2|\Phi_{z,g}(J,\tau:J'\tau')|^2}{W^{(0)}{}_{J,\tau}-W^{(0)}{}_{J',\tau'}}R \text{ ergs}, \tag{1b}$$

where $|\Phi_{z,g}(J,\tau:J'\tau')|^2$ is the line strength for the transition $J,\tau\rightarrow J',\tau'$ for a field along the space-fixed axis, z, interacting with a dipole moment along the molecule-fixed axis, g; this quantity is given in the CHK tables; $\mu_g{}^2$ is the square of the component of the electric dipole moment along the molecule-fixed axis g;

$$R=\frac{M^2}{J^*(J^*+1)(2J^*+1)}, \quad |M|\leq J^*=J \text{ if } J=J'$$

or

$$R=\frac{J^{*2}-M^2}{J^*(4J^{*2}-1)}, \quad |M|\leq J^*-1 \text{ where } J^*=J \text{ if } J=J'+1$$
$$\text{or } J^*=J' \text{ if } J=J'-1$$

The primed summation indicates that the term J', $\tau'=J,\tau$ is omitted.

The paper of Golden and Wilson[5] gives an identical formulation of this solution in addition to a more general discussion of the problem for the case of degeneracy, a situation which has no bearing on the present problem.

The calculations themselves are straightforward. We have used three-point interpolation in the CHK tables for the line strengths. Three-place logarithmic interpolation was used for cases where the line strength varied rapidly with the asymmetry coefficient, κ. (κ is defined as $(2b-a-c)/(a-c)$ where a, b, and c are the maximum, intermediate, and minimum reciprocal moments of inertia.)

Interpolation seemed unsatisfactory for the line strength of the 5_0-5_1, and the $4_{-3}-3_1$ transitions, so we have calculated these two direction-cosine matrix elements exactly by using the method of CHK.[6] KHC have investigated interpolation errors in the paper[1] and the operation seems justified in the other cases.

[6] Cross, Hainer, and King, J. Chem. Phys. 12, 210 (1944).
[7] See reference 5.
[8] E. U. Condon and G. H. Shortley, *Theory of Atomic Spectra* (Cambridge University Press, London, 1935).

For HDO we have used $\kappa=-.685$, $(a-c)/2=8.495$ cm^{-1} and $(a+c)/2=14.88$ cm^{-1}, the latter two parameters being one-half the difference and the sum of the extreme reciprocal moments of HDO. These parameters were deduced from the KHC paper.[1] The term value differences $W^{(0)}{}_{J,\tau}-W^{(0)}{}_{J,\tau'}$ must be calculated by using a rigid rotor model with the above parameters. In general the most important term is the one with the smallest energy difference in the denominator, and this usually corresponds to the transition frequency measured in the microwave region. Since this energy difference is therefore known very accurately, the major term in the above summation is thus known to an accuracy limited only by the validity of the interpolation of the line strength. The other terms essentially form a small correction factor so that rigid rotor term values are sufficiently accurate for use in their denominator. Hence we do not calculate the rigid rotor Stark effect as given in the Golden and Wilson tables,[5] but the Stark effect based on rigid rotor wave functions and corrected for centrifugal distortion.

Trouble was encountered in calculating the 3_1 Stark perturbation for there are two near terms; one is the 3_0, the other is the 4_{-3} level. The 3_0-3_1 energy denominator is immediately calculated from the observed absorption frequency, but the $4_{-3}-3_1$ energy term is known rather inaccurately and is listed by KHC[1] as 1.13 cm^{-1}. We therefore brought into the calculations at this point a frequency ν_{34} to stand for the expected $4_{-3}-3_1$ absorption frequency, and carried the calculations through with this additional unknown. The other unknowns are the static dipole moment μ, and the angle δ between the dipole moment and the molecule-fixed principal axis of the intermediate moment of inertia. The resulting Stark shift in the 3_0-3_1 absorption may then be given in the form

$$\Delta\nu=\left(\frac{\mu E}{hc}\right)^2 10^4\left\{\sin^2\delta(A+BM^2)+\cos^2\delta\left[\frac{C(16-M^2)}{\nu_{34}}+D+FM^2\right]\right\} \text{Mc/sec.}, \tag{2}$$

where A, B, C, D, and F are constants calculable by the procedure outlined above, and E is the electric field in kilovolts/cm, h is Planck's constant and c is the speed of light.

The observed Stark shift was measured to have the form

$$\Delta\nu=(0.577+0.087M^2)E^2 \text{ Mc/sec.} \tag{3}$$

If the predicted ratio of the M-dependent and M-independent term in Eq. (2) is set equal to the observed ratio in Eq. (3), we obtain ν_{34} in terms of A, B, C, D, F, and δ. The angle is known approximately as 20° 30',[1] and to this approximation a value for ν_{34} may be calculated. This procedure was carried out roughly and gave a value of 20,000 Mc/sec or .67 cm^{-1} for this frequency,

TABLE I. Theoretical and experimental Stark shift.

2_1-2_2	$\Delta\nu_{\text{theor.}}=\left(\frac{\mu E}{hc}\right)^2\{\sin^2\delta(64.50M^2+.01506)+\cos^2\delta(.00709M^2+.2163)\}$
	$\Delta\nu_{\text{obs.}}=(.0545+2.36M^2)E^2$
3_0-3_1	$\Delta\nu_{\text{theor.}}=\left(\frac{\mu E}{hc}\right)^2\{\sin^2\delta(3.178M^2+.3052)+\cos^2\delta[(.1280+.2880\kappa)M^2-4.608\kappa-.987]\}$
	$\Delta\nu_{\text{obs.}}=(.577+.087M^2)E^2$
$4_{-3}-3_1$	$\Delta\nu_{\text{theor.}}=\left(\frac{\mu E}{hc}\right)^2\{\sin^2\delta(1.607M^2-.1461)+\cos^2\delta[(.2184+.5760\kappa)M^2-2.159-9.216\kappa]\}$
	$\Delta\nu_{\text{obs.}}=1.056E^2$
5_0-5_1	$\Delta\nu_{\text{theor.}}=\left(\frac{\mu E}{hc}\right)^2\{\sin^2\delta(2.636M^2+.0135)+\cos^2\delta(.00621M^2-.1093)\}$
	$\Delta\nu_{\text{obs.}}=(-.027+.0950M^2)E^2$

$\Delta\nu$ in Mc/sec.
μ is the electric dipole moment in e.s.u. cm
h is Planck's constant in erg sec.
c is speed of light in cm/sec.
E is field strength in kilovolts/cm
M is the magnetic quantum number
κ is the parameter of asymmetry.

instead of 34,000 Mc/sec or 1.13 cm^{-1} as predicted by the rigid rotor approximation. The only absorption in water mixtures which we have found in this region is one at 20,460.40 Mc/sec.

It was then evident that the calculation should be carried out with ν_{34} taken as 20,460.40 Mc/sec; and that the theoretical Stark pattern for the 20,460.40 Mc/sec absorption should be computed on the basis of its being a $4_{-3}-3_1$ transition to check this identification with the observed Stark pattern.

The observed Stark splitting was so good even with an estimated value for δ that we assumed the 20,460.40 Mc/sec to be due to the $4_{-3}-3_1$ transition in HDO.

We may now look at the complete picture on the basis of this tentative identification to expose any inconsistencies. Since the rigid rotor predicted frequencies are so close to the observed frequencies for $\Delta J=0$ transition, it may be assumed that centrifugal distortion in the two levels involved in each case is approximately the same. In any case, for an approximation using rigid rotor wave functions both levels must be described geometrically by the single angle parameter δ, which we shall call δ_J. Since we have four J states involved, in the transitions, $J=2\rightarrow2$, $3\rightarrow3$, $3\rightarrow4$, and $5\rightarrow5$, there are only four values of δ_J which need be carried throughout the calculations. It must be remembered that from this point of view δ_J is essentially only a parameter which may or may not be related simply to a physical angle in the molecule, but it is the "effective" value of this angle for the transitions $J=2\rightarrow2$, $3\rightarrow3$, $3\rightarrow4$, $5\rightarrow5$, etc.

To be entirely consistent the direction-cosine matrix elements will vary with δ, since they are a function of κ alone and it may be shown that in HDO

$$d\kappa\cong-.0043d\delta_J$$

with $d\delta_J$ in degrees. For a variation of δ by one degree, κ will change by .6 percent and for all matrix elements except for the $4_{-3}-3_1$ term the corresponding change in the matrix elements will be no more than one-fifth of this, or about 0.1 percent. Only the $4_{-3}-3_1$ matrix element was therefore entered explicitly into the calculation as

$$|\Phi_{xy}|^2=(-.4954-.1158)(16-M^2);$$

this expression is in error by .3 percent at $\kappa=-.8$, and $-.6$ with no error at $\kappa=-.7$.

The theoretical Stark effect may then be written as in Table I. The experimentally observed Stark shifts are also listed in Table I. By imposing the condition that the ratio of the M-dependent to M-independent coefficients in both the observed and calculated Stark formulae be equal, δ_2 and δ_5 may be determined uniquely. With values of δ so determined, the dipole moment may be obtained by using the condition that both the observed and calculated Stark formulae have the same magnitude. The μ's and δ's so determined are listed in Table II.

The 3_0-3_1 and $4_{-3}-3_1$ transitions must be handled differently since κ, δ, and μ enter explicitly into the Stark effect of these two transitions. The situation is under-determined, and so no explicit values for those parameters may be obtained. It would naturally be desirable to have κ_J and δ_J for these two transitions turn out to be identical since the 3_1 term participates in both. However, as we have indicated above, δ_J must be considered only a parameter, or an effective angle in a rigid-rotor Stark-effect calculation. Also it would be well to have μ close to the value determined from the $J=2$ and $J=5$ transitions. Knowing the desired solutions then, one particular solution is: $\mu_{33}=1.85$, $\mu_{34}=1.83$, $\delta_{33}=19°\,50'$, and $\kappa=-.696$. This solution seems satisfactory from a physical point of view, and no further discussion of data reduction need be given.

Incidental to the observation on the 3_0-3_1 HDO absorption we have also measured the half-line breadth at half intensity, $\Delta\nu$, as .010±.001 cm^{-1} at 20 mm pressure. This extrapolates to a line breadth at one atmos-

TABLE II. Deduced molecular parameters.

	μ	δ
2_1-2_2	1.84±1%	20° 57′±1%
3_0-3_1*	1.85	19° 50′
$4_{-3}-3_1$*	1.83	19° 50′
5_0-5_1	1.83±2%	20° 44′±2%

* For $\kappa=-.696$.

phere of .38±.04 cm^{-1}. Townes and Merritt[3] have published a value of .27±.05 cm^{-1} for the 5_0-5_1 line breadth extrapolated to one atmosphere pressure. The two measurements agree rather well.

SUMMARY

For four different transitions of low J the static dipole moment of HDO is seen to be a constant 1.84±.01. Centrifugal distortion makes no radical change in the electric moment between the $J=2$ to $J=5$ states. The angle between the moment of inertia ellipsoid and the symmetry axis δ apparently undergoes no radical change, and may be determined as 20° 30′±30′; the value of the HOD angle is then 104°±30′. The value of δ is in good agreement with the determination of this angle from the rigid rotor parameters as given by KHC.[1] Further, the asymmetry parameter may be shown to be about −.696 from the Stark data. This value of κ is also in agreement with the KHC determination. It should be noted that though a value of κ had to be known before the Stark data could be reduced, this value needed to be known only roughly. It might be best to say that Stark effect observations are capable of giving information on molecular structure which at least checks otherwise determined knowledge, and beyond that it gives information for a particular pair of rotational states instead of an average value over a number of rotational states. It may be seen from the above identification of the $4_{-3}-3_1$ transition that the Stark effect is also a very useful tool to aid in assigning transition term values.[9]

We have previously published similar observations on the Stark effect for the $5_{-1}-6_{-5}$ transition in H_2O.[10] In this case the dipole moment proved to be about 5 percent higher than 1.84 debye, the measured result for HDO. A value of 1.84 debye is generally given for the dipole moment of H_2O and D_2O as measured from the temperature dependence of the polarization.[11] It has been pointed out to us by E. B. Wilson, Jr. that the dipole moment is of interest to correlate experimental and theoretical studies of the line shape and intensity in this transition.

Van Vleck[12] has shown that if a value of the dipole moment of 1.84 debye is used and the line breadth parameter is adjusted to fit the observed line shape, the calculated peak absorption for the $5_{-1}-6_{-5}$ absorption in H_2O is low by about 20 percent. If the moment observed in microwave Stark measurement for this transition is used, the discrepancy is reduced to 10 percent and the agreement of theory with experiment is markedly enhanced. Van Vleck mentions other effects which could also contribute to this discrepancy, so that for the present one can only say that these absorption studies are not in disagreement with the high dipole moment determined from the Stark effect.

ACKNOWLEDGMENT

The author is grateful for the assistance of J. G. Ingersoll, T. Wentink, and R. Hillger in taking the experimental data upon which this paper depends.

[9] For similar use of the Stark effect for transition identification in SO_2, see Dailey, Golden, and Wilson, Phys. Rev. **72**, 871 (1947). Previously the author has suggested (Phys. Rev. **74**, 1245 (1948)) that the 20,460.40 Mc/sec absorption might be due to D_2O. The argument, though not incorrect, is not so conclusive as the interlocking evidence presented here to assign it to the $4_{-3}-3_1$ transition in HDO.

[10] Golden, Wentink, Hillger, and Strandberg, Phys. Rev. **73**, 92 (1948).

[11] See, for instance, Technical Report II, "Tables of Dipole Moments," Laboratory for Insulation Research, M.I.T.

[12] J. H. Van Vleck, Phys. Rev. **71**, 425 (1947).

Triplet-Singlet Transitions in Organic Molecules. Lifetime Measurements of the Triplet State*

DONALD S. MCCLURE
Department of Chemistry, University of California, Berkeley, California
(Received December 20, 1948)

The emission lifetimes of the metastable triplet states (phosphorescent states) of a large variety of organic molecules have been measured. The lifetimes are in the range from 10^{-4} to about 10 seconds. It is shown that the transition probabilities corresponding to the shorter lifetimes are of the same magnitude as found in the light atoms of which the molecule is composed. The longer lifetimes, on the order of seconds, are found only among the aromatic compounds. A consideration of the perturbing singlet states in aromatic compounds shows that the matrix elements for the intercombination must be very much smaller than those responsible for the intercombination in the free carbon atoms. Direct evidence that the long-lived states of the aromatic compounds are triplet states is obtained by showing that as the atomic number of chemically similar substituents is increased (e.g. substitute Br for Cl), the transition probability increases approximately in proportion to the increase in the square of the spin-orbit interaction energy of the substituent atom. The luminescences are usually observable only when the substance is dissolved in a rigid solvent, and the effect of such a solvent on the lifetimes is discussed. Experimental data relating singlet-triplet absorption strength to triplet state lifetime is presented.

THE work of Lewis and Kasha[1,2] has brought to the attention of spectroscopists the possibility of studying the triplet states of complex molecules. Before their work, very little was known about such states, and no systematic investigation of them had been attempted. It was known, however, that in rigid media, many organic compounds containing multiple bonds, notably the aromatic compounds, have two emission bands, contrary to the usual opinion that only a fluorescence band should exist. The second band was always found at greater wave-lengths and had a greater lifetime; in some cases many seconds, in contrast to the fluorescence lifetime which are usually between 10^{-6} and 10^{-8} second. Lewis and Kasha interpreted these long-lived, lower energy states as the metastable triplet states of the molecules where they were found. They also interpreted the extremely weak absorption bands of many substances as being due to singlet-triplet absorptions, and found many new examples both of weak absorption bands and of luminescences in rigid media. A considerable amount of indirect evidence supported the contentions of these workers, but it was not until Lewis and Calvin[3] measured the paramagnetism of fluorescein in its metastable (2.5-second lifetime) state, that direct evidence of a triplet state was obtained. This, and the later work of Lewis, Calvin and Kasha[4] on the same molecule, proved that there are two unpaired electrons per excited molecule when fluorescein is in its metastable electronic state.

Both the existence and the method of study of metastable triplet states were established by the work just outlined. The study of the other triplet states of the term manifold could be undertaken if sufficiently high concentrations of metastable molecules were obtainable. This is possible in many cases. In the present paper, we shall deal only with the lowest triplet state, and shall be primarily concerned with its lifetime.

A low lying metastable triplet state can be present in any molecule having a multiple bond (possibly also in some others, although we shall not deal with them). The type of multiple bond will serve for the purposes of this paper as a broad classification of organic molecules. The experimental results of the lifetime measurements made on several of these classes of molecules are presented in this paper. Direct evidence that the metastable states are triplet states is found on interpreting these results. The lifetimes are qualitatively explained by comparison with intercombination processes in atomic systems, and by approximate calculations. It is also shown that the aromatic compounds have anomalously long-lived states. Selection rules for intercombinations in polyatomic molecules have recently been given.[5] Further theoretical work on the subject is planned.

I. EXPERIMENTAL

Lifetimes were measured with a mechanical phosphoroscope consisting of a pair of half-sectors mounted on a common shaft in such a way that during half a revolution of the shaft, the sample was exposed to the exciting light, and during the other half-revolution, the exciting light was shut off and a detector observed the after-glow. The detector was a photo-multiplier tube, the anode resistor of which was connected directly across the vertical plates of a cathode-ray tube. For lifetime measurements between 3×10^{-4} sec. and 0.03 sec., a synchronous motor turned the phosphoroscope disks at 30 r.p.s. while the oscilloscope sweep was exactly 60 c.p.s. Thus a decay curve and a zero intensity base line appeared on the screen for each revolution of the phosphoroscope. A disk with 20 narrow equally

* Presented before the Symposium on Molecular Structure and Spectroscopy at the Ohio State University, June 1948.
[1] G. N. Lewis and M. Kasha, J. Am. Chem. Soc. **66**, 2100 (1944).
[2] G. N. Lewis and M. Kasha, J. Am. Chem. Soc. **67**, 994 (1945).
[3] G. N. Lewis and M. Calvin, J. Am. Chem. Soc. **67**, 1232 (1945).
[4] G. N. Lewis, M. Calvin, and M. Kasha, J. Chem. Phys. (to be published).
[5] D. S. McClure, J. Chem. Phys. **17**, 665 (1949).

TABLE I. Comparison of lifetimes in polar and non-polar rigid solvents.*

	Polar	Non-polar
P-dibromo benzene	0.00030±3 sec.	0.00033±3 sec.
β-iodo naphthalene	0.0025±1 sec.	0.0024±1 sec.
P-dichloro benzene	0.016±1 sec.	0.017±1 sec.
O-dichloro benzene	0.018±1 sec.	0.018±1 sec.
α-fluoro naphthalene	2.13±10 sec.	1.99±10 sec.

* Non-polar solvent: 4 parts methyl cyclohexane, 1 part isopentane. Polar solvent: 5 parts ether, 5 parts isopentane, 2 parts alcohol (E.P.A.). These solvents form clear rigid glasses at 77°K.

spaced notches was mounted on the motor shaft so that the notches on its periphery reduced the flux between the poles of a small electromagnet every 1/20 revolution. This supplied timing markers for the oscilloscope screen. The decay curve and timing marks were photographed and analyzed. An adaptation of this method enabled measurements to be made in the region 0.03–0.3 sec., but few substances fell in this range. For lifetimes of 0.2 sec. or greater a repeated decay pattern was not necessary, and as the resolving time was no problem, the disks were manually turned from the illuminating position to the observation position. The 1 and 5 sec. sweeps for this range were obtained from mechanically operated potentiometers. Calibrating markers were obtained from a pulse generator connected both to the oscilloscope and to a counter. The pulse generator was calibrated by measuring the time for 100 counts. The calibration did not vary more than one percent over periods of several weeks.

The vertical deflections on the oscilloscope screen were proved to be sufficiently linear by calibration with a point light source, using the inverse square law to determine accurately the relative intensities of light falling on the photo-multiplier tube.

The resolving time of the phosphoroscope was 10^{-4} sec. at the narrowest slit widths used, so the shortest lifetimes measured were somewhat greater than this. The errors were no greater than 10 percent for all ranges. Probable errors are given with each measurement where the number given is *the error in the last decimal place.* The lifetime values that are given in this paper are mean lifetimes, i.e.,

$$\tau=\frac{t_2-t_1}{2.31\times\log I_1/I_2}.$$

The substances studied were in a rigid glassy solution at liquid nitrogen temperature. A small quartz Dewar and a quartz sample tube allowed exciting light of wave-lengths up to the transmission limit of the solvent to enter the sample tube. The use of rigid solutions is discussed by Lewis and Kasha.[1] The light source was a commercial carbon arc having high ultraviolet emission. A water cell and various filters were used to select the radiation desired for a particular sample.

II. THE USE OF RIGID MEDIA

The use of a rigid medium requires some discussion because we want to assume that the measured molecular lifetimes bear some relation to the natural lifetimes of the molecular states.

In the first place, it is necessary to have the substance immersed in a dense phase of some type, as otherwise it would be very difficult to observe the emission from the triplet state. The reasons are as follows. The direct excitation to the triplet state is such a slow process that one cannot in this way build up sufficient emission intensities as to be easily observable. It is therefore necessary to excite the molecule to its upper singlet states and to rely on the process of radiationless internal conversion to carry molecules into the triplet state. By far the greatest fraction of this process takes place when the molecules are in their lowest excited singlet state, before they radiate. Some type of perturbation causes this singlet to become mixed with the metastable triplet, so that for a part of the time, the molecule is in the lowest singlet, and for the other part of the time, it is in an isoenergetic vibrational level of the metastable triplet. If the molecule is isolated, the numbers emitting from the two states will be proportional to the rate of radiation from the two states. Therefore, practically all of the radiation comes from the singlet, because the radiation rate from this state is some 10^5 times greater than from the triplet (see Section III). On the other hand, if the molecule can lose to its surroundings the vibrational energy it has when in the vibrationally excited triplet, it will go without radiation to the lowest vibrational levels of the metastable triplet. Barring collisional deactivation of the triplet molecules, the relative numbers emitting from the two states will then be proportional to the number in the two states. Since this ratio may be on the order of unity (see, e.g., Table VI), a large amount of triplet radiation may be observed. The excess vibrational energy of the triplet state must therefore be removed by collisions, and therefore the molecule must be in a sufficiently dense phase in order for the phosphorescence of the organic molecule to be observable.

Once a large number of molecules have reached the low lying vibrational levels of the triplet state through the action of the medium, the same medium must be such as not to remove additional energy from the molecule and send it without radiating to the ground state. If an appreciable fraction of the process of going to the ground state is by thermal deactivation, the measured lifetimes will not be the natural ones. In order for thermal deactivation to occur, electronic energy of the excited molecules must be converted into kinetic energy of the surrounding molecules. As is well known, this is a relatively inefficient process compared to the removal of vibrational energy from the same molecule. The momentum transfer from an electron to a molecule is inefficient because of the large mass difference. Never-

theless, the high collision rate in a liquid overcomes this and we usually find that complete thermal deactivation of the triplet state occurs in liquids. If we gradually cool a liquid containing an organic phosphor, the luminescence increases in intensity as the viscosity of the liquid increases. If there is no thermal quenching in the solid state, both the intensity and lifetime of the luminescence should be constant with temperature. No quantum yield measurements have been completed as yet, but there are some data on the temperature independence of the lifetime. Lewis, Lipkin, and Magel[6] showed that the lifetime of the metastable state of fluorescein is the same at 77°K as it is at 20°K. (All of the lifetimes to be reported in this paper are measured in a rigid glass at 77°K.) It therefore seems likely that the rigid glass may be a medium which can remove vibrational energy from a molecule, but cannot remove electronic energy.

Another fact which indicates that collisional deactivation does not alter triplet state lifetimes is that the decay curves are exponential. This does not prove a complete lack of collisional processes, but if as little as 10 percent of the decay process were a second order thermal deactivation process, this could have been detected as a deviation from the exponential decay law. The deviations from the exponential decay law actually observed were always traced to the presence of impurities, and indeed, the exponential form became one of the criteria of purity. The decay curves were observed over a period of one or two lifetimes.

Collision processes are not the only ones which can affect the lifetimes. Dispersion forces, induced polarization forces and dipole-dipole forces also come into play. Not enough work has been done as yet to estimate accurately the effects of these forces. Table I shows that the lifetimes of a few aromatic halogen compounds are the same in a polar as in a non-polar rigid solvent. This shows that the polarization forces are not very important. Dispersion forces are usually of greater importance in molecules having multiple bonds than are polarization forces. For a molecule in a metastable triplet state, only the higher triplet states of the molecule enter into the calculation of the dispersion force. These are probably closer to the metastable triplet state than the perturbing singlets are to the ground state, so the dispersion forces should be greater in the metastable state than in the ground state. But the mixing in of these higher triplet states should not cause much change in the intercombination probability.

There is one substance, biacetyl, whose triplet state lifetime has been measured in both the vapor phase and in a rigid glass. The emission lifetime of the vapor has been reported[7] as 1.65×10^{-3}, and 1.40×10^{-3} sec., while the author obtained 1.30×10^{-3} sec. The lifetime is temperature dependent at high temperatures, probably because of thermal activation to a state from which transitions to the ground state are more rapid than from the triplet state. The lifetime is reported to be about 0.8×10^{-3} sec. at 338°K.[8] The lifetime measured in a rigid solvent (E.P.A., see note to Table I), at 77°K is 2.25×10^{-3} sec. Probably a large part of the increase over the vapor phase measurement is attributable to the temperature effect, so that any solvent effect would increase the lifetime by only 20 or 30 percent. This example shows that none of the factors mentioned have an important effect on the lifetime of the luminescence of this substance.

For all the reasons just discussed, we may conclude that it is very unlikely that lifetimes of metastable states are changed by as much as a factor of two when the molecule is embedded in a rigid medium. Absolute quantum yield measurements in progress at this laboratory will be the best experimental evidence showing whether or not this conclusion was really justified. Throughout the remainder of this paper, it will be assumed that the measured molecular lifetimes are the same as the true molecular lifetimes.

III. ESTIMATION OF TRANSITION PROBABILITIES

Triplet-singlet transitions occur because the spin-orbit interaction (or other spin and orbital dependent forces) mixes certain singlet states with the triplet state. The square of the amount of singlet character in the triplet state is proportional to the probability of the intercombination transition. The result of a first-order perturbation calculation of the intercombination probability in an atom or molecule is

$$\frac{1}{\tau_{3n}}=P_{3n}=P_{1n}\left(\frac{H_{13}}{\Delta E}\right)^2\left(\frac{\nu_3}{\nu_1}\right)^3 \qquad (1)$$

where the contribution from only one perturbing state is being considered. P_{1n} is the transition probability between the perturbing singlet and the normal state. ν_1 and ν_3 are the frequencies for transitions between the normal state and the perturbing singlet and between the normal state and the triplet. ΔE is the energy difference between the triplet and the perturbing singlet. The quantity H_{13} is the matrix element of the spin-orbit operator between the triplet and the perturbing singlet. In atoms this consists of a radial part, ζ, and an angular part, and is dependent on the configuration of the atom. $\zeta/\Delta E$ is approximately the first-order correction to the wave function in the perturbation calculation applied to the atom when the angular part is considered to be close to unity. The values of ζ are known for most of the atoms, as they are derivable from atomic spectra. It is much more difficult to determine the values of H_{13} for molecules, and this will not be attempted in the present paper. For the approximate

[6] G. N. Lewis, D. Lipkin, and T. Magel, J. Am. Chem. Soc. **63**, 3005 (1941).

[7] G. M. Almy and S. Anderson, J. Chem. Phys. **8**, 805 (1940); R. D. Rawcliff, Rev. Sci. Inst. **13**, 414 (1942).

[8] G. M. Almy and P. R. Gillette, J. Chem. Phys. **11**, 188 (1943).

TABLE II. Effects of heavy atom substituents on phosphorescence lifetime and spectra of naphthalene derivatives, and comparison with spectra and strength of ordinary absorption bands.

(a) Triplet-singlet emission band

Substituent	α-isomer ζ cm^{-1}	ν_P cm^{-1}	τ (sec.)	$10^{-5}\tau\zeta^2$	β-isomer ν_P cm^{-1}	τ (sec.)	$10^{-5}\tau\zeta^2$
F	272	20,970*	1.5±1	1.11	—	—	—
Cl	587	20,700	0.30±4	1.03	21,000	0.47±4	1.62
Br	2460	20,700	0.018±2	1.10	21,100	0.021±1	1.29
I	5060	19,000*	0.0025±1	0.64	21,040	0.0025±1	0.64
OH**	152				21,100	1.30±5	0.30
SH	382				20,800	0.28±1	0.41
H	—	21,300	2.6±2	—	—	—	—

(b) Singlet-singlet absorption bands*** (β-halogen naphthalenes only)

Substituent	$\tilde{\nu}_1$ cm^{-1}	f_1	$\tilde{\nu}_2$ cm^{-1}	f_2	$\tilde{\nu}_3$ cm^{-1}	f_3
H	31,200	0.0010	35,000	0.214	45,300	1.1
Cl	31,080	0.0037	34,620	0.112	44,000	1.4
Br	31,050	0.0039	34,600	0.127	43,900	1.4
I	30,900	0.0026	34,300	0.145	41,100	1.4

* These values from the work of R. V. Nauman, thesis, University of California, 1947. All others from Lewis and Kasha, J. Am. Chem. Soc. 66, 2100 (1944). The highest frequency of the emission band is given.

** The OH compound is to be compared with the SH but not with the halogen compounds.

*** There are three regions of absorption in the near ultraviolet which probably correspond to three electronic transitions. The *average* frequencies of these regions are designated in the table as $\tilde{\nu}_1$, $\tilde{\nu}_2$, $\tilde{\nu}_3$. In the case of the first band, a correction must be made for the overlapping of the second, and in the case of the third, the band is partly beyond the ordinary range of solution spectra work and the integration is somewhat inaccurate.

TABLE III. Effects of heavy atom substituents on spectra of benzene derivatives.

(a) Tetraphenyl group IV compounds

Element	Triplet-singlet emission band ζ	ν_P cm^{-1}	τ (sec.)	$10^{-3}\tau\zeta^2$	Near ultraviolet absorption band $\tilde{\nu}_a$ cm^{-1}	f
C*	(28)	28,500	5.4±2	4	38,800	0.015
Si	142	28,200	1.24±5	25	38,100	0.015
Sn	2097	28,400	0.0030±2	14	38,900	0.015
Pb**	7294	23,900	0.010±1	530	>38,500	0.028

(b) Triphenyl group V compounds

Element	ζ	ν_P cm^{-1}	τ (sec.)	$10^{-3}\tau\zeta^2$	$\tilde{\nu}_a$ cm^{-1}	f
N	(70)	25,500	0.49±4	2.5	33,300	0.57
P	(231)	25,200	0.014±2	0.8	38,000	0.30
As	1500	25,500	0.0016±3	3.6	40,000	0.33

(c) Halogen derivatives

Element	ζ	ν_P cm^{-1}	τ (sec.)	$10^{-3}\tau\zeta^2$	$\tilde{\nu}_a$ cm^{-1}	f
F	272	Too weak to measure			39,120	0.00816
Cl	587		0.004±1	1.4	38,540	0.00284
Br	2460		(0.0001)***	0.7	38,100	0.00249
I	5060				38,580	0.0134
H	28	29,400	7.0±5		40,100	0.00147

* Triphenyl methane was used.

** The Pb compound is out of line not only because of the relatively long lifetime but also because of the position of the triplet level and the f of the lowest singlet-singlet transition. There is no adequate explanation as yet.

*** This value was obtained by extrapolating from a number of chloro and bromo compounds whose luminescence lifetimes were measurable. The data of Table IV were used.

determination of intercombination transition probabilities in molecules, it is often accurate enough to use the ζ-value of the atoms of which the molecule is composed. The angular part of the atomic matrix element will be sufficiently close to unity for this purpose. Since ζ is approximately a radial integral over $1/r^3$ for the triplet state of the atom, its main contributions come from near the nucleus. We therefore expect that the ζ-value for the heaviest atom in the excited system of the molecule will be a reasonable approximation to the H_{13} value for the molecule.

Without at first going into great detail, one can make some rough estimates, based merely on the types of atoms appearing in the molecule. The values of ζ can be found for most atoms in Condon and Shortley[9] but because of configuration interactions, the ζ-values for some of the first and second period atoms cannot be given. Reasonable values to use in Eq. (1) were obtained, however, by extrapolating from nearby atoms of the periodic table, using the fact that the ζ-values vary with the fourth power of the effective atomic number. These estimated values are enclosed in parentheses in the tables in which they appear (Tables II and III). Using these values of ζ and taking $\Delta E = 10{,}000$ cm^{-1}, $P_{1n} = 10^8$ sec.$^{-1}$, and $(\nu_1/\nu_3)^3 = \frac{1}{2}$, we can give the following estimates of triplet state lifetimes of molecules containing various types of atoms: carbon—0.003 sec.; nitrogen—0.0004 sec.; oxygen—0.0001 sec. In organic molecules containing several different atoms, the heaviest one in the excited system would be expected to have the dominant effect on the lifetime.

One could make more refined estimates for a particular organic compound if enough were known about the perturbing states. Unfortunately, it is not easy to decide which ones they are. This has been done, however, for two classes of compounds. In the following sections on the aliphatic ketones and on the aromatic hydrocarbons, a comparison of estimated and measured lifetimes will be made after it is shown which states of the term manifold of the molecule perturb the metastable triplet. It will be seen that the lifetimes of the aliphatic ketones agree with the estimated ones, and that indeed most lifetimes can be estimated by this simple procedure, but that the lifetimes of the aromatic compounds cannot be estimated in this way. Before further discussing the estimation of lifetimes, we shall bring up an important consequence of Eq. (1).

IV. THE EFFECT OF HEAVY ATOM SUBSTITUENTS ON LIFETIMES

Direct verification that the long lifetime of the metastable state of fluorescein is due to its multiplicity of three came from the measurements of the paramagnetism of the metastable state.[3,4] Nearly as direct evidence for the triplet state hypothesis has been obtained for a variety of other molecules by simply studying the effect of heavy atom substituents on the lifetimes.

[9] E. U. Condon and G. H. Shortley, *Theory of Atomic Spectra* (Cambridge University Press, London, 1935).

The spin-orbit interaction energy increases very rapidly with atomic number, and in heavy atoms it becomes greater than the electrostatic energy, which stays approximately constant as the atomic number increases. At the same time, the intercombination probabilities increase. The electron coupling gradually changes from $L\cdot S$ to $j\cdot j$. These effects of increasing atomic number should be observable in molecular intercombinations. In fact, if such effects are found in a group of molecules differing only in the atomic number of an atom not directly in the excited system of the molecule, it may be inferred that the transitions so affected are singlet-triplet transitions. The molecules chosen for study were aromatic nuclei with various heavy atoms attached. For example, the halogen naphthalenes, Table II, and the $(\phi)_nX$ compounds, Table III, where ϕ=phenyl, X is some element in main groups IV to VII, and n is the smallest valence of X. In Tables II and III, it is seen that on replacing the heavy atom, X, by the next heavier one, neither the position nor the intensity of the singlet-singlet bands or the position of the triplet level are greatly altered, but the lifetime of the triplet state is markedly decreased. Thus all the factors on the right side of Eq. (1) except ζ remain approximately constant, and one would expect the relation

$$\tau_a/\tau_b=(\zeta_b/\zeta_a)^2 \qquad (2)$$

to be approximately obeyed. This is equivalent to saying that $\tau\zeta^2$ is constant throughout a series of similar compounds such as the halogen naphthalenes. The tables show that this relationship is obeyed rather well by the naphthalenes, and not quite as well by the $(\phi)_nX$ compounds. Some further examples which support the validity of (2) are: diphenylene oxide $\tau\zeta^2=1.3\times10^{-5}$ and the corresponding selenide, $\tau\zeta^2=1.7\times10^{-5}$; the $\tau\zeta^2\times10^4$ values for the p-halogen acetophenones are: chloro, 1.4; bromo, 4.0; iodo, 2.3. The fact that (2) is approximately obeyed is good evidence that spin-dependent forces are responsible for the transitions. We can infer from the similarity to the spectra of the unsubstituted compounds that the corresponding transitions in them are also intercombinations and thus the phosphorescence of benzene and naphthalene are established as intercombination transitions.

Another type of comparison illustrating the atomic number effect is shown in Table IV. The lifetime ratios should be about the same for compounds of differing structure. The actual lifetime ratios are fairly constant, but about twice the ratio to be expected from the simple theory.

One must recognize the limitations of the treatment which has been given. The values of ζ depend on the electron configuration in the atom. We have used the value of ζ corresponding to the lowest lying configuration of the atom; which may or may not be a good approximation to the true matrix element for the molecule. Nevertheless, the extent of the agreement is remarkable in view of the simplicity of the assumptions. In later more exact work, atomic and molecular orbital calculations may be found to improve the agreement. We are justified at this stage in drawing the important conclusion that the atomic number effect described constitutes good evidence that spin dependent forces are responsible for the electronic transitions we observe as phosphorescence in organic molecules.

TABLE IV. The atomic number effect in the polyhalogen benzenes. Lifetimes are given in seconds.

X	p-di-X	1,3,5 tri-X	1,2,4,5 tetra-X	$\left(\frac{\zeta_{Br}}{\zeta_{Cl}}\right)^2$
Cl	0.016	0.022	0.018	
Br	0.0003	0.00074	0.00055	
Ratio	53	30	33	17.5

V. ALIPHATIC KETONES

It was stated at the end of Section III that the most important perturbing state in the aliphatic ketones could be located with some certainty, and that the measured lifetimes compared favorably with those calculated using Eq. (1) and the atomic ζ-value for oxygen. We have not proved that the emission of long duration (about 0.001 sec.) is due to a triplet-singlet transition, but in view of the long lifetime, no other type of transition seems possible. An attempt to study the atomic number effect in the α- and α-γ-halogen acetones was made, but the bromo- and iodo-compounds had metastable state lifetimes which were too short for the present apparatus to measure. It will be assumed in the remainder of this paper that the metastable state is a triplet state.

The identification of the principal perturbing singlet state is based on a study of the behavior of the ketones toward methyl substitution in the α- and γ-positions. In Table V, the f values for the transitions of interest in the methyl substituted acetones are presented.[10] The f of the 35,000 cm^{-1} transition is practically unaffected by methyl substitution while that of the metastable state is markedly decreased. The f values of the 51,000 cm^{-1} transition[11] parallel those of the metastable state very closely. The ratios shown in the last column are roughly constant. The f values of the 60,000 cm^{-1} transition[11] increase as methyl substitution proceeds.

The fact that the f-number of the triplet-singlet transition varies with methyl substitution in the same way as the 51,000 cm^{-1} transition, is evidence that the latter is the principal perturbing state. The lifetime of

[10] The f value for the triplet level is determined from the experimental lifetime and from $f=1.50/\nu^2\tau$, with ν in cm^{-1} and τ in sec. The average frequency of the emission band for all the compounds was nearly the same and equal to 23,000 cm^{-1}. Undoubtedly a modification of this formula should be used here, but the values given are at least proportional to the correct ones. See Section IX.

[11] R. S. Holdsworth and A. B. F. Duncan, Chem. Rev. 41, 311 (1947).

TABLE V. Lifetimes of carbonyl luminescences and comparison of f numbers of singlet states with f numbers of triplet states.

Ketone	$\tau \times 10^3$ sec.	$f(ST)$ $\times 10^6$	f(35,000 cm^{-1}) $\times 10^4$	f(51,000 cm^{-1}) $\times 10^2$	Ratio $\frac{f(ST)}{f(51{,}000)}$ $\times 10^4$
Di-methyl	0.6	4.7	4.54	2.0	2.4
Methyl-ethyl	0.85	3.33	5.82	1.8	1.9
Di-ethyl	1.26	2.25	4.50	0.77	2.9
Methyl isopropyl	1.7	1.6	5.14	0.95	1.7
Di-isopropyl	3.77	0.75	6.86	0.18	4.2
Di-t-butyl	8.6	0.33	6.30	0.16	2.1

TABLE VI. Triplet state lifetimes of polynuclear hydrocarbons.

	Symmetry group	Max ν of fluor. cm^{-1}	Max ν of phos. cm^{-1}	$\frac{\Phi_P}{\Phi_F}$ (approx)*	τ (sec.)
Triphenylene	D_{3h}	29,100	23,800	1.2	15.9±3
Coronene	D_{6h}	23,600	19,100	1	9.4±2
Benzene	D_{6h}	38,000	29,400	1	7.0±5
Fluorene	C_{2v}	33,200	23,750	0.7	4.9±2
Phenanthrene	C_{2v}	28,700	21,600	0.3	3.3±2
Naphthalene	D_{2h}	31,750	21,300	0.01	2.6±2
Chrysene	C_{2h}	27,450	19,800	0.03	2.5±1
1,2,5,6 dibenz-anthracene	C_{2h}	25,300	18,300	0.01	1.5±1
1,2 benz-anthracene	C_s	26,100	16,500	0.001	0.3±1
Pyrene	D_{2h}	27,000	16,800	0.001	*ca.* 0.2
Anthracene	D_{2h}	26,600	14,700**	0.0001	—

* Φ_P/Φ_F is the ratio of phosphorescence yield to fluorescence yield. A study of internal conversion between the singlet states and the metastable triplet has been made by Dr. M. Kasha and is soon to be published. He has kindly permitted me to use some of his data to complete this column. The significance of Φ_P/Φ_F in the study of internal conversion was first pointed out by Dr. Kasha.

** Lewis and Kasha, see reference 1. On account of the weakness of the emission and its presence in the infra-red region, the lifetime could not be measured.

the luminescence of acetone can be calculated on this basis using Eq. (1). Taking $\zeta = 152$ cm^{-1}, the estimated value for oxygen; $\nu_1 = 51{,}500$ cm^{-1}; $\nu_3 = 30{,}000$ cm^{-1} and $f_1 = 0.020$, we find $\tau_3 = 0.0029$ sec. The actual value, 0.0006 sec., is five times shorter than this. A calculation shows that if the two other nearby states (at 35,000 cm^{-1} and 60,000 cm^{-1}) contribute to the intercombination probability, the lifetime is only slightly decreased, namely to 0.002 sec. Without doubt, the use of the radial atomic integral as an approximation to the matrix element for acetone is rather crude, and the discrepancy could easily disappear if a better value were used. The calculated lifetimes of the other aliphatic ketones are in error by about the same factor, in view of the last column of Table V. The order of magnitude of the result is correct, however, and we expect Eq. (1) using the atomic ζ-value to give approximately the right lifetimes for molecules similar to the aliphatic ketones. The rough estimates of Section III are not very far from what is actually observed. Although a comprehensive study has not been made of many other classes of molecules (classification based on the type of multiple bond), most of the examples encountered support the conclusion that Eq. (1) in the way we have used it leads to nearly the correct triplet state lifetime. Some other examples are to be found in Section VIII.

VI. POLYNUCLEAR HYDROCARBONS

The lifetimes of the polynuclear hydrocarbons are on the order of seconds, which is much longer than in the other types of organic compounds studied, and longer than the estimates of Section III would lead one to expect. The estimates were based on the use of the ζ-value for the lowest lying electron configuration of the carbon atom as an approximation to the matrix element for the singlet-triplet perturbation in the molecule. Apparently in this case, it is a very poor approximation to do this. The lifetimes of some of these compounds are listed in Table VI, along with other data which will be discussed later.

If enough information were available, one could make a better estimate of the discrepancy between observed and calculated lifetimes. The necessary information is a knowledge of the position and symmetry of the excited singlet levels of the molecule, the ground→excited-singlet state transition probability, and the selection rules governing the singlet-triplet perturbations in the molecule. The latter have recently been derived,[5] but only a part of the other necessary information is available. It is possible, however, to estimate the lifetime of the metastable triplet state of benzene, and to estimate the maximum lifetime to be expected for other polynuclear hydrocarbons (under the assumption that ζ is a good approximation to the spin-orbit interaction energy). As was shown by Shull,[12] the metastable triplet state of benzene is perturbed by the $^1B_{1u}$ state. As suggested by Shull and later confirmed by the author,[5] the metastable triplet state must, as a result, be $^3B_{2u}$. In order to use Eq. (1), we must know the position of the perturbing singlet level, i.e., the $^1B_{1u}$ level.

Shull's assignment of $^1B_{1u}$ as the perturbing singlet was based on the discovery of a β_{2g} vibrational interval

TABLE VII. Comparison of calculated and observed f-numbers for triplet states of polynuclear hydrocarbons.

Compound	$E(^1L_b)$ cm^{-1}	$E(^3L_a)$ cm^{-1}	$f(^1L_b)$ meas.	$10^8 \times f(^3L_a)$ meas.	$10^8 \times f(^3L_a)$ calc. Eq. (1)	Ratio $\left(\frac{\text{calc.}}{\text{meas.}}\right)$
Benzene	38,000	29,400	0.00147	0.0246	1.56	64
Naphthalene	32,000	21,300	0.002	0.123	1.14	9
Phenanthrene	28,300	21,600	0.003	0.081	5.2	64
Chrysene	27,500	19,800	0.005	0.154	6.6	43
Triphenylene	29,200	23,800	0.012	0.0177	31.5	1780
1,2 benz-anthracene	25,800	16,500	0.003	1.85	2.7	1.5

in the triplet-singlet emission spectrum, and is thus the first time that definite experimental evidence has been adduced to distinguish between a B_{1u} and a B_{2u} state. Other assignments[13] have made use of theoretical calculations of doubtful validity. This fact is mentioned here because it seems to be necessary to reverse the

[12] H. Shull, J. Chem. Phys. **17**, 295 (1949).

[13] See C. C. J. Roothan and R. S. Mulliken, J. Chem. Phys. **16**, 118 (1948) for references and discussion.

present assignments of the first two excited singlet levels of benzene. The lowest singlet has been assigned the symmetry $^1B_{2u}$, and the second $^1B_{1u}$. Using the spectral similarities of the polynuclear hydrocarbons,[14] the lowest excited singlet, in the nomenclature of Klevens and Platt, is ^1L_b and the lowest triplet is ^3L_a, and is associated with (belongs to the same electron configuration as) the second excited singlet, ^1L_a. The perturbing singlet must not, therefore, be the second excited singlet, but the first, the ^1L_b state. The selection rules then require ^1L_b to be $^1B_{1u}$, since ^3L_a has already been assigned $^3B_{2u}$. This is opposite from the assignment of previous workers cited.

Having located the position of the perturbing singlet state in benzene, we can use the data for this state in Eq. (1) to estimate the lifetime of the triplet state under the assumption that "normal" spin-orbit coupling takes place. Using the analogies between the spectrum of benzene and the other polynuclear hydrocarbons[14] enables us to predict maximum lifetimes for the other hydrocarbons.

In Table VII are presented the f-numbers of the triplet→ground-state transitions computed using Eq. (1) with the data for the ^1L_b state of the hydrocarbon, and using the ζ-value for the lowest configuration of atomic carbon. The ratio of this f-number to the true f-number (obtained from the lifetime by the formula of reference 10) is also given. Most of the calculated f-numbers are many times too high. In addition, one must remember that these f's are minimum values, since only the ^1L_b state is considered as a perturbing state. Consideration of only one state is probably a good approximation for benzene, but in the less symmetrical molecules, other states certainly interact with the metastable triplet state, causing the f-number calculated by Eq. (1) to be even larger. There are probably no restrictions on the perturbing states in the case of 1,2 benzanthracene, so that the near agreement between calculated and observed f-numbers is fortuitous. One can conclude, therefore, on the basis of Table VII, that the lifetimes of the aromatic hydrocarbons are considerably longer than would at first be expected, and that some prohibition in addition to the change of multiplicity restriction must be operative.

In the case of benzene, one might at first think of the electronic symmetry prohibition, but the use of the experimental $^1A_{1g}\rightarrow{}^1B_{1u}$ transition probability (strength of the 2600A band) has already taken this into account. In most of the other molecules, no such vibrational prohibition exists, yet the lifetimes remain anomalously long. Actual calculation of the matrix elements for spin-orbit interaction, using the method of antisymmetrized products of molecular orbitals fails to show where the difficulty lies, the calculated matrix elements being of the same order of magnitude as those for the free carbon atom.[15]

Table VI gives some further data on the polynuclear hydrocarbons. The ratio of phosphorescence to fluorescence (only the order of magnitude is given) varies strikingly throughout the series of compounds, and illustrates one of the difficulties encountered in the study of phosphorescence. In the case of the last three compounds listed, the triplet emission band is extremely weak, and the lifetime measurements were difficult to make. The triplet emission bands of 20-methyl cholanthrene and of fluoro benzene could not be found, probably because of their extreme weakness. This involves the theory of internal conversion, which we have already mentioned in Section II, but it is a large subject and cannot be entered into here.

TABLE VIII. Triplet state lifetimes of substituted aromatic compounds (light atom substituents).

(a) Benzene derivatives			(b) Naphthalene derivatives		
Substance	τ (sec.)	νp^* cm^{-1}	Substance	τ (sec.)	νp cm^{-1}
Benzene	7.0±5	29,400	Naphthalene	2.6±2	21,300
Toluene	8.8±2	28,800	α-methyl naphthalene	2.5±2	20,850
Aniline	4.7±3	26,800	α-amino naphthalene	1.5±1	19,000
Phenol	2.9±1	28,600	α-naphthol	1.9±1	20,500**
Fluoro benzene	too weak to measure		β-naphthol	1.3±1	21,100**
Benzoic acid	2.5±2	27,200	α-fluoro naphthalene	1.5±1	20,970
Benzoate ion	0.7±1	27,700	β-naphthoic acid	2.5±2	20,900
Anisole	3.0±1	28,200	Methyl β-naphthyl ketone	0.95±5	20,700†
Aceto-phenone	0.008±2	26,000**	α-nitro naphthalene	0.049±2	19,200**

*The maximum frequency of the long-lived emission band is from the work of R. V. Nauman except where noted. See R. V. Nauman thesis, University of California, 1947.
**G. N. Lewis and M. Kasha, reference 1.
†M. Kasha, private communication.

TABLE IX. Triplet state lifetimes of nitro compounds.

	νp^* cm^{-1}	τ (sec.)
α-nitro naphthalene	19,200	0.05
2-nitro fluorene	20,600	0.13
p-nitro biphenyl	20,500	0.080
1,5 dinitro naphthalene	19,900	0.11

* G. N. Lewis and M. Kasha, reference 1.

VII. SUBSTITUTED AROMATIC COMPOUNDS

In Table VIII we give the lifetimes of some substituted benzenes and naphthalenes. The long lifetimes are characteristic of all but the carbonyl and nitro derivatives. It can be seen that the symmetry is not correlated with the lifetime. The somewhat shorter lifetimes of aniline and phenol compared to toluene, can be explained on the basis of the atomic number effect of Section IV.

The carbonyl lifetimes can be explained in the following way. The molecule can be thought of as an aromatic ring perturbed by a carbonyl group if the interaction between these two parts is not too great. It appears

[14] H. B. Klevens and J. R. Platt, J. Chem. Phys. 17, 470 (1949).

[15] D. S. McClure, unpublished work.

TABLE X. Relation of lifetime to absorption strength.

Compound	Lifetime from absorption band* (sec.)	Measured lifetime (sec.)
Benzene	0.20−1.5**	7.0±5
Bromo benzene	0.0030±5	(0.0001)***
P-dibromo benzene	0.00153±6	0.00033±3
β-bromo naphthalene	0.010±3	0.021±1
β-iodo naphthalene	0.0019±1	0.0025±1

* All these absorption bands had to be corrected for the overlap of the main absorption bands. This overlap is appreciable even though the 0−0 bands of the two transitions are in some cases 10,000 cm^{-1} apart. An exponential curve fitted to the tail of the main band and extrapolated into the region of the triplet band was assumed to give the right correction. The spectra were taken on the Beckmann spectrophotometer in solution at room temperature, while the lifetimes were measured in rigid E.P.A. (see note to Table I) at 77°K.

** These are the minimum and maximum values. The integration over the bands at room temperature is very inaccurate.

*** See note to Table III(c).

justifiable to make this assumption when considering the lowest triplet states of the aromatic carbonyl compounds because of the results obtained. If the lowest triplet states of the two "parent molecules" are alone considered, the perturbation theory gives fairly simple results for the energy and lifetime of the lowest triplet state of the "compound" molecule. If E is the energy of the triplet state of the "compound" molecule, E_1 and E_2 the energies of the parent molecules, and h_{ij} the matrix element of the perturbation involving the two states, the secular equation is

$$\begin{vmatrix} E_1+h_{11}-E & h_{12} \\ h_{12} & E_2+h_{22}-E \end{vmatrix} = 0.$$

The two values of E are thus

$$E_a = E_1+h_{11}+\frac{h_{12}^2}{\Delta E+\Delta h_{ii}} \quad \text{and} \quad E_b = E_2+h_{22}-\frac{h_{12}^2}{\Delta E+\Delta h_{ii}}$$

and the corrected wave functions for the perturbed states are

$$\psi_a = \psi_1\left(1-\frac{h_{12}^2}{\Delta E^2}\right)^{\frac{1}{2}}+\psi_2\frac{h_{12}}{\Delta E}, \quad \psi_b = \psi_1\frac{h_{12}}{\Delta E}+\left(1-\frac{h_{12}^2}{\Delta E^2}\right)^{\frac{1}{2}}\psi_2.$$

The lifetime of the lowest triplet state of the "compound" molecule (say state b) is then approximately given by

$$\frac{1}{\tau_b} = \frac{1}{\tau_1}\left(1-\frac{h_{12}^2}{\Delta E^2}\right)+\frac{1}{\tau_2}\left(\frac{h_{12}}{\Delta E}\right)^2.$$

Even if h_{12} could be evaluated accurately, this formula would have only qualitative significance because of the rather severe use of perturbation theory. Nevertheless, it shows that the triplet state lifetimes lie between the lifetimes of the two parent compounds, and we can also deduce that in energy, lifetime and spectrum, the compound molecule will more nearly resemble that parent molecule whose triplet energy level lies the lower. If we suppose that h_{12} is approximately given by the difference E_2-E_b, we can make rough comparisons with experiment. As an example, we can consider that acetophenone consists of an acetone-like part and a benzene-like part. The triplet level of the benzene molecule is at 29,400 cm^{-1}, that of acetone is at 26,000 cm^{-1}, while that of acetophenone is at 24,000 cm^{-1}. Thus h_{12} is 2000 cm^{-1} and $(h_{12}/\Delta E)^2$ is 0.35, so that the lifetime of acetophenone should be roughly three times that of acetone. It is actually about ten times that of acetone. In this case, we expect, and find, that the spectrum and lifetime of acetophenone are characteristic of ketones. In the case of methyl β-naphthyl ketone, the triplet level of the hydrocarbon part is below that of the acetone part and the lifetime and spectrum of the combination are more similar to naphthalene than to acetone. In this case the data are: naphthalene, 21,300 cm^{-1}, 2.6 sec.: acetone 26,000 cm^{-1}, 0.0006 sec.: methyl β-naphthyl ketone 20,800 cm^{-1}, 0.95 sec. The calculated value of τ for the combination would be 0.04 sec. These considerations give satisfactory results for a number of other side groups such as the nitrile, carboxyl and nitroso. Thus we can correctly predict the approximate lifetimes of many complex molecules from the information we have about the simple ones.

The lifetimes of the aromatic nitro compounds cannot be explained so simply. Interaction between the nitro group and the ring is too large in this case. The lifetimes are all shorter than in the unsubstituted ring compounds. Nitro benzene has an extremely weak luminescence and nitro methane shows no appreciable long lived luminescence. This constitutes a further barrier to the interpretation. Table IX gives the lifetimes and the maximum frequency of the emission band (position of the triplet level) for a group of aromatic nitro compounds.

An interesting effect of substitution in an aromatic compound is the apparent steric hindrance effect on the lifetimes of the biphenyls. *oo'* difluor biphenyl has its lowest triplet level at 25,700 cm^{-1} and the lifetime for this state is 0.88±4 sec., while the *pp'* compound has its triplet level at 23,000 cm^{-1} and a lifetime of 3.2±2 sec. The *pp'* compound is very close to biphenyl in these properties. For biphenyl we have 22,800 cm^{-1} and 3.6±2 sec.

VIII. OTHER COMPOUNDS

A small amount of data on the triplet state lifetimes of some of the other classes of organic compounds has been obtained. Some of the nitrogen analogs of the polynuclear aromatic hydrocarbons, e.g., pyridine and quinoline, have the long lifetimes characteristic of the corresponding hydrocarbons. One which does not is pyrazine (a benzene ring with two nitrogens para to each other), whose lifetime is 0.020±2 sec. The reason why this should behave differently from the aromatics is not known, but a knowledge of the term scheme of the molecule might give the answer. The straight chain

amidinium dye $NH_2-CH=CH-CH=NH_2^+$ can be described by the same metallic model as the aromatic ring compounds[16] and might be expected to behave as they do. It's lifetime, however, is 0.0030 ± 2 sec., approximately what one would expect for a carbon compound according to the estimates of Section III.

The luminescence of the ethylenic compounds has not been studied as yet because of the necessity for exciting them in the far quartz or vacuum region of the ultraviolet. It may well be, in view of Mulliken's theory of the triplet state of ethylene,[17] that no luminescence will be found. If it is assumed that the step-out on the long wave end of the absorption spectrum of cyclohexene[18] (also present in the spectra of other ethylenic compounds) is due to a singlet-triplet transition, the lifetime calculated from this band is 0.002 to 0.005 sec., which is in the range estimated in Section III for carbon-containing compounds. Overlapping by the strong singlet-singlet band prevents a more accurate estimate.

It was assumed by Lewis and Kasha[2] that the characteristic band of the nitroso compounds at 7500A is due to a singlet-triplet transition. The absorption strength of the aliphatic nitroso compounds appears to be too great if the entire band in this region is due to the intercombination. Using the published data[19] for the compound 1-chloro-1-nitrosocyclohexane, the calculated lifetime is found to be 4.2×10^{-6} sec. Making proper allowance for the inaccuracy of the relation used to relate absorption strength to emission lifetime (see next section), the value just obtained seems too short for a singlet-triplet transition in this type of molecule. There is also evidence for the lack of any atomic number effect, as examples of bromo and chloro nitroso compounds having the same absorption strength may be found (see reference 19). In view of the similarity of these compounds to the carbonyl compounds, there may be a triplet band hidden by the singlet band. The luminescences have not been studied as yet because of the difficulties of measuring weak infra-red radiation.

[16] W. T. Simpson, J. Chem. Phys. **16**, 1124 (1948). I am indebted to Dr. Simpson for letting me have some of this compound.

[17] R. S. Mulliken, Rev. Mod. Phys. **14**, 265 (1942).

[18] H. Stuckeln, H. Thayer, and P. Willis, J. Am. Chem. Soc. **62**, 1717 (1940). I am indebted to Professor E. P. Carr for some of the original data from this paper.

[19] D. L. Hammick and M. W. Lister, J. Chem. Soc. **1937**; 1,489.

IX. THE CALCULATION OF LIFETIMES FROM THE ABSORPTION STRENGTH

We have done this several times in the previous section, and we calculated f values from lifetimes in Section V. Lewis and Kasha[2] discussed this problem and were able to give a few examples of the application of the well known equation (their Eq. (1)) for the atomic case to molecules. Since that time, it has been possible to test the accuracy of this equation by comparing measured triplet state lifetimes with the corresponding integrated singlet-triplet absorption bands. The results are given in Table X. In calculating the lifetimes from the absorption band, n^2 has been set equal to 1.0, and $g_u/g_l=3$. In two of the examples the measured lifetime is considerably shorter than that found from the absorption band, while in the other three it is appreciably greater. Judging from these results therefore, the estimates of lifetimes we have made in Section VIII cannot be considered reliable to within less than a factor of five. The equation which has been derived for isolated atoms is admittedly a poor approximation for molecules embedded in a rigid medium or in a liquid solution. The fact that internal conversion and changes of molecular configuration take place can be allowed for in deriving a similar equation for molecules, but it is difficult to evaluate the parameters which appear in the final equation. We will therefore not go further into this subject, but leave it for some future investigation.

ACKNOWLEDGMENTS

I wish to thank Professor G. E. Gibson for his help in this work. I am also indebted to Dr. David Bohm for suggesting some of the interpretation of the data which has been made and to Dr. M. Kasha for many fruitful discussions of various problems. I also wish to thank the Dow Chemical Company for a fellowship, and the Shell Development Company for a grant-in-aid, both of which assisted in the progress of this work.

THE JOURNAL OF CHEMICAL PHYSICS VOLUME 17, NUMBER 10 OCTOBER, 1949

The Tensile Strengths of Liquids. I. Thermodynamic Considerations*,**

SIDNEY W. BENSON AND EDWARD GERJUOY
The University of Southern California, Los Angeles, California

(Received January 3, 1949)

An investigation is made of the thermodynamic stability of liquids under tension. Comparisons of the Helmholtz free energies show that small samples of liquid under tension are unstable with respect to two-phase liquid-vapor equilibrium at the same volume and temperature.

Defining the tensile strength as the negative pressure at which $(\partial P/\partial V)_T=0$ for the liquid, it is possible to calculate "maximum" possible tensile strengths from equations of state. The van der Waals and Berthelot equations in reduced form can be adapted to such explicit calculation and give values much lower, and therefore much closer to experimental values, than previous calculations. For non-associated liquids at 27°C, the van der Waals maximum tensile strengths are about 150 atmos. whereas the Berthelot values are about 750 atmos. The temperature dependence for the two equations is about 1 and 6 atmos. °C, respectively.

Comparisons with observation of the calculated reduced liquid volume, energy of vaporization, coefficient of thermal expansion, and bulk compressibility support the use of the van der Waals and Berthelot equations in computing liquid properties.

INTRODUCTION

DURING the past hundred years the tensile strengths of liquids have been investigated both experimentally and theoretically by a number of workers. It is surprising therefore that at the present time there is so little real information as opposed to conjecture concerning this very important property. A review of the subject has recently been presented by Temperley and Chambers.[1] From this source and others[2–5] it seems fair to conclude that our experimental knowledge of the tensile strength of liquids is most uncertain. A survey of the results of different investigators reveals "observed" values of the tensile strength differing by factors of 100 or more. Similar differences occur even in the repeated measurements made by the same investigator. Thus for water, the liquid which has received the most attention experimentally, observed values of the tensile strength range from zero to upward of 150 atmospheres. There are similar disparities for the other liquids which have been studied.

Although there have been many theoretical studies of the problem of liquid tensile strength,[6–10] it may be said that at present, the phenomenon still awaits rigorous formulation. Different approaches have led to estimates which differ by orders of magnitude from each other and which have been uniformly much higher than the highest reported experimental values. To take the case of water again, these estimates range from about 500 atmospheres to over 10,000 atmospheres.[1,4,9] It is quite possible that the disparities between theoretical estimates and experimental values may be accounted for by the presence of gas bubbles, suspended particles, voids in the container walls, or dissolved matter. It is also quite possible that the low values which have been reported for tensile strength may be due to difficulties or errors inherent in the particular experimental techniques which have been employed. The present paper is not concerned with these latter considerations, however, but is restricted to a discussion of the problem of pure, gas-free, isothermal liquids.

I. CRITERIA FOR RUPTURE IN A LIQUID UNDER TENSION

We can define the tensile strength of a liquid as the maximum tension which the liquid can maintain at constant temperature. It will have physical significance if there is a unique tension above which the liquid becomes mechanically unstable*** (in the sense that an infinitesimal increase in tension produces an infinite increase in volume). This may be expressed analytically as: $(\partial P/\partial V)_T=0$ or in terms of the coefficient of extensibility: $\beta\equiv-(1/V)(\partial V/\partial P)_T=\infty$.

Such a condition must generally be employed with caution since it is also satisfied by a liquid and vapor system in two-phase equilibrium. However the two-phase equilibrium can be maintained only at positive pressures. Consequently, the above relations are a legiti-

* Part of the contents of this paper were reported on at the Symposium on Cavitation held at San Diego, August 27, 1948, and sponsored jointly by the Marine Physics Laboragory of the University of California and the Naval Electronics Laboratory at San Diego.

** This investigation was sponsored by the ONR under Task Order Contract No. N6 ori-77/2 at the University of Southern California.

[1] Temperley and Chambers, Proc. Phys. Soc. **58**, 420 (1946).
[2] R. S. Vincent, Proc. Phys. Soc. **53**, 126 (1941); *Ibid.* **55**, 41 (1943).
[3] Vincent and Simmonds, Proc. Phys. Soc. **55**, 376 (1943).
[4] H. N. V. Temperley, Proc. Phys. Soc. **58**, 436 (1946); *Ibid.* **59**, 199 (1947).
[5] Knapp and Hollander, Trans. A.S.M.E. **70**, 419 (1948).
[6] Briggs, Johnson, and Mason, J. Acous. Soc. Am. **19**, 664 (1947).
[7] R. B. Dean, J. App. Phys. **15**, 446 (1944).
[8] R. Fürth, Proc. Camb. Phil. Soc. **37**, 276 (1941).
[9] J. Frenkel, *Kinetic Theory of Liquids* (Oxford University Press, New York, 1946), Chapter VII.
[10] E. Gerjuoy, Phys. Rev. **73**, 538 (1948).

*** It should, however, be noted that it is by no means obvious that a liquid has a definite tensile strength, even in one simple type of experiment, i.e., that rupture always occurs at a definite value of the tensile stress, independent of the shape and magnitude of the containing vessel. This point is discussed in more detail in a forthcoming paper.

TABLE I. Reduced tensile strengths from the van der Waals equation.

θ	$\phi_{min.}$	$-\pi_{min.}$	$d\pi_{min.}/d\theta$
0.500	0.500	4.00	16.0
0.600	0.536	2.54	13.2
0.650	0.556	1.91	12.0
0.700	0.580	1.35	10.8
0.800	0.635	0.37	8.8
0.844 (27/32)	0.667 (2/3)	0	8.0

TABLE II. Reduced tensile strengths computed from the Berthelot equation.

θ	$\phi_{min.}$	$-\pi_{min.}$	$d\pi_{min.}/d\theta$
0.500	0.426	18.7	94.9
0.600	0.457	11.0	61.5
0.650	0.475	8.20	50.3
0.700	0.497	5.95	41.1
0.800	0.552	2.56	27.6
0.900	0.642	0.23	17.7
0.919	0.667 (2/3)	0	16.0

mate criterion for rupture under tension, provided, of course, that they do actually yield roots corresponding to negative pressures.

If we compare the Helmholtz free energies of two different samples of a liquid at the same temperature and same volume, V, one under a tension P and the other at its normal vapor pressure P_0 but containing a spherical bubble, then the condition that the extended liquid be more stable is easily shown to be:

$$P \leqslant 5.5(\sigma^3/V_0\beta)^{\frac{1}{3}} - P_0.$$

On substituting reasonable values in this equation we find that small volumes of a liquid ($\sim$10 cc) may be stable down to negative pressures of about 0.1 atmosphere.**** Under any significant tensions, therefore, liquids will be metastable with respect to vapor formation. Rupture in such systems is therefore most probably a thermodynamically irreversible process comparable to the onset of the explosion limit in a mixture of gases. Any rigorous theoretical treatment of the rupture phenomenon must thus involve a dynamical or kinetic treatment of the metastable system and its approach to equilibrium. No such ambitious program is attempted in this paper. Rather it is our primary concern at this time to determine what, if any, significant information about the tensile strength can be obtained from basically thermodynamic considerations. We begin, in the following section, by investigating the applicability of two well-known equations of state, the van der Waals and Berthelot, to the calculation of maximum tensile strengths. In such a calculation we assume tacitly that the equation of state represents all stable states of the liquid, and is valid. The tensile strength in the region of metastability can then be inferred by following the $P-V$ isotherms to negative pressures where they describe first metastable and then obviously unstable states. Our calculations indicate that the metastable region extends from slightly below the vapor pressure to the minimum on the isotherm.

If the equation of state is to be given credence, it is apparent that such a procedure yields an upper bound to the tensile strength. The calculations described in the final section indicate that at positive pressures the equations of state do yield fairly good representations of the liquid. It is thus not unreasonable to use these equations at negative pressures.

Any naturally occurring mechanism in the liquid which permits it to go from its metastable one-phase state to its stable, two-phase, liquid-vapor equilibrium state may make inaccessible parts of the metastable region, thereby reducing the tensile strength. A particular mechanism whereby such an instability may occur is investigated in a forthcoming paper. By comparing the results of such an investigation with the results of this paper, it is possible to evaluate more critically the likelihood that the maximum possible strengths here calculated will about equal the maximum strengths attainable in the laboratory under ideal conditions.

**** A sample of water at 27°C (volume, 10^{-3} cc) will be stable down to a tension of 0.25 atmosphere. On the other hand a 10 cc sample will be unstable as soon as its vapor pressure is reached.

II. TENSILE STRENGTHS FROM THE VAN DER WAALS EQUATION

Most simple models of the liquid state yield an expression very close to the van der Waals equation as a first approximation. The latter is itself a semi-empirical equation which can be derived by assuming a microscopically random and uniform molecular distribution function for the liquid and complete communality of its free volume. With such assumptions the form of the equation becomes independent of the choice of any particular intermolecular potential. While originally derived to account for the behavior of non-ideal gases, it has had considerable success in predicting liquid behavior for non-associated liquids. Temperley[4] has shown that the observed data on the maximum superheating of liquids are in good qualitative agreement with values calculated from the van der Waals equation.

In order to extend Temperley's method and obtain explicit values of tensile strength it is best to work with the reduced form of the equation:

$$\pi = 8\theta/(3\phi-1) - 3/\phi^2. \tag{1}$$

Applying the condition for instability, we find:

$$(\partial\pi/\partial\phi)_\theta = V_c/P_c(\partial P/\partial V)_T = 0$$
$$= -(24\theta/(3\phi-1)^2) + 6/\phi^3. \tag{2}$$

On expanding this expression, it becomes:

$$\phi^3 - (9/4\theta)\phi^2 + (3/2\theta)\phi - (1/4\theta) = 0. \tag{3}$$

From Eqs. (2) and (1) it is possible to obtain simple, explicit relations for both θ and $\pi_{\min.}$ in terms of $\phi_{\min.}$:

$$\theta=\tfrac{1}{4}[(3\phi-1)^2/\phi^3], \tag{4}$$

$$\pi_{\min.}=3/\phi^2-2/\phi^3. \tag{5}$$

From Eq. (5) we find that $\pi_{\min.}$ will be zero when $\phi=\frac{2}{3}$ which corresponds to a reduced temperature, $\theta=27/32=0.844$. This is the value computed by Temperley,[4] which he interprets as the maximum temperature above which a liquid is incapable of existing at zero pressure. He identifies it as the maximum temperature of superheating.

Equation (3) may have three positive roots and no negative roots. One of these roots lies between $0\leqq\phi\leqq\frac{1}{3}$. This belongs to the physically meaningless portion of the van der Waals isotherm for which π is always negative. The largest root of Eq. (3) corresponds to a maximum in the isotherm for which π is positive. It is usually associated with the minimum volume of the supercooled vapor. The third root corresponds to the minimum in the isotherm and yields negative values for π, for values of θ below 0.844. For this range of θ, ϕ lies between $\frac{1}{3}$ and $\frac{2}{3}$ and may be easily computed from Eq. (3) by standard methods. Table I shows the values of $\phi_{\min.}$ and $\pi_{\min.}$ corresponding to different values of θ.

We see that the values computed for $\pi_{\min.}$ in Table I, in contrast to previous calculations, are of quite reasonable order of magnitude when compared with experimental values. For example, they range from a tensile strength of 60 atmos. (if $P_c=30$ atmos.) to 120 atmos. ($P_c=60$ atmos.) at a value of $\theta=0.63$, which corresponds roughly to the normal boiling point for unassociated liquids.

The variation of tensile strength with temperature is of interest and can be computed from Eq. (1).

$$\frac{d\pi_{\min.}}{d\theta}=\left(\frac{\partial\pi}{\partial\theta}\right)_\phi+\left(\frac{\partial\pi}{\partial\phi}\right)_\theta\frac{d\phi}{d\theta}=\left(\frac{\partial\pi_{\min.}}{\partial\theta}\right)_\phi=\frac{8}{3\phi-1}. \tag{6}$$

Values of this derivative are listed in Table I. In terms of the normal variables we have:

$$\left(\frac{\partial P}{\partial T}\right)_V=\left(\frac{\partial\pi}{\partial\theta}\right)_\phi\cdot\frac{P_c}{T_c}=\frac{1}{3\phi-1}\cdot\frac{3R}{V_c}. \tag{7}$$

The latter step results from the substitution $P_c/T_c=3R/8V_c$, obtained from the van der Waals critical isotherm. Since $3R/V_c$ is about 1 atmos./°C for most liquids, we see that the variation of tensile strength with temperature is about 1 to 2 atmos./°C in the range of interest. At the normal boiling point ($\theta=0.63$) it is about 1.5 atmos./°C.

III. TENSILE STRENGTHS FROM THE BERTHELOT EQUATION

In reduced form, the Berthelot equation is given by:

$$\pi=8\theta/(3\phi-1)-(3/\theta\phi^2). \tag{8}$$

Applying the previously described treatment:

$$\left(\frac{\partial\pi}{\partial\phi}\right)_\theta=-\frac{24\theta}{3\phi-1}+\frac{6}{\theta\phi^3}=0, \tag{9}$$

$$\theta=((3\phi-1)/2)\cdot\phi^{-\frac{3}{2}}, \tag{10}$$

$$\pi_{\min.}=\frac{2}{\phi^3}\left\{\frac{3\phi-2}{3\phi-1}\right\}. \tag{11}$$

Just as with the van der Waals equation, $\pi_{\min.}$ becomes zero when $\phi=\frac{2}{3}$, corresponding to $\theta=(27/32)^{\frac{1}{2}}=0.919$. In expanded form Eq. (9) becomes:

$$\phi^3-\frac{9}{4\theta^2}\phi^2+\frac{3}{2\theta^2}\phi-\frac{1}{4\theta^2}=0. \tag{12}$$

It differs from the corresponding van der Waals equation only in having θ^2 in place of θ. Once more the desired root lies between $\frac{1}{3}\leqq\phi\leqq\frac{2}{3}$. Values of $\phi_{\min.}$ and $\pi_{\min.}$ for different values of θ are given in Table II.

The variation in tensile strength with temperature is given by:

$$\frac{d\pi_{\min.}}{d\theta}=\left(\frac{\partial\pi}{\partial\theta}\right)_\phi=\frac{8}{3\phi-1}+\frac{3}{\theta^2\phi^2}. \tag{13}$$

In order to obtain some indication of the validity which may be ascribed to these calculations of tensile strength, we have computed other physical properties from the two equations of state. These are discussed in the following section. The results suggest that the maximum possible tensile strengths of liquids lie somewhere between the values computed from the van der Waals and Berthelot equations. The results would warrant a stronger conclusion than merely "suggest" were it not for the fact that our calculations are limited to positive pressures. There are as yet no data (other than the still experimentally uncertain tensile strengths themselves) with which the equations of state could be tested at negative pressures.†

IV. CALCULATIONS OF THE PHYSICAL PROPERTIES OF LIQUIDS FROM THE VAN DER WAALS AND BERTHELOT EQUATIONS

At temperatures near or below the reduced boiling point, the reduced pressure may be neglected in comparison with the other two terms in the equations of state. This approximation makes it possible to obtain relatively simple expressions for the reduced volume, energy of vaporization, coefficient of thermal expansion, and bulk compressibility of liquids. To obtain explicit values the only data needed are the boiling point, critical temperature, and critical pressure.

Although these equations are not supposed to be applicable to associated liquids, it was thought that the

† Experiments to measure the extensibility of a liquid under tension are in preparation at this University.

values obtained for such liquids would be of some interest, and so water and ethyl alcohol were included in the tables.

A. Reduced Volume at the Boiling Point[11]

$$\phi_b(\text{v.d.W.})=\frac{9}{16\theta_b}\left[1-\left(1-\frac{32}{27}\theta_b\right)^{\frac{1}{3}}\right], \quad (14)$$

$$\phi_b(\text{Ber.})=\frac{9}{16\theta_b^2}\left[1-\left(1-\frac{32}{27}\theta_b^2\right)^{\frac{1}{3}}\right]. \quad (15)$$

TABLE III. Calculated values of the reduced volumes of liquids.

	Carbon tetrachloride	Benzene	Ethyl alcohol	Water
T_b °K (obs.)	349.9	353.4	351.4	373.2
T_c °K (obs.)	556.3	561.7	516.3	647.3
θ_b(obs.)	0.629	0.629	0.680	0.577
V_b(obs.) cc/mole	103.9	95.6	62.5	18.77
V_c(obs.) cc/mole	276.1	256.5	167.5	56.3
ϕ_b(obs.)	0.376	0.375	0.373	0.333
ϕ_b(v.d.W.) Eq. (14)	0.443	0.443	0.462	0.427
ϕ_b(Ber.) Eq. (15)	0.385	0.385	0.398	0.374

B. Energies of Vaporization at the Boiling Point

$$E_{\text{vap.}}(\text{v.d.W.})=9RT_b/8\theta_b\phi_b, \quad (16)$$

$$E_{\text{vap.}}(\text{Ber.})=9RT_b/4\theta_b^2\phi_b. \quad (17)$$

TABLE IV. Calculated values of the energy of vaporization.

	$E_{\text{vap.}}$(obs.) K cal./mole	$E_{\text{vap.}}$(v.d.W.) Eq. 16	$E_{\text{vap.}}$(Ber.) Eq. 17
Carbon tetrachloride	6.47	2.81	10.28
Benzene	6.66	2.84	10.38
Ethyl alcohol	8.73	2.50	14.56
Water	8.98	3.25	21.4

C. Coefficient of Thermal Expansion at the Boiling Point

$$\alpha=(1/V)(\partial V/\partial T)_P, \quad (18)$$

$$\alpha(\text{v.d.W.})=\frac{1}{T_b}\left[\frac{8\theta_b\phi_b}{9-16\theta_b\phi_b}\right], \quad (19)$$

$$\alpha(\text{Ber.})=\frac{1}{T_b}\left[\frac{16\phi_b\theta_b^2}{9-16\phi_b\theta_b^2}\right]. \quad (20)$$

TABLE V. Calculated values of the coefficient of thermal expansion.

	α(obs.) °C$^{-1}\times10^3$	α(v.d.W.—Eq. 19) °C$^{-1}\times10^3$	α(Ber.—Eq. 20) °C$^{-1}\times10^3$
Carbon tetrachloride	1.36	1.40	0.80
Benzene	1.37	1.38	0.79
Ethyl alcohol	1.33	1.80	1.03
Water	0.76	10.4	0.56

[11] S. W. Benson, J. Phys. and Coll. Chem. **52**, 1060 (1948).

D. Coefficient of Compressibility at the Boiling Point

$$\beta=-(1/V)(\partial V/\partial P)_T,$$

$$\beta(\text{v.d.W.})=\frac{8\theta_b\phi_b^3}{27P_c}\left[1-\frac{48}{27}\theta_b\phi_b\right]^{-1}, \quad (21)$$

$$\beta(\text{Ber.})=\frac{8\theta_b^3\phi_b^3}{27P_c}\left[1-\frac{48}{27}\theta_b^2\phi_b\right]^{-1}. \quad (22)$$

TABLE VI. Calculated values of the coefficient of compressibility.

	β(obs.) $\times10^4$ atmos.$^{-1}$	β(v.d.W.) $\times10^4$ atmos.$^{-1}$ (Eq. 21)	β(Ber.) $\times10^4$ atmos.$^{-1}$ (Eq. 22)
Carbon tetrachloride	1.70	7.1	1.28
Benzene	1.50	7.6	1.20
Ethyl alcohol	1.70	7.1	1.38
Water	0.48	1.09	0.18

E. Critical Pressure and Tensile Strength

For both the van der Waals and Berthelot equations, the critical pressure is given by: $P_c=3RT_c/8V_c$. Calculated values are shown in Table VII. The tensile strengths were calculated at the normal boiling points and at room temperature by interpolation from the data in Tables I and II. Temperature coefficients of tensile strength were similarly obtained.

TABLE VII. Calculated values of critical pressure and maximum tensile strength.

	Carbon tetrachloride	Benzene	Ethyl alcohol	Water
P_c(obs.) atmos.	45.0	47.9	63.1	217.7
P_c(calc.) atmos.	62.7	67.4	95	354
Max. tensile strength at b.p. (v.d.W.) atmos.	96	103	99	627
Max. tensile strength at b.p. (Ber.) atmos.	428	455	442	3680
Max. tensile strength at 27°C (v.d.W.) atmos.	153 (θ=0.540)	164 (θ=0.534)	179 (θ=0.580)	996 (θ=0.464)
Max. tensile strength at 27°C (Ber.) atmos.	702	754	790	4800
Temp. coeff. of tensile strength at b.p. (v.d.W.) atmos./°C	1.0	1.1	1.9	4.7
Temp. coeff. of tensile strength at b.p. (Ber.) atmos./°C	6.1	6.6	8.3	23
Temp. coeff. of tensile strength at 27°C (v.d.W.) atmos./°C	1.2	1.3	2.5	5.8
Temp. coeff. of tensile strength at 27°C (Ber.) atmos./°C	6.5	7.1	12.5	38

The observed values for the physical constants used in the preceding tables were taken from Landolt-Bornstein and the I.C.T. The values for ϕ_b used in computing $E_{\text{vap.}}$, α and β, were the values calculated from Eqs. (14) and (15), respectively, rather than ϕ_b observed.

We see that both equations predict values of the reduced volume which are too high. The Berthelot is fairly close while the van der Waals is in error by 28 percent in the worst case, water. The critical pressures are also high by about 30–50 percent. For all the other constants, however, the two equations together bracket the observed values. The Berthelot equation predicts too "tight" a liquid, whereas the van der Waals predicts too "loose" a structure.

It seems quite reasonable, therefore, to suppose that the true maximum possible tensile strengths lie between the values predicted by these two equations.†† Certainly the maximum possible tensile strength should not lie far outside the range between these equations if they represent liquids as well at negative pressures as they do at positive pressures. In the case of the associated liquids such as water, the predictions must be given much less credence.

†† One of the authors (S. W. Benson) has developed an empirical, reduced equation of state similar in form to the Berthelot equation which gives much better values for all of the physical properties at positive pressures. It predicts tensile strengths intermediate between the two equations and closer to the van der Waals results.

Infra-Red Spectra of Propane, 1-Deuteropropane, and 2-Deuteropropane and Some Revisions in the Vibrational Assignments for Propane

H. L. McMURRY, V. THORNTON, AND F. E. CONDON
Phillips Petroleum Company, Research Department, Bartlesville, Oklahoma

(Received January 21, 1949)

The infra-red spectra of propane, 1-deuteropropane, and 2-deuteropropane are presented. The spectrum of propane does not have the bands at 720 and 1179 cm^{-1} reported by Wu and Barker.

The vibrational modes of the three molecules are described. The 748-cm^{-1} band in the propane spectrum is unambiguously assigned to rocking of the CH_2 group about an axis normal to the molecular axis and in the C_s plane; and the 1053-cm^{-1} band is unambiguously assigned to rocking of the CH_2 group about an axis normal to the C_s plane.

Unambiguous assignments for the remaining bands below 1350 cm^{-1} in the propane spectrum were not possible without an elaborate theoretical treatment beyond the scope of this paper.

I. INTRODUCTION

IT has been empirically established that there are many molecular groupings each of which produces one or more infra-red bands at definite wave-lengths.[1] Valuable applications of these correlations to molecular structure determination have been possible without knowing the vibrational origins of the bands. However, more detailed information as to the origin of infra-red bands will extend their usefulness for structural interpretation. Thus, for example, the vibrational origin of a band observed when polarized radiation is sent through an oriented polymer must be known if the dependence of the band intensity on the direction of polarization is to be interpreted.

For determining more about the origins of bands in the spectra of paraffinic hydrocarbons from a detailed study of the propane spectrum, the infra-red spectra of 1-deuteropropane and 2-deuteropropane have been obtained.

II. EXPERIMENTAL

The propane was Phillips Research Grade material certified to be 99.99 mole percent by the National Bureau of Standards.

Each deuteropropane was prepared from the corresponding Grignard reagent prepared in the usual way from one mole of propyl chloride, previously purified by fractional distillation. The flask containing the Grignard reagent was evacuated to less than 1 mm Hg pressure and was finally heated for a short time with boiling water to remove propane and propylene produced during formation of the Grignard reagent, and most of the ether. The flask was then cooled in ice and air was admitted, simply by turning a three-way stopcock, through a Drierite-filled drying tube and a dry ice-cooled trap. Immediately thereafter, 0.6 mole deuterium oxide (99.8 percent) was slowly dropped onto the ice-cooled Grignard reagent. The generated deuteropropane was caught in the aforementioned dry ice-cooled trap and finally was purified by low temperature fractional distillation.

Figure 1 presents the transmission curves for these substances in the gas phase at 29 C from spectra obtained with a Perkin-Elmer Model 12B spectrometer with a rocksalt prism. The most likely contaminants of each deuteropropane were propane, propylene, the other deuteropropane, and diethyl ether, each of which could have been detected in a concentration of one percent or more. None of these impurities were detected, except for about three percent of propylene in the 2-deuteropropane. The dashed line in Fig. 1 shows the 2-deuteropropane spectrum corrected for three percent of propylene.

Except for the absence of bands at 720 and 1179 cm^{-1} and for the relative intensities of the bands at 1150 and 1165 cm^{-1}, the propane spectrum in Fig. 1 agrees with

[1] For example, see Barnes, Gore, Stafford, and Williams, Anal. Chem. **20**, 402 (1948).

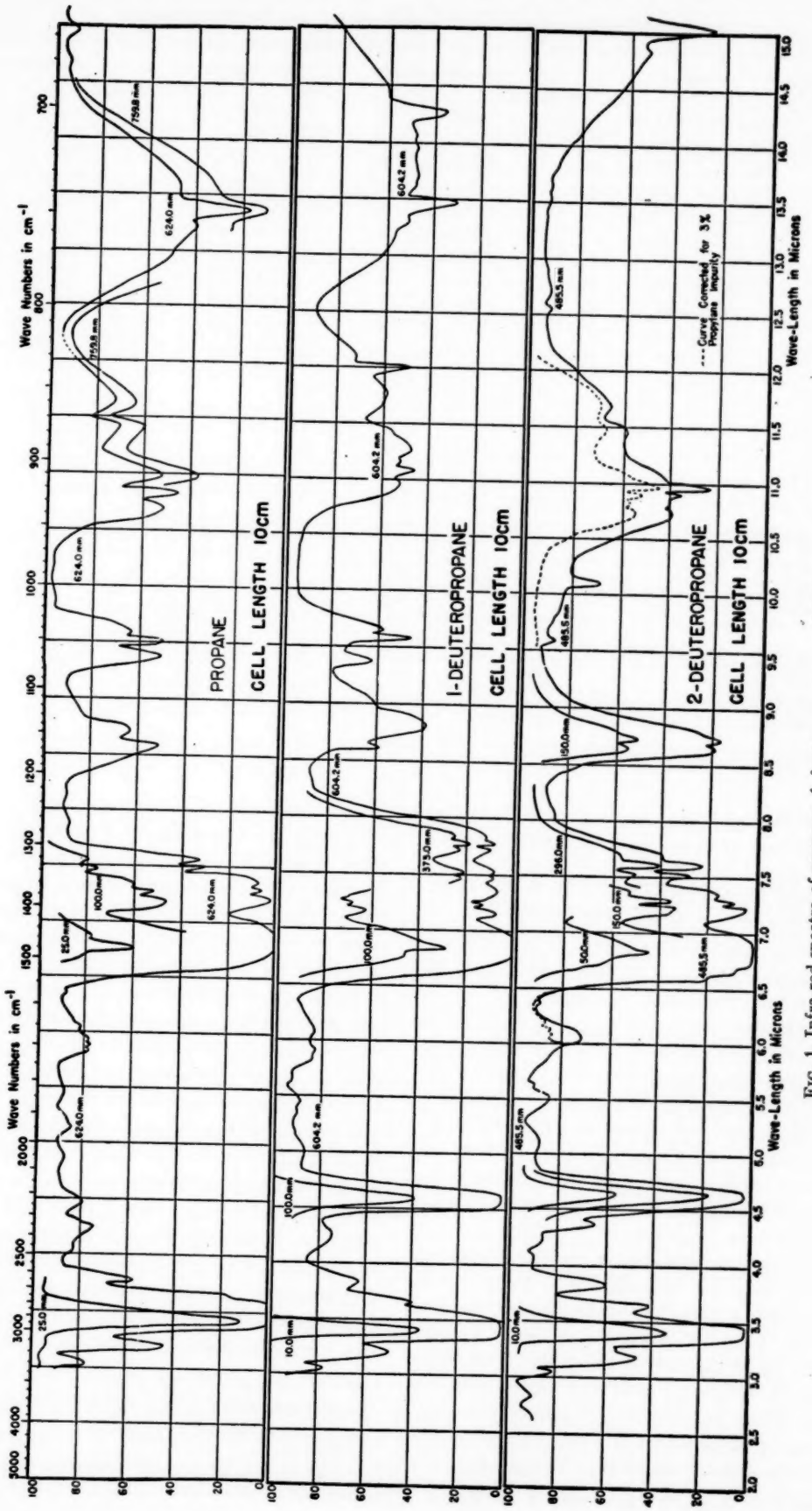

FIG. 1. Infra-red spectra of propane, 1-deuteropropane and 2-deuteropropane.

TABLE I. Vibrations of propane, 1-deuteropropane, and 2-deuteropropane.[a]

Designation[b]	Propane[c-e] C_{2v}		1-Deuteropropane[c,d,f,g] C_s		1-Deuteropropane[g] C_1	2-Deuteropropane[c,d,h] C_s	
S_1, D_1, R_1	$(CH_3)_{ex,\alpha}+(CH_3)_{ex,\gamma}$	A_1	$(CH_2D)_{a',\alpha}$	A'	$(CH_2D)_{a',\alpha}$	$(CH_3)_{ex,\alpha}+(CH_3)_{ex,\gamma}$	A'
S_2, D_2, R_2	$(CH_3)_{ex,\alpha}-(CH_3)_{ex,\gamma}$	B_1	$(CH_3)_{ex,\gamma}$	A'	$(CH_3)_{ex,\gamma}$	$(CH_3)_{ex,\alpha}-(CH_3)_{ex,\gamma}$	A''
S_3, D_3, R_3	$(CH_3)_{ey,\alpha}-(CH_3)_{ey,\gamma}$	B_2	$(CH_2D)_{a'',\alpha}$	A''	$(CH_2D)_{a'',\alpha}$	$(CH_3)_{ey,\alpha}-(CH_3)_{ey,\gamma}$	A'
S_4, D_4, R_4	$(CH_3)_{ey,\alpha}+(CH_3)_{ey,\gamma}$	A_2	$(CH_3)_{ey,\gamma}$	A''	$(CH_3)_{ey,\gamma}$	$(CH_3)_{ey,\alpha}+(CH_3)_{ey,\gamma}$	A''
S_5, D_5	$(CH_3)_{a_1,\alpha}+(CH_3)_{a_1,\gamma}$	A_1	$(CH_2D)_{a',\alpha}$	A'	$(CH_2D)_{a'\,\alpha}$	$(CH_3)_{a_1,\alpha}+(CH_3)_{a_1,\gamma}$	A'
S_6, D_6	$(CH_3)_{a_1,\alpha}-(CH_3)_{a_1,\gamma}$	B_1	$(CH_3)_{a_1,\gamma}$	A'	$(CH_3)_{a_1,\gamma}$	$(CH_3)_{a_1,\alpha}-(CH_3)_{a_1,\gamma}$	A''
R_5	$(CH_3)_{a_2,\alpha}+(CH_3)_{a_2,\gamma}$	A_2	$(CH_2D)_{a'',\alpha}$	A''	$(CH_2D)_{a'',\alpha}$	$(CH_3)_{a_2,\gamma}+(CH_3)_{a_2,\alpha}$	A''
R_6	$(CH_3)_{a_2,\alpha}-(CH_3)_{a_2,\gamma}$	B_2	$(CH_3)_{a_2,\gamma}$	A''	$(CH_3)_{a_2,\gamma}$	$(CH_3)_{a_2,\alpha}-(CH_3)_{a_2,\gamma}$	A'
S_7, D_7	$(CH_2)_{a_1,\beta}$	A_1	$(CH_2)_{a_1,\beta}$	A'	$(CH_2)_{a_1,\beta}$	$(CHD)_{a',\beta}$	A'
R_7	$(CH_2)_{a_2,\beta}$	A_2	$(CH_2)_{a_2,\beta}$	A''	$(CH_2)_{a_2,\beta}$	$(CHD)_{a'',\beta}$	A''
R_8	$(CH_2)_{b_2,\beta}$	B_1	$(CH_2)_{b_2,\beta}$	A'	$(CH_2)_{b_2,\beta}$	$(CHD)_{a'',\beta}$	A''
S_9, R_9	$(CH_2)_{b_1,\beta}$	B_2	$(CH_2)_{b_1,\beta}$	A''	$(CH_2)_{b_1,\beta}$	$(CHD)_{a',\beta}$	A'
S_{10}	$(C_3)_{a_1}$	A_1	$(C_3)_{a'}$	A'	C_3	$(C_3)_{a'}$	A'
S_{11}	$(C_3)_{b_1}$	B_1	$(C_3)_{a'}$	A'	C_3	$(C_3)_{a''}$	A''
D_8	$(C_3)_{a_1}$	A_1	$(C_3)_{a'}$	A'	C_3	$(C_3)_{a'}$	A'

[a] Some of the modes described here would not result in conservation of angular momentum. This refinement is omitted because of the qualitative nature of these descriptions.

[b] The letters S, D, and R in column 1 indicate whether the propane vibrations in column 2 are stretching (S), deformation (D), or rocking or twisting (R). Thus the combination $(CH_3)_{ex,\alpha}+(CH_3)_{ex,\gamma}$ belongs in all three categories while $(CH_2)_{b_2,\beta}$ involves only a rocking motion of the CH_2 group. The subscripts in column 1 serve to designate vibrations specific to propane. However, the deuteropropane vibrations described in columns 3, 4, and 5 exhibit the same S, D, or R character as the propane vibrations in the same line.

[c] The symbols in capital letters appearing after each combination denote the group representation to which the combination belongs. See Section III for details about the formation of these combinations.

[d] The stretching and deformation modes S_1-S_6 and D_1-D_6 make use of the single symmetric, and the degenerate pair of unsymmetric, vibrations of the CH_3 group.

[e] Since the plane of the CH_2 group is normal to the C_3 plane the symmetry designations for this group differ from those for the molecule as a whole. Thus the unsymmetrical stretching motion S_9 of this group has the symmetry b_1 as far as the CH_2 group is concerned but it has the symmetry B_2 as far as the propane molecule as a whole is concerned.

[f] When a D atom is substituted on a CH_3 group to give the C_s isomer of 1-deuteropropane, propane vibrations of types A_1 and B_1 yield A' vibrations of 1-deuteropropane. Similarly, B_2 and A_2 propane vibrations yield A'' 1-deuteropropane vibrations.

[g] Only the group vibrations are given for the 1-deuteropropanes. The ways in which these interact to give the molecular vibration modes have not been indicated.

[h] In 2-deuteropropane the symmetry plane is normal to the C_3 plane. Therefore, B_1 and B_2 propane vibrations become A'' and A' 2-deuteropropane vibrations, respectively.

that of Wu and Barker.[2] Apparently the bands in their spectrum at 720 and 1179 cm^{-1} are foreign to propane.

III. VIBRATIONAL MODES OF PROPANE, 1-DEUTEROPROPANE, AND 2-DEUTEROPROPANE

Without free rotation, equilibrium configurations of propane, 1-deuteropropane, and 2-deuteropropane belong to one of the symmetry classes, C_{2v}, C_s, or C_1. Plausible equilibrium forms for propane are the C_{2v} form shown in Fig. 2, another C_{2v} form in which both methyl groups have been rotated 60° about their z axes in Fig. 2, and a C_s form in which only one methyl group has been rotated 60° about its z axis. The simplicity of the propane spectrum suggests that only one equilibrium form needs to be considered and the vibrational analysis herein applies to propane with either of the C_{2v} configurations.

If each of the deuteropropanes is considered derived from propane with a C_{2v} configuration, 2-deuteropropane has only one equilibrium configuration with C_s symmetry while 1-deuteropropane has two configurations, one with the deuterium in the plane of the three carbons with C_s symmetry and the other with the deuterium out of this plane with C_1 symmetry.

Each of these molecules has 27 vibrational modes of which 21 are infra-red active for the C_{2v} symmetry and all are active for C_s symmetry or C_1 symmetry. All vibrations of all models are Raman active. All but the three modes of the C_3 skeleton may be described qualitatively as combinations of vibrations within the CH_3, CH_2, CH_2D, and CHD groups, and of rocking or twisting of these groups. These descriptions may be simplified by divorcing the motions of the end groups from the center group, and by considering the stretching, deformation, and rocking modes not to interact.[3] Such combinations are listed in Table I. The symbolism used in Table I is related to the axes used in Fig. 2 where each group is given its own set of x, y, and z axes. The groups are distinguished by the letters α, β, and γ, as shown in Fig. 2. The modes for each group are described in terms of the representations of its symmetry class (C_{3v} for CH_3; C_s for CH_2D, CHD; and C_{2v} for CH_2). A symbol $(CH_3)_{a_1,\alpha}$ denotes an a_1 vibration within the α-CH_3 group. Similarly $(CH_3)_{ex,\gamma}$ denotes a degenerate (e) vibration within the γ-CH_3 group which transforms in the same manner as an x displacement of this group. Lower-case letters are used, as above, to describe the symmetry properties of vibrations *within* the groups, upper-case letters to describe vibrations of the whole molecule.

[2] V. L. Wu and E. F. Barker, J. Chem. Phys. **9**, 487 (1941).

[3] Only motions of different symmetry type can be rigorously separated in this manner.

TABLE II. Infra-red bands of propane, 1-deuteropropane, and 2-deuteropropane.

Propane			1-Deuteropropane			2-Deuteropropane		
ν(cm^{-1})	$\lambda(\mu)$	Description[a]	ν(cm^{-1})	$\lambda(\mu)$	Description[a]	ν(cm^{-1})	$\lambda(\mu)$	Description[a]
736.3	13.581	*R* w	692.9	14.433	*R* w	665.1	15.037	*Q* sh m
			700.9	14.268	*Q* sh w	673.8	14.841	*P* w
			712.3	14.039	*P* w			
747.5	13.376	*Q* sh m				853.6	11.715	w
756.6	13.218	*R* w	724.8	13.797	*R* w			
			743.2	13.455	*Q* sh w	877.1	11.401	w
			751.7	13.303	*P* w			
858.4	11.650	*R* w	758.2	13.189	w	911.3	10.973	*Q*? s[b]
875.6	11.421	*P* w				917.2	10.902	sh w
911.3	10.973	*R* sh w	834.1	11.989	*Q* sh w	925.5	10.804	w
923.3	10.832	*Q* sh w				932.4	10.725	w
935.4	10.690	*P* sh w	848.9	11.780	broad w			
						990.5	10.096	(i)
1043.1	9.587	*R* sh w	874	11.44	w	1041.4	9.602	(i)
1052.0	9.506	*P* sh w						
1067.0	9.373	*Q* sh w				1142.9	8.750	*Q*? sh m
			888	11.26	broad w	1155.9	8.651	*P*? m
1146.3	8.723	w						
1164.5	8.587	sh w	896.6	11.153	*R*? w			
			902.7	11.078	*Q* w	1316	7.602	*Q*? m
1323	7.560	sh w	911.3	10.973	*P*? w	1330	7.517	sh m
			1030	9.708	sh w			
1336	7.485	sh w	1044.0	9.579	sh w	1362	7.341	m
						1373	7.281	m
1359	7.357	*R*? m	1057.4	9.456	sh w			
1373	7.281	*Q*? sh m	1134.6	8.814	broad w	1384	7.227	m
1390	7.194	m						
1456	6.870	m	1162.1	8.605	sh w	1465	6.824	*Q*? sh m
1478	6.767	*Q*? sh m						
			1277	7.829	*R* sh m	1656	6.042	w
			1285	7.778	*Q* sh m			
1699	5.886	w	1294	7.726	*P* sh m			
1842	5.430	w	1330	7.517	sh m	*1820*	5.49	w
			1340	7.463	sh m			
			1382	7.238	sh m	*1950*	5.12	w
1940	5.155	w	1394	7.173	sh m			
			1463	6.835	*Q*? m	2154	4.643	sh s
2250	4.445	w	1473	6.790	m			
						2285	4.377	w
2350	4.255	w	1648	6.068	w	2350	4.255	w
						2450	4.082	w
2647	3.778	w	1691	5.913	w			
						2610	4.831	w
2938	3.403	s	1715	5.831	w			
			1840	5.434	w	2738	3.652	m
			2000	5.000	w			
3138	3.186	s	2169	4.610	m			
						2938	3.403	s
3311	3.020	m	2350	4.255	w	3099	3.226	m
						3138	3.186	w
			2610	3.831	w	3311	3.020	w
			2738	3.652	w			
			2938	3.403	s			
			3119	3.206	w			
			3287	3.042	w			

[a] The band intensities have been indexed according to the value of $I = 1/p \log 1/t$, where t is the transmission and p the pressure in mm. Values of I in the ranges >0.01; <0.01 >0.001; <0.001 are used for strong (s), medium (m), and weak (w), respectively.
[b] Part of this absorption is caused by propylene impurity.

IV. VIBRATIONAL ANALYSIS

The bands in the infra-red spectra of propane, 1-deuteropropane, and 2-deuteropropane are listed in Table II together with notations of their intensities and structures. In all three spectra, the C—H stretching vibrations superpose in the unresolved bands at 2938 cm^{-1}. As expected, the C—D stretching vibrations are displaced: to 2169 cm^{-1} in the spectra of 1-deuteropropane and 2154 cm^{-1} in the spectrum of 2-deuteropropane.

The propane bands at 748 and 1053 cm^{-1} are strongly displaced in the spectrum of 2-deuteropropane but are

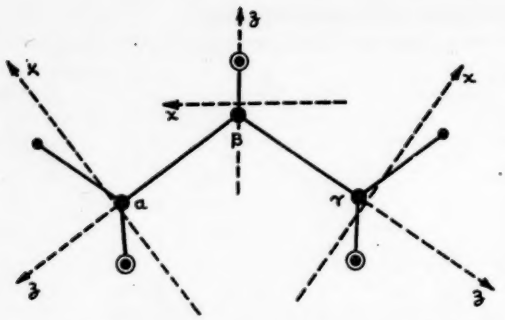

FIG. 2. Equilibrium configuration of propane. The two CH_3 groups and the CH_2 group have been given right-handed systems of axes. These groups are denoted, respectively, by the letters α, β, γ (see text).

only slightly displaced in the spectrum of 1-deuteropropane.[4] Therefore, these bands must be associated with vibrations of the CH_2 group. The CH_2 stretching and deformation vibrations occur at higher frequencies, and the rocking mode R_7 is forbidden.[5] The shape of the 748-cm^{-1} band results from a B_2 moment;[6] therefore, this band must be associated with the R_9 motion in which CH_2 group rocks approximately about the x axis in Fig. 2. This agrees with the mode assigned to the 725-cm^{-1} band in the spectra of long chain paraffins by Sheppard and Sutherland, and Sutherland and Vallance-Jones.[7] Their conclusion was based on the study of the spectra of a fully deuterated paraffin and of oriented polyethylenes irradiated with polarized radiation. The shape of the 1053-cm^{-1} band results from a B_1 moment; therefore, this band must be associated with the R_8 motion in which the CH_2 group rocks around the y axis in Fig. 2.

The 743-cm^{-1} band in the spectrum of 1-deuteropropane, corresponding to the 748-cm^{-1} band in the propane spectrum, is accompanied by a similar band at 701 cm^{-1}, which has no counterpart in the spectra of propane and 2-deuteropropane. This 701-cm^{-1} band is conceivably associated with the CH_2 rocking motion, analogous to R_9, in the unsymmetrical form of 1-deuteropropane.

The bands at 870 and 923 cm^{-1} in the propane spectrum are clearly of the A_1 and B_1 types, respectively. The conclusions already made reduce the possible assignments for these bands to the alternatives, S_{10} and R_1 for the 870-cm^{-1} band, and S_{11} and R_2 for the 923-cm^{-1} band. The bands next higher in frequency come at 1160 and 1336 cm^{-1}. The shape of the former is not distinctive and that of the latter is obscured by additional absorption on its short wave-length side. The possibilities for assigning these bands cannot be limited as they can be for the 870 and 923 cm^{-1} bands. The spectrum of 1-deuteropropane shows bands near all of these frequencies and attempts to use this spectrum to clarify further the propane assignments have not been successful. The bands beyond 1336 cm^{-1}, not well resolved in Fig. 1, are typical of the spectra of paraffin hydrocarbons and are known to be associated with deformation and stretching vibrations of CH_2 and CH_3 groups.

V. ACKNOWLEDGMENTS

Mr. F. E. Frey was instrumental in initiating this work. Miss Nora Potts prepared the spectrograms. Professor J. Rud Nielsen of Oklahoma University supplied the Raman data.

[4] In the Raman spectrum of propane a line at 1064 cm^{-1} is the only line near 1053 cm^{-1}. The Raman spectrum of 1-deuteropropane has a corresponding line at 1048 cm^{-1}; but the Raman spectrum of 2-deuteropropane has no line corresponding to these in position or intensity. From unpublished findings of J. Rud Nielsen.

[5] The vibrational mode R_7 would be active in the C_s propane isomer. If a C_{2v} and a C_s isomer are present together, the bands in the spectrum of one must be weak or the spectra of both isomers must largely superpose. In any case, if the R_7 vibration of the C_s isomer produced a band in the propane spectrum its counterpart in 2-deuteropropane would be strongly shifted. There is no obvious indication of such a phenomenon.

[6] The application of band shapes to the analysis of the propane spectrum has been discussed by Wu and Barker (reference 2). The general principles have been given by Badger and Zumwalt (J. Chem. Phys. 6, 711 (1938)). For propane the A_1 bands have P and R branches with the Q branch weak or absent, the B_2 bands have strong Q branches and weak P and R branches, and the B_1 bands have P, Q, and R branches of comparable intensity.

[7] Cf. G. B. B. M. Sutherland and A. Vallance-Jones, Nature 160, 567 (1947); N. Sheppard and G. B. B. M. Sutherland, Nature 159, 739 (1947).

The Consistency of the Thermodynamic Data for Water Substance Vapor Phase to 550°C. Part VII.[1]

FREDERICK G. KEYES
Department of Chemistry, Massachusetts Institute of Technology, Cambridge, Massachusetts

(Received February 11, 1949)

A comprehensive investigation of the thermodynamic consistency of the large body of steam data above 150°C has been completed using the new thermodynamic scale information supplied by Professor J. A. Beattie to test the consistency of measured vapor pressures, specific volumes, enthalpies at saturation and superheat and specific heats. As an aid in correlation and unification a new form of equation of state is employed which has some validity through the critical region. The results of the investigation indicate a satisfactory state of thermodynamic consistency over the liquid-vapor range with respect to vapor pressures and saturation volumes deduced from the measured vaporization quantities using the Beattie corrections to the international temperature scale. The consistency test includes also verification of the accuracy and usefulness of the new functional relation for the vapor phase, $p=F(v, T)$ whose parameters were determined from the measured superheat p-v-T data. The superheat enthalpy data to 550°C at zero pressure is however not consistent with the present theoretical information pertaining to C_p^0. The computed enthalpies of the vapor to 550°C and pressures of 300 kg/cm² are satisfactory provided an empirical correction term is subtracted from the theoretical values of C_p^0. The accuracy of the Keenan-Keyes steam tables values of specific volume, pressure, and enthalpy is confirmed.

INTRODUCTION

THE cooperating experts[a] attending the Third International Steam Tables Conference, sponsored by the American Society of Mechanical Engineers, and held in Washington, Cambridge, and New York in September, 1934, brought to the meetings critical correlations of the experimental data obtained in the course of an extensive international program of steam properties measurement. The correlations presented formed the basis for the skeleton tables of steam and liquid water properties subsequently published.[2] In the course of the meetings it became apparent that the degree of accuracy attained for water substance properties above 200°C was very satisfactory and a doubt was in consequence suggested that the available knowledge of the properties below 200°C, regarded as entirely sufficient at the time of the London Conference in 1929, might not be of comparable accuracy. At the final session of the 1934 Conference a resolution was passed expressing the hope that the experimental programs would be continued by the several national groups with special reference to water substance properties in the lower temperature range.

Thus, it was considered desirable that the enthalpy measurements be continued at the Imperial College of Science, London, that the group at the National Bureau of Standards carry out new measurements of saturation properties from 0 to 100°C using their highly developed thermal method and include also an investigation similar to that volunteered by the Reichsanstalt group relative to new measurements of the saturation pressure in the lower range of temperature. The group at the Massachusetts Institute of Technology agreed to continue the measurements of enthalpy change with pressure in the range 0 to 150°C begun in 1932. The foregoing commitments have been largely completed and published. In addition there has also appeared an important investigation independent of the steam research program by James A. Beattie and his collaborators[3] on the relation of the 1927 international scale of temperature to the nitrogen gas thermometer scale. The ensemble of information pertaining to low temperature steam and thermometric data has been correlatively treated for thermodynamic consistency in a recent paper.[1—Part VI]

The published directly-measured volume data[1—Part IV, b] for water substance extends to 460°C and 360 atmos., the measured enthalpy values in the superheat to 600°C,[4] and the vapor pressures of three independent

[1] Parts I–VI have appeared as follows: Part I. Frederick G. Keyes, Proc. Am. Acad. **68**, 505 (1933); Part II. Smith, Keyes, and Gerry, *ibid.* **69**, No. 3, 137 (1934); Part III. Leighton B. Smith and Frederick G. Keyes, *ibid.* **69**, No. 7, 285 (1934); Part IV. Keyes, Smith, and Gerry, *ibid.* **70**, No. 8, 319 (1936); Part V. Samuel C. Collins and Frederick G. Keyes, *ibid.* **72**, No. 8, 283 (1938); Part VI. Frederick G. Keyes, J. Chem. Phys. **15**, No. 8, 602 (1947).

[a] The technical delegates were: *United States:* H. N. Davis, H. C. Dickinson, J. H. Keenan, F. G. Keyes, C. N. LePage, G. A. Orrok, N. S. Osborne and L. B. Smith; *Great Britain:* G. S. Callendar, A. C. G. Egerton, H. L. Guy, I. V. Robinson; *Germany:* H. Hausen, F. Henning, W. Koch, F. Michel, E. Schmidt.

[2] Mech. Eng. **57**, 710 (1935).

[3] The following nine papers have been published to date: Part I. Beattie, Jacobus, and Gaines, Proc. Am. Acad. **66**, 167 (1930). Part II. Beattie, Benedict, and Blaisdell, *ibid.* **71**, 327 (1937). Part III. J. A. Beattie and B. E. Blaisdell, *ibid.* **71**, 361 (1937). Part IV. Beattie, Blaisdell, and Kaminsky, *ibid.* **71**, 375 (1937). Part V. Beattie, Huang, and Benedict, *ibid.* **72**, 137 (1938). Part VI. Beattie, Jacobus, Gaines, Jr., and Benedict, *ibid.* **74**, 327 (1941). Part VII. Beattie, Benedict, and Kaye, *ibid.* **74**, 343 (1941). Part VIII. Beattie, Blaisdell, Kaye, Gerry, and Johnson, *ibid.* **74**, 371 (1941). Part IX. Beattie, Blaisdell, and Kaye, *ibid.* **74**, 389 (1941).

[b] The earlier measurements were made at pressures to about 11 atmos. and to 190°C by Knoblauch, Linde, and Klebe, Mitteilung über Forschungsarbeiten auf dem Gebeite des Ingenieurswesens, Heft 21 (1905).

[4] A. C. G. Egerton and G. S. Callendar reported their extensive

investigations are complete from 140°C to the critical temperature.[5] There are also available extensive measurements of the vapor superheat specific heat capacity[6] and the Joule-Thomson quantity $(dT/dp)_h$,[7] where T is the thermodynamic temperature, p the pressure, and h the enthalpy of unit mass. Since the correlative treatment of the volume data for the third conference published as Part IV, an excellent analysis of the enthalpy measurements of J. Havlíček and L. Miškowský has appeared by Jan Jüza.[8] He showed that the volumes deduced for superheated steam from the enthalpy measurements of Havlíček and Miškowský through use of the relation $(\partial h/\partial p)_T = \partial v\tau/\partial \tau_1 (\tau = T^{-1})$ were in good agreement with the direct measurements.

The formulations of the volume data of Jüza[8] and the writer have however been of the form $v = f(p, T)$, a form generally preferred by engineers because most practical problems are presented in terms of the independent variables, pressure and temperature. These formulations ($f(p, T)$) are valid however only to about 12 cc per g, and indeed no formulation of this type is known which admits of accurate representation of volume data to the critical condition.

The usefulness of a reliable formulation of the form $p = F(v, T)$ which represents the data through the critical region is of considerable practical convenience[9–11, e] and also of interest in view of the important investigations of J. E. Mayer and his associates[12] on the mechanism of condensation culminating in the critical state. A semi-empirical equation of the foregoing general form is proposed in this paper and employed to represent the volume observations to values less than the critical volume. The formulation leads also to inferences bearing on the suggestions Mayer has shown follow from his theory of the condensation phenomenon.

From the practical point of view an equation which allows of accurate representation of pressure-volume-temperature data is a virtual necessity for thermodynamic calculations and can be used for the tabulation of constant pressure properties although the form of representation employed is $p = F(v, T)$. Indeed with modern mechanical means of carrying out numerical computations the often expressed predilection for a correlating equation of the form $v = f(p, T)$ loses point particularly if the properties in the critical region can be represented.

The temperature scale used in all the measurements made by the participants in the steam program was that adopted by international agreement in 1927.[13] In the present paper however, as in the recent paper (reference 1, Part VI) use will be made of the comparisons of the nitrogen gas thermometer readings with the indications of the platinum resistance thermometer according to the 1927 specifications, the international scale, carried out by James A. Beattie and his associates.[3, d] The scale differences available, however, do not extend beyond the sulfur boiling point, but the effects of the differences determined by Beattie are more pronounced over the region of phase equilibrium of water ($t_c = 374.15$°C) while the variations introduced in computing the enthalpy, entropy, or other thermodynamic functions due to imperfect knowledge of the thermodynamic scale become of smaller consequence above the critical temperature or in the superheat region.

The intent of the present paper is to review the available fundamental experimental data for water substance

measurements of the enthalpy of superheated steam in the following publications of the Brit. Elec. and Allied Ind. Res. Ass., as follows: Part I. J/T79 An Investigation of the Errors of Determination of Total Heat of Steam by the Condenser Method. Part II. J/T83 Investigation of the Total Heat of Steam by the Condenser Method. Part III. J/T99 Same title as Part II. Further Measurements to 175 kg per g. Part IV. J/T115 Same title as Part II. Experiments with high temperature apparatus and extension of the measurements above 200 kg per sq. cm and 500°C. (600°C was reached). Jaraslav Havlíček and Ladeslav Miškowský, Helv. Chim. Acta **9**, 161 (1936). Enthalpies to 400 kg per sq. cm and from 150° to 550°C.

[5] Osborne, Stimson, Fiock, and Ginnings, Bur. Stand. J. Research **10**, 155 (1933). A. C. G. Egerton and G. S. Callendar, Phil. Trans. Roy. Soc. **231A**, 147 (1932). See also an important note on the flow method measurements by the authors in the publication, Brit. Elec. and Allied Res. Assoc., J/T87 (August 31, 1934). The values from this work used in the present paper are from the latter reference. Also see reference I, Part II. The foregoing references relate to the measurements of vapor pressures under the international steam properties program in which no measurements were reported below 100°C. Reliance for the lower pressures was placed on the critical evaluation of the older measurements as given in the *Wärmetabellen* by Holborn, Scheel, and Henning (Vieweg und Sohn Braunschweig, Germany, 1919). An important later paper on the vapor pressures from 75° to 125°C is that of H. Moser and A. Zmaczynski, Physik. Zeits **40**, 221 (1939).

[6] O. Knoblauch and W. Koch, Zeit. ver. deut. Eng. **72**, 1733 (1928). W. Koch, Forschungsarbeiten auf dem Gebeite des Ingenieurwesens **3**, 1 (1932); **3**, 189 (1932).

[7] H. N. Davis, Mech. Eng. **47**, 107 (1925); R. V. Kleinschmidt, Mech. Eng. **48**, 155 (1926); H. N. Davis and J. H. Keenan, World Eng. Conf. Report No. 455, Tokyo (1929).

[8] Jan Jüza, Engineering **146**, 1 (1938).

[9] Benedict, Webb, and Rubin, J. Chem. Phys. **8**, 334 (1940); J. Chem. Phys. **10**, 747 (1942).

[e] Benedict and his co-workers (see reference 9) have shown that the volume properties of the hydrocarbon substances, methane, ethane, propane, and *n*-butane can be represented with substantial accuracy through the critical region and into the liquid phase by analytical additions to the equation of Beattie and Bridgeman (see reference 10). The number of additional constants required is only three more than occurs in the original Beattie-Bridgeman equation and by making use of an extension of the combination rules for the equation of state constants suited to the Beattie-Bridgeman equation, the properties of binary and even ternary mixtures of the four substances can be represented for some properties with an error of a part in two hundred.

The Beattie-Bridgeman equation in its original form cannot however be used to represent the volume properties of a pronouncedly polar substance of which water and ammonia are examples, even for large volumes, except at very high temperatures; a fact demonstrated in the Part IV paper on water substance. The situation has been discussed in detail by Walter H. Stockmayer (see reference 11) from the point of view of the theory of intramolecular force, both for pure polar substances and mixtures of polar and non-polar species.

[10] J. A. Beattie and O. C. Bridgeman, J. Am. Chem. Soc. **49**, 1665 (1927).

[11] W. H. Stockmayer, J. Chem. Phys. **9**, 863 (1941).

[12] J. E. Mayer and S. F. Harrison, J. Chem. Phys. **6**, 87 (1938); J. E. Mayer and M. G. Mayer, *Statistical Mechanics* (John Wiley and Sons Inc., New York, 1940).

[13] G. K. Burgess, Bur. Stand. J. Research **1**, 635 (1927).

[d] There is reason to believe, however, that the international scale may depart from the thermodynamic scale by as much as a degree at 1000°C.

in the gaseous phase, mainly from the point of view of thermodynamic consistency, and to suggest what appear to be the most likely values for important thermodynamic quantities to 600°C. Further measurements suggested by the present investigation would be desirable partly for practical reasons in view of the use of steam at higher pressures and temperatures in power generation and partly also for reasons relating to the theory of intramolecular forces in view of the highly polar character of water.

The liquid phase of water will not be given attention except incidentally, relative to a consideration of the critical region on the vapor side of the "dome." The pressure-temperature formulation for the liquid given in the paper, Part III, failed as an extrapolation device to saturation in the latter region. Additional accurate volume data at high densities and to a temperature of at least 600°C would be desirable above the pressure range of the old steam research program (340 atmos.) and extending to perhaps 5000 atmos. The additional data would provide material for promoting an understanding of the exceptional behavior of water in the liquid and highly compressed vapor phase, in particular the rapid rise of the coefficient $(\partial p/\partial T)_v$ with temperature which in the case of water substance is in contrast to the near constancy of the coefficient for other liquids, ethyl ether or isopentane, for example. Thus, from Amagat's data at the constant volume for 10.5 atmos. at 0°C, $(\Delta p/\Delta T)_v$ is 0.33 in the range 0–10°C, 3.2 for 10–20°, and 5.9 for 20–30°. However the volume for 2130 atmos. and 0°C for the same temperature ranges shows $(\Delta p/\Delta T)_v$ to be respectively for the same temperature intervals 14.4, 15.4, and 17.1, a very marked diminution in the scale of variation of the coefficient. By way of rough summary, the behavior of water as regards the course of $(\partial p/\partial T)_v$ for liquid water approaches that of liquid ethyl ether, or liquid isopentane, only at volumes corresponding to pressures far higher than the saturation pressure. There is also great need for the high density data at higher temperatures for the interpretation of geological phenomena.

THE REPRESENTATION OF THE VOLUME DATA IN THE FORM $p=F(v, T)$

The equations proposed and used for correlating volume data are exceedingly numerous since the equation of van der Waals was published. The first quantitatively accurate relationship of the van der Waals type[14, e] satisfactory for substances in the gas or liquid phase in the region where constancy of $(\partial p/\partial T)_v$ is a good approximation, failed however to bridge the values to the liquid phase volume near the critical region. In the intervening years, however, much has been learned regarding the origin of intermolecular forces and the theory of the equation of state. Theory and empirical guides have led to the possibility of representing the properties of the gas phase with accuracy to volumes three to fourfold the critical. Knowledge of the structure of the liquid phase has also made substantial progress although the problem may by no means be considered solved.

The specific form of equation here used to correlate the observed data for steam was originally based on the attempt to compare the series form of temperature function given by the theory with the second virial coefficients derived from the experimental volume data. The required numerous terms of the series expression for the second virial coefficient derived from the theory for polar substances below the critical temperatures are far too cumbersome for practical purposes and a closed empirical expression was sought. Walter H. Stockmayer[11] has recently examined the empirical form proposed for the second virial coefficient, namely $B(T)=\beta - A_0\tau \exp C_2\tau^2 (\tau = T^{-1})$, and in the case of the water molecule found it to be a fair equivalent of the theoretical series form. The theory as at present developed also gives the higher virial coefficients in series form.[12, f] The following function $\varphi(v, T)$ has however been constructed on the basis of an examination of the extensive data for steam. The following form is the equivalent of a closed expression for the theoretical series form of representation and valid for representing the volume data to values of the order of the critical volume.

$$\log RT/pv = \log\omega/v + \psi\omega/v^2, \tag{1}$$

where ω represents $v-\delta$, the symbol δ representing the expression $\beta \exp(-\alpha/v)$. The quantity ψ is a temperature-density function $\psi=\psi_0(1+\bar{\psi}_1\rho+\cdots)$ where $\psi_0 = \bar{A}_0\tau \exp c_2\tau^2$. The symbol $\bar{A}_0 \equiv \bar{A}_0/R$ and $\bar{\psi}_1$, etc., can be expressed in terms of ψ_0 and τ.

At very large volumes and high temperatures Eq. (1) becomes

$$p = RT/(v-\beta) \exp(-\bar{A}_0\tau/v), \tag{1a}$$

identical in form with the equation of Dieterici. Expansion of the exponential brings Eq. (1a) into the form due to van der Waals, namely

$$p = (RT/v-\beta) - (A_0/v^2), \tag{1b}$$

provided the second term of the right hand member is taken to be a sufficient approximation for $A_0/(v-\beta)v$.

An intermediate approximation of (1) follows by expanding $1/\omega$ to the expression $1/v+\beta/v^2(1-\alpha/v)$ and

[14] F. G. Keyes, Am. Soc. Refrig. Eng. 1, 9 (1914).

[e] In this paper the older data for helium, hydrogen, nitrogen, oxygen, air, carbon dioxide are shown capable of accurate representation to high densities above the critical temperature, while the liquid phase of isopentane was also shown to be representable by the same form but involving different constants. The equation, $p=RT/v-\delta-A/(v+1)^2$ where $\delta=\beta \exp^d(-\alpha/v)$, now appears to be the general limiting form of Eq. (1) for high temperatures relative to the critical state.

[f] See Chapters 13 and 14 of *Statistical Mechanics*, by Mayer and Mayer (see reference 12) for a presentation of the modern theory of imperfect gases and the authors' theory of condensation culminating in the critical state.

ψ_0 to $A_0/R\tau(1+c_2\tau^2)$. Thus we find equation

$$p=RT/v[1+\beta/v(1-\alpha/v)] -A_0/v^2(1+c_2\tau^2)(1+d_1/v-d_2/v^2). \quad (1c)$$

The Beattie-Bridgeman equation[10] is usually written in the following form:

$$p=RT/v^2[v+B_0(1-b/v)][1-(c/v)\cdot\tau^3] -A_0/v^2(1-a/v), \quad (1d)$$

or by rearrangement as follows:

$$p=RT/v\left[1+\frac{B_0}{v}(1-b/v)\right] -A_0/v^2\left(1+\frac{RC}{A_0}\tau^2\right)[1+D_1/v-D_2/v^2]. \quad (2)$$

The first term of the right-hand member of Eq. (2) is identical with Eq. (1c). The second term is similar in form to (1c) where D_1 and D_2 are also temperature functions.

It will be observed that at high temperatures Eq. (1c) as an approximation for high temperatures, can be written:

$$p=(RT/v-\delta)-[A_0/(v-d_1/2)^2],$$

which is also essentially identical with an equation used by the writer[14] more than thirty years ago and found to represent the "permanent" gases, nitrogen, air, oxygen, hydrogen, etc., to considerable pressures (1000 atmos.) at temperatures from 0° to 200°C. However in general in the region below and above the critical temperature, Eq. (1d) has been shown to be satisfastory[15] to volumes of about 12 to 15 cc per g.

A convenient procedure in applying Eq. (1) for the evaluation of the parameters is suggested by the following expansion.

$$v\log RT/pv=(-\beta+\psi_0)+\text{terms in the density } (\rho). \quad (3)$$

Accordingly by plotting the combination of observable quantities, $v\log RT/pv$, as ordinates for constant temperatures with the density as abscissas, values of the quantity $-\beta+\psi_0$[g] may be found from the axis intersection of $v\log RT/pv$ for zero density. Designating the latter quantity by the symbol z_0 for brevity, a second plot can be made of z_0 *versus* $\tau\cdot 10^{c_2\tau^2}$, where c_2 is estimated to a first approximation by using a corresponding states rule.[15] By successive trials a value of c_2 can be found which brings z_0 into satisfactory linear relation to $\tau\cdot 10^{c_2\tau^2}$.[h]

To verify the value of β and obtain an estimate of α, p/T may be plotted *versus* T^{-1} or τ or $\tau\cdot 10^{c_2\tau^2}$ for constant volumes. The lines will be nearly linear at high temperatures and the intersections with the ordinate axis for $\tau=0$ gives the values of $R/v-\delta$ which may be designated $f(v)$. Since $\log\delta=\log(v-f(v))=\log\beta-\alpha/v$, the values of β and α are easily found.

The slope of the lines at $\tau\rightarrow 0$ may also be used to give values of $A_0/v^2(1+c_2\tau^2)$ from which A_0 may be obtained and also an estimate of c_2 in favorable cases.

Following a decision on the values of β and ψ_0, the quantity $[(v^2/\omega\log RT/p\omega)1/\psi_0-1]$ abbreviated to $(\varphi-1)$ for constant temperatures may be computed. The quantity φ requires a knowledge of α for computing the variable $\omega=v-\delta$, where δ is the expression $\beta\exp(-\alpha\rho)$. A value of α can be found by trial, if not from $ap\tau$ *versus* τ plotting, which brings $(\varphi-1)$ into linear or approximately linear relation to the density, ρ, and which also passes through the origin: $(\varphi-1)=0$; $\rho=0$.[i] A rough estimate of α for use with common logarithms is $\frac{1}{5}$ to $\frac{1}{6}$ of β. The relation $(\varphi-1)=\bar{\psi}_1\rho+\bar{\psi}_2\rho^2$ or $v(\varphi-1)=\bar{\psi}_1+\bar{\psi}_2\rho$ is sufficient in the case of steam to represent volumes to about the critical volume above the critical temperature, T_c. Below T_c and to the critical temperature, $a\bar{\psi}_2$ term does not appear to be required. Also it appears from the data available for steam that a break or hiatus in the course of $\bar{\psi}_1$ as a function of temperature occurs in the critical region, a situation described in detail later in the present paper.

The equations for δ, ψ_0, $\bar{\psi}_{11}$, $\bar{\psi}_{12}$, etc., for steam follow, where τ is T^{-1} ($T=273.16+t_T$°C) and exp refers to

[15] J. A. Beattie and O. C. Bridgeman, Proc. Am. Acad. **63**, 229 (1938); F. G. Keyes, J. Am. Chem. Soc. **60**, 1761 (1938); J. A. Beattie and W. H. Stockmayer, Reports on Progress in Physics **7**, 195 (1940).

[g] The theory of the equation of state makes clear that the quantity β, formally representing fourfold the aggregate volume of the molecules, is an allowable practical approximation *for equation of state formulations* only when the magnitude of the "attraction terms" of the intermolecular potential are very great relative to the positive branch, or otherwise expressed, when the temperature range of considered $p-v-T$ properties is very low. The case of steam is representative of a substance where apparently for all temperatures even to the point of perceptible chemical instability of the molecule, the elastic sphere model of repelling force or positive potential is a sufficient approximation for the construction of an accurate $p-v-T$ correlative equation. Helium is representative, however, of the opposite extreme where except for temperatures below 20°K, the positive potential must be assumed a function of the distance between centers of the helium atoms. The requirements of the situation have been briefly discussed by F. G. Keyes and J. L. Oncley in Chem. Rev. **19**, 209 (1936); J. O. Hirschfelder and W. S. Roseveare, J. Chem. Phys. **43**, 15 (1939); F. G. Keyes, *Temperature* (Reinhold Publishing Company, New York, 1941), p. 41.

[h] In the case of ammonia it is not clear that adsorption effects have been entirely eliminated, which may account possibly for the necessity of expressing c_2 as a function of τ of the form "c_2"$=c_2/(1+c_4\tau^4+c_5\tau^5)$. See however, W. H. Stockmayer (see reference 11), in particular Fig. 1, p. 865.

[i] The accuracy with which β may be obtained from the z_0,ρ information may, because of a too restricted range of temperature, be insufficient and some adjustment will be needed to cause $(\varphi-1)$ to assume the value zero, as ρ approaches zero, when apparently no value of α can be found to accomplish the result. For volumes not less than 15 cc per gram, δ in the form $\beta(1-\alpha\rho)$ may replace the exponential form. Moreover for some substances data at densities less than 0.05 g/cc tend to be increasing in error at decreasing densities due to adsorption of the substance on the container walls while simultaneously the departure from the ideal gas expression decreases rapidly. Accordingly in the present state of our knowledge of gas properties for pure substances it is reasonable to omit measurements at densities less than 0.05 g/cc in favor of taking an abundance of data at increasing densities to beyond the critical density.

TABLE I. Vapor pressures computed from saturation volumes.

1[a]	2*	3[b]	4[c]	5[d]	6[e]	7[f]
0		206381.0	0.006025	0.006026		
50		12038.6	0.12180	0.12179		
100		1673.4	0.9999	1.00000		
150	0.0211	392.80	4.695	4.695		4.696
170	0.0340	242.809	7.810	7.811	7.818	7.812
180	0.041	194.011	9.887	9.887	9.894	9.888
190	0.048	156.488	12.377	12.375	12.382	12.377
200	0.0554	127.305	15.331	15.329	15.336	15.331
210	0.0624	104.359	18.811	18.807	18.814	18.808
220	0.0695	86.141	22.872	22.867	22.874	22.868
230	0.0763	71.541	27.579	27.573	27.578	27.574
240	0.0832	59.732	32.997	32.994	32.998	32.993
250	0.0898	50.105	39.196	39.197	39.198	39.194
260	0.0962	42.191	46.254	46.256	46.258	46.251
270	0.1023	35.636	54.231	54.247	54.250	54.240
280	0.1080	30.165	63.226	63.250	63.255	63.243
290	0.1135	25.565	73.322	73.351	73.358	73.345
300	0.1187	21.66	84.64	84.65	84.66	84.64
310	0.1231	18.34	97.22	97.24	97.26	97.22
320	0.1276	15.47	111.22	111.23	111.25	111.20
330	0.1320	12.98	126.75	126.74	126.76	126.71
340	0.1352	10.80	143.91	143.93	143.93	143.89
350	0.1383	8.82	162.94	162.92	162.94	162.89
360	0.1410	6.96	184.01	183.98	184.01	183.96
370	0.1430	4.96	207.10	207.43	207.56	207.39
374.37		3.066**	217.44	218.26		

* The values of $T-\Theta$ and $d\Theta/dt$ were obtained from a formula supplied by Professor Beattie using 444.7 for the temperature of the sulphur, N.B.P.
** Hans Eck (reference 19) obtained by the closed tube method a critical volume of 3.066 cc/g, critical pressure 218.26 atmos., critical temperature on Θ scale 374.23°C. Osborne, Stimson, and Ginnings (see reference 5) selected 374.15 for t_c and 218.35 atmos. for p_c. Smith, Keyes, and Gerry[1–Part II] observed 374.11 for t_c, 218.17 atmos. for p_c.
[a] Thermodynamic scale temperatures derived by applying the J. A. Beattie differences listed in column 2.
[b] Saturation volumes, v_s, calculated from gamma-measurements by Osborne, Stimson, and Ginnings (see reference 16).
[c] Pressures computed by inserting v_s of column 3 in the Eq. of state 1, 4, using the corresponding temperatures of column 1.
[d] Vapor pressure values taken from the tabulation given in Table III of reference 5, changed to correspond to the scale of column 1.
[e] The A. C. Egerton and G. S. Callendar revised values, reference 5, but changed to correspond to the scale of column 1.
[f] Smith, Keyes, and Gerry measurements, reference 1, Part II, changed to correspond to the scale of column 1.

common logarithms.

$$\delta = 2.0624\exp(-0.38\rho),$$

$$\psi_0 = \bar{A}_0\tau\exp(c_2\tau^2) = 1260.17\tau\exp(7.424\cdot10^4\tau^2),$$

$$T<T_c,\quad \bar{\psi}_{11} = \bar{A}_1\psi_0\tau\exp(2c_2\tau^2) = 305.6\psi_0\tau\exp(2\cdot7.424\cdot10^4\tau^2),^{j} \qquad (4)$$

$$T>T_c,\quad \bar{\psi}_{12} = (479.76+141.5\cdot10^3\tau)\psi_0\tau,$$

$$\bar{\psi}_{22} = \frac{75.364-27.505\psi_0}{\psi_0^3};$$

$$\frac{R}{M} = \frac{82.0566}{18.016} = 4.55465.$$

For the representation of the vapor phase volumes to the critical temperature five constants are required in addition to the universal gas constant, namely β, A_0, c_2, α, A_1. Above the critical temperature three additional quantities proved to be necessary. The volume data for steam are represented by the above formulation with fidelity[k] and will be used to explore the thermodynamic consistency of the extensive body of directly measured thermal data obtained by the participants in the international program of research in the thermodynamic properties of water substances sponsored by the American Society of Mechanical Engineers.

[j] An equation of state of form 1 was given in reference 1, part VI. The Eq. (ψ_1) given in that paper is however equivalent to $\psi_0\bar{\psi}_1$ of the present paper and is of a slightly different form.

TABLE II. Liquid phase volumes at saturation calculated using equation of state 5.

t_s	v_s calc. (5)	v_s O.S.G. 1939	v_s Eck
340[a]	1.6395	1.639	
350	1.7387	1.741	1.745
360	1.8836	1.894	1.894
370	2.114	2.225[b]	2.211
374.15+0.142		3.1	
374.23+0.142			3.066

[a] Each temperature was increased by 0.142°C to bring the observed temperature to the thermodynamic scale as given by the J. A. Beattie results.
[b] The volume at 370° was verified by Osborne, Stimson, and Ginnings (see reference 16) by direct observation and found to be in agreement with the volume deduced from the thermal magnitude γ through the Clapeyron-like relation.

TABLE III. Vapor phase volumes at saturation calculated using Eqs. 1, 4, $t<t_c$.

t_T	$v_s\Theta$	$v_s{}^T$	p_s Eq. $t<t_c$	$p_s{}^T$
370	4.932	4.957[a]	207.11	207.43
371	4.681	4.746	209.41	209.92
372	4.40	4.469	211.20	212.44
373	4.05	4.141	214.07	215.00
374	3.47	3.687	215.92	217.59

[a] No definite indication of the effect of carry-over of liquid water was found in either γ- or β-experiments even at temperatures up to and including 373°C. At 374°C, however, the determination of both γ and β was scattered much more widely than would be accounted for by inaccuracies of measurements. The value deduced from the γ-data is in agreement with a directly determined value obtained by Osborne, Stimson, and Ginnings, see reference 16.

VAPOR PRESSURES, VAPORIZATION QUANTITIES, AND SATURATION VAPOR VOLUMES

The vapor pressures below 150°C have been discussed in the earlier paper[1–Part VI] while above this temperature to the critical state each of the three participants[5] in the steam research program has included a detailed comparison of measured values with the independently observed pressures. The accord of the data of the three investigators, two of whom employed the static and the third a dynamic method, is very satisfying. The difference in the assigned pressures at temperatures on the international scale of 1927 nowhere differ much more than an amount corresponding to the order of ±0.01 dp/dT except for a range of some twenty degrees under the critical temperature. Moreover the newer measurements are in substantial accord with the measurements to the critical temperature of Holborn and Henning and of Holborn and Bauman published in the first decade.

Expressed as pressure differences, ±0.01°C corre-

[k] Paper No. 4 (reference 1—Part IV) contains a formulation (Eq. (9)) of a considerable part of the same data in the form $v=\varphi(p, T)$. However, it was not found possible to represent the volumes accurately below fourfold the critical volume.

sponds to a part in 3700 at 150°C, a part in 6000 at 250°, a part in 7100 at 300°, and a part in 8200 at 350°.[1] The values of $dp/d\Theta$ have been computed by differentiation of the equations of formulations (on the international temperature, Θ, scale) employed by each of the three investigators. The agreement of the derivative values is the order of a part in four thousand.

The vaporization quantity,[16] γ, is the heat required to transfer a unit of substance as saturated vapor under equilibrium conditions, from a closed vessel at constant temperature. The magnitude of γ is given by the thermodynamic expression $v_g T dp/dT$. Accordingly, γ having been measured, the volume of the saturated vapor, v_g, at the thermodynamic temperature T may be computed, given $dp/d\Theta$ and also $d\Theta/dT$. The values of v_g computed from the γ-observations upon substitution into the formulation equation based on the volume data, should give the vapor pressure in agreement with direct measurement.

The data available for carrying out the consistency test suggested in the foregoing scheme consist of a large amount of highly precise measurements of γ over the whole of the saturation region of water, namely 0°C to substantially the critical temperature. Confidence in the vapor pressure values and the derivatives rests as already stated on three independent investigations in agreement to the order of a part in five thousand.

The volume data over the temperature range of the liquid phase and to 460° have been verified by duplicate measurements using different containers. The conclusions from a correlative study[1—Part IV] indicate that in the range of volume measurements from 50 cc/g downward the precision is on average a part in two thousand. The measurements by the method of confinement with mercury for larger volumes, 150 cc/g to 50 cc/g, are, however, of lower precision, about one part per thousand. The foregoing estimate of precision is confirmed by the study made by Jan Jüza[8] who deduced volumes for steam through the relation $(\partial v\tau/\partial\tau)_p=(\partial h/\partial p)_T$ employing the enthalpy measurements of Havlíček and Miškowský[4] to 550°C and 290 átmos. The derived values of volume by Jüza extending to 12 cc/g are substantially in accord with the directly measured volumes and support the view that knowledge of the $p-v-T$ properties[17] for steam to 12 cc/g are accurate to at least a part in a thousand to 550°C. (Table I). The measured liquid volumes[1—Part III] are apparently of comparable accuracy. The data for a comprehensive test of thermodynamic consistency over the saturation range are accordingly available.

There remains, however, the uncertainty inherent in the lack of information on the degree of approximation of the international scale to the thermodynamic scale of temperature. This knowledge can be supplied by carrying out at fixed temperatures comparisons of the indications of the platinum resistance thermometer with the readings of the gas thermometer. The most recent comparisons of resistance and gas thermometers with modern experimental resources, as stated in Part VI of this series, have been carried out over a number of years by James A. Beattie and his collaborators.[3] The scale differences, $T-\Theta$, where T refers to thermodynamic temperature and Θ to the international scale of 1927, have been provided through the courtesy of Professor Beattie, and extend to the boiling point of sulfur, 444.6° (Θ scale). The data are collected in Table I.

The results of the consistency test in Table I will be evident on comparing the pressures "p_{calc}" with the "observed" pressures as given by the three independent observers. The latter pressures are however the smoothed observations corrected to the J. A. Beattie scale of thermodynamic temperatures. The following procedure was used in carrying out the computations.

Each value of γ was transferred from the Θ scale used in making the original measurements to the T scale; the scale differences appearing in the second column of Table I. From a list of values of $d\Theta/dt$ obtained by differentiating Beattie's equation for $(T-\Theta)$ the values of $T(dp/dT)=T(dp/d\Theta)\cdot(d\Theta/dT)$ were next obtained for computing $v_g=\gamma/T(dp/dT)$. (The values of $dp/d\Theta$ listed by Osborne, Stimson, Fiock, and Ginnings were used).[5]

THE SATURATION VOLUMES NEAR THE CRITICAL REGION

The general thermal method for measuring saturation quantities for the liquid-gas phases, devised by Nathan S. Osborne and used by Osborne, Stimson, Fiock, and Ginnings[17] in the steam research program, is undoubtedly the most complete and reliable that has been suggested and applied.

Jacob and Fritz,[18] also collaborators in the steam research program working at the Physikalisch-technischen Reichsanstalt, contributed numerous and valuable observations on the heat of vaporization of water to high pressures from which saturation vapor volumes were deduced through the Clapeyron relation.

Saturation volumes in the critical region were measured directly by Hans Eck[19] using fused quartz tubes.[m]

[1] The accord of the independently measured values as the critical temperature is approached becomes less.

[16] Osborne, Stimson, and Ginnings, J. Research Nat. Bur. Stand. **18**, 389 (1937).

[17] N. S. Osborne, Bur. Stand. J. Research **4**, 609 (1930). Osborne, Stimson, and Fiock, Bur. Stand. J. Research **5**, 411 (1930); **8**, 321 (1932); **9**, 807 (1932); **13**, 699 (1934). Osborne, Stimson, and Ginnings, J. Research Nat. Bur. Stand. **18**, 389 (1937); **23**, 261 (1939). Heats of evaporation and the heat capacity measurements of liquid water are contained in the following publication: Osborne, Stimson, and Ginnings, J. Research Nat. Bur. Stand. **23**, 197 (1939).

[18] M. Jacob and W. Fritz, Zeits. des Vereins Deut. Ing. **73**, 629 (1929). Tech. Mech. und Therm. **1**, 236 (1930). M. Jacob and W. Fritz, Forschung auf dem Gebiete des Ingenieurwesens **4**, 1 (1933). M. Jacob, Zeits. f. tech. Physik **3**, 83 (1935). M. Jacob, Physik. Zeits. **36**, 413 (1935).

[19] Hans Eck, Physik. Zeits. **40**, 3 (1939).

[m] The closed tube method devised by Sidney Young is the most satisfactory older method of obtaining saturation volumes in the

Eck measured the critical quantities not only for water but also for D_2O and in the conduct of the observations care was exercised with regard to the solubility of the quartz and the influence of gravity on the density distribution of the phases. The measurements extend from (Θ) 350° to 374.23°C in the case of H_2O.

The values of the saturation volumes of both liquid and vapor from 340°C ($v_s = 10.795$ cc/g) to the critical temperature, t_c, may also be obtained from the directly measured superheat volumes by graphical extrapolation, but with decreasing accuracy as t_c is approached. The disabilities of extrapolation are caused by the rapid increase in the value of $(dv/dt)_{sat}$ on the liquid phase side and on the vapor side of the dome, as the saturation pressure is approached. The known forms of equation of state for the vapor phase have not been sufficiently exact for representing values of volume less than 12 to 15 cc per gram and accordingly extrapolation by this route cannot be used with confidence in the critical region.

There exists for water substance a considerable body of volume data in the superheat field at temperatures below and above the critical temperature. It will be observed from Table I that the formulation Eqs., (1) and (4), for the volume data give the saturation pressures with substantial accuracy to 370°C when the saturation vapor volumes deduced from the γ-values[16, 17] are inserted in Eq. (1) ($t < t_c$). In what follows a survey of the available observational data for a short range of temperature will be given using Eqs. (1) and (4) as a correlative aid for saturation volumes from 370°C to the critical volume.

The earlier extrapolations to saturation by the writer and collaborators (reference 1, Part III) of the isothermal liquid volumes corresponding to some twenty degrees below the critical pressure were not satisfactory. Since the earlier formulation of the liquid volumes, a better correlation form for the liquid has been devised for the range close to the critical temperature which results in greater accuracy when used to extrapolate to the saturation liquid volumes. Figure 1 represents the course of the saturation volumes corresponding to 160 atmos. (about 348.4°C) and volumes extending to beyond the critical pressure (about 218.2 atmos.). This is the so-called dome for water substance.

Reference has already been made to the pronounced analytical difficulty, if not impossibility, of representing the behavior of the superheated vapor of steam over the range of temperature below the critical temperature and above the critical state with a single form.

The volume range, for which pressures computed with either of the forms (Eq. (4)) corresponding to $t < t_c$ or $t > t_c$ will be in agreement with the observed pressures, is from 20 cc per g. By way of example for 20 cc/g and 400°C the pressure computed using the form for $t < t_c$ is 123.39 atmos. compared with the observed pressure 123.44 atmos., while at 10 cc/g the corresponding pressures are 198.63 and 196.91 atmos. The difference in the behavior of the vapor above and below the critical tem-

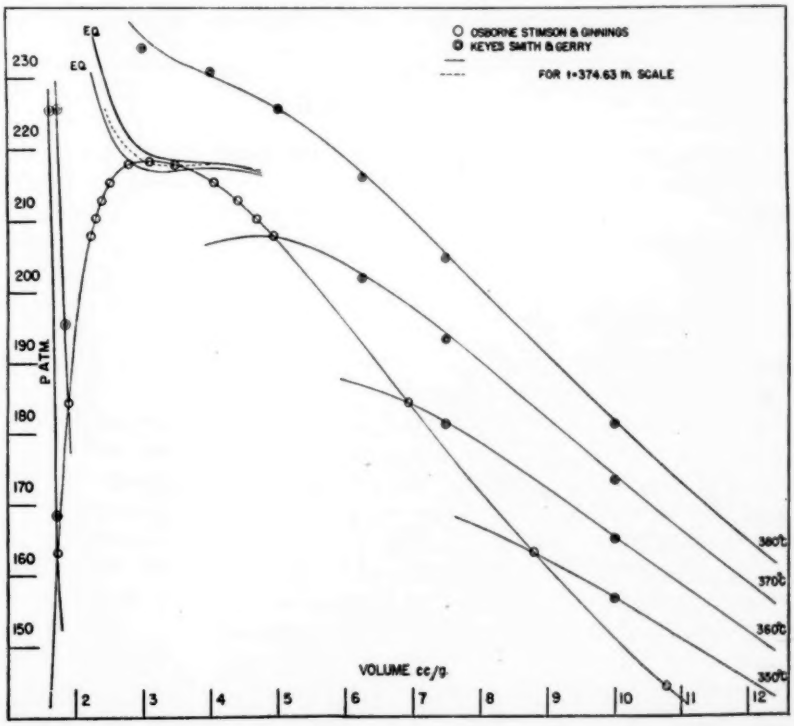

FIG. 1. The critical region of steam. Continuous lines computed with Eqs. (1), (4), and (5). The dotted isotherm is computed using an assumed critical temperature 0.26° larger than Eck reported ($t_T = 374.23 + 0.14$). The upper critical isotherm is for $t < t_c$ (Eq. (4)); the lower $t < t_c$ (t_T374.15+0.14).

critical region. The method has not usually yielded values, as far as known, of an accuracy comparable to that obtainable with the thermal method. The Young method has been employed recently, however, by Eck in the case of water close to the critical region with satisfactory results.

perature made itself evident when the values of $\bar{\psi}_1$, deduced from the observed data were plotted *versus* $\psi_0^2 \cdot 10^{c_2\tau^2}$ for the range 40° to 460°C. The values of $\bar{\psi}_{11}$ exhibited a sharp divergence in trend at the point corresponding closely to 374°C. The situation is described analytically by the difference in the two forms for $\bar{\psi}=(\bar{\psi}_1+\bar{\psi}_2\rho\cdots)$.

THE REPRESENTATION OF LIQUID VOLUMES NEAR THE CRITICAL STATE

The p-v-T properties of the liquid phase of water differ considerably from those of any substance for which data are available. The difference has been briefly alluded to in the early part of this paper and is marked by the behavior of the quantity $(\partial p/\partial T)_v$ which, in the case of liquid ethyl ether or carbon dioxide as examples, is nearly constant with increasing temperature.

The present formulation for the liquid phase is based on the isotherms, 340, 350, 360, and has for its main object the extrapolation of the compressed isothermal liquid phase volumes to the saturation pressure. The following formula was obtained:

$$\begin{aligned} &\psi_0 \text{ the same as given under Eq. (4)} \\ &\bar{\psi}_{1f}=(259.37+9.508\cdot 10^4\tau\psi_0)\tau\psi_0 \\ &\log\delta_f=0.3143729-(0.38+a)\rho+b\rho^2 \\ &a=2.8378\cdot 10^{16}\tau^7 \exp 12c_2\tau^2 \\ &b=1.7607\cdot 10^{26}\tau^{10} \exp 6c_2\tau^2 \end{aligned} \Big\}\text{base 10.} \qquad (5)$$

The volumes of the liquid phase corresponding to the normal vapor pressure of water were computed using the form Eq. (1) with the expressions for $\bar{\psi}_{1f}$ and δ_f given in Eq. (5) above. The formulation has, however, no validity outside of the range of temperatures upon which it is based. It does, however, indicate the possibility of using the same general form for the condensed phase as proved satisfactory for the vapor phase. The saturation volumes for the liquid phase are given in Table II with corresponding values reported by Osborne, Stimson and Ginnings,[16,17] and Eck.[19]

The vapor phase saturation volumes beginning with 370° on the T scale have been computed for each degree by using Eqs. (4) for $t<t_c$, i.e., the same equation used for computing the pressures in Table I from the volumes deduced from γ-data.[17, n] The data are assembled in Table III in the first column of which appear the temperatures on the T scale making use of the J. A. Beattie differences from the Θ scale. The second column contains values listed by Osborne, Stimson, and Ginnings[17] for Θ temperatures of the same numerical magnitude as the T scale and given for purposes of comparison with the volumes in column 3 which have been deduced from the γ-values of Osborne, Stimson, and Ginnings using the identical procedure described for obtaining the saturation volumes of Table I from γ-values. The volumes in column 3 substituted into the equation of state for the vapor $t<t_c$ give the pressures in column 4 which may be compared with the measured vapor pressures of column 5 on the T scale.

It will be noted in Fig. 1 that as the 370° isotherm approaches the saturation pressure, it tends to become more nearly parallel to the volume axis. The effect of this tendency is to make the pressure insensitive to a

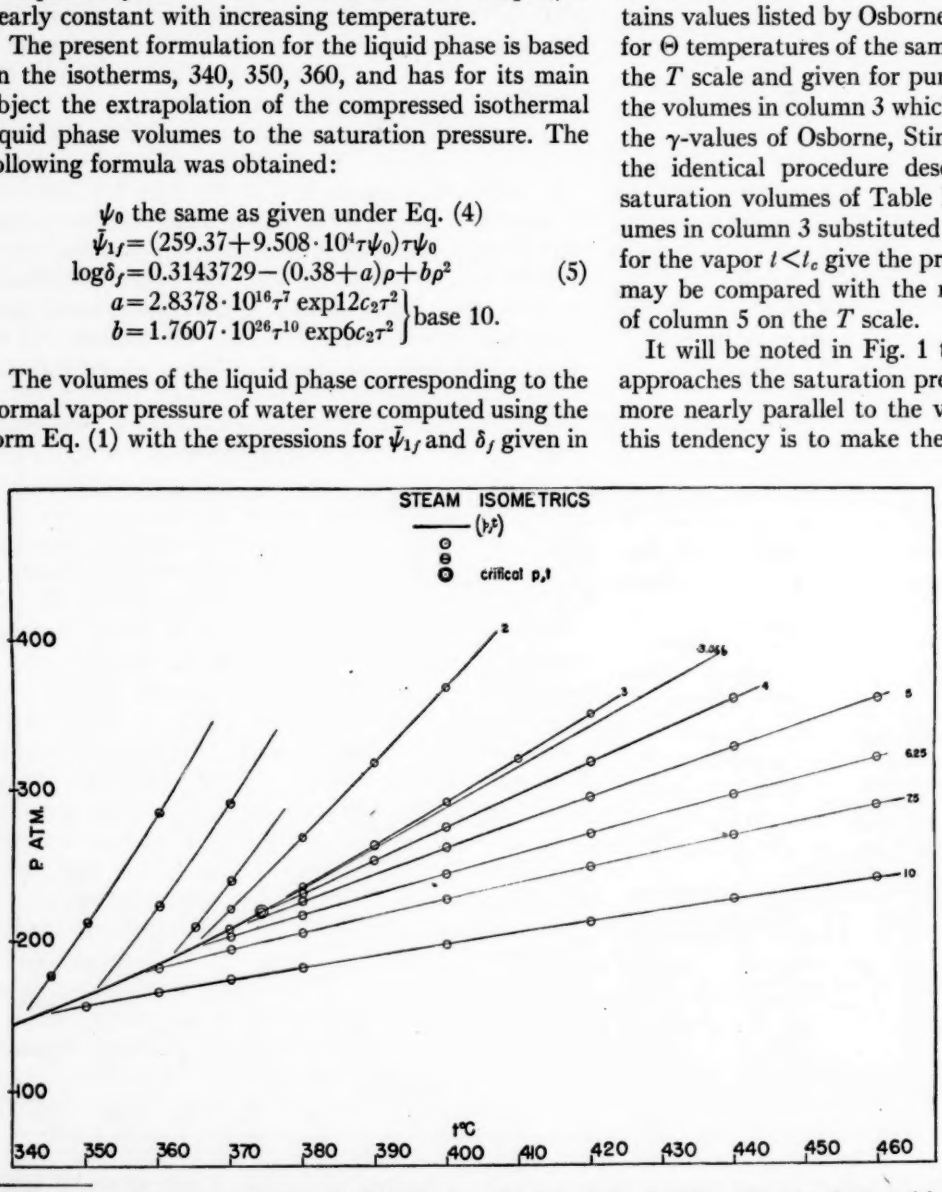

FIG. 2. The isometrics for the vapor are perhaps everywhere concave to the t axis for $v>v_c$. The critical isometric 3.066 cc/g interpolated from the data appears to be linear. For $v<v_c$ the isometrics are concave viewed from the pressure axis.

[n] The mean observed γ-values were plotted *versus* the international scale temperature increased by the J. A. Beattie correction. The values of γ were then read for even T scale temperatures from which volumes were computed.

change in volume. Accordingly with rising temperature an increasingly considerable change in vapor volume is needed to bring the computed pressure into agreement with the measured vapor pressure. Since it is not believed that above 370°C the volumes are in error nearly as much as would be implied by the pressure differences, it is concluded that an element in the equation of state may have eluded recognition.

Part of the available data in the critical region has been used to construct Fig. 1 where the full lines have been drawn using values computed by means of the equation of state. There are several comments suggested by a consideration of the data represented in the figure.

An item of first importance is that the amount of data required to make further progress in understanding the behavior of a fluid in the critical region should be far greater than is now available. The volumes of water under pressure should be measured for each two degrees from about 365° to perhaps ten degrees above the critical temperature and to pressures of 1000 atmos. There are now available only data for isometrics 2, 3, 4, and 5 cc/g, the spacing of which is now recognized to be far too coarse and the temperature intervals should also, as stated for the liquid phase, be spaced two degrees apart instead of ten, up to perhaps 420°C. The volume spacing should be by quarter cubic centimeters.

A piece of the critical isotherm computed from the equation for $t>t_c$ is shown in Fig. 1 and it lies above the isotherm representation for the $t<t_c$ formulation to the extent of 1.5 atmos. A third piece of isotherm appears as a dotted line computed for 374.63° (T scale) and the $t<t_c$ equation. There seems little likelihood however that the observations of critical temperature can be in error by 0.26 degree.

It is evident that in so far as the equations represent the available data with accuracy, the critical isotherm is "flat," or $(\partial p/\partial v)_{t_c}$ is zero as well as $(\partial^2 p/\partial v^2)_{t_c}$. The situation is not entirely satisfactory however in view of the failure of the computed $(\partial^2 p/\partial T^2)_v$ Fig. 3 for the critical isotherm to assume the value zero for the critical density.

Figure 2 is a representation of the isometrics in the critical region and indicates for water substance what appears to be a general fact, namely that the isometrics on the vapor side of the vapor pressure curve are concave to the temperature axis. However as the volumes diminish towards the critical volume, the isometrics assume a more nearly linear aspect becoming practically linear for the critical volume. Isometrics for lesser volumes (liquid) than the critical are, however, convex to the temperature axis.

The foregoing property of the isometrics of each homogeneous phase means that $\partial^2 p/\partial T^2$ is negative for the vapor phase and positive for the liquid phase, but zero possibly to high pressures for the isometric of the critical volume.

An examination of the first and second derivatives of

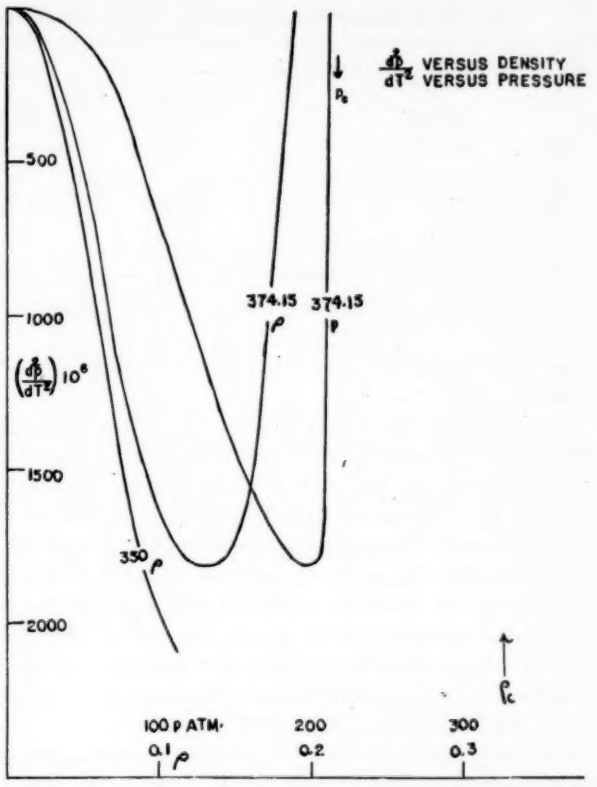

FIG. 3. Isothermal values of $(\partial^2 p/\partial T^2)_v$ computed from Eqs. (1) and (4) *versus* density and pressure. To be consistent with Fig. (2) the isotherm should cross the density axis at ρ_c.

Eq. (1) shows that isothermal values of $(\partial^2 p/\partial T^2)_v$ in relation to density are negative for the equation for $t<t_c$, $v>v_c$ and progress with increasing curvature as the saturation condition is approached. The isotherm of the critical temperature however passes through a minimum, increases, and becomes zero. The equation for the liquid phase gives values of $(\partial^2 p/\partial T^2)_v$ which are uniformly positive.

The following equation is obtained from Eq. (1):°

$$(\partial^2 p/\partial T^2)_v = -p\tau^2[\tau^2(\partial^2\psi/\partial\tau^2) - (\tau\cdot\partial\psi/\partial\tau)^2\omega\rho^2]^\circ\omega\rho^2. \quad (6)$$

Figure 3 represents graphically the computed values of the second derivatives at constant temperature in relation to density for $t<t_c$, which makes evident the decreasing curvature of the isometrics as successively higher temperatures are considered. The 374.29 (T scale) isotherm passes to a minimum after which it moves toward zero. The liquid water values of the second derivative lie wholly on the positive side of Fig. 3 and cannot be shown with any clarity of detail on Fig. 3 because of the relatively small change of density with pressure.

It may be noted that the isotherm in Fig. 3 for 374.29 does not cross to zero (linear isometric) at the critical

° The differentiation of the equation for ψ is facilitated by using the operators,

$$\partial/\partial T = -\tau^2\partial/\partial\tau; \quad \partial^2/\partial T^2 = \tau^2(2\tau\partial/\partial\tau + \tau^2\partial^2/\partial\tau^2).$$

TABLE IV. Enthalpy difference relative to 0°C, obtained by subtracting the quantities computed from Eqs. (7) and (8).

t	H^0 O.S.G. i.j.	H^0 E and C i.j.	H^0 H and M i.j.	$(H^0-2501.09)-\int C_p^0 dT$(VI) O.S.G.	E and C	H and M	t	$(H^0-2501.09)-\int C_p^0$(VII) O.S.G.	E and C	H and M
0	2501.09			0.00			0	0		
100	2688.42			0.14			100	+0.44		
200		2879.16			−0.66		200		+0.15	
300		3075.20			−1.62		300		−0.09	
400		3277.03	3277.5		−3.20	−2.73	400		−0.50	+0.03
450		3380.01	3380.6		−4.39	−3.80	450		−1.00	−0.41
500		3484.53	3485.5		−5.75	−4.78	500		−1.56	−0.59
550		3591.80	3592.5		−6.11	−5.41	550		−0.92	−0.22

density as it should if the implications of Fig. 2 are taken literally.

The course of the critical isotherm is represented as a function of pressure as well as density in Fig. 3, and the intersection of the zero axis of $(\partial^2 p/\partial T^2)_v$ occurs a little short of the critical pressure whereas the course of the derivative with density exhibits intersection at a density value roughly 0.2 g per cc instead of 0.326 g per cc. The reason for the large apparent difference lies in the very great compressibility of the fluid which becomes infinite at the critical volume. The situation however emphasizes the superiority of the density as independent variables in judging the degree of completeness with which a proposed equation represents the critical region. It will be observed also that the progressive diminution of the accord of pressures in Table III from 370° to 374°C is only relatively less striking as an indication of the failure of exact representation of the fluid properties immediately under the critical temperature as compared with the course of the $(\partial^2 p/\partial T^2)$ derivative *versus* density diagram.

THE ENTHALPY OF SUPERHEATED STEAM

Measurements of the enthalpy of superheated steam have been carried out by two independent groups of investigators.[4] The range of pressure extends to 387 atmos. of temperature and to 600°C. A comparison of the measured values with similar values computed through the use of the Eqs. (1) and (4) is given in Table V.

A fundamental requirement for the computation of the enthalpy is a knowledge of the heat capacity corresponding to indefinitely reduced pressure. The equation for C_p^0 given in the previous paper,[1—Part VI] (Eq. (9)) is based on A. R. Gordon's[20] values with addition of the "centrifugal stretching" term calculated by E. B. Wilson, Jr.;[21] a calculation later verified by C. C. Stephenson and H. O. McMahon[22] through the recomputation of the rotational partition function from Randall, Dennison, Ginsburg, and Weber's[23] data. There is a point of particular interest in comparing the direct measurements of enthalpy at low pressure adjusted for pressure independence through the use of the enthalpy pressure dependent term of Eq. (10) of the Part VI paper with the integral of the Gordon-Wilson expression and a second equation.

The lowest pressures of recorded enthalpies are 5 kg/cm² for the Egerton and Callendar observations, and 1 kg/cm² for the values given by Havlíček and Mišikowský. There are available also the saturation enthalpies of Osborne, Stimson, and Ginnings[17] at 0, 100°, and higher temperatures. The pressure dependent portion of the enthalpy is not large for these low pressures and it may be evaluated with confidence from Table XII of Part IV and Table V of Part VI. The measured enthalpies reduced by the pressure dependent terms are solely temperature functions proportional to the integral of the specific heat of steam at indefinitely reduced pressure. Relative to the zero pressure enthalpy at 0°C, Table IV contains the amounts by which the "observed" enthalpies (H^0) exceed the following two specific heat integrals. Equation (7) is obtained from the Gordon values with addition of the E. B. Wilson, Jr. term, while Eq. (8) is the same equation diminished by a term.

$$\int C_p^0 dT(\text{VI}) = 1.4722(T-T_0) + 3.8863\cdot 10^{-4}(T^2-T_0^2) + 110.16\log_{10} T/T_0, \quad (7)$$

$$\int C_p^0 dT(\text{VII}) = C_p^0 dT(\text{VI}) - 9.49\cdot 10^{-9}(T^3-T_0^3). \quad (8)$$

The differences of Table IV derived through the use of Eq. (7) are outside the limit of error of the observations for temperatures beginning at 400°C. Moreover the differences are systematic. The differences based on Eq. (8) are within the probable error of the enthalpy measurements although of the same sign. It is notable that agreement of the independently measured values is excellent.

Table V contains on the first two horizontal lines for each temperature computations for the enthalpy using Eqs. (7) and (8), according to the following:

$$h = \int_{T_0}^{T} C_v^0 dT + \int_0^{\rho} (\partial p\tau/\partial\tau) v^2 d\rho + pv + E_0. \quad (9)$$

[20] A. R. Gordon, J. Chem. Phys. **2**, 65 (1934).
[21] E. B. Wilson, Jr., J. Chem. Phys. **4**, 526 (1936).
[22] C. C. Stephenson and H. O. McMahon, J. Chem. Phys. **7**, 614 (1939).
[23] Randall, Dennison, Ginsburg, and Weber, Phys. Rev. **52**, 160 (1937).

TABLE V. Enthalpy of superheated steam above the critical temperature. Values are in international joules.

	kg/cm²	1	25	50	100	150	200	250	300	350	400
400°C	VI calc.[a]	3278.6	3241.7	3200.6	3107.0	2993.4	2845.9	2627.8			
	VII calc.[b]	3275.9	3239.0	3197.9	3104.3	2990.7	2843.2	2625.1			
	Steam Table[c]	3276.1	3239.4	3197.8	3102.6	2984.7	2833.2	2611.1	2231.2		
	E. and C. 1939[d]	3275.5	3238.3	3196.5	3098.5	2979.6	2826.0				
	H. and M.(J) 1938[e]	3276.0	3238.7	3197.3	3100.6	2983.8	2832.3				
	K. (VDI) 1937[f]	3273.1	3234.6	3193.1	3099.4	2981.3	2832.2	2605.4	2195.6		
450°C	VI calc.	3383.0	3352.7	3319.6	3247.7	3167.0	3075.6	2970.0	2844.2		
	VII calc.	3379.6	3349.3	3316.2	3244.3	3163.6	3072.2	2966.6	2840.8		
	Steam Table	3379.8	3350.0	3316.7	3245.8	3165.5	3073.9	2968.0	2842.4		
	E. and C. 1939	3378.8	3348.8	3316.2	3242.9	3159.6	3061.7				
	H. and M.(J) 1938	3379.4	3349.3	3316.2	3243.8	3163.0	3071.3	2966.2	2842.7		
	K. (VDI) 1937	3376.9	3345.9	3312.8	3242.9	3163.8	3071.3	2962.9	2835.6		
500°C	VI calc.	3489.1	3463.6	3436.1	3378.1	3315.6	3248.3	3175.9	3098.1	3014.6	2925.4
	VII calc.	3484.9	3459.4	3431.9	3373.9	3311.4	3244.1	3171.7	3094.0	3010.4	2921.2
	Steam Table	3485.1	3460.0	3433.0	3376.6	3315.0	3249.7	3179.0	3101.9	3019.6	2929.1*
	E. and C. 1939	3483.5	3458.5	3432.6	3373.1	3310.3	3235.4				
	H. and M.(J) 1938	3484.5	3459.8	3432.6	3375.2	3313.3	3246.7	3175.1	3098.5	3016.5	
	K. (VDI) 1937	3483.2	3457.7	3430.5	3374.8	3315.4	3250.9	3179.3	3098.5		
550°C	VI calc.	3596.8	3575.0	3551.7	3503.4	3452.8	3399.8	3344.8	3289.7		
	VII calc.	3591.7	3569.9	3546.6	3498.3	3447.7	3394.7	3339.7	3284.6		
	Steam Table	3591.9	3570.8	3548.0	3500.7	3451.9	3400.3	3346.5	3290.5		
	E. and C. 1939	3590.9	3569.0	3547.3	3497.9	3447.2					
	H. and M.(J) 1938	3591.6	3570.3	3548.1	3500.8	3451.4	3399.1	3344.2	3287.3		
	K. (VDI) 1937	3592.0	3570.3	3548.1	3502.0	3453.5	3402.4	3347.6	3290.2		

[a] Refers to the use of Eqs. (1), (4), and (7).
[b] Refers to the use of Eqs. (1), (4), and (8).
[c] Refers to *Thermodynamic Properties of Steam*, J. H. Keenan and F. G. Keyes, (John Wiley and Sons, Inc., New York).
[d] Refers to the Brit. Elec. and Allied Ind. Research Ass., Technical Report J/T115, p. 14, Table 6. 1 kg/cm² values extrapolated.
[e] Refers to the J. Havliček and L. Miškowský measurements as smoothed by Jan Jůza.
[f] Refers to the Koch VDI Wasserdampftafeln (Verlag. Julius Springer, Berlin, 1937).
* Extrapolated beyond limit of Steam Tables.

From Eq. (1) the following equation for the second integral term of the right member of Eq. (9) will be obtained.

$$\int_0^\rho (\partial p\tau/\partial\tau)v^2 d\rho = -R/M\int_0^\rho \exp[-\psi(\omega/v^2)]\partial\psi/\partial\tau\cdot d\rho. \quad (10)$$

The integral of Eq. (10) may be readily solved in series form. However the integral may also be obtained easily by computing the integrand for several values of the density for constant temperature and integrals found in the usual way by measuring the areas under the curve formed on a graph by the integrand *versus* density. The value of the integrand per unit mass takes at infinite volume the value $R/M\psi_0 T(1+2c_2\tau^2)$, thereafter rising slowly with density to a maximum. Computation of the enthalpies for constant pressure may be obtained by computing the densities for the desired pressures using Eqs. (1) and (4).

The isotherm, Table V, 400°C, lies 25.8° above the critical temperature and for pressures approaching 150 kg/cm² and higher, the enthalpy is changing rapidly with pressure. It is to be noted also that the thermodynamic properties of a fluid during measurement are less easily maintained in true thermodynamic equilibrium in or near the critical region particularly when a "flow" method is used.[24] However in the case of the 400° isotherm the measurements reported by Egerton and Callendar and by Havliček and Miškowský are in good agreement, and lack of agreement in the computed values suggests a defect in the formulating equation as the region of the critical volume is approached. The values of W. Koch[25] (VDI Steam Tables) are deduced from his steam tables based upon heat capacity measurements[p] obtained by the use of a "flow" calorimeter.[6]

The accord of the computed values, using Eq. (8), with the observed values reported by the three independent investigators participating in the steam research program is satisfactory throughout except for the 400° isotherm above 150 kg/cm². The computed enthalpies using the completely theoretical Eq. (7) for the integral zero pressure specific heats give higher values and for this reason justify the conclusion that either the theo-

[24] Abnormalities, relative to classical conceptions of the behavior of a fluid at or near the critical density, were observed in the case of steam prior to 1910 by Professor H. L. Callendar. The results of the observations were comprehensively summarized and discussed by Max Jacob in the course of four lectures delivered at the University of London in May 1931, and reprinted in Engineering **132**, 143 (1931). An important paper bearing on the Callendar observations and containing new experimental material is contained in the publication by W. Koch, Forschung auf dem Gebiete des Ingenieurwesens **3**, 189 (1932). See also Tapp, Stacie, and Maass, Canadian J. Research **9**, 217 (1933) and later papers.

[25] W. Koch, VDI-Wasserdampftafeln (Verlag. Julius Springer, Berlin, 1937).

[p] Using the Eq. $(\partial h/\partial T)_p = C_p$ and $(\partial C_p/\partial p)_T = T(\partial^2 v/\partial T^2)_p$, the enthalpy and volume may be obtained.

TABLE VI. Enthalpy of saturated vapor.

t°C	150	200	300	350	360
VII calc.[a]	2745.0	2792.1	2752.0	2557.6	2466.7
Steam Table[b]	2744.9	2790.5	2747.0	2561.0	2481.9
E. and C.[c]	2746.1	2793.0	2748.9	2564.0	2481.9
K. (VDI)[d]	2744.0	2792.1	2746.5	2561.4	2481.5
O. S. and G.[e]	2746.1	2792.5	2748.6	2564.7	2480.7

[a] Refers to the use of Eqs. (1), (4), and (8).
[b] Refers to J. H. Keenan and G. F. Keyes, *Thermodynamic Properties of Steam* (John Wiley and Sons, Inc., New York, 1936).
[c] Refers to the 1939 Callendar steam tables compiled and edited by G. S. Callendar and A. C. G. Egerton (Edward Arnold, London, 1939).
[d] Refers to the Koch VDI Wasserdampftafeln (Verlag. Julius Springer, Berlin, 1937).
[e] Refers to N. S. Osborne, H. F. Stimson, and D. C. Ginnings, J. Research Nat. Bur. Stand. **23**, 261 (1939).

retical equation requires reconsideration on the basis of additional spectroscopic data or that the volume data forming the basis for evaluating the density dependent integral in Eq. (9) are in error. Additional volume data in the critical region are indeed required before a satisfactory analytical representation of the pressure-sensitive critical state can be formulated. However examination of the Havlíček and Miškowský enthalpy data by Jüza[8] led to the conclusion that the volume data reported by Keyes, Smith and Gerry[1–Part IV] were consistent and accurate. A brief reference to the procedure used by Jüza will aid in sensing the implications of the situation.

The results of the smoothed enthalpy measurements are reported as set down in Table V, and it is not difficult to obtain accurate values of $(\partial h/\partial p)_T$ from the isotherms. The latter differential quantity is one member of the following equation whose integral follows:

$$(\partial v\tau/\partial \tau)_p=(\partial h/\partial p)_T, \tag{11}$$

$$(v\tau)_1-(v\tau)_0=\int (\partial h/\partial p)_T d\tau$$

$$=\int_{\tau_0}^{\tau_1}[f_0(\tau)+f_1(\tau)p+\cdots]d\tau, \tag{12}$$

where $f_0(\tau)$, $f_1(\tau)$ etc., are temperature functions evaluated from the coefficients of the pressure terms for each of the enthalpy isotherms.

The quantity $(v\tau)_0$ denotes a reference point along each isobar and Jüza selected a value from the 400° isotherm of the K.S.G. data for the constant in each series of deductions of volumes represented by successive values of $(v\tau)$. The volume data obtained are therefore at least valuable as a test of the consistency of the independent volume data. The accuracy of the H. and M. data has been well substantiated by the enthalpy measurements of Egerton and Callendar as well as by the enthalpies reported by Koch based on the use of his C_p data.[6] We are accordingly led to regard the directly measured volume data as substantiated. Confirmation of the quality of the formulation Eqs. (1) and (4), representing the volume data is afforded by the comparisons of computed vapor pressures and observed pressures in Table I.[q] The conclusion from the evidence now available is that it would be desirable to extend the spectroscopic observations on water vapor to provide the basis for additional computations of the quantity C_p^0.

TABLE VII. Specific heat of the saturated vapor. Values in international joules.

t	200	300	330	340	350
Koch[6]		6.08	9.80	12.18	15.98
Calc. 1, 4	1.30	5.98	9.37	11.98	16.97

It will be observed from Table V that the Steam Tables[26] values of enthalpy are throughout in satisfactory accord with the observed values; the agreement tending to be in better accord with the H. and M. values and Koch's values above 150 kg per cm².

ENTHALPY OF SATURATED VAPOR

The Eqs. (1), (4), (8), and (9) have been employed to compute the saturation values of enthalpy and the results are given in Table VI along with values taken directly from three standard tables at the temperature listed without adjustment. The agreement of the computed values is satisfactory except at 350°C and 360°C. The cause of the difference in enthalpy computed from the measured values at the latter temperature is not understood, particularly in view of the excellent accord shown in Table I between the computed and observed vapor pressures.

THE SPECIFIC HEAT OF THE SATURATED VAPOR

The only experimentally related values available have been obtained by extrapolation through the use of Koch's empirical equations based on superheat region measurements. The specific heat increases with great rapidity as the critical temperature is approached, becoming infinite at that temperature. A few values computed by the use of Eqs. (1) and (4) are given in Table VII. The values labeled "Koch" refer to values using W. Koch's[6] equations.

The computations, VII calc., have been made by using the following equation:

$$C_p=C_v^0+\int T(\partial^2 p/\partial T^2)_v dv+T(\partial p/\partial T)_v(\partial v/\partial T)_p, \tag{13}$$

and employing C_v^0 derived from Eq. (8).

It is a pleasure to acknowledge the computational assistance of Miss Barbara M. Healy in the preparation of this paper.

[q] It is true that the formulation equation used in computing the pressures of Table I are for $t<t_c$ whereas Table V employs the $\bar{\psi}$ relationships for $t>t_c$. However either equation will lead to the same pressures for equal temperatures with volumes greater than 20 cc/g. Below 20 cc/g the pressures are well represented, less satisfactorily for isotherm 380° and 400°C, but otherwise well to 4 cc/g.

[26] J. H. Keenan and F. G. Keyes, *Thermodynamic Properties of Steam* (John Wiley and Sons, Inc., New York, 1936).

Macroscopic Space Charge in Electrolytes during Electrolysis

CHARLES ALBERT REED* AND WILLIAM SCHRIEVER
University of Oklahoma, Norman, Oklahoma

(Received January 27, 1949)

Since the publication of Hittorf's famous paper in 1853 it has been assumed, in general, that macroscopic space charge does *not* exist in an electrolyte during electrolysis. An apparatus and procedures were developed which made possible reproducible data on potential distribution in an electrolyte. In a uniform column of electrolyte the potential rise was found to be a non-linear function of the distance from the cathode, and it was shown that this non-linearity could *not* have been due to concentration changes caused by the electrolysis, but must have been due to macroscopic space charges in the electrolyte. Calculations showed *the space charge to be positive very close to the cathode, negative in the next quarter of the column, positive for the next nearly three-quarters of the column and negative very close to the anode.*

The eight electrolytes studied were 0.0024*N* solutions of $CuSo_4$, $CuCl_2$, $ZnSO_4$, $ZnCl_2$, $Zn(C_2H_3O_2)_2$, $NiSO_4$, $NiCl_2$ and $Al_2(SO_4)_3$. The pure metal was used for the electrodes in each case. Each column of electrolyte was 8 cm×8 cm×40 cm long, and the constant potential difference was 8.000 volts. The largest observed space charge at the end of 15 minutes was in $CuSO_4$ at 2 mm from the anode; it was an excess of 2×10^6 Cu^{++} ions over SO_4^{--} ions per cm^3, which is an excess of only 3 Cu^{++} ions for every 10^{12} Cu^{++} ions originally present.

Although the space charges were all very small, they had very appreciable effects on the potential gradients, which also were calculated. *The potential gradients in the different electrolytes were not constant,* but had maximum deviations from constancy of from 5 to 20 percent in the explorable part of the column (to within 1 mm of each electrode). The *average* potential gradients in the explorable part were from 1.1 to 23 percent less than the 8/40 volt/cm. Thus Ohm's law was found not to hold even over the explorable part of the column.

EVER since the publication of Hittorf's[1] famous paper in 1853 it has been assumed, in general, that, in every small element of volume of an electrolyte of uniform concentration and undergoing electrolysis, the sum of the charges on the negative ions is equal to the sum of the charges on the positive ions, namely, that during electrolysis *macroscopic* space charge does not exist. Apparently Hittorf based this assumption on some experimental results which were reported by Faraday[2] in about 1833, and which were quoted by Hittorf.

A few examples of modern workers who assume electrical neutrality in a uniform electrolyte during electrolysis are Nernst,[3] Newman,[4] Falkenhagen,[5] and MacInnes.[6] Although none of these writers makes a specific statement concerning macroscopic space charge in electrolytes, statements which these writers do make can be true only if such space charge does *not* exist.

Macroscopic space charge is known to exist in a uniformly ionized column of gas which is conducting an electric current. This phenomenon has been investigated both experimentally and theoretically by a number of workers, including Zeleney,[7] Child,[8] Walker,[9] Robb,[10] Thomson,[11] and Mie.[12] These investigators found a positive space charge in the cathode half of the column of gas, and a negative space charge in the anode half of the column, and that the magnitude of the space charge increased as an electrode was approached.

Since a column of electrolyte is also uniformly ionized throughout, and since the current, in each of the uniformly ionized columns of gas and electrolyte, consists of positive ions moving toward the cathode together with negative ions moving toward the anode, it seems reasonable to expect that macroscopic space charges *might* exist in an electrolyte during electrolysis. This conjecture led the senior author, in 1924, to begin a series of researches designed to test the hypothesis that macroscopic space charges exist in electrolytes during electrolysis, and to determine the distribution of the charge should any be found to exist.

THE POTENTIAL DISTRIBUTION REQUIRED FOR SPACE CHARGE

Consider a rectangular column of electrolyte, contained in an accurately made glass trough having a uniform section, between two plane metal electrodes each having an area equal to that of the column and at a distance d from each other. Suppose that the potential difference V_d of these current electrodes is maintained constant and that the cathode is grounded. Let V be the potential in the electrolyte at a point P

* Submitted as a dissertation in partial fulfillment of the requirements for the degree Doctor of Philosophy in July, 1948 by Mr. Reed who is now Associate Professor of Physics at Clemson College, Clemson, South Carolina.

[1] W. Hittorf, "On the migration of ions during electrolysis," Pogg. Ann. **89**, 177 (1853).

[2] Michael Faraday, *Experimental Researches in Electricity* (E. P. Dutton and Company, New York), pp. 238, 240.

[3] Walter Nernst, *Theoretical Chemistry* (MacMillan Company, Ltd., London, 1923), fifth edition, p. 424.

[4] F. H. Newman, *Electrolytic Conduction* (John Wiley and Sons, Inc., New York, 1931), p. 36.

[5] Hans Falkenhagen, *Electrolytes* (Oxford University Press, London, 1934), pp. 2, 82.

[6] D. A. MacInnes, *Principles of Electrochemistry* (Reinhold Publishing Corporation, New York, 1939), p. 53.

[7] J. Zeleney, Phil. Mag. **46**, 120 (1898).

[8] C. D. Child, Ann. d. Physik **65**, 152 (1898).

[9] G. W. Walker, Phil. Mag. **8**, 650 (1904).

[10] A. A. Robb, Phil. Mag. **10**, 237, 664 (1905).

[11] J. J. Thomson, *Conduction of Electricity through Gases* (Cambridge University Press, London, 1906), p. 84.

[12] G. Mie, Ann. d. Physik **13**, 857 (1904).

which is at a distance x from the cathode, and let ϵ be the dielectric constant of the solution. Under these conditions Poisson's equation takes the form,

$$d^2V/dx^2 = -4\pi\rho/\epsilon, \quad (1)$$

where ρ is the space charge at P.

After the current through the electrolyte has been established for a time t electrical double layers and other space-charge effects may exist *very close* to the electrodes. Also concentration changes close to the electrodes may cause certain electromotive forces. All such phenomena may be assumed to be confined to a rather thin layer next to each current electrode. Let the thickness of that layer next to the cathode be Δx, and let the potential rise through it due to these effects be e'. The potential rise due to the resistance of the layer may be written $IR_{\Delta x}$, and the potential rise due to the resistance of the column between Δx and x may be written $k(x-\Delta x)$. Since e', $IR_{\Delta x}$ and $k\Delta x$ are constants independent of the location of the point P, at any time t the potential at P may be expressed,

$$V = e + kx + \varphi(x), \quad (2)$$

where $e = e' + IR_{\Delta x} - k\Delta x$, and $\varphi(x)$ is the potential rise between Δx and x due to space charge, if any, in that region.

If there had been no unique potential rises and electromotive forces at the electrode surfaces and in the thin layers next to the electrodes, then at time $t=0$ the potential at any point x would be given by,

$$V_0' = (V_d/d)x. \quad (3)$$

V_0' differed from the actual potential, $V_0 = e_0 + k_0x$ (where e_0 and k_0 may be different from e and k) only by a linear function of x.

If the deviation D be defined as $V - V_0'$ then,

$$D = e + kx + \varphi(x) - (V_dx/d). \quad (4)$$

Since

$$d^2V/dx^2 = d^2D/dx^2 = -4\pi\rho/\epsilon, \quad (5)$$

the space charge ρ will be zero unless $\varphi(x)$ is a *non-linear* function of x. Thus space charge may exist in the column of electrolyte (i.e., for $x > \Delta x$) only if V, and therefore D, is a non-linear function of x. The quantity D was measured experimentally with a quadrant electrometer.

RESULTS OF PRELIMINARY WORK

Roller[13] found the potential gradient not to be constant in a column of HCl solution between platinum electrodes; this gave an indication of space charge. Cameron,[14] investigating a solution of $CuSO_4$ between copper electrodes with improved apparatus, found even better evidence of space charge. Both workers determined the potential gradient by measuring the potential difference between two small pointer electrodes maintained at a fixed distance apart and placed at various positions along the column of electrolyte. The indicated space charges were found to be small everywhere, but were largest near the current electrodes. Reproducibility of data was not achieved.

Mitchell,[15] using better apparatus and $CuSO_4$ solution, measured the potential difference between a single pointer exploring electrode and the grounded cathode, as a function of time. From such data he calculated the potential distribution along the column at any instant and found it to be a non-linear function of the distance from the cathode. Again good reproducibility of data was not achieved. Reed,[16] using a "standard-curve method" (which will be described later) and essentially Mitchell's apparatus, developed a procedure for preparing the current electrodes, which together made possible good reproducibility of the deviation-time data. In fact, his data revealed irregularities in the special porcelain trough which he was using. His data gave excellent indications of space charge.

Brooking,[17] employing a new, large and accurately made plate glass trough and heavy optical bench equipment to hold the current and pointer electrodes, obtained accurately reproducible data with a 0.0024 normal solution of $CuSO_4$. He used the standard-curve method as well as Reed's method of preparing the current electrodes. He found the space charge in the explorable part of the electrolyte to be *negative* in the *cathode* end of the column and *positive* in the *anode* end of the column. However, it was also possible to show that the space charge was positive *very close* to the cathode and negative *very close* to the anode, but these regions were too near the electrodes to be investigated experimentally. Brooking's data showed that four space-charge regions existed in his electrolyte, alternately positive and negative, in contrast to the two regions which exist in gases.

Rice,[18] using Brooking's apparatus, found that the space charge increased with increasing potential difference of the current electrodes, and that the temperature of the solution had a negligible effect on the space-charge provided that the temperature of the solution did not *change* during a deviation-time run. His runs at 9.000 volts checked those of Brooking.

Carson[19] enclosed Brooking's apparatus in a cabinet lined with thick heat-insulating material to prevent rapid temperature changes, and found that the space

[13] Duane Roller, *On Space Charge in Electrolytes I.* (Thesis: University of Oklahoma, 1925).

[14] John N. Cameron, *On Space Charge in Electrolytes II.* (Thesis: University of Oklahoma, 1926).

[15] J. Taylor Mitchell, *On the Departures from Ohm's Law in a Conducting Electrolyte* (Thesis: University of Oklahoma, 1928).

[16] Charles A. Reed, *Deviation from Ohm's Law in a Conducting Electrolyte I.* (Thesis: University of Oklahoma, 1929).

[17] Leslie E. Brooking, *Deviations from Ohm's Law in a Conducting Electrolyte II.* (Thesis: University of Oklahoma, 1932).

[18] Kenneth A. Rice, *Space Charge in a Conducting Copper Sulphate Solution* (Thesis: University of Oklahoma, 1933).

[19] Roe Carson's work is summarized in the thesis of John L. Dalke, *Macroscopic Space Charge Near the Electrodes in a Conducting Electrolyte* (University of Oklahoma, 1939).

charge increased with increasing concentration. He found also that, when the current was maintained for a number of hours, the deviations in the central part of the trough were greater than those near the electrodes, and that the *positive* space charge next to the cathode then extended out into the solution sufficiently far to be measured. No measurements were made to determine the possible existence of concentration changes which may have existed because of the relatively long time that the current existed.

Martin[20] showed that the deviations observed by Brooking and others could not have been due to changes in concentration of the solution caused by the electric current. He measured the resistance, by an alternating current method, between two wire electrodes 1 mm long and 1 mm apart immersed in the column of electrolyte of Brooking's apparatus, both before and after the current through the column had existed for 15 minutes, the maximum time used by Brooking. The wire electrode assembly was calibrated by immersing it in copper sulfate solutions of various known concentrations in the neighborhood of $0.0024N$, and it was found possible to measure changes of 2 percent (of $0.0024N$), or less. To account for the deviations observed by Brooking would have required concentration changes of as much as 16 percent. Not the slightest evidence of concentration change was observed by Martin.

While these researches were in progress Coehn and Schnurman[21] published their observations on the streaming of bubbles backward from a point cathode in dilute sulfuric acid. They interpreted their observations as evidence of space charge in the electrolyte near the electrode.

THE OBJECT OF THE PRESENT INVESTIGATION

The purposes of the present investigation were to establish beyond all reasonable doubt the existence of macroscopic space charges in electrolytes during electrolysis; to determine the space charge distributions in different electrolytes conducting current between two plane parallel electrodes in a rectangular trough of uniform cross section; and to determine the effect of these space charges on the distributions of the potential gradient in these electrolytes.

THE APPARATUS

The assembly of instruments and the various pieces of apparatus which were used is schematically illustrated in Fig. 1. The trough T which contained the electrolyte was made of pieces of plane plate glass cemented together so that the space inside was 41 cm long by 8 cm wide by 9 cm deep. The width of the trough was constant to within 0.1 mm. The column of electrolyte between the electrodes was made to be a rectangular parallelopiped 40 cm by 8 cm by 8 cm.

Each electrolyte studied was a 0.0024 normal solution of a metallic salt, and the metal of the electrodes was the same as that of the metallic ion. The current electrodes *Ca* and *An* were made of pure metal sheet approximately $\frac{1}{8}$-inch thick. They were made quite flat and cut so as to fit nicely between the sides of the trough.

The exploring electrode, or pointer P, was made by sealing a Number 30 B. & S. gauge wire (of the same metal as the current electrodes) into a glass tube which had been drawn to a long narrow point. About one cm length of this long point was bent at right angles to the axis of the tube and the end was carefully ground off so as to expose only the cross section of the Number 30 wire. This glass tube was mounted vertically through a horizontal brass turntable from which it was insulated by polystyrene rods. A suitable mechanism was provided which made it possible to adjust the exposed tip of the wire so that it lay exactly on the axis of the turntable. This made it possible to keep the tip at one point in the electrolyte and yet have it face either the cathode or the anode.

The two current electrode assemblies and the pointer assembly were mounted on three heavy cast iron riders which slid on a carefully ground Leitz optical bench. Each current electrode assembly provided screw adjustments with which the plane of the electrode was made accurately normal to the sides and bottom of the trough. This optical bench and a flat plank on which the trough rested, were mounted on heavy steel cross bars which were provided with leveling screws. These cross bars also carried an accurate Brown and Sharpe steel scale with a 1/20 mm vernier slider; this was used to measure the location of the tip of the pointer with respect to either electrode, as well as to adjust the distance between the current electrodes.

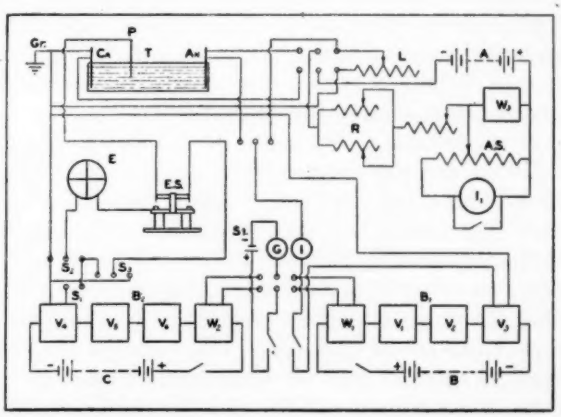

FIG. 1. Schematic diagram of the apparatus. Battery A supplied the current through the electrolyte T; it could be measured by the galvanometer I_1. The potential difference between the cathode and anode was maintained constant with the aid of potentiometer B_1 and the rheostats R. The potential of the pointer P was measured with the potentiometer B_2 for which the balance was indicated by the quadrant electrometer E. The potentiometer currents were adjusted with the aid of the Weston standard cell St. and the galvanometer G.

[20] Paul J. Martin, *Concentration Variations in a Conducting Electrolyte* (Thesis: University of Oklahoma, 1938).
[21] Coehn and Schnurman, Zeits. f. Physik **46**, 354 (1928).

TABLE I. Reproducibility of data after correction by the standard curve method.*

Time (minutes)	First run S	First run D	First run D.C.	Second run S	Second run D	Second run D.C.
1	3.8	18	14	−1.0	17	16
2	9.0	26	24	3.8	26	25
3	13.0	33	32	8.8	34	33
4	16.0	38	38	12.5	40	38
5	18.5	43	43	15.8	46	44
6	20.2	46	47	17.5	49	47
7	21.8	49	50	19.0	52	50
8	22.5	50	52	20.2	54	52
9	23.2	51	54	20.8	55	54
10	24.0	52	55	21.8	57	56
11	24.2	53	55	22.5	58	58
12	24.5	55	57	22.5	58	59
13	25.0	54	58	22.0	57	57
14	25.2	54	57	22.2	57	59
15	25.2	54	58	22.5	58	58

* Data were taken in a $CuCl_2$ solution at a point 2 cm from the cathode. The first run was made on June 9, 1947 and the second run on June 14, 1947. Pointer-cathode chemical e.m.f. correction: First run, 37 mv; second run, 39 mv. Pointer distortion correction, −8 mv for each run. Corrected linear rise of potential: First run, 429 mv; second run, 431 mv. Balancing potentiometer setting: First run, 440 mv; second run, 450 mv. *S* is the electrometer deflection in mm. *D* is the deviation in mv. *D.C.* is the deviation corrected by the standard curve method.

The Electrical Circuits

The current through the electrolyte was supplied by the battery of dry cells A, and was adjusted by means of the resistance R which consisted of a 3200-ohm rheostat in parallel with a 200-ohm rheostat, and these in series with two 900-ohm rheostats. The potential difference between the cathode Ca and the anode An was maintained at 8.000 volts and was measured by use of the potentiometer B_1 in which the portable galvanometer I indicated the balance. The resistance boxes marked V were Leeds & Northrup four-dial boxes and those marked W were Wolff plug boxes.

The potential difference between the pointer P and the grounded cathode (or grounded anode) was measured with the potentiometer B_2 in which the balance was indicated by the quadrant electrometer E. This electrometer also indicated the deviation D directly by the size of its deflection. Its needle potential was kept at 112.5 volts and the sensitivity of the electrometer was 1.72 millivolts per mm with a scale distance of one meter. This instrument was remodeled and equipped with polystyrene insulators; leaks were not detected even on the most humid hot days. The switches S_1, S_2, S_3 and $E.S.$ made it possible to check the calibration of the electrometer at any time. The currents for both potentiometers B_1 and B_2 were adjusted by use of the Weston standard cell St. and the portable galvanometer G. The electrometer switch $E.S.$ was also provided with polystyrene insulators.

The auxiliary resistance L, equal to that of the column of electrolyte, was so arranged that the current could be switched through it when the electrodes were disconnected from the battery. This procedure prevented rapid variation in the current through the electrolyte when that circuit was again closed. The resistance box W_3, the Ayrton shunt $A.S.$ and the L. & N. Type "P" galvanometer I_1 were used to measure the current through the electrolyte. The trough with its accessories, the electrometer and the electrometer switch were housed in a heat-insulated cabinet within which rapid changes in temperature did not occur. All leads to the electrodes and the electrometer had excellent electrical insulation. The temperature in the cabinet was maintained near 30°C.

PROCEDURE

The deviations from a linear rise of potential, the distributions of space charges, and the distributions of electric potential gradient were determined for 0.0024N solutions of the following eight salts: cupric sulfate, cupric chloride, zinc sulfate, zinc chloride, zinc acetate, nickel sulfate, nickel chloride and aluminum sulfate.

Since the correctness of our conclusions can be judged only after careful consideration of the procedure used to obtain the data, the essential parts of this procedure will be described somewhat in detail.

After the electrodes had been carefully prepared according to a routine which made possible the reproduction of data, the pointer was located at the desired point x in the column of electrolyte, the potential difference of the electrodes was adjusted to 8.000 volts, the current was switched to the auxiliary resistor L which was adjusted so that its potential difference was also 8.000 volts, after which the solution was thoroughly stirred and permitted to rest undisturbed for at least 15 minutes so that all parts of the fluid would be at rest.

With the pointer potentiometer B_2 set so as to balance the corrected linear rise of potential to the point x (namely, (8.000 volts/40 cm)$\cdot x$ cm plus certain corrections which will be explained below), the current from battery A was switched to the electrolyte and, immediately following this, one pair of electrometer quadrants was connected to the pointer, and the other pair to the potentiometer B_2, by means of switches $E.S.$ and, S_1 and S_2. The potential difference between the current electrodes was maintained at 8.000 volts by small adjustments in the rheostats R, and the electrometer deflection was noted and recorded each minute after the switches were closed, for a period of 15 minutes. These electrometer deflections gave the deviations D at the end of each minute. The switch $E.S.$ was reversed, the potential difference across Box V_4 was reduced to zero, the switch S_1 was opened, the electrolyte current was switched to the auxiliary resistor L, the solution was thoroughly stirred, the pointer was moved to a new position, and the solution was again left undisturbed for a period of 15 minutes. The apparatus was then ready for the next deviation-time run.

From $x=0$ to $x=20$ cm the pointer potentials were measured with respect to the cathode. From $x=20$ cm to $x=40$ cm the pointer potentials were measured with

respect to the anode. In the latter case the ground connection was shifted from cathode to anode.

Corrections Applied to the Rise of Potential $V_d x/d$

The slight chemical differences between the metals of the cathode and the pointer caused a "chemical e.m.f." to exist. This was measured just before each run by noting the deflection of the electrometer when no current existed in the electrolyte. The magnitude was found to be independent of the position of the pointer in the column of electrolyte, and it varied little over the period of a day. Its magnitude varied from some 5 mv for $ZnSO_4$ to some 400 mv for $NiSO_4$. Proper allowance for this e.m.f. was made in the setting of the pointer potentiometer.

Another correction was necessary because of the physical size of the glass-covered pointer electrode. This pointer distorted the equipotential surfaces in its neighborhood and thus the potential at the face of the pointer was somewhat different from what it would have been at that point in the electrolyte, had the pointer not been there. When a series of deviation-time runs was made with the exposed face of the pointer electrode at one point in the trough, but first facing the cathode and then the anode, the deviations for the two orientations differed by a constant amount, which was independent of the position of the pointer along the trough but did depend on the size of the glass covering. One-half of this difference was applied as a correction in order to make the proper setting of the pointer potentiometer. In the case of the copper pointer this correction was 8 mv.

The deviations D used in plotting the deviation-time curves were always calculated from the linear rise of potential which had been corrected for both the chemical e.m.f. and the pointer distortion of the equipotential surfaces. Thus, if due consideration is given to the signs of these corrections,

$$V_0' = (V_d/d)x + \text{pointer e.m.f.} + \text{distortion correction.} \quad (6)$$

Use of Standard Curves

In conformity with the experience of earlier workers on this problem it was found that repeated deviation-time curves at the same point in the trough did not duplicate each other, but that there was a progressive change as the electrodes were used again and again. Investigation showed that this was due, principally, to the "aging" of the electrodes, i.e., to changes at the surface of the metal. It was not found possible to eliminate this aging effect either by a special cleaning procedure or by a special manner of manipulating the apparatus.

However, it was found that good reproduction of data could be obtained by compensating for this aging effect in the following manner. Two "standard points" were chosen, one at $x=20$ cm for measurements with respect to cathode, and one at $x=36$ cm for measurements with respect to the anode. A deviation-time run was made at the standard point, then one was made at any desired point, then another at the standard point. This procedure was continued until all the data for a given electrolyte were obtained. The points for a "standard" deviation-time curve were then computed from all the runs at the standard point, by averaging all these deviations at the end of each minute. To correct the data for a run at any other point, the data for the runs at the standard point, taken just before and just after it, were averaged at each minute. The correction at any time t was then taken as the difference between the mean of these two deviations and the deviation of the standard curve for that time. This correction was added to the observed deviation at that time. All data were corrected in this manner.

In many cases the aging effect progressed so slowly that it was possible to make deviation-time runs at several points between each pair of runs at the standard point. The correction for any one datum was computed on the assumption that the effect of aging was a linear function of the time that the electrodes were used. Thus if n runs were made between two runs at the standard point, then the correction for an observed deviation of the kth run at a desired point, was obtained by adding $k/(n+1)$ of the difference between corresponding deviations of the two runs at the standard point, to the corresponding deviation of the first of these runs, and then subtracting that result from the corresponding datum of the standard curve.

The degree of reproducibility of the data obtained after employing these corrections may be seen in Table I, which shows two rather typical sets of data taken 5 days apart with $CuCl_2$ solution at a point 2 cm from the cathode. In general data taken in the anode half of the trough were more perfectly reproducible than those taken in the cathode half of the trough.

Graphical Representation of Data

The corrected deviation-time data for the $ZnSO_4$ solution are shown by the right-hand set of curves in Fig. 2. The number near the right-hand end of each curve indicates the distance in cm that the pointer was from the cathode. On this same figure are three curves showing how the deviations varied with distance from cathode, at the end of 5, 10 and 15 minutes. The data for these curves were obtained from the set of deviation-time curves.

Data for the other seven electrolytes were obtained and treated in the same manner. Only the deviation-distance curves are shown for these solutions in Fig. 3, together with that for zinc sulfate. The deviations for $CuSO_4$ range from +66 mv near the cathode to −20 mv near the anode, whereas those for $NiSO_4$ range from +535 mv near the cathode to −1313 mv

near the anode. Thus to show the shapes of the curves it was necessary to plot them to three different scales. It was so difficult to obtain reproducible results for the aluminum sulphate solution between aluminum electrodes, that data were obtained only for the anode half of the column of electrolyte.

CALCULATIONS OF POTENTIAL GRADIENT AND SPACE CHARGE

The electric potential gradients at points along the column of electrolyte were calculated from the deviation-distance curve for each of the eight electrolytes by the same method that was first used on Brooking's data.

Let the potentials at points x_1, x_0 and x_2 be respectively V_1, V_0 and V_2; let $x_1=x_0-\Delta x$ and $x_2=x_0+\Delta x$, the two Δx's being small and equal in magnitude; let D_1, D_0 and D_2 be the deviations at the three points; and let K be the potential gradient for the strictly linear rise of potential, which was $V_a/d=8000$ mv/400 mm $=20$ mv/mm. Then,

$$V_0=Kx_0+D_0, \tag{7}$$

$$V_1=K(x_0-\Delta x)+D_1, \tag{8}$$

and

$$V_2=K(x_0+\Delta x)+D_2. \tag{9}$$

From these it may be shown that the potential gradient at x_0 will be given by,

$$\left(\frac{dV}{dx}\right)_{x_0}=K+\frac{D_2-D_1}{2\Delta x}=20\frac{\text{mv}}{\text{mm}}+\frac{D_2-D_1}{2\Delta x}. \tag{10}$$

From Eq. (10) it is evident that the potential gradients at points $[x_0-(\Delta x/2)]$ and $[x_0+(\Delta x/2)]$ are, respectively, $K+(D_0-D_1)/\Delta x$ and $K+(D_2-D_0)/\Delta x$. Thus the gradient of the field strength at the point x_0 will be given by,

$$(d^2V/dx^2)_{x_0}=(D_1+D_2-2D_0)/(\Delta x)^2, \tag{11}$$

and the space charge at x_0 will be given by,

$$\rho=\frac{\epsilon}{4\pi}\left(\frac{2D_0-D_1-D_2}{(\Delta x)^2}\right). \tag{12}$$

The dielectric constant of water is 80. If the deviations are in millivolts, Δx is in mm and the space charge ρ is

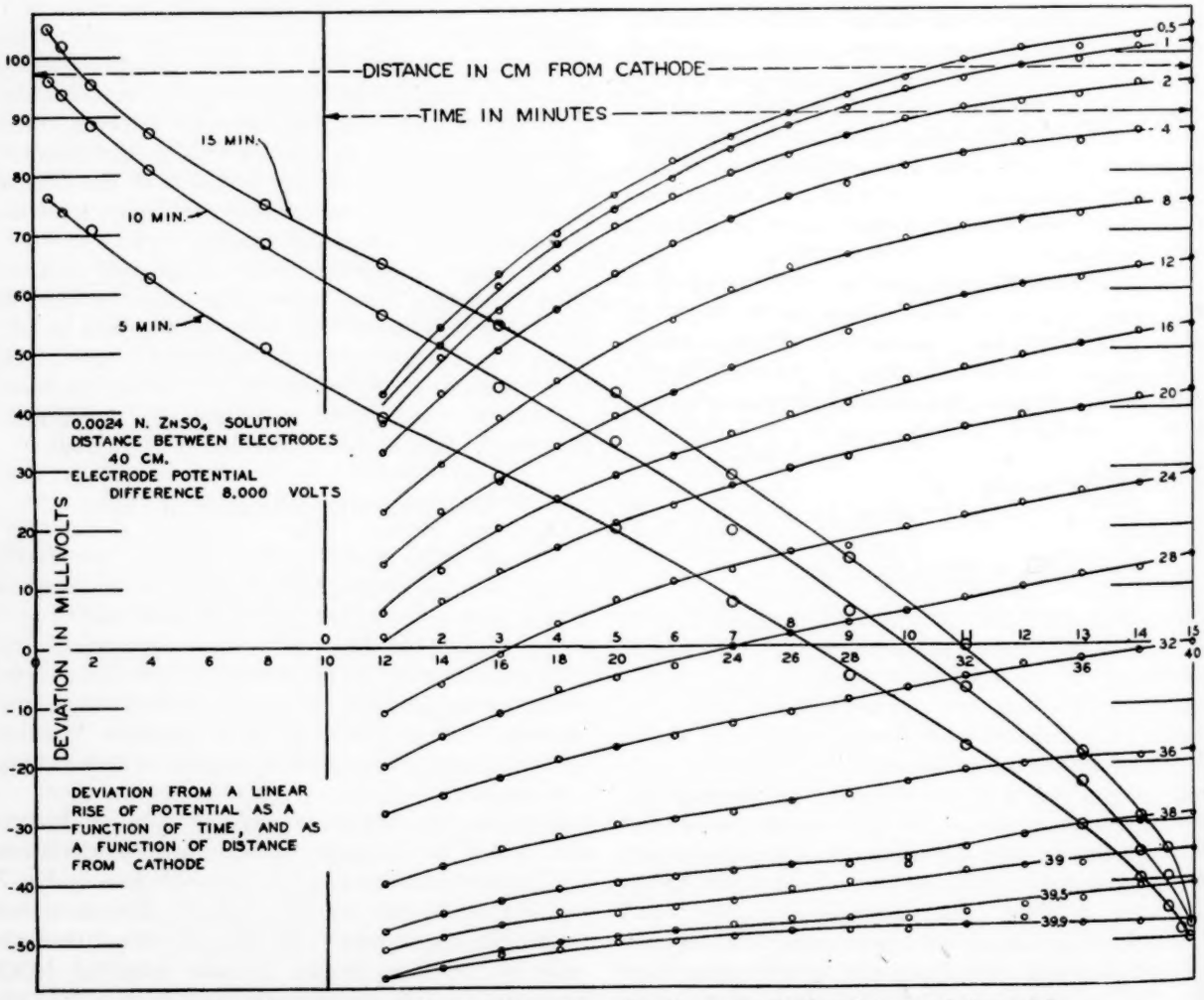

FIG. 2. Deviation-time curves for 16 positions along the column of a $ZnSO_4$ solution, and the resulting deviation-distance curves at three different times.

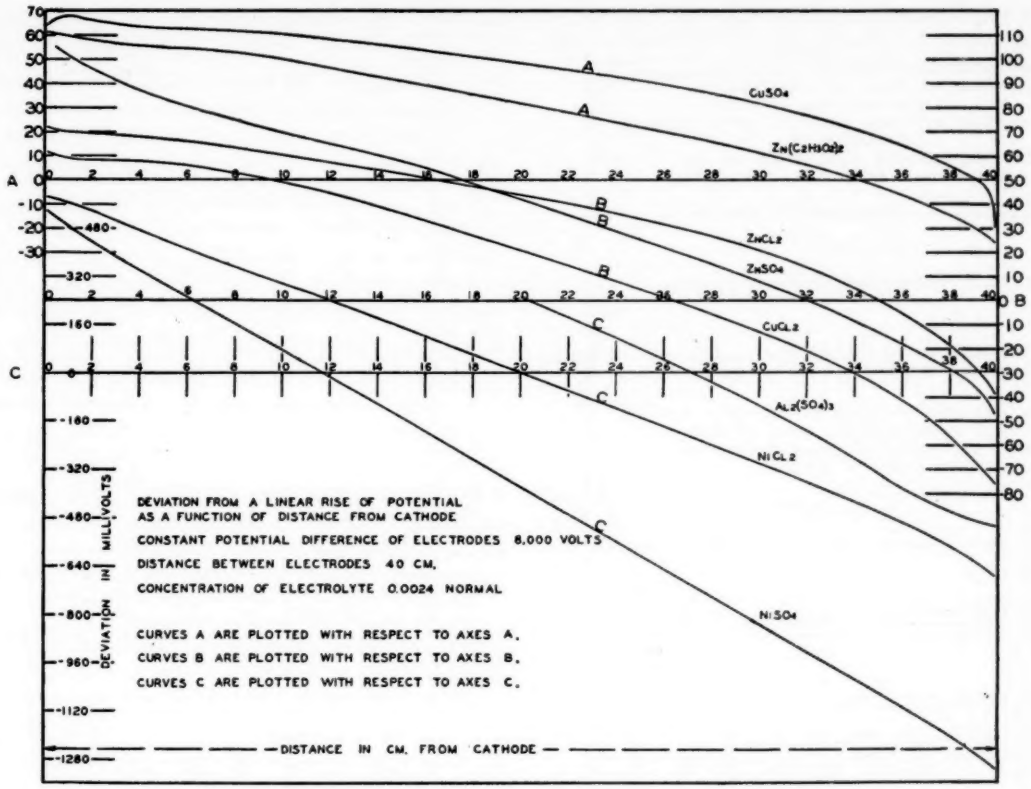
CuSO4
Zn(C2H3O2)2
ZnCL2
ZnSO4
CuCL2
Al2(SO4)3
NiCL2
NiSO4
DEVIATION FROM A LINEAR RISE OF POTENTIAL AS A FUNCTION OF DISTANCE FROM CATHODE
CONSTANT POTENTIAL DIFFERENCE OF ELECTRODES 8.000 VOLTS
DISTANCE BETWEEN ELECTRODES 40 CM.
CONCENTRATION OF ELECTROLYTE 0.0024 NORMAL
CURVES A ARE PLOTTED WITH RESPECT TO AXES A.
CURVES B ARE PLOTTED WITH RESPECT TO AXES B.
CURVES C ARE PLOTTED WITH RESPECT TO AXES C.
DEVIATION IN MILLIVOLTS
DISTANCE IN CM. FROM CATHODE

FIG. 3. Deviation from a linear rise of potential as a function of distance from cathode, for eight electrolytes, after current existed 15 minutes.

desired in statcoulombs/cm^3, then

$$\rho = 2.12\times 10^{-3}\left(\frac{2D_0 - D_1 - D_2}{(\Delta x)^2}\right). \qquad (13)$$

In order to facilitate the computations of the numerous values of the potential gradient and the space charge, the deviation-time and the corresponding deviation-distance curves were plotted to a large scale on sheets of profile paper 17 by 22 inches in size. In fact, Fig. 2 is a photographic reproduction of one such sheet of curves. Sets of D_1, D_0 and D_2 were read from a deviation-distance curve at points all along the curve, and then Eqs. (10) and (13) were applied to these data.

The calculated values of the potential gradient, at the end of 15 minutes, are shown plotted as functions of the distance from the cathode in Fig. 4, for each of the eight electrolytes. The dashed line for each curve shows the average value of the existing potential gradients in the explorable part of the column of electrolyte. The horizontal line marked "20" on the gradient axis shows the potential gradient that would have existed if there had been no space charge and no special phenomena near and at each electrode surface in that electrolyte.

The calculated values of the space charge, at the end of 15 minutes, are shown plotted as functions of the distance from the cathode in Fig. 5, for each of the eight electrolytes. Note that the zero ordinate for each curve lies at about the level of the horizontal section of that curve. Note also that only in the case of $NiCl_2$ and $CuSO_4$ did the positive space charge next to the cathode extend out into the solution far enough to be measured, and that only in the case of $Al_2(SO_4)_3$ did the negative space charge next to the anode extend out into the explorable part of the column.

Test of Another Method

All the experiments described thus far were carried out with a constant potential difference between the current electrodes, under which condition there was a small change of current with time. It was thought that some of the difficulties arising from the progressive aging of the electrodes could be eliminated by maintaining the current constant during the 15 minute interval. A complete set of data for the $CuSO_4$ solution was obtained by this method, and the usual calculations were made. The results agreed almost exactly with those obtained by the method of constant potential difference for this solution. Since the constant current method was more laborious and more difficult to carry out, only the method of constant potential difference was used with the other seven electrolytes, and all the data described here were obtained by the constant potential method.

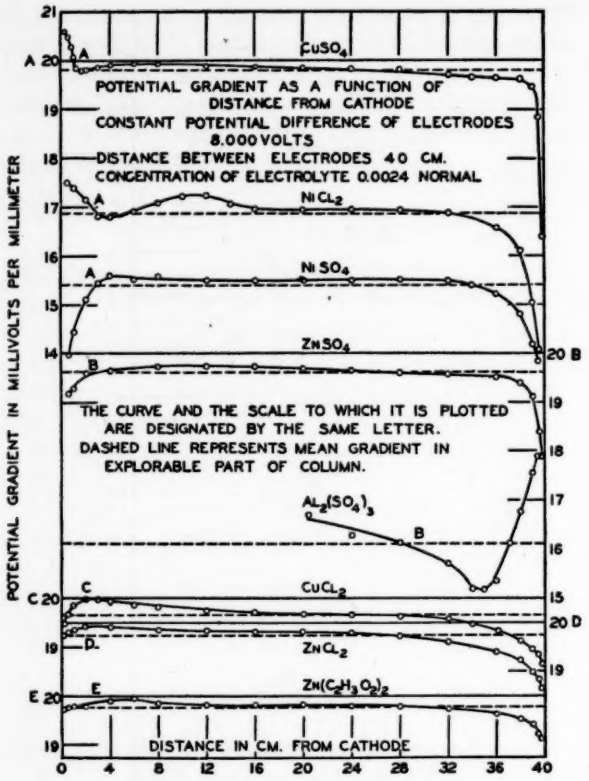
POTENTIAL GRADIENT AS A FUNCTION OF DISTANCE FROM CATHODE
CONSTANT POTENTIAL DIFFERENCE OF ELECTRODES 8.000 VOLTS
DISTANCE BETWEEN ELECTRODES 40 CM.
CONCENTRATION OF ELECTROLYTE 0.0024 NORMAL
CuSO4
NiCl2
NiSO4
ZnSO4
THE CURVE AND THE SCALE TO WHICH IT IS PLOTTED ARE DESIGNATED BY THE SAME LETTER.
DASHED LINE REPRESENTS MEAN GRADIENT IN EXPLORABLE PART OF COLUMN.
Al2(SO4)3
CuCl2
ZnCl2
Zn(C2H3O2)2
POTENTIAL GRADIENT IN MILLIVOLTS PER MILLIMETER
DISTANCE IN CM. FROM CATHODE

FIG. 4. Curves showing how the electric potential gradient varied along a uniform column of electrolyte after electrolysis had taken place for 15 minutes. If there had been no space charge and no special effects very close to each electrode surface, the potential gradient in each case would have been 20 mv/mm.

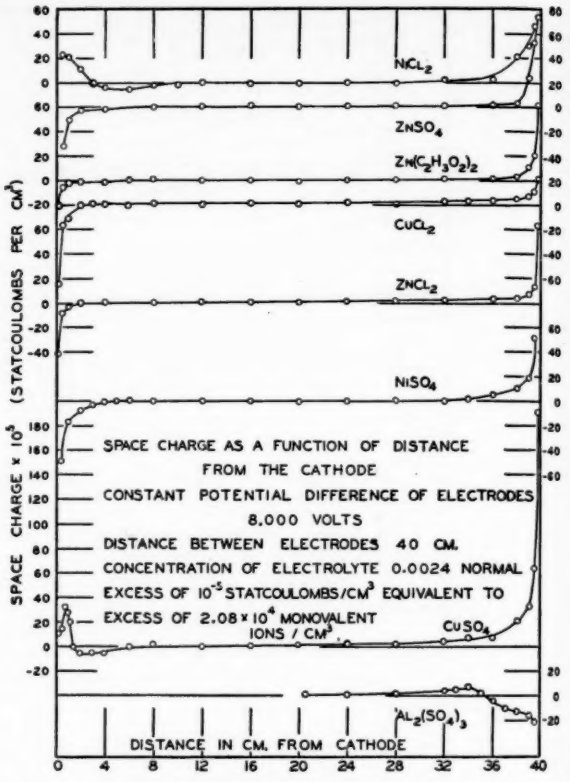

FIG. 5. Curves showing how the macroscopic space charge varied along a uniform column of electrolyte after electrolysis had taken place for 15 minutes. Note that the zero ordinate for each curve is at the level of the horizontal part of that curve.

DISCUSSION OF RESULTS

Three factors imposed limitations on the reproducibility of the data. In the first place it was very difficult to reproduce a given initial condition of the electrodes. Much time was spent on each of the four metals to devise a procedure that was at least fairly satisfactory. Each of these involved cleaning in an acid solution, polishing with very fine emery cloth while wet, again cleaning with acid solution, and finally washing with distilled water and using immediately without drying. The copper and the zinc electrodes also were "aged" by having the usual current in the trough turned on for 12 or 18 hours before data were taken.

The second factor was the aging of the electrodes while the deviation-time runs were being made. This factor was satisfactorily dealt with by use of the standard curve method which has been described already. However, it was also found necessary to clean the electrodes and to change the electrolyte periodically in order to maintain reproducibility.

Sensitivity of the Apparatus

The third factor involved the limitations of the apparatus. Reproduction of the setting of the pointer could be made with an estimated mistake of ± 2 mv. The position of coincidence of the pointer with an electrode surface caused an estimated mistake of ± 1 mv. The electrometer deflections could be read to an estimated mistake of ± 1 mv. The potential difference between the current electrodes could be held constant to within ± 0.2 mv. The balancing potential for the electrometer could be maintained constant to within about ± 0.1 mv. The total estimated mistake which might occur in a deviation determination was thus estimated to be approximately ± 4 mv.

Each point on a plotted deviation-time curve was the average of the values obtained in from 2 to 8 runs. The differences between the value obtained in a run, from that of the mean which was plotted, was only from 1 to 3 mv for the $CuSO_4$, $CuCl_2$, $ZnSO_4$ and $ZnCl_2$ solutions. For the $Zn(C_2H_3O_2)$ and $NiSO_4$ solutions the differences were from 2 to 5 mv. In $NiCl_2$ and $Al_2(SO_4)_3$ solutions some of the differences were as much as 15 mv but, since the deviations themselves were very large, the percentages of inaccuracy were not worse than those for the copper solutions. Thus for all except $NiCl_2$ and $Al_2(SO_4)_3$ the reproducibility was as good as, or better than, was expected.

Effect of Concentration Changes

The solution level was maintained to within ± 1 mm by adding distilled water from time to time. This made

for an inaccuracy in the concentration of less than 1 percent (of $0.0024N$). To test the effect of this, deviation-time runs were made with concentrations of 105 percent, 100 percent and 95 percent of $0.0024N$. The observed deviation-time curves agreed well within the estimated mistake. Therefore the evaporation had an entirely negligible effect on the data.

Possible concentration changes caused by the electrolysis were investigated by Martin (mentioned earlier) and found to be negligible. Such concentration changes would be expected to be very small since the current was only 5×10^{-5} amp./cm² and since the mobilities of the ions are only some 0.0005 (cm/sec.)/(volt/cm). Therefore in 15 minutes such an ion would move only about one mm. Further, if the current had produced appreciable concentration changes, an increase in potential gradient should have occurred in the cathode region and a decrease in the anode region. Actually decreases in gradient were observed out in the solution near both electrodes. In $CuSO_4$ and $NiCl_2$ near the cathode, and in $Al_2(SO_4)_3$ near the anode, an increase was observed close to the electrode and a decrease further out from the electrode. Thus it would appear that concentration changes could not have caused the observed deviations which have been attributed to space charges.

The Deviation-Distance Curves

Since the deviations in the metal of the cathode and in the metal of the anode must be zero, the deviation-distance curve must start at $D=0$ at the cathode and end at $D=0$ at the anode. Further, it is to be observed that each curve is concave upward near the cathode end, and concave downward near the anode end. Therefore, somewhere close to the cathode this deviation-distance curve must have an inflection point; it must also have an inflection point somewhere near the anode and it must therefore have a third inflection point somewhere in between. Except in the case of $CuSO_4$ and $NiCl_2$ solutions near the cathode, and the $Al_2(SO_4)_3$ solution near the anode, the inflection points near the electrodes occurred too close to the electrodes to be observed.

Some of the curves near the cathode end appear to have little concavity upward because of the small scale to which they are reproduced. However, in these regions many runs were made in order to establish that a concavity actually existed.

The effects of these inflections in the deviation-distance curves are shown clearly by the corresponding potential gradient curves in Fig. 4 and by the space charge curves in Fig. 5.

Space Charge-Distance Curves

At the location of each inflection point in a deviation-distance curve, there occurs a change in sign of the space charge. For most of the solutions, in the explorable part of the columns, there occurred *negative* space charge in the *cathode* part of the column and *positive* space charge in the *anode* part. However, since the inflection points occurred very near the electrodes, there must have been, in *every* case, a positive space charge very near the cathode and a negative space charge very near the anode. For the $CuSO_4$ and $NiCl_2$ solutions these positive space charges near the cathode actually existed far enough out in the solution to be observed (see Fig. 5), and for the $Al_2(SO_4)_3$ solution the negative space charge near the anode existed far enough out in the solution to be observed.

Thus one is led to conclude that, when a column of electrolyte undergoes electrolysis, there exist in the column four space charge regions; from cathode to anode these are: (1) a narrow region of positive space charge near the cathode, (2) a broad region of negative space charge, (3) an even broader region of positive space charge, and (4) a narrow region of negative space charge next to the anode.

TABLE II. Observed space charges.

Compound	Distance in cm. from cathode	Excess charge per cm³ (e.s.u.)	Excess number of ions per cm³	Relative excess of ions. One in every
$CuSO_4$	0.5	$+16\times10^{-5}$	2×10^{6}	40×10^{11}
	20	$+1\times10^{-5}$	1×10^{4}	700×10^{11}
	39.8	$+180\times10^{-5}$	2×10^{6}	4×10^{11}
$CuCl_2$	0.5	-64×10^{-5}	1×10^{6}	10×10^{11}
	20	$+1\times10^{-5}$	1×10^{4}	700×10^{11}
	39.8	$+21\times10^{-5}$	2×10^{5}	40×10^{11}
$ZnSO_4$	0.6	-32×10^{-5}	3×10^{5}	30×10^{11}
	20	negligible		
	39.8	$+74\times10^{-5}$	8×10^{5}	10×10^{11}
$ZnCl_2$	0.5	-42×10^{-5}	8×10^{5}	20×10^{11}
	20	negligible		
	39.8	$+64\times10^{-5}$	7×10^{5}	10×10^{11}
$Zn(C_2H_3O_2)_2$	0.5	-21×10^{-5}	4×10^{5}	40×10^{11}
	20	negligible		
	39.8	$+64\times10^{-5}$	7×10^{5}	10×10^{11}
$NiSO_4$	0.5	-49×10^{-5}	5×10^{5}	10×10^{11}
	20	negligible		
	39.5	$+51\times10^{-5}$	5×10^{5}	10×10^{11}
$NiCl_2$	0.5	$+11\times10^{-5}$	2×10^{5}	30×10^{11}
	20	negligible		
	39.5	$+47\times10^{-5}$	5×10^{5}	10×10^{11}
$Al_2(SO_4)_3$	0.5	No data for cathode half of column		
	20	$+2\times10^{-5}$	1×10^{4}	500×10^{11}
	39.5	-21×10^{-5}	4×10^{5}	20×10^{11}

The Potential Gradient Curves

The potential gradient curves in Fig. 4 indicate clearly that in a uniform column of electrolyte during electrolysis the potential gradient is far from constant especially near the electrodes. The *mean* potential gradient in the *explorable* part of the column ($x=0.1$ cm to $x=39.9$ cm) for each electrolyte is indicated by the dashed horizontal line. The percentage difference of this value from the linear rise of potential value of

20 mv/mm is for $CuSO_4$ 1.1 percent, $CuCl_2$ 1.7 percent, $ZnSO_4$ 1.9 percent, $ZnCl_2$ 1.4 percent, $Zn(C_2H_3O_2)_2$ 1.1 percent, $NiSO_4$ 23 percent, $NiCl_2$ 16 percent, and $Al_2(SO_4)_3$ 16 percent. These curves show clearly that, in conductivity measurements, care must be taken, not only to eliminate the large potential drops at, and near, the electrode surfaces by some suitable method, but also to eliminate the broader regions where the potential gradients are not constant. If the potential gradient is not constant but is some known function of x, then the conductance may be calculated by use of a suitable integration.

Magnitude of the Space Charges

The magnitudes of the space charges at three points along the column are shown for each solution in Table II. The greatest space charge observed, 180×10^{-5} statcoulomb/cm^3, existed in the $CuSO_4$ solution at 2 mm from the anode. This represents an excess of 2×10^6 Cu^{++} ions over SO_4^{--} ions per cm^3. The relative excess is still only one ion for every 4×10^{11} Cu^{++} ions originally present. Such an excess appears trivial. However, as can be observed in Fig. 4, the effects of the space charges on the potential gradients are not trivial by any means.

CONCLUSIONS

Experiments with eight 0.0024N solutions of salts of four metals demonstrate beyond all reasonable doubt that macroscopic space charges exist in an electrolyte during electrolysis, and that these space charges occur in four distinct regions of the column of electrolyte, the charges in the regions being alternately positive and negative in going from cathode to anode.

Such space charges, although small, have very appreciable effects on the distribution of the potential gradient along a uniform column of electrolyte.

The fall of potential along a uniform column of electrolyte, carrying a direct current is, in general, not a linear function of distance along the column, i.e., Ohm's law does not hold.

Any direct current method of determining the conductivity of an electrolyte must take into account the effects of space charge as well as the complicated effects very close to the electrode surfaces.

It appears that electrical neutrality (lack of space charge) of an electrolyte during electrolysis is *assumed* at the present time because of work which Faraday did in about 1833, and because no one has knowingly got into sufficiently great trouble with this assumption since that time.

ACKNOWLEDGMENTS

The writers acknowledge with thanks the gifts of the 99 percent pure sheet zinc from the Matthiessen and Hegeler Zinc Company; the electrolytic refined sheet nickel from The International Nickel Company; the pure nickel wire from the Driver Harris Company; and the 99.987 percent pure aluminum sheet from the Aluminum Company of America. The sheet copper electrodes were made of electrolytic copper and were purchased from a supply house.

THE JOURNAL OF CHEMICAL PHYSICS VOLUME 17, NUMBER 10 OCTOBER, 1949

Changes in the Crystal Structure of AgBr When Exposed to X-Rays

J. C. M. BRENTANO AND L. V. C. SPENCER*
Northwestern University, Evanston, Illinois

(Received February 14, 1949)

Controversial evidence has appeared in the literature concerning the constancy of the lattice parameter of AgBr with varying exposure to radiation. This paper gives in detail experiments showing that the lattice parameter does not change appreciably with increasing exposure to x-rays.

INTRODUCTION

At the Minneapolis meeting of the American Physical Society in 1946, we reported on some precision determinations of the lattice spacing of silver bromide.[1] Measurements on this same subject had been published in 1943 by B. Hess.[2] In the September, 1947, issue of *Physica*, Burgers and Mesritz describe measurements similar to those of Hess, but with results which are at variance.[3] They do not refer to our publication, and their measurements were done with basically the same methods as used by Hess and with similar photographic materials, so that the conflicting evidence of their results and those of Hess leaves the question open as to the correct answer. It seems thus of interest to go into somewhat greater detail regarding our measurements.

The significance of such measurements derives from a theory of the latent image formation proposed by Huggins as an alternative to that of Gurney and Mott. According to this theory[4] the photographic latent image

* At present at the National Bureau of Standards, Washington, D. C.

[1] J. C. M. Brentano and L. V. C. Spencer, Phys. Rev. **71**, 142 (1947).

[2] B. Hess, Physik. Zeits. **44**, 245 (1943).

[3] W. G. Burgers and E. A. Mesritz, Physica **13**, 490 (1947).

[4] M. L. Huggins, J. Chem. Phys. **11**, 412 (1943).

is associated with local domains in which the silver bromide assumes a $B3$ structure. Huggins shows that a change from the normal $B1$ to the $B3$ structure would involve little energy and would be facilitated by the presence of irregularities or foreign ions in the crystal. Since the density of the $B3$ structure should be smaller than that of the $B1$, one might think that the formation throughout the crystal of $B3$ regions would result in a slightly smaller lattice constant, through compression of the crystal.

B. Hess reported that over a range of exposures in which the developed image increases in density with exposure, the lattice constant increases by as much as 20×10^{-4} angstrom unit; while over part of the solarization range, the lattice constant decreases by about the same amount. This effect, if real, might be interpreted as support for Huggins' theory.

The purpose of our experiment was to examine the diffraction pattern of crystals of silver bromide for varying exposures to x-rays in order to determine whether a regular change with exposure occurs. One reason for using silver bromide crystals and not a photographic emulsion is that an effect of the kind indicated above should be essentially related to the silver bromide lattice and should not depend upon the particular dispersion of the silver bromide in the form of an emulsion in gelatin. Further, by adjusting the conditions of precipitation, silver bromide crystals can be made of somewhat greater size than offered by the grains of a photographic emulsion, so that more accurate measurements of the spacing become possible.

EXPERIMENTAL PROCEDURE

The x-ray diffraction pattern was recorded photographically by means of a back reflection camera conforming in approximation with the parafocusing condition.[5] (See Fig. 1.) V-shaped fiducial marks were cut in the camera to serve as reference marks. (The background radiation reproduced these clearly on the recording film.)

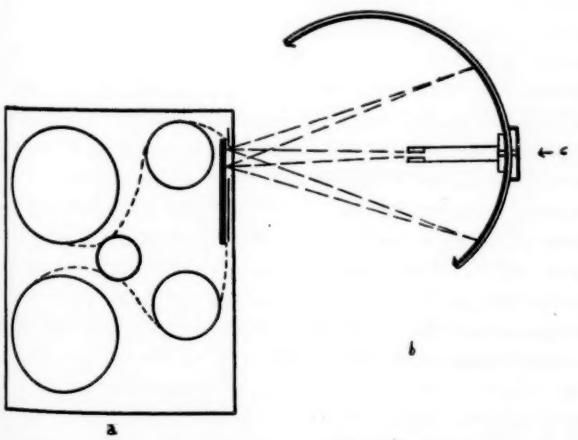

FIG. 1. Design of apparatus: (a) Motion picture camera; (b) Recording camera; (c) X-ray source.

[5] J. C. M. Brentano, J. App. Phys. **17**, 429 (1946).

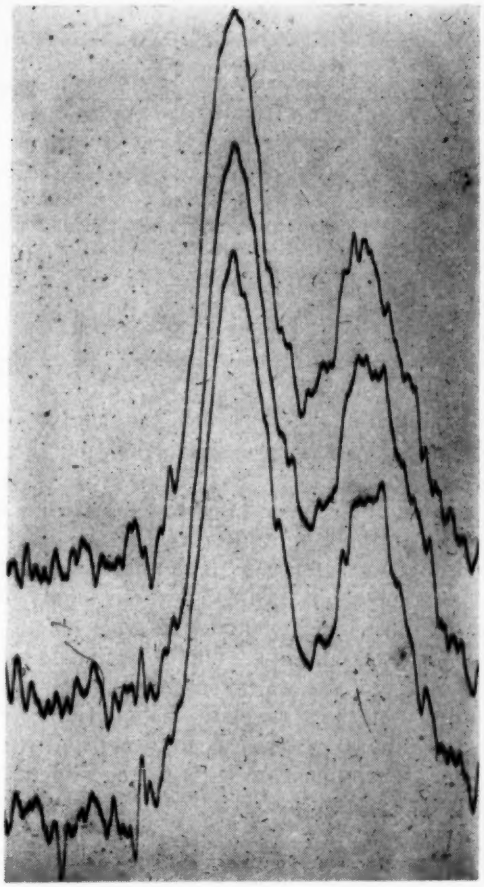

FIG. 2. Three parallel microdensitometer tracings from one of the films used, showing the definition obtained in these experiments. The tracing of the fiducial mark to which the position of the peaks was referred is not shown.

The silver bromide was exposed as a thick, flat layer on the surface of 16-mm movie film from which the emulsion had been removed. This film was moved at a uniform rate in an adapted movie camera. A paper-covered rectangular slot in the wall of the movie camera allowed the incident x-rays to strike the silver bromide and the diffracted x-rays to strike the recording film. Long strips of film could be used which could be moved at such a speed as to reduce the "element exposure" (exposure received by each powder element) to the desired value.

The distance between recording film and powder was 15.56 cm. Cobalt $K\alpha$ radiation was used in combination with an iron filter. Reflection from the 310 planes gave a line for which the diffraction angle 2θ is approximately 158°. This line was recorded on both sides of the camera.

The accuracy of the measurements required maintaining an approximately constant temperature. For this reason the temperature of the room was controlled to within 1° centigrade during any single exposure.

TABLE I.

Element exposure	Variation from mean lattice spacing	σ (Standard deviation)
39 sec.	-0.5×10^{-4}A	0.6×10^{-4}A
116 sec.	0.0×10^{-4}A	
193 sec.	-0.7×10^{-4}A	
270 sec.	0.5×10^{-4}A	
365 sec.	0.0×10^{-4}A	
424 sec.	-0.5×10^{-4}A	
88 min.	1.0×10^{-4}A	
123 min.	-0.2×10^{-4}A	
158 min.	-0.5×10^{-4}A	
193 min.	1.1×10^{-4}A	

Exposures taken at different room temperatures could be correlated by making a correction for the temperature.

The photographic patterns were evaluated in reference to the neighboring fiducial marks by means of a recording microdensitometer.[6] The film was scanned in several parallel bands. Three of these bands passed through the lines being evaluated and the fourth along the upper or lower edge of the film, so as to pass through the tips of the V-shaped fiducial marks. All tracings were recorded on the same plate, the last tracing reproducing the fiducial notches as extremely sharp magnified V's. (A sample plate without the fiducial mark tracing is reproduced in Fig. 2.)

EXPERIMENTAL RESULTS

Some of the results which we obtained are given in Table I. Each value for the variation of d from the mean of all determinations of the lattice constant is the average of six different measurements on the film.

A study of the variations in the distance between lines of the doublet and between the calibration peaks indicates that if the cause of the deviations is due alone to the imperfect estimates of the position of the line peak and the calibration peak, σ would have been approximately 0.4×10^{-4} angstrom unit. The slight variations in temperature could account for the difference.

Displacement of the surface of the AgBr backward and forward due to varying thickness would lead to a broader peak; however, since different runs were made over the same section of AgBr, a definite shift of spacing corresponding to an increase in the exposure which each element received should have been observable. Apparent change in spacing due to distortion of the camera mounting could only have been very small.

[6] J. C. M. Brentano, Rev. Sci. Inst. **16**, 309–315 (1945).

Measurements were also made using Eastman K x-ray film instead of the pure silver bromide. The results again gave no evidence of a shift of the diffraction line with increasing exposure. Although the grain size was smaller in this case, accuracy comparable to that obtained with pure silver bromide could be achieved (σ in this case was 1.4×10^{-4}A). Some of the above factors affecting definition were eliminated with this Eastman Kodak film owing to the fact that it had uniform thickness. Also, our technique was somewhat better developed when measurements on commercial film were made.

We undertook measurements of relative line widths using the same arrangement and comparing the line contour by superposition. No systematic change could be observed for the small range of exposures, while for extremely long exposures a broadening occurs which is to be expected owing to the accumulation of photolytic silver. Silver diffraction lines begin to appear then also. (No broadening could be noticed over the exposure range of Table I.)

DISCUSSION

The lack of change of spacing with exposure for the two cases where conditions were favorable for measurements is not in conflict with the Huggins theory if it may be assumed that the domains of the $B3$ structure are extremely small. It removes, however, the correlation which is offered by the experiments of Hess, since the effects which he reported should have been clearly observable with the materials which we examined.

On a broader basis we differ in our interpretation somewhat from that suggested by Hess, who attached significance to the gradual change of the lattice constant. We feel inclined to regard the process of exposure in the range of increasing densities as a process in which some of the grains have been affected by having received varying amounts of energy while others are unaffected. We should thus expect that any change of lattice due to exposure in that range should in the first place lead to line broadening, since the line would result from the superposition of the contributions from crystalline domains which have been affected by the exposure and others which have not. We were, in fact, in the first place looking for such a broadening as a means for determining the statistical distribution of lattice changes with increasing exposure from line contour. For this reason also, we did not attempt to make measurements in the range of very small exposures, since the small exposure would essentially mean a small number of grains affected.

The Vapor-Phase Photo Decomposition of Hydrogen Peroxide

DAVID H. VOLMAN
Division of Chemistry, College of Agriculture, University of California, Davis, California
(Received February 14, 1949)

The decomposition of hydrogen peroxide vapor initiated by light of wave-length 2537A was studied. The quantum yield of the reaction was found to be 1.7±0.4, essentially independent of pressure of peroxide and intensity of absorbed light. The reaction products were water and oxygen only. The rate of the reaction was found to be independent of temperature and was not affected by the addition of oxygen, nitrogen or water to the reaction mixture. The reaction scheme proposed is

$$H_2O_2+h\nu\rightarrow 2\,OH$$
$$OH+H_2O_2\rightarrow H_2O+HO_2$$
$$HO_2+HO_2\rightarrow H_2O_2+O_2$$

this leads to a maximum quantum yield of 2.

INTRODUCTION

FEW studies of the vapor-phase photo-chemistry of H_2O_2 have been made. This is somewhat surprising since H_2O_2 is, with the exception of H_2O, the only stable molecule containing H and O atoms exclusively, and is of considerable importance in problems associated with reactions in the system H_2-O_2. Moreover, the H_2O_2 molecule is comparatively simple. Experimental difficulties arising from the low vapor pressure of H_2O_2 at room temperature, thermal decomposition at moderate temperatures and reactivity with mercury have been deterrents to extensive studies.

The spectrum of H_2O_2 vapor has recently been studied by Holt, McLane, and Oldenberg.[1] This work summarizes and explains discrepancies in earlier investigations. It is clear that the absorption is continuous and without a maximum in the region studied (3100–1850A).

Urey, Dawsey, and Rice[2] consider three primary processes.

$$H_2O_2+h\nu\rightarrow H_2O+O, \quad (1)$$

$$H_2O_2+h\nu\rightarrow 2\,OH, \quad (2)$$

$$H_2O_2+h\nu\rightarrow HO_2+H. \quad (3)$$

Of these equations, (1) appears to have a low probability and need not be further considered. The energy change for dissociation into two OH radicals, Eq. (2), has been approximated at 50.9 kcal. by thermochemical equations.[1] A simultaneous publication by Walsh[3] gives the dissociation energy of the OO bond in H_2O_2 as approximately 56 kcal. The recent data of Walsh also gives the dissociation energy of reaction (3) as 78 kcal. These values are somewhat higher than those calculated by Urey, Dawsey, and Rice.[2] However, the wave-length corresponding to an energy of 78 kcal. is 3670A which is well beyond the limit of absorption observed in the gas phase and near the limit of absorption by high concentrations in aqueous solution. Hence, sufficient energy is available in absorbed light to effect either primary process (2) or (3) over most, if not all, of the absorption range.

Urey, Dawsey, and Rice[2] have demonstrated that H atoms are absent in the products of an electric discharge operating in H_2O_2 vapor. In these experiments the emission spectra of excited OH was observed. These authors reason that the inelastic collisional process is more probable if the optical transition is permitted by the selection rules, and, hence, the favored optical process should be a dissociation into OH radicals. Fluorescence studies by the same authors with absorbed light of 2000–2100A show that OH radicals are formed in the irradiated system. Work of von Elbe[4] on the reaction of radicals from H_2O_2 with H_2 and CO also indicates the formation of OH radicals. Although the evidence for the formation of OH is undisputable, evidence that process (3) does not occur is lacking. Sharma,[5] indeed, concludes that H atoms are produced since he has observed that cupric oxide is reduced in an absorption tube containing H_2O_2 under irradiation.

The work of Bates[6] and Volman[7] on the Hg sensitized reaction between H_2 and O_2 has shown that an important reaction is

$$H+O_2\rightarrow HO_2, \quad (4)$$

and that subsequently HO_2 radicals react to give H_2O_2,

$$HO_2+HO_2\rightarrow H_2O_2+O_2. \quad (5)$$

This sequence of reactions suggests that addition of O_2 to H_2O_2 should decrease the rate of over-all H_2O_2 decomposition if H atoms are produced by primary process (3), because the net result is no reaction. Experiments with added gases including oxygen are described below.

The products of the photo-decomposition of H_2O_2 in aqueous solution are only O_2 and H_2O.[8] It has been tacitly assumed that these are also the products in the

[1] Holt, McLane, and Oldenberg, J. Chem. Phys. **16**, 225 (1948).
[2] Urey, Dawsey, and Rice, J. Am. Chem. Soc. **51**, 1371 (1929).
[3] A. D. Walsh, J. Chem. Soc. 331 (1948).
[4] G. von Elbe, J. Am. Chem. Soc. **54**, 821 (1932).
[5] R. S. Sharma, Proc. Acad. Sci. (India) **4**, 51 (1934).
[6] J. R. Bates, J. Chem. Phys. **1**, 457 (1933).
[7] D. H. Volman, J. Chem. Phys. **14**, 707 (1946).
[8] G. Kornfeld, Zeits. f. wiss. Phot. **21**, 66 (1921).

gas phase.[9] However, no experiments directed at detecting H_2 in the products have been reported. It is evident that such information is of importance in establishing the decomposition mechanism. Thus H_2 could conceivably be formed not only from H atoms but also by the postulated mechanism[10,11]

$$OH+OH \rightarrow H_2+O_2. \quad (6)$$

The author's experiments on the vapor phase reaction between ozone and hydrogen peroxide[7] also indicate the possibility of H_2 formation by this mechanism. Evidence for the non-formation of H_2 is presented here.

EXPERIMENTAL

Apparatus

The apparatus used to study the photochemical reaction is shown diagrammatically in Fig. 1. An aqueous solution approximately 90 percent by weight H_2O_2[12] was kept in storage vessel, *A*. This was stored usually at dry ice temperature to minimize decomposition and reaction with stopcock lubricant. The reaction was followed by measuring pressure changes with a manometer filled with dibutyl phthalate, *M*. In early experiments a glass "click" gauge was used to measure pressures, but comparative experiments established the fact that no complexities were introduced by use of the phthalate. The reaction tube, *R*, was a quartz jacketed vessel with quartz to Pyrex seals. Constant temperature water circulated in the outer jacket. The entire chamber was contained within a helical mercury resonance arc of the rare gas-mercury discharge type.

The effective absorbed light may be taken as 2537A since the resonance light source emits almost entirely 1849 and 2537A mercury emission lines. The quartz layers and liquid water barrier in the light path would eliminate 1849A radiation.

The H_2O_2 was outgassed by repeated warming, freezing and pumping out and introduced into the reaction tube while maintaining the storage vessel at about 19°C. The combined pressures of H_2O_2 and H_2O were adjusted to 1.62 mm Hg. As will be shown below, the H_2O_2 pressure was 1.23 mm.

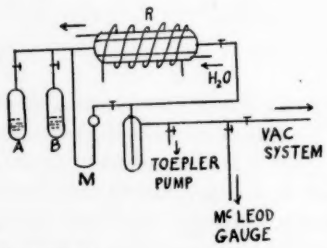

FIG. 1. Reaction system.

Products of the Reaction

Analysis of the non-condensable decomposition products using a Blacet-Leighton gas microanalysis apparatus indicated that hydrogen was absent in the products. This point was checked by use of three experimental methods: the reaction of the gas with heated copper oxide; the combustion with oxygen over glowing platinum; and a determination that all of the non-condensable gas was O_2 by reaction with phosphorus. Although very small amounts of hydrogen would escape detection by these techniques, it seems safe to say that the upper limit of hydrogen gas cannot exceed about 0.2 percent and that it is probably completely absent.

Variation of Temperature

The temperature was varied by controlling the temperature of water in the jacket around the reaction tube. Figure 2 shows the course of the reaction over the temperature range covered. The curve in each case is the experimental curve derived from the 30° experiment, while the experimental points are for the indicated temperature. An attempt to follow the photo-chemical reaction at 75° was unsuccessful due to appreciable thermal decomposition.

It may be observed that in each case the pressure approaches a maximum. From the fact that no hydrogen is formed and the over-all decomposition equation

$$2\,H_2O_2 \rightarrow 2\,H_2O+O_2, \quad (7)$$

the initial H_2O_2 pressure may be calculated from the value of the maximum. This is the value referred to above.

Added Gases

The effect of adding O_2, N_2, and H_2O to the H_2O_2, H_2O gas mixture was studied at a single temperature, 30°. In Fig. 3 the results are represented graphically by comparison of each experiment with the experiment at 30° without added gas, represented by the curve. The experimental points are the ones obtained for the experiments with added gas.

The Quantum Yield

The quantum yield of the reaction was determined by using acetone as an actinometer. Acetone vapor was introduced into the reaction vessel at 70°C and the initial photo-chemical rate was determined on the basis of pressure increase in the system. At 70°C the decomposition of acetone[13] may be expressed by the over-all equation

$$(CH_3)_2CO+h\nu \rightarrow C_2H_6+CO. \quad (8)$$

[9] G. K. Rollefson and M. Burton, *Photochemistry and the Mechanism of Chemical Reactions* (Prentice-Hall, Inc., New York, 1939), p. 178.

[10] Rodebush, Wende, and Campbell, J. Am. Chem. Soc. **59**, 1924 (1937).

[11] Rodebush, Keizer, McKee, and Quagliano, J. Am. Chem. Soc. **69**, 538 (1947).

[12] The hydrogen peroxide sample was kindly supplied by the Buffalo Electrochemical Company, Buffalo, New York.

[13] D. S. Herr and W. A. Noyes, Jr., J. Am. Chem. Soc. **62**, 2052 (1940).

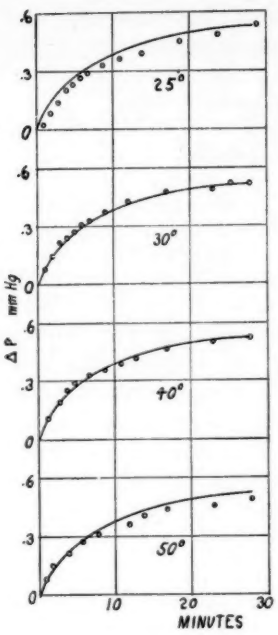

FIG. 2. Course of the reaction at various temperatures. The curve is in each case the 30° experimental curve. The experimental points are for the indicated temperature.

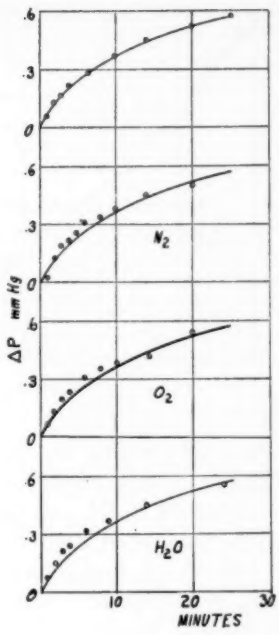

FIG. 3. Course of the reaction with added gases at 30°. The curve is in each case the 30° experimental curve without added gas, top curve. The experimental points are for the indicated added gas.

Herr and Noyes[13] have shown that above 60° the ratio of C_2H_6/CO is unity.

The acetone pressure was 2.16 mm Hg. At this low pressure, the absorption may be expressed by the first term of the logarithmic expansion

$$I_0-I/I_0=\epsilon cl. \tag{9}$$

Using this expression also for H_2O_2, the geometry of the system need not be considered and the quantum yield of H_2O_2 decomposition may be calculated from the quantum yield of acetone photolysis, Φ_a, the absorption coefficients of acetone and H_2O_2, ϵ_a and ϵ_p, the initial concentrations of acetone and H_2O_2, c_a and c_p, and the rates of decomposition of acetone and H_2O_2, n_a and n_p.

$$\Phi_p=n_p/I_p, \tag{10}$$

$$\Phi_a=n_a/I_a, \tag{11}$$

$$\Phi_p=(n_pI_a/n_aI_p)\Phi_a, \tag{12}$$

$$\Phi_p=(n_{pa}c_a/n_{ap}c_p)\Phi_a. \tag{13}$$

The absorption coefficient for H_2O_2 is calculated as 19.6 at 2537A from the Eq. (14) for c in moles per liter,

$$\log_{10}(I_0/I)=\epsilon cl, \tag{14}$$

using the absorption data of Holt, McLane, and Oldenberg.[1] The absorption coefficient of acetone for the same wave-length is 7.0.[14] Φ_a is dependent on concentration and intensity of absorbed light but at 70°C is rapidly approaching unity for all conditions and is certainly between 0.6 and 1.0.[13] Taking Φ_a, therefore, as 0.8 ± 0.2, the value of Φ_p is calculated as 1.7 ± 0.4.

[14] C. W. Porter and C. Iddings, J. Am. Chem. Soc. **48**, 40 (1926).

DISCUSSION

In Fig. 4, the curves of Figs. 2 and 3 are represented on a $\log p$ *vs.* t plot. Deviation from linearity is not very serious until almost three-fourths of the peroxide has been decomposed. Since the quantity of light absorbed varies continuously with the pressure of H_2O_2, the incident light being constant, this does not imply that the reaction is unimolecular. Rather, it may be explained on the linear relationship between the quantity of light absorbed and concentration of absorbing species at the low pressures used. Mathematically then the decomposition rate may be expressed by the equation,

$$-\{d[H_2O_2]/dt\}=kI_{\text{abs.}}, \tag{15}$$

and, since $I_{\text{abs.}}$ is directly proportional to the pressure,

$$-\{d[H_2O_2]/dt\}=k'[H_2O_2], \tag{16}$$

for a constant I_0. Since this equation is moderately well followed, it may be concluded that the quantum yield of the reaction is, in fact, independent of both the pressure of H_2O_2 and $I_{\text{abs.}}$.

Since the experiments with added O_2 indicate that H atoms are absent, the primary process is as represented by Eq. (2), and the entire mechanism is adequately explained by the set of reactions.

$$H_2O_2+h\nu\rightarrow 2\,OH,\ k_1I_a \tag{2}$$

$$OH+H_2O_2\rightarrow H_2O+HO_2,\ k_2 \tag{15}$$

$$HO_2+HO_2\rightarrow H_2O_2+O_2,\ k_3 \tag{5}$$

$$OH+OH\rightarrow H_2O_2,\ k_4. \tag{16}$$

Reaction (15) has been used by Taube and Bray[15] to maintain the chain in the reaction between H_2O_2 and

[15] H. Taube and W. C. Bray, J. Am. Chem. Soc. **62**, 3357 (1940).

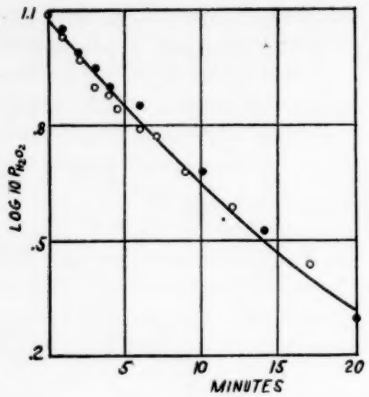

FIG. 4. Log of H_2O_2 pressure *versus* time for duplicate experiments at 30°.

ozone. ΔF for this reaction is given as -25.3 kcal. Reaction (5) has proven useful in discussions involving systems of H atoms and oxygen.[6,7] ΔF for this reaction may be calculated from the data of Yost and Russell[16] as -30.0 kcal. Recombination of OH radicals to form H_2O_2, reaction (16), may be involved at the lowest pressures as shown in the following argument.

Using the steady state treatment for the concentration of free radicals, the sequence (2), (15), (5) leads to the kinetic equation

$$-\frac{d[H_2O_2]}{dt}=2k_1I_{abs.}. \qquad (17)$$

This sequence would lead to a maximum quantum yield of 2.0 which is consistent with the experimental determination. A quantum yield of less than 2.0 and deviation from linearity in Fig. 4 may be accounted for by Eq. (16). If this reaction is used, the kinetic equation becomes

$$-\frac{d[H_2O_2]}{dt}=k_2[H_2O_2]\frac{-k_2[H_2O_2]+(k_2^2[H_2O_2]^2+16k_1k_4I_{abs.})^{\frac{1}{2}}}{4k_4}.$$

A reaction such as (16) might be expected to be a 3 body or wall reaction. The observation that adding gases to the reaction mixture does not appreciably affect the reaction indicates that (16) is not important.

The gases O_2 and H_2O added are also reaction products. Since they have no appreciable effect it may be concluded that equilibria involving the products are not involved.

The quantum yield of H_2O_2 decomposition in liquid water solution has been reported as varying between 1 and 500 depending upon experimental conditions.[17] The careful work of Heidt[18] has shown that at low concentrations the quantum yield is in the region 1–2 in agreement with the vapor phase value reported here.

The observation that the rate of the reaction is temperature independent over the range studied is additional evidence that the rate depends only upon the rate of radiation absorption. If the recombination reaction is eliminated, then the secondary reactions postulated effect a sequence independent of temperature.

[16] D. M. Yost and H. Russell, Jr., *Systematic Inorganic Chemistry* (Prentice-Hall, Inc., New York, 1944), p. 268.

[17] See reference 9, p. 379.

[18] L. J. Heidt, J. Am. Chem. Soc. **54**, 2840 (1932).

The Exchange Reaction between the Hydrogen Halides and the Halogens in the Gaseous State

HAROLD W. DODGEN AND W. F. LIBBY
*Institute for Nuclear Studies and Department of Chemistry, University of Chicago**

(Received February 22, 1949)

It has been shown that hydrogen fluoride and fluorine gases do not undergo an exchange reaction at room temperature and that heating to 200°C for a matter of an hour or so in a brass vessel is necessary to accomplish exchange. Evidence is obtained that even in this case the observed exchange is heterogeneous and catalyzed by the metal fluorides on the wall of the vessel. Illumination by the light of a mercury arc did not accomplish the exchange under conditions such that an activation free energy of some 9 Kcal/mole for the reaction between a fluorine atom and the fluorine molecule or fluorine atom and HF molecule would have been necessary to prevent exchange.

A rapid exchange reaction in the dark at room temperature has been observed to occur between chlorine and HCl in the gaseous state. This is taken as evidence that the hydrogen halides exchange with the halogens through the formation of an intermediate complex of the general formula HX_3, and some discussion of the improbability of the alternative atomic mechanism is given. The non-existence of the HX_3 mechanism in the case of the fluorine system is explained by the absence of electrons in the higher shells which are thought to be the main bonding forces involved in the stabilization of the HX_3 complex in the case of chlorine, bromine, and iodine, and also by the polar character of the hydrogen-fluorine bond in HF, increasing the probability of an alternative HX_3 complex formation in which the hydrogen rests between the fluorine on the HF molecule and the fluorine molecule itself, thus keeping it clearly labeled and rendering interchange on dissociation of the complex unlikely.

I. INTRODUCTION

THE occurrence of a very rapid exchange reaction between HBr and Br_2 in the gaseous state at room temperature was noted by Brezhneva, Roginskii and Shilinskii in 1936,[1] and thoroughly confirmed by the later work of Liberatore and Wiig.[2a, b] A similar reaction was observed to occur in the case of iodine both in the gaseous state and when dissolved in dry pentane.[3] The present paper describes in some detail tests made on the fluorine-HF system[4] and reports briefly on the discovery of a fast reaction in the HCl-chlorine system.

The analogous exchange reaction for the aqueous solution has been very carefully studied for the three heavier halogens, and found to be immeasurably rapid in all three cases.[5–8] Halford has made a strong argument that extremely rapid reaction in the $Cl^- - Cl_2$ case probably proceeds through a Cl_3^- intermediate[5] with a specific rate constant greater than 10^5 liters per mole per minute at room temperature.

Two mechanisms have been proposed for this exchange reaction when occurring in the gaseous state: (1) An atomic mechanism, in which it is supposed that the halogen atoms exchange with ease with both the hydrogen halides and halogen molecules, has been particularly espoused by Liberatore and Wiig[2a, b] in the case of the $HBr - Br_2$ exchange. In this mechanism it is necessary to assume that the halogen atoms are produced thermally since the rate is not perceptibly diminished by shielding from light, and the use of particularly weak radiobromine sources has shown no perceptible effect on the rate in the case of the $HBr - Br_2$ exchange.[3] (2) The molecular mechanism in which an intermediate of the general formula HX_3 is postulated to exist at very low concentrations, this HX_3 molecule having at least two halogen atoms in equivalent positions insofar as their location with respect to hydrogen is concerned, so that the dissociation of the complex will accomplish exchange. The fact that all three halogens, chlorine, bromine and iodine, appear to possess extremely rapid rates at room temperature requires in all three cases that the activation free energy for the formation of such complex must be less than about 11 Kcal. One envisages two possible models for the HX_3 intermediate, one in which the three halogen atoms are at the corners of an equilateral triangle with the hydrogen symmetrically placed above or below the plane of the halogens, and the other having all four atoms in one plane with the hydrogen symmetrically placed with respect to two of the halogen atoms. Some argument has been presented for this mechanism in the case of the hydrogen-bromine exchange *versus* the atomic mechanism.[3] This point will be discussed further in later sections.

II. EXPERIMENTAL

A. Description of Apparatus

The apparatus used in the study of the fluorine-HF exchange consisted of brass and copper tubing silver-

* This work was assisted by the ONR under Task Order III of Contract N6ori20 with the University of Chicago.

[1] Brezhneva, Roginskii, and Shilinskii, Acta Physicochimica URSS **5**, 549 (1936).

[2a] L. C. Liberatore and E. O. Wiig, J. Chem. Phys. **8**, 165 (1940).

[2b] L. C. Liberatore and E. O. Wiig, J. Chem. Phys. **8**, 349 (1940).

[3] W. F. Libby, J. Chem. Phys. **8**, 348 (1940).

[4] The initial tests on this reaction were conducted at the SAM Laboratories in New York City during the war by Dr. Walter Moore and Drs. Francis Bonner and Jacob Bigeleison, all of whom reported no detectible exchange at room temperatures in periods of the order of an hour. The present work was undertaken to confirm these early findings, and to obtain an estimate of the temperature at which the reaction does start.

[5] F. A. Long and A. R. Olson, J. Am. Chem. Soc. **58**, 2214 (1936).

[6] Olson, Porter, Long, and Halford, J. Am. Chem. Soc. **58**, 2467 (1936).

[7] R. W. Dodson and R. D. Fowler, J. Am. Chem. Soc. **61**, 1215 (1939).

[8] R. S. Halford, J. Am. Chem. Soc. **62**, 3233 (1940).

soldered at the joints and with the DuPont polytetrafluoroethylene ("Teflon") plastic as valve seat and packing material. The valves were Kerotest diaphragm packless or repacked Hoke needle valves. The pressure gauges were bronze tube Dura gauges. The fluorine was purchased from the Penn Salt Company and appeared to be of around 99 percent quality. The HF was the standard Harshaw product. A considerable quantity of the HF was allowed to escape from the cylinder as a purification measure, but no purification was attempted on the fluorine gas itself. A sketch of the equipment is shown in Fig. 1.

The radiofluorine F^{18} (half-life 112 minutes) was made by condensing liquid HF into a 4-in. length of $\frac{1}{2}$-in. copper tubing silver-soldered at one end with a Teflon packed Hoke needle valve at the other. The sample was placed within a few inches of the lithium target on the University of Chicago cyclotron and the fast neutrons from the deuteron bombarded target used to accomplish the $(n, 2n)$ reaction of F^{19}. After the irradiation and thorough shaking to insure uniform distribution of the F^{18} in the liquid HF, the apparatus constituted a source of radioactive HF some of which was mixed with fluorine gas in the 1.5-liter reaction vessel and the rest of which was saved for determination of the radioactivity present in the original sample. A decay curve taken over a period of two half-lives showed that no contaminating activities were present. The counter used had a 10-mil aluminum wall to which was attached with Teflon gaskets a brass enclosing jacket in which the gaseous HF or fluorine samples could be admitted for counting. The volume of this gas space around the counter was 67 cc. An initial count of some 5000 counts per minute for 50 cm of HF was the standard activity produced by a bombardment of about three hours with an 8-mev deuteron beam current of about 30 micro-amperes. A special arrangement was used for measuring the pressure more accurately than the Dura gauges could be read, consisting of 1-mil brass diaphragm separating an air space connected to a mercury manometer from the fluorine-HF system, and the "click gauge" principle was used to read the pressure within about 0.5 mm. The reaction chamber was wound with heater coils and packed with insulation so that elevated temperatures could be obtained. The volume of the leads to the chambers was small as compared to its 1.5-liter volume. The temperatures were recorded by means of a copper-constantan thermocouple fastened directly to the brass reaction chamber.

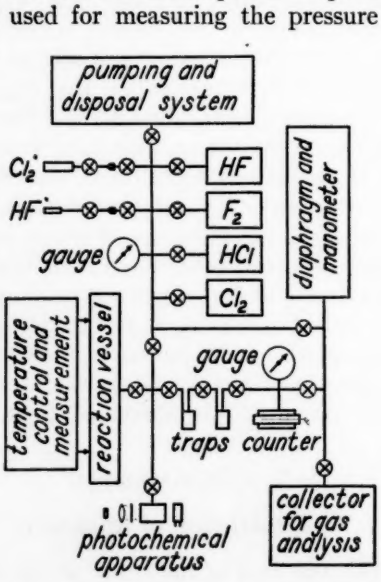

FIG. 1. A schematic diagram of the apparatus.

In the photochemical test a special chamber was substituted which had a length of 5 cm, a diameter of 3.5 cm, a volume of 48 cc, and two clear fluorocarbon plastic windows consisting of poly-monochlorotrifluoroethylene (now sold by the M. W. Kellogg Company) were used. The windows were sealed to the brass chamber simply by pressure set, the plastic possessing enough pliability to make the seal, and it being completely inert to both fluorine and HF even in the presence of radiation from a mercury arc. Our measured absorption coefficients of fluorine of 0.0496 per cm per atm (0°C) (base 10 logs) and 0.172 at 3650 A° and 3130 A° agree well with the values 0.04 (extrapolated) and 0.18 of Von Wartenberg *et al.*[9] and show that no absorbing impurities were present in the fluorine.

The separation of the HF and fluorine gases was accomplished by condensation of the HF out of the fluorine gas in a liquid nitrogen bath followed by immersion of the trap in CO_2 acetone. Two traps were used between the reaction chamber and the counter so a thorough separation was assured. The pressure of the gas in the counting chamber was measured carefully with the click gauge arrangement. The total quantity of gas drawn off for analysis was estimated to be less than 5 percent of that in the reaction chamber, hence the effect on the rate due to the small pressure change was ignored. After measurement the fluorine was pumped through a disposal system consisting of about 5 pounds of finely divided sodium bromide in a brass chamber connected between the apparatus and the pump. A cold trap between the disposal chamber and the pump was used to condense the bromine generated by the reaction. The HF was measured by allowing it to vaporize from the trap into the counting volume, and after measurement was taken through the same disposal system, being condensed in the bromine cold trap. Eventually the contents of this cold trap were removed with an aspirator pump and so passed into the sewage.

The few tests done on the HCl—Cl exchange were conducted in the same equipment, it being necessary in this case, however, to analyze the two gas fractions for HCl and Cl_2 because the separation obtained by distillation was not complete. The chemical analysis

[9] Von Wartenberg, Sprenger, and Taylor, Zeits. f. physik Chemie 61–8 (1931).

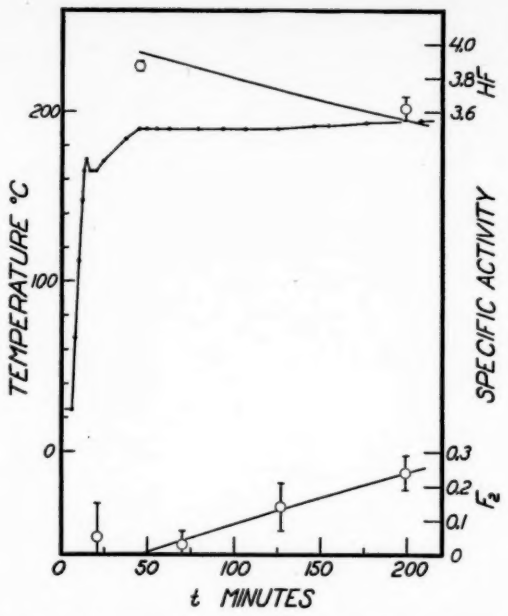

FIG. 2. The observed specific activities and temperatures as a function of time during Run No. 4. The specific activity curves were drawn with $t_{\frac{1}{2}}=610$ minutes, $Y_\infty=1.49$, and Yo (HF) $=3.95$. The discrepancies for HF are probably due to uncertainty in the degree of polymerization of HF.

was carried out by allowing the chlorine to oxidize iodide which was then titrated with thiosulfate. The reaction between iodate and iodide, which consumes acid quantitatively, was then used to determine the HCl. Further work is projected on this problem when a more appropriate cold bath will be used, and it is hoped that better separation will be obtained.

B. Data on the F_2-HF Exchange

Most of the experimental data obtained on this reaction are contained in Tables I and II and Figs. 2 and 3.

In addition, an attempt was made to induce the exchange photo-chemically, with the kind assistance of Mr. George Zimmerman. The conditions were as follows: The smaller cell described above in section II A with fluorocarbon windows was used. The cell was filled with 36.0 cm HF and 29.7 cm of fluorine and illuminated for 30 minutes with the full radiation (3650A) of a H-4 mercury arc. The specific activity of the HF initially was 0.92 ± 0.02, and the specific activity of the fluorine finally was 0.04 ± 0.04. Complete exchange would have resulted in a specific activity for the fluorine of 0.40, so we conclude that within the error of the experiment which was some 10 percent there was no exchange. It is estimated that somewhat more than 4×10^{12} fluorine atoms were generated per cc per second. The cell contained 10^{19} molecules of F_2 per cc.

It was suspected that even the exchange observed at high temperatures in the F_2-HF system was not homogeneous. An experiment was performed to test the heterogeneity of this reaction. The treatment of the vessels with F_2 and HF had of course formed a layer of copper and zinc fluorides on the surface of the brass which might conceivably exchange with the HF and then with the F_2 to accomplish a heterogeneous catalysis of the reaction. The following experiment therefore was performed:

Step 1: The tank was filled with 68 cm of radioactive HF at 23°C.

Step 2: The tank was heated to a temperature of 270°C for 80 minutes.

Step 3: The radioactive HF was pumped out of the tank and inert fluorine admitted at a pressure of 68.5 cm at 270°C.

Step 4: After heating for 80 minutes the specific activity of the fluorine was measured to be 0.10 ± 0.01. The specific activities of the HF when added was 2.51 ± 0.02 and 2.48 ± 0.02 when removed.

The specific activity of 0.10 in the fluorine cannot be explained by HF which had not been pumped out of the tank because it would require a residual HF pressure of some 6 cm. We conclude therefore that there was indeed some heterogeneous catalysis and that most likely a considerable part of the observed exchange in runs 4 and 5 was heterogeneous in character.

All of the data given above for the radioactivity of the various samples have been corrected for decay of the radiofluorine using the time of mixing of the gases as reference points.

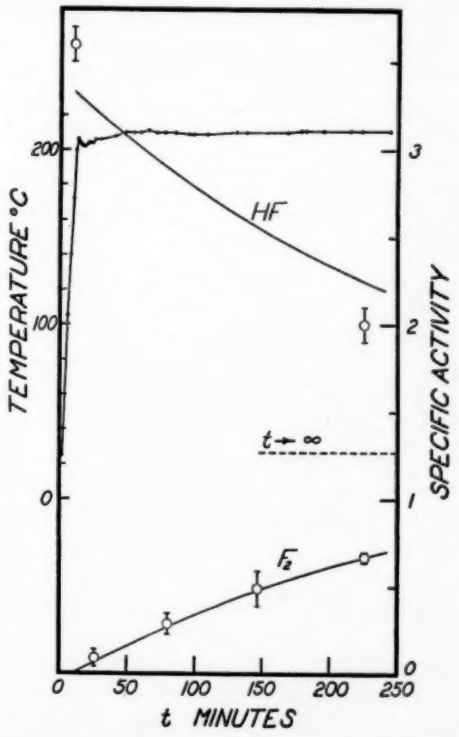

FIG. 3. The observed specific activities and temperatures as a function of time during Run No. 5. The specific activity curves were drawn with $t_{\frac{1}{2}}=200$ minutes $Y_\infty=1.27$, and Yo (HF) $=3.34$. The discrepancies for HF are probably due to uncertainty in the degree of polymerization of HF.

TABLE I. Experiments showing no exchange.

Run no.	Temp. (°C)	Time (min.)	Pressure of HF (cm Hg at 24°C)	Pressure of F_2 (cm Hg at 24°C)	Exchange observed (percent of equilibrium)
1	24	92	31	46	0±3
2	100–140*	20*	36	38	0±4

* HF and F_2 were in contact for 150 minutes total time, 20 minutes of which were at temperatures of 100–140°C.

C. The Experimental Data on the Thermal Non-Photo-chemical Exchange Reaction between HCl and Cl_2**

The equipment described above for the HF+F_2 exchange was used in this case. The inertness of the fluoride-covered metal surfaces to F_2+HF chemical attack of the underlying metal was thought to be a fair guarantee of the inertness of these surfaces to Cl_2+HCl, thus greatly decreasing the chance for heterogeneous catalysis of the reaction. In addition, since the apparatus was constructed entirely of metal we could be very certain of the absence of light. The tank was filled with 27.5 cm of radioactive Cl_2 (37.0 min. Cl^{38}) and 47.9 cm of ordinary HCl at 25°. About 3 minutes were required to introduce the HCl and the mixture stood for about 9 minutes longer. At the end of this time liquid nitrogen was placed on a trap connected with the tank and a valve opened. Condensation occurred rapidly at first, but about 12 minutes were required to completely freeze down the mixture. The estimated contact time at room temperature is 20 minutes with a possible error of 5 minutes. The material in the trap was then allowed to warm and after certain practice the fraction of the gas evolved immediately was taken as HCl and the residual taken as Cl_2. These fractions were analyzed and counted. The HCl fraction analyzed 96.8-mole percent HCl, and 3.2-mole percent Cl_2. The Cl_2 fraction analyzed 53.5 percent HCl and 46.5 percent Cl_2. The initial count rate for the radiochlorine introduced in the mixture was 11,230 per minute for 27.5 cm of chlorine, or a specific activity of 20.4±0.1. From this one calculates that the specific activity at complete exchange should be 11.0±0.1, correcting the counts for decay, of course, back to the time of introduction of gas.

The observed counts for the HCl fraction were 2,640±50 at a pressure of 23.8 cm; and 2,590±80 at 16.7-cm pressure for the chlorine-rich fraction. Calculating the specific activities of the HCl and Cl_2 from these data, one finds them to be 10.8±0.2 for the HCl and 10.5±0.5 for the Cl_2—complete exchange within the experimental error.

It appears, therefore, that the Cl_2+HCl case probably is rapid, with a reaction which probably is homogeneous and certainly non-photo-chemical at room temperature.

** This work was performed in collaboration with Mr. W. H. Johnston, who intends to investigate the reaction further.

III. DISCUSSION

A. The Improbability of the Atomic Mechanism

It appears that chlorine, bromine, and iodine all partake in a reaction so rapid at room temperature as to be very difficult of measurement, and that in the case of bromine at least this reaction is most likely homogeneous and certainly non-photo-chemical. It is tempting to suppose that this exchange reaction proceeds through the mechanism

$$HX^*+X \underset{k_1}{\overset{k_1}{\rightleftarrows}} HX+X^* \qquad (1)$$

to

$$X^*+X_2 \underset{\frac{1}{2}k_2}{\overset{k_2}{\rightleftarrows}} X+X^*X \qquad (2)$$

the source of the halogen atoms being the thermal equilibrium. It does seem, however, that this is unlikely when one calculates the maximum rates of exchange at all times by means of collision theory.

The differential equation governing the rate of change of the specific activity of the halogen is:

$$\frac{d\ln(Y_\infty - Y)}{dt} = -\frac{k_1 k_2 No[X]}{2RT}\left(\frac{(HX)+2(X_2)}{k_1(HX)+k_2(X_2)}\right) \qquad (3)$$

where No is Avogadro's constant, $[X]$ is the pressure in atmospheres of the atomic species, and k_1 and k_2 are the specific rate constants of reactions (1) and (2) in cc per molecule per sec. The derivation of this equation involves the obviously justifiable assumptions that the fraction of the halogen atoms which are radioactive is small and that the fraction of radioactive atoms present as atoms is small.

In order to calculate a maximum interchange rate for this mechanism we shall make the following assumptions: (1) $k_1 \gg k_2$. This means the halogen atom population will be in equilibrium at all times with the initially radioactive species, assuming it to be the HX molecule. However, by inspection of Eq. (3) it is clear that the calculated maximum rate will be essentially the same regardless of which reaction we assume to be faster and which species is initially radioactive. (2) The population of halogen atoms will be that given by thermal equilibrium, in other words the radioactivity itself will be sufficiently low as to leave this population unaffected. (3) Zero activation energy for reaction 2 will be assumed, which of course means essentially zero activation energy for reaction 1, also. (4) The collision cross sections for reaction 2 will be taken essentially as the viscosity radii. Actually for the purpose of generalizing the result we shall assume that the collision diameter, σ, be related to the atomic weight, M, of the halogen involved.

$$\sigma^2(A^\circ) = (M)^{\frac{1}{3}}. \qquad (4)$$

(5) The heats of dissociation of the halogen molecules,

TABLE II. Higher temperature experiments showing some exchange.

Run no.	Temp. (°C)	Time (min.)	Pressure of HF (cm Hg at 24°C)	Pressure of F_2 (cm Hg at 24°C)	Specific activity of HF*	Specific activity of F_2*	Exchange observed (percent of equilibrium)
3	200–270†	40†	28	26	—	—	60
4	190	0	35.3	37.8	3.87±0.03	—	0
(cf. Fig. 2)							
	190	25	35.3	37.8	—	0.03±0.04	2±7
	190	82	35.3	37.8	—	0.14±0.07	9.6±5
	190	154	35.3	37.8	3.62±0.07	0.24±0.05	16±3
5	210	0	35.6	36.6	3.6 ±0.1	—	0
(cf. Fig. 3)							
	210	17	35.6	36.6	—	0.09±0.05	8±4
	210	70	35.6	36.6	—	0.29±0.06	23±5
	210	138	35.6	36.6	—	0.49±0.10	40±8
	210	217	35.6	36.6	2.0±0.1	0.67±0.03	54±3

* The specific activities are calculated by dividing the observed counts by the product of the pressure and the average number of fluorine atoms per gas molecule, i.e., 2 in the case of F_2 and a number between 1 and 2.5 in the case of HF, as determined by the data of K. Fredenhagen, Zeits. p. anorg. allgem. Chemie **218**, 161 (1934).

† The HF-F_2 mixture was heated from 24 to 270°C in 90 minutes. During 40 minutes the mixture was at temperatures between 200 and 270°C.

$\Delta H°$, are independent of temperature and the entropy of dissociation is approximated as 25 entropy units.

On these assumptions we first calculate the steady state population of halogen atoms in terms of the pressure of halogen molecules in atmospheres. The result is

$$[X]=[X_2]^{\frac{1}{2}}\exp\{25/2R-\Delta H°/2RT\}. \quad (5)$$

The specific rate constant, k_2, is equal to the collision frequency at unit concentrations and will be given by

$$k_2=\sigma^2\left(\frac{8\pi RT(M_1+M_2)}{M_1M_2}\right)^{\frac{1}{2}}, \quad (6)$$

which becomes

$$k_2=10^{-16}(12\pi RT)^{\frac{1}{2}} \quad (7)$$

upon application of Eq. (4). Solving Eq. (3) for the half-time for exchange one obtains

$$t_{\frac{1}{2}}=\frac{2RT\ln 2}{k_1k_2No[X]}\left(\frac{k_1[\mathrm{HX}]+k_2[X_2]}{[\mathrm{HX}]+2[X_2]}\right), \quad (8)$$

and by applying assumption (1) and Eqs. (4), (5), and (7) the result for the minimum half-time for exchange is

$$t_{\frac{1}{2}}=6.30\times10^{-14}T^{\frac{1}{2}}\exp\left\{\frac{\Delta H°}{2RT}\right\}\frac{[\mathrm{HX}]}{[X_2]^{\frac{1}{2}}([\mathrm{HX}]+2[X_2])}. \quad (9)$$

For 25°C and $[\mathrm{HX}]=[X_2]=$ one atmosphere one finds the expression

$$\log_{10}t_{\frac{1}{2}}(\mathrm{sec.})=-12.4+\frac{\Delta H°(\mathrm{kcal/mole})}{2.7} \quad (10)$$

as a general expression for the expected minimum half-time for exchange by the atomic mechanism for any of the homogeneous systems. Figure 4 presents a general relation in the range of measurable half-times. From this it is clear that the heats of dissociation would have to be less than some 38 Kcal/mole to account for the experimentally observed speed on this mechanism. The result is not entirely unreasonable for iodine, one of the least carefully studied cases, but is quite unreasonable for either bromine or chlorine. Table III summarizes the values for these heats of dissociation of all the halogens as reported in the literature. These data make it seem extremely improbable that the bromine, and certainly very improbable that the chlorine, could proceed by the atomic mechanism.

B. The HX_3 Molecular Complex Mechanism

In view of the conclusion above that the atomic mechanism is unlikely, one is forced to consider the obvious alternative mechanism, which involves the formation of an intermediate molecule of the general formula HX_3. It is of course necessary in this formulation that at least two of the halogens in the HX_3 molecule be equivalent insofar as their location with respect to the hydrogen atom is concerned, so that on dissociation the radioactive atom will be interchanged. Consideration of the rates observed leads one to the additional conclusion that the activation free energy for the formation of the HX_3 complex must not exceed about 11 Kcal/mole. It has been reported[2b] that the

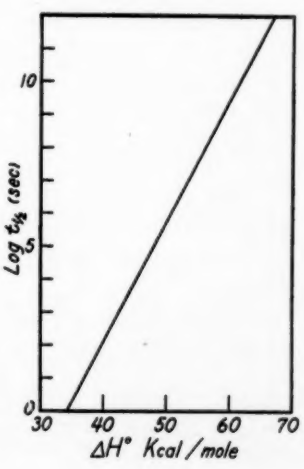

FIG. 4. The minimum half-time for exchange at 25°C *vs.* the heat of dissociation of the halogen as calculated by collision theory according to the atomic mechanism.

TABLE III. Literature values for the heats of dissociation of the halogens (all values in Kcal/mole).

Fluorine		Chlorine		Bromine		Iodine	
69	(10)	58.5	(16)	45.2	(16)	35.2	(16)
63.5±0.7	(11)	57.5	(10)	45.23	(20)	35.4	(22)
76±2	(12)	56.9	(17)	44±10	(21)	36.34±0.1	(23)
63.3	(13)	57.1±2.1	(18)			35.51±0.05	(24)
76±2	(14)	56.9	(19)				
70	(15)						

Eyring-Hirshfelder calculations suggest that this is an unreasonably low figure. On the other hand, it is well known that the ions of X_3^- exist in aqueous solution for all three of the heavier halogens, their stabilities decreasing from iodine to chlorine. But even in the case of chlorine the ion is sufficiently stable to have been detected and its dissociation constant measured.[25] It seems therefore that a rather strong affinity exists of halogen molecules for halogen ions, this affinity decreasing from iodine through chlorine. If one imagines that the polar character of the HX molecule can be carried over to the complex HX_3, it seems not unreasonable to suppose that the affinity demonstrated in aqueous solution may exist in the gaseous state and result in the formation of such a molecule to an extent sufficient to catalyze the exchange reaction. It is not clear whether the intermediate will be a pyramidal type with the three halogens ot the corners of an equilateral triangle with the hydrogen symmetrically placed above or below the plane of the halogens, or if some other model may apply. The pyramidal model seems reasonable and it certainly satisfies the condition of the equivalence of the halogen atoms necessary to exchange. The authors suppose that the lower activation free energy for the formation of this complex is probably due to the inadequacy of the methods of calculation for the types of forces stabilizing the complex. It is of course clear that the HX_3 complex need not be sufficiently stable to be detected by pressure measurements on mixing of HX and X_2 gases. Experiments of this sort with HBr and Br_2 have given negative results. Liberatore and Wiig[2b] have made the argument that this mechanism should also occur for the organic halides such as ethyl bromide exchanging with Br_2. It is our opinion that this is not necessarily so in that the carbon-bromine bond will be more covalent and the ionic type of resonance structure required to stabilize the X_3^- ion will be much more favored in the case of HX_3 than in the case of RX_3. It is also possible that steric factors may prevent an alkyl radical playing the role that the hydrogen atom plays in stabilizing such a complex. We have seen instances recently of extraordinary bonding properties in the hydrogen atoms of such molecules as diborane.[26]

The slowness of the rate with fluorine can be understood either on this mechanism or on the atomic mechanism. In the case of the atomic mechanism the high dissociation heat of course predicts a very slow rate at room temperature and the result of the photo-chemical experiment (see section C) indicates that a homogeneous reaction would not occur rapidly even at 200°C. The molecular complex mechanism is hardly expected to apply for two reasons: (1) the attractive forces between fluorine molecules and fluoride ion are probably much weaker than in the case of the other three halogens in that these attractive forces probably arise from interactions among the electrons in the shells higher than the second. Further, the high bond energy of HF of ~150 Kcal would be against the formation of a complex in which the HF bond is stretched as would probably be the case for any complex which would give exchange. (2) In addition, the strong polar character of the bond between hydrogen and fluorine will have a great tendency to pull the hydrogen down between two of the fluorines to give a HX_3 molecule which may have a certain stability which may indeed exceed that for the other halogens, but not satisfying the requirement that the atom joined to the hydrogen in the HX molecule become equivalent with those constituting the X_2 molecule when the complex is formed. In other words the radioactive HF molecule could conceivably join itself to a non-radioactive fluorine molecule and dissociate off again without ever losing its radioactivity. The result of run number 1, Table I, shows that the activation free energy for the formation of a complex which would give exchange is >20 Kcal per mole at 24°C and the failure of the reaction to occur homogeneously at 200°C indicates an activation free energy of >30 Kcal per mole at 200°C if one use viscosity radii at both temperatures. These values seem not unreasonable in view of the above discussion.

C. The Failure to Observe Exchange in the Photochemical Experiment

By using viscosity radii and assuming about one collision in 500 between fluorine atoms leads to recombination by a termolecular process we calculate a steady

[10] Stackel, Zeits. f. Electrochemie **36**, 375–6 (1930).
[11] Wartenberg and J. Taylor, NGW Gott. Math. P. Clas. No. 1 (1930); Frank, Zeits. f. Physik. Chemie **120**, 144 (1926).
[12] Desai, Nature **128**, 34 (1931).
[13] Wartenberg, Sprenger, and Taylor, Zeits. f. Physik. Chemie. Børd. Fest. 61–8 (1931).
[14] Desai, Proc. Roy. Soc. (I) **A136**, 76–82 (1932).
[15] Dodenstein, Jockusch, and Shing Hou Chong, Zeits. anorg. allgem. Chemie **231**, 24–33 (1937).
[16] Kuhn, Zeits. Physik **39**, 77–91 (1926).
[17] Giauque and Overstreet, J. Am. Chem. Soc. **54**, 1731–44 (1932).
[18] Trautz and Ader, Zeits. f. anorg. allgem. Chemie **218**, 104–10 (1934).
[19] Cherton, Bull. Soc. Roy. Sci. Liege **11**, 54–60 (1942).
[20] Gordon and Barnes, J. Chem. Phys. **1**, 692 (1933).
[21] Blewett, Phys. Rev. **49**, 900–3 (1936).
[22] W. G. Brown, Phys. Rev. **38**, 709–11 (1931).
[23] G. M. Murphy, J. Chem. Phys. **4**, 344–50 (1936).
[24] Perlman and Rollefson, J. Chem. Phys. **9**, 362–9 (1941).
[25] M. S. Sherrill and E. F. Izard, J. Am. Chem. Soc. **53**, 1667 (1931).
[26] K. S. Pitzer, J. Am. Chem. Soc. **67**, 1126 (1945).

state concentration of 4×10^{12} fluorine atoms per cc for our rate of production of some 4×10^{12} atoms per cc per second. The probable mean life of 5 seconds for diffusion to the walls gives a steady state concentration of 2×10^{13} atoms per cc. Since it is likely that a fluorine atom would have to undergo more than one collision with a fluoride coated wall in order to react we conclude that the termolecular processes determine the steady state concentration over most of the volume of the vessel and that in either case the steady state concentration of fluorine atoms was some 10^{12} atoms per cc. One might well worry about the failure to observe exchange under these conditions. However, by application of Eq. (3), with viscosity radii and the above concentration of fluorine atoms we are forced to assume that the exchange of fluorine atoms with either HF or F_2 molecules must have a free energy of activation in the sense of the Eyring rate theory of about 9 Kcal per mole. This seems not an unreasonable value. It seems likely that more intense illumination and/or slightly elevated temperatures will actually accomplish this exchange, and such an investigation would appear to offer real opportunities for studying the reaction of fluorine atoms with HF and F_2 molecules.

THE JOURNAL OF CHEMICAL PHYSICS VOLUME 17, NUMBER 10 OCTOBER, 1949

Thermodynamic Properties of Oxygen Fluoride and Chlorine Fluoride from Spectroscopic Data*

ROBERT L. POTTER
Department of Chemistry, University of Pittsburgh, Pittsburgh, Pennsylvania

(Received February 21, 1949)

Spectroscopic and electron diffraction data have been combined to make calculations of the free energy, entropy, and heat capacity of OF_2 to the rigid rotator-harmonic oscillator approximation between 298.16° and 1500°K. The spectrum of ClF is known well enough to calculate these properties to the next approximation from 298.16° to 2000°K. Thermal data have been combined with these results to give the complete thermodynamic properties of these two fluorine compounds. It is pointed out that the accepted dissociation energy of F_2 is too high, and calculations show that it must be close to 1.5 ev per molecule.

THE thermodynamic properties of fluorine compounds are difficult to measure directly because of experimental difficulties. However, in cases of gaseous compounds where spectroscopic data are adequate, these properties may be calculated by standard methods of statistical mechanics.

Oxygen fluoride was first reported by Lebeau and Damiens.[1] The molecule is similar to the water molecule and belongs to point group C_{2v}. Hence, it has a symmetry number $\sigma=2$. A triatomic asymmetric molecule has three non-degenerate fundamentals. The vibrational infra-red spectrum of OF_2 has been studied by Hettner, Pohlman, and Schumacher[2] and the fundamentals observed by them have been reassigned by Sutherland and Penney.[3] The three fundamentals are $\gamma_1=833$ cm^{-1}, $\gamma_2=492$ cm^{-1}, and $\gamma_3=1110$ cm^{-1}.

Although no rotational spectrum of OF_2 has been observed, electron-diffraction measurements have been made which give sufficient information to allow the rotational constants to be calculated. Sutton and Brockway[4] and Boersch[5] have made these measurements, and Brockway[6] has summarized these electron-diffraction experiments. He gives $\alpha_{FOF}=100\pm5°$ and $r_{OF}=1.41\pm0.05$A for the bond angle and oxygen-fluoride distance, respectively. With these figures one calculates $I_1=88.94_7\times10^{-40}$ g cm^2, $I_2=73.59_2\times10^{-40}$ g cm^2, and $I_3=15.35_3\times10^{-40}$ g cm^2. The atomic weights of oxygen and fluorine were taken as 16.000 and 19.000, respectively.[7] The molecule was considered to be a rigid rotator and the vibrations to be those of harmonic oscillators. The method of calculations was adapted from Mayer and Mayer;[8] the physical constants were those of Dumond and Cohen[9] and Birge.[10] The constant in the free energy equation is 7.2797 ($R=1.98646$ cal.), and the second radiation constant C_2 is 1.4384_8. With these values, the thermodynamic properties of OF_2 may

* Contribution No. 710 from the Department of Chemistry, University of Pittsburgh.

[1] P. Lebeau and A. Damiens, Comptes Rendus **185**, 652 (1927).

[2] Hettner, Pohlman, and Schumacher, Zeits. f. Physik **96**, 203 (1935).

[3] G. B. B. M. Sutherland and W. G. Penney, Proc. Roy. Soc. London **A156**, 678 (1936).

[4] L. E. Sutton and L. O. Brockway, J. Am. Chem. Soc. **57**, 473 (1935).

[5] H. Boersch, Sitz. ber. Akad. Wiss. Wien. **144**, 1 (1935); Monatsch. **65**, 311 (1935).

[6] L. O. Brockway, Rev. Mod. Phys. **8**, 231 (1936).

[7] Thirteenth Report of the Committee on the Atomic Weights of the International Union of Chemistry, J. Am. Chem. Soc. **69**, 731 (1947).

[8] Mayer and Mayer, *Statistical Mechanics* (John Wiley & Sons, Inc., New York, 1940).

[9] J. W. M. Dumond and E. R. Cohen, Rev. Mod. Phys. **20**, 82 (1948).

[10] Raymond T. Birge, Rev. Mod. Phys. **13**, 233 (1941).

TABLE I. Thermodynamic functions of OF_2.

T °K	$-(F^0-H_0^0)/T$	S^0	C_p^0
	cal./deg.mole	cal./deg.mole	cal./deg.mole
298.16	50.31	58.93	10.08
300	50.36	59.00	10.10
350	51.72	60.60	10.63
400	52.91	62.04	11.08
500	55.00	64.60	11.79
600	56.79	66.79	12.29
700	58.36	68.71	12.65
800	59.76	70.42	12.90
900	61.03	71.95	13.09
1000	62.20	73.34	13.23
1100	63.27	74.61	13.34
1200	64.26	75.77	13.42
1300	65.19	76.85	13.49
1400	66.06	77.85	13.54
1500	66.88	78.79	13.58

be calculated. The values of $-(F^0-H_0^0)/T$, S^0, and C_p^0 are listed in Table I. It is to be noted that these values do not include nuclear spin and that they refer to OF_2 in the ideal gas state at one atmosphere pressure.

If a reliable heat of formation of OF_2 were known, the complete thermodynamic properties of OF_2 would be available. Ruff and Menzel[11] give $\Delta H_f = 4.6 \pm 2$ kcal., Von Wartenburg and Klinkott[12] give $\Delta H_f = 11 \pm 2$ kcal., and later Von Wartenburg[13] gives as an average $\Delta H_f = 9.0$ kcal. Bichowsky and Rossini[14] give $\Delta H_f = 5.5$ kcal. from an analysis of these data. Thermodynamic functions of oxygen[15] and of fluorine,[16] when combined with values for OF_2 and the value of ΔH_f selected by Bichowsky and Rossini, lead to $\Delta H_0^0 = 6080$ cal./mole; $\Delta H^0_{298.16} = 5500$ cal./mole; and $\Delta F^0_{298.16} = 9720$ cal./mole. The determinations of ΔH_f were not made at 25°C, but their accuracy is such as to make it senseless to attempt the slight correction to 25°C. These are the best figures available for the thermodynamic properties of OF_2. The entropy at 298.16°K is in agreement with that given by Kelley.[17]

In 1928, Ruff[18] and co-workers reported a new compound of fluorine, ClF. The rotation-vibration spectrum has been investigated by Wahrhaftig[19] and the vibration spectrum by Schmitz and Schumacher.[20] Wahrhaftig observed the electronic transitions $^3\Pi_0^+ \leftarrow {}^1\Sigma^+$ and from these transitions he has obtained values of the ground state constants. He gives $\omega_e'' = 793.2$ cm^{-1}, $\omega_e''x_e'' = 9.9$ cm^{-1}, $B_e'' = 0.518$ cm^{-1}, and $\alpha_e'' = 0.006$ cm^{-1}. The excited state lies 19,826 cm^{-1} above the ground state[20] which is non-degenerate. Schmitz and Schumacher have observed this transition and they give $\omega_e'' = 780.4$ cm^{-1} and $\omega_e''x_e'' = 4$ cm^{-1}. The difference is small and the uncertainty in the thermodynamic properties is negligible at 2000°K and is small at 298.16°K. With an uncertainty of 12.8 cm^{-1} in ω_e'', the probable error in the free energy is about 0.2 percent over the temperature range from 298.16 to 2000°K. The probable error in the entropy increases from 0.027 percent at 298.16°K to 0.12 percent at 2000°K, while the heat capacity may be in error by 0.15 percent at 298.16°, but the error has decreased to 0.007 percent at 2000°K. For consistency, the data of Wahrhaftig was used for both rotation and vibration.

TABLE II. Thermodynamic functions of isotopic ClF.

T °K	$-(F^0-H_0^0)/T$	S^0	C_p^0
	cal./deg.mole	cal./deg.mole	cal./deg.mole
298.16	44.904	52.045	7.672
300	44.948	52.092	7.680
350	46.056	53.292	7.895
400	47.029	54.358	8.072
500	48.684	56.189	8.348
600	50.067	57.731	8.534
700	51.259	59.057	8.666
800	52.308	60.221	8.762
900	53.246	61.257	8.836
1000	54.094	62.191	8.894
1100	54.870	63.041	8.942
1200	55.584	63.821	8.983
1300	56.245	64.542	9.019
1400	56.862	65.212	9.050
1500	57.440	65.837	9.079
1600	57.983	66.424	9.106
1700	58.496	66.977	9.130
1800	58.982	67.500	9.153
1900	59.444	67.995	9.175
2000	59.883	68.466	9.196

The procedure outlined by Mayer and Mayer[8] for diatomic molecules was used to calculate the thermodynamic functions. The expansion of their equation 7.42 is not valid for the constants of ClF below 900°K and hence the equation was used without expansion to evaluate the correction terms for the state sum of the molecule considered as a rigid rotator and harmonic oscillator. It is to be noted that Wahrhaftig's data refer to $Cl^{35}F$. The molecular constants were changed to those of $Cl^{37}F$ by standard methods.[21] The atomic weights were taken from Hahn, Flügge, and Mattauch[22] as were the abundances of the two isotopes of chlorine. The ratio of chemical to physical atomic weights was taken from Birge.[10] The thermodynamic functions were calculated for both isotopic molecules and the results mixed according to the abundance of the two molecules. The entropy of mixing was omitted. The contribution of the excited state to the state sum is negligible at

[11] O. Ruff and W. Menzel, Zeits. f. anorg. u. allgem. Chem. **190**, 257 (1930).
[12] H. Von Wartenburg and G. Klinkott, Zeits. f. anorg. u. allgem. Chem. **193**, 409 (1930).
[13] H. Von Wartenburg, Zeits. f. anorg. u. allgem. Chem. **200**, 235 (1931).
[14] Bichowsky and Rossini, *Thermochemistry of Chemical Substances* (Reinhold Publishing Corporation, New York, 1936).
[15] H. W. Woolley, J. Research Nat. Bur. Standards **40**, 163 (1948).
[16] G. M. Murphy and J. E. Vance, J. Chem. Phys. **7**, 806 (1939).
[17] K. K. Kelley, Bur. Mines Bull. **434** (1941), IX, "Entropies of Inorganic Substances."
[18] O. Ruff, Zeits. f. anorg. u. allgem. Chem. **176**, 258 (1928).
[19] A. Wahrhaftig, J. Chem. Phys. **10**, 248 (1942).
[20] H. Schmitz and H. Schumacher, Zeits. f. Naturforsch. **2a**, 358 (1947).
[21] Herzberg, *Molecular Spectra* (Prentice-Hall, Inc., New York, 1939).
[22] O. Hahn, S. Flügge, and J. Mattauch, Physik. Zeits. **41**, 1 (1940).

TABLE III. Molecular constants.

OF_2	$Cl^{35}F$
$\nu_1 = 833\ cm^{-1}$	$\omega_e = 793.2\ cm^{-1}$
$\nu_2 = 492\ cm^{-1}$	$\omega_e x_e = 9.9\ cm^{-1}$
$\nu_3 = 1100\ cm^{-1}$	$B_e = 0.518\ cm^{-1}$
	$\alpha_e = 0.006\ cm^{-1}$
$I_1 = I_2 + I_3 = 88.94_7 \times 10^{-40}$ g cm²	
$I_2 = 73.59_3 \times 10^{-40}$ g cm²	
$I_3 = 15.35_3 \times 10^{-40}$ g cm²	

2000°K. The free energy, entropy, and heat capacity are shown in Table II. These quantities do not include nuclear spin and they refer to the hypothetical ideal gas at one atmosphere pressure.

If a reliable heat of formation of ClF were known, the complete thermodynamic properties of ClF would be known. Ruff[23] gives values of ΔH_f ranging from −22 kcal. to −27.4 kcal. Bichowsky and Rossini[14] reviewed these data and they give $\Delta H_f = -25.7$ kcal. Schmitz and Schumacher[24] give a more recent value of $\Delta H_f = -15 \pm .5$ kcal./mole. This determination did not involve the formation of HF but that of NaF(*s*), and as the work of Schmitz and Schumacher on the heat of formation of NaF(*s*) is in accord with that of Von Wartenburg and Fitzner,[25] the ΔH_f of ClF was taken as −15.0 kcal. This heat of formation was obtained at 18°C, but was used at 25°C without correction because of the uncertainty of 500 cal. which would make any such correction worthless. The thermodynamic functions of Cl_2 were taken from Giauque and Overstreet[26] and those of F_2 from Murphy and Vance.[16] These lead to the values of $\Delta H_0^0 = -15{,}000$ cal./mole, $\Delta H^0_{298.16} = -15{,}000$ cal./mole, and $\Delta F^0_{298.16} = -15{,}330$ cal./mole.

Both Wahrhaftig[19] and Schmitz and Schumacher[20] report the dissociation energy of ClF. If the products of dissociation are $Cl(^2P_{\frac{3}{2}})$ and $F(^2P_{\frac{3}{2}})$, then ΔH^0_0 for the dissociation of ClF into normal atoms is 60.31 kcal./mole. The dissociation energy of Cl_2 into normal atoms is 2.481 ev according to Herzberg.[21] Hence the dissociation energy for the reaction

$$F_2 = 2F \quad \Delta H_0^0 = 33{,}400 \text{ cal.},$$

or the dissociation energy of F_2 into normal atoms would be 1.45 ev. If the heat of formation given by Bichowsky and Rossini[14] for ClF is used, the dissociation energy of F_2 would be 0.52 ev. If the products of dissociation of ClF are both normal atoms, then the dissociation energy of F_2 would be raised to 1.55 ev. On the other hand, if the products of dissociation of ClF are two excited atoms, or if only the chlorine is excited, the dissociation energy of F_2 would be smaller. Schmitz and Schumacher[20] give 21,257 cm^{-1} for the predissociation limit of ClF, and this gives an upper limiting value of the dissociation energy of ClF. This is still too low to raise the dissociation energy of F_2 to a value such as 2.8 ev given by Herzberg.[21]

If the heat of dissociation of HF into atoms were known, another path would be available from which the dissociation energy of F_2 could be obtained. (This has been considered by Murphy and Vance.[16]) Kirkpatrick and Salant[27] have estimated the dissociation energy of HF to be 140,000 cal./mole from their values of ω_e and $\omega_e x_e$, assuming a Morse function. Usually a Morse function gives an upper limiting value to the true dissociation energy. Combining this value with the heat of dissociation of HF into molecules[16] and with the dissociation energy of H_2,[28] one finds 2.08 ev for the dissociation energy of F_2. If the calculation is reversed assuming the heat of dissociation of F_2 obtained from the ClF data (33,400 cal./mole), one obtains 132,500 cal./mole for the dissociation energy of HF into atoms.

The dissociation energy of F_2 from the two paths is 1.45 ev and 2.08 ev, and both of these are smaller than the corresponding value for chlorine and they bracket the dissociation energy of bromine. It has been assumed in the past that the dissociation energy of F_2 is greater than that of chlorine, but in view of the irregular behavior of the first row elements, it is not inconceivable that these values may be closer to the true value of the heat of dissociation of F_2 than the value 2.75 ev selected by Murphy and Vance.[16]

In order to obtain a heat of dissociation of F_2, of the order of magnitude that Herzberg[21] and Murphy and Vance[16] quote, it would be necessary to have the heat of formation of ClF close to zero. Unless Schmitz and Schumacher[24] made some gross error in their heat of formation of ClF, or unless the spectrum of ClF has been misinterpreted, it is apparent that the heat of dissociation of F_2 is smaller than hitherto thought. Until another path is investigated, it seems that the best value for the heat of dissociation of F_2 is 1.5 ev.

The thermodynamic functions of $OF_2(g)$ and ClF(*g*) in the ideal gas state are presented in Tables I and II, respectively, while the molecular constants used are collected in Table III. The standard entropy of $OF_2(g)$ can be taken as $S^0_{298.16} = 58.9 \pm 0.2$ *E.U.*; and the standard entropy of ClF(*g*) can be taken as $S^0_{298.16} = 52.05 \pm 0.01$ *E.U.*

[23] O. Ruff, Zeits. f. angew. Chem. **42**, 806 (1929); O. Ruff and F. Laass, Zeits. f. anorg. u. allgem. Chem. **183**, 214 (1929); O. Ruff and W. Menzel, *ibid.* **198**, 375 (1931).

[24] H. Schmitz and H. Schumacher, Zeits. f. Naturforsch. **2a**, 362 (1947).

[25] H. Von Wartenburg and O. Fitzner, Zeits. f. anorg. u. allgem. Chem. **151**, 313 (1926).

[26] W. F. Giauque and R. Overstreet, J. Am. Chem. Soc. **54**, 1731 (1932).

[27] D. E. Kirkpatrick and E. O. Salant, Phys. Rev. **48**, 945 (1935).

[28] H. Beutler, Zeits. f. physik. Chemie **B29**, 315 (1935).

Application of a General Theory of the Formation of Liquid Films to Solutions of Lanthanum Chloride

LAWRENCE BAYLOR ROBINSON
Department of Physics, Howard University, Washington, D. C.
(Received March 15, 1949)

A general theory of the formation of liquid films is applied to the case of lanthanum chloride. The hyperelliptic integrals involved are approximated with elliptic integrals. The small values of the zeta-potentials make reliable assignments of the values of the "corrected surface tensions" difficult.

INTRODUCTION

LANGMUIR'S theory for the formation of liquid films of solutions of uni-univalent electrolytes in narrow capillaries was presented in a more general form by this writer.[1] It was shown that the thickness of such films could be represented as a hyperelliptic integral (Eq. (9) of reference 1):

$$\Delta r = K\int_{y_1}^{y_2} \frac{dy}{(a_n y^n + a_{n-1}y^{n-1} + \cdots + a_0)^{\frac{1}{2}}}. \quad (1)$$

The numerical computations necessary to the evaluation of such an integral are in general prohibitive and hence none were attempted in the previous article. When the general theory is applied to the case of lanthanum chloride, a hyperelliptic integral results which can be shown to have values between two elliptic integrals. The maximum and minimum values as represented by the elliptic integrals can be made to approach each other as closely as one likes and, as such, the value of the hyperelliptic integral can be determined quite accurately. Some of the details of the necessary mathematical transformations as well as the numerical computations are given here. Such computations not only give the corrected surface tentions, but also have intrinsic interest in that they represent a method of approximating the value of a *hyperelliptic integral* by means of *elliptic integrals.*

An interpretation of the results is given at the end of this article.

MATHEMATICAL FORMULATION

Negative Zeta-Potentials

When Langmuir's theory is applied to the case of 3-1 electrolytes, hyperelliptic integrals become involved. All of the equations listed in reference 1 from (1) through (6) are valid and are not repeated here. It is known experimentally that some of the zeta-potentials are negative whereas those of the more concentrated solutions are positive.[2] According to the theory, the potential at the solution-air interface must have the same sign as that of the zeta-potential. In order to determine the value of this potential, it is necessary to solve a fourth-degree equation. It is convenient to use different transformations for the positive and negative cases in order that the root of the equation which fixes the solution-air potential will be automatically selected. The method of selecting the proper root has been discussed in previous papers.

The transformation for the case of negative potentials follows immediately below. Take

La^{+++} as ionic species 1; $z_1=+3$,
H^+ as ionic species 2; $z_2=+1$,
OH^- and Cl^- as ionic species 3; $z_3=-1$.

Let:

$$y=\exp(+\eta) \quad \text{and} \quad K=\exp(+m). \quad (2)$$

The equation relating the film thickness to the potentials and concentrations of the ionic species becomes:

$$d\theta=\left[\frac{6c_1+c_2}{c_3}\right]^{\frac{1}{2}} \times \frac{y^{\frac{1}{2}}dy}{\left[y^4-\dfrac{c_1K^{-3}+c_2K^{-1}+c_3K}{c_3}y^3+c_2/c_3y^2+c_1/c_3\right]^{\frac{1}{2}}}. \quad (3)$$

The c's refer to the concentration of the various ionic species. In effecting a simplification of notation, Eq. (3) is written as

$$d\theta = Ly^{\frac{1}{2}}Q^{-\frac{1}{2}}dy, \quad (4)$$

where

$$Q\equiv y^4+a_1y^3+a_2y^2+a_4,$$

$$L\equiv\left[\frac{6c_1+c_2}{c_3}\right]^{\frac{1}{2}}; \quad a_1\equiv-\frac{c_1K^{-3}+c_2K^{-1}+c_3K}{c_3},$$

$$a_2\equiv c_2/c_3; \quad a_4\equiv c_1/c_3; \quad c_3\equiv c_2+3c_1.$$

The constants a_2 and a_4 are determined from the concentration of the ionic species in the solution; a_1 depends on the concentrations and also K, which serves as the lower limit when the integration is performed. It is worth while to point out in some detail how both a_1 and K can be computed. When the film thickness is sufficiently large so that van der Waals' or other short range forces are of no consequence, there are three types

[1] L. B. Robinson, J. Chem. Phys. **16**, 734 (1948).
[2] L. A. Wood and L. B. Robinson, J. Am. Chem. Soc. **69**, 1862 (1947).

of forces in equilibrium at the level of the meniscus in the capillary tube, according to Langmuir's interpretation. One force results from the weight of the solution in the capillary, pulling down on the film (the film itself is also a part of solution in the capillary), tends to make the film thinner. The pressure is regarded here as negative, since it acts downward, and it is computed by the following relation:

$$p_1=-(d-\beta)hg, \tag{6}$$

where d and β are the density of the solution and air, respectively, h is the capillary vise, and g is the acceleration of gravity. The second force originates in the pressure resulting from the surface tension of the cylindrical surface and tends to make the film thicker; this pressure is determined by the formula given below:

$$p_2=(d-\beta)(hg/2). \tag{7}$$

The third force in equilibrium results from the difference between the osmotic pressure in the bulk solution and that at the air-solution interface of the wetting film. According to van't Hoff's simple law, the osmotic pressure is given by $p=nkT$, where n is the number of ions per cm³. It is also assumed that the ions at the air interface obey the Boltzmann distribution and hence:

$$n=\sum_{i=1}^{s} n_i \exp(-z_i\epsilon\psi/kT),$$

or

$$n=\sum_{i=1}^{s} n_i K^{z_i}; \tag{8}$$

in the bulk solution the osmotic pressure is $p=\sum_i n_i kT$. Thus the difference in osmotic pressure tending to make the film thicker is:

$$p_3=\sum_{i=1}^{s} n_i kT(K^{z_i}-1). \tag{9}$$

At equilibrium the sum of these three pressures is zero and therefore:

$$\sum_i n_i kT(K^{z_i}-1)-(d-\beta)hg/2=0. \tag{10}$$

Using $N_i=10^{-3}C_iN$, where N is Avogadro's number, one can transform Eq. (10) into:

$$10^{-3}NkT[c_1K^{-3}+c_2K^{-1}+(c_2+3c_1)K-(4c_1+2c_2)]=(d-\beta)hg/2. \tag{11}$$

The above equation can be rewritten in the following form:

$$\frac{c_1K^{-3}+c_2K^{-1}+(c_2+3c_1)K}{c_2+3c_1}=\frac{1}{c_2+3c_1}\left[4c_1+2c_2+\frac{500(d-\beta)hg}{NkT}\right]. \tag{12}$$

The left-hand side of Eq. (12) is identically the negative of a_1 as defined by (5) and hence a_1 can be computed even through K is not known (every term on the right-hand side of (12) is known).

When the left-hand side of (12) is equated to a_1, the equation given below is obtained.

$$K^4+a_1K^3+a_2K^2+a_4=0. \tag{13}$$

It is apparent that the roots of (13) are identical with those of $Q=0$ in Eq. (4). The proper value of K can be found and ψ_m, the potential at the air interface can be evaluated. Q has two real and two complex zeros. If K_1 and K_2 are taken as the real zeros, then Q becomes

$$Q=(y-K_1)(y-K_2)(y^2+2\lambda' y+\mu'), \tag{14}$$

where $\lambda'=-(K_3e^{i\theta_3}+K_3e^{-i\theta_3})$; $\mu'=-K_3^2$, θ_3 is the argument of the complex roots, and $i^2=-1$. Consequently (2) may be written as:

$$\Delta r=\frac{L}{K}\int_{y_1}^{y_2}\frac{y^{\frac{1}{2}}}{[(y-K_1)(y-K_2)(y^2+2\lambda' y+\mu')]^{\frac{1}{2}}}dy, \tag{15}$$

where y_1 corresponds to ψ_m and y_2 to the measured ζ-potential. This equation is the hyperelliptic type as discussed in reference 1; the approximate solution is given below.

If the $y^{\frac{1}{2}}$ factor did not appear in the numerator, the solution of (15) could be had in terms of elliptic functions. Even as it stands, it can be seen that the integral has a value always between an elliptic integral multiplied by $y_1^{\frac{1}{2}}$ and $y_2^{\frac{1}{2}}$. The interval between y_1 and y_2 can be broken up into any number of smaller intervals; then one can find two numerical values between which Δr must always lie. Choosing the interval (over which the integration is performed) smaller and smaller makes these values approach each other more closely so that Δr may be determined quite accurately.

Let the interval between y_1 and y_2 be broken up into subintervals, the end points of which are y_i and y_j ($y_j>y_i$ and $y_j<1$) for each interval. It follows that

$$y_j^{\frac{1}{2}}\int_{y_i}^{y_j}Q^{-\frac{1}{2}}dy>\int_{y_i}^{y_j}y^{\frac{1}{2}}Q^{-\frac{1}{2}}dy>y_i\int_{y_i}^{y_j}Q^{-\frac{1}{2}}dy. \tag{16}$$

The integral $\int Q^{-\frac{1}{2}}dy$ can be evaluated readily if it is reduced to the Lagrangian form. Q is factored into two quadratic forms with real coefficients and is written:

$$Q=(y^2+2\lambda y+\mu)(y^2+2\lambda' y+\mu'). \tag{17}$$

Then, as usual, let y become $(p+qt)/(1+t)$, from which

$$y^2+2\lambda y+\mu=H(t^2+2ft+b^2)/(1+t)^2, \tag{18}$$

where

$$\left.\begin{aligned} H&=q^2+2\lambda q+\mu.\\ b^2&=(p^2+2\lambda p+\mu)/(q^2+2\lambda q+\mu).\end{aligned}\right\} \tag{19}$$

Likewise:

$$y^2+2\lambda' y+\mu'=H'(t^2+2f't+b'^2)/(1+t)^2, \tag{20}$$

where H' and f', and b'^2 are the same functions of p, q, λ', and μ' as H, f, and b^2 are of p, q, λ, and μ. Equations (18) and (20) hold for any arbitrary values of p and q. However, f and f' can be made to equal zero simultaneously by choosing p and q such that:

$$\left.\begin{aligned} p&\equiv\frac{(\mu-\mu')+W}{2(\lambda'-\lambda)},\\ q&\equiv\frac{(\mu-\mu')-W}{2(\lambda'-\lambda)},\end{aligned}\right\} \tag{21}$$

and

$$W^2\equiv(\mu+\mu'-2\lambda\lambda')^2-4(\mu-\lambda^2)(\mu'-\lambda'^2). \tag{22}$$

It can be shown that W^2 is always positive for all values of λ, λ', μ, and μ' and hence p and q are always real. After the substitutions are made, the elliptic integral can be written as

$$\int_{y_1}^{y_2} Q^{-\frac{1}{2}}dy=\frac{q-p}{(HH')^{\frac{1}{2}}}\int_{t_1}^{t_2}\frac{dt}{[-(t^2-b^2)(t^2-b'^2)]^{\frac{1}{2}}}. \tag{23}$$

The other transformations which are made in order that the integral be evaluated depend upon the numerical values of t_1, t_2, b, and b'. One can see from an examination of Table I and also the relation $t=(p-y)/(y-q)$ that $b'>t>b$; consequently the integrand in (23) is real. The following transformations are necessary to convert (23) in a form so that it can be evaluated from tables:

$$\left.\begin{aligned} t^2&=b'^2-(b'^2-b^2)\sin^2\phi,\\ b'^2\sin^2\alpha&=b'^2-b^2.\end{aligned}\right\} \tag{24}$$

When Eq. (24) is substituted in (23), the integral given by Eq. (25) is used to compute the thicknesses of the films.

$$I=\int_{\phi_1}^{\phi_2}\frac{d\phi}{(1-\sin^2\alpha\sin^2\phi)^{\frac{1}{2}}}. \tag{25}$$

The film thicknesses are calculated by using the inequality (16). The limits ϕ_1 and ϕ_2 (corresponding to y_1 and y_2, respectively) are selected sufficiently close to each other so that

$$y_2^{\frac{1}{2}}\int_{\phi_1}^{\phi_2}\frac{d\phi}{(1-\sin^2\alpha\sin^2\phi)^{\frac{1}{2}}} \tag{6}$$

is almost equal to

$$y_1^{\frac{1}{2}}\int_{\phi_1}^{\phi_2}\frac{d\phi}{(1-\sin^2\alpha\sin^2\phi)^{\frac{1}{2}}}.$$

These integrals are multiplied by

$$M\equiv\frac{L}{K}\frac{q-p}{b'(HH')^{\frac{1}{2}}}. \tag{27}$$

This multiplicative factor comes from (3), (23), and (25); from Eq. (3), $\Delta\theta=K\Delta r$. In calculating the values for the curve in Fig. 1, the two integrals in (26) were usually selected so that the two extremes differed by not more than about 1 or 2 angstrom units; in the most extreme cases, the difference was never more than 6 angstrom units.

Positive Zeta-Potentials

In the solutions in which the zeta-potentials are positive, it is convenient that

$$y\equiv\exp(-\eta)\quad\text{and}\quad K\equiv\exp(-m), \tag{28}$$

instead of Eq. (2). The ionic species 1, 2, and 3 are the same as in the first transformation.

Equation (29) then replaces Eq. (3).

$$d\theta=-\left[\frac{6c_1+c_2}{c_1}\right]^{\frac{1}{2}}\times\frac{y^{-\frac{1}{2}}dy}{\left[y^4+\frac{c_2}{c_1}y^2-\frac{c_1K^3+c_2K+c_3K^{-1}}{c_1}y+\frac{c_3}{c_1}\right]^{\frac{1}{2}}}. \tag{29}$$

This equation may be rewritten as

$$\Delta r=-\frac{L}{K}\int_{y_1}^{y_2}\frac{y^{-\frac{1}{2}}}{(y^4+a_1y^2+a_2y+a_3)^{\frac{1}{2}}}dy, \tag{30}$$

where

$$\left.\begin{aligned} L&\equiv\left[\frac{6c_1+c_2}{c_1}\right]^{\frac{1}{2}};\quad a_1=c_2/c_1;\\ a_2&\equiv-\frac{c_1K^3+c_2K+c_3K^{-1}}{c_1};\\ a_3&\equiv c_3/c_1\equiv\frac{3c_1+c_2}{c_1}=a_1+3.\end{aligned}\right\} \tag{31}$$

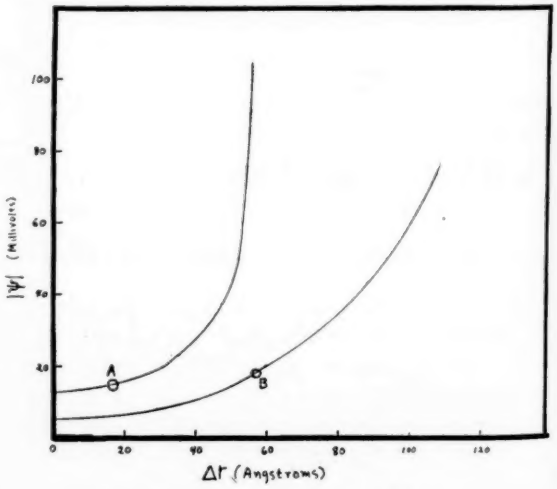

FIG. 1. Zeta-potential *vs.* film thickness.

TABLE I. Parameters for the evaluation of film thicknesses.

	Concentration of lanthanum chloride solutions			
	1.00×10	2.50×10	1.00×10	5.00×10
$c_1(\times 10^6)$	1000	250	100	50
$c_2(\times 10^6)$	1	1	1	1
$c_3(\times 10^6)$	3001	751	301	151
$(\times 10^8)$	39.28		124.1	
K	0.8184	0.6562	0.6155	0.5301
K'	1.1936	1.3926	2.0114	2.7380
$d-\beta$	0.9973	0.9971	0.9971	0.9971
λ	−1.0060	−1.0244	−1.3085	−1.6340
μ	0.9768	0.9138	1.2320	1.4514
λ'	1.0060	1.0244	0.2855	0.2569
μ'	3.0732	3.2917	0.2688	0.2281
$\psi_{m(mv)}$	5.15	10.8	12.5	16.3
$\zeta_{(mv)}$	16.4	2.0	14.5	15.0
W	6.0979		2.3264	
p	0.9944		1.0320	
q	−2.0364		−0.4276	
H	9.2209		2.5339	
H'	3.1229		0.2075	
b	0.0617		0.3991	
b'	1.9414		9.2677	
t_1	0.0617		0.3991	
α(degrees)	87.53		88.18	
$M(\times 10^8)$	27.994		−38.09	
η	−0.6385		−0.5646	
y_2	0.5281		0.5686	
$y_1(=K)$	0.8184		0.6156	
t_2	0.1818		0.4651	
ϕ_1(degrees)	84.95		88.52	
Δr(angstroms)	56	0	18	0

From equilibrium conditions, one sees that

$$K^4+a_1K^3+a_2K+a_3=0, \tag{32}$$

from which the different values of K and also a_1 are formed by using a procedure similar to that following Eq. (5). One then treats Eq. (30) in the same fashion as (3) and (16) were treated with p, q, and all other parameters defined exactly as in the first case.

As before, the integral is evaluated by computing several small increments and subsequently adding all of the successive increments to those which have been previously calculated. Since $y=\exp(-\eta)$, and $y^{-\frac{1}{2}}=\exp(+\eta/2)$, it follows that $y^{-\frac{1}{2}}\int Q^{-\frac{1}{2}}dy$ goes to infinity as the potential does. This, however, presents no difficulty in evaluating the increments for $y^{-\frac{1}{2}}\int Q^{-\frac{1}{2}}dy$; in the region where $y^{-\frac{1}{2}}$ begins to become large so that the difference between y_i and y_j to be considered must be very small, the increment of the elliptic integral in this corresponding region approaches zero. Actually, the elliptic integral attains its full value, very nearly, at about 80 millivolts so that all of the many increments to be added between 80 mv and infinity are practically negligible. The curve showing the variation of the film thickness with potential for this case is also shown in Fig. 1.

INTERPRETATION OF COMPUTATIONS

The values of the zeta-potential listed in Table I have been used to compute the wetting film thicknesses for lanthanum chloride solutions of concentrations 10^{-3} and 10^{-4} mole/liter. When the minimum potential in the film, at the air-solution interface, is larger than the zeta-potential, no film of any significant size can form according to Langmuir's theory. Any film which would form would be controlled by van der Waals' and other short range forces. Because of this consideration, the value of the wetting film is taken as zero for the 2.50×10^{-4} and the 5.0×10^{-5} mole/liter solutions as in both cases the ζ-potentials were less than the air-solution potentials. Table I is not completely filled out for these solutions since many of the entries were not required as no computations were made. Table I shows all of the necessary parameters used to evaluate Δr (the film thickness) as well as the computed values of Δr. Table II shows the "corrected surface tensions" when three samples of water with varying ionic concentrations are taken as having surface tension equal to unity. The minimum is eliminated in the case of lanathum chloride as predicted by Langmuir.

TABLE II. Corrected surface tensions for lanthanum chloride solutions.

Concentration	Δr (angstroms)	Langmuir correction factor	Apparent relative surface tension	Corrected relative surface tension
Reference water: ionic concentration 4.2×10^{-6} mole/liter				
Water	548	(1.000,00)	(1.000,00)	(1.000,00)
0.00005	0	1.000,40	0.999,85	1.000,25
0.00010	18	1.000,39	0.999,84	1.000,23
0.00025	0	1.000,40	0.999,81	1.000,21
0.00100	56	1.000,36	0.999,87	1.000,23
Reference water: ionic concentration 2.0×10^{-6} mole/liter				
Water	508	(1.000,00)	(1.000,00)	(1.000,00)
0.00005	0	1.000,37	0.999,85	1.000,22
0.00010	18	1.000,36	0.999,84	1.000,20
0.00025	0	1.000,37	0.999,81	1.000,18
0.00100	56	1.000,33	0.999,87	1.000,20
Reference water: ionic concentraotin 0.95×10^{-6} mole/liter				
Water	442	(1.000,00)	(1.000,00)	(1.000,00)
0.00005	0	1.000,32	0.999,85	1.000,17
0.00010	18	1.000,31	0.999,84	1.000,15
0.00025	0	1.000,32	0.999,81	1.000,13
0.00100	56	1.000,28	0.999,87	1.000,15

That no regularity in the corrected data is observed is not surprising. The corrected surface tensions have the following sources of error inherent in them: (a) the experimental error in determining the streaming potentials (used to compute the zeta-potentials); and (b) the unknown value of the ratio of the dielectric constant of the electric double layer to its viscosity which is necessary to convert streaming potential data to zeta-potentials. In case the potentials were as large as 80 millivolts, it is quite apparent from the graph that errors of these types might be quite insignificant. But such small potential values as are obtained experimentally make it possible that an error of from two to three millivolts (especially in the case of the 10^{-4} and 5×10^{-5} solutions) in the zeta-potential could make a difference of from 0 to 30

angstroms in the film thickness. This difference in turn would cause significant changes in the calculated "corrected surface tensions." Actually the zeta-potential is not reproducible to more than two or three millivolts. No significant error results from the mathematical approximations.

It seems apparent that the original capillary rise data of Jones and Ray can be interpreted without assuming that a minimum exists in the surface tension-concentration curve. In order to compare the corrected values with the theory one needs to know the zeta-potentials with a higher degree of accuracy. The curves given in Fig. 1 will still be valid, but points A and B will have different locations on the curves.

THE JOURNAL OF CHEMICAL PHYSICS VOLUME 17, NUMBER 10 OCTOBER, 1949

On the Non-Equilibrium Theory of Absolute Reaction Rates

HUGH M. HULBURT
Department of Chemistry, Catholic University of America, Washington, D. C.

AND

JOSEPH O. HIRSCHFELDER
Department of Chemistry, University of Wisconsin, Madison, Wisconsin

(Received February 23, 1949)

The ensemble of point masses representing reaction complexes in configuration space is treated as an ideal gas by methods of exact kinetic theory. Hydrodynamic equations for the mean motion of the ensemble are derived. The theory of compressible flow is used to show that under a very wide range of conditions, the energy distribution characteristic of the reactants in a chemical reaction is maintained in the reaction complex at least until it passes through the activated state.

THE current theory of reaction rates[1] is limited in its rigorous application to reversible reactions proceeding at dynamic equilibrium. Ever since its proposal, the theoretical applicability of this theory to irreversible reactions or to the rate of approach to equilibrium has been a subject of discussion.[2] Recently two attempts have been made to make more precise the limits of its applicability. Kramers[3] has extended the classical theory of Brownian motion to calculate, in terms of an empirical "friction factor," the rate at which point masses diffuse over a one-dimensional potential energy barrier under conditions that the mean flow is nearly zero, and the energy distribution of the masses consequently nearly that of equilibrium. This implies that the energy barrier is relatively high ($>20kT$). Eyring and Zwolinski[4] verify Kramer's general conclusions by a different type of calculation in which a specific rate of reaction is assigned to each quantum state of the reaction complex. Over-all rates are calculated for different sets of assumptions concerning the magnitudes of these specific reaction rates. Making spot checks supposed to cover the extremes likely to be encountered, they find that the non-equilibrium rate for a unimolecular reaction may deviate by no more than 20 percent from its equilibrium value, in general agreement with Kramer's estimates.

It is the purpose of this paper to present a third approach to the theory of the rate of an irreversible reaction which is not restricted to slow reactions and which leads to some immediate qualitative conclusions concerning the rate of approach to equilibrium.

We proceed from the view that a chemical reaction can be represented by the motion of a mass-point in the configuration space of the reacting complex. In the interests of clarity, we list the principle restrictions and assumptions which this involves:

1. We suppose the reaction complex to remain in the same electronic quantum state throughout its motion. Reactions involving excited reactants or products will need special consideration.
2. We suppose the point-mass to obey the classical Hamilton's equations of motion.

Previous considerations[5,6] have shown that, except possibly for reactions of atomic hydrogen and its isotopes, this assumption introduces no serious error as long as the rate of reaction must be averaged over a normal distribution of reactant energies.

When each possible reaction complex is represented by a point mass in configuration space, the macroscopic course of the reaction will be represented by a distribution of such point-masses with varying density in space and moving with varying velocities. For such a distribution it is possible to derive macroscopic differential equations governing the average density, average momentum and average energy of the fluid system. These are the hydrodynamic equations of the system. Chapman and Cowling[7] give the derivation for a real mon-

[1] Glasstone, Laidler, and Eyring, *The Theory of Rate Processes* (McGraw-Hill Book Company, Inc., New York, 1941).
[2] Fowler and Guggenheim, *Statistical Thermodynamics* (Cambridge University Press, London, 1940).
[3] H. A. Kramers, Physica **7**, 284 (1940).
[4] Eyring and Zwolinski, J. Am. Chem. Soc. **69**, 2702 (1947).
[5] J. O. Hirschfelder and E. P. Wigner, J. Chem. Phys. **7**, 616 (1939).
[6] H. M. Hulburt and J. O. Hirschfelder, J. Chem. Phys. **11**, 276 (1943).
[7] Chapman and Cowling, *The Mathematical Theory of Non-Uniform Gases* (Cambridge University Press, London, 1942).

atomic gas in three dimensions. This treatment is extended to n dimensions in the appendix to this paper. It is strictly valid only when one can assume (1) conservation of mass, momentum and energy between molecules in every collision, and (2) that no more than two molecules need be considered to interact at any time. Kirkwood[8] and Born and Green[9] have shown how this treatment needs to be modified for condensed systems. The essential result is the introduction of new terms in the expressions for the coefficients of viscosity, diffusion, thermal conductivity and thermal diffusion. Presumably these are represented to a first approximation by the Eyring theory of viscosity[1] and extension to other transport properties.

It is possible, therefore, to represent a chemical reaction by the motion of a fluid in the configuration space of the reaction complex. This fluid is compressible and moves in a potential energy field which governs its rate of flow in part. Somewhere in configuration space there are sources and sinks, the strengths of which complete the data required to calculate in principle, the flow pattern of this representative fluid.

It has been shown[7] that if the reaction complexes have the velocity distribution of equilibrium, the fluid viscosity is zero. In the case of a real gas, of course, collisions bring about interactions which destroy the equilibrium velocity distribution and introduce fluid friction. In the case of a reaction-complex gas, we shall suppose these collisions to be so rare as to be negligible. It is thus frictionless, even though not in equilibrium.

We shall now write down the differential equations of motion of the representative fluid and proceed to investigate the possible states of steady motion. The equations of motion are:

$$\frac{D\rho}{Dt}+\rho\sum_i\frac{\partial v^i}{\partial q^i}=0, \tag{1}$$

$$\frac{Dv^i}{Dt}=-\frac{1}{\rho}\sum_k\frac{\partial \Pi_{ik}}{\partial q^k}-\frac{1}{m}\frac{\partial V}{\partial q^i}, \tag{2}$$

where $D/Dt=\partial/\partial t+\sum_i v^i(\partial/\partial q^i)$, Π_{ik}=pressure tensor, ρ=fluid density, V=potential energy per reaction complex, m=mass of a representative point, v^i=ith component of mean velocity of the representative fluid. Since there are no collisions between complexes, there is no exchange of energy between any portion of our representative fluid and its surroundings and the flow is adiabatic in the thermodynamic sense. Moreover, the fluid is a monatomic gas and the hydrostatic pressure is

$$p=\rho kT/m. \tag{3}$$

Its internal energy is

$$E=(3r-6)kT/2,$$

where r is the number of atoms in the reaction complex. ($3r-6$ is the number of degrees of freedom in configuration space).

A word may be said concerning the interpretation of the pressure of this fluid in configuration space. As in the kinetic theory of an ordinary gas, the hydrostatic pressure, as well as the temperature, is proportional to the difference between the mean kinetic energy of the molecules and the kinetic energy of the mean motion of the molecules. In a reversible reaction, the averaging is carried out over reaction complexes traveling in all directions. The hydrodynamic velocity is thus proportional to the difference between the forward and reverse rates. If, as we have assumed, there is no interaction between complexes, this is a completely additive superposition of the motions of complexes originating as reactants on the motion of complexes originating as products. Even in a completely irreversible reaction, however, there will be an effective pressure, since some of the complexes moving forward along the reaction path will be reflected by the potential energy gradients. Thus the net forward rate of motion at any point will not be the forward velocity of an individual complex, but rather the average over incident and reflected complexes.

A further simplification is frequently possible. It has been shown[5,6] that whenever the potential energy surface is such that the Schrödinger equation for the reaction complex is separable into "fast" coordinates normal to the reaction path and a "slow" coordinate along the reaction path, the many-dimensional problem can be replaced by a one-dimensional one. The representative fluid can now be considered to move uniformly in every cross section of 3-space. There is a separate potential energy surface, however, for each vibrational state, and transitions between vibrational levels may be induced by potential energy gradients as well as by interaction between complexes. Alternatively, one may consider a single surface (that for the lowest vibrational level) on which move point-masses with internal energy. A vibrational transition now produces an exchange between the internal and translational energies of the point-mass. This is an apparent dissipation of energy and may be treated like a friction term, though the "viscosity" will not be Newtonian but a function of velocity.

This one-dimensional treatment will be feasible whenever the potential energy surface permits one of the variables of the Schrödinger equation to be separated out, at least approximately. This appears often to be the case in practice, although more detailed knowledge of actual energy surfaces would be desirable to test the point.

In the one-dimensional case, the equations of motion become

$$\frac{\partial\rho}{\partial t}+u\frac{\partial\rho}{\partial x}+\rho\frac{\partial u}{\partial x}=0, \tag{5}$$

$$\frac{\partial u}{\partial t}+u\frac{\partial u}{\partial x}=-\frac{1}{\rho}\frac{\partial p}{\partial x}-\frac{1}{\rho}\frac{\partial \Pi}{\partial x}-\frac{1}{m}\frac{\partial V}{\partial x}, \tag{6}$$

[8] J. G. Kirkwood, J. Chem. Phys. **14**, 180 (1946).
[9] M. Born and D. Green, Proc. Roy. Soc. **A190**, 455 (1947) and earlier.

where Π = the frictional part of the pressure tensor. The pressure is still that of an ideal gas and the internal energy lies between $(1/2)kT$ and $(3r-7)kT/2$ per complex, approaching the latter value for high temperatures and equipartition. These are, of course, equilibrium values, but we suppose, as usual, that local pressures and temperatures can be assigned which preserve the equilibrium functional form for the thermodynamic quantities throughout the flow pattern.

Even when more than one degree of freedom can be treated classically, the one-dimensional form of Eqs. (5) and (6) may be valid. To show this, suppose the reaction complex to be vibrationally quantized in a three-dimensional configuration space. This means that all but two internal degrees of freedom are treated quantally and there is a separate energy surface for each set of these quantum numbers. The representative fluid is then a monatomic gas in three dimensions. Alternatively, if internal energy is allowed the reaction complex, a single surface may be used. Now if the potential energy surface is such that it can be expressed as a product of two factors, one involving distance normal to the reaction path, the other parallel to it, the situation is analogous to the flow of a compressible fluid through a pipe of variable cross section for which the area is known as a function of the distance from one end. The equilibrium density is given by

$$\rho_1=\rho_0 e^{-V(x,y)/kT}=\rho_0 e^{-V_1(x)/kT}\cdot e^{-[V(x,y)-V_1(x)]/kT}=\rho\sigma, \quad (7)$$

where

$$\sigma=\exp\{-[V(x,y)-V_1(x)]/kT\};\qquad \rho=\rho_0\exp[-V_1(x)/kT]. \quad (8)$$

Here σ plays the role of the variable area. If $V(x, y)$ is in fact independent of y in some region, the one-dimensional equations apply strictly in that region. Thus an energy surface in the form of a flat bottomed channel with perpendicular sides reduces to the one-dimensional case. The flow is uniform in any cross section and Eq. (5) becomes

$$\frac{\partial(\rho\sigma)}{\partial t}+u\frac{\partial(\rho\sigma)}{\partial x}+(\rho\sigma)\frac{\partial u}{\partial x}=0. \quad (9)$$

Returning to the one-dimensional case, it has been shown[5] that there is a dominant tendency to retain a given vibrational quantum number when the potential energy changes suddenly, compensated in part by a smaller tendency to retain the initial vibrational *energy*. If, as is usual, the vibration frequencies become lower as the complex becomes activated, this means that any induced transitions as the barrier is approached will tend to be into higher vibrational states, thus reducing the density and pressure of the complex-fluid as it approaches the barrier even more than occurs by reflection without change of vibration quantum number. The steady state of flow must satisfy Eqs. (5) and (6) when $\partial\rho/\partial t=\partial u/\partial t=0$. The integration of this set of equations is well-known in acoustics and aerodynamics. Two important cases arise. First, we consider that only infinitesimal variations in density and pressure occur. For $\Pi=0$ and $\sigma=\sigma_0$, we have

$$u du=-dp/\rho-dW/\rho, \quad (10)$$

$$u d\rho=-\rho du, \quad (11)$$

where

$$dW=(\rho/m)dV. \quad (12)$$

Note that W is the volume density of potential energy and dW the body force on unit volume of fluid. Eliminating du from Eqs. (10) and (11)

$$u^2=dp/d\rho+dW/d\rho. \quad (13)$$

Since the flow is adiabatic

$$dp/d\rho=\gamma(p/\rho)=\gamma kT/m. \quad (14)$$

Hence

$$u^2=\frac{\gamma kT}{m}\left[1+\frac{m}{\gamma kT}\frac{dW}{d\rho}\right]. \quad (15)$$

If the density is that of equilibrium

$$\rho=\rho_0\exp\{-(V-V_0)/kT\},$$

and

$$u^2=(\gamma-1)kT/m, \quad (16)$$

where, for our reaction complex, $C_v=(3r-7)k/2$, and

$$\gamma=1+2/(3r-7). \quad (17)$$

We see that, as in a real gas, an infinitesimal disturbance can persist only for a fixed velocity of fluid relative to the disturbance, *viz.*, the velocity of sound. Moreover, this velocity is diminished by the presence of a potential gradient of the normal type (i.e., $dW/d\rho$ negative).

The second important case arises when we consider the possibility that a finite discontinuity in pressure, density and velocity persist in steady flow at some point on the energy profile. In a real fluid, such a discontinuity is called a "shock wave," and its properties and the conditions of its stability are well known.[10,11] These conditions need to be re-examined, however, for the possible influence of the potential energy gradient, taken as zero in the aerodynamic case.

Consider flow relative to the wave front in which there are jumps u_2-u_1, p_2-p_1, $\rho_2-\rho_1$ in the velocity, pressure and density, respectively. Then conservation of mass at the wave front requires

$$\rho_1 u_1=\rho_2 u_2. \quad (18)$$

[10] MacColl and Taylor, "Propagation of Plane Disturbances," Chapter III in Durand, *Aerodynamic Theory* (J. Springer, Berlin, 1935), Vol. III, pp. 209–250.

[11] Liepman and Puckett, *Introduction to Aerodynamics* (John Wiley and Sons, Inc, New York, 1947), Chapter IV.

Conservation of momentum in a differential length is expressed by

$$\rho u du = -dp - \rho d\Phi, \tag{19}$$

where $\Phi = V/m$. Putting $dW = \rho d\Phi$, this equation can be integrated to read

$$\rho_2 u_2^2 - \rho_1 u_1^2 = p_1 - p_2 + W_1 - W_2. \tag{20}$$

But W is a continuous function of x even though ρ is not. Hence at the shock wave $W_1 = W_2$ and, using Eq. (18),

$$u_2 - u_1 = \frac{p_1}{\rho_1 u_1} - \frac{p_2}{\rho_2 u_2}, \tag{21}$$

just as if there were no potential energy field. Conservation of energy requires in general

$$\frac{u_1^2}{2} + C_p T_1 + \Phi_1 = \frac{u_2^2}{2} + C_p T_2 + \Phi_2, \tag{22}$$

which, for an ideal gas at the shock front may be written

$$u_2^2 - u_1^2 = \frac{2\gamma}{\gamma - 1}\left(\frac{p_1}{\rho_1} - \frac{p_2}{\rho_2}\right), \tag{23}$$

since

$$C_p = \frac{k\gamma}{m(\gamma - 1)} \quad \text{and} \quad \Phi_1 = \Phi_2.$$

From Eqs. (18), (21), and (23) we derive the usual Rankine-Hugoniot equation for the pressure ratio as a function of the density ratio on the two sides of the shock wave

$$\frac{p_2}{p_1} = \left[\left(\frac{\rho_2}{\rho_1}\right)\left(\frac{\gamma+1}{\gamma-1}\right) - 1\right] \Big/ \left[\frac{\gamma+1}{\gamma-1} - \frac{\rho_2}{\rho_1}\right]. \tag{24}$$

This is to be compared with the isentropic line

$$p_2/p_1 = (\rho_2/\rho_1)^\gamma. \tag{25}$$

It is clear that Eq. (24) lies to the right of Eq. (25), i.e., toward higher densities, provided p_2/p_1 and ρ_2/ρ_1 are greater than 1.0. This corresponds to an entropy rise upon passage through the shock wave. On the other hand, if p_2/p_1 and ρ_2/ρ_1 are less than 1.0, passage through the shock corresponds to an entropy decrease. Therefore, a stable shock wave can persist only if fluid passing through it experiences a rise in density and pressure. We have seen that deviations from the equilibrium density distribution due to reflection by the potential energy surface can only accentuate and not counteract the normal density gradient. Hence no shock wave can persist between initial and activated states, but may develop after the flow passes the activated state into a region of increasing density.

Since the shock wave brings about an increase in entropy, more kinetic energy must be lost in passing through it than is predicted by Bernouilli's theorem for adiabatic compressible flow. This dissipation requires vibrational transitions in the reaction complexes, and from its impossibility we may conclude that the population of the vibrational levels of the reaction complex cannot show any net change between initial and activated states, so long as we exclude interaction between reaction complexes. The collision of a reaction complex with another body, of course, furnishes another mechanism for inducing vibrational transitions. So long as these collisions occur in the "reactants" region of configuration space, far from the activated state, we should be inclined to include them in whatever mechanism maintains the initial distribution of complexes over their vibrational levels. Collisions occurring near the activated state will be three-body collisions and will be relatively rare, particularly in gas reactions. Furthermore, as we have seen, there is a marked persistence of vibrational quantum number in all molecular collisions. Hence one might expect on physical grounds that the "external" collisions will have only a small effect on the energy distribution.

Our method does not, of course, predict boundary or initial values for the pressure, density and velocity of flow. We cannot, therefore, assign values to the initial density distribution without considering the problem of the rate of activation under non-equilibrium conditions. However, it is very unlikely that the ratio of activated complexes to non-activated ones should be large, and, under these conditions, the complex-fluid flow must be adiabatic as far as the activated state, at least.

In conclusion, we have shown that very general considerations based on the application of the laws of thermodynamics to a complex-fluid reveal that no changes in the energy distribution among the several degrees of freedom of a reaction complex can occur before the activated state is reached unless the complex suffers a collision with a third body. The rarity of this occurrence, together with the low probability of collisional transfer of vibrational energy lends us confidence in the application of the Eyring theory of absolute reaction rates to processes not at equilibrium.

APPENDIX

If it be assumed that the motion of the nuclei may be treated by the laws of classical mechanics, the reaction complex consisting of r nuclei moving in the field of their electrons has the kinetic energy

$$T = \tfrac{1}{2} \sum_{i,j}^{3r} m_i \dot{x}^i \dot{x}^j, \tag{A1}$$

and the potential energy $V(x^i)$ equal to the electronic energy of the system. It is always possible to find a coordinate system q^i, such that the kinetic energy exclusive of that of the center of mass takes the form

$$T = \tfrac{1}{2} m \sum_{i=1}^{3r-6} (\dot{q}^i)^2. \tag{A2}$$

Thus the reaction complex may be represented by a point of mass

m in $3r-6$ dimensional q-space. Its equations of motion are

$$\frac{\partial H}{\partial q^i}=-\dot{p}_i;\quad \frac{\partial H}{\partial p_i}=\dot{q}^i, \tag{A3}$$

where $H=T+V$ is the Hamiltonian of the system.

In an actual chemical reaction, there will be a distribution of these representative points in phase space which is characterized by the function $f(q^i, p_i, t)$, where q^i and p_i stand for the entire set of generalized coordinates and momenta, respectively, and t is the time. The function f is defined to give the number of systems having coordinates with values in the range q^i to q^i+dq^i and momenta in the range p_i to p_i+dp_i at the instant t.* The function f is the density-in-phase of the assembly of systems under consideration. By Liouville's theorem, this is conserved in time, so that any given set of phase points occupies the same volume throughout their motion. Thus we may write

$$\frac{Df}{Dt}=\frac{\partial f}{\partial t}+\dot{p}_i\frac{\partial f}{\partial p_i}+\dot{q}^i\frac{\partial f}{\partial q^i}=0. \tag{A4}$$†

The average value, $\bar{\phi}$, of any property ϕ of the point masses in a small volume $dq=dq^1dq^2\cdots dq^{3r-6}$ of configuration space is given by

$$\begin{aligned} n\bar{\phi}dq&=dq\int f\phi dp,\\ \bar{\phi}&=\frac{1}{n}\int f\phi dp, \end{aligned} \tag{A5}$$

where n is the number density of point masses in configuration space and $dp=dp_1dp_2\cdots dp_{3r-6}$. In particular, the density itself is given by taking $\phi=1$:

$$n=\int f dp. \tag{A6}$$

The average rate of change of a property ϕ may be expressed by use of Eq. (A4):

$$\begin{aligned} n\frac{d\bar{\phi}}{dt}&=\int\phi\frac{\partial f}{\partial t}dp+\int\phi\dot{p}_i\frac{\partial f}{\partial p_i}dp+\int\phi\dot{q}^i\frac{\partial f}{\partial q^i}dp\\ &=\int\frac{\partial(f\phi)}{\partial t}dp-\int f\frac{\partial\phi}{\partial t}dp+\dot{p}_i\int\phi\frac{\partial f}{\partial p_i}dp\\ &\qquad+\int\frac{\partial(f\phi\dot{q}^i)}{\partial q^i}dp-\int f\frac{\partial(\phi\dot{q}^i)}{\partial q^i}dp, \end{aligned} \tag{A7}$$

where we take $\dot{p}_i$ and $\dot{q}^i$ to be independent of p_i and q^i. Making the hypothesis that $f\phi$ vanishes at $+\infty$ and $-\infty$, the third term may be integrated by parts to give

$$\dot{p}_i\int\phi\frac{\partial f}{\partial p_i}dp=-\dot{p}_i\int f\frac{\partial\phi}{\partial p_i}dp.$$

Using this result and Eq. (A5), Eq. (A7) becomes

$$n\frac{d\bar{\phi}}{dt}=\frac{\partial(n\phi)}{\partial t}+\frac{\partial}{\partial q^i}(n\langle\phi\dot{q}^i\rangle)-n\left\{\dot{p}_i\frac{\langle\partial\phi\rangle}{\partial p_i}+\frac{\langle\partial\phi\rangle}{\partial t}+\frac{\langle\partial(\phi\dot{q}^i)\rangle}{\partial q^i}\right\}, \tag{A8}$$

where angular brackets denote average values.

It is often convenient to express f as a function of the *peculiar momentum*, $P_i=p_i-\bar{p}_i$. Here the average momentum, $\bar{p}_i$, is a function of both t and q^i, whereas p_i is a coordinate independent of q^i. Thus we have

$$\left.\begin{aligned} \frac{\partial\phi}{\partial p_i}&=\frac{\partial\phi}{\partial P_i}\\ \frac{\partial\phi}{\partial t}&=\frac{\partial\phi}{\partial t}+\frac{\partial\phi}{\partial P_i}\frac{\partial P_i}{\partial t}=\frac{\partial\phi}{\partial t}-\frac{\partial\phi}{\partial P_i}\frac{\partial\bar{p}_i}{\partial t}\\ \frac{\partial\phi}{\partial q^i}&=\frac{\partial\phi}{\partial q^i}+\frac{\partial\phi}{\partial P_j}\frac{\partial P_j}{\partial q^i}=\frac{\partial\phi}{\partial q^i}-\frac{\partial\phi}{\partial P_j}\frac{\partial P_j}{\partial q^i} \end{aligned}\right\}, \tag{A9}$$

in which the variables are now P_i, q^i, and t. Furthermore,

$$P_i=m\dot{Q}_i,\quad \text{where}\quad \dot{Q}_i=\dot{q}^i-\langle\dot{q}^i\rangle,$$

provided we make the definition $\bar{p}_i=\dfrac{\partial\bar{T}}{\partial\langle\dot{q}^i\rangle}$. Substituting Eq. (A9) into Eq. (A8)

$$\begin{aligned} n\frac{\partial\bar{\phi}}{\partial t}=\frac{D(n\bar{\phi})}{Dt}+\frac{\partial}{\partial q^i}\left(\frac{n}{m}\langle\phi P_i\rangle\right)-n\Big\{&\left\langle\frac{\partial\phi}{\partial P_i}\right\rangle\left(\dot{p}_i-\frac{D\bar{p}_i}{Dt}\right)+\left\langle\frac{D\phi}{Dt}\right\rangle\\ &+\frac{1}{m}\left\langle\frac{\partial(\phi P_i)}{\partial q^i}\right\rangle-\frac{1}{m}\left\langle\frac{\partial\bar{p}_i}{\partial q^j}\right\rangle\left\langle\frac{\partial(\phi P_j)}{\partial P_i}\right\rangle\Big\}, \end{aligned} \tag{A10}$$

where we have written

$$\frac{D}{Dt}=\frac{\partial}{\partial t}+\frac{\bar{p}_i}{m}\frac{\partial}{\partial q^i}. \tag{A11}$$

Taking $\phi=1$ gives us the equation of change of density in configuration space:

$$\frac{Dn}{Dt}+\frac{n}{m}\frac{\partial\bar{p}_i}{\partial q^i}=0. \tag{A12}$$

Writing $v^i=\bar{p}_i/m$ and $\rho=mn$, this becomes the usual equation of continuity for a continuous medium.

$$\frac{D\rho}{Dt}+\frac{\rho\partial v^i}{\partial q^i}=0. \tag{A12a}$$

Taking $\phi=P_k$ we obtain the equation of momentum. Since $\bar{P}_k=0$,

$$\left\langle\frac{\partial P_k}{\partial P_i}\right\rangle=\delta_{ik};\quad\left\langle\frac{DP_k}{Dt}\right\rangle=0;$$
$$\left\langle\frac{\partial(P_iP_k)}{\partial q^i}\right\rangle=0,\quad\text{and}\quad\left\langle\frac{\partial(P_kP_j)}{\partial P_i}\right\rangle=0;$$

Eq. (A10) becomes

$$\frac{D\bar{p}_k}{Dt}=\dot{p}_k-\frac{1}{n}\frac{\partial\Pi_{ik}}{\partial q^i}, \tag{A13}$$

or, in terms of v^i and ρ,

$$\frac{Dv^i}{Dt}=\dot{v}^i-\frac{1}{\rho}\frac{\partial\Pi_{ik}}{\partial q^i}, \tag{A13a}$$

where

$$\Pi_{ik}=\frac{n}{m}\langle P_iP_k\rangle,$$

is by definition the pressure tensor. This is the usual hydrodynamic equation.

The distribution function f must be known in order to determine the form of the pressure tensor, Π_{ik}. Taking $f=A\exp(-H/kT)$, as in equilibrium, we find from Eqs. (A5) and (A6)

$$n=A(2\pi mkT)^{3r-6/2}e^{-V/kT}, \tag{A14}$$

$$\Pi_{ik}=nkT\delta_{ik}=\Pi. \tag{A15}$$

The complex-fluid thus has the equation of state and internal energy of an ideal gas and hence one can define all the usual thermodynamic functions for it as for an ideal gas.

* This is the function $\hat{f}$ of Kirkwood, reference 8.

† Henceforth, any term in which a subscript or superscript is repeated is to be summed for all $3r-6$ values of the subscript or superscript. Thus

$$\dot{p}_i\frac{\partial f}{\partial p_i}\equiv\sum_{i=1}^{3r-6}\dot{p}_i\frac{\partial f}{\partial p_i}.$$

The Calculation of Ionic Resonance Energies

RALPH G. PEARSON
Department of Chemistry, Northwestern University, Evanston, Illinois
(Received March 1, 1949)

A molecular orbital calculation is made of the bond energy between dissimilar atoms, A–B. The principle of the geometric mean and experimental bond energies between similar atoms are used to evaluate the exchange integral. The other parameter needed is the difference in coulombic energy of an electron on atom A and on atom B. This is related to the difference in Pauling's empirical electronegativity values. Numerical results are given for non-polar bonds and the best polar bonds and comparison is made with experimental bond energies.

INTRODUCTION

PAULING[1] first introduced the concept of "ionic resonance energy" to account for the experimental fact that a bond between two dissimilar atoms ($A-B$) is generally stronger than could be accounted for on the basis of either the arithmetic or geometric mean of the bond strengths between similar atoms ($A-A$ and $B-B$). His explanation in terms of a resonance between ideal covalent and ideal ionic structures is open to some criticism[2] but his general conclusion that the extra, or stabilization energy increased with increasing polarity of the bond is undoubtedly correct. An empirical equation was proposed in which the stabilization energy is proportional to the square of the difference in electronegativities of the bonded atoms. Mulliken[3] treated the problem of bonding between dissimilar atoms by a molecular orbital method and showed that Pauling's empirical equation was justified as an approximate solution to a more complex equation. The purpose of this paper is to extend Mulliken's work by some actual calculations of the "ionic resonance energies" and to compare with the values deduced from the most recent bond energies.

CALCULATIONS

The wave function for each of the two electrons in the bond $A-B$ will be represented as

$$\psi_{AB}=a\psi_A+b\psi_B \tag{1}$$

where ψ_A and ψ_B are appropriate atomic orbitals and a and b numerical coefficients. Solution of the secular equation gives for the lowest energy[3]

$$(1-S^2)E_1=\frac{q_A+q_B}{2}-S\beta_{AB}+\left\{\left(\beta_{AB}-S\left(\frac{q_A+q_B}{2}\right)\right)^2+\frac{(q_A-q_B)^2}{4}(1-S^2)\right\}^{\frac{1}{2}} \tag{2}$$

where q, β and S have their usual meaning. If the coefficients a and b were equal in (1) then the resulting energy would be

$$(1+S)E_0=\frac{q_A+q_B}{2}+\beta_{AB}. \tag{3}$$

The difference between E_1 and E_0 then represents the "ionic resonance energy" or the extra bond energy due to the polarity of the bond. In Pauling's terminology it would be due to the contribution of the ionic structure A^-B^+ (assuming A more electronegative than B). If the usual convention of neglecting the overlap integral S is followed (we shall consider the validity of this later) Eqs. (2) and (3) simplify considerably,

$$E_1=\frac{q_A+q_B}{2}+\left\{\frac{(q_A-q_B)^2}{4}+\beta_{AB}^2\right\}^{\frac{1}{2}} \tag{4}$$

$$E_0=\frac{q_A+q_B}{2}+\beta_{AB}. \tag{5}$$

It can readily be seen that E_1-E_0 will always be a positive quantity in terms of β (corresponding to a negative energy since q and β are negative). To calculate bonding energies we must evaluate the quantities β_{AB} and (q_A-q_B), the exchange integral and the difference in the coulombic energies of an electron on atoms A and B. The absolute values of q_A and q_B are not needed since they cancel in the calculation of the energy of formation of the bonded atoms from the separated atoms. For β_{AB} we shall make the reasonable assumption that it can be represented as the geometric mean of β_{AA} and β_{BB}.[4]

$$\beta_{AB}=(\beta_{AA}\beta_{BB})^{\frac{1}{2}}=\tfrac{1}{2}(E_{A_2}E_{B_2})^{\frac{1}{2}} \tag{6}$$

where E_{A_2} is the bond energy of $A-A$ etc. For q_A-q_B we shall follow Mulliken[3,5] and assume that this difference is equal to the difference between the term values for the separated atoms with the conditions that the separated atoms be maintained in the same valence state as for the equilibrium distance and that both electrons of the bond circulate over both nuclei. This leads to the approximation:

$$q_A-q_B=(I_A+E_A)/2-(I_B+E_B)/2, \tag{7}$$

[1] See L. Pauling, *The Nature of the Chemical Bond* (Cornell University Press, Ithaca, New York, 1940), Chapter II for a complete discussion.
[2] A. Burawoy, Trans. Faraday Soc. **39**, 79 (1943).
[3] R. S. Mulliken, J. Chem. Phys. **3**, 573 (1935).
[4] L. Pauling and J. Sherman, J. Am. Chem. Soc. **59**, 1450 (1937).
[5] R. S. Mulliken, J. Chem. Phys. **2**, 782 (1934).

where I refers to the ionization potential and E to the electron affinity for the atom in the appropriate state. The corrections for the state to be used in the calculations become involved for the polyvalent atoms but Mulliken has shown that, for the cases where calculations can be made, there is a close correspondence between the function $(I+E)/2$ and Pauling's empirical electronegativity function. Thus, expressing the energies in kcal.,

$$(I_A+E_A)/2-(I_B+E_B)/2=65(X_A-X_B) \qquad (8)$$

where X_A refers to Pauling's electronegativity value for atom A etc. We shall accordingly use the X values given by Pauling[1] for all calculations of q_A-q_B.

Table I shows the results of the calculations made. The quantity $-2\beta_{AB}$ is the bond energy of a pure covalent bond ($a=b$ in Eq. (1)),

$$-\beta\{4+[(X_A-X_B)^2(65)^2/\beta^2]\}^{\frac{1}{2}}$$

is the bond energy of the best polar bond, and E_{AB} is the experimental bond energy. Table II gives the experimental values of the single bond energies between similar atoms and the electronegativity values used.

Next let us consider the effect of including the overlap integral which was neglected in the preceeding calculations. If we define the new quantity

$$\beta_{AB}{}^*=\beta_{AB}-S\left(\frac{q_A+q_B}{2}\right), \qquad (9)$$

then Eqs. (2) and (3) become

$$E_1=\frac{q_A+q_B}{2}+\frac{-S\beta_{AB}{}^*+\{\beta_{AB}{}^{2*}+[(q_A-q_B)^2/4](1-S^2)\}^{\frac{1}{2}}}{1-S^2} \qquad (10)$$

$$E_0=\frac{q_A+q_B}{2}+\frac{\beta_{AB}{}^*}{1+S}. \qquad (11)$$

If the value of S is known, the $\beta_{AA}{}^*$ and $\beta_{BB}{}^*$ can be calculated from known bond energies between similar bonds as before. The use of the geometric mean for the evaluation of $\beta_{AB}{}^*$ leads to some difficulty, but if the principle of the arithmetic mean is used, and if a constant value of S is assumed, then it follows that

$$\beta_{AB}=\frac{\beta_{AA}+\beta_{BB}}{2} \qquad (12)$$

$$\beta_{AB}{}^*=\frac{\beta_{AA}{}^*+\beta_{BB}{}^*}{2}=\frac{E_{A_2}+E_{B_2}}{4}(1+S), \qquad (13)$$

which should be a fair approximation for bonds between atoms whose values of β are not too different.

Some calculations were made in this way of the bond energy of HCl with S equal to 0.0, 0.5 and 0.8. The corresponding energies are 100, 96 and 92 kcal. Similar results are obtained with other bonds. Evidently the bond energies are not sensitive to the value of S used, providing that a constant value can be used throughout. This is similar to the results of Wheland[6] who investigated the effect of the overlap integral on calculated resonance energies of aromatic compounds. The general conclusions drawn may not be true, of course, for bonds between atoms of quite different values of β and hence of the overlap integral.

[6] G. W. Wheland, J. Am. Chem. Soc. **63**, 2025 (1941).

TABLE I. Bond energies for dissimilar atoms.*

Bond	$-2\beta_{AB}$	$-\beta\left(4+\frac{(X_A-X_B)^2(65)^2}{\beta^2}\right)^{\frac{1}{2}}$	E_{AB} (Experimental)
H–Cl	77 kcal.	97 kcal.	103 kcal.
Br–Cl	51	53	53
I–Cl	45	59	50
O–Cl	44	55	49
C–Cl	68	76	78
Si–Cl	51	93	90
Ge–Cl	44	95	100
P–Cl	50	77	76
As–Cl	44	78	70
S–Cl	56	65	65
Li–Cl	39	136	119
Na–Cl	32	140	98
K–Cl	26	145	101
Rb–Cl	25	145	101
Cs–Cl	24	151	103
N–Cl	46	46	46
Si–O	39	117	103
C–O	52	83	80
N–O	35	48	52
C–S	66	66	62
C–N	54	63	66
I–Br	41	49	43
C–Br	61	64	67
P–Br	45	64	62
N–Br	41	43	45
C–H	91	95	98
N–H	62	85	93
O–H	60	109	110
S–H	75	79	83
P–H	68	68	76
As–H	59	59	57
Si–H	68	71	76
Li–H	52	88	58
Na–H	43	89	47
K–H	35	92	43
Rb–H	34	91	39
As–Br	40	66	58
Si–Br	46	80	76
Li–Br	35	122	105
Na–Br	29	127	88
K–Br	23	132	91
Rb–Br	23	132	91
P–I	40	44	42
As–I	35	44	43
C–I	54	54	52
Na–I	25	101	72
K–I	21	106	76
Rb–I	20	106	76
Cs–I	19	112	78

* The sources of these bond energies are Gaydon, *Dissociation Energies and Spectra of Diatomic Molecules* (Chapman and Hall, London, 1947); Skinner, Trans. Far. Soc. **41**, 645 (1945) and Pitzer, J. Am. Chem. Soc. **70**, 2140 (1948). The carbon-iodine value is from Butler and Polanyi, Trans. Far. Soc. **39**, 19 (1943). Generally only bond energies on which there is agreement to two or three kilocalories by the several sources are used in the tables. In several cases where one author's value was selected, care was taken to insure internal consistency with all bonds involving that element.

TABLE II. Bond energies for similar atoms.*

Element	Single bond energy	Electronegativity (X)
Hydrogen	104 kcal.	2.1
Chlorine	57	3.0
Bromine	46	2.8
Iodine	36	2.4
Lithium	26	1.0
Sodium	18	0.9
Potassium	12	0.8
Rubidium	11	0.8
Cesium	10	0.7
Phosphorous	44	2.1
Arsenic	34	2.0
Sulfur	54	2.5
Carbon	80	2.5
Oxygen	34	3.5
Nitrogen	37	3.0
Silicon	45	1.8
Germanium	34	1.7

*From the same sources as Table I.

DISCUSSION

Considering the crudities of the approximations used, the results in Table I are encouraging. It must be remembered that the comparison is to be made between experimental values of the bond energies and the values in the third column compared to the second column. Those cases where the agreement is poor are readily understandable. They are bonds which are highly polar and essentially ionic in nature. The calculated bond energies are always in excess of the observed. Now for such bonds the electronegativities used are not very good because the piling up of the electrons on the more negative atom will reduce the electronegativity of that atom and increase the electronegativity of the more positive atom. Hence the real difference in electronegativity becomes less and the "ionic resonance energy" is correspondingly reduced. For example, to give agreement with experiment in the case of sodium chloride, the X value of chlorine should be reduced by 0.35 unit and the X value of sodium increased by the same amount.

The difficulty really lies in the approximation of using one-half of the ionization potential and one-half the electron affinity to represent the term value of an electron on a combined atom. Actually the weight to be given to each quantity should depend on the plarity of the bond. For a highly positive atom the electron affinity will be of little importance because the probability of finding both electrons simultaneously on that atom is very small. For a highly negative atom the electron affinity will be of great importance because both electrons will be on that atom most of the time. The effect is clearly shown in the alkali hydrides. Hydrogen, which has a small electron affinity is forced to be highly negative in these compounds. Hence the true binding energy is much less than that calculated by Eq. (4) and in fact approaches the bond energy that would result if X_A was equal to X_B. Evidently the electronegativity value to be used for hydrogen in the hydrides is less than that used for the hydrogen in, say, hydrogen chloride.

The empirical equation developed by Pauling[1] for the "ionic resonance energy" is an expansion of Eq. (4) as was pointed out by Mulliken.[3] It corresponds to an average value of β equal to -46 kcal. This is somewhat larger than the values of β deduced from Table II (about -20 kcal.). The effect is to make the empirical equation fit the data over a wider range of electronegativity differences. Actually the energies calculated from the simplified equation and the more complete expression do not differ appreciably, the more complete equation being better for small electronegativity differences and the empirical equation being better for large electronegativity differences. Since Pauling's X values were originally derived from experimental "ionic resonance energies" it might appear illegitimate to use them now to calculate the same quantities. It is our purpose here to justify the substitution of electronegativity differences for differences in coulombic energies as given by Eqs. (7) and (8). One possible advantage of the more complete treatment developed here would be in its application to calculations of resonance energies and electronic distributions of systems involving more than one kind of atom.

Structural Investigations by Means of Nuclear Magnetism. I. Rigid Crystal Lattices

H. S. GUTOWSKY,* G. B. KISTIAKOWSKY, G. E. PAKE,**† AND E. M. PURCELL
Gibbs Chemical Laboratory and the Lyman Laboratory of Physics, Harvard University, Cambridge, Massachusetts
(Received March 7, 1949)

Experimental absorption line shapes at nuclear magnetic resonance are given for several simple assemblies of nuclei, with spin ½, in the solid state at temperatures between 90° and 95°K. Analysis of these data is facilitated by the theory of Van Vleck which relates the second moment of the absorption line in a rigid lattice to nuclear spins, gyromagnetic ratios, and internuclear distances, and which provides, therefore, an objective and general method for determining structural parameters from the experimental line shapes.

1,2-dichloroethane exhibits a proton resonance with line structure characteristic of nuclear magnetic moments interacting in pairs to produce the broadening of the absorption line. Consideration of both fine structure and second moment leads to an inferred H−H distance of 1.71±0.02A in the $-CH_2Cl$ group. In conjunction with the expected C−H bond distance of from 1.09A to 1.10A, this implies that the H−C−H bond angle is between 4° 30′ and 9° *less* than tetrahedral. Absorption line shapes for the proton resonance in 1,1,1-trichloroethane and ammonium chloride are given as characteristic respectively of equilateral three-spin and tetrahedral four-spin systems. Less conclusive studies of perfluoroethane and diborane are presented. A detailed analysis of data on ammonium fluoride, chloride, and bromide yields a value of 1.025±0.005A for the N−H distance in the ammonium ion. Some general aspects of the use of nuclear magnetism in structural investigations are discussed briefly.

1. INTRODUCTION

THE development of experimental methods[1,2] for observing nuclear magnetism has provided a means for investigating certain aspects of molecular and crystal structure.[3,4] A substance containing magnetic nuclei and subjected to a strong magnetic field displays a resonance absorption at some radio frequency. The frequency on which the absorption is centered depends only on the strength of the magnetic field and the gyromagnetic ratio of the nuclear spins involved. The width and shape of the absorption line, however, depend on magnetic interactions[3,5] among neighboring nuclei, and hence upon the configuration of atoms in the immediate vicinity of a magnetic nucleus. Not only the distances and angles characteristic of the local configuration are involved, but also the motion of a nucleus and that of its neighbors. It is therefore possible to infer something about the configuration and motion of a small group of atoms from a study of the shape of a nuclear magnetic absorption line, provided one is equipped with an adequate theory of the effects. We shall describe in this and subsequent papers a series of experiments that illustrate the application of the method to a number of substances. Although much remains to be done in refining both the theory and the experimental techniques, it appears that some new and useful structural information is accessible by the present means.

In this paper, the first of a projected series of three, we discuss the width and shape of absorption lines in structures that are *rigid* in the sense that the local configuration of atoms is effectively stationary or frozen for times as long as 10^{-4} to 10^{-5} seconds, except for the ever present thermal vibrations of the crystal lattice. If the lattice is rigid by this criterion, the shape of the absorption line does not differ sensibly from one that would be observed in an absolutely stationary configuration, and the calculation of the theoretical line shape for a hypothetical structure can proceed on the assumption of fixed positions for a given nucleus and its neighbors.

Lack of rigidity, in the above sense, is made evident in general by a marked narrowing of the absorption line, whose width therefore affords a clue to the existence of internal motion in the crystal.[6,7] In such cases it may be possible to infer something about the type of motion involved, and its rapidity. A second paper will describe results obtained with several molecular crystals that show evidence of internal motion. The third paper will describe a particularly striking case of internal motion, already reported briefly,[8] that of ammonium salts.

In these experiments the substances investigated were solids normally diamagnetic, except for the nuclear paramagnetism. The nucleus involved was the proton in all but one case, in which it was fluorine. The resonance absorption was observed at a frequency of 29 Mc/sec., by means of a radiofrequency bridge. The measurements extended over the temperature range +20° to −185°C.

2. THE STRUCTURE OF THE ABSORPTION LINE IN CERTAIN SIMPLE CASES

The application of a magnetic field $\mathbf{H}_0$ to a nucleus of spin I removes its spatial degeneracy and establishes a set of equally spaced Zeeman energy levels, $2I+1$ in number. The level spacing, in energy, is $g\beta H_0$, where β

* Now at Department of Chemistry, University of Illinois, Urbana, Illinois.
** Now at Department of Physics, Washington University, St. Louis, Missouri.
† Predoctoral Fellow of the National Research Council.
[1] Purcell, Torrey, and Pound, Phys. Rev. **69**, 37 (1946).
[2] Bloch, Hansen, and Packard, Phys. Rev. **69**, 127 (1946).
[3] G. E. Pake, J. Chem. Phys. **16**, 327 (1948).
[4] E. M. Purcell, Science **107**, 433 (1948).
[5] J. H. Van Vleck, Phys. Rev. **74**, 1168 (1948).
[6] Bloembergen, Purcell, and Pound, Phys. Rev. **73**, 679 (1948).
[7] N. L. Alpert, Phys. Rev. **75**, 398 (1949).
[8] H. S. Gutowsky and G. E. Pake, J. Chem. Phys. **16**, 1164 (1948).

is the nuclear magneton, 5.049×10^{-24} ergs/gauss, and $g\beta I$ is the nuclear magnetic moment. If $g\beta H_0$ is large compared to all other interactions involving the nuclear spin—as it always is in our experiments—a system composed of a large number of such nuclei can be described in terms of these $2I+1$ Zeeman levels and their population. Transitions from one to another of the levels may be induced by the application of a weak oscillatory magnetic field, at the frequency of resonance $\nu=g\beta H_0/h^{-1}$ and perpendicular to $\mathbf{H}_0$. For protons, as an example, with $H_0=10{,}000$ gauss, $\nu=42.6$ Mc/sec. In thermal equilibrium, the population of the levels corresponds to a Boltzmann distribution and there is a net absorption of energy from the radiofrequency field; it is this effect which is measured in our experiments.

However, in addition to the externally applied magnetic field, local magnetic fields originating with neighboring nuclear magnetic dipoles are effective in contributing small energy terms responsible, at least in part, for the finite width and structure of the absorption line. The Hamiltonian for the system of nuclear dipoles will be written as the sum of three terms:

$$\mathcal{H}=\mathcal{H}^{(0)}+\mathcal{H}^{(1)}+\mathcal{H}^{(2)}. \tag{1}$$

Here

$$\mathcal{H}^{(0)}=-\sum_j g_j\beta I_{zj}H_0, \tag{2}$$

represents the Zeeman energy of the nuclear dipoles in the large external magnetic field $\mathbf{H}_0$, which is taken in the $\mathbf{Z}$ direction, and

$$\mathcal{H}^{(1)}=\sum_{j>k} g^2\beta^2[\mathbf{I}_j\cdot\mathbf{I}_k r_{jk}^{-3}-3\mathbf{I}_j\cdot\mathbf{r}_{jk}\mathbf{I}_k\cdot\mathbf{r}_{jk}r_{jk}^{-5}] +\sum_{j,f} g_jg_f\beta^2[\mathbf{I}_j\cdot\mathbf{I}_f r_{jf}^{-3}-3\mathbf{I}_j\cdot\mathbf{r}_{jf}\mathbf{I}_f\cdot\mathbf{r}_{jf}r_{jf}^{-5}], \tag{3}$$

represents the mutual energy of the nuclear dipoles. In this equation $\mathbf{r}_{jk}$ is the vector connecting nuclei j and k, and r_{jk} is the internuclear distance. The subscripts j and k refer to the nuclear species at resonance, and the subscripts f refer to all other nuclear species in the sample.

The contribution $\mathcal{H}^{(2)}$ to the total Hamiltonian of the absorbing nuclei includes, for nuclei with spin $I>\frac{1}{2}$, an electric quadrupole energy proportional to the gradient of the crystalline electric field, as well as energy terms contributed by the electronic magnetic moments of paramagnetic ions, if any, in the lattice. We are considering only absorbing nuclei with spin $\frac{1}{2}$, and hence no electric quadrupole moments, so their quadrupole energies are zero. It is perhaps worthwhile to note that nuclei identified in Eq. (3) by subscripts f may possess electric quadrupole moments without affecting this conclusion. In addition, if attention is further restricted to diamagnetic samples, there will be no energy contributions from electronic magnetic moments and $\mathcal{H}^{(2)}$ may be disregarded completely in these applications.

Van Vleck[5] shows that, except where g_f is very nearly equal to g,[9] the only portion of $\mathcal{H}^{(1)}$ that is effective in broadening the absorption line at $\nu=g\beta H_0/h^{-1}$ is

$$\mathcal{H}_{\text{eff.}}^{(1)}=\tfrac{1}{2}g^2\beta^2\sum_{j>k}(\mathbf{I}_j\cdot\mathbf{I}_k-3I_{zj}I_{zk})r_{jk}^{-3}(3\cos^2\theta_{jk}-1) -g\beta^2\sum_{j,f} g_f r_{jf}^{-3}I_{zj}I_{zf}(3\cos^2\theta_{jf}-1), \tag{4}$$

where θ_{jk} is the angle between $\mathbf{r}_{jk}$ and $\mathbf{H}_0$. It is in considering $\mathcal{H}^{(1)}$ in the subsequent discussion that the nuclei are assumed to be in a rigid crystal lattice, i.e., nuclear motion, whether random or regular, does not occur at a high enough frequency or with a large enough amplitude to narrow the line from the breadth predicted on the basis of Eq. (4) for a static configuration. In principle, $\mathcal{H}_{\text{eff.}}^{(1)}$ may be treated as perturbing the Zeeman levels of $\mathcal{H}^{(0)}$, and the solution of this perturbation problem will yield the detailed structure of the

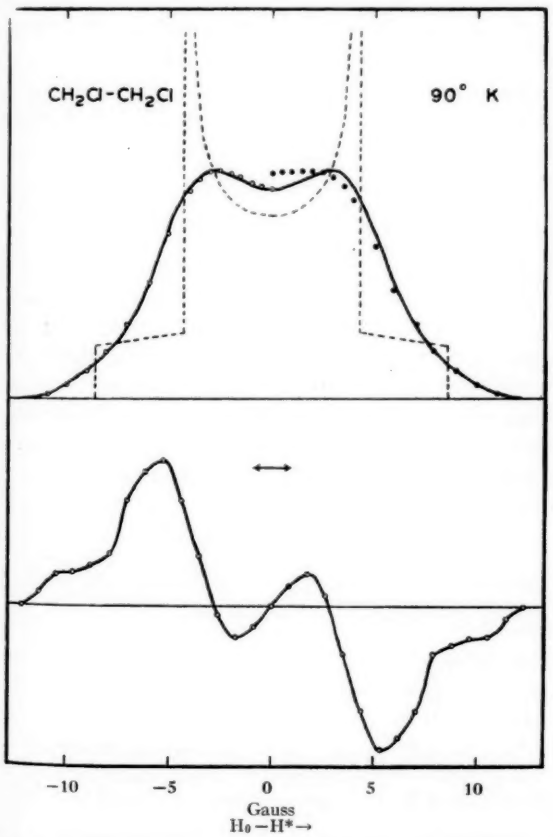

FIG. 1. A two-spin system with $I=\frac{1}{2}$: The proton magnetic resonance absorption line and its derivative in solid 1,2-dichloroethane at 90°K. The solid lines represent experimental data. In the upper part of the figure the open circles in the left-half are theoretical values computed for a proton separation of 1.70A and the points in the right-half are for 1.72A. The dashed curve is the theoretical line shape for a crystal powder with a proton separation of 1.70A and in which magnetic interactions are confined to pairs of nuclei.

[9] If two different nuclei should happen to have g-values such that the separation between their resonances is the order of the width of one of the resonances, perturbation methods appropriate for a continuum would be required. However, such a near coincidence of g-values is expected to be rare.

absorption line. This procedure was followed by Pake in studies of the proton resonance in crystalline hydrates in which each proton is predominantly in the local magnetic field of its partner in a given water molecule. The structure of the corresponding absorption line is given thus by a solution of the perturbation problem for a two-proton system.[3]

Experimental and theoretical results for a similar two-spin system, the protons in 1,2-dichloroethane, are shown in Fig. 1 for the crystal powder. In this molecule the small chlorine and the zero C^{12} nuclear magnetic moments and also the relatively large end-end intramolecular distances provide a system that to a good approximation can be considered as the simple two-spin case. The dashed curve in the upper part of Fig. 1 has the shape that would arise from a crystal powder in which the magnetic dipole interactions are confined completely to pairs of protons; the separation between peaks is $3\mu r^{-3}$, where $\mu=gI$ is the nuclear magnetic moment in nuclear magnetons[10] and r, the proton-proton distance, is taken as 1.70A. In reality, other neighboring nuclei and also the inhomogeneity of the external field H_0 contribute an additional broadening effect. The open and filled circles plotted in the upper part of the figure represent the smoothed out absorption lines that result when additional broadening is introduced according to a Gauss error function. The broadening functions used and the details of the calculations are discussed below in Section 6a. The lower part of the figure gives the first derivative of the absorption line which is the quantity measured by the modulation type apparatus used.[3] The solid line drawn in the upper part of the figure is the line shape obtained by graphical integration of the observed derivative.

Although the two-spin problem is relatively simple, the addition of even one more spin to the "elementary dipole-interaction cell" leads to considerable complexity. Experimental results for 1,1,1-trichloroethane CH_3-CCl_3, for example, show a fine structure of the proton line at temperatures below about 120°K. (See Fig. 3 in Section 6b.) The structure of this line is determined in main by the magnetic interactions of the three protons which lie presumably on the vertices of an equilateral triangle normal to the C−C axis of the 1,1,1-trichloroethane molecule. Calculation of the structure of the line is complicated by the degeneracy of the Zeeman levels for which the three protons have a resultant magnetic quantum number $m_I=+\frac{1}{2}$ or $-\frac{1}{2}$. Mr. R. Bersohn[11] has solved the secular equation arising from these degenerate levels, obtaining the effects on the absorption line of the magnetic dipole interaction. The transition probabilities, which are relatively involved functions of triangle orientation, have been obtained, and also the resultant line shape for a powder sample. A detailed discussion of the equilateral three-spin system, and also an analysis of four like spins in a tetrahedral configuration, will be published at a later date. It is noteworthy here, however, that the general character of the experimental absorption line in Fig. 3 is obtained in the calculation of Bersohn.

3. COMPUTATION OF THE SECOND MOMENT OF THE ABSORPTION LINE

With the inclusion of more than three nuclei in the elementary dipole-interaction cell, detailed perturbation calculation of the line structure becomes prohibitively tedious. A more easily applied analysis of the experimental data on line structure is provided by Van Vleck,[5] who has expressed $\langle\nu^2\rangle_{Av}$, the average value of the frequency-square over the absorption line, as the trace of a matrix. Since it is a well-known theorem of transformation theory that the trace is independent of the representation, one is free to compute the trace for any representation, in particular for that in which each nuclear spin is individually space quantized. In this way, the previously encountered difficulty in solving the secular equation is avoided.

The second moment of the absorption line is defined as the average value of $(\nu-\nu_0)^2$ over the symmetrical line shape;

$$\langle(\nu-\nu_0)^2\rangle_{Av}=\langle(\Delta\nu)^2\rangle_{Av}=\langle\nu^2\rangle_{Av}-\nu_0^2. \tag{5}$$

Experimentally it is more convenient to vary the external magnetic field H_0, and thus to vary ν_0, instead of ν, and in these experiments the second moment is measured as the average value of $(\Delta H)^2=(H_0-H^*)^2$ over the line shape. Here H^* is the resonance value of the external magnetic field for an applied radiofrequency ν_0. We shall denote the root-second-moment, $\langle(\Delta H)^2\rangle_{Av}^{\frac{1}{2}}$, by ΔH_2 which is related to the quantities in Eq. (5) as follows:

$$\Delta H_2=(h/g\beta)\langle(\Delta\nu)^2\rangle_{Av}^{\frac{1}{2}}. \tag{6}$$

From Eq. (4), the value of the second moment may be written according to Van Vleck as

$$\Delta H_2^2=\frac{3}{2}\frac{I(I+1)}{N}g^2\beta^2\sum_{j>k}(3\cos^2\theta_{jk}-1)^2r_{jk}^{-6}$$
$$+\frac{1}{3}\frac{\beta^2}{N}\sum_{i,f}I_f(I_f+1)g_f^2(3\cos^2\theta_{if}-1)^2r_{if}^{-6}, \tag{7}$$

where N is the number of the nuclei at resonance which are present in the elementary dipole-interaction cell. Only magnetic dipole broadening is considered in obtaining this relation.

Eq. (7) gives the value of the second moment for a particular orientation of the dipole-interaction cell with respect to $\mathbf{H}_0$. However, it is usually necessary to work

[10] The values used for nuclear magnetic moments and nuclear spins are those given by H. H. Goldsmith and D. R. Inglis, Brookhaven National Laboratory Report BNL-I-5, October 1, 1948. Isotopic abundances are those appearing in the Sept. 1946 Segré Chart, available in Vol. I. "The Science and Engineering of Nuclear Power" (Addison-Wesley Press, Inc., Cambridge, Mass., 1947).

[11] R. Bersohn, private communication.

with crystalline powders, in which the constituent microcrystals are presumed to be randomly distributed among all directions in space. Averaging $(3\cos^2\theta_{jk}-1)^2$ in Eq. (7) over a sphere, one obtains for powder samples the relation

$$\Delta H_2^2=\frac{6}{5}\frac{I(I+1)}{N}g^2\beta^2\sum_{j>k}r_{jk}^{-6}+\frac{4}{15}\frac{\beta^2}{N}\sum_{j,f}I_f(I_f+1)g_f^2r_{jf}^{-6}. \quad (8)$$

To compute the second moment by this expression involves merely a knowledge of the g-values, nuclear spins, and inter-atomic distances. Experimental values of ΔH_2^2 may be computed directly from the measured derivative of the absorption line, as illustrated by Pake and Purcell,[12] and comparison with theoretical values may help determine the validity of any assumed structure. The dependence of the second moment on I_f and also the calculations in Section 6c for diborane suggest nuclear spins may be obtained in favorable instances from observed second moments in rigid lattices of known structure.

In principle, what we have called the "elementary dipole-interaction cell" should include the entire sample. However, the inverse sixth power of the internuclear distances in Eq. (8) allows one to ignore in a first approximation neighbors outside the crystal unit cell, and, for example, in certain molecular crystals, the second moment may be computed to fair approximation using the molecule itself as the elementary cell. Thus, in the application of Eq. (8) to the proton resonance in diborane, B_2H_6, the fundamental cell was assumed to be the B_2H_6 molecule, so that $N=6$, and the only "foreign" nuclei are the two boron nuclei. Of course, to obtain accuracy it is essential to know the basic elements of the crystal structure and to compute the broadening effects of first nearest and even second or third nearest neighbors outside the elementary dipole-interaction cell. Even so, evaluation of ΔH_2^2 from Eq. (8) compares favorably with the complexity often met in the analysis of data obtained by other methods for investigating molecular structure. Moreover, x-ray and electron diffraction methods yield relatively inexact information concerning the location of light nuclei, particularly protons, whose magnetic properties are ideal for resonance absorption experiments.

4. APPARATUS AND EXPERIMENTAL PROCEDURE

With the exception of a cooling assembly, the apparatus and experimental procedure used in these experiments was the same as that previously reported.[3] The disappearance of the structure of the absorption lines in liquids and the low melting points of most of the compounds of interest required the use of low temperatures. The $\frac{3}{4}$-in. gap of the available permanent magnet prevented introduction of a dewar, so cooling was effected by conduction.[8] A sectional view of the all copper and brass design is shown in Fig. 2. The block containing the sample and radio-frequency coil is of copper and the double bottomed can is of brass. The connection to the r.-f. bridge circuit is made via the coaxial brass tubing which was silver plated for higher electrical conductivity. The inner tube is insulated from the block and outer brass tube by "Teflon" spacers (duPont Company perfluoro polyethylene). Though conduction cooling is inherently inefficient, the design proved satisfactory for these experiments. Temperatures as low as 90°K were obtained with liquid nitrogen, which was used at a rate of four to five liters an hour. We are grateful for the generous cooperation of the Linde Air Products Company who supplied the liquid nitrogen.

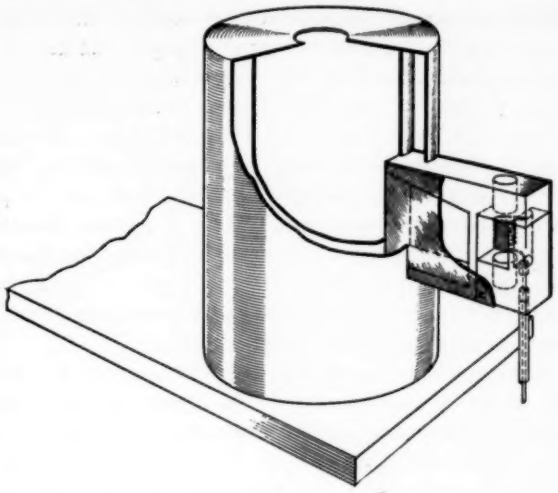

FIG. 2. Cooling assembly.

Solid and liquid samples were placed in standard pyrex test tubes, 1-cm O.D.×11-cm long, stoppered to prevent condensation of water vapor on the sample. For gases, the test tubes were fused on 500 cc or liter flasks which were evacuated and filled from a vacuum system. No single crystals were used in these experiments. The r.-f. coil in the cooling block in which the test tubes were inserted was of the same dimensions used previously.[3] The temperature was measured by means of a copper-constantan thermocouple inserted directly in the samples. The lowest attainable temperatures varied somewhat among the samples, depending on thermal contact and heat conductivity.

The line shapes were plotted at constant frequency, which was 29.0 Mc/sec. for proton resonances and 27.2 Mc/sec. for F^{19} resonances. The magnetic field was modulated at 30 cycles/sec. to provide the sensitivity essential for observing the broad, weak signals characteristic of solids. Therefore,[6] the directly measured quantity is the first derivative of the absorption line, provided the ratio of the modulation to line width is

[12] G. E. Pake and E. M. Purcell, Phys. Rev. 74, 1184 (1948).

sufficiently small. In general, the smallest modulation compatible with adequate signal strength was used; the total modulation sweep (two amplitudes) is represented in the figures by horizontal arrows drawn to scale. The usage of the term "line width" herein follows a previous definition[8] of δH as the width in gauss between the most widely separated maximum and minimum on the derivative curve. In most instances the line shape obtained by graphical integration is shown as well as the directly observed first derivative. The ordinate in the figures represents the intensity of the absorption signal and is given in arbitrary units for each sample.

Brief mention may be made of two sources of trouble for which allowance should be made in any future design. When modulation larger than four gauss was used, sufficiently strong eddy currents were induced in the cooling block at low temperatures to vibrate the whole assembly, thereby giving a spurious 30 cycle signal. In our apparatus this was eliminated by driving bakelite shims between the cooling block and the pole faces. The other source of difficulty was the temperature dependence of the r.-f. bridge circuit. The capacities in the sample arm of the circuit were located in a brass box joined to the cooling block by three inches of the thin-walled coaxial brass tubing, which also maintained thermal contact. No attempt was made to use capacities with low or balanced thermal coefficients and this, perhaps as well as dimensional changes in the coil and cooling block, caused pronounced balance drifts on cooling or warming. Moreover, balance instability was markedly greater at low temperatures.

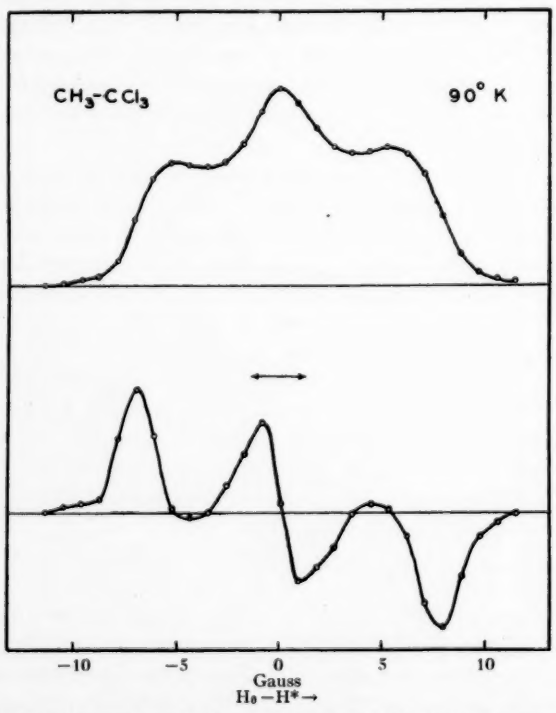

FIG. 3. An equilateral three-spin system with $I=\frac{1}{2}$: The proton magnetic resonance absorption line and its derivative in solid 1,1,1-trichloroethane at 90°K.

5. MATERIALS

The sources of the various samples investigated are given below:

CH_2Cl-CH_2Cl 1,2-dichloroethane (ethylene chloride): C.P., Eastman Kodak Company, 132.

CH_3-CCl_3 1,1,1-trichloroethane (methyl chloroform): Eastman Kodak Company, practical grade material, P 3613, purified by recrystallization, infra-red spectroscopically pure.

C_2F_6 perfluoroethane (hexafluoroethane; ethforane): We are indebted to Professor J. H. Simons, Fluorine Laboratory, Pennsylvania State College, for the loan of this sample. Undoubtedly 95 percent pure and possibly better than 98 percent; however, it was less than 99.6 percent pure. Possible impurities in order of their probable concentration are CHF_3, $CBrF_3$, C_2HF_5, C_2BrF_5.

NH_4F Ammonium fluoride: C.P., Eimer and Amend.

NH_4Cl Ammonium Chloride: reagent grade, General Chemical Co.

NH_4Br ammonium bromide: analytical reagent, Mallinckrodt Chemical Works.

$B_2{}^{10}H_6$ diborane: 96±0.4 percent B^{10}. This sample was prepared by the reaction between $B^{10}F_3$ etherate and an ether solution of lithium aluminum hydride.[13] The latter was supplied through the kindness of Dr. A. E. Finholt, Metal Hydrides, Inc., Beverly Mass. The $B^{10}F_3$ was generated by the thermal decomposition, under vacuum, of the $B^{10}F_3$:CaF_2 complex obtained from the Clinton Laboratories with the approval of the Isotopes Branch, AEC. The diborane was purified by repeated passage through acetone-dry ice and melting CS_2 traps; the vapor pressure of the diborane at the latter temperature was approximately 235 mm.

C_2H_4 ethylene: 99.5 percent, USP, Ohio Chemical and Mfg. Company.

C_2H_6 ethane: 95 percent, Ohio Chemical and Mfg. Company.

Si_2H_6 disilane: The sample was prepared by the reaction of Si_2Cl_6 with an ether solution of lithium aluminum hydride.[14] The Si_2Cl_6 was at least 95 per-

[13] Finholt, Bond, Jr., and Schlesinger, J. Am. Chem. Soc. **69**, 1199 (1947).

[14] Finholt, Bond, Jr., Wilzbach, and Schlesinger, J. Am. Chem. Soc. **69**, 2692 (1947).

cent pure and was generously supplied by Prof. W. C. Schumb of M.I.T. The disilane was purified in the same fashion as the diborane. The most likely impurity is SiH_4 which was removed in main by discarding the most volatile third of the preparation.

6. RESULTS

a. 1,2-dichloroethane: a two-spin system.

The derivative curve observed for the proton resonance in 1,2-dichloroethane at 90°K is given in Fig. 1. The line shape is typical of a crystal powder in which magnetic dipole interactions are confined mainly to proton pairs. Following the procedure of Pake,[3] one finds by inspection of the line shape that the doublet separation $3\mu r^{-3}$ is about 8.8 gauss, which corresponds to an H—H separation of approximately 1.69A. The near agreement of this value with other determinations,[15] as well as our observation that the line width and shape remain essentially the same from 90°K to 165°K, indicates that the 1,2-dichloroethane molecules may be treated as stationary over this temperature range. Thus the observed line broadening can be used in conjunction with Eq. (8) to obtain quantitative structural information. The second moment of the derivative curve given in Fig. 1 is 18.2 gauss.[2] Two other curves, not quite as symmetrical and not shown here, give values of 16.4 and 16.6 gauss.[2] However, we will confine our attention to the most symmetrical curve observed for each sample, as it is considered most reliable.[16]

Contributions to the observed second moment have been classed as arising from magnetic field inhomogeneity, intra- and also intermolecular magnetic dipole interactions. With the permanent magnet used in these experiments, the broadening by field inhomogeneity of the already broad lines in solids is comparatively very small. The line width δH in liquids is often fixed by the field inhomogeneity,[6] and the line widths of about 0.3 to 0.4 gauss observed for liquids using this magnet indicate that the inhomogeneity contribution to the second moment is only 0.02 to 0.04 gauss^2 at the most.[17] This contribution is neglected therefore.

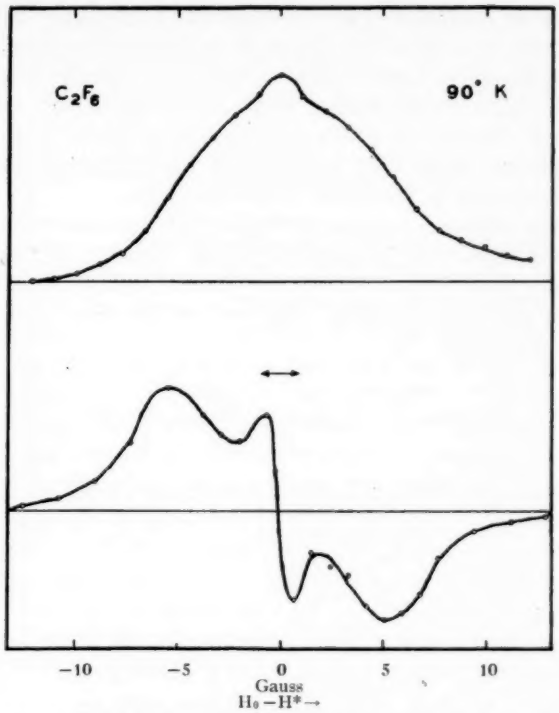

FIG. 4. The fluorine magnetic resonance absorption line and its derivative in solid perfluoroethane at 90°K.

Considering next the intramolecular broadening, by assuming tetrahedral bond angles, a trans-staggered C_{2h} configuration,[18] and C—H, C—Cl, and C—C bond distances[15] of 1.10, 1.78, and 1.54A respectively, Eq. (8) gives 12.56 gauss^2 for a single molecule; of this only 0.05 gauss^2 is caused by chlorine and a total of 1.94 gauss^2 is external to a given proton pair. This does not include the effects of the small percentages of deuterium and C^{13}. However, not only are both of these effects negligibly small (about 0.10 gauss^2) but they are also opposite in sign and effectively cancel. Inasmuch as the crystal structure of 1,2-dichloroethane is not available, an exact calculation of the intermolecular broadening is not possible. However, ethane provides a means of estimating an upper limit to this quantity, since the introduction of the larger chlorine atoms reduces the closeness of packing of the remaining hydrogen atoms. The molecular[15] and crystal[19] structure of ethane gives an approximate intermolecular broadening of 9 gauss^2. Simple removal of a proton from each CH_3 group, without allowing for increase of intermolecular distances, reduces the second moment to $\frac{2}{3}$ of the ethane value. Thus 6 gauss^2 may be taken as a quantity greater than the actual intermolecular contribution. When combined with the intramolecular broadening of 12.6 gauss^2, a theoretical second moment of 18.6 gauss^2 results, which

[15] Simmons, Gordy, and Smith, Phys. Rev. **74**, 243 (1948); L. G. Smith, J. Chem. Phys. **17**, 139 (1949).

[16] Asymmetry of data is caused by changes in the zero of the apparatus, and also by drifts in the r.-f. bridge balance which results in curves intermediate between absorption and dispersion (see reference 6). The difficulty of establishing the resonance center accurately in these curves and the sensitivity of the second moment to the choice of center combine to invalidate such data. However, they are included for qualitative comparison only, in the absence of other results.

[17] For a perfect Gaussian line shape $\delta H/\Delta H_2=2$. Actual line shapes appear to be intermediate between Gauss and Lorenz functions (see reference 12) and observed values of $\delta H/\Delta H_2$ vary between 2 and 3. We assume herein that the second moment of the inhomogeneity broadening can be added to the magnetic dipole broadening. This is rigorous for Gaussian functions.

[18] G. Herzberg, *Infrared and Raman Spectra of Polyatomic Molecules* (D. Van Nostrand Company, Inc., New York, 1945), p. 346 ff.

[19] R. W. G. Wyckoff, *The Structure of Crystals* (The Chemical Catalog Company, Inc., New York, 1931), second edition, p. 381; H. Mark and E. Pohland, Zeits. f. Krist. **62**, 103 (1925).

is to be compared with the observed 18.2 gauss². The agreement is fortuitous since the actual intermolecular broadening is undoubtedly considerably smaller than the suggested maximum of 6 gauss². Moreover, the H−H distance of 1.80A in the assumed model is prohibitively larger than the value of 1.69A suggested by the qualitative line shape considerations.

The difficulty imposed by the lack of crystal structure information may be resolved in this instance by combining line shape and second moment considerations. The line shape function, $f(\mathrm{H})$, for the two-spin system has been given[3] as

$$f(\mathrm{H})=\int_{-\infty}^{+\infty} p(\mathrm{H}_0-\mathrm{H}^*)S(\mathrm{H}-\mathrm{H}_0)d\mathrm{H}_0, \qquad (9)$$

where $p(\mathrm{H}_0-\mathrm{H}^*)d\mathrm{H}_0$ is the probability that a fine structure component line has its center in the region $d\mathrm{H}_0$ and $S(\mathrm{H}-\mathrm{H}_0)=\exp[-(\mathrm{H}-\mathrm{H}_0)^2/2(\Delta\mathrm{H}_2^2)_E$ takes into account broadening $(\Delta\mathrm{H}_2^2)_E$ external to the pair. Theoretical line shapes were computed for H−H distances of 1.70 and 1.72A, that is for α's of 4.30 and 4.15 gauss and $(\Delta\mathrm{H}_2^2)_E$ of 3.4 and 4.4 gauss² respectively. The latter were obtained by subtracting the second moment contribution of the pair, $0.8\alpha^2$, from the experimental value of 18.2 gauss². α is defined as $(3/2)\mu r^{-3}$. The results are shown in Fig. 1. Agreement between the experimental line shape and the points computed for an H−H distance of 1.70A is reasonable and it is suggested on the basis of the data available that the distance is 1.71±0.02A. This value gives an H−C−H angle between 100° 20′ and 103° 40′ if the C−H bond distance is 1.10A, or between 101° 40′ and 105° 0′ if the C−H bond distance is 1.09A. Since these possibilities are significantly smaller than 109° 28′, the results indicate a distortion of the bond angles from tetrahedral. When the crystal structure be comes known it can be used to evaluate the intermolecular broadening of the line and thereby give a check on the proposed H−H distance, which corresponds to intermolecular broadening of about 1.5 gauss².

b. 1,1,1-trichloroethane: an equilateral three-spin system.

The measured derivative of the proton resonance in 1,1,1-trichloroethane at 90°K and the corresponding absorption line are given in Fig. 3. These data are presented primarily for their bearing on the matter of the line shape for the three-spin system discussed in Section 2. The second moment of the absorption line is 18.7 gauss² which is smaller than the intramolecular value of 21.2 gauss² computed using the same bond distances as for 1,2-dichloroethane and assuming tetrahedral angles. When allowance is made for the broadening by neighboring molecules, the experimental value is approximately 5 gauss² too small; this is not too surprising, for the line width, which undergoes a transition[8] in the region 135° to 155°, still may not have reached a constant value at 90°K. However, it is a good example of a three-spin system, for the chlorine broadening is very small, 0.02 gauss², and the intermolecular broadening is probably not much more than 2 to 3 gauss². The substance should be investigated at lower temperatures for if the reported second moment is the rigid lattice value, then there is appreciable distortion of the H−H distances from the assumed values.

c. Perfluoroethane: an externally broadened three-spin system.

The derivative curve observed for the fluorine resonance in perfluoroethane at 90°K and the corresponding absorption line are given in Fig. 4. Data on this compound are of interest in connection with the magnitude of the intermolecular broadening and its effect on line shape. Also a check is furnished on the effect of modulation. The second moment of the curve shown in Fig. 4 is 14.90 gauss²; it was observed using a rather high modulation of 1.8 gauss. Another equally symmetrical curve, not shown here, which was obtained with 1.0 gauss modulation, has a second moment of 15.35 gauss², indicating that the modulations used do not perturb the observations appreciably.[20] The intramolecular broadening in perfluoroethane is 7.45 gauss², based on a D_{3d} configuration with tetrahedral angles and C−F and C−C bond distances of 1.35 and 1.45A respec-

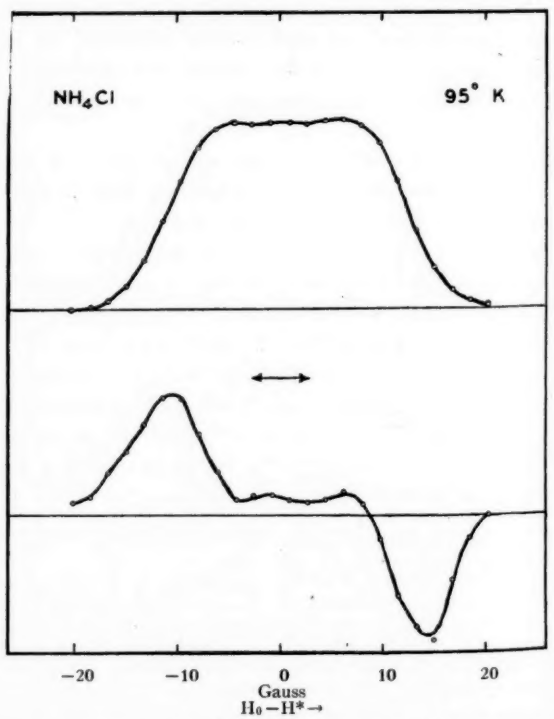

FIG. 5. A tetrahedral four-spin system with $I=\frac{1}{2}$: The proton magnetic resonance absorption line and its derivative in ammonium chloride at 95°K.

[20] These data were observed using a Teflon coil form external to the r.-f. coil containing the sample. While fluorine in the Teflon contributed to the signal, other observations indicate such contributions to the second moment were small.

TABLE I. The N−H bond distance in the ammonium ion† in ammonium halides.

X	$(\Delta H_2^2)_0$ at 95°K	$(\Delta H_2^2)_{H-X}$	$(\Delta H_2^2)_{H-H'}$	N−H distance in NH_4^+
F	58.5 gauss²	3.0 gauss²	4.7 gauss²	1.024A
Cl	57.0±3.0	0.1	6.4	1.025±0.01
Br	51.8	0.7	4.5	1.039*

* Approximate only due to incomplete rigidity of crystal lattice.
† An electron diffraction value of 0.95±0.07Å has been given by V. E. Lashkarev and I. D. Usyskin, C.A. **28**, 386 (1934).

tively.[21] Crystal structure data are not available to give an independent evaluation of the intermolecular broadening; however, the difference of 7.65 gauss² between the average experimental second moment and the intramolecular broadening is perhaps a bit large* when compared with the value of 9 gauss² estimated for ethane. The distortion of the line shape from the three-spin case, as observed in 1,1,1-trichloroethane, is probably a result of the large interactions external to each three-spin system, in which the broadening is only 5.5 gauss². Although perfluoroethane shows a sharp line-width transition at about 105°K, the line width is constant for nearly ten degrees above 90°K and this, along with the above data, indicates that the crystal lattice may be treated as stationary at 90°K.

d. The ammonium ion: a tetrahedral four-spin system.

Various data on the proton resonance have been reported earlier[3] for several ammonium salts, including a value for the N−H distance within the ammonium ion. Here, the details are given of a more exact calculation of this distance. Figure 5 shows the derivative curve observed for the proton resonance and the corresponding absorption line in ammonium chloride at 95°K. Line width versus temperature curves for ammonium fluoride and chloride indicate that the crystal lattice is rigid in these salts at 95°K. Ammonium bromide exhibits a line-width transition at 108°K and its absorption line may not have reached a rigid lattice second moment value at 95°K. At this temperature the derivative curve for the bromide is very similar to that given for the chloride, with a shorter plateau in the center. In the fluoride this plateau is completely absent. Experimental values of the second moment at 95°K are 58.5, 57.0±3.0, and 51.8 gauss² for the fluoride, chloride, and bromide respectively. The second moment for the chloride is from two acceptable derivative curves.

Four types of dipole interactions broaden the proton absorption lines in the ammonium halides, NH_4X. These are: (a) H−H in a given ammonium ion, (b) N−H in a given ammonium ion, (c) H−X, and (d) H−H in different ammonium ions. That is, the observed second moment $(\Delta H_2^2)_0$ is set equal to

$$(\Delta H_2^2)_0=(\Delta H_2^2)_{H-H}+(\Delta H_2^2)_{N-H}+(\Delta H_2^2)_{H-X}+(\Delta H_2^2)_{H-H'} \quad (10)$$
$$=\frac{56.50}{r^6}+\frac{2.21}{r^6}+(\Delta H_2^2)_{H-X}+(\Delta H_2^2)_{H-H'},$$

where r is the N−H distance in the ammonium ion, for which a tetrahedral configuration is assumed. The first two of the terms in Eq. (10) are very sensitive to r whereas the last two are not. So if the latter are computed for an approximate value of r, its accurate value can be computed directly from Eq. (10).

The crystal structure of ammonium fluoride is hexagonal, of the ZnO type.[22] $(\Delta H_2^2)_{H-X}$ and $(\Delta H_2^2)_{H-H'}$ were computed assuming a value of 1.025A for r, using

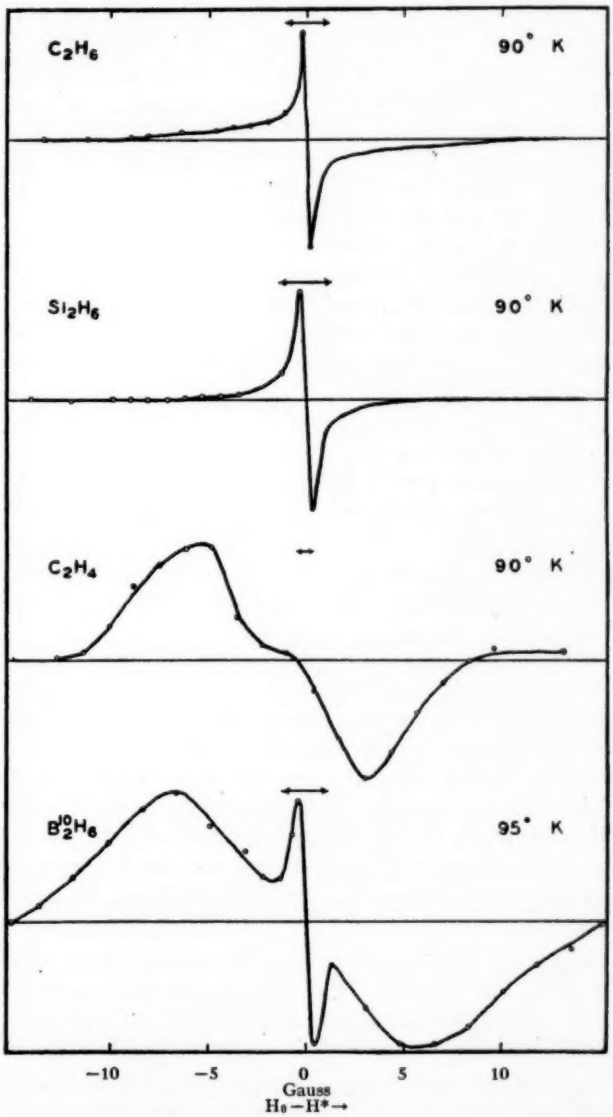

FIG. 6. Derivatives of the proton magnetic resonance absorption lines in ethane, disilane, ethylene, and diborane at 90° to 95°K.

[21] E. L. Pace and J. G. Aston, J. Am. Chem. Soc. **70**, 566 (1948).
* *Note added in proof.*—Recent reports [see e.g. W. F. Edgell and A. Roberts, J. Chem. Phys. **16**, 1002 (1948)] suggest a smaller C−F distance. The resulting increase in the computed intramolecular broadening provides an adequate interpretation of this apparent discrepancy.
[22] W. Zachariasen, Zeits. f. physik. Chemie **127**, 218 (1927).

TABLE II. Theoretical calculations of ΔH_2^2 for the proton absorption line in diborane as a function of structure and nuclear spin I of B^{10}.

Model	$(\Delta H_2^2)_{H-H}$	$(\Delta H_2^2)_{B-H}{}^{I=1}$	$(\Delta H_2^2)_{B-H}{}^{I=3}$	$(\Delta H_2^2)_E$	$\Delta H_2^2(I=1)$	$\Delta H_2^2(I=3)$
ethane-like	9.0 gauss^2	1.9 gauss^2	7.6 gauss^2	7.5 gauss^2	18.2 gauss^2	24.1 gauss^2
ethylene-bridge	17.1	2.7	10.7	5.5	25.3	33.3
4 proton bridge	47.3	2.7	10.4	~7	57.0	64.7

in this instance the room temperature unit cell dimensions. Neither the x-ray data nor simple electrostatics serve to establish completely the angular orientation of the ammonium ions in the unit cell. The interionic broadening is dependent on the orientation, with $(\Delta H_2^2)_{H-F}$ varying from 2.5 to 3.8 gauss^2 and $(\Delta H_2^2)_{H-H'}$ from 4.3 to 5.0 gauss^2. An orientation, in which closest interionic distances are the sum of ionic radii, gives values of about 3.0 and 4.7 gauss^2. The effect of low temperature on the unit cell dimensions will introduce a small positive correction, less than the uncertainty in the adapted intermediate values. The substitution of these values in Eq. (10) yields 1.024A for the N−H bond distance in ammonium fluoride.

The crystal structure of ammonium chloride is cubic, CsCl type, and the size of the unit cube has been reported[23] as 3.820A at 88°K. Electrostatic considerations suggest that the ammonium ion at the center of the unit cube has a C_2 axis perpendicular to a cube face, with a plane of symmetry which contains the C_2 axis and the diagonal of the cube face. On this basis $(\Delta H_2^2)_{H-Cl}$ and $(\Delta H_2^2)_{H-H'}$ were determined to be 0.1 and 6.4 gauss^2 respectively. The application of Eq. (10) to these values gives an r of 1.025±0.01A.

A similar set of calculations was made for ammonium bromide, employing the crystal structure[24] at 128°K. The larger apparent N−H bond distance of 1.039A in this instance is a probable result of motion in the crystal lattice at 95°K. $(\Delta H_2^2)_0$ at 101°K, only six degrees warmer, was 40 gauss^2, so the value for r in the bromide may be considered merely as qualitative, an upper limit.

The various results are summarized in Table I. The close agreement between the N−H distances of 1.024 and 1.025±0.01A in the fluoride and chloride is fortuitous perhaps, in view of the hydrogen bonding in the fluoride. Moreover, only one satisfactory derivative curve was obtained for the fluoride, and the signal with this compound was weak, with a resultant decrease in accuracy. The N−H bond distance in the ammonium ion may be considered as 1.025±0.005A on the basis of these data.

e. Diborane.

The initial impetus to our research program was the possibility of investigating the structure of diborane.[25] The results reported herein for diborane are inconclusive, primarily since definite proof is lacking for the rigidity of the crystal lattice at the lowest temperature obtained in our apparatus. However, diborane is an excellent example of a type of structural problem to which the methods of nuclear magnetism are well suited.

Until the rotational structure of certain infra-red bands was reported recently[26] as favoring the ethylene-bridge model, there was little evidence clearly supporting either the ethane-like or the ethylene-bridge structure for diborane. Prior to this, the successful use of nuclear magnetic experiments to obtain an accurate proton separation in a two-spin system[3] suggested to us that it might be possible to apply the same methods to the more complex diborane case. The diborane was prepared with concentrated B^{10} for at that time the spin of B^{10} was considered to be 1 and its nuclear magnetic moment 0.598; thus B^{10} would give markedly smaller perturbing effects on the proton absorption line than the normally predominant (81.6 percent) B^{11} of spin $\frac{3}{2}$ and moment 2.686. A typical derivative curve observed for the proton resonance in this diborane at a temperature of about 95°K is given in Fig. 6. The second moment of this curve is 27.0 gauss^2. The second moments of two other curves observed at temperatures between 90 and 95°K are 23.0 and 23.5 gauss^2. The first of these has a pronounced zero drift while the second is slightly asymmetric. These values have a spread larger than usual since they were observed in the initial experiments at a high noise level before stabler operating conditions were obtained. The melting point of diborane is 107.7°K and the data were obtained at temperatures only 12 to 18° lower, so it is possible that the observed line was narrowed by some residual molecular motion in the solid; it was not convenient to check line width *versus* temperature in this narrow range to verify lattice rigidity.

Theoretical calculations of the second moment are summarized in Table II for three models which have been proposed[25] for diborane. The intermolecular broadening $(\Delta H_2^2)_E$ was calculated from the reported crystal structure;[19] the B−H contributions to this term are small so the same value can be used for B^{10} spins of 1 or 3. These results were interpreted[8] earlier as affording support for the ethylene-bridge structure, using the then accepted value of 1 for the nuclear spin of B^{10}. However, since that time an investigation[27] of the spin of B^{10} has given a value of 3, and comparison of the

[23] L. Vegard and S. Hillesund, Anhandl. Norske Vid-Akad. Oslo, Mat-Naturv. Kl. No. 8 (1942); Chem. Zentr. I, 930 (1943).
[24] J. Weigle and H. Saini, Helv. Phys. Acta 9, 515 (1936).
[25] For general reviews of the problem see J. H. Bauer, Chem. Rev. 31, 43 (1942); R. P. Bell and H. J. Emeléus, Quart. Rev. 2, 132 (1948).
[26] W. C. Price, J. Chem. Phys. 15, 614 (1947); 16, 894 (1948).
[27] Gordy, Ring, and Burg, Phys. Rev. 74, 1191 (1948); M. Goldhaber, Phys. Rev. 74, 1194 (1948).

corresponding theoretical second moments with the experimental data is inconclusive. In addition to possible narrowing of the absorption line by molecular motion, any measurement of the second moment tends to be low because the signal is called zero, of necessity, when it becomes about equal to noise. But such a decision cuts off the tails of the absorption line, which give a considerable contribution to the second moment. Still, the differences between the theoretical second moments for the models are large enough so that in principle nuclear magnetism can distinguish the correct one. Thus, it is planned to determine the second moment at lower temperatures and at a lower noise level that should permit conclusive comparisons.

The derivative curves shown in Fig. 6 for the proton resonance in diborane, ethylene, ethane and disilane indicate an interesting similarity between diborane and ethylene. The melting point of ethylene is 103.8°K, four degrees below that of diborane. Both ethylene and diborane exhibit broad absorption lines 10° to 15° below their melting points. On the other hand, ethane and disilane with melting points of 101.0° and 140.7°K, show very narrow, liquid-like absorption lines at temperatures 10° and 50°, respectively, below their melting points. The second moment of the ethylene curve in Fig. 6 is 13.1 gauss^2. The intramolecular broadening for ethylene is 11.0 gauss^2, computed for C=C and C—H bond distances of 1.353A and 1.071A and an H—C—H bond angle of 119° 55′.[28] The intermolecular broadening should be 6 to 8 gauss^2 by analogy to ethane, as verified by an approximate calculation from the crystal structure.[29] Thus, the theoretical second moment is about 17 to 19 gauss^2. The smaller observed value suggests the likelihood of a similar effect in diborane. Prediction of the line shapes for any of the diborane models would require an extremely lengthy calculation. It can not be inferred from the similarity between the diborane and perfluoroethane derivative curves that diborane has an ethane-like structure.

7. DISCUSSION

The experimental results reported herein are essentially of an exploratory nature and serve to illustrate the potentialities of nuclear magnetism as a method for the determination of molecular structure. One of the chief values of the method lies in its general ability, outlined above, to obtain accurate proton distances in the simpler hydrogen-containing substances. Some degree of rigor is obtained by using the second moment of the absorption line as a quantitative measure of line shape and width and relating it to the theoretical treatment of Van Vleck.

The limitations and necessary precautions are several and more or less obvious. It is mandatory for the sample to be at a low enough temperature that the absorption line is not narrowed by motion of the particles in the solid. The power level of operation and the nuclear relaxation time must be such that the absorption line is not distorted by saturation effects. The sensitivity and stability of the detection system must be high, for the second moments are greatly influenced by the edges of the absorption line where the signal is weak. Fortunately, the symmetry of the absorption lines provides a good criterion for the accuracy of the data. Insofar as systematic errors are concerned, the calibration of field strength is a likely source. The use of the permanent magnet wound with a d.c. driven coil to vary the field permitted an accurate "permanent" calibration of change in field strength *versus* d.c. coil current. It is estimated that errors in field strength calibration introduced no more than ±1.5 percent error in the reported experimental values for the second moment. Though no attempt was made to determine the best possible experimental reproducibility of the second moment, the perfluoroethane results suggest that a reproducibility of ±2 percent is easily feasible. The dependence of the second moment on the inverse sixth power of the internuclear distances gives a correspondingly lower error in the distances. Greater accuracy is theoretically obtainable by using single crystals but not necessarily enough to justify their preparation in general. Only in unusually simple cases would this method be likely to suffice in itself to give a complete structural analysis. The evaluation of the intermolecular broadening of the absorption lines depends on some knowledge of the crystal structure and in the cases discussed herein the value of the intermolecular broadening is great enough to influence derived interatomic distances by as much as 5 percent. In brief, the method is well suited for investigating the more elusive aspects of a structure whose gross features are known independently.

Attention may be called again to the narrow absorption lines observed in solid ethane and disilane. The line widths δH are 0.5 and 0.6 gauss respectively, only slightly broader than the usual 0.2 to 0.3 gauss width in liquids. The inferred relatively high rotational mobility of ethane and particularly disilane in the solid state at such low temperatures is surprising, even when possible impurity effects are considered. A subsequent paper will discuss a number of such observations in more detail.

8. ACKNOWLEDGMENT

It is a pleasure to thank Dr. J. R. Arnold for several early conversations concerning the application of nuclear magnetism to the diborane problem and to the ammonium halides. We are particularly indebted to Mr. Richard Bersohn for his interest and aid in the interpretation of the data and in making some of the initial calculations. The continued interest of Professor J. H. Van Vleck in the theoretical aspects of the work has been stimulating and helpful.

Facilities for the experimental work were provided in part through a Frederick Gardner Cottrell Special Grant-in-Aid from the Research Corporation.

[28] W. S. Galloway and E. F. Barker, J. Chem. Phys. **10**, 88 (1942).

[29] C. W. Bunn, Trans. Faraday Soc. **40**, 23 (1944).

Spectroscopic Investigation of the Carbon Monoxide-Oxygen Reaction*

GEORGE A. HORNBECK AND HELEN S. HOPFIELD
Applied Physics Laboratory, The Johns Hopkins University, Silver Spring, Maryland
(Received March 8, 1949)

High dispersion spectrograms of CO-oxygen explosions in a spherical vessel have been obtained. Under conditions affording maximum contrast between the banded spectrum and the continuum, the $^3\Sigma_u^- - ^3\Sigma_g^-$ and the $^1\Sigma_g^+ - ^3\Sigma_g^-$ transitions of the neutral oxygen molecule have been observed in emission. Additional spectroscopic information on the absorption by OH radicals in flames has been obtained.

I. INTRODUCTION

RECENT developments in the field of combustion have led to a renewed interest in the molecules and radicals involved in the fundamental processes of combustion. Many investigators have approached this problem with spectroscopic studies of the radiation emitted from flames of various mixtures of combustible gases. The combustion of CO and oxygen is frequently chosen for such studies because it is one of the simplest polymolecular mixtures which will burn with high luminosity. The major portion of the spectroscopic work on the CO-oxygen flame has been done by Gaydon,[1–7] Kondratjew,[8–13] and Weston.[14,15] Of these, Kondratjew is the only investigator who obtained the fine structure of the emission bands, but because of their complexity he did not report his work. The results obtained by these investigators led them to conclude that carbon dioxide is the most probable emitter in the spectrum of the CO-oxygen flame.[16] This assignment of the flame bands lying in the visible and ultra-violet region (3000–4500A) to the CO_2 molecule is inconclusive for the following reasons: (1) Most of the work on the CO flame bands was done on instruments of moderate dispersion. (2) The strong continuous background which is characteristic of CO-oxygen combustion generally prevents sufficient contrast to resolve the structural part of the spestrum. (3) Absorption studies of CO_2 in the visible and ultraviolet show that the first absorption band lies below 1700A.[17]

Since the experimental evidence does not irrevocably support the CO_2 molecule as the emitter of the flame bands, a spectroscopic study of the CO-oxygen flame has been carried out by the authors in the visible and ultraviolet regions as well as the photographic infra-red with the purpose of reducing the ambiguities associated with the identity of this spectrum.

II. EXPERIMENTAL

The apparatus used for producing the CO-oxygen explosion flames consists of a spherical vessel, and a gas metering system which is electrically controlled by a set of magnetic solenoid valves. A schematic arrangement of this combustion system is shown in Fig. 1. The 7-liter explosion vessel was made of two mild steel hemispheres separated by a steel spacer ring which contains two 1-in. quartz windows diametrically centered. The combustible mixture is ignited at the center of the vessel by a pair of tungsten electrodes, with $\frac{1}{4}$-in. separation, connected to a common ignition spark coil. Preliminary tests disclosed the Fe spectrum superposed on the CO-oxygen flame spectrum. The Fe spectrum was eliminated by gold plating the walls of the vessel.

Commercially prepared carbon monoxide and oxygen were used in these experiments. It was necessary, however, to free the carbon monoxide from iron carbonyl which would otherwise deposit out on the windows and walls of the explosion vessel. This was achieved in the

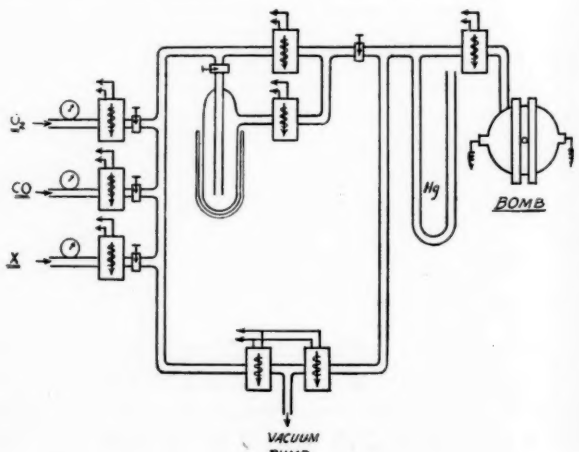

FIG. 1. Schematic diagram of the explosion apparatus.

* The work described in this paper has been supported by the Bureau of Ordnance, U. S. Navy, under Contract NOrd-7386.

[1] A. G. Gaydon, Proc. Roy. Soc. **A176**, 505 (1940).
[2] A. G. Gaydon, Proc. Roy. Soc. **A178**, 61 (1941).
[3] A. G. Gaydon, Proc. Roy. Soc. **A181**, 197 (1942).
[4] A. G. Gaydon and W. G. Penney, Nature **150**, 406 (1942).
[5] A. G. Gaydon, Proc. Roy. Soc. **A182**, 199 (1943).
[6] A. G. Gaydon, Proc. Roy. Soc. **A183**, 111 (1944).
[7] A. G. Gaydon, *Spectroscopy and Combustion Theory* (Chapman and Hall, Ltd., London, 1942).
[8] V. Kondratjew, Zeits. f. Physik **63**, 322 (1930).
[9] V. Kondratjew, J. Phys. Chem. (U.S.S.R.) **8**, 124 (1936).
[10] V. Kondratjew, Acta Physicochimica (U.R.S.S.) **6**, 748 (1937).
[11] V. Kondratjew, J. Phys. Chem. (U.S.S.R.) **11**, 331 (1938).
[12] V. Kondratjew, Acta Physicochimica (U.R.S.S.) **10**, 805 (1939).
[13] V. Kondratjew, J. Phys. Chem. (U.S.S.R.) **13**, 169 (1939).
[14] F. R. Weston, Proc. Roy. Soc. **A109**, 177 (1925).
[15] F. R. Weston, Proc. Roy. Soc. **A109**, 523 (1925).
[16] A. Fowler and A. G. Gaydon, Proc. Roy. Soc. **A142**, 362 (1933).
[17] W. C. Price and D. M. Simpson, Proc. Roy. Soc. **A169**, 501 (1938).

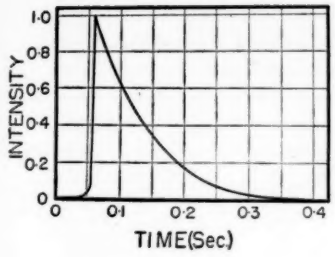

FIG. 2. Intensity-time curve of the radiation from a stoichiometric explosion of CO-oxygen as obtained from an oscillographic recording.

usual manner by passing the CO through a pyrex tube containing crushed porcelain which was heated to 300–350°C by means of a constant temperature furnace.

The radiation from one explosion of a stoichiometric mixture of CO-oxygen at an initial pressure of one atmosphere is sufficiently intense in the visible and ultra-violet to properly expose an Eastman II-O photographic plate in the second order of a 2-meter grating spectrograph with a 25-micron slit. Most of this photographic density is obtained in about 0.1 second, as shown by the intensity—time distribution curve of a single explosion in Fig. 2.

III. RESULTS AND DISCUSSION

The Runge Bands

The spectrum obtained from the brilliant flash which accompanies an explosion of CO and oxygen in a closed vessel consists of banded structure superposed on a continuous background. It has been found[18] that the intensities of the continuous background and the banded structure are different non-linear functions of the percent of oxygen in an explosive mixture. This is shown in Fig. 3, which also indicates that spectrograms of optimum contrast will be obtained with an O_2/CO ratio of two parts oxygen to one part CO. It is interesting to note that this fuel ratio is the inverse of stoichiometric.

Spectroscopic studies of the CO-oxygen reaction, employing the optimum fuel ratio described above, have been carried out in the ultraviolet and visible as well as the photographic infra-red. A spectrogram of the explosion flame in the region from 3000–5000A was obtained using a 21-foot grating spectrograph with a dispersion of 0.6A/mm. Plates with good density and high contrast were obtained from 150 explosions, equivalent to a total burning time of approximately 35 seconds. Measurements of the rotational structure made from these plates identified the banded structure in this region as the Runge bands.[19] Our measurements are in good agreement (generally better than 0.2 cm^{-1}) with those of Lochte-Holtgreven and Dieke[20] on the bands obtained by Runge[21] with a high tension arc in oxygen. This band system has been attributed[22] to the

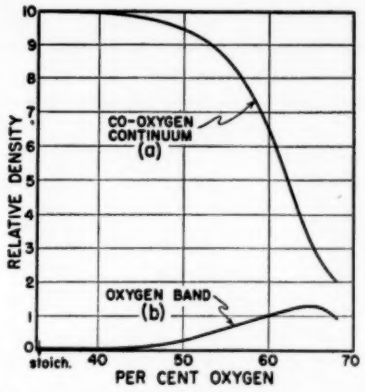

FIG. 3. Curve (a): Density of the continuum at 3400A as a function of percent oxygen, normalized to stoichiometric density. Curve (b): The difference in density between the banded structure (~3400A) and the adjacent continuum as a function of percent oxygen. The data for these curves are based on spectrograms of single CO-oxygen explosions taken with a 2-meter grating spectrograph.

$^3\sum_u^- - {}^3\sum_g^-$ transition of the neutral oxygen molecule. The following bands (v', v'') of this system, where v' and v'' refer to the vibrational levels of the upper and lower electronic states respectively, have been identified from the spectrogram of the explosion flame: (0, 12), (0, 13), (2, 15), (0, 14), (2, 16), (0, 15), (1, 16), (0, 16), (1, 17), (0, 17), (1, 18), (2, 19), (0, 18), (1, 19), (2, 20), (0, 19), (1, 20), (2, 21). Further structure is visible at both ends of this range, but is either too faint or too confused to be easily identified. A densitometer tracing

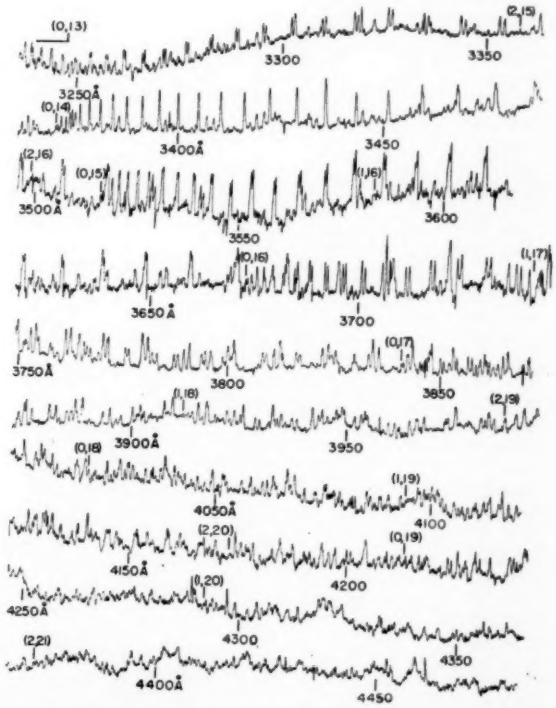

FIG. 4. Densitometer tracing of the Runge bands as obtained from CO-oxygen explosions photographed in the second order of a 21-foot grating spectrograph.

[18] G. A. Hornbeck, J. Chem. Phys. **16**, 845 (1948).
[19] G. A. Hornbeck, J. Chem. Phys. **16**, 1005 (1948).
[20] W. W. Lochte-Holtgreven and G. H. Dieke, Ann. d. Physik 3, 937 (1929).
[21] C. Runge, Physica, l. s. 254 (1921).
[22] R. S. Mulliken, Phys. Rev. **32**, 186 (1928).

TABLE I. $^1\Sigma_g^+ - {}^3\Sigma_g^-$ transitions of O_2.

(0, 0) Band		
λ, A	Intensity	Remarks
7593.73*	14	Band head
7594.97*	20	wide
7596.05*	9	diffuse
7597.24*	9	
7598.47*	8	wide
7600.02*	6	wide
7601.57*	4	
7602.11*	3	
7603.37*	3	
7604.26*	3	
7605.52*	3	
7606.60*	3	
7607.89*	2	
7609.26*	2	
7610.58*	2	
7612.15*	2	
7613.60	2	
7614.95*	2	
7615.47	2	
7616.1*	1	
7617.03	2	
7619.06	2	
7620.56	2	
7622.96*	2	
7624.34*	2	
7626.93*	2	
7628.32*	2	wide
7630.86*	2	
7631.94*	2	wide
7632.94	1	
7634.98*	2	
7636.19*	2	
7637.59	1	
7639.36*	2	
7640.66*	2	
7641.31	1	
7642.70	1	
7644.05*	2	
7645.17*	2	
7646.77	1	wide
7648.86*	3	
7649.97*	3	
7652.50	1	
7653.93*	3	
7655.03	3	
7659.31*	3	
7660.33*	3	
—*	Obscured by K line	
7665.73*	2	
7670.45*	3	
7671.58*	4	
7676.38*	3	
7677.55*	3	
7682.64*	3	
7683.85*	8	(1, 1) head
7689.03*	5	(1, 1)
7690.17*	5	(1, 1)
7695.69*	4	(1, 1)
7696.82*	4	(1, 1)
7702.53*	4	
7703.61*	4	
7709.68*	3	
7710.76*	4	
7717.08*	3	(1, 1)
7718.16*	3	
7724.66	3	(1, 1)
7725.74	4	(1, 1)
7732.58	3	
7733.66	4	(1, 1)

(0, 0) Band—*Continued*		
λ, A	Intensity	Remarks
7740.77	3	
7741.79	3	
7749.16	3	(1, 1)
7750.28	3	(1, 1) diffuse
7757.70	2	
7758.82	2	
7766.65	2	
7767.52	3	(1, 1)
7775.89	2	
7776.85	2	
7785.34	3	(2, 2) wide
7786.34	2	
7794.79	2	(1, 1) diffuse
7795.89	3	(1, 1) diffuse
7805.09	2	
7806.10	2	
7815.35	2	(2, 2)
7816.41	2	
7826.11	2	(1, 1)
7827.20	2	(1, 1)
7836.93	2	
7837.84	2	
7848.04	2	
7849.19	2	
7859.60	2	
7860.62	2	
7871.45	2	(1, 1)
7872.71	2	(1, 1)
7884.19	2	(2, 2); (3, 3) wide
7885.48	2	(2, 2); (3, 3) diffuse
7896.16	1	(3, 3)
7897.09	1	(3, 3)
7908.90	2	(2, 2)
7909.99	1	
7922.32	1	
7923.18	1	
7935.11	1	(2, 2)
7936.33	1	(1, 1)
7948.20	1	(1, 1)
7949.36	1	(1, 1)

(1, 1) Band		
7683.85	8	Band head; also (0, 0)
7685.18	7	
7685.77*	3	diffuse
7687.05*	3	diffuse
7688.06*	3	
7689.03*	5	(0, 0)
—*	Obscured by (0, 0)	
7691.60*	2	
7692.39*	2	
7693.65*	2	
7694.63*	2	
7695.69*	4	(0, 0)
7696.82*	4	(0, 0)
—*	Obscured by K line	
7700.09*	2	
7701.16*	2	diffuse
7702.53*	4	(0, 0)
7704.81*	2	
7706.73	1	
7708.16	2	
7712.07	1	
7713.63*	1	
7714.51	1	
7715.96*	2	

* Recorded by previous observers.

TABLE I.—*Continued.*

(1, 1) Band—*Continued*		
λ, A	Intensity	Remarks
7717.08*	3	(0, 0)
7720.17*	2	
7721.39*	2	
7724.66*	3	(0, 0)
7725.74*	4	(0, 0)
7728.90*	2	
7730.11*	2	
7733.66*	4	(0, 0)
7734.88*	2	
7738.70*	2	
7739.79*	2	
7743.80*	2	
7745.09*	2	
7749.16*	3	(0, 0) wide
7750.28*	3	(0, 0) wide
7755.08	2	
7756.21	2	
7761.09	2	
7762.21	2	
7767.52	3	(0, 0)
7768.36	2	
7773.67	2	
7774.72	2	
7780.36	4	(2, 2) diffuse
7781.33	3	(2, 2)
7787.44	2	(2, 2)
7788.60	2	(2, 2)
7794.79	2	(0, 0) diffuse
7795.89	3	(0, 0) diffuse
7802.15	2	
7803.19	2	
7809.85	2	(2, 2)
7811.00	2	(2, 2)
7817.91	2	
7818.98	2	(2, 2)
7826.11	3	(0, 0)
7827.20	2	(0, 0)
7834.67	2	(2, 2)
7835.77	2	
7843.54	2	
7844.61	2	(2, 2)
7852.69	2	
7853.73	2	
7862.10	2	
7863.11	2	(2, 2)
7871.45	2	(0, 0)
7872.71	2	(0, 0)
7881.71	2	(3, 3) wide
7882.64	2	(3, 3)
7891.87	2	(2, 2), (3, 3)
7892.99	2	(2, 2), (3, 3)
7902.50	1	
7903.68	2	
7913.53	1	
7914.66	1	
7924.92	2	(2, 2)
7926.07	1	(2, 2)
7936.33	1	(0, 0)
7937.48	1	
7948.30	2	(0, 0)
7949.36	2	(0, 0)
7960.48	1	
7961.64	1	
7972.95	1	(2, 2)
7974.12	1	(2, 2)
7986.20	1	
7986.97	1	
7999.37	1	wide
8000.43	1	

(2, 2) Band		
λ, A	Intensity	Remarks
7779.03	2	Band head; wide
7780.36	4	(1, 1) diffuse
7781.33	3	(0, 1)
7782.16	2	
7783.55	2	wide
7785.34	3	(0, 0) wide
7787.44	2	(1, 1)
7788.60	2	(1, 1)
7789.78	1	
7791.53	1	diffuse
7792.91	1	wide
7797.35	1	
7799.05	1	
7800.32	1	
7804.	1	
7807.96	1	wide
7809.85	2	(1, 1)
7811.00	2	(1, 1)
7814.3	1	
7815.35	2	(0, 0)
7818.98	2	(1, 1)
7820.23	1	diffuse
7823.36	1	
7824.56	1	
7828.38	1	
7829.38	1	
7833.34	1	wide
7834.67	2	(1, 1)
7838.88	1	
7840.07	1	
7844.61	2	(1, 1)
7845.69	1	
7850.50	1	
7851.66	1	
7856.66	1	wide
7857.89	2	wide
7863.11	2	(1, 1)
7864.28	1	
7869.90	1	
7871.09	1	
7876.92	1	
7877.97	1	
7884.19	2	(3, 3) wide
7885.48	2	(3, 3) wide
7891.87	2	(1, 1), (3, 3)
7892.99	2	(1, 1), (3, 3)
7899.67	1	(3, 3)
7900.79	1	(3, 3)
7907.84	1	wide
7908.90	2	(0, 0) wide
7916.08	1	
7917.29	1	
7924.92	2	(1, 1)
7926.07	1	(1, 1)
7934.11	1	
7935.11	1	(0, 0)
7943.33	1	
7944.53	1	
7952.46	1	wide
7953.93	1	
7962.91	1	
7964.05	1	
7972.95	1	(1, 1)
7974.12	1	(1, 1)
7983.60	1	
7984.65	1	wide
7994.64	1	
7995.75	1	

TABLE I.—*Continued.*

(3, 3) Band		
λ, A	Intensity	Remarks
7879.17	2	Band head; wide
7880.70	2	wide
7881.71	2	(1, 1) wide
7882.64	2	(1, 1)
7884.19	2	(0, 0); (2, 2) wide
7885.48	2	(0, 0); (2, 2) wide
7887.61	1	wide
7889.84	1	wide
7891.87	2	(1, 1); (2, 2)
7892.99	2	(1, 1); (2, 2)
7896.16	1	(0, 0)
7897.09	1	(0, 0)
7898.08	1	wide
7899.67	1	(2, 2)
7900.79	1	(2, 2)

Additional Band Heads	
Band	λ, Head
0, 1	8597.8
1, 2	8697.8
2, 3	8803.

of these Runge bands obtained from the CO-oxygen explosion flame is shown in Fig. 4.

In order to determine whether the $^3\Sigma_u^- - ^3\Sigma_g^-$ transition of oxygen occurs in flames other than explosion flames, the self-sustained flame** of CO-oxygen was studied for comparison. Densitometer tracings of the region from 3370–3400A of the bomb and burner spectra are shown in Fig. 5. It will be noted that the (0, 14) band of the Schumann-Runge system is equally well developed in the bomb and burner spectra. However,

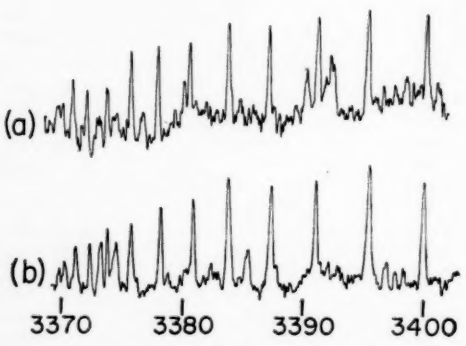

FIG. 5. Curve (a): A densitometer tracing of a portion of the (0, 14) Runge band as obtained from a reduced pressure burner using CO and oxygen. Curve (b): A densitometer tracing of the same portion of the (0, 14) Runge band as obtained from the CO-oxygen explosion flame.

** Spectrograms of the CO-oxygen flame were obtained from a reduced pressure burner using a 2-meter grating spectrograph. This burner affords a wide pressure range (20–760 mm) of combustion of CO and oxygen and seldom requires rekindling. The electrically controlled manostats on the fuel reservoirs preclude the necessity of high pumping capacity, as well as increase the ease with which a stable flame is established.

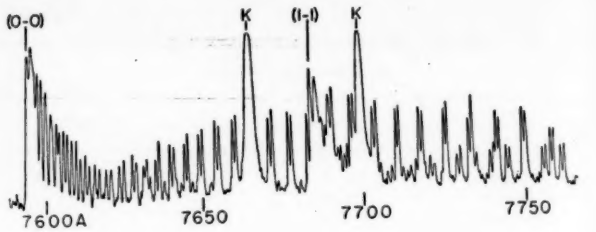

FIG. 6. Densitometer tracing of the $^1\Sigma_g^+ - ^3\Sigma_g^-$ emission bands of O_2.

some of the other bands of the system are less pronounced in the burner flame than in the bomb spectrum, and spectrograms of the burner flame show additional structure which is not attributable to the Schumann-Runge system. Furthermore, the continuum is not so well suppressed by excess oxygen in the self-sustained flame as in the explosion flame. This may be due to the temperature and pressure differences in the two cases. Nevertheless, the reaction which gives rise to the Runge bands must occur in both the self-sustained and the explosion flame.

Photographic Infra-Red Bands of O_2

The CO-oxygen explosion, using the same pressure and oxygen-fuel ratio as before, has also been photographed in the region 7200–8800A, in the first order of a 2-meter grating spectrograph. Several bands of the so-called "atmospheric absorption" system of O_2 have been obtained in emission.[23] This system has been attributed to a $^1\Sigma_g^+ - ^3\Sigma_g^-$ transition of the neutral oxygen molecule, the final level being the ground state.[24] We have identified the following bands of this system: (0, 0), (1, 1), (2, 2), (3, 3), (0, 1), (1, 2), and (2, 3). The first two of these bands have been observed before (in absorption). Rotational structure of the (0, 0) band has been measured by Dieke and Babcock.[25] Mecke and Baumann[26] have published measurements of additional lines of the (0, 0) band and also measurements of the (1, 1) band structure. Our measurements of the rotational structure are generally in good agreement with these published results, but many additional rotational lines of these bands appear on our spectrograms.

The distribution of intensity as obtained in emission is markedly different from that previously obtained in

[23] Herman, Hopfield, Hornbeck, and Silverman, J. Chem. Phys. 17, 220 (1949).
[24] R. S. Mulliken, Phys. Rev. 32, 880 (1928).
[25] G. H. Dieke and H. D. Babcock, Proc. Nat. Acad. Sci. 13, 670 (1927).
[26] R. Mecke and W. Baumann, Zeits. f. Physik 73, 139 (1932).

absorption because of the higher temperatures involved. The peak intensity is shifted away from the origin of the band in both R and P branches, the intensity maximum in the R branch being quite near the head of the band. Many additional lines are therefore observed in both branches of the previously known bands. The head of the (1, 1) band is observed in emission at $\lambda = 7683.8$A, while in absorption no lines of this band were observed below 7685.7A, probably because of their low intensity.

Measurements from these plates of the rotational structure of the (0, 0), (1, 1), (2, 2), and (3, 3) bands, as well as the heads of the (0, 1), (1, 2), and (2, 3) bands,[23] are listed in Table I. Because of the inadequate dispersion and the extensive overlapping of bands, it is not feasible to analyze the bands completely from the plates which have been obtained. Some faint lines which appear among the identified lines, especially in the (0, 0) band, may be due to the isotopic O_2 molecules. Figure 6 shows a densitometer tracing of some of these bands.

OH Bands in Emission and Absorption

The absorption of OH bands in flames is frequently used as a means of determining the concentration of the free radical. However, it is generally necessary to use an external source of continuum in conjunction with a flame. The OH bands can readily be obtained in absorption or in emission in the explosion flame depending upon the quantity of stoichiometric mixture present in the bomb at the time of firing. In the case of the CO and oxygen explosion with its small trace of hydrogen impurity, the OH band at 3064A occurs in emission at all firing pressures below $\simeq 0.6$ of an atmosphere. At 0.6 of an atmosphere the $Q_1 7$ branch shows absorption of the continuum while the other branches of the band are indistinguishable from the continuum. Explosions at higher initial pressures will bring other branches of the band into absorption. Although the pressure at which this transition takes place with other gases such as hydrocarbons has not been established, it is known that they too will yield OH in absorption or in emission depending on the pressure at which the reaction takes place. In addition to the (0, 0) OH band at 3064A, the (1, 0), (2, 0), and the (3, 0) bands at 2811, 2609, and 2444A have been observed in absorption in this explosion. Figure 7 shows a densitometer tracing of the absorption of the continuum by the different branches of the (0, 0) OH band.

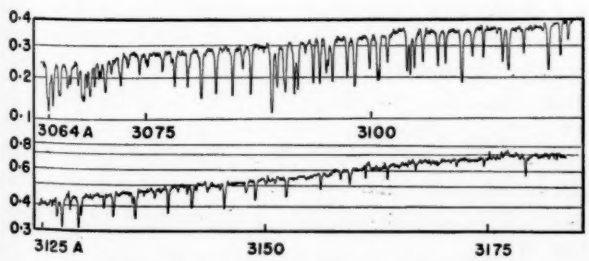

FIG. 7. Densitometer tracing of the (0, 0) OH band in absorption.

Experimental evidence of the relatively long life of the OH radical was found with the aid of a cylindrical bomb. The bomb was capable of being fired from either end or the center, and a stoichiometric mixture was used in order to provide a strong continuum. If the bomb is fired at the far end, and the spectrograph views the propagating flame front through the unburned gas, the OH bands appear in emission. When the bomb is fired at the end nearer the spectrograph, and the flame is viewed through the burned gas, there is little evidence of the OH bands in either absorption or emission. This indicates that although the OH bands are emitted only in the flame front, they are absorbed by free OH radicals whose life time behind the flame front is long relative to their radiative life. It is also interesting to note that if the bomb is fired at the center, the OH bands appear in absorption.

IV. CONCLUSION

The most significant result of this investigation was the identification of the Runge bands in the CO-oxygen flame. It had previously been assumed by other investigators that there is insufficient energy in flame sources to excite atoms or molecules to high electronic states. In view of the relatively high excitation energy (6.09 ev) required to produce the Runge bands, it may be necessary to reconsider the existing mechanisms which have been proposed for the CO-oxygen reaction.

One of the important spectroscopic problems of this reaction, which is still unsolved, is the origin of the continuum. The continuum, which is known to extend from the near ultra-violet to the photographic infra-red, constitutes a large percentage of the total radiation in this region when the combustible mixture is in stoichiometric proportion. The preferential suppression of the continuum with excess oxygen indicates the existence of competing mechanisms in the CO-oxygen reaction, and the presence of excess oxygen may establish a preferred reaction which does not give rise to a continuum.

Although there is sufficient energy in the flame to produce the ${}^3\Sigma_u^- - {}^3\Sigma_g^-$ transition of O_2, we found no spectroscopic evidence of atomic oxygen which has an excitation energy of 1 ev less than the Runge bands.

The experimental evidence that OH bands are absorbed by the burned gases necessitates a judicious choice of experimental technique in temperature studies where the OH iso-intensity method is employed.

V. ACKNOWLEDGMENTS

We are indebted to Dr. R. C. Herman for helpful suggestions and general encouragement, and to Mr. B. W. Bullock for his assistance in experimental matters. We wish to express our appreciation to Dr. E. F. Fiock, and also to Dr. B. Lewis and Dr. G. von Elbe for valuable discussions. We wish to thank Professor G. H. Dieke for his interest in the problem and for making available to us the 21-foot Paschen spectrograph at The Johns Hopkins University.

The Statistical Mechanical Theory of Transport Processes.

III. The Coefficients of Shear and Bulk Viscosity of Liquids*

JOHN G. KIRKWOOD, FRANK P. BUFF, AND MELVIN S. GREEN**
The Gates and Crellin Laboratories of Chemistry, California Institute of Technology, Pasadena, California

(Received March 17, 1949)

A molecular theory of the coefficients of shear and bulk viscosity of monatomic liquids is developed on the basis of the general theory of transport processes presented in the first article of this series. With the use of the Lennard-Jones potential and a reasonable analytic approximation to the experimental radial distribution function, calculations of the coefficients of shear and bulk viscosity of liquid argon at 89°K have been carried out. The theory leads explicitly to ratios of the coefficients to the friction constant of the theory of Brownian motion. With a preliminary estimate of the friction constant, a value of the shear viscosity of liquid argon in moderately good agreement with experiment is obtained.

I

THE general statistical mechanical theory of transport processes, developed in the first article (SMTI) of this series,[1] has as an objective the determination of the coefficients of viscosity, diffusion and heat conductivity of fluids in terms of molecular variables. It is the purpose of the present article to present a detailed theory of the coefficients of shear and bulk viscosity of liquids based upon the general theory. The starting point is provided by the differential equations of the Chandrasekhar[2] type for the probability distribution functions in the phase space of sets of one, two, and three molecules of the liquid, which were derived from the molecular standpoint in SMTI. An alternative approach is provided by the kinetic theory of liquids of Born and Green.[3] While their theory parallels our own and duplicates many of its general results, it differs in the manner in which dissipative terms are introduced into the equations satisfied by the distribution functions. Although Born and Green have presented an interesting qualitative discussion of the coefficient of shear viscosity of liquids, they have not yet succeeded in constructing solutions of their equations for the distribution functions in sufficiently explicit form to yield concrete results.

The macroscopic hydrodynamics of viscous fluids is described by the equations of continuity and motion,

$$\nabla\cdot(\rho\mathbf{u})+\partial\rho/\partial t=0,$$
$$\rho(d\mathbf{u}/dt)=\mathbf{X}+\nabla\cdot\boldsymbol{\sigma},$$

where ρ is the density, $\mathbf{u}$ the particle velocity, $\mathbf{X}$ the external body force, and $\boldsymbol{\sigma}$ the stress tensor, supplemented by the Newtonian expression for the stress tensor,

$$\boldsymbol{\sigma}=-\{p+[(2\eta/3)]-\phi)\nabla\cdot\mathbf{u}\}\mathbf{I}+2\eta\dot{\boldsymbol{\epsilon}},$$

where p is the equilibrium pressure of the fluid, $\dot{\boldsymbol{\epsilon}}$ the rate of strain, and η and ϕ are the coefficients of shear and bulk viscosity. The stress tensor is determined by molecular distribution functions and intermolecular forces in the manner described by Eq. (26) of SMTI. There are two types of terms, one arising from momentum transport and one from the direct transmission of intermolecular forces, which is determined by the average density of molecular pairs. In thermodynamic equilibrium the stress reduces to a uniform normal pressure, the first term of which is the ideal gas contribution. The second term arising from intermolecular forces has no shear components, since the pair density, proportional to the radial distribution function of the theory of liquids, possesses spherical symmetry. Departure from equilibrium resulting from hydrodynamic flow leads to perturbations in the molecular distribution functions proportional to the components of the rate of strain. In liquids the momentum transport contribution to these terms is very small relative to the contribution from intermolecular forces. The latter contribution arises from the perturbation in the pair density. This perturbation consists of two parts, one spherically symmetric, which determines the bulk viscosity ϕ, and one having the symmetry of a surface harmonic of order two, which determines the shear viscosity.

By means of the general equations of SMTI, the perturbations in the pertinent molecular distribution functions have been constructed and the ratios η/ζ and ϕ/ζ of the two coefficients of viscosity to the Brownian motion friction constant ζ have been expressed in terms of definite integrals involving the potential of intermolecular force and the equilibrium radial distribution function. Calculations have been carried out for liquid argon at 89°K with the use of the Lennard-Jones potential of intermolecular force and the Eisenstein-Gingrich radial distribution function. The result of the calculation is

$$\eta/\zeta=2.63\times10^{6}\ \text{cm}^{-1}.$$

* This work was carried out under Task Order XIII of Contract N6onr-244 between the Office of Naval Research and the California Institute of Technology.

** Present Address: Natural Sciences Staff, College of the University of Chicago, Chicago, Illinois.

[1] J. G. Kirkwood, J. Chem. Phys. **14**, 180 (1946).

[2] S. Chandrasekhar, Rev. Mod. Phys. **15**, 1 (1945). (Chandrasekhar's equations are derived from the phenomenological theory of Brownian motion.)

[3] M. Born and H. S. Green, Proc. Roy. Soc. **A188**, 10 (1946) and **190**, 455 (1947); H. S. Green, Proc. Roy. Soc. **A189**, 103 (1947).

Although the theory of the friction constant ζ was presented in SMTI, it has not yet been possible to calculate it accurately. Our preliminary estimate, $\zeta=4.84\times10^{-10}$ g sec.$^{-1}$, leads to a shear viscosity η of 1.27×10^{-3} poise, in fair agreement with the experimental value, 2.39×10^{-3} poise. Calculations relating to the bulk viscosity are postponed for treatment in a subsequent article.

II

In SMTI, the macroscopic observables of a system of N molecules were put into correspondence with average values determined by probability densities $\bar{f}^{(n)}(\mathbf{p},\mathbf{q};t)$ in the phase space $(\mathbf{p},\mathbf{q})$ of subsets of n molecules

$$\bar{f}^{(n)}(\mathbf{p},\mathbf{q};t)=\int\int \bar{f}^{(N)}(\mathbf{p},\mathbf{q},\mathbf{P},\mathbf{Q};t)\mathbf{dPdQ},$$
$$\bar{f}^{(N)}(\mathbf{p},\mathbf{q},\mathbf{P},\mathbf{Q};t)=\frac{1}{\tau}\int_0^\tau f^{(N)}(\mathbf{p},\mathbf{q},\mathbf{P},\mathbf{Q};t+s)ds, \tag{1}$$

where $(\mathbf{P},\mathbf{Q})$ is the phase space of the residual set of $N-n$ molecules and $f^{(N)}(\mathbf{p},\mathbf{q},\mathbf{P},\mathbf{Q};t)$ is the probability density in the complete phase space of an example of the appropriate statistical ensemble, from which a system is sampled in the process of preparation at time t with specified values of the molar variables determining its macroscopic state. The interval τ is determined by the time resolution of the instruments employed in the measurement of the macroscopic observables. If the shortest period macroscopically resolved is long relative to the Brownian motion correlation time, it was made plausible that in liquids, the macroscopic description would not sensibly depend upon the smoothing time τ, provided τ is long relative to the correlation time. For the representation of average values of functions of the configuration coordinates of small sets of n molecules, it is convenient to define number densities $\rho^{(n)}(\mathbf{q};t)$ by the relation,

$$\rho^{(n)}(\mathbf{q};t)=\frac{N!}{(N-n)!}\int \bar{f}^{(n)}(\mathbf{p},\mathbf{q};t)\mathbf{dp}. \tag{2}$$

The mass density ρ of hydrodynamic theory at a point $\mathbf{R}$ in a fluid and the particle velocity $\mathbf{u}$ are then determined by the relation,

$$\rho(\mathbf{R})=m\rho^{(1)}(\mathbf{R}),$$
$$\rho\mathbf{u}=N\int \mathbf{p}\bar{f}^{(1)}(\mathbf{R},\mathbf{p})d\mathbf{p}, \tag{3}$$

where m is the mass of a molecule. The distribution functions $\bar{f}^{(n)}$ were shown to satisfy partial differential equations, SMTI, Eq. (60), of the type derived by Chandrasekhar[2] on the basis of the phenomenological theory of Brownian motion. The use of these equations to determine the molecular distribution functions of a fluid in a state of stationary viscous flow will be presented in Section III.

In a system of molecules for which the potential of intermolecular force V_N can be represented in the form,

$$V_N=\sum_{i<k=1}^{N} V(R_{ik}), \tag{4}$$

where $V(R_{ik})$ is a function, say of the Lennard-Jones type, of the distance R_{ik} between the pair of molecules (ik), the stress tensor $\boldsymbol{\sigma}$ is given by SMTI, Eq. (26). In the notation of Eqs. (2) and (3), this equation becomes,

$$\boldsymbol{\sigma}=-\rho^{(1)}\left[\frac{\langle\mathbf{pp}\rangle_{Av}}{m}-m\mathbf{uu}\right]+\tfrac{1}{2}\int\frac{\mathbf{R}_{12}\mathbf{R}_{12}}{R_{12}}\frac{dV}{dR_{12}}\rho^{(2)}(\mathbf{R},\mathbf{R}_{12})dv_{12}, \tag{5}$$
$$\rho^{(1)}\langle\mathbf{pp}\rangle_{Av}=N\int\mathbf{pp}\bar{f}^{(1)}(\mathbf{p},\mathbf{R})\mathbf{dp},$$

where $\rho^{(2)}(\mathbf{R},\mathbf{R}_{12})$ is the number density of pairs, one member of which is situated at point $\mathbf{R}$ and the other at point $\mathbf{R}_{12}$ relative to the position of the first. The integration in the second term of Eq. (5), the contribution of intermolecular forces to the stress tensor, extends over the relative configuration space $\mathbf{R}_{12}$ of the representative pair. The first term represents the momentum transfer contribution, important in gases, but almost negligible in liquids.

In a liquid in a state of stationary viscous flow, the distribution functions are perturbed in such a manner that the stress tensor takes on the extended Newtonian form. In Section III, it will be shown that with neglect of non-linear terms in the rate of strain, $\dot{\boldsymbol{\epsilon}}$,

$$-\rho^{(1)}\left[\frac{\langle\mathbf{pp}\rangle_{Av}}{m}-m\mathbf{uu}\right]\rho^{(1)}=-\rho^{(1)}kT\mathbf{1}+\rho\frac{kT}{\zeta}\dot{\boldsymbol{\epsilon}}, \tag{6}$$
$$\zeta=kT/D,\quad \dot{\boldsymbol{\epsilon}}=Sym\nabla\mathbf{u},$$

where ζ is the Brownian motion friction constant and D is the coefficient of self-diffusion of the liquid. The pair density, $\rho^{(2)}$, determining the contribution of intermolecular forces to the stress tensor is conveniently written in the form,

$$\rho^{(2)}(\mathbf{R},\mathbf{R}_{12})=\rho^{(1)}(\mathbf{R})\rho^{(1)}(\mathbf{R}+\mathbf{R}_{12})g^{(2)}(\mathbf{R},\mathbf{R}_{12}), \tag{7}$$

a relation defining the pair correlation function $g^{(2)}(\mathbf{R},\mathbf{R}_{12})$. In Section III, it will be shown that $g^{(2)}$ can be expanded in the components of the rate of strain as,

$$g^{(2)}=g_0^{(2)}(R_{12})\left\{1+\frac{\zeta}{2kT}\left[\frac{\mathbf{R}_{12}\cdot\dot{\boldsymbol{\epsilon}}\cdot\mathbf{R}_{12}}{R_{12}^2}-\tfrac{1}{3}\nabla\cdot\mathbf{u}\right]\psi_2(R_{12})+\frac{\zeta}{6kT}(\nabla\cdot\mathbf{u})\psi_0(R_{12})\right\}, \tag{8}$$

where $g_0^{(2)}(R_{12})$ is the radial distribution function of the fluid in thermodynamic equilibrium and $\psi_0(R_{12})$

and $\psi_2(R_{12})$ satisfy certain ordinary differential equations, presently to be derived from the general theory of the probability densities, $\bar{f}^{(n)}$.

Substitution of the momentum contribution of Eq. (6) and the perturbed pair density of Eqs. (7) and (8) into Eq. (5) yields the stress tensor,

$$\sigma = -[p+(2/3\eta-\phi)\nabla\cdot\mathbf{u}]\mathbf{1}+2\eta\dot{\epsilon},$$
$$p=\frac{NkT}{V}-\frac{2\pi N^2}{3V^2}\int_0^\infty R^3\frac{dV}{dR}g_0^{(2)}(R)dR, \tag{9}$$

where p is the equilibrium pressure of the liquid at the given temperature and uniform number density $\rho^{(1)}$, equal to the ratio of Avogadro's number N and the molal volume V. The coefficients of shear viscosity η and bulk viscosity ϕ are then given by the expressions

$$\eta=\rho\frac{kT}{2\zeta}+\frac{\pi\zeta}{15kT}\frac{N^2}{V^2}\int_0^\infty R^3\frac{dV}{dR}\psi_2(R)g_0^{(2)}(R)dR,$$
$$\phi=\rho\frac{kT}{3\zeta}+\frac{\pi\zeta}{9kT}\frac{N^2}{V^2}\int_0^\infty R^3\frac{dV}{dR}\psi_0(R)g_0^{(2)}(R)dR, \tag{10}$$

where, as subsequent calculations will show, the initial terms arising from momentum transport are of minor importance in liquids.

In order to evaluate the integrals of Eqs. (10), as well as to solve the differential equations determining the perturbation functions $\psi_0(R)$ and $\psi_2(R)$, it is necessary to know the equilibrium radial distribution function $g_0^{(2)}(R)$ and the potential of intermolecular force $V(R)$. The potential $V(R)$ is conveniently approximated by the Lennard-Jones expression,

$$V(R)=\epsilon\left(\frac{1}{x^n}-\frac{1}{x^6}\right),$$
$$x=R/a_0. \tag{11}$$

In applications of the theory presently to be made to liquid argon, we shall use parameters, n, ϵ, and a_0, determined by Rushbrooke[4] and Corner.[5] The values are: $n=11.4$; $\epsilon=6.82\times10^{-14}$ erg; $a_0=3.43$A.

The radial distribution function $g_0^{(2)}(R)$ is of course determined by the potential of intermolecular force $V(R)$ and the thermodynamic variables.[6] It is also accessible to experimental measurement, since it determines the intensity of x-rays scattered by a liquid as a function of scattering angle. In the applications to follow, we shall make use of the radial distribution function data for argon of Eisenstein and Gingrich.[7] This function possesses a series of peaks with amplitude rapidly diminishing as R increases. Since it is found that the integrals of Eq. (10) are in the main determined by the first peak of the radial distribution function, the other factor being of very short range, we have constructed the following analytical approximation to $g_0^{(2)}(R)$,

$$g_0^{(2)}(R)=(a_1/R)^s\exp\left\{\left(\frac{a_m}{a_1}\right)^t-\left(\frac{a_m}{R}\right)^t\right\};\quad 0\le R\le a_1,$$
$$=1;\quad R<a_1, \tag{12}$$

which represents quite well the first peaks of the Eisenstein-Gingrich curves. It has the important advantage of allowing the integration of the differential equations satisfied by the perturbation function ψ_0 and ψ_2, in terms of confluent hypergeometric functions. Two of the parameters $a_1=4.5$A and $t=14$ are determined from the Eisenstein-Gingrich data to be relatively insensitive to temperature. For liquid argon at 89°K and 1.2 atmos., the remaining parameters were determined with the use of the Lennard-Jones potential, Eq. (11), the theoretical equation of state, given by the second of Eq. (9), and the energy of vaporization,

$$E_v=-\frac{2\pi N^2}{V}\int_0^\infty R^2V(R)g_0^{(2)}(R)dR. \tag{13}$$

They were found to have the values, $a_m=3.55$A and $s=7.01$. This calibration was found to be necessary, since the Eisenstein-Gingrich functions fail to satisfy the equation of state, due to the extreme sensitivity of the cohesive pressure, arising from intermolecular forces, to the relative position of the first peak of $g_0^{(2)}(R)$ and the position of the minimum of the Lennard-Jones potential. With the adjusted parameters, the peak of the empirical function, Eq. (12), lies at 3.73A and corresponds to a coordination number of 8.1, both in good agreement with the experimental results of Eisenstein and Gingrich.

III

The determination of the perturbations from equilibrium of the distribution functions $\bar{f}^{(1)}(\mathbf{p},\mathbf{R})$ and $\rho^{(2)}(\mathbf{R},\mathbf{R}_{12})$ in a liquid in a state of stationary viscous flow is based upon the use of the Chandrasekhar equations, SMTI, Eq. (59) and Eq. (60), derived from the standpoint of molecular dynamics in the first paper of this series. In order to determine the momentum contribution to the stress tensor, we employ the equation [SMTI (59)]

$$\frac{\partial\bar{f}^{(1)}}{\partial t}+\frac{\mathbf{p}}{m}\cdot\nabla_{\mathbf{R}}\bar{f}^{(1)}+\nabla_{\mathbf{p}}\cdot\mathbf{F}^{(1)}\bar{f}^{(1)}$$
$$=\zeta\nabla_{\mathbf{p}}\cdot\left\{\left(\frac{\mathbf{p}}{m}-\mathbf{u}\right)\bar{f}^{(1)}+kT\nabla_{\mathbf{p}}\bar{f}^{(1)}\right\}, \tag{14}$$
$$\mathbf{F}^{(1)}={}^{(1)}\langle\mathbf{F}\rangle_{Av}{}^0+{}^{(1)}\mathbf{F}^+,$$

[4] G. S. Rushbrooke, Proc. Roy. Soc. (Edin.) **60**, 182 (1940).
[5] J. Corner, Trans. Faraday Soc. **35**, 711 (1939).
[6] J. G. Kirkwood and E. M. Boggs, J. Chem. Phys. **10**, 394 (1942).
[7] A. Eisenstein and N. S. Gingrich, Phys. Rev. **62**, 261 (1942).

where ζ is the friction constant of the theory of Brownian motion, ${}^{(1)}\langle\mathbf{F}\rangle_{Av}{}^{0}$ is the average in the equilibrium ensemble of the total intermolecular force acting on a molecule situated at point $\mathbf{R}$, and ${}^{(1)}\mathbf{F}^{+}$ is the perturbation arising from the departure of $\rho^{(2)}$ from equilibrium. Upon multiplication of both sides of Eq. (14) by $(\mathbf{p}/m-\mathbf{u})(\mathbf{p}/m-\mathbf{u})$ and integration over momentum space, we find with the use of Green's theorem that

$$\langle\mathbf{\Pi\Pi}\rangle_{Av}-mkT\mathbf{1}=-\frac{m}{2\zeta}\left\{\langle\mathbf{\Pi\Pi}\rangle_{Av}\cdot\nabla\mathbf{u}+\langle\mathbf{\Pi}\cdot\nabla\mathbf{u}\mathbf{\Pi}\rangle_{Av}+\mathbf{u}\cdot\nabla\langle\mathbf{\Pi\Pi}\rangle_{Av}+\frac{\partial\langle\mathbf{\Pi\Pi}\rangle_{Av}}{\partial t}\right\}, \quad (15)$$
$$\mathbf{\Pi}=\mathbf{p}-m\mathbf{u},$$

with the neglect of non-linear terms in all perturbations from equilibrium. In the stationary case, Eq. (15) leads at once to Eq. (6), in the linear approximation, and the momentum transfer contribution to the stress tensor is evaluated.

In order to determine the pair density $\rho^{(2)}$, from which the intermolecular force contribution to the stress tensor is to be calculated, we employ Eq. (60) of SMTI in the form appropriate to $\bar{f}^{(2)}(\mathbf{p}_1, \mathbf{R}_1, \mathbf{p}_2, \mathbf{R}_2; t)$ in the phase space of molecular pairs,

$$\frac{\partial\bar{f}^{(2)}}{\partial t}+\frac{\mathbf{p}_1}{m}\cdot\nabla_{\mathbf{p}_1}\bar{f}^{(2)}+\frac{\mathbf{p}_2}{m}\cdot\nabla_{\mathbf{R}_2}\bar{f}^{(2)}+\nabla_{\mathbf{p}_1}\cdot\mathbf{F}_1{}^{(2)}\bar{f}^{(2)}+\nabla_{\mathbf{p}_2}\cdot\mathbf{F}_2{}^{(2)}\bar{f}^{(2)}$$
$$=\nabla_{\mathbf{p}_1}\cdot\zeta_1{}^{(2)}\cdot\left\{\left(\frac{\mathbf{p}_1}{m}-\mathbf{u}_1\right)\bar{f}^{(2)}+kT\nabla_{\mathbf{p}_1}\bar{f}^{(2)}\right\} \quad (16)$$
$$+\nabla_{\mathbf{p}_2}\cdot\zeta_2{}^{(2)}\cdot\left\{\left(\frac{\mathbf{p}_2}{m}-\mathbf{u}_2\right)\bar{f}^{(2)}+kT\nabla_{\mathbf{p}_2}\bar{f}^{(2)}\right\};$$
$$\mathbf{F}_1{}^{(2)}={}^{(2)}\langle\mathbf{F}_1\rangle_{Av}{}^{0}+{}^{(2)}\mathbf{F}_1{}^{+}; \quad \mathbf{F}_2{}^{(2)}={}^{(2)}\langle\mathbf{F}_2\rangle_{Av}{}^{0}+{}^{(2)}\mathbf{F}_2{}^{+},$$

where ${}^{(2)}\langle\mathbf{F}_1\rangle_{Av}{}^{0}$ is the mean force acting on the first molecule of the pair in the unperturbed equilibrium ensemble, subject to the condition that the configuration $(\mathbf{R}_1, \mathbf{R}_2)$ of the pair is fixed, and ${}^{(2)}\mathbf{F}_1{}^{+}$ is the perturbation arising from the departure of $\rho^{(3)}$, the density in triplet configuration space from equilibrium. The friction tensor $\zeta^{(2)}$ is a second rank tensor in the six-dimensional configuration space of the pair, related to intermolecular forces in the manner prescribed in SMTI. The vectors $\mathbf{u}_1$ and $\mathbf{u}_2$ are the particle velocities of three-dimensional hydrodynamics, defined by Eq. (3), at the respective positions $\mathbf{R}_1$ and $\mathbf{R}_2$ of the pair. Integration of both sides of Eq. (16) over the momentum space of both molecules leads to the equation of continuity in pair configuration space,

$$\frac{\partial\rho^{(2)}}{\partial t}+\nabla_{\mathbf{R}_1}\cdot\mathbf{j}_1{}^{(2)}+\nabla_{\mathbf{R}_2}\cdot\mathbf{j}_2{}^{(2)}=0, \quad (17)$$
$$\mathbf{j}_\alpha{}^{(2)}=\frac{N(N-1)}{m}\int\int\mathbf{p}_\alpha\bar{f}^{(2)}(\mathbf{p}_1, \mathbf{p}_2, \mathbf{R}_1, \mathbf{R}_2; t)d\mathbf{p}_1d\mathbf{p}_2,$$

with $\mathbf{j}_\alpha{}^{(2)}$ the number current density in pair space projected on the 3-space of molecule α. Multiplication of both sides of Eq. (16) by $\mathbf{p}_1$ and $\mathbf{p}_2$ respectively, followed by integration over momentum space yields the equations,

$$m\frac{\partial\mathbf{j}_1{}^{(2)}}{\partial t}=-kT\nabla_{\mathbf{R}_1}\rho^{(2)}+\mathbf{F}_1{}^{(2)}\rho^{(2)}-\zeta_1{}^{(2)}\cdot[\mathbf{j}_1{}^{(2)}-\mathbf{u}_1\rho^{(2)}],$$
$$m\frac{\partial\mathbf{j}_2{}^{(2)}}{\partial t}=-kT\nabla_{\mathbf{R}_2}\rho^{(2)}+\mathbf{F}_2{}^{(2)}\rho^{(2)}-\zeta_2{}^{(2)}\cdot[\mathbf{j}_2{}^{(2)}-\mathbf{u}_2\rho^{(2)}], \quad (18)$$

with the neglect of non-linear terms in $\mathbf{u}_1$ and $\mathbf{u}_2$ and of terms of the order of $1/\zeta$ in the departure of the non-diagonal terms in $\langle\mathbf{p}_\alpha\mathbf{p}_\alpha\rangle_{Av}{}^{(2)}/m$ from their vanishing equilibrium values. Similar equations are obtained by the same procedure from Eq. (14),

$$m\frac{\partial\mathbf{j}_\alpha{}^{(1)}}{\partial t}=-kT\nabla_{\mathbf{R}_\alpha}\rho^{(1)}(\mathbf{R}_\alpha)+\mathbf{F}_\alpha{}^{(1)}\rho^{(1)}(\mathbf{R}_\alpha),$$
$$\frac{\partial\rho^{(1)}(\mathbf{R}_\alpha)}{\partial t}+\nabla_{\mathbf{R}_\alpha}\cdot\mathbf{j}_\alpha{}^{(1)}=0, \quad \alpha=1, 2, \quad (19)$$
$$\mathbf{j}_\alpha{}^{(1)}=\rho^{(1)}(\mathbf{R}_\alpha)\mathbf{u}(\mathbf{R}_\alpha).$$

We now introduce the simplifications,

$$\zeta_1{}^{(2)}=\zeta_2{}^{(2)}=\zeta\mathbf{1},$$
$$\mathbf{F}_\alpha{}^{(2)}-\mathbf{F}_\alpha{}^{(1)}=kT\nabla_{\mathbf{R}_\alpha}\log g_0{}^{(2)}(R_{12}); \quad \alpha=1, 2, \quad (20)$$

where ζ is the singlet friction constant of Eq. (14) and $g_0{}^{(2)}$ is the equilibrium radial distribution function. The first of Eqs. (20) implies the neglect of the dependence of the friction tensor $\zeta^{(2)}$ on the relative configuration of the pair, and the second approximates the mean intermolecular force difference by its equilibrium value.[8] Thus it is a well known result of equilibrium statistical mechanics that,

$$g_0{}^{(2)}=\exp(-(W^{(2)}-W_1{}^{(1)}-W_2{}^{(1)})/kT),$$
$${}^{0}\langle\mathbf{F}_\alpha\rangle_{Av}{}^{(2)}=-\nabla_{\mathbf{R}_\alpha}W^{(2)}(R_{12}), \quad \alpha=1, 2, \quad (21)$$
$${}^{0}\langle\mathbf{F}_\alpha\rangle_{Av}{}^{(1)}=-\nabla_{\mathbf{R}_\alpha}W^{(1)}(R_\alpha),$$

where $W^{(1)}$ and $W^{(2)}$ are the potentials of mean force in singlet space and pair space, respectively.

Introduction of Eq. (7) into Eqs. (17) and (18) and elimination of $\rho^{(1)}(\mathbf{R}_1)$ and $\rho^{(2)}(\mathbf{R}_2)$ by means of Eqs. (19) leads, with neglect of the inertial terms, to the

[8] See J. G. Kirkwood, J. Chem. Phys. 3, 300 (1935).

following equation for the correlation function,

$$\nabla_{\mathbf{R}}\cdot\{\nabla_{\mathbf{R}}g^{(2)}-(\nabla_{\mathbf{R}}\log g_0^{(2)})g^{(2)}\}$$
$$-\frac{\zeta}{2kT}\frac{\partial g^{(2)}}{\partial t}=\frac{\zeta}{2kT}\mathbf{R}\cdot\dot{\boldsymbol{\epsilon}}\cdot\nabla_{\mathbf{R}}g^{(2)},$$
$$\mathbf{j}_{12}^{(2)}=-\frac{2kT}{\zeta}\{\nabla_{\mathbf{R}}g^{(2)}-(\nabla_{\mathbf{R}}\log g_0^{(2)})g^{(2)}\}, \tag{22}$$
$$\rho^{(1)}(\mathbf{R}_1)\rho^{(1)}(\mathbf{R}_2)\mathbf{j}_{12}^{(2)}=[\mathbf{j}_2^{(2)}-\rho^{(2)}\mathbf{u}_2]$$
$$-[\mathbf{j}_1^{(2)}-\rho^{(2)}\mathbf{u}_1],$$
$$g^{(2)}(\mathbf{R}_1,\mathbf{R})=g^{(2)}(\mathbf{R});\quad \mathbf{R}=\mathbf{R}_2-\mathbf{R}_1;$$
$$\mathbf{u}_2-\mathbf{u}_1=\mathbf{R}\cdot\nabla\mathbf{u},$$

where $\mathbf{j}_{12}^{(2)}$ is the excess probability current density in relative pair space, vanishing at $R\to\infty$ by definition and is conditioned by the absence of sources or sinks in the pair density distribution.

Introduction of Eq. (8) into Eq. (22) and linearization with respect to the components of the rate of strain $\dot{\boldsymbol{\epsilon}}$ leads, in the stationary case to the following ordinary differential equation for the functions $\psi_2(R)$ and $\psi_0(R)$,

$$\frac{d}{dR}\left(R^2g_0^{(2)}\frac{d\psi_2}{dR}\right)-6g_0^{(2)}\psi_2=R^3\frac{dg_0^{(2)}}{dR},$$
$$\frac{d}{dR}\left(R^2g_0^{(2)}\frac{d\psi_0}{dR}\right)=R^3\frac{dg_0^{(2)}}{dR}. \tag{23}$$

In coordinate representation $\psi_2(R)$ is the coefficient of surface harmonics of order two, arising from the shear component of the rate of strain, and $\psi_0(R)$ is the coefficient of the surface harmonic of order zero, arising from the dilatational component. The excess probability current density in the relative pair space is given by

$$\mathbf{j}_{12}^{(2)}=-g_0^{(2)}\left\{\nabla_{\mathbf{R}}\left[\frac{\mathbf{R}\cdot\dot{\boldsymbol{\epsilon}}\cdot\mathbf{R}}{R^2}-\tfrac{1}{3}\nabla\cdot\mathbf{u}\right]\psi_2(R)\right.$$
$$\left.+\tfrac{1}{3}(\nabla\cdot\mathbf{u})\psi_0(R)\right\}. \tag{24}$$

The requirement that $\mathbf{j}_{12}^{(2)}$ vanish at $R=\infty$ and that there be no sources or sinks in pair space leads to the boundary conditions,

$$\lim_{R\to\infty}\psi_2(R)=0, \tag{25a}$$
$$\lim_{R\to 0}R^2g_0^{(2)}\frac{d\psi_2(R)}{dR}=0, \tag{25b}$$
$$\lim_{R\to\infty}\frac{d\psi_0(R)}{dR}=0, \tag{25c}$$
$$\lim_{R\to 0}R^2g_0^{(2)}\frac{d\psi_0(R)}{dR}=0, \tag{25d}$$

subject to which Eqs. (23) are to be solved. In addition, ψ_2, $d\psi_2/dR$, and $d\psi_0/dR$ must be continuous for all $0\leq R\leq\infty$, a condition which must be applied at the cut-off point, $R=a_1$, of the approximate radial distribution function, Eq. (12), in order to ensure continuity of the pair current at this point.

IV

The solution of the ψ_2 Eq. (23a) is based on use of the approximate representation of $g_0^{(2)}$ given in Eq. (12). Since $R^2/2$ is a particular solution, we only have to investigate the homogeneous equation

$$x^2\frac{d^2\psi_2}{dx^2}+\left\{2+x\frac{d\log g_0^{(2)}}{dx}\right\}x\frac{d\psi_2}{dx}-6\psi_2=0;\quad x=\frac{R}{a_0}. \tag{26}$$

For $x_1<x$, Eq. (26) reduces to Euler's equation so that the solution satisfying the boundary condition at infinity, Eq. (25a), is given by

$$\psi_2=K_2/x^3;\quad x_1<x. \tag{27}$$

Substitution of the first peak approximation in Eq. (26) leads to the following differential equation for $0\leq x\leq x_1$

$$z^2\frac{d^2\psi_2}{dz^2}+(2k-z)z\frac{d\psi_2}{dz}+(k+m-\tfrac{1}{2})(k-m-\tfrac{1}{2})\psi_2=0,$$
$$k=\tfrac{1}{2}+\frac{s-1}{2t};\quad m=\frac{1}{t}\left(\left(\frac{s-1}{2}\right)^2+6\right)^{\frac{1}{2}};\quad z=\left(\frac{x_m}{x}\right)^t. \tag{28}$$

Two linearly independent solutions of this equation are found to be $e^{z/2}z^{-k}W_{k,m}(z)$ and $e^{z/2}z^{-k}W_{-k,m}(-z)$, where $W_{k,m}(z)$ is the Whittaker confluent hypergeometric function.[9] We note that the generalized hypergeometric function is given by

$${}_pF_q(\alpha_1,\alpha_2,\cdots\alpha_p;\ \rho_1,\ \rho_2,\cdots\rho_q;z)=\sum_{n=0}^{\infty}\frac{\Gamma(\alpha_1+n)\Gamma(\alpha_2+n)\cdots\Gamma(\alpha_p+n)\Gamma(\rho_1)\Gamma(\rho_2)\cdots\Gamma(\rho_q)z^n}{\Gamma(\alpha_1)\Gamma(\alpha_2)\cdots\Gamma(\alpha_p)\Gamma(\rho_1+n)\Gamma(\rho_2+n)\cdots\Gamma(\rho_q+n)n!}. \tag{29}$$

[9] For discussion of this function, see Whittaker and Watson, *Modern Analysis* (The Macmillan Company, New York, 1943).

In order to satisfy the boundary condition at the origin, Eq. (25b), it is seen from the asymptotic expansion of $W_{k,m}(z)$

$$W_{k,m}(z)\sim e^{-z/2}z^{k}\ {}_2F_0(\tfrac{1}{2}-m-k,\tfrac{1}{2}+m-k;-z^{-1}) \quad |\arg z|<3\pi/2 \tag{30}$$

that $e^{z/2}z^{-k}W_{-k,m}(-z)$ is not an admissible solution. Thus for $0\leq x\leq x_1$, with

$$y_1(z)=e^{z/2}z^{-k}W_{k,m}(z),$$
$$\psi_2=(a_0^2x^2/2)+K_1y_1(z). \tag{31}$$

The derivative of $y_1(z)$ is readily obtained from the Mellin-Barnes type contour integral representation of $W_{k,m}(z)$

$$W_{k,m}(z)=\frac{e^{-z/2}z^{k}}{2\pi i}\times\int_{-\infty i}^{+\infty i}\frac{\Gamma(v)\Gamma(-v-k+m+\frac{1}{2})\Gamma(-v-k-m+\frac{1}{2})z^{v}dv}{\Gamma(-k-m+\frac{1}{2})\Gamma(-k+m+\frac{1}{2})}, \tag{32}$$

with the result

$$\frac{dy_1(z)}{dx}=\frac{6}{tx}z^{-k}e^{z/2}W_{k-1,m}(z). \tag{33}$$

The constants K_1 and K_2 are determined by the requirement that ψ_2 and $d\psi_2/dx$ be continuous at x_1. With use of Eq. (33) we find after some elementary calculations that

$$K_1=-a_0^2x_1^2K_3=-\frac{a_0^2x_1^2(5/2)z_1^{k}e^{-z_1}}{3W_{k,m}(z_1)+\frac{6}{t}W_{k-1,m}(z_1)},$$

$$K_2=-a_0^2x_1^5K_4 \tag{34}$$
$$=-\frac{a_0^2x_1^5\left\{W_{k,m}(z_1)-\frac{3}{t}W_{k-1,m}(z_1)\right\}}{3W_{k,m}(z_1)+\frac{6}{t}W_{k-1,m}(z_1)},$$

$$z_1=\left(\frac{x_m}{x_1}\right)^{t}.$$

Since in our numerical example $z_1=3.67\times10^{-2}$, $W_{k,m}(z_1)$ is easily computed by means of the relation

$$W_{k,m}(z)=z^{(1/2)+m}e^{-z/2}\frac{\Gamma(-2m)}{\Gamma(\frac{1}{2}-m-k)}\times{}_1F_1(\tfrac{1}{2}+m-k;1+2m;z)$$
$$+z^{(1/2)-m}e^{-z/2}\frac{\Gamma(2m)}{\Gamma(\frac{1}{2}+m-k)}\times{}_1F_1(\tfrac{1}{2}-m-k;1-2m;z), \tag{35}$$

only a few terms in the power series being required.

Substitution of ψ_2 given by Eqs. (27) and (31) into Eq. (10) and use of the potential $V(x)$, Eq. (11), leads to the following result for the coefficient of shear viscosity,

$$\eta=\frac{\zeta\pi N^2a_0^5}{15kTv^2}\left[\frac{1}{2}\int_0^{x_1}x^5g_0^{(2)}(x)\frac{dV(x)}{dx}dx+K_4x_1^5V(x_1)\right.$$
$$\left.+K_3\frac{\epsilon x_1^{2+s}e^{z_1}}{tx_m^{3+s}}\left\{\frac{nI_{n-3}}{x_m^{n-6}}-6I_3\right\}\right]+\frac{NmkT}{2v\zeta}, \tag{36}$$

$$I_\alpha=I_\alpha(\infty)-I(z_1),$$

$$I(z)=\int_0^{z}y_1(z)e^{-z}z^{(\alpha+s/t)-1}dz.$$

The value of $I_\alpha(\infty)$ is conveniently calculated with use of Eq. (32) and Barnes lemma (reference 9, p. 289).

$$I_\alpha(\infty)=\frac{1}{2\pi i}\int_{-\infty i}^{+\infty i}\frac{\Gamma(v)\Gamma(-v-k-m+\frac{1}{2})\Gamma(-v-k+m+\frac{1}{2})\Gamma\left(v+\frac{\alpha+s}{t}\right)dv}{\Gamma(-k-m+\frac{1}{2})\Gamma(-k+m+\frac{1}{2})} \tag{37}$$
$$=\frac{\Gamma\left(\frac{\alpha+s}{t}-k-m+\frac{1}{2}\right)\Gamma\left(\frac{\alpha+s}{t}-k+m+\frac{1}{2}\right)}{\Gamma\left(\frac{\alpha+s}{t}+1-2k\right)};\quad t>n-2.$$

Use of Eq. (35) and Kummer's formula

$$e^{-z}{}_1F_1(\tfrac{1}{2}+m-k;1+2m;z)={}_1F_1(\tfrac{1}{2}+m+k;1+2m;-z), \tag{38}$$

immediately leads to the result

$$I_\alpha(z_1)=I_\alpha{}^{m}(z_1)+I_\alpha{}^{-m}(z_1), \tag{39}$$

where

$$I_\alpha^\beta(z_1)=\frac{\Gamma(-2\beta)}{\Gamma(\frac{1}{2}-\beta-k)}\frac{z_1^{(\alpha+s/t)-k+1/2+\beta}}{\left(\frac{\alpha+s}{t}-k+\frac{1}{2}+\beta\right)}{}_2F_2\left(\tfrac{1}{2}+\beta+k,\right.$$

$$\left.\frac{\alpha+s}{t}-k+\tfrac{1}{2}+\beta;\ 1+2\beta,\ \frac{\alpha+s}{t}-k+\tfrac{3}{2}+\beta;\ -z_1\right).$$

We have carried out the numerical calculation of η for liquid argon at 89°K

$$\eta=2.63\times10^{6}\zeta+\frac{8.53\times10^{-15}}{\zeta}\text{ poise}$$

the second term arising from momentum transport being negligible in comparison with the first. It is of interest to note that by defining an effective radius by the relationship $\zeta=6\pi\eta R_{\text{eff}}$, $R_{\text{eff}}=2.0$A at 89°K, while the actual radius, taken to be one half the distance between nearest neighbors is 1.9A.

In order to check our theory with experiment it is necessary to calculate the friction constant. As a preliminary estimate we find that

$$\zeta^2=\frac{4\pi a_0\rho}{3}\int_0^\infty x^2\left(\frac{d^2V}{dx^2}+\frac{2}{x}\frac{dV}{dx}\right)g_0^{(2)}dx, \tag{40}$$

which for liquid argon at 89°K, using Eqs. (11) and (12) leads to $\zeta=4.84\times10^{-10}$ g sec.$^{-1}$. With this value of the friction constant, the calculated coefficient of shear viscosity for liquid argon at 89°K is 1.27×10^{-3} poise which is in moderately good agreement with the extrapolated experimental determination of 2.39×10^{-3} poise.[10]

The solution of the ψ_0 Eq. (23b), subject to the boundary condition at the origin, Eq. (25d), is given by

$$\psi_0=a_0^2\int_\infty^x\frac{d\xi}{\xi^2g_0^{(2)}}\int_0^\xi\frac{dg_0^{(2)}}{dw}w^3dw+\psi_0(\infty), \tag{41}$$

$$\psi_0\sim\frac{c}{x}+\psi_0(\infty)\quad\text{for } x \text{ large.}$$

[10] N. S. Rudenko and L. W. Schubnikow, Physik. Zeits. Sowjetunion **6**, 470 (1934).

In order to evaluate $\psi_0(\infty)$ we consider Eq. (22) for the case of a periodic dilation of frequency ω. For large x, we obtain

$$\frac{d}{dx}\left(x^2\frac{d\psi_0}{dx}\right)-\frac{i\omega\zeta a_0^2}{2kT}x^2\psi_0=0, \tag{42}$$

with the solution

$$\psi_0\sim\frac{A(\omega)}{x}\exp\left(-\left[\frac{a_0}{2}\left(\frac{\omega\zeta}{kT}\right)^{\frac{1}{2}}x(1+i)\right]\right)$$

$$\frac{B(\omega)}{x}\exp\left(\left[\frac{a_0}{2}\left(\frac{\omega\zeta}{kT}\right)^{\frac{1}{2}}x(1+i)\right]\right). \tag{43}$$

The boundary condition at infinity Eq. (25c) requires that $B(\omega)=0$. For the case of zero frequency of dilation

$$\psi_0\sim\lim_{\omega\to0}\frac{A(\omega)}{x}\exp\left\{-\left[\frac{a_0}{2}\left(\frac{\omega\zeta}{kT}\right)^{\frac{1}{2}}x(1+i)\right]\right\}=\frac{C}{x}. \tag{44}$$

Comparison of (41) and (44) shows that ψ_0 vanishes at infinity. We thus obtain the following expression for the coefficient of bulk viscosity

$$\phi=\frac{NmkT}{3v\zeta}+\frac{\zeta\pi a_0^5N^2}{9kT}\int_0^\infty x^3\frac{dV}{dx}g_0^{(2)}dx$$

$$\times\int_\infty^x\frac{d\xi}{\xi^2g_0^{(2)}}\int_0^\xi w^3\frac{dg_0^{(2)}}{dw}dw. \tag{45}$$

Numerical calculations of the coefficient of bulk viscosity are postponed for later treatment, since the result appears to be extraordinarily sensitive to the equilibrium radial distribution function and it is believed that a better approximation than that of Eq. (12) is required. For the same reason, our numerical estimate of the shear viscosity is to be considered preliminary and subject to revision. From recent ultrasonic absorption measurements of Galt,[11] an upper bound to the ratio ϕ/η is estimated to be $\frac{1}{3}$ for liquid argon at 85°K. However, in the absence of an experimental value of the heat conductivity, the calculation of the absolute value of ϕ is not possible.

[11] J. G. Galt, J. Chem. Phys. **16**, 505 (1948).

The Effect of Electric Fields on the Decomposition of Ethane by Alpha-Rays

NELSON T. WILLIAMS* AND HARRY ESSEX
Department of Chemistry, Syracuse University, Syracuse, New York
(Received January 6, 1949)

In the decomposition of ethane by alpha-rays the reaction is largely initiated by splitting of molecules on ionization and by splitting of molecules without ionization on electron collision. The application of even a weak electric field results in an increased ion yield in ethane, a phenomenon which has not been observed in other gases studied by this method, and this is attributed to inhibition by the field of a reaction involving ions which decreases the amount of non-condensed gas produced. The application of higher fields results in another increase in the ion yield due to the collisions of electrons accelerated by the field which cause splitting with or without attachment. At the lower pressure, a final constancy of the ion yield at high fields can be attributed to the final attachment of all of the free electrons to molecular fragments. The reaction at the higher pressure was not followed to sufficiently high values of X/p to exhibit the same high field effect.

THE experimental procedure of this work followed that described in a recent paper[1] by the authors on the alpha-ray decomposition of nitrous oxide, the principal change being that liquid nitrogen instead of liquid oxygen was used to condense out the ethane when measuring the pressure of non-condensed gaseous products because of the higher vapor pressure of ethane at low temperatures. The ethane was obtained from a cylinder supplied by the Ohio Chemical Company and was purified by passing through solutions of ammoniacal cuprous chloride, sulfuric acid, bromine water, and potassium hydroxide, followed by drying over anhydrous calcium chloride. The gas was further purified by fractional distillation from liquid oxygen, the first and last fractions being discarded in each of four successive distillations. The purified gas was then transferred to the reaction system at the desired pressure.

The decomposition of ethane by alpha-rays has been studied by Mund and Koch[2] who observed the formation of liquid products and of a gaseous product which was not condensed by liquid air. Lind and Bardwell[3] have also investigated the reaction and they also observed the formation of liquid products of formula $C_nH_{1.85n}$, as well as hydrogen, methane, propane, butane, and pentane, but no ethylene. The latter authors found that 1.7 molecules of ethane were decomposed per ion pair, or 1.5 molecules of hydrogen plus methane were produced per ion pair, about five molecules of hydrogen being obtained for each molecule of methane. In both of these studies the fraction of the ethane decomposed was much larger than that reported in the present work. No chemical analysis of the products was made in the present work. The reaction was followed by measuring the pressure of the gaseous products which were not condensed by liquid nitrogen, i.e., hydrogen and methane.

The results are listed in Table I and are shown graphically in Fig. 1. The ion yield as given here is the number of molecules of non-condensed gaseous products produced per ion pair. It should be noted that even the highest field strength employed was below the value required to produce ionization by collision due to the field, as is apparent from the appearance of the current-potential curve. The ion yield curve at 200 mm was not investigated at as high a value of X/p as at 85 mm because the higher voltage required in the former case caused electrical difficulties.

DISCUSSION

The most unusual feature of the ion yield—X/p curve for ethane—is the initial rise in ion yield with increased field strength. This is the first time that this phenomenon has been observed. Its probable significance will be discussed later.

After the initial rise followed by a horizontal section, above an X/p value of approximately 6 volts/cm/mm C_2H_6, the ion yield again increases and this is evidently the phenomenon generally observed, namely, the onset

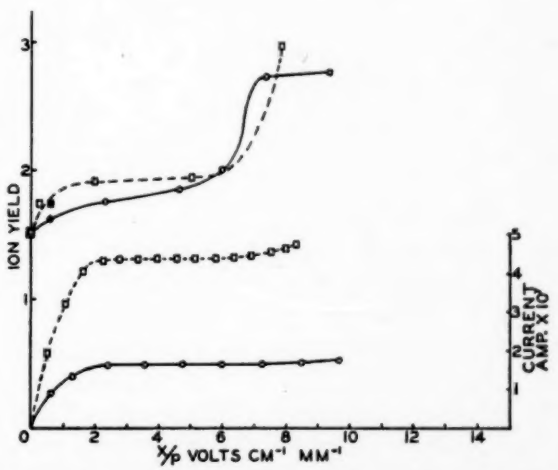

FIG. 1. The two upper curves show the variations in ion yield with X/p, the dashed curve at 200 mm, the solid curve at 85 mm pressure. Values of ion yield at fields sufficient to give half-saturation currents are indicated by solid points. The two lower curves are typical current $-X/p$ curves at 200 mm (dashed line) and 85 mm (solid line), respectively.

* Du Pont Fellow, 1947–48.
[1] N. T. Williams and H. Essex, J. Chem. Phys. **16**, 1153 (1948).
[2] W. Mund and W. Koch, Bull. soc. chim. Belg. **34**, 119 (1925).
[3] S. C. Lind and D. C. Bardwell, J. Am. Chem. Soc. **48**, 2335 (1926).

TABLE I. Ethane decomposition. Ion yields at 200 mm pressure and 21°C.

X/p	Duration of run in hours	Increase of pressure of non-condensed gases in mm	Saturation current amp. $\times 10^7$	Ion yield
0	267.33	0.1369	4.30	1.47
0	186.25	0.0978	4.37	1.49
0	182.50	0.0924	4.32	1.45
0	251.25	0.1447	4.41	1.61
0	208.50	0.1189	4.41	1.60
0	208.00	0.1177	4.25	1.65
			average	1.54
0.2*	433.00	0.2725	4.38	1.77
0.2*	161.75	0.1002	4.41	1.74
			average	1.76
0.6**	185.67	0.1123	4.37	1.71
0.6**	279.20	0.1748	4.36	1.77
0.6**	162.50	0.1064	4.42	1.83
0.6**	234.50	0.1423	4.40	1.71
0.6**	161.00	0.0922	4.24	1.67
			average	1.74
2.0	185.75	0.1293	4.36	1.97
2.0	186.50	0.1227	4.26	1.91
2.0	183.25	0.1200	4.26	1.90
			average	1.93
5.1	212.55	0.1532	4.48	1.99
5.1	160.50	0.1067	4.25	1.93
			average	1.96
7.9	144.00	0.1590	4.59	2.98
	Ion yields at 85 mm pressure and 21°C.			
0	377.25	0.0798	1.69	1.55
0	259.75	0.0533	1.69	1.50
			average	1.53
0.6**	237.50	0.0521	1.68	1.61
0.6**	210.00	0.0470	1.69	1.64
			average	1.63
2.3	200.75	0.0485	1.69	1.77
4.7	190.25	0.0480	1.68	1.86
6.1	241.75	0.0665	1.68	2.02
7.5	240.00	0.0899	1.70	2.72
9.4	253.75	0.1023	1.80	2.77

* X/p values at quarter-saturation current.
** X/p values at half-saturation current.

of a reaction initiated by more severe electron collisions with molecules. Data on electron energies in ethane as a function of X/p are not available, but maximum energies may be calculated roughly using the kinetic theory equation for the terminal energy E_t of an electron in a gas as a function of X/p in which only elastic collisions are assumed.[4] This equation may be stated in the form

$$E_t = k((M/m)^{\frac{1}{2}}/\sigma^2)(X/p),$$

where M is the mass of a molecule of the gas, m is the mass of the electron, and σ is the diameter of a molecule of the gas. Substitution of the proper numerical values in this equation shows that the terminal energy acquired by an electron at any value of X/p in nitrous oxide is 1.9 times as great as the terminal energy the electron would acquire in ethane. The point of inflection on the ion yield curve in nitrous oxide[1] probably corresponds to the decomposition

$$N_2O \rightarrow N_2 + O, \quad (1)$$

which requires about 1.8 ev. The value of X/p at the considered point of inflection on the ethane ion yield curve ($\sim$6.5) is 3 or 4 times the value of X/p of the corresponding point of inflection on the N_2O curve which indicates that the reaction occurring on electron collision in ethane is one requiring about double the electron energy required for the N_2O decomposition. The energy necessary to break the first C—H bond in ethane, i.e., for the reaction

$$C_2H_6 \rightarrow C_2H_5 + H, \quad (2)$$

is about 4.2 ev,[5] and the energy required to break the C—C bond in ethane, i.e., for the reaction

$$C_2H_6 \rightarrow 2\,CH_3, \quad (3)$$

is about 3.7 ev.[5] According to Faltings,[6] the split in the photo-chemical decomposition of ethane is into two methyl radicals, and according to Steacie and Cunningham[7] and Steacie and Potvin[8] in the mercury- and cadmium-sensitized photo-decomposition the split is into an ethyl radical and a hydrogen atom. Presumably the decompositions (2) and/or (3) on electron collision may occur either with or without attachment of the electron to one of the fragments. The flattening off of the ion yield at high X/p values at the lower pressure may be explained, as in the case of nitrous oxide,[1] by the final attachment of all of the free electrons to molecular fragments. Apparently the ion yield at the higher pressure was not followed to sufficiently high values of X/p to exhibit the same high field strength effect.

From data in Rutherford, Chadwick, and Ellis[9] it can be calculated that in ethane one alpha-particle expends 26.9 ev per ion pair. Therefore, as about 80 percent of the ionization is secondary,[9] the average energy of the electrons expelled by an alpha-particle (delta-rays) is 108 ev. As most of the ionization is by electrons, the positive ions to be expected when an alpha-particle travels through ethane may be obtained from mass-spectrographic data of Hipple[10] and of Stevenson and Hipple.[11] The paper by Stevenson and Hipple shows the effect of varying electron energy on the frequency distribution of the various positive ions, and it is interest-

[4] L. B. Loeb, *Kinetic Theory of Gases* (McGraw-Hill Book Company, Inc., New York, 1927), p. 501.

[5] E. W. R. Steacie, *Atomic and Free Radical Reactions* (Reinhold Publishing Corporation, New York, 1946), p. 79.
[6] K. Faltings, Ber. d. D. Chem. Ges. **72B**, 1207 (1939).
[7] E. W. R. Steacie and R. L. Cunningham, J. Chem. Phys. **8**, 800 (1940).
[8] E. W. R. Steacie and R. Potvin, J. Chem. Phys. **7**, 782 (1939).
[9] Rutherford, Chadwick, and Ellis, *Radiations from Radioactive Substances* (Cambridge University Press, London, 1930), pp. 81, 145.
[10] J. A. Hipple, Jr., Phys. Rev. **53**, 530 (1938).
[11] D. P. Stevenson and J. A. Hipple, Jr., J. Am. Chem. Soc. **64**, 1588 (1942).

ing to note that there is little change in this distribution when the bombarding electrons have energies from 30 to 175 volts. The only negative ion reported is H^-.

From the relative abundance of the positive ions produced in ethane on ionization by electrons the mechanism of the alpha-ray decomposition of ethane in the absence of a field may be approximately visualized. The important primary processes of ionization are:[10]

$$C_2H_6 \rightarrow C_2H_6^+ + e^-, \quad (4)$$

$$C_2H_6 \rightarrow C_2H_5^+ + H + e^-, \quad (5)$$

$$C_2H_6 \rightarrow C_2H_4^+ + H_2 + e^-, \quad (6)$$

$$C_2H_6 \rightarrow C_2H_3^+ + H_2 + H + e^-, \quad (7)$$

$$C_2H_6 \rightarrow C_2H_2^+ + 2H_2 + e^-. \quad (8)$$

It seems probable that these, together with reactions (2) and/or (3), constitute the important primary processes which result in decomposition at no field. If we assume that the positive ions yield only products condensed by liquid nitrogen and that each H atom reacts with ethane to produce a molecule of hydrogen, then using the frequency distribution obtained by Stevenson and Hipple[11] we obtain 1.1 molecules of non-condensed gas per ion pair *due to the primary ionization process.* Since the ion yield obtained at no field is 1.5, it appears that 1.5 minus 1.1, or 0.4, is the ion yield due to molecule splitting, without ionization, on electron collision.

Steacie[12] has given what he considers the most reliable values for the activation energies of the possible subsequent reactions which the radicals H, CH_3, and C_2H_5 may undergo. In these experiments the most probable reactions in the gas phase are:

$$H + C_2H_6 \rightarrow C_2H_5 + H_2 \quad E_A = 6.7 \text{ kcal.} \quad (9)$$

and

$$CH_3 + C_2H_6 \rightarrow CH_4 + C_2H_5 \quad E_A = 8 \text{ kcal.} \quad (10)$$

The reaction:

$$2C_2H_5 \rightarrow C_4H_{10} \quad E_A = \text{small}, \quad (11)$$

may occur to some extent in the gas phase because the ethyl radicals would not be removed by reaction with ethane molecules. Other reactions in the gas phase which involve only radicals are very improbable because of the very minute concentrations of the radicals. Faltings[6] has explained the photo-chemical decomposition of ethane by a methyl radical mechanism in which the radicals combine with each other to give the products. However, since his radical concentrations were larger than those obtained in this work by at least several powers of ten, reaction between radicals in the gas phase is much less probable here. Also at the low pressures of these experiments most of the ions should be neutralized at the wall and therefore most of the reaction between radicals in these experiments would be expected to occur on the walls.

At both pressures, the ion yield increases with the field strength as the field is increased from zero to saturation. This shows that a reaction *involving ions* which decreases the amount of non-condensed gas produced is stopped by the field. The ions $C_2H_5^+$ and H^- have been shown in the mass-spectrograph[10,11] studies to be produced by electron bombardment of ethane. In a field, the $C_2H_5^+$ ions would be neutralized at the negative electrode yielding C_4H_{10} and the H^--ions at the positive electrode yielding H_2, whereas in the absence of a field the $C_2H_5^+$ and H^- would be neutralized at the wall and some of them would react with each other to give ethane.

The greater effect of the field at high pressure can be explained on the basis of the competing wall reactions:

$$C_2H_5 + H \text{ at wall} \rightarrow C_2H_6, \quad (12)$$

and

$$H + H \text{ at wall} \rightarrow H_2. \quad (13)$$

At the lower pressure the rates of both reaction (12) and reaction (13) are slower. However, to the extent that reaction (3) with (10) is the source of C_2H_5, reaction (12) will decrease relative to (13) and correspondingly more hydrogen is produced at the wall. Consequently, on applying a field there will be a smaller increase in the hydrogen produced and a smaller increase in the ion yield (molecules of gas not condensed per ion pair). If this is the explanation of the smaller effect of the field at the low pressure, it would seem to imply a larger ion yield at no field at low pressure, whereas our measurements show no effect of pressure on the ion yield at no field. The agreement in the ion yield at the two pressures at no field may be fortuitous and due to experimental errors, but it is possible to explain such a phenomenon. It may be that at the higher pressure the production of methane by reaction (10) compensates for the increased amount of reaction (12) which takes place at this pressure.

[12] See reference 5, p. 519.

Letters to the Editor

THIS section will accept reports of new work, provided these are terse and contain few figures, and especially few half-tone cuts. The Editorial Board will not hold itself responsible for opinions expressed by the correspondents. Contributions to this section should not exceed 600 words in length and must reach the office of the Managing Editor not later than the 15th of the month preceding that of the issue in which the letter is to appear. No proof will be sent to the authors. The usual publication charge ($4.00 per page) will not be made and no reprints will be furnished free.

Anomalous Negative Peaks in Mass Spectra

A. G. SHARKEY, JR. AND R. A. FRIEDEL
Bureau of Mines, Synthetic Liquid Fuels, Research and Development Branch, Bruceton, Pennsylvania
August 15, 1949

IN the mass spectra of the gases O_2, N_2, CO, and CO_2, negative peaks have been found approximately two mass units lower than the peaks of the positive molecular ions. Arnot[1] and Sloane and Press,[2] using mass spectrometer tubes of special design, observed negative peaks corresponding roughly in mass to positive ions of these same gases. For the present work a conventional spectrometer was used (Consolidated Model 21-102).

The mechanism for negative ion formation that seems most probable is that proposed by Arnot[1] and Arnot and Beckett.[3] In this process, the positive ion captures an electron at the metal surface and is neutralized but left excited. This is followed by either: (1) capture of another electron forming a negative ion of the same type, or (2) transfer of the energy of the positive ion to another type atom on the surface, which in turn captures an electron forming a negative ion of another type.

Negative peaks have been observed with various ion sources while using the same analyzer section of the mass spectrometer tube. This indicates that the source of the negative peaks is in the region of the exit slit of the analyzer section and probably arises from a non-conducting layer on the exit slit plate. A schematic diagram of this possible source of negative ions from carbon monoxide is given in Fig. 1. With field conditions set to focus positive ions of mass 26, mass 28 ions will have a larger radius and strike some point (as shown) on the exit slit plate. This spot on the plate will then act as the source of negative ions, which are deflected by the magnetic field, collected, and recorded as a negative peak at 26.2 on the mass scale. The difference in radius of the "mass 26.2" and mass 28 ions is approximately two millimeters. Assuming that the negative ions CO^- are formed with very low energy, the radius of the path of these ions would be about this value, making it possible for them to be collected. In Fig. 2 is shown a negative peak near mass 26.2 on a portion of a CO spectrum.

Table I gives the ratio of negative to positive ions for the gases studied thus far. These values are of the same order of magnitude as the probabilities of conversion given by Arnot[1] for O_2, 0.42×10^{-4}, and CO_2, 2.3×10^{-4}.

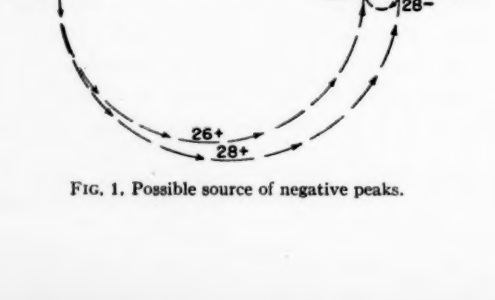

FIG. 1. Possible source of negative peaks.

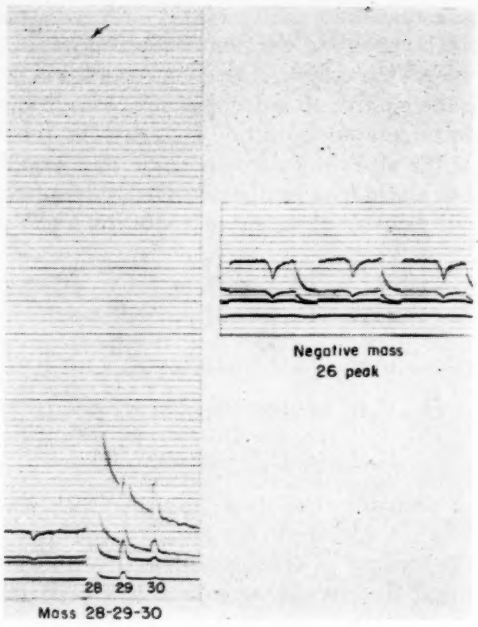

FIG. 2. Portion of CO spectrum.

TABLE I. Ratio of negative to positive ion peaks for various gases.

N_2	2.9×10^{-4}
O_2	3.5×10^{-4}
CO	4.5×10^{-4}
CO_2	5.9×10^{-4}

The negative ion N_2^- is known to be unstable and was not detected by Arnot,[1] but in the present work on N_2 a negative peak near 26.2 was found. This may be due to a negative ion of another type, according to Arnot's mechanism (2) (see above). However, the detection of N_2^- is feasible in the present case because of the short distance traversed to the collector. Further, negative peaks in the spectra of all four gases appear to have the same shape. If a transfer of energy were involved, the ions formed would possibly have a large energy spread giving broad peaks. Therefore, the negative peak in the spectrum of N_2 is probably due to N_2^-.

It was difficult to obtain an accurate peak height *vs.* pressure relationship because of the size of the peak; however, as nearly as could be determined, this relationship was linear up to three times normal operating pressure. Any negative ions from hydrocarbons formed by this process would not be detected because of the much larger positive ion peaks occurring at the same masses.

We would like to express our appreciation to Dr. J. A. Hipple for his helpful discussion concerning a possible source of the negative ions.

[1] F. L. Arnot, Proc. Roy. Soc. (London) **A158**, 137–156 (1937).
[2] R. H. Sloane and R. Press, Proc. Roy. Soc. (London) **A168**, 284–301 (1938).
[3] F. L. Arnot and C. Beckett, Proc. Roy. Soc. (London) **A168**, 103–122 (1938).

C^{13} Isotope Effect in the Decarboxylation of Malonic Acid

JACOB BIGELEISEN AND LEWIS FRIEDMAN*
Brookhaven National Laboratory, Upton, New York
August 17, 1949

IN a recent publication by one of us,[1] a theoretical treatment of the C^{14} isotope effect in the decarboxylation of malonic acid was given. The results of the theory are in sharp disagreement with the experiments of Yankwich and Calvin.[2] The recent experiments

of Lindsay, McElcheran, and Thode[3] on the C^{13} isotope effect in the decomposition of oxalic acid into CO_2, CO, and H_2O are of the order of magnitude predicted for malonic acid. The isotope effects should be comparable in the decarboxylation of oxalic and malonic acids. We have studied the isotope effect in the decarboxylation of malonic acid by following the isotopic composition of the CO_2 liberated from ordinary malonic acid.

The decomposition of malonic acid gives $C^{13}O_2$ and $C^{12}O_2$ according to the following equations

$$C^{12}H_2(C^{12}OOH)_2 \xrightarrow{k_1} C^{12}O_2 + C^{12}H_3C^{12}OOH \quad (1)$$

$$C^{13}H_2(C^{12}OOH)_2 \xrightarrow{k_2} C^{12}O_2 + C^{13}H_3COOH \quad (2)$$

$$C^{12}H_2 \begin{cases} C^{13}OOH \\ C^{12}OOH \end{cases} \xrightarrow{k_3} C^{13}O_2 + C^{12}H_3COOH \quad (3)$$

$$\xrightarrow{k_4} C^{12}O_2 + C^{12}H_3C^{13}OOH. \quad (4)$$

Since the reaction is first order, the ratio $C^{13}O_2/C^{12}O_2$ is at any time, t,

$$C^{13}O_2/C^{12}O_2 = \frac{k_3 M_3^0(1-e^{-(k_3+k_4)t})}{(k_3+k_4)\left[M_1^0(1-e^{-k_1 t}) + M_2^0(1-e^{-k_2 t}) + \frac{k_4}{k_3+k_4} M_3^0(1-e^{-(k_3+k_4)t})\right]},$$

where M_1^0, M_2^0, and M_3^0 are the initial amounts of the malonic acids in Eqs. (1)–(3). If α is the average fraction of C^{13} in natural carbon and if we assume that there is no fractionation in the formation of malonic acid, then we get

$$C^{13}O_2/C^{12}O_2 = \frac{2\alpha k_3}{(1-\alpha)k_1} \text{ at small } t$$

and

$$C^{13}O_2/C^{12}O_2 = \frac{2\alpha k_3}{(1-\alpha)(k_3+k_4)} \text{ at } t=\infty.$$

Implicit in these equations are the approximations that $k_2\alpha \simeq k_1\alpha$, $k_4\alpha \simeq k_3\alpha \simeq (k_1/2)\alpha$. These assumptions are justified by our results.

C. P. malonic acid was further purified by fractional crystallization from water at about 20°C. The sample used in experiment 2 (M.P. 137–137.5°C) was 99.2 percent pure by acidimetric titration. Samples of the order of 5 grams were decomposed in a thermostated (137.5±0.5°C) vacuum system. The CO_2 was separated from the acetic acid by cold traps. A sample of the CO_2 was collected after a small amount of decomposition and another sample was taken for analysis after completion of the reaction. A portion of the purified malonic acid was oxidized completely to CO_2 by KIO_3 and $K_2Cr_2O_7$ in a mixture of syrupy H_3PO_4 and 30 percent fuming H_2SO_4. Determination of the ratio of $C^{13}O_2/C^{12}O_2$ from the oxidation gives directly $\alpha/(1-\alpha)$. The samples were analyzed with a Consolidated-Nier isotope ratio mass spectrometer. During the course of analysis frequent determinations were made on samples of tank CO_2 to check the precision and reproducibility of the mass spectrometer. The results are given in Table I. The values of $k_1/2k_3$ were corrected back to zero time. For the calculation of k_4/k_3 the values of $t\infty$ were corrected for the amount of sample of different isotopic composition removed at $t\epsilon$. Our results for tank CO_2 and the CO_2 from the combustion of the malonic acid are in good agreement with each other and the results of Nier and Gulbransen[4] (0.0111±0.0002). The close agreement between tank CO_2 and the combustion sample justify our assumption in regard to fractionation in the formation of the two C^{13} malonic acids. It should be pointed out that malonic acid sample 1 was purified in a different manner and contained some NaCl, which does not take part in the reaction. The discrepancy between the tank CO_2 analyses as well as the other samples in the two different sets of experiments resulted from the differences

TABLE I.

Exp.	Sample	$C^{13}O_2/C^{12}O_2$	Av. dev.	$k_1/2k_3$	k_4/k_3
1	$t=\epsilon$	0.010587	0.024%	1.039±0.001	
1	Tank CO_2	0.010986	0.024%		
1	$t=\infty$	0.010902	Single Det.		1.020
2	$t=\epsilon$	0.010918	0.008%	1.035±0.001	
2	Tank CO_2	0.011287	0.078%		
2	Combustion	0.011303	0.047%		
2	$t=\infty$	0.011200	0.10 %		1.019±0.001
Theory				1.021	1.0198

in the operating characteristics of the spectrometer over a period of several weeks. In any given experiment the reproducibility was excellent as shown by the average deviations, which were usually taken from three or more independent determinations.

The theoretical values were calculated according to the method previously given[1] for C^{14}. The theoretical value for k_4/k_3 is in excellent agreement with experiment. The discrepancy between the theoretical and experimental values for $k_1/2k_3$ results from the fact that the malonic acid vibrations cannot be completely approximated by an XY_2 model. The vibrations within the carboxyl group should be taken into account as both our experiments and those on oxalic acid show. The C^{14} experiments on malonic acid[2] measure k_4/k_3 in the above notation. Both theory and the C^{13} experiments on oxalic and malonic acids are not consistent with the large isotope effects reported[2] for C^{14} substitution in malonic and brom-malonic acids.

* Research carried out under the auspices of the AEC.

[1] J. Bigeleisen, J. Chem. Phys. **17**, 425 (1949).
[2] P. E. Yankwich and M. Calvin, J. Chem. Phys. **17**, 109 (1949).
[3] Lindsay, McElcheran, and Thode, J. Chem. Phys. **17**, 589 (1949).
[4] A. O. Nier and E. A. Gulbransen, J. Am. Chem. Soc. **61**, 697 (1939).

Contribution to the Thermodynamics of High Polymer Solutions. V. Solubility of Heterogenous Polymers

G. GAVORET AND MICHEL MAGAT
Laboratoire de Chimie-Physique, Faculté des Sciences, Paris
August 19, 1949

IN an article in course of publication[1] we give some results on precipitation limits of narrow fractions and mixtures of fractions of GRS, precipitated by ethanol from toluene solutions. We came to the conclusion that the precipitation limit for mixtures was not determined by the *number average molecular weight* as previously suggested on the basis of a statistical treatment,[2] but was dependent on an average of a rather higher order than the weight average.

Lately Stockmayer[3] has corrected the results of Scott and has shown that the precipitation limit is determined by the relation

$$2\mu_c = (1+x_w^{-1/2})^2 - \frac{(x_z^{1/2}-x_w^{1/2})^2}{x_w \cdot x_z^{1/2}}, \quad (1)$$

where x_w is the weight average and x_z the z average of the number of segments.[4]

In the absence of published data Stockmayer could not check his formula experimentally. It was interesting to attempt a verification with our data. To make a rigorous test one would have to determine μ-values independently, say from osmotic pressure measurements, and to make all the comparisons at critical concentrations. This is prohibitively long and the precise determination of the precipitation limit at the rather high critical concentrations is difficult. We have hence proceeded in a different way. A calibration curve, molecular weight, *viz.*, concentration of alcohol at the precipitation point, was established from experiments on narrow fractions, for which $\bar{M}_n \approx \bar{M}_w \approx \bar{M}_z$; the real concentration of the polymer at the precipitation point being $\varphi_P = 1.10^{-2}$. From this plot and the experimentally determined amount of alcohol required for precipitation of mixtures of frac-

TABLE I.

No.	Molecular weight of fractions	Composition of the mixture by weight	E.E.M.W.	10^{-3} M_{St}	M_n	M_w	M_z
8	75 20	9.62 90.38	30.0± 1	27.8	21.5	25.3	35.7
9	220 1	88.4 11.6	250 ±35	207	8.3	194	220
10	220 1	46.0 54.0	170 ±15	148	1.8	101	219
11	220 1	13.15 86.85	125 ±10	102	1.15	29.9	189.5

tions, one can obtain the experimental equivalent molecular weight of the fraction-mixture (E.E.M.W.). The E.E.M.W. can be then compared to calculated $\bar{M}_n$, $\bar{M}_w$, $\bar{M}_z$ values and to the molecular weight of the hypothetical fraction $\bar{M}_{St}$, that according to (1) would have the same precipitation point as the mixture used.

$\bar{M}_{St}$ was calculated from:

$$(1+x_{St}^{-1/2})^2=2\mu_e=(1+x_w^{-1/2})^2-\frac{(x_z^{1/2}-x_w^{1/2})^2}{x_w\cdot x_z^{1/2}}. \qquad (2)$$

Table I gives the results obtained in a few characteristic cases (all the molecular weights in thousands). The agreement between E.E.M.W. and M_{St} without being perfect is much better then between E.E.M.W. and the other averages and can be judged as satisfactory, in view of the unavoidable errors in the molecular weights of fractions.

[1] G. Gavoret and M. Magat, J. Chimie Phys. (to be published).
[2] R. L. Scott, J. Chem. Phys. **13**, 178 (1945). M. Magat, J. Chimie Phys. to be published.
[3] W. H. Stockmayer, J. Chem. Phys. **17**, 588 (1949).
[4] In the note published by Stockmayer the sign before the second term is given as positive but from the context one can deduce that in reality it should be negative.

A Preferentially Oil Soluble Carrier for Radiocobalt-60

J. R. WHITE
Socony-Vacuum Laboratories, Paulsboro, New Jersey
August 15, 1949

A FREQUENTLY met with industrial problem is the quantitative measurement of the location and flow of liquids through porous media or behind barriers to visibility and access. One attack on this measurement problem is to incorporate a gamma-active material in the liquid and to trace the movement of the liquid with a Geiger counter or other radiation detector located externally to the system barriers. When the flowing liquid consists in mutually little soluble liquid pairs, such as water and oil, it is generally desirable that the gamma-active tracer be confined to only one liquid phase.

The cobaltous salt of the dodecyl ester of tetrahydrophthallic acid, having the structural formula,

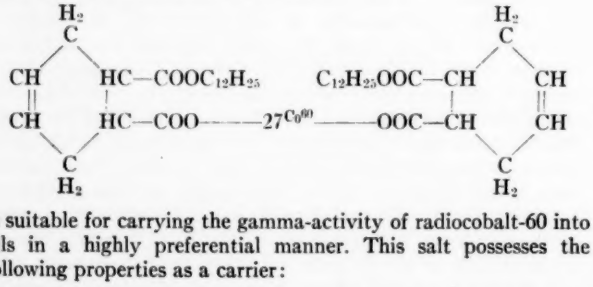

is suitable for carrying the gamma-activity of radiocobalt-60 into oils in a highly preferential manner. This salt possesses the following properties as a carrier:

1. Solubility to the extent of 1.5 percent by weight of the salt in acid washed kerosene at 25°C.
2. A kerosene over water distribution coefficient in excess of 200 at 25°C provided that the water have a *p*H of seven and not contain cations exchangeable with cobaltous ion.
3. Thermal stability to temperatures in excess of 100°C.
4. Hydrolytic stability in contact with water at *p*H-7.
5. Stability toward photolysis provoked by sunlight.

This organic salt has been synthesized from samples of Atomic Energy Commission irradiated cobaltic oxide (Co_2O_3). The oxide has been digested to solution with 12*N* hydrochloric acid and adjusted to *p*H-5 with sodium hydroxide solution. A water solution of the sodium salt of the organic acid has been admixed with the cobaltous chloride solution in appropriate mole proportions, whence the cobaltous salt of the organic acid precipitates. The precipitated salt suspended in the water phase has been directly extracted into a desired oil by gentle agitation of contacting phases of oil and water containing suspended salt. Any excess cobaltous chloride has then been removed from the oil phase by repeated water washing. Large samples of oil containing as much as 0.03 mc/ml have been prepared by this procedure.

Condensation Coefficient and Adsorption

HANS M. CASSEL
Pittsburgh, Pennsylvania
August 15, 1949

THE condensation coefficient, defined as the ratio, α, of the observed rate of evaporation to the gas kinetically computed excess of molecules striking the surface of the condensed phase per unit time, has recently been discussed by G. Wyllie[1] from the standpoint of Volmer's theory of phase transitions.[2] Accordingly, evaporation and condensation have to be considered as (at least) two-step processes, the exchanged molecules passing through the adsorbed state at the interface. To describe the rate of transition from the substrate into the adsorbed film Wyllie introduces the simplest possible hypothesis, namely that this is given by $A(\Gamma_0-\Gamma)$, where A depends on the temperature, and Γ is the superficial concentration, the subscript referring to the state of equilibrium. Regarding the exchange between the film and the vapor phase he assumes that the adsorption isotherm is that of an ideal two-dimensional gas: $\Gamma=\tau bp$. Here, τ is the "verweilzeit"[3] in the adsorbed state, determining the rate of desorption, $b=(2\pi mkT)^{-\frac{1}{2}}$, and p is the vapor pressure. On this basis, Wyllie derives the expression

$$\alpha=A/(1/\tau+A).$$

It is quite obvious that the restriction to low pressure adsorption limits the validity of this theory unnecessarily, and that a better approximation can be obtained on the assumption of a Langmuir type adsorption isotherm

$$\Gamma=\tau bp/(1+\tau\beta bp). \qquad (1)$$

This implies that the occupied fraction of the surface, $\beta\Gamma$, is blocked to impinging molecules, and the condensation efficiency correspondingly reduced. On this basis, the result is

$$\Gamma=(A\Gamma_0+bp)/(1/\tau+A+\beta bp) \qquad (2)$$

and

$$\alpha=A/(1/\tau+A+\beta bp)(1+\tau\beta bp_0). \qquad (3)$$

This means that α becomes dependent on the pressure and, therefore, must be smaller for condensation than for evaporation. It should be noticed that the factor $(1+\tau\beta bp_0)$, being always greater than $(1+\beta\Gamma_0)$, may surpass the amount 2 if τ is great enough. Provided that $1/\tau$ can be neglected in comparison to A, the maximum condensation coefficient that may be attained is

$$\alpha_{max}=1/(1+\tau\beta bp_0). \qquad (4)$$

One has to be aware that Langmuir type adsorption can be expected only at temperatures higher than the critical temperature of the film which in the case of van der Waals' forces is half the critical temperature of its substance in bulk.[4] At lower temperatures the cohesive interaction between adatoms will contribute to

the adsorption energy and, thereby, to the longevity in the adsorbed state. This would diminish α even more pronouncedly, were it not for the rapid decrease of the saturation pressure. Therefore, it is not surprising that α-values close to unity have been found for Hg. On the other hand, almost as high values, reported for CCl_4 at temperatures very near the critical film temperature,[5,6] are hard to reconcile with the simple picture here presented.

The preceding considerations are restricted to liquids, not because the free mobility of adatoms is insufficient on the surface of crystals, but because the structure of the crystalline surface permits of substrate-film transitions only at certain active centers, i.e. at the "half-crystal" sites of Stranski.[2] Primarily by this reason, surface diffusion, as another rate-determining step, has to be taken into account in the kinetics of sublimation.

[1] G. Wyllie, Proc. Roy. Soc. **A197**, 383 (1949).
[2] Max Volmer, *Kinetik der Phasenbildung* (Theodor Steinkopff, Dresden, 1939).
[3] Leonard B. Loeb, *Kinetic Theory of Gases* (McGraw-Hill Book Company, Inc., New York, 1927), p. 330.
[4] H. M. Cassel, J. Phys. Chem. **48**, 195 (1944).
[5] M. Baranaev, J. Phys. Chem. USSR **13**, 1635 (1939).
[6] W. Prueger, Zeits. f. Physik **115**, 202 (1940).

Calculations of the Lower Excited Levels of Benzene

C. C. J. ROOTHAAN*
Department of Physics, The University of Chicago, Chicago, Illinois
AND
ROBERT G. PARR
Department of Chemistry, Carnegie Institute of Technology, Pittsburgh, Pennsylvania
July 26, 1949

In a 1938 paper under the above title,[1] Goeppert-Mayer and Sklar employed the method of antisymmetrized products of molecular orbitals to calculate the lower excited electronic energy levels of the benzene molecule. Using no other empirical data than the carbon-carbon distance, and considering the six π-electrons alone, they obtained excitation energies which agreed fairly well with experiment[2] (see second and last columns in Table I). It was noticed later by London,[3] and independently by Goeppert-Mayer and McCallum,[4] however, that repetition of the calculation including the small, but numerous, initially neglected terms yields results which are less encouraging (see third column in Table I).

Recently it has been found that Goeppert-Mayer and Sklar (and London) used incorrect values for certain integrals.[5] We wish to call attention to the results that are obtained when correction is made for this. When the Goeppert-Mayer-Sklar work is repeated,[6,7] the energies which are found are bad (see fourth column in Table I), but the energies one gets upon redoing the London calculation are very encouraging (see next to last column in Table I).

TABLE I. Electronic energy levels of benzene (ev).

Level	Goeppert-Mayer Sklar[b] (I, N)[a]	London[c] (I)[a]	Craig Parr[d] (N)[a]	Roothaan Parr[e]	Observed[f]
$^1E_{1u}(^1\Gamma_{12})$	8.0	11.1	6.7	9.7	7.0
$^1B_{1u}(^1\Gamma_{10})$	5.8	8.8	4.2	7.2	6.2
$^1B_{2u}(^1\Gamma_9)$	5.0	7.3	3.7	5.8	4.9
$^3B_{2u}(^3\Gamma_{10})$	3.0	7.2	1.5	5.6	—
$^3E_{1u}(^3\Gamma_{12})$	2.2	5.8	0.8	4.3	—
$^3B_{1u}(^3\Gamma_9)$	1.5	4.5	0.2	3.0	3.8[g]
$^1A_{1g}(^1\Gamma_1)$	0.0	0.0	0.0	0.0	0.0

[a] I denotes incorrect integrals (see reference 5); N denotes neglect of hybrid, exchange, and penetration integrals involving non-neighboring carbon atoms.
[b] Reference 1.
[c] Reference 3.
[d] References 6 and 7.
[e] These values have been calculated independently by both authors, and have been essentially confirmed by Mulliken [R. S. Mulliken, "Report on Molecular Orbital Theory," J. de Chim. Phys. (to be published)].
[f] Reference 2.
[g] The investigations of H. Shull, J. Chem. Phys. **17**, 295 (1949) and D. S. McClure, J. Chem. Phys. **17**, 665 (1949), indicate that this observed level may have the symmetry $^3B_{2u}$. If this is the case, the calculated triplet levels fall in the wrong order, since the 3.8 ev level is definitely the lowest triplet level (see reference 2).

* On leave of absence from The Catholic University of America, Washington, D. C.
[1] M. Goeppert-Mayer and A. L. Sklar, J. Chem. Phys. **6**, 645 (1938).
[2] C. C. J. Roothaan and R. S. Mulliken, J. Chem. Phys. **16**, 118 (1948).
[3] A. London, J. Chem. Phys. **13**, 396 (1945).
[4] M. Goeppert-Mayer and K. J. McCallum, Rev. Mod. Phys. **14**, 248 (1942).
[5] R. G. Parr and B. L. Crawford, Jr., J. Chem. Phys. **16**, 1049 (1948).
[6] R. G. Parr, Ph.D. Thesis, University of Minnesota, 1947; B. L. Crawford, Jr. and R. G. Parr, J. Chem. Phys. **17**, 726 (1949).
[7] D. P. Craig, "Polar Structures in the theory of conjugated molecules, Part 4" (to be published). We are greatly indebted to Dr. Craig for allowing us to see his manuscript.

Dynamic Properties of Polymeric Materials

BASIL A. DUNELL* AND ARTHUR V. TOBOLSKY
The Textile Foundation and Frick Chemical Laboratory, Princeton University, Princeton, New Jersey
August 17, 1949

CONSIDERABLE interest is attached to the problem of the mechanical properties (dynamic modulus G_{dyn} and dynamic viscosity η_{dyn}) of high polymers subjected to harmonic vibrations of varying frequencies. In particular, it has been observed that $\eta_{dyn}\omega$ is relatively independent of frequency $\omega/2\pi$ over a considerable frequency range.[1-4] The question has also arisen as to whether a relationship exists between the dynamic energy losses and static phenomena such as creep.

Kuhn has shown how, in a material for which the creep curve is linear with logarithmic time, one may predict the dynamic losses in free vibration experiments.[5] In the course of his theoretical arguments he described the mechanical system approximately in terms of a distribution of relaxation times which is a rectangular function on a logarithmic plot, namely,

$$\left.\begin{aligned} G(\tau)d(\log\tau) &= G_0 \quad a<\tau<b \\ &= 0 \quad a>\tau,\ \tau>b \end{aligned}\right\}. \tag{1}$$

This distribution of relaxation times had previously been extensively investigated by Becker for ferromagnetic hysteretic behavior.[6] The same function was also shown to fit stress relaxation data in polyisobutylene.[7]

By use of the distribution function (1), the correlation between stress relaxation and dynamic properties is exact and remarkably simple, and is mathematically even more direct than the correlation between creep data and dynamic properties. If stress relaxation is linear when plotted against logarithmic time, the data can be expressed in terms of the distribution function (1), where a and b are, respectively, smaller than and greater than the smallest and largest recorded times. For dynamic experiments in which $1/b \ll \omega \ll 1/a$, the following very simple relationship exists:

$$\eta_{dyn}\omega = \frac{\pi}{2\epsilon_0 \log_e 10} \begin{pmatrix}\text{slope of relaxation curve plotted} \\ \text{vs. } \log_{10} \text{ time}\end{pmatrix}, \tag{2}$$

where ϵ_0 is the fixed strain at which the stress relaxation measurement is being carried out.

This relationship was applied to stress relaxation data[8] for rubbers, and the predicted values of $\eta_{dyn}\omega$ were compared with observed values of $\eta_{dyn}\omega$ for the same rubber stocks.[3] Also experimental data were obtained for stress relaxation and dynamic properties of various textile fibers, and comparison between $\eta_{dyn}\omega$ values predicted from Eq. (2) and observed values was made. These comparisons are shown in Table I. It is clear from this table that an order of magnitude agreement exists between the observed and calculated values. In most cases the losses predicted from stress relaxation data are less than the observed dynamic losses. Papers detailing the theoretical and experimental developments will appear soon in the *Textile Research Journal*.

TABLE I.

Material	Temp. °C	Calc'd $\eta_{dyn\omega}$ dynes/cm²	Observed $\eta_{dyn\omega}$ dynes/cm²
Hevea gum stock	40°	0.026×10^{8}	0.24×10^{8}
	100°	0.045×10^{8}	0.13×10^{8}
Hevea tread stock	40°	0.48×10^{8}	2.5×10^{8}
	100°	0.55×10^{8}	1.1×10^{8}
GR-S gum stock	40°	0.11×10^{6}	0.85×10^{6}
	100°	0.11×10^{6}	0.42×10^{6}
GR-S tread stock	40°	1.1×10^{6}	7.8×10^{6}
	100°	0.40×10^{8}	3.0×10^{6}
Butaprene gum	40°	0.17×10^{6}	1.7×10^{6}
	100°	0.25×10^{6}	0.70×10^{6}
Butaprene tread	40°	0.42×10^{6}	4.1×10^{6}
	100°	0.40×10^{6}	1.5×10^{6}
Neoprene gum	40°	0.33×10^{6}	0.85×10^{6}
	100°	0.33×10^{6}	0.68×10^{6}
Neoprene tread	40°	0.82×10^{6}	3.9×10^{6}
	100°	0.86×10^{6}	2.0×10^{6}
Nylon	20°	0.8×10^{9}	3.8×10^{9}
Viscose rayon	20°	1.4×10^{9}	4.8×10^{9}
Acetate rayon	20°	1.2×10^{9}	1.5×10^{9}
Feather keratin	20°	0.70×10^{9}	1.5×10^{9}
Raw silk	20°	2.3×10^{9}	3.8×10^{9}
Polyethylene	20°	0.18×10^{9}	0.82×10^{9}

Grateful acknowledgment is made to the ONR which supported this work through Contract No. N7-onr-374, Task Order I.

* Research Fellow of Textile Research Institute.

[1] A. L. Kimball and D. E. Lovell, Phys. Rev. **30**, 948 (1927).
[2] Gehman, Woodford, and Stambaugh, Ind. and Eng. Chem. **33**, 1032 (1941).
[3] Dillon, Prettyman, and Hall, J. App. Phys. **15**, 309 (1944).
[4] Palandri, Rubber Age **64**, 45 (1948).
[5] Kuhn, Künzle, and Preissmann, Helv. Chim. Acta **30**, 307, 464, 839 (1947).
[6] R. Becker, *Probleme der technischen Magnetisierungskurve* (Verlag J. Springer, Berlin, 1938), p. 103.
R. Becker and W. Döring, *Ferromagnetismus* (Verlag J. Springer, Berlin, 1939), p. 254.
[7] Andrews, Hofman-Bang, and Tobolsky, J. Polymer Sci. **3**, 669 (1948).
[8] Tobolsky, Prettyman, and Dillon, J. App. Phys. **15**, 380 (1944); also unpublished data obtained during this same investigation.

A Kinetic Mechanism for Ion-Exchange

ARTHUR W. ADAMSON AND JACK J. GROSSMAN
Department of Chemistry, The University of Southern California, Los Angeles, California

August 15, 1949

IT has generally been observed that the velocity of the zeolitic exchange of monovalent ions in dilute solution obeys simple mass action rate equations.[1–4] It does not necessarily follow, however, that a chemical exchange process is rate controlling. Thus, Boyd, Adamson, and Myers[4] showed that for tracer exchange the observed mass action rate equation was predicted on the basis of diffusion through a bounding liquid film. This mechanism, moreover, explained the dependence of the exchange velocity on the particle size and stirring rate.

The present paper extends the film diffusion hypothesis to the more common case of exchange of macro-concentrations of both ions. The equilibrium constant for the exchange process $A^+ + BR = AR + B^+$ may be written as

$$K = \bar{C}_B N_A / \bar{C}_A N_B. \tag{1}$$

The thermodynamic activities have been assumed equal to the molar concentrations in solution and to the mole fractions N_A and N_B in the resin phase.

The permeation of the ions through the liquid film is given by Fick's first law

$$P_A = -D_A(\partial C_A/\partial l) = D_A(C_A - \bar{C}_A)/l$$
$$P_B = -D_B(\partial C_B/\partial l) = D_B(C_B - \bar{C}_B)/l. \tag{2}$$

It is assumed that the concentrations of A^+ and B^+ vary linearly from C_A and C_B, the average solution concentrations, to $\bar{C}_A$ and $\bar{C}_B$ at the surface of the resin particle, over a region of effective thickness l. $\bar{C}_A$ and $\bar{C}_B$ are taken to be those concentrations in equilibrium with the instantaneous composition of the exchanger, and hence by (1)

$$\bar{C}_A = \bar{a}/(1+\bar{C}_B/\bar{C}_A) = \bar{a}/(1+KN_B/N_A), \tag{3}$$

where $\bar{a} = \bar{C}_A + \bar{C}_B$. It follows, by a material balance, that

$$\Sigma P_A = d(\chi\bar{C}_A)/dt + d(EN_A)/dt \tag{4}$$
$$\Sigma(P_A + P_B) = d(\chi\bar{a})/dt, \tag{5}$$

where Σ is the surface area/g of resin of exchange capacity E equivalents/g, and χ is the "interstitial" volume/g. The variations in $\chi\bar{C}_A$ and $\chi\bar{a}$ can be neglected if the solution is dilute, so to a first approximation, the net transfer rate may be set equal to zero, i.e. $P_A + P_B = 0$. By means of (2), (3), and (5) it follows that

$$\bar{a} = \frac{(D_A C_A + D_B C_B)(KN_B + N_A)}{D_A N_A + KD_B N_B} \tag{6}$$

and then from (2), (3), (5), and (6), the permeations of the two ions are

$$P_A = -P_B = \frac{D_A D_B (KC_A N_B - C_B N_A)}{l(D_A N_A + KD_B N_B)}. \tag{7}$$

Setting $d(\chi\bar{C}_A)/dt = 0$ in Eq. (4), the differential rate equation becomes

$$dN_A/dt = \frac{\Sigma D_A D_B (KC_A N_B - C_B N_A)}{El(D_A N_A + KD_B N_B)}. \tag{8}$$

Two cases will be considered. For constant outer solution concentration, (8) becomes

$$dN_A/dt = \frac{\Sigma D_A[C_A^0 - (C_A^0 + C_B^0/K)N_A]}{El[1 + (D_A/KD_B - 1)N_A]} \tag{9}$$

and for variable solution concentration, where $C_B = 0$ and $C_A = C_A^0$ at $t = 0$

$$dN_A/dt = \frac{\Sigma W D_A[K(1-N_A)(C_A^0 V/WE - N_A) - N_A^2]}{VKl[1 + (D_A/KD_B - 1)N_A]} \tag{10}$$

where V is the total volume of solution and W the weight of ion-exchanger. The quantity D_A/KD_B is of the order of unity for the exchange of monovalent ions, and if N_A remains small throughout the exchange reaction, the bracketed expression in the denominator may be set equal to unity. With this approximation, (8) becomes a mass action type rate equation and the special cases, (9) and (10), give on integration

$$\ln(1 - N_A/N_A^\infty) = -kt \tag{11}$$

$$\frac{N_A^\infty}{2\alpha - (1+\alpha)N_A^\infty} \frac{\ln\alpha(N_A + N_A^\infty) - (1+\alpha)N_A^\infty N_A}{\alpha(N_A^\infty - N_A)} = k't, \tag{12}$$

where $\alpha = C_A^0 V/WE$. N_A^∞ is the mole fraction of A^+ on resin sites at equilibrium, and k and k' are

$$k = \frac{\Sigma D_A C_A^0 N_A^\infty}{El} \tag{11a}$$

$$k' = \Sigma W D_A / Vl. \tag{12a}$$

Equations (11) and (12) are identical with the first and second order mass action equations that have been observed experimentally, except for the different significance of the rate constants, (11a) and (12a).

This demonstration of the similarity of the film diffusion and mass action equations makes it apparent that the presently available rate data does not permit differentiation between film diffusion and chemical exchange as the rate controlling process. Such differentiation would be possible, however, under conditions such that the expression in the denominator of (9) cannot be taken as unity. Thus, the complete integral of (9) is

$$\ln\left(1 - \frac{N_A}{N_A^\infty}\right) + \frac{C_A^0(D_A - KD_B)N_A}{(C_A^0 D_A + C_B^0 D_B)N_A^\infty} = -\frac{\Sigma D_A D_B (KC_A^0 + C_B^0)C_A^0}{ElN_A^\infty(C_A^0 D_A + C_B^0 D_B)}t \tag{13}$$

and if C_B^0 be kept equal to zero, it reduces to

$$\ln(1-N_A)+(1-KD_B/D_A)N_A=-(\Sigma D_B K C_A^0/El)t. \quad (14)$$

Since N_A no longer remains small, the correction term in (9) cannot be neglected and its effect may be maximized further by choice of a system for which KD_B/D_A is large (e.g., Cs^+-H^+ exchange). These conditions can be met experimentally, and this means of testing the validity of the film diffusion mechanism is currently under investigation, as well as the more obvious approach of varying the particle sizes and flow or stirring rate.

[1] F. C. Nachod and W. Wood, J. Am. Chem. Soc. **66**, 1380 (1944).
[2] H. A. Thomas, J. Am. Chem. Soc. **66**, 1664 (1944).
[3] W. Juda and M. Carron, J. Am. Chem. Soc. **70**, 3295 (1948).
[4] Boyd, Adamson, and Myers, Jr., J. Am. Chem. Soc. **69**, 2836 (1947).

Availability of Radioantimony-Beryllium Neutron Sources

OAK Ridge National Laboratory has developed a relatively inexpensive radioantimony-beryllium neutron source which is now available for distribution to users in the United States. These sources will be allocated through the Isotopes Division, U. S. Atomic Energy Commission.

The sources use a core of 32 grams of antimony metal surrounded by a $\frac{3}{16}$ in.-thick beryllium metal cup, the assembly being enclosed in an aluminum jacket. The outside dimensions of this jacket are as follows:

Cylinder containing source	$1\frac{3}{16}$ in. diameter$\times 1\frac{3}{16}$ in. long
Aluminum plate protruding from one end	$\frac{5}{8}$ in.
Hole in plate for handling	$\frac{1}{4}$ in.
Over-all length of assembly	$1\frac{3}{4}$ in.

The entire unit is placed in the pile and the antimony activated to the desired level. Antimony 122 (half-life 2.8 days) and antimony 124 (half-life 60 days, gamma-ray energy 1.72 Mev) are both formed in this irradiation, but the source can stand for two weeks before shipment to allow the Sb 122 to decay. Saturation activity of the Sb 124 is approximately 3.5 curies; however, normally an activation time of 120 days will be used which will give an activity of about 2.6 curies. A source activated for 69 days and cooled for 16 days gave an unshielded gamma-radiation reading of about 20 roentgens/hour at one foot. Other readings followed the inverse square very closely. Shorter activation periods may be arranged if a lower activity is satisfactory. After the activity of the Sb 124 has decayed, it may be reactivated by reinsertion in the pile.

It has been found that the saturated source will emit a total of about 8×10^6 neutrons per second or 9.8×10^4 neutrons/cm²/second at one inch, if it is assumed that the source behaves as a point source. The neutrons are approximately monoenergetic.*

The shipping container for the source will weigh approximately 350 pounds and should be returned to Oak Ridge National Laboratory within three weeks after date of shipment. A customer will have to make arrangements beforehand to provide a suitable storage space for the source; a lead pig with walls four inches thick would probably be sufficient.

It is planned to charge for the source and the irradiation separately, thus allowing the requestor to choose one, two or more months' irradiation time. The itemized costs of the source are as follows:

Antimony-beryllium Source	$44.00
Service Irradiation of Source	$43.00/month
Returnable Deposit on Container	$400.00.

* The following are references to articles dealing with the subject of the energy of the neutron: Collins, Waldman and Guth, Phys. Rev. **56**, 878 (1939); D. J. Hughes and C. Eggler, Phys. Rev. **72**, 902 (1947); A. Wattenberg, Phys. Rev. **71**, 497 (1947).

The Critical Point of Heterogeneous Polymers

H. TOMPA
Research Laboratory, Courtaulds, Ltd., Berkshire, England
August 31, 1949

IN a recent note Stockmayer[1] derived equations giving the concentration of the solvent and the value of the interaction constant at the critical point of solutions of heterogeneous polymers which conform to the Flory-Huggins theory. Stockmayer's conclusion is that the critical point depends on the weight- and z-average molecular weights and not on the number-average molecular weight as previously believed.[2]

It is well, however, to consider carefully the significance of the critical point. By definition a critical point is a point in the phase diagram at which two coexisting phases become identical. The point derived by Stockmayer satisfies this condition. But while for a two-component system a small change of concentration, at constant temperature and pressure, leads one into the homogeneous region, it must not be assumed that this is necessarily the case for a multi-component system, and, in fact, it will not be so in general. The thermodynamic reason for this is that for a two-component system such a change is one at which the intensive variables remain constant, while for a multi-component system even at the critical point changes at constant temperature and pressure are possible in which the chemical potentials are not constant. In general, a change along a line in the phase diagram joining the point representing the pure solvent and the point representing a given heterogeneous polymer involves changes of chemical potentials even at the critical point and leads in one direction into the heterogeneous region. In other words, even if such a line may pass through a critical point, it is not necessarily a tangent to the binodial there, but cuts the two-phase boundary there and at another point, and passes through the two-phase region between these points. Solutions of the given polymer will separate into two phases in a certain range of concentrations even for values of the interaction constant μ which are below that given by Stockmayer; the minimum value of μ for which this holds is the one at which the line touches the two-phase boundary, but the point of contact is not, in general, a critical point, and the coexisting phase has a different composition.

These conditions are brought out in the diagrams given by the author in a recent publication[3] for the case in which the heterogeneous polymer consists of two species only (Figs. 6 and 7). It is easily confirmed that Stockmayer's Eqs. (6) and (7) reduce to those given by the author for the case of two-polymer components,

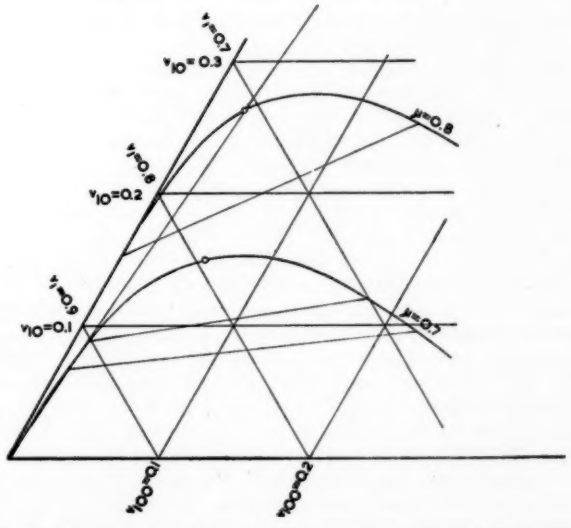

FIG. 1. Corner of phase diagram of the system solvent and two polymers of chain-lengths 10 and 100, with binodials for μ=0.7 and 0.8. o critical points, v volume fractions.

Eqs. (15) and (16).[3] The part near the solvent corner of the triangular diagram for the case of two polymers of chain-lengths 10 and 100 is shown in Fig. 1, together with the binodials for $\mu=0.7$ and 0.8. The critical points are also shown, as well as several tie lines. The line joining the pure solvent ($v_1=1$) to the point representing a polymer of composition $v_{10}^{c}=0.9105$, $v_{100}^{c}=0.0895$, passes through the critical point of the binodial for $\mu=0.8$ ($v_1=0.7096$, $v_{10}=0.2644$, $v_{100}=0.0260$) and cuts this binodial again near $v_1=1$. It also cuts the binodial for $\mu=0.7$ at about $v_1=0.920$, $v_{10}=0.073$, $v_{100}=0.007$, and again near $v_1=1$, and the least value of μ for which separation into two phases is possible, is somewhat below 0.7. For this polymer Stockmayer's equation for the critical point gives 0.8; on the assumption that the critical point is determined by the number average molecular weight, the critical value would be 0.849, even further from the minimum value.

[1] W. H. Stockmayer, J. Chem. Phys. **17**, 588 (1949).
[2] Robert L. Scott, J. Chem. Phys. **13**, 178 (1945).
[3] H. Tompa, Trans. Faraday Soc. (submitted for publication).

Solubilization in Swollen Micelles*

H. B. KLEVENS
Division of Agricultural Biochemistry, University of Minnesota. St. Paul 1, Minnesota
August 29, 1949

RECENTLY, additional evidence to indicate that there are at least two different loci of solubilization in soap micelles has been obtained. Previous indications were based on the fact that there were characteristic differences observed when solubilization data (moles oil dissolved *vs.* moles soap) were plotted. In the case of non-polar solubilization, the curves were convex toward the concentration axis; for dyes or polar compounds, curves were linear or concave toward this axis.[1] Long-chain alcohol solubilization (as *n*-heptanol) show this latter effect.[2] Micelles were found to increase in size in the presence of hydrocarbons[3] and it has been indicated that long-chain alcohols do not swell micelles.[4] It is apparent that the hydrocarbons are solubilized by being incorporated in the micelle center while the polar molecules upon solubilization are oriented, in the micelle, as are the soap molecules, with their hydrocarbon chains lying roughly parallel to those of the soap molecules and their polar-hydrogen-bonding head toward the water.[1,2] If this hypothesis is correct, it should be possible to prepare a swollen micelle (soap solution essentially saturated with polar compound such as a long-chain alcohol) which would solubilize more hydrocarbon than the same concentration of soap alone.

Soap solutions were shaken with *n*-heptanol for more than 24 hours in sealed ampules and then *n*-heptane was added. Saturation was determined by an increase in turbidity. The data in Fig. 1 show this enhancement of solubilization in comparing the systems potassium *n*-tetradecanoate: *n*-heptanol: *n*-heptane and potassium *n*-tetradecanoate: *n*-heptane. The presence of the long-chain alcohol in potassium tetradecanoate increases the solubilization of *n*-heptane as much as fourfold. This is much more than would be solubilized if an amount of potassium tetradecanoate equivalent to the alcohol were added to the original soap concentration. The enhancement of solubilization is also much more marked than would be found if an equivalent amount of potassium *n*-heptanoate in place of *n*-heptanol were added to the soap solution. Thus, since there is this observed increase in solubilization and since the solubilizations of *n*-heptane and *n*-heptanol are independent of each other in the same soap solution (i.e., they are not additive), it must follow that there are at least two loci of solubilization in the soap micelle. Quite similar results have been obtained with added long-chain amines and mercaptans and their effect on the increase of solubilization. These data, with additional results on the alcohol systems, will be reported more in detail in a forthcoming publication.

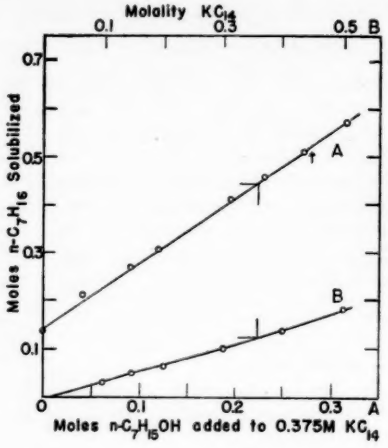

FIG. 1. Comparison of the solubilization of *n*-heptane in *n*-tetradecanoate (B) and in 0.375 M *n*-tetradecanoate with added *n*-heptanol (A). Arrow indicates saturation point of *n*-heptanol in 0.375 M potassium *n*-tetradecanoate.

An explanation of this greatly enhanced solubilization can possibly be found by consideration of the change in the geometry of the micelle. The addition of 0.75 mole *n*-heptanol per mole *n*-tetradecanoate (at 0.375 M soap), the chain-length of the alcohol being considerably shorter than that of the soap, would result in a considerable increase in the curvature of the micelle surface. This would result in an increase in the short axis and a decrease in the long axis of the prolate spheroid micelle.[5] More micelles would form and the total volume available for solubilization of the *n*-heptane would increase. Calculations, based on these assumptions, agree with the experimental findings.

Further, an extremely turbid system is observed when one exceeds the saturation of a long-chain alcohol in a soap solution. Addition of a hydrocarbon to this emulsion results in an enhancement of solubility of the alcohol as evidenced by a marked decrease in turbidity until a transparent system is obtained. A turbid emulsion (a gel at room temperature) is again found upon further hydrocarbon addition. As much as 8–10 times the normal solubilization of *n*-heptane in soap solutions is possible in such *n*-heptanol: *n*-tetradecanoate systems where the initial alcohol concentration exceeds its solubility in the soap solution.

* Paper No. 2498, Sci. J. Series, Minnesota Agricultural Experiment Station.
[1] H. B. Klevens, Am. Chem. Soc. meeting, New York, New York (September 15–19, 1947); J. Am. Oil Chem. Soc. **25** (1949).
[2] W. D. Harkins and H. Oppenheimer, J. Am. Chem. Soc. **71**, 808 (1949).
[3] See, for example, review by J. W. McBain, *Advances in Colloid Science* (Interscience Publishers, Inc., New York, 1942), Vol. 1.
[4] W. D. Harkins and R. Mittelman, mentioned in reference 2.
[5] H. B. Klevens, Colloid Symposium, Cambridge, Massachusetts (June 23–25, 1948); J. Colloid Sci. (in press).

Simplified Technique for Surface Area Determination by Adsorption of Nitrogen

W. V. LOEBENSTEIN AND V. R. DEITZ
National Bureau of Standards, Washington, D. C.
September 1, 1949

THE determination of surface area of solid adsorbents by the *BET* method has been one of the most important developments in recent times in the field of surface chemistry. It is based upon the determination of the amounts of nitrogen adsorbed at liquid oxygen or liquid nitrogen temperatures at two or more equilibrium pressures.

A new simplified method has been developed in this laboratory for determining surface areas by nitrogen adsorption. It is based upon the preferential adsorption of nitrogen from nitrogen-helium mixtures at liquid oxygen temperatures. The method proposed has the particular advantage that a vacuum pumping system is not required. Also, less time is consumed in completing

a determination than with the conventional method and without sacrifice of accuracy. The proposed assembly is adaptable to a portable piece of equipment for surface area measurements.

The apparatus includes a U-shaped adsorption tube, one arm of which is capillary tubing and the other contains the sample. A gas entering the tube has intimate access to all parts of the sample before leaving. Calibrated gas burets of approximately equal volume are connected to each of the two arms of the adsorption tube. Both burets are equipped with hand-operated mercury leveling bulbs.

The sample contained in the adsorption tube is freed from conflicting impurities, such as air and moisture, by heating in a continuous stream of helium. Before making the dead-space-calibration, the exit connection is closed and the furnace surrounding the adsorption tube replaced by a Dewar flask containing liquid oxygen. A quantity of helium is next drawn into the system filling the sample tube and only one of the burets. The resultant pressure is designated as p_1. When the helium is expanded so as to include the second buret, as well, its pressure becomes p_2. The "dead-space" volume may be calculated according to the easily derivable relationship:

$$V/T=[p_2/(p_1-p_2)](V_2/T_0)-V_1/T_0,$$

where V = geometrical volume of dead space, T = temperature of liquid O_2 or N_2 bath, V_2 = volume of buret No. 2, V_1 = volume of buret No. 1, p_2 = pressure of helium in the system including both burets and dead space, p_1 = pressure of same quantity of helium when compressed into the volume of No. 1 buret and the dead space, and T_0 = room temperature.

A measured amount of nitrogen is then introduced and the helium-nitrogen mixture is passed from one gas buret through the sample to the other buret. This process is repeated until a constant pressure reading is obtained. The liquid oxygen bath is not removed between the time of calibration and nitrogen adsorption. An additional quantity of nitrogen is added for each subsequent adsorption point. In the calculation it is necessary to subtract the partial pressure of the helium from the total pressure to obtain that due to the nitrogen. The surface area may be then calculated from the adsorption data in the well-known procedure of Brunauer, Emmet, and Teller.

It has been shown for a number of adsorbents, such as silica gel, coconut-shell charcoal, an activated clay, titania, and bone char, that the pressure of helium has very little, if any, influence on the adsorption of nitrogen at liquid oxygen temperature. For example, values for surface area of 60, 61, 61 m^2/g were obtained for a sample of bone char with the respective partial pressure of helium of 80, 79, and 405 mm Hg. The value obtained for the same sample in the absence of helium in a conventional system was 59 m^2/g.

Carrier-Free Radioisotopes from Cyclotron Targets. I. Preparation and Isolation of Sn^{113} and In^{114} from Cadmium*

ROY D. MAXWELL,** HERMAN R. HAYMOND, DONALD R. BOMBERGER, WARREN M. GARRISON, AND JOSEPH G. HAMILTON

Crocker Laboratory and Divisions of Medical Physics, Experimental Medicine, and Radiology; University of California, Berkeley and San Francisco, California

August 29, 1949

THE cyclotron is the only practical source of many carrier-free[1] radioisotopes. The preparation and radiochemical isolation of a number of these activities, produced in the 60-in. cyclotron of Crocker Laboratory, will be presented in this paper and in subsequent papers of this series. In most cases the carrier-free radioisotopes were prepared for use in biological systems and the final preparations were in the form of isotonic saline solutions at a range of pH from 5 to 8.

The present paper reports the radiochemical isolation of carrier-free Sn^{113} and In^{114} produced by bombarding cadmium with 38-Mev alpha-particles. At this energy, Sn^{113} and In^{114} are produced in a thick target by the nuclear reactions:[2] $Cd^{110}(\alpha, n)Sn^{113}$, $Cd^{111}(\alpha, 2n)Sn^{113}$, $Cd^{112}(\alpha, 3n)Sn^{113}$, $Cd^{111}(\alpha, p)In^{114}$, $Cd^{113}(\alpha, pn)In^{114}$. The shorter-lived tin and indium activities, together with the possible radioisotopes of silver produced by (n, p) reactions, were allowed to decay out prior to the chemical separations.

The target, a block of C.P. cadmium metal, soft-soldered to a water-cooled copper plate, was bombarded with 38-Mev alpha-particles for a total of 450 μa-hr. at an average beam intensity of 3.4 μa. After aging for one week, the bombarded surface was milled off and dissolved in a minimum volume of 16N HNO_3.

A 0.2 g of target cadmium nitrate was dissolved in 25 ml of water, and the tin and indium activities were carried quantitatively on 10 mg of $Fe(OH)_3$ precipitated with NH_4OH. The $Fe(OH)_3$ was dissolved in 15 ml of 36N H_2SO_4 and transferred to an all-glass distilling flask.[3,4] The 9N HBr was added dropwise while a stream of CO_2 was bubbled through the solution at 220°C. The distillate containing the carrier-free Sn^{113}, HBr, Br_2, and traces of H_2SO_4 was caught in a series of traps filled with 12N HCl; the indium activity remained in the residue. Carrier-free radio-tin collected in HNO_3 or H_2SO_4 forms a radiocolloid[5,6] and is adsorbed onto the walls of the containing vessel. The 12N HCl keeps the radio-tin in solution, presumably as the chlorostannate complex. The trap contents were treated with 5 ml of 16N HNO_3 to destroy HBr, 15 mg of citric acid were added and the solution was evaporated on a steam bath to the 1- to 2-ml volume of H_2SO_4 carried over in the distillation. Citric acid prevents the formation of radiocolloid after removal of HCl.

The H_2SO_4 solution was diluted with 25 ml of water and the radio-tin was carried down on $Fe(OH)_3$ precipitated with NH_4OH: The $Fe(OH)_3$ was dissolved in 8N HCl and iron was extracted with isopropyl ether. The aqueous phase, containing HCl, Sn^{113}, and equilibrium amounts of the In^{113} daughter, was evaporated to dryness on 10 mg of sodium citrate. The activity dissolved quantitatively in distilled water.

The carrier-free Sn^{113} was identified by its 105-day half-life and by the 0.39-Mev conversion electron of the In^{113} daughter.[7] The indium fraction from a chemical separation of an equilibrium mixture using tin and indium carriers, showed the 105-min. period of In^{113}.

The residue from the tin distillation, containing Fe^{+++} and In^{114}, was neutralized with NH_4OH. The $Fe(OH)_3$ plus indium activity was dissolved in 8N HCl, and extracted with isopropyl ether. The HCl solution of In^{114} was evaporated to dryness on 10 mg of NaCl. The activity dissolved quantitatively with the addition of distilled water. The In^{114} was identified by the assigned 48-day half-life and by the 0.19-Mev conversion electron.[7,8]

The authors wish to express their appreciation to Professor G. T. Seaborg for his interest in this work, to Mr. T. Putnam and B. Rossi and the 60-in. cyclotron staff for bombardments, and to Mrs. Alberta Mozley and Mrs. Helen Haydon for technical assistance.

* This document is based on work performed under Contract No. W-7405-eng-48-A for the AEC.

** Lieutenant Colonel, U. S. Army, now stationed at Walter Reed Hospital, Washington, D. C.

[1] This term is used to indicate that no stable isotopic carriers have been intentionally added. In a "carrier-free" separation the specific activity is determined by the chemical purity of the reagents.

[2] G. T. Seaborg and I. Perlman, Rev. Mod. Phys. **20**, 585 (1948).

[3] J. A. Scherrer, J. Research Nat. Bur. Stand. **21**, 95 (1938).

[4] Schwaibold, Borchers, and Nagel, Biochem. Zeits. **306**, 113 (1940).

[5] O. Hahn, *Applied Radiochemistry* (Cornell University Press, Ithaca, New York, 1936).

[6] The colloidal properties of carrier-free radio-tin are being investigated. These results will be published elsewhere.

[7] S. W. Barnes, Phys. Rev. **56**, 414 (1939).

[8] J. L. Lawson and J. M. Cork, Phys. Rev. **57**, 982 (1940).

Carrier-Free Radioisotopes from Cyclotron Targets. II. Preparation and Isolation of Cd^{109} from Silver*

ROY D. MAXWELL,** HERMAN R. HAYMOND, WARREN M. GARRISON, AND JOSEPH G. HAMILTON

Crocker Laboratory and Divisions of Medical Physics, Experimental Medicine, and Radiology; University of California, Berkeley and San Francisco, California

August 29, 1949

THE radionuclide, Cd^{109}, produced by the nuclear reaction $Ag^{109}(d, 2n)$[1] has been isolated without added isotopic carrier by a solvent-extraction procedure based on the selective solubility of cadmium pyridine thiocyanate in chloroform. Radioactive palladium, 13-hr. Pd^{109}, produced by the reaction $Ag^{109}(n, p)$, was allowed to decay out prior to the separation of 185-day Cd^{109}. This activity, however, is not extracted with cadmium and the method may be used in isolating 6.7-hr. Cd^{107} from an un-aged target.

The target was a block of spectrographically pure silver[2] ($\frac{1}{4}$ in. thick), soldered to a water-cooled copper plate. It was bombarded with 19-Mev deuterons for a total of 100 μa-hr. in the 60-in. cyclotron at Crocker Laboratory. The bombarded surface of the silver was removed from the target by milling off to a depth of $\frac{1}{8}$ in.

The silver turnings were dissolved in a minimum volume of 16N HNO_3 and the solution was evaporated to dryness on a steam bath. The $AgNO_3$ plus activity was dissolved in 25 ml of H_2O and the silver was complexed with excess NH_4CNS. The solution was adjusted to pH 5 with sodium acetate and the Cd^{109} was extracted with chloroform containing 5 percent pyridine. This procedure, originally developed[3] for the separation of micro amounts of cadmium, quantitatively extracted Cd^{109} from solutions containing presumably less than 10^{-8} g of stable cadmium.

To remove traces of silver, the chloroform phase was evaporated to dryness on a steam bath, redissolved in 2 to 3 ml of 1 percent H_2SO_4, and extracted with 0.005 percent dithizone in chloroform.[4] The final solution of Cd^{109} contained less than one microgram of silver.

A small portion of the activity was added to a solution containing silver and cadmium in carrier amounts, and the silver was precipitated as AgCl. Ninety-nine percent of the activity remained in the supernatant.

Absorption measurements in aluminum showed conversion electrons of approximately 0.1 Mev and the 22-kev x-ray of the Ag^{109} daughter. These data agree with the previously reported values.[1]

The authors wish to express their appreciation to the crew of the 60-in. cyclotron for the bombardments, and to Mrs. Alberta Mozley and Mrs. Helen Haydon for technical assistance in counting.

* This document is based on work performed under Contract No. W-7405-eng-48-A for the AEC.

** Lieutenant Colonel, U. S. Army, now stationed at Walter Reed Hospital, Washington, D. C.

[1] A. C. Helmholz, Phys. Rev. **70**, 982 (1946).

[2] The silver was obtained from Johnson Mathey and Company. Cadmium was not detected by spectrographic analysis.

[3] H. Fischer and G. Leopoldi, Mikrochim. Acta **1**, 30 (1937).

[4] E. B. Sandell, *Colorimetric Determination of Traces of Metals* (Interscience Publishers, Inc., New York, 1944).

The Critical Points of Ternary Systems with a Polymer Component

H. TOMPA

Research Laboratory, Courtaulds, Ltd., Berkshire, England

August 31, 1949

IN a recent paper R. L. Scott[1] has derived two equations giving the critical or plait points of ternary systems containing one-polymer component. As these equations are of the third and fourth order, respectively, they have twelve solutions, of which Scott has shown two to be spurious; he has shown how to calculate the remaining ten roots for polymers of infinite chain-length, and has indicated how to obtain the roots for large polymers as expansions by the reciprocal chain-length.

It is the purpose of this note to show that one more of the solutions is spurious and to indicate a numerical method for calculating the nine plait points for any value of the chain-length, should this be required.

Introducing constants $\mu_1=\mu_{12}+\mu_{13}-\mu_{23}$ and similarly, μ_2 and μ_3, Scott's Eqs. (26) and (27)[2] can be written, in his notation:

$$\varphi_1(1-\mu_2\varphi_2)(1-m\mu_3\varphi_3)+\varphi_2(1-\mu_1\varphi_1)(1-m\mu_3\varphi_3)+m\varphi_3(1-\mu_1\varphi_1)(1-\mu_2\varphi_2)=0, \quad (1)$$

$$\varphi_3(1-\mu_1\varphi_1)[\varphi_1(1-m\mu_3\varphi_3)+m\varphi_3(1-\mu_1\varphi_1)]+\varphi_3(1-\mu_2\varphi_2).[\varphi_2(1-m\mu_3\varphi_3)+m\varphi_3(1-\mu_2\varphi_2)]-[\varphi_1(1-\mu_2\varphi_2)+\varphi_2(1-\mu_1\varphi_1)]^2=0. \quad (2)$$

Equation (1) is symmetrical with respect to the volume fractions φ, except for the intrusion of m_1, while Eq. (2) is not; it can, however, be made symmetrical most easily by introducing new variables U, V, and W, defined by

$$U=\varphi_1/(1-\mu_1\varphi_1), \quad V=\varphi_2/(1-\mu_2\varphi_2), \quad W=m\varphi_3/(1-m\mu_3\varphi_3). \quad (3)$$

Equations (1) and (2) then become

$$U+V+W=0 \quad (4)$$

$$U(1+\mu_1U)^2+V(1+\mu_2V)^2+mW(1+\mu_3W)^2=0, \quad (5)$$

where Eq. (4) has been used to simplify Eq. (5). These equations together with Eq. (6)

$$U/(1+\mu_1U)+V/(1+\mu_2V)+W/m(1+\mu_3W)=1 \quad (6)$$

which results from $\varphi_1+\varphi_2+\varphi_3=1$, have nine roots and determine the nine critical points. It is easily confirmed that for infinite chain-length ($m=\infty$), nine of the ten points given by Scott satisfy these equations, while the point given by his Eq. (47) does not and is spurious. Incidentally, this solution satisfies his Eqs. (26) and (27) for all values of m. This solution, and the other two spurious ones quoted by Scott, are introduced during the algebraic manipulation of the equations by the necessity of multiplying with factors of the form $1-\mu_i\varphi_i$; had n_1 and n_3, or n_2 and n_3, been used in the fundamental equations of the plait points (Scott's Eqs. (20) and (21)), instead of n_1 and n_2, then three other spurious solutions would have been introduced. None of these spurious roots appear if the plait points are calculated from the expression for the free energy of mixing for "one mole of sites," $n_1+n_2+mn_3=1$, using two of the φ as independent variables, in extension of the treatment of Van der Waals and Kohnstamm[3] for divariant binary systems to divariant ternary systems.

Solutions for any value of m can be obtained by assuming a trial value of U and calculating V and W from Eqs. (4) and (6); Eq. (6) reduces to a quadratic for given U, Eq. (5) is then used to ascertain whether the chosen value of U is correct; if it is not, the value of the l.h.s. of Eq. (5) can be used as a guide for the choice of a better U; the process may be repeated until Eq. (5) is satisfied to any desired degree of accuracy.

Equations (4), (5), and (6) can be written in terms of the φ's in the following symmetrical forms:

$$\varphi_1/(1-\mu_1\varphi_1)+\varphi_2/(1-\mu_2\varphi_2)+m\varphi_3/(1-m\mu_3\varphi_3)=0 \quad (7)$$

$$\varphi_1/(1-\mu_1\varphi_1)^3+\varphi_2/(1-\mu_2\varphi_2)^3+m^2\varphi_3/(1-m\mu_3\varphi_3)^3=0 \quad (8)$$

$$\varphi_1+\varphi_2+\varphi_3=1. \quad (9)$$

After multiplication these equations are of the third, seventh, and first order, respectively; they have therefore twenty-one solutions, of which the following are spurious: $\varphi_1=1/\mu_1$, $\varphi_2=1/\mu_2$, $\varphi_3=1-1/\mu_1-1/\mu_2$, and two analogous ones, three times each, and three solutions at infinity, obtained by making the equations three solutions at infinity, obtained by making the equations homogeneous by means of a fourth variable z in the form (1, −1, 0, 0), (−1, 0, 1, 0), and (0, 1, −1, 0). We are thus left with nine genuine critical points.

The author is grateful to Mr. J. Crank and Dr. J. G. Oldroyd for helpful discussion of some of the points arising in this note.

[1] R. L. Scott, J. Chem. Phys. **17**, 268 (1949).

[2] The + sign in front of φ_3 in the third line of Eq. (27) should be replaced by a − sign.

[3] Van der Waals and Kohnstamm, *Lehrbuch der Thermostatik* (Leipzig, 1927).